

Project Report
ASAP-6
Volume 1

Proceedings of the Adaptive Sensor Array Processing (ASAP) Workshop 11-12 March 1998

990 91908661

G.M. O'Donovan
Editor

15 May 1998

Lincoln Laboratory
MASSACHUSETTS INSTITUTE OF TECHNOLOGY
LEXINGTON, MASSACHUSETTS



Prepared for the Defense Advanced Research Projects Agency and the Department of the Navy under
Air Force Contract F19628-95-C-0002.

Approved for public release; distribution is unlimited.

DTIC QUALITY INSPECTED 2

This report is based on studies performed at Lincoln Laboratory, a center for research operated by Massachusetts Institute of Technology. The work was sponsored in part by the Defense Advanced Research Projects Agency and in part by the Department of the Navy under Air Force Contract F19628-95-C-0002.

This report may be reproduced to satisfy needs of U.S. Government agencies.

The ESC Public Affairs Office has reviewed this report, and it is releasable to the National Technical Information Service, where it will be available to the general public, including foreign nationals.

This technical report has been reviewed and is approved for publication.
FOR THE COMMANDER

Gary Tungian
Gary Tungian

Administrative Contracting Officer
Directorate of Contracted Support Management

Non-Lincoln Recipients

PLEASE DO NOT RETURN

Permission is given to destroy this document
when it is no longer needed.

MASSACHUSETTS INSTITUTE OF TECHNOLOGY
LINCOLN LABORATORY

**PROCEEDINGS OF THE ADAPTIVE SENSOR ARRAY
PROCESSING (ASAP) WORKSHOP
11-12 MARCH 1998**

G.M. O'DONOVAN
EDITOR
Division 10

PROJECT REPORT ASAP-6, VOLUME 1

15 MAY 1998

DTIC QUALITY INSPECTED 3

Approved for public release; distribution is unlimited.

LEXINGTON

MASSACHUSETTS

1998 ASAP Workshop Theme

This year marks the sixth annual ASAP workshop, which is sponsored jointly by the DARPA Sensor Technology, Tactical Technology, and Information Systems Offices, and the Navy AEGIS and E2C Program Offices. This unique joint sponsorship is the result of this year's workshop focus and the many organizations that are developing adaptive signal processing technologies to address critical national defense concerns.

In 1997 the workshop focused on the synergy between the sonar and radar communities and their approaches to adaptive signal processing problems. This year we will continue expanding this interaction by providing a forum in which important new developments may be presented and discussed within the context of national defense. The theme for this year's workshop will be adaptive sensor fusion, which extends the concept of an array to a "system of systems." This theme is strengthened by the inclusion of adaptive techniques for model-based image processing and SAR to complement sonar and radar.

In 1997 a companion meeting, the High Performance Embedded Computing (HPEC) workshop, focused on embedded computing architectures and the real-time implementation of advanced adaptive techniques on these architectures. This year HPEC will be held on 23-24 September 1998. The Workshop will feature case study examples of high performance embedded computing implementations.

We welcome your participation in the sixth annual ASAP workshop.



Dr. Mark Davis
DARPA/ISO
Foliage Penetration Radar
Program Manager

Major Dan Gammon
DARPA/STO
Advanced Signal Processing
Program Manager



Capt. Dan Meyer
US Navy/PMS-400
AEGIS
Program Manager

Dr. Allan Steinhardt
DARPA/TTO
Maritime Systems
Program Manager



Mr. Fred Lee
US Navy/PMA-231 AD
E2C Advanced Development
Deputy Program Manager

Advisory Committee

Arthur Baggeroer / MIT
Lloyd Griffiths / George Mason University
Kenneth Senne / MIT Lincoln Laboratory

Technical Program Coordinator

Christ D. Richmond

Workshop Administrator

Cindy Pelley

ADAPTIVE SENSOR ARRAY PROCESSING WORKSHOP 11-12 MARCH 1998

SPEAKER PRESENTATIONS

VOLUME 1

SPEAKER	TITLE	PAGES
Thomas Miller Raytheon Systems Co.	Keynote Address Adaptive Processing: An Implementation Perspective	1-25
	POSTER PRECIS	
Daniel Fuhrman Washington University	The Subspace Tracking Loop	27-44
Timothy Barton MIT Lincoln Laboratory	Mutual Coherence Parameter Estimation	45-68
John Hoffman, Louis Vasquez, Charles Farthing and Clarence Ng Systems Engineering Group, Inc. Kenneth Johnson Naval Surface Warfare Center	Adaptive Distributed Clutter Improvement Factor (ADDCIF)	69-86
Daniel Kreithen, Carl Pearson and Christ Richmond MIT Lincoln Laboratory	Adaptive Sidelobe Blanker: Threshold Setting and Performance in Inhomogeneous Clutter	87-102
Yaron Seliktar, Douglas Williams and Jeff Holder Georgia Institute of Technology	Adaptive Monopulse Processing in the Presence of TSI and Mainbeam Jamming	103-120

Nicholas Pulsone and Edward Baranoski MIT Lincoln Laboratory	Adaptive Wideband Interference Suppression for a Beam-space Application (AN/SPY-1)	121-138
Matthew Nelson and Ralph Chatham Dynamics Technology, Inc.	Synthetic Aperture Sonar	139-155
Travis Slocumb SAIC	SESSION I: Radar Array Processing	157-167
Gary Hatke MIT Lincoln Laboratory	Space-Time Adaptive Processing Applied to GPS Adaptive Arrays	169-193
Joseph Guerci SAIC	Covariance Matrix Tapers: A Unifying Framework for Robust Adaptive Array Beamforming	195-214
J. Scott Goldstein MIT Lincoln Laboratory I. Reed University of Southern California L. Scharf University of Colorado	A New Interpretation of the Wiener Filter	215-233
S. Unnikrishna Pillai, Y. Kim, and Joseph Guerci Polytechnic University	Strategies for Minimal Sample Support STAP	235-261
Daniel Rabideau MIT Lincoln Laboratory	Advanced STAP for TSI Modulated Clutter	263-287
Mark Davis DARPA	SESSION II: SAR	289-294
Charles Le and Scott Hensley Jet Propulsion Laboratory	RFI Rejection in Wideband SAR Signals Using LMS Adaptive Filters	295-331
Mitchell Mirkin MIT Lincoln Laboratory	Adaptive Dual Aperture Clutter Cancellation	333-353

Stuart DeGraaf Northrop Grumman Corp.	Adaptive SAR Imaging and its Impact on ATD/R and Image Exploitation	355-373
Lloyd Griffiths George Mason University	SESSION III: Detection and Estimation 1	375-380
A. Lee Swindlehurst Brigham Young University Petre Stoica Uppsala University	On the Use of Unstructured Array Models for Space-Time Adaptive Processing	381-403
Christ Richmond MIT Lincoln Laboratory	Performance of the Adaptive Sidelobe Blanker Detection Algorithm in the Presence of Signal Mismatch	405-431
Steven Smith MIT Lincoln Laboratory	Estimation for Synthetic Bandwidth Processing	433-456
Gregory Duckworth BBN Technology	SESSION IV: Sonar 1	457
Howard Lazoff BBN Technologies	Target Tracking Using Fuzzy Logic Association Techniques	459-470
Henry Cox Orincon	Some Improvements to Dominant Mode Rejection Adaptive Beamforming	471-486
James Ward and Lisa Zurk MIT Lincoln Laboratory Arthur Baggeroer Massachusetts Institute of Technology	Rapidly Adaptive Matched Field Processing for Nonstationary Environments	487-509

**Adaptive Processing:
An Implementation Perspective**

DR. THOMAS W. MILLER
RAYTHEON SYSTEMS COMPANY

11 MARCH 1998

Outline

- The Past
 - Background
 - Overview of Past Applications
- The Present
 - Implementation Issues
 - Example Applications
 - *A/J for GPS*
 - *Acoustic Noise Reduction*
 - *STAP for Sonar*
 - *Fighter Radars*
 - *Hot Clutter*
 - Thumbing Through the Abstracts
- The Future
 - Application Areas
 - Trends

In The Beginning...

there was

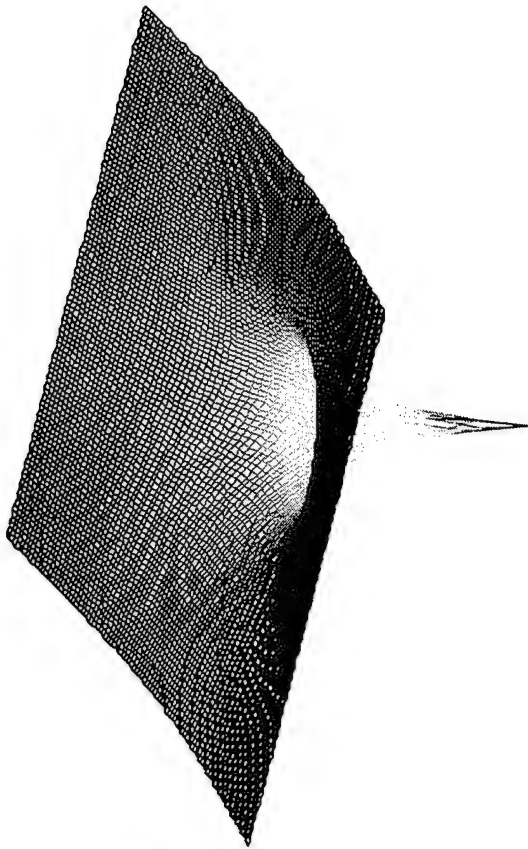
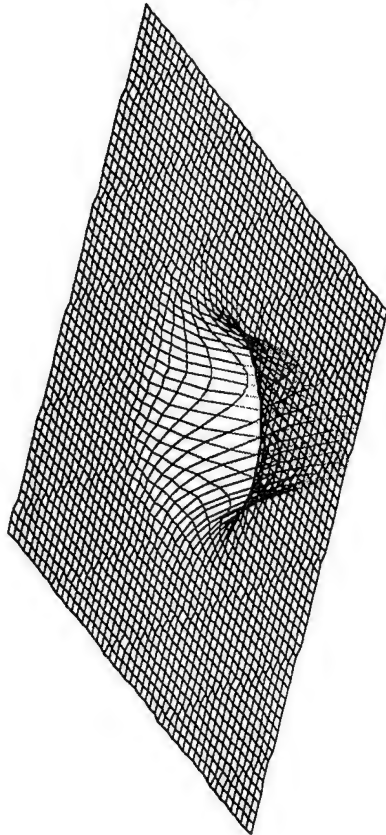
$$\underline{w} = R_{xx}^{-1} \underline{d}$$

**and it was very good,
but it was difficult to implement.**

A Comparison

$$E = mc^2$$

$$\underline{W} = R_{xx}^{-1} \underline{d}$$

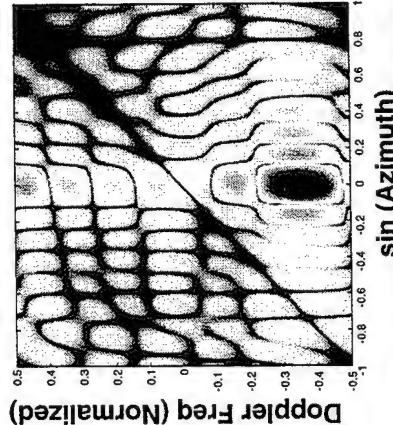
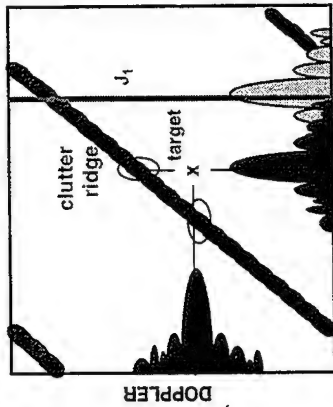


Space-Time Continuum

Space-Time Processing

It's not yet a basic tenet of the universe, but its importance is growing...

30 Years of Adaptation



FUNCTIONS		ALGORITHMS	
	Hot Clutter		
	Irregular Arrays		
	STAP Processing		
	Digital Beamforming		
	Super-Resolution		
	Adaptive Filtering		
	Sidelobe Cancellers		
	Fully Adaptive Beamforming with Null-Steering		
		QR Methods / SVD	
		Maximum Likelihood	
		Matrix Inverse Algorithms	
		Search Algorithm / Sequential Gradient	
		LMS Algorithm / Howells-Applebaum Algorithm	
		Phase Only	Phase Only

1968 1978 1988 1998

The Top Ten Words and Phrases...

...guaranteed to glaze a program manager's eyes
(... or smoke out the true believers)

10. taxonomy

9. conjugate gradient

8. recursive least squares

7. Cramer-Rao bound

6. Toeplitz / Hermitian

5. Q-R decomposition

4. beamspace / element space / space-time

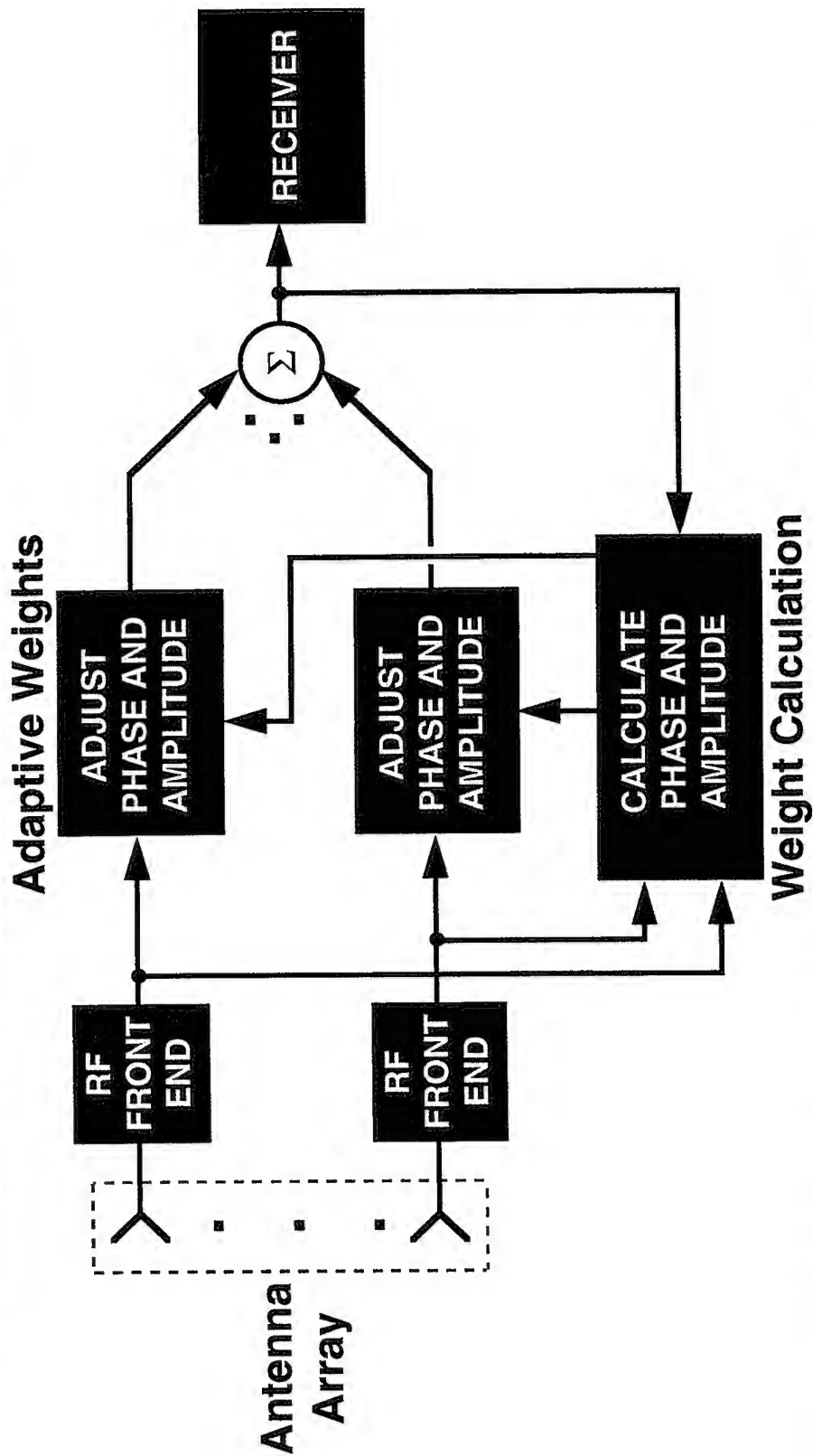
3. Gram-Schmidt orthogonalization

2. singular value decomposition

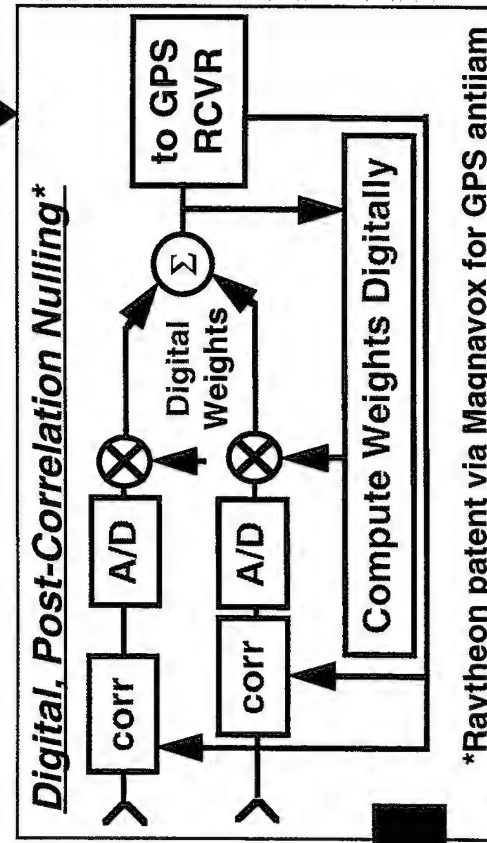
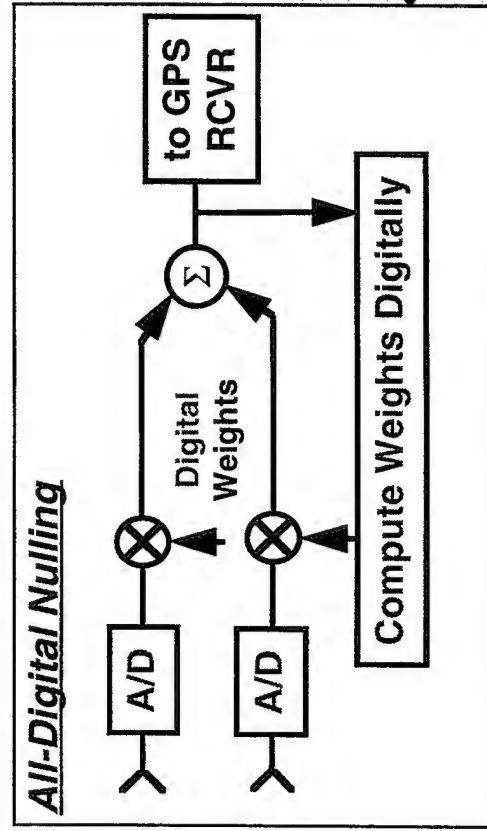
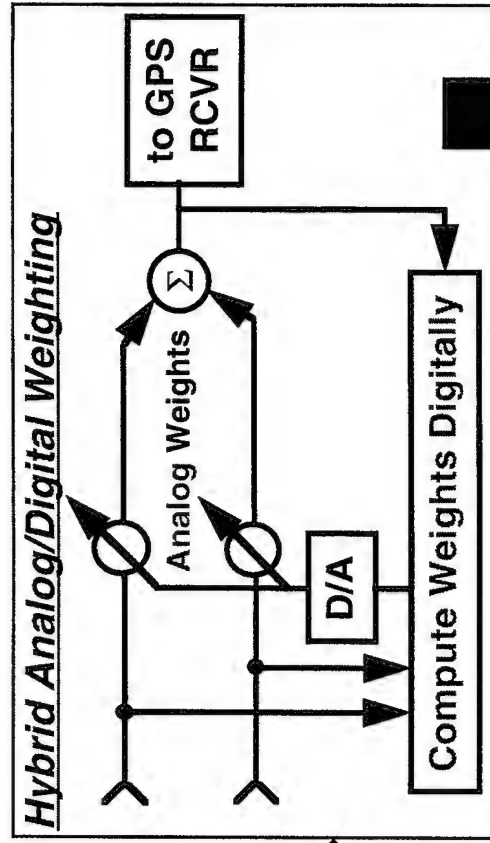
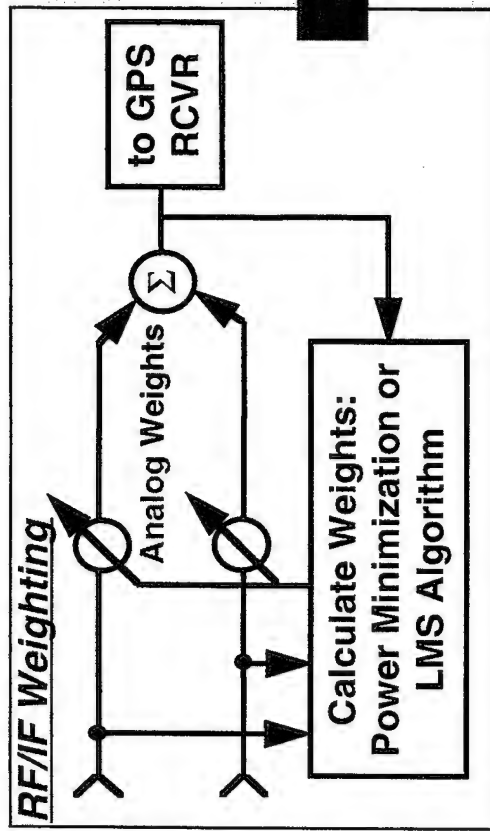
1. eigen-anything

The Theory

An Adaptive Array Can Be Implemented Using Various Combinations of Digital and Analog Technologies



From Theory to Practice: GPS Receiver Example



Potential Pitfalls

Common Factors

- channel matching
- multipath and hot clutter
- polarization
- rotating antenna
- antenna calibration
- VSWR reflections

Digital Implementations

- limited bandwidth
- limited dynamic range
- high computational loads

Analog Implementations

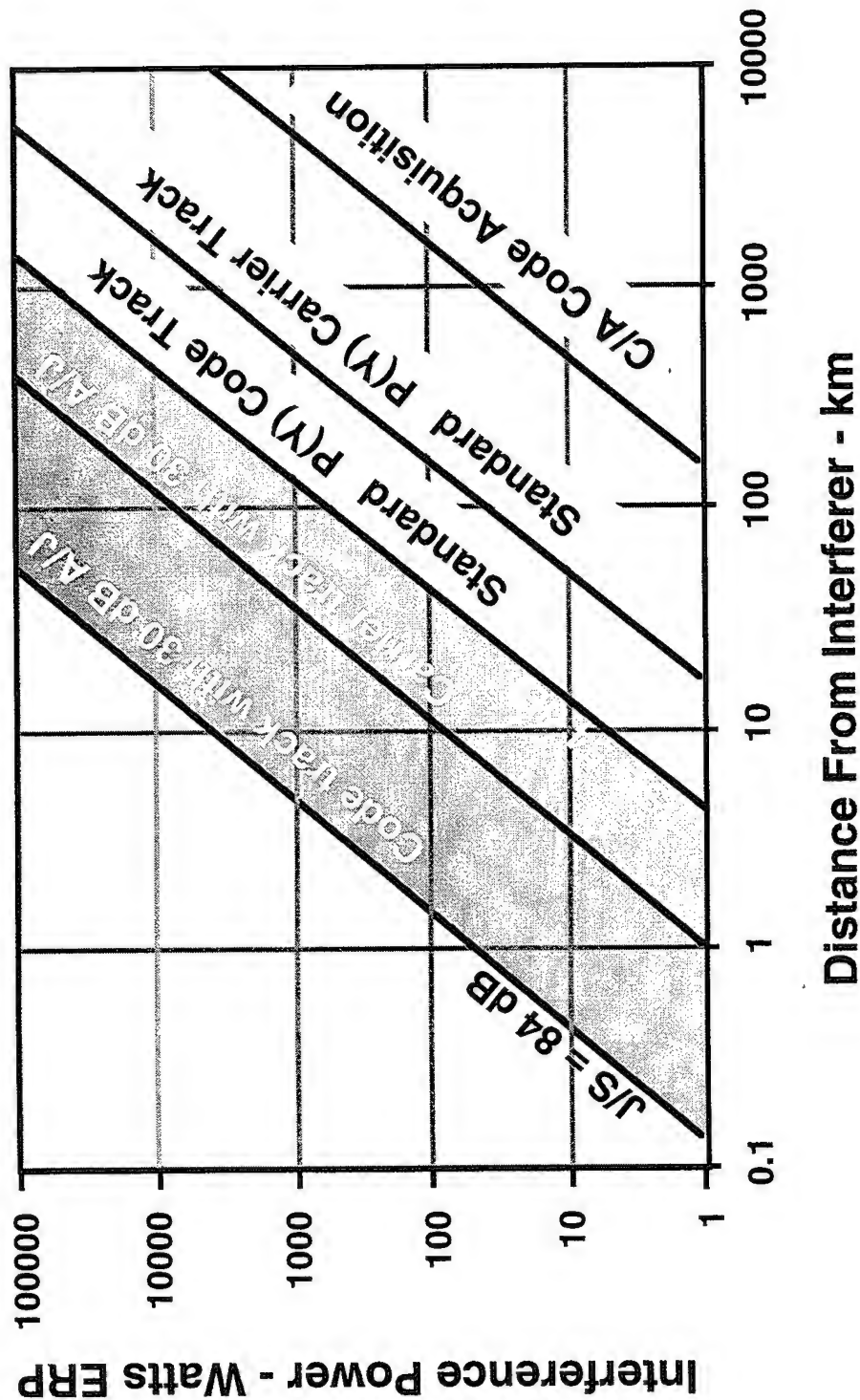
- phase shift in the feedback loops
- slow convergence
- limited accuracy
- signal distortion
- difficult to use equalization
- loop instability caused by large interferer
- correlator d.c. offset, dynamic range limitations

Outline

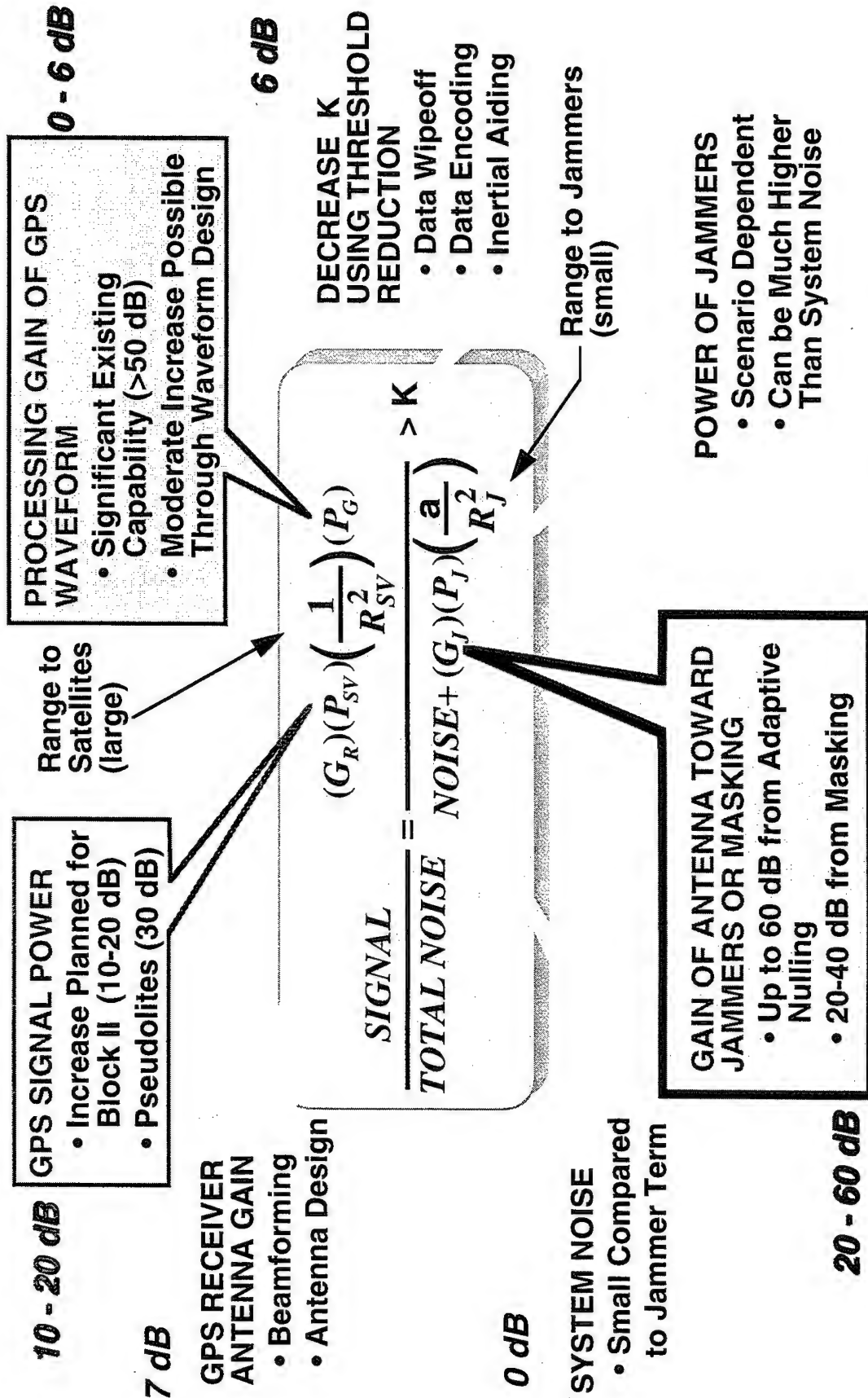
- The Past
 - Background
 - Overview of Past Applications
- The Present
 - Implementation Issues
 - Example Applications
 - *A/J for GPS*
 - *Acoustic Noise Reduction*
 - *STAP for Sonar*
 - *Fighter Radars*
 - *Hot Clutter*
 - Thumbing Through the Abstracts
- The Future
 - Application Areas
 - Trends

Effect of Interference on GPS Receivers

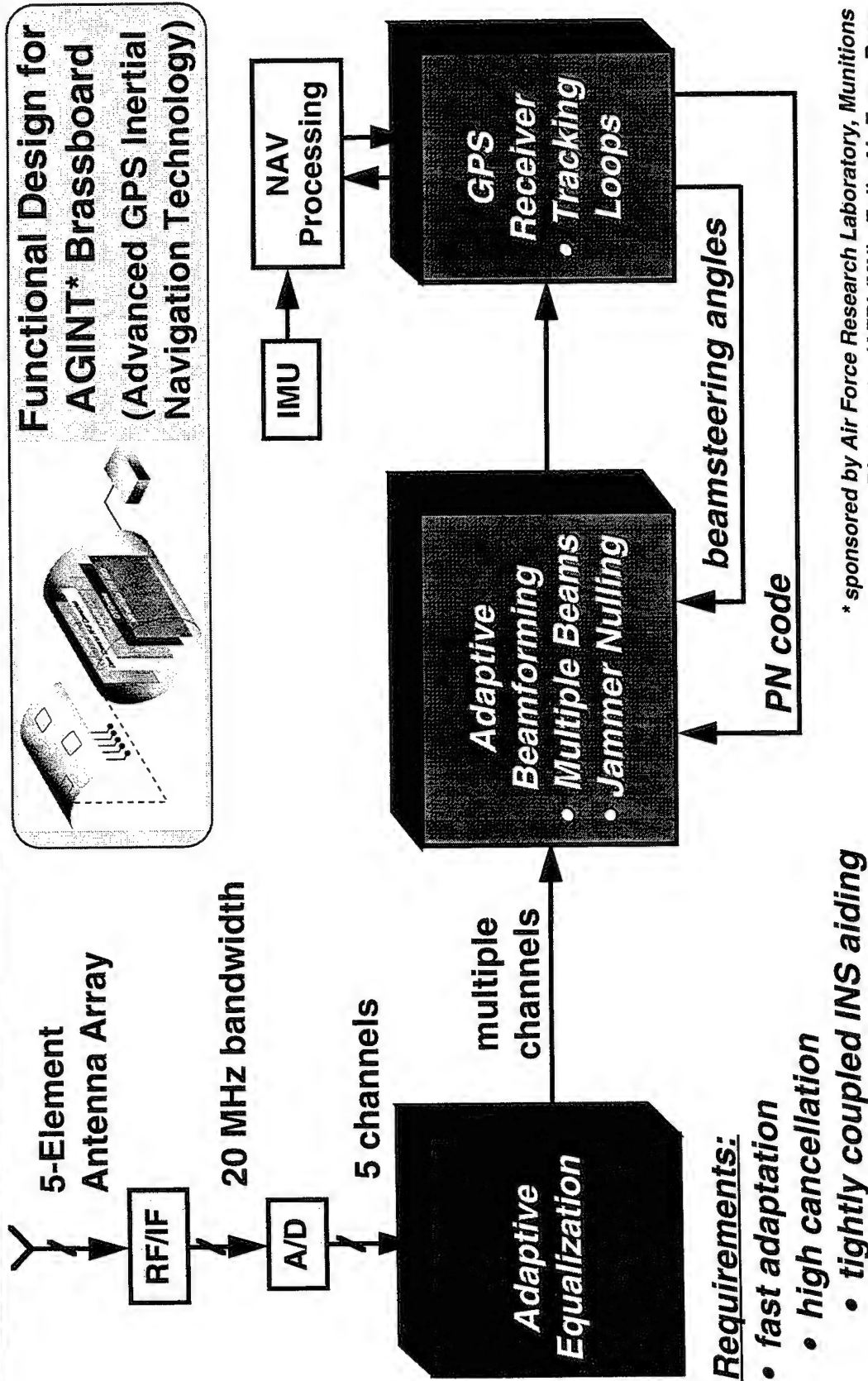
GPS Navigation



Raytheon The Bottom Line: Improving SNR (GPS Receiver Example)

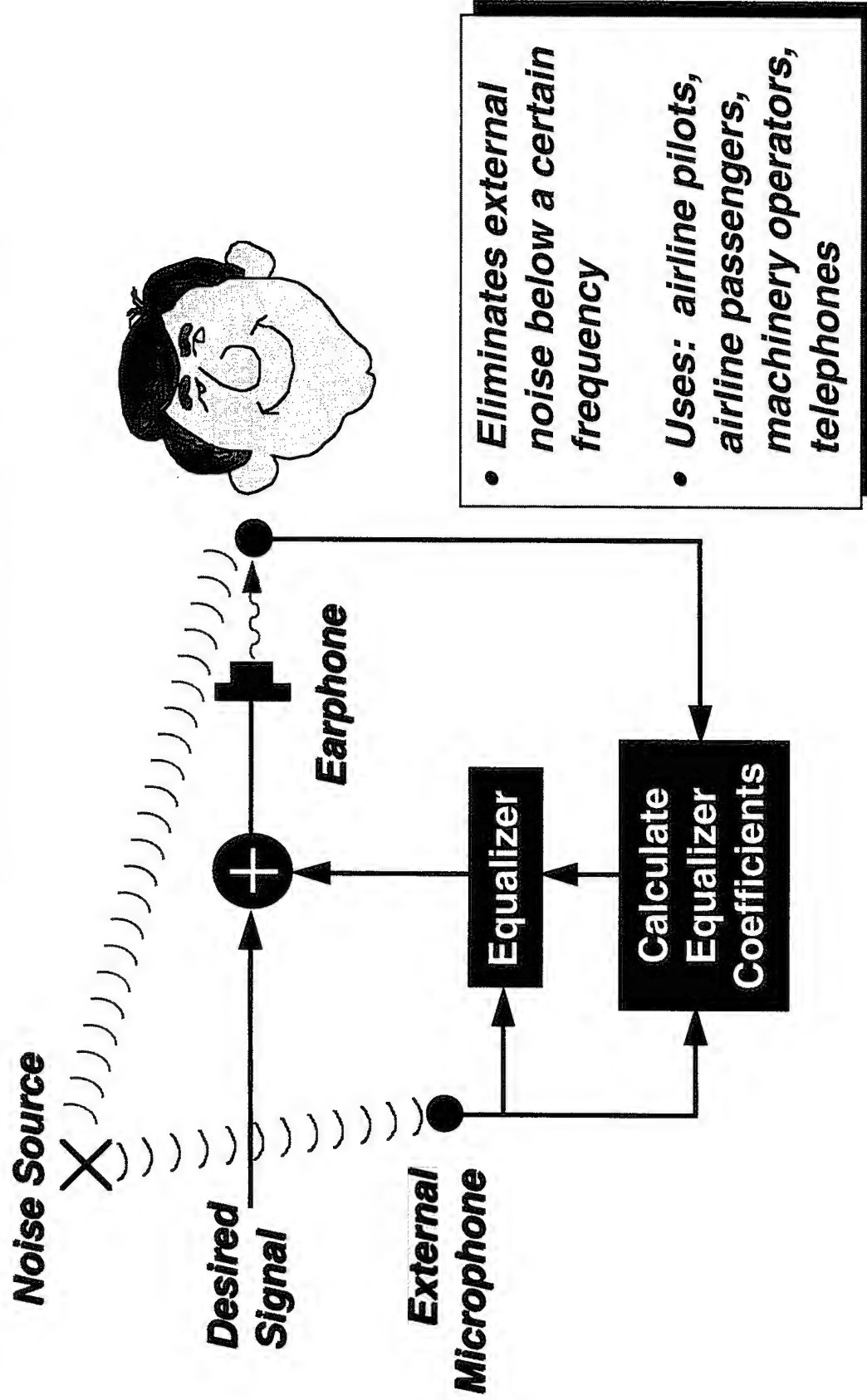


Current Research: GPS Applications

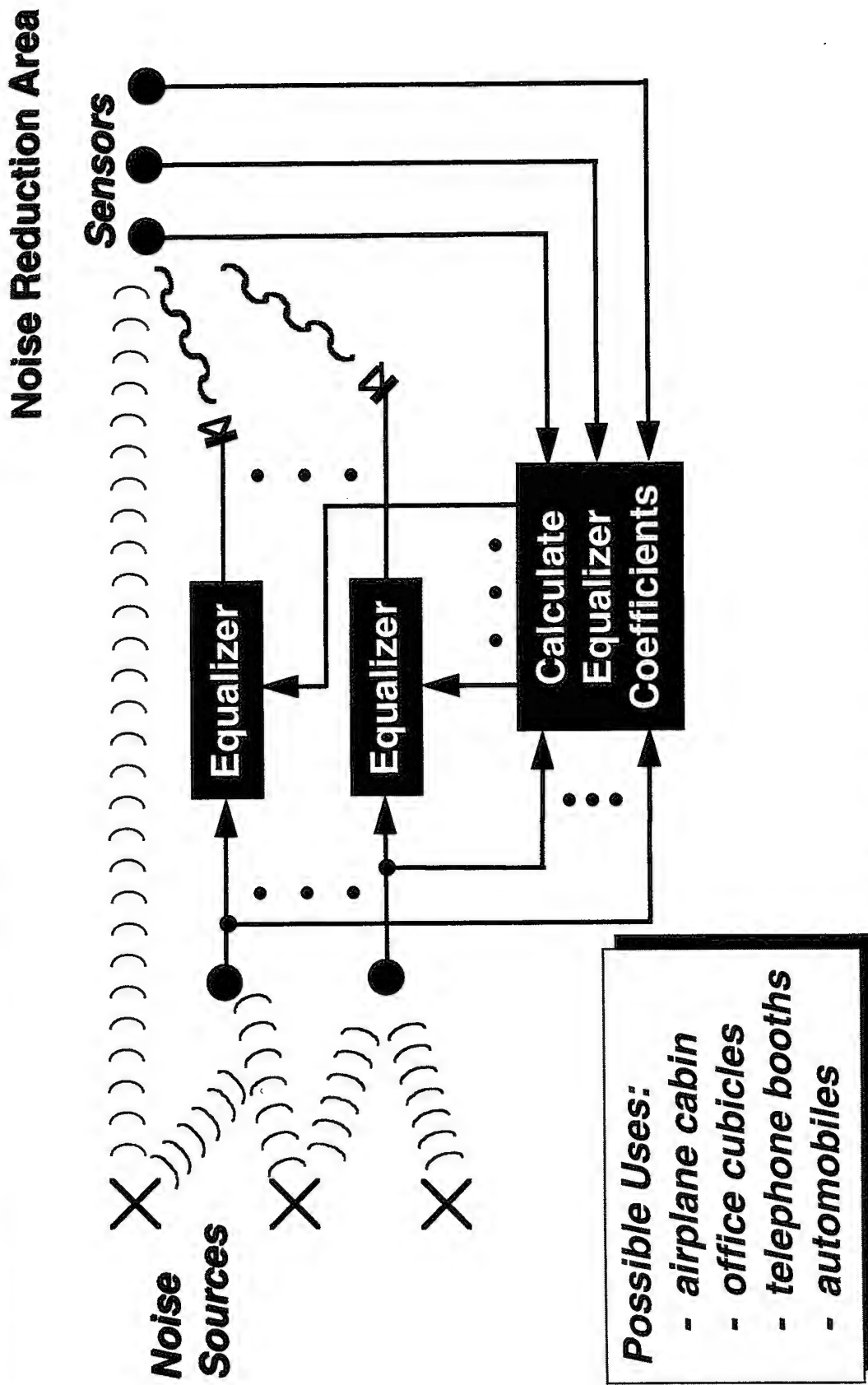


* sponsored by Air Force Research Laboratory, Munitions Directorate (AFRL/MN), Eglin Air Force Base
<http://www.munitions.eglin.af.mil/public/mnngn/mnngnhome.html>

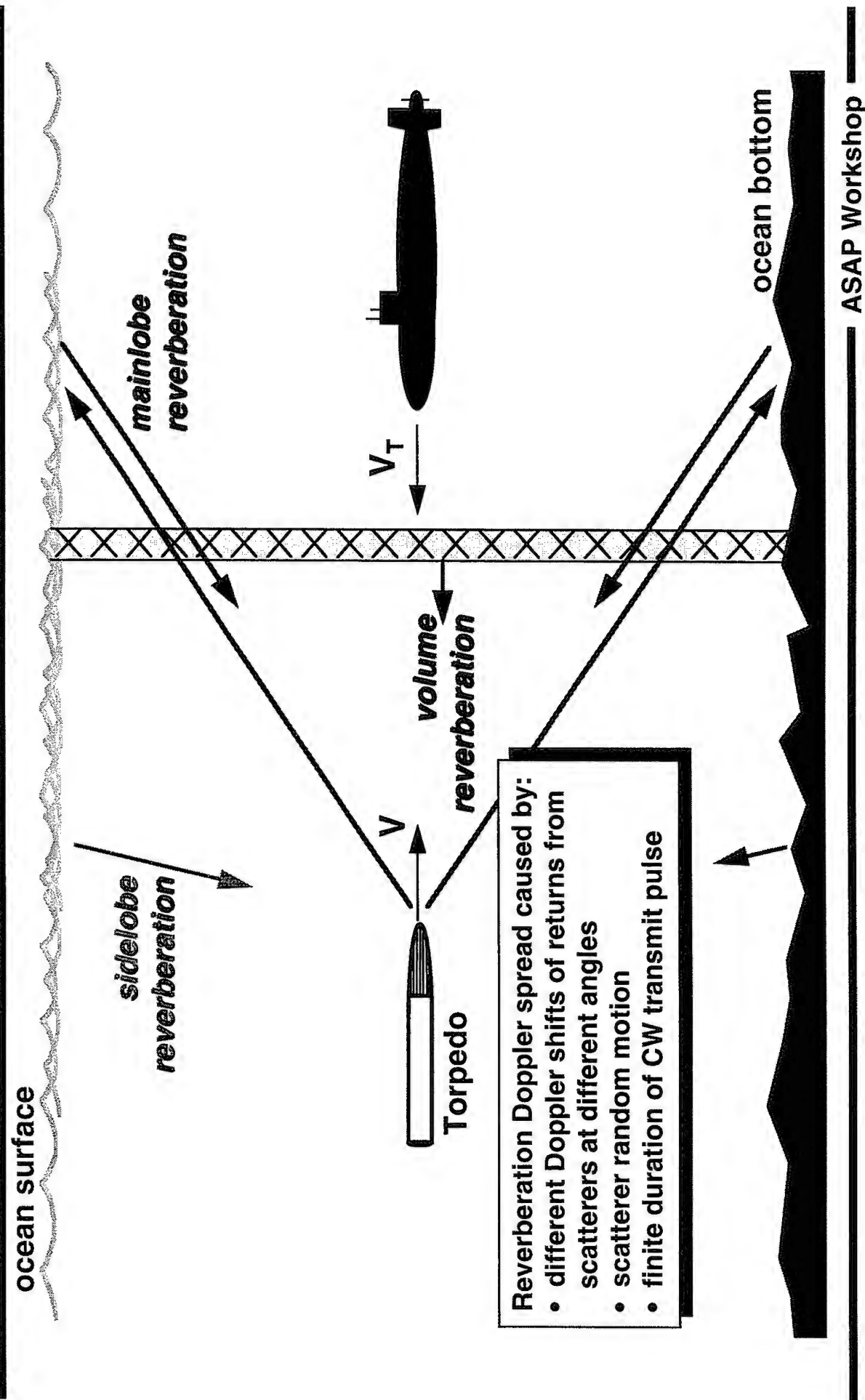
Acoustic Applications: Noise Cancellation Earphones



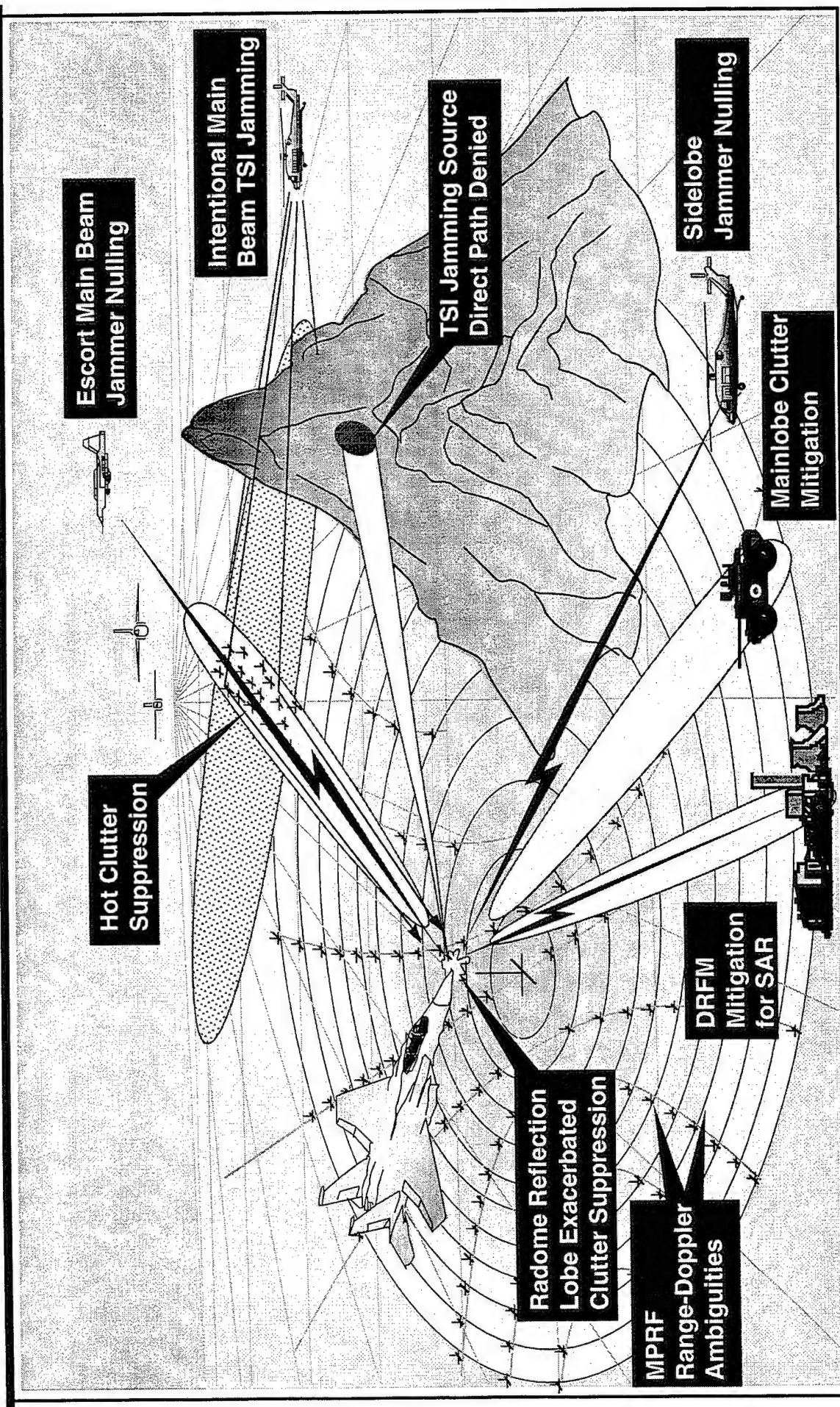
Acoustic Applications: Area Quieting



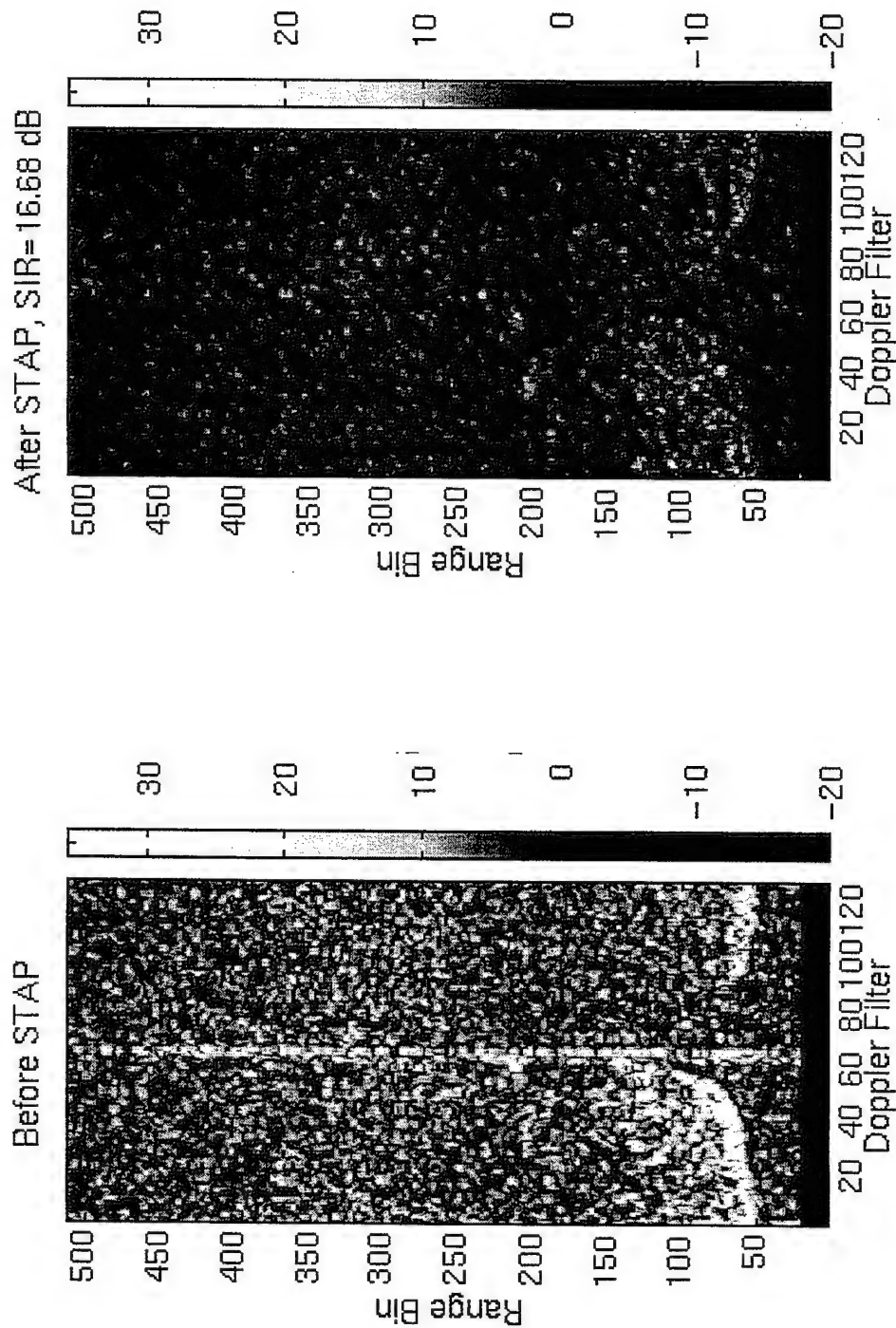
Sonar Application: Shallow Water Reverberation



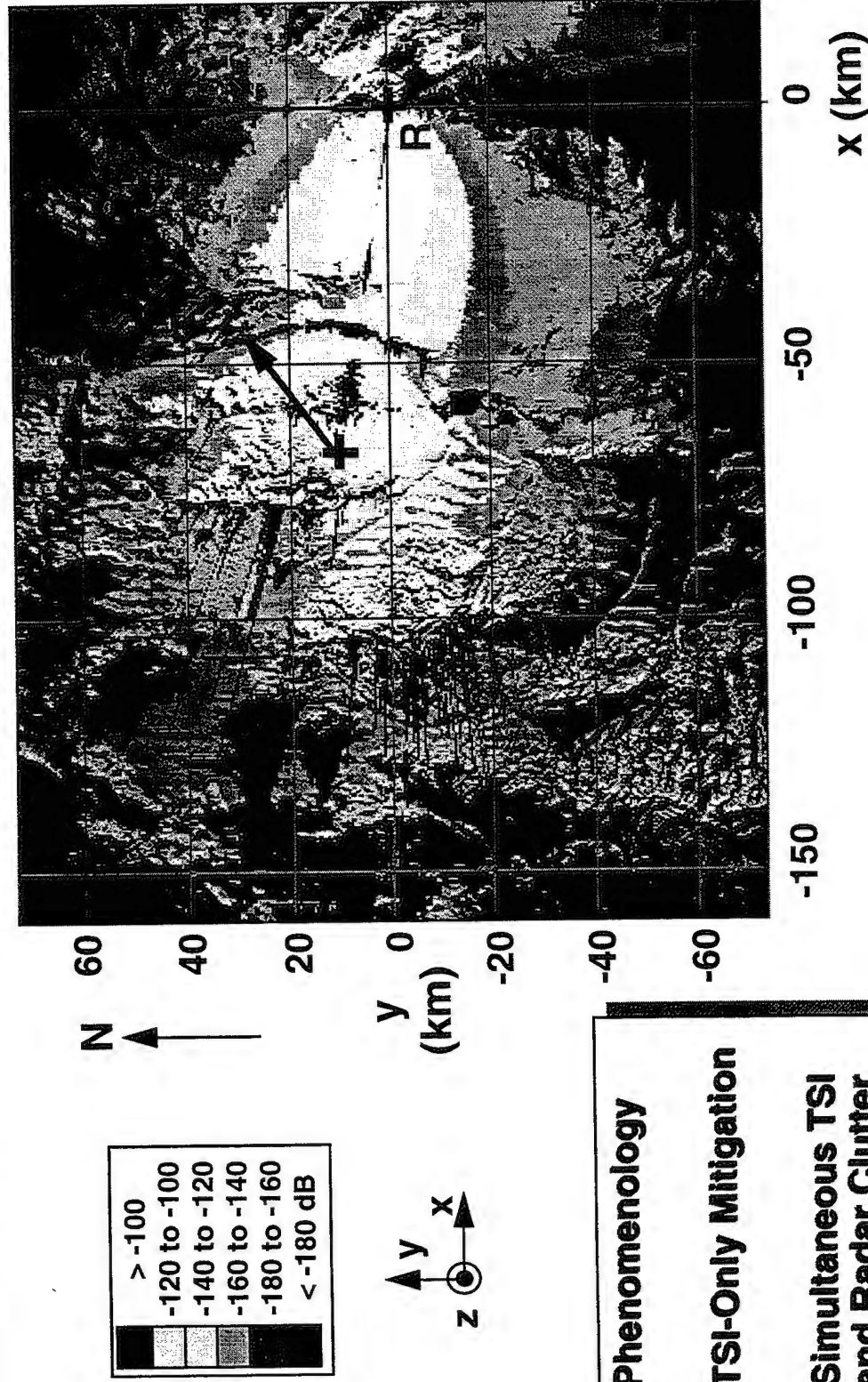
Raytheon Adaptive Processing for Future Fighters



Sidelobe Clutter Mitigation with Flight Test Data

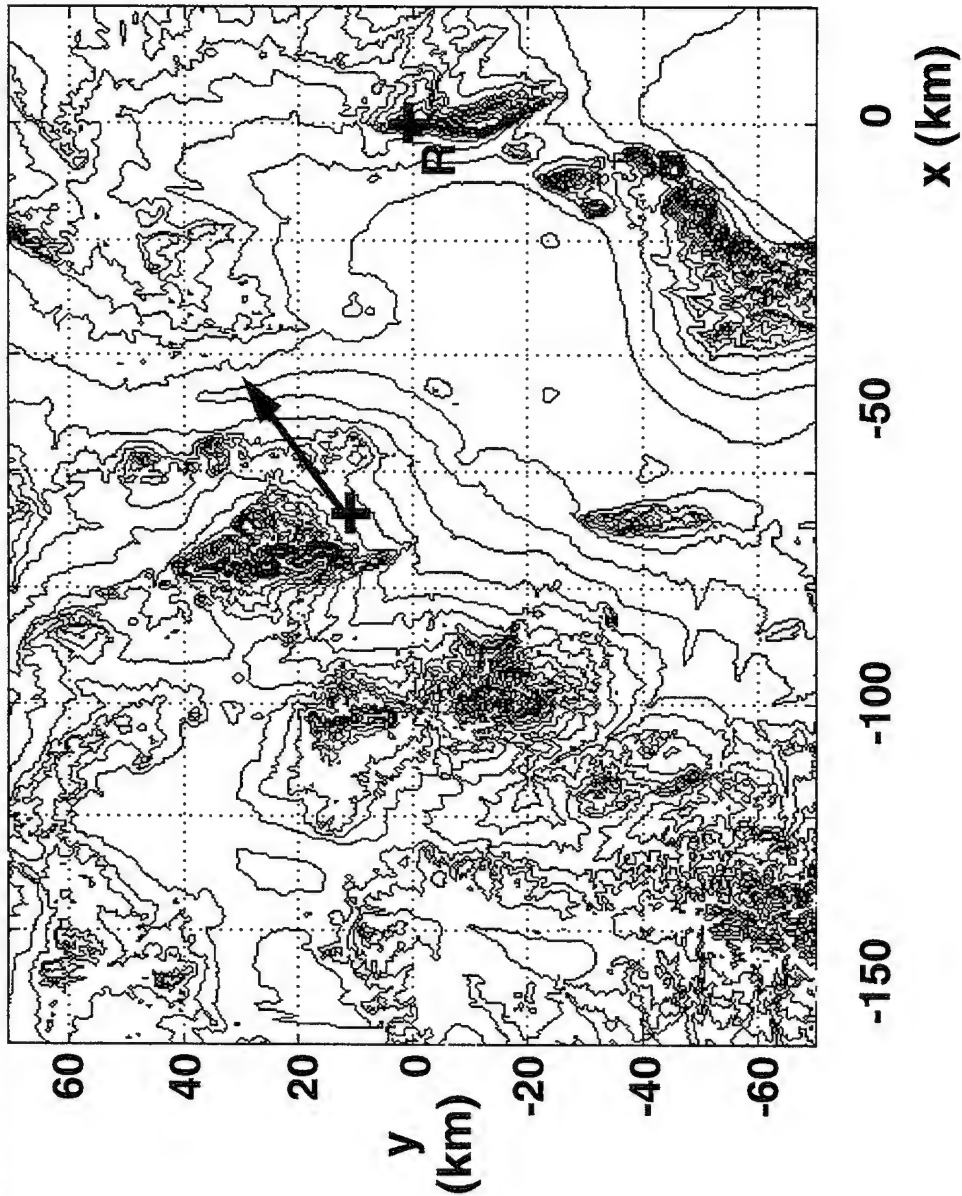


Raytheon Simulated Hot Clutter Example: Airborne Jammer



- Phenomenology
- TSI-Only Mitigation
- Simultaneous TSI and Radar Clutter Mitigation

White Sands Missile Range (WSMR) 1200-3200 m 100 m contours



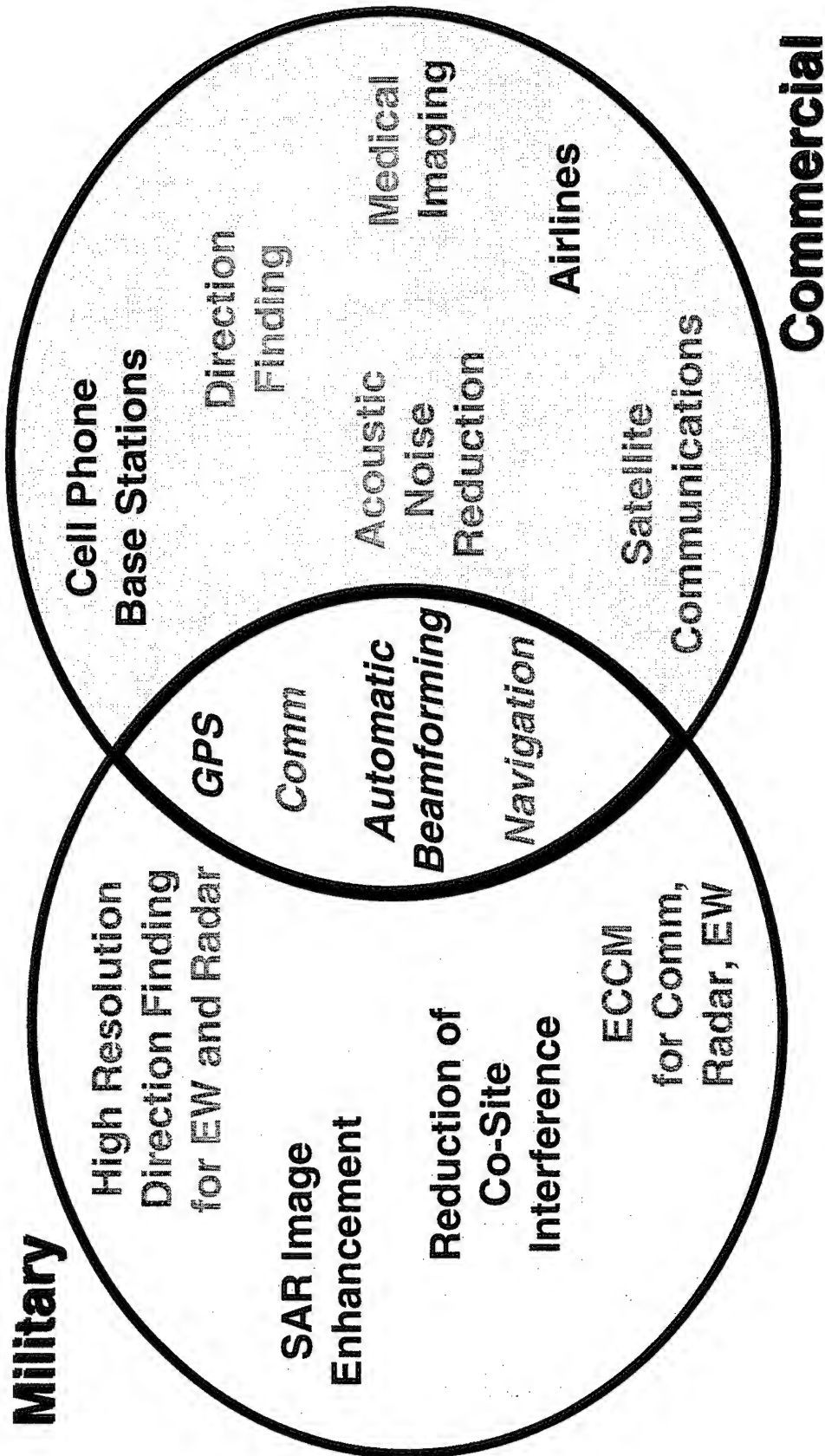
Thumbing Through the Abstracts

What to Look for Today and Tomorrow:

<ul style="list-style-type: none"> • solutions to combined hot clutter/cold clutter mitigation 	<ul style="list-style-type: none"> • <i>sample support for STAP processing</i>
<ul style="list-style-type: none"> • <i>minimizing signal distortion in adaptive arrays</i> 	<ul style="list-style-type: none"> • adaptive processing for SAR <ul style="list-style-type: none"> – image enhancement – interference rejection
<ul style="list-style-type: none"> • sub-banding vs. tapped-delay filtering 	<ul style="list-style-type: none"> • <i>synthetic aperture sonar</i>
<ul style="list-style-type: none"> • <i>angle finding after mainbeam nulling in TSI</i> 	<ul style="list-style-type: none"> • overcoming array calibration errors
<ul style="list-style-type: none"> • use of wavelets to optimize computational throughput 	<ul style="list-style-type: none"> • <i>synthetic wideband processing</i>

Applications to SONAR, COMM, RADAR, GPS

Application Areas to Watch

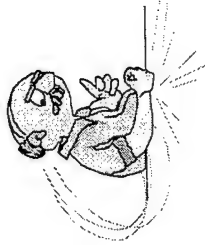


Future Directions

- **Trend toward all-digital implementations**

- *currently sampling at 50 MHz*
- *faster/cheaper/smaller/broader band applications*
- *more beams, deeper nulls, more degrees of freedom*

Do More!!



- **Denser signal environment increases need**

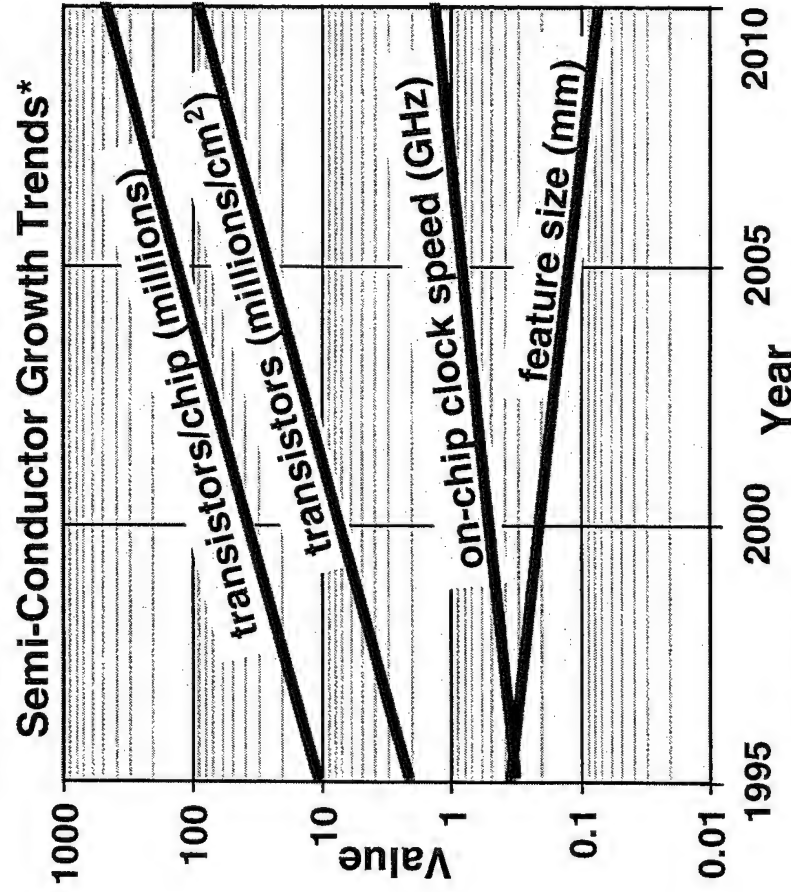
- *satellite proliferation*
- *co-channel interference*
- *wideband applications*

- **And often, “suboptimal” solutions as we continue to outpace processing capability and budgets**

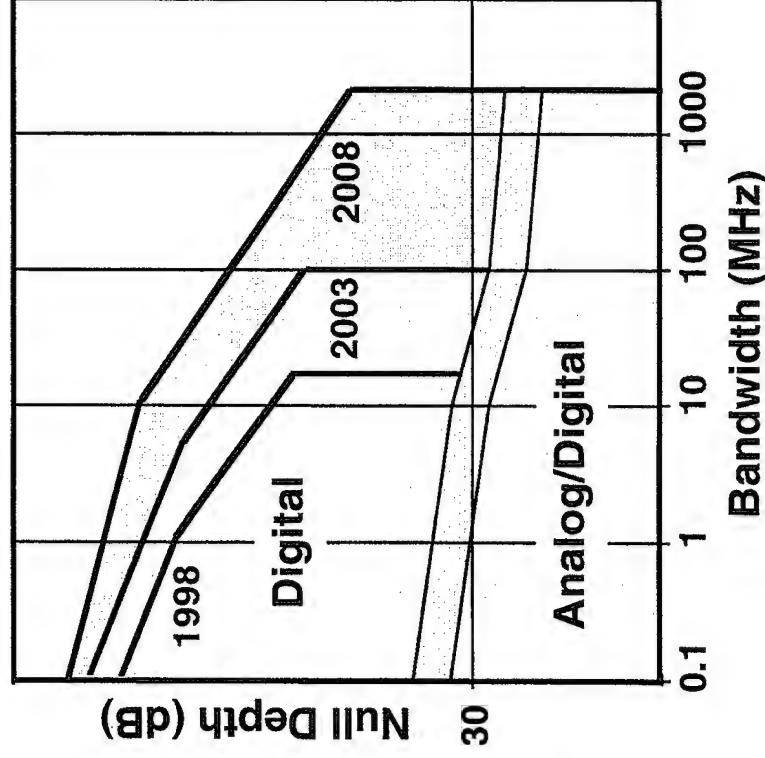


Supporting Technologies

- Digital Processing Trends Support Improved Capability and Lower Cost



* Source: Semiconductor Industry Association



- *Not the only story; must also consider I/O, Architectures, Software*
- *Additional Challenge: Low-Cost RF Front End*

What's Next ...

There will still be

$$\underline{w} = R_{xx}^{-1} \underline{d}$$

**but with new applications and
improved ways to implement them.**

The Subspace Tracking Loop

Daniel R. Fuhrmann

Department of Electrical Engineering
Campus Box 1127
Washington University
St. Louis, MO 63130
tel: (314) 935-6163
email: danf@saturn.wustl.edu

Abstract An algorithm for tracking the principal components of a time-varying covariance matrix is proposed. Unlike previous algorithms for subspace tracking, our method is based explicitly on a dynamic model for the time-varying subspace. The subspace $S(t)$, as a function of time, is considered as a trajectory in a Grassmann manifold, and is given a coordinate representation via the projection matrix $P(t)$. A general dynamic model for trajectories in the space of projection matrices (of fixed size N and rank K) is given by the differential equation

$$\dot{P}(t) = A(t)P(t) - P(t)A(t)$$

where $A(t)$ is a skew-symmetric matrix. If $A(t)$ is held constant, then this equation describes a constant-velocity trajectory along a geodesic, which has the closed-form expression

$$P(t) = e^{A(t)P(0)}e^{-At}$$

Our goal is to observe a sequence of data vectors $x(0), x(T), x(2T), \dots$ where $x(t)$ lies in or near the range space of $P(t)$, and using our dynamic model, estimate the trajectory $P(t)$ along with the constant or slowly time varying matrix A . Specifically, one iteration of our algorithm, applied for each new data vector x_i is as follows:

- 1) $B = xx^H P - Pxx^H$
- 2) $A \leftarrow \text{FILTER } \{A, B\}$
- 3) $P \leftarrow e^{AP}e^{-A}$

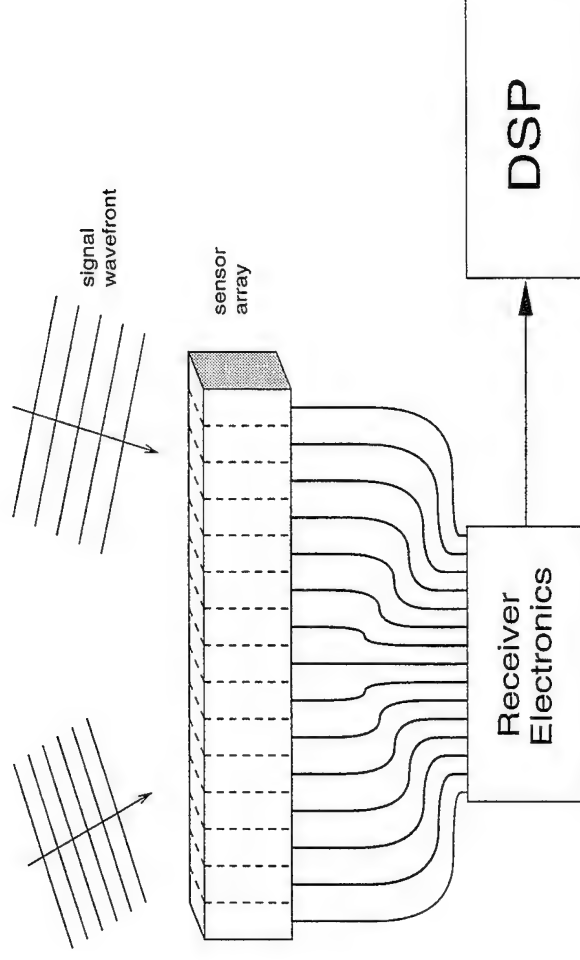
The structure of this tracking algorithm bears some resemblance to a phase-locked loop, and in fact steps 1, 2, and 3 above can be viewed as the analogues of a mixer, a loop filter and a VCO, respectively. With this analogy in mind we have termed this algorithm the subspace tracking loop (STL). Analysis of this loop can be accomplished by first linearizing steps (1) and (3) above. As with the classical PLL, the amplitude of the input signal determines the loop gain, and because this is a discrete-time control system, the unknown gain can cause stability to be an issue. Proper design of the loop filter (step 2 above) is critical for overall system performance.

THE SUBSPACE TRACKING LOOP

Daniel R. Fuhrmann

Electronic Systems and Signals Research Laboratory
Department of Electrical Engineering
Washington University
St. Louis, Missouri

Sensor Array Signal Processing



Model equation:

$$\mathbf{z}(t) = \sum_{i=1}^M \mathbf{a}(\theta_i) s_i(t) + \mathbf{n}(t)$$

Subspace Methods

There is a class of signal processing methods for emitter location and adaptive beamforming which exploit the fact that the principal components of the data lie in the M -dimensional signal subspace $S = \text{span}(\mathbf{a}(\theta_1) \cdots \mathbf{a}(\theta_M))$.

These methods require the computation or estimation of the principal eigenvectors of the observation covariance matrix:

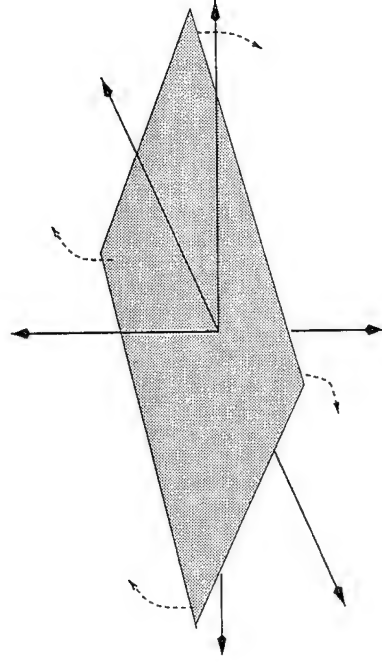
$$\mathbf{R} = \text{E}\{\mathbf{z}\mathbf{z}^H\} = \mathbf{A}(\Theta)\mathbf{R}_s\mathbf{A}^H(\Theta) + \mathbf{R}_n$$

Subspace Tracking

- Subspace methods depend on one's ability to determine accurately the signal subspace.
- If the emitters and/or the platform are moving, the signal subspace is *moving* and must be *tracked*.
- The **subspace tracking problem** is to estimate the signal subspace of $\mathbf{R}(t)$, call it $S(t)$, given a discrete sequence of observations $\mathbf{z}(0), \mathbf{z}(T), \mathbf{z}(2T), \dots, \mathbf{z}(KT), \dots$

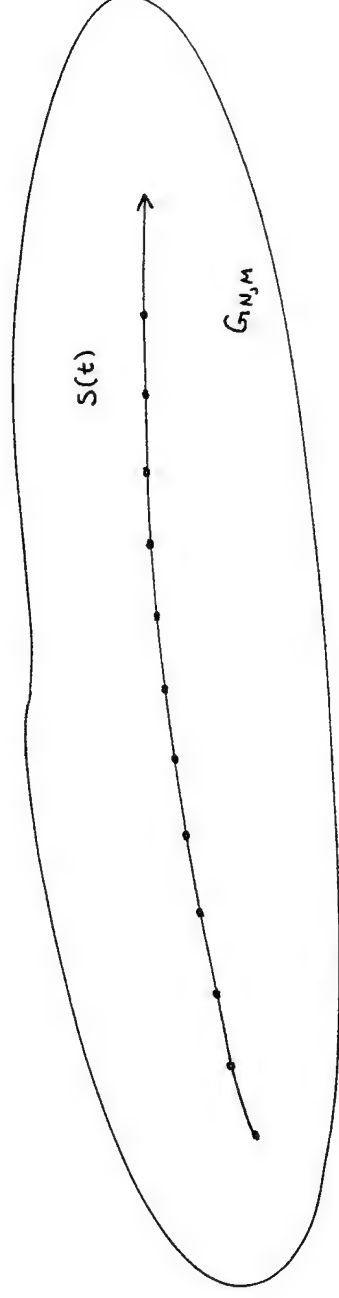
Equivalent Geometrical Problem

- The subspace tracking problem is very much like the problem of tracking a moving plane, only in higher dimensions.



- We use the geometric properties of the set of all signal subspaces (the *Grassmann manifold*) to develop models of subspace motion, and signal processing algorithms based on these models.

Grassmann Manifold



The Grassmann manifold $G_{N,M}$ is the set of all M -dimensional subspaces of \mathbb{R}^N . (Analysis carries over easily to the complex case).

An M -dimensional subspace S is a point in $G_{N,M}$.

A subspace S is uniquely identified by a projection matrix \mathbf{P} . The set of rank- M $N \times N$ projection matrices, which we call $P_{N,M}$, is isomorphic to $G_{N,M}$. We seek algorithms for *tracking* $\mathbf{P}(t)$ on its trajectory through $P_{N,M}$.

Mathematics of Subspace Motion

A smooth curve through $P_{N,M}$ satisfies a differential equation of the form

$$\dot{\mathbf{P}}(t) = \mathbf{A}(t)\mathbf{P}(t) - \mathbf{P}(t)\mathbf{A}(t)$$

where \mathbf{A} is a *skew-symmetric* matrix.

A *geodesic* curve through $P_{N,M}$ satisfies the differential equation

$$\dot{\mathbf{P}}(t) = \mathbf{A}\mathbf{P}(t) - \mathbf{P}(t)\mathbf{A}$$

where

$$\mathbf{A} = \dot{\mathbf{P}}(0)\mathbf{P}(0) - \mathbf{P}(0)\dot{\mathbf{P}}(0) \ .$$

The solution is

$$\mathbf{P}(t) = e^{\mathbf{A}t}\mathbf{P}(0)e^{-\mathbf{A}t} \ .$$

Canonical Representation of Geodesics

The skew-symmetric matrix \mathbf{A} which defines a geodesic has a decomposition of the form

$$\mathbf{A} = \begin{bmatrix} \mathbf{U}_1 & \mathbf{U}_3 \end{bmatrix} \begin{bmatrix} 0 & -\Omega \\ \Omega & 0 \end{bmatrix} \begin{bmatrix} \mathbf{U}_1^T \\ \mathbf{U}_3^T \end{bmatrix}$$

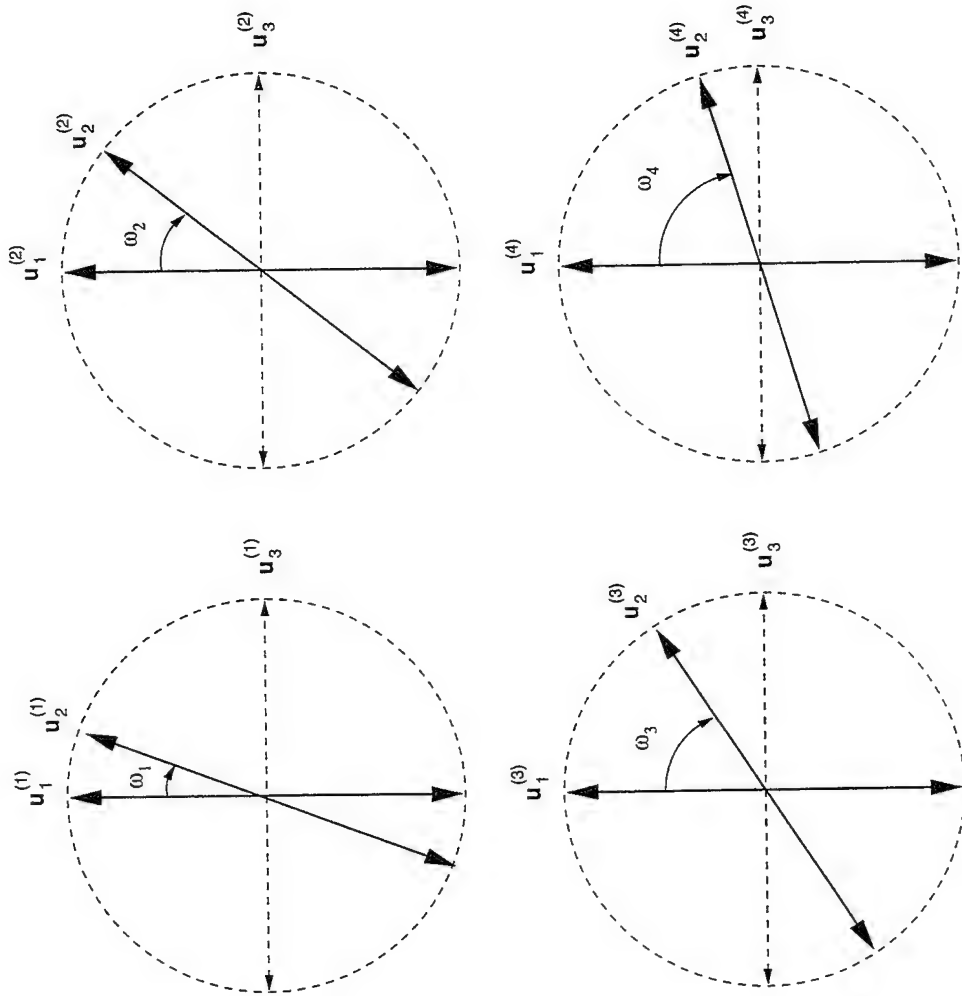
Furthermore,

$$e^{\mathbf{A}} = \begin{bmatrix} \mathbf{U}_1 & \mathbf{U}_3 \end{bmatrix} \begin{bmatrix} \cos \Omega & -\sin \Omega \\ \sin \Omega & \cos \Omega \end{bmatrix} \begin{bmatrix} \mathbf{U}_1^T \\ \mathbf{U}_3^T \end{bmatrix}$$

For all t , the SVD of $\mathbf{P}(t)\mathbf{P}(t+1)$ is $\mathbf{U}_1(\cos \Omega)\mathbf{U}_2^T$. \mathbf{U}_3 is \mathbf{U}_2 rotated orthogonal to \mathbf{U}_1 .

We call the \mathbf{A} the *velocity matrix* for the geodesic curve.

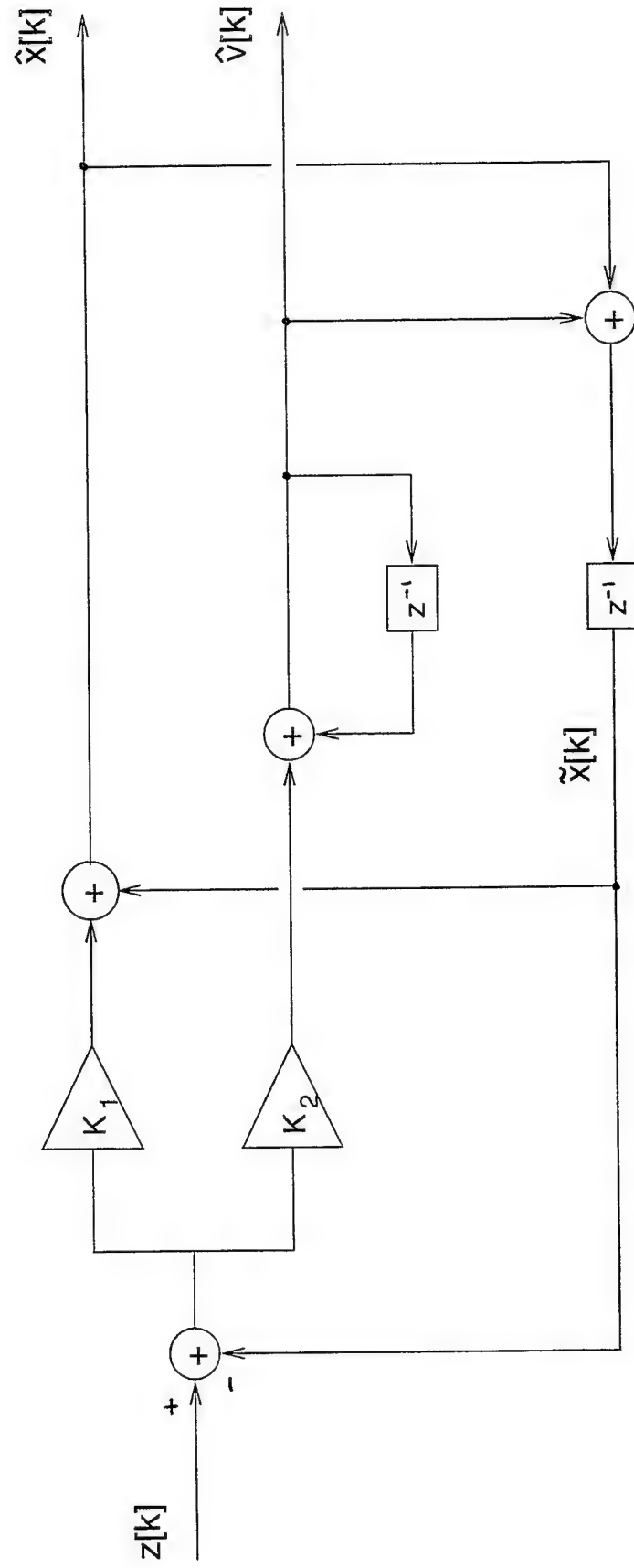
Graphical Depiction of Subspace Motion



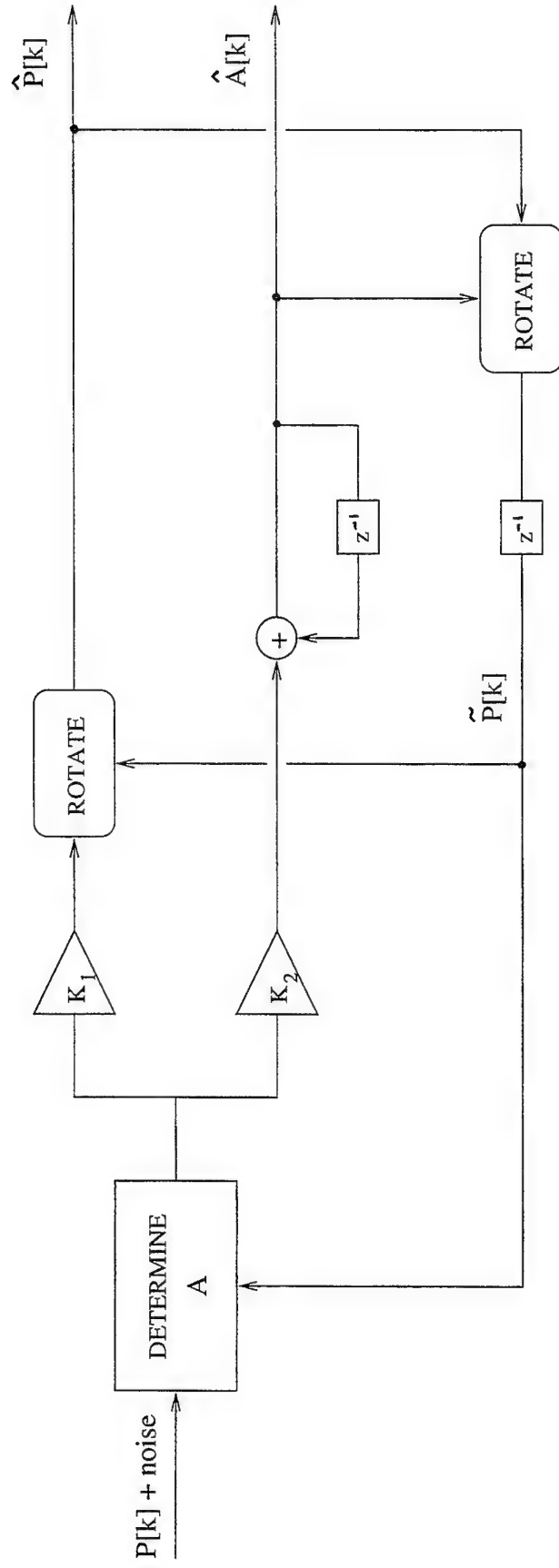
Our Approach to Subspace Tracking

- Treat \mathbf{P} as a *position* in $P_{N,M}$
- Treat \mathbf{A} as a *velocity* in $P_{N,M}$
- Borrow concepts from Kalman filtering for position-velocity tracking
- " $\mathbf{P}_2 - \mathbf{P}_1$ " means find the geodesic (defined by \mathbf{A}) which connects \mathbf{P}_1 and \mathbf{P}_2 .
- " $\mathbf{P} + \mathbf{A}$ " means $e^{\mathbf{A}}\mathbf{P}e^{-\mathbf{A}}$
- \mathbf{A} matrices are added in the usual way

Simple Position-Velocity Kalman Filter



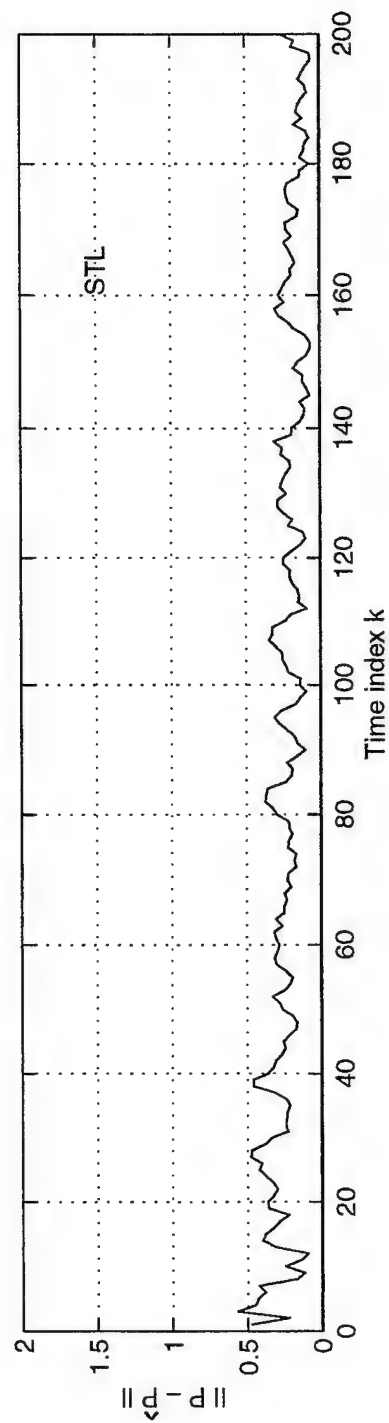
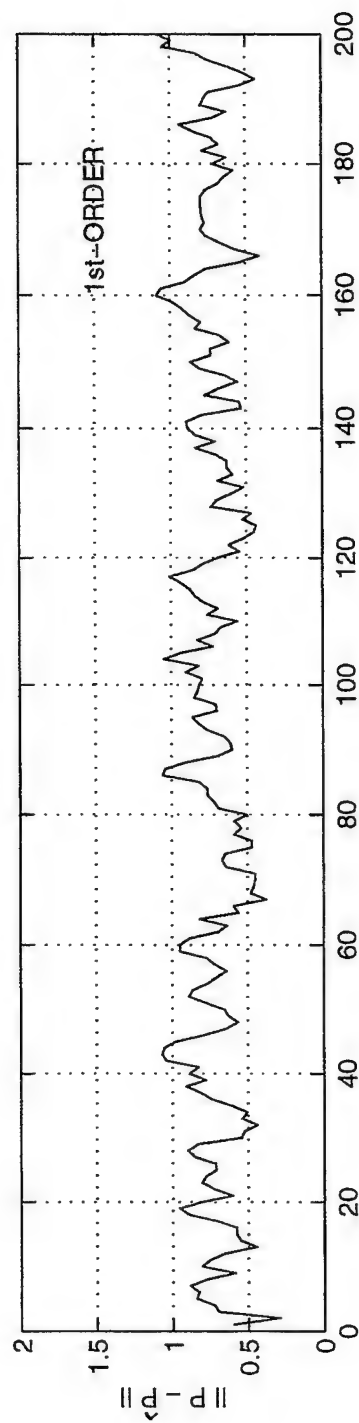
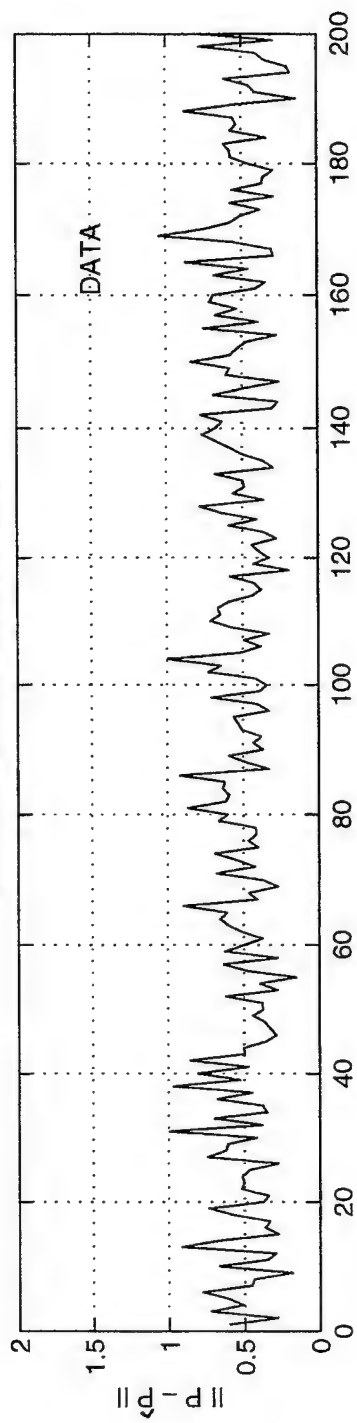
The Subspace Tracking Loop



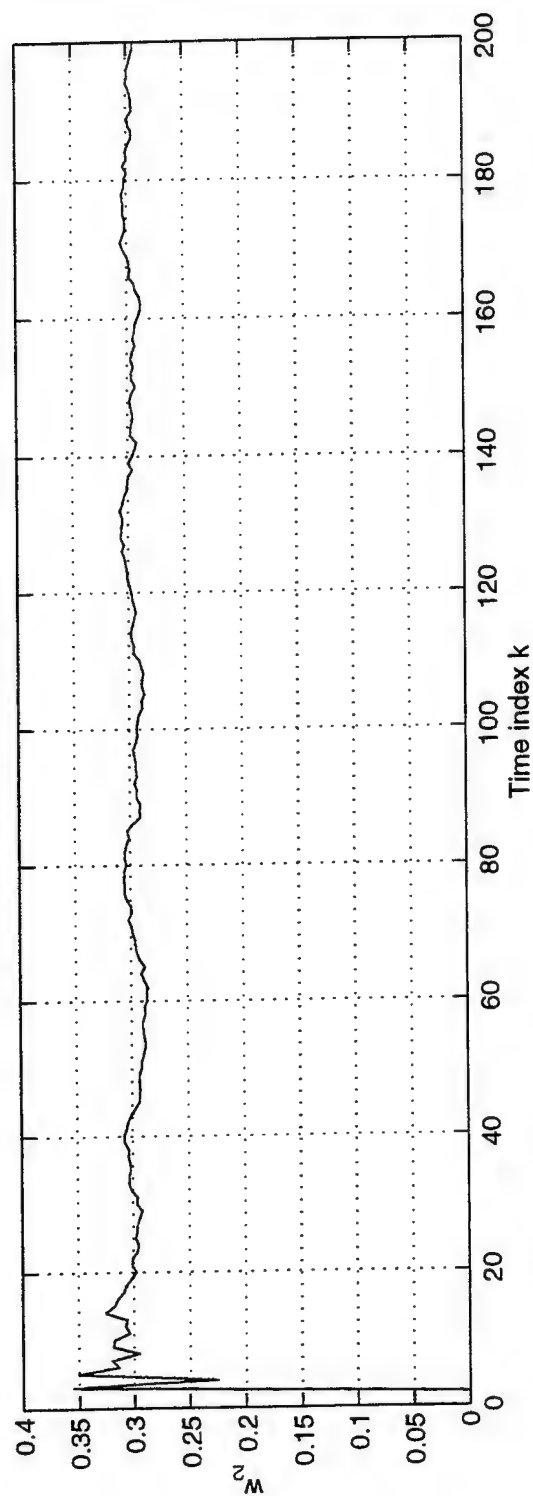
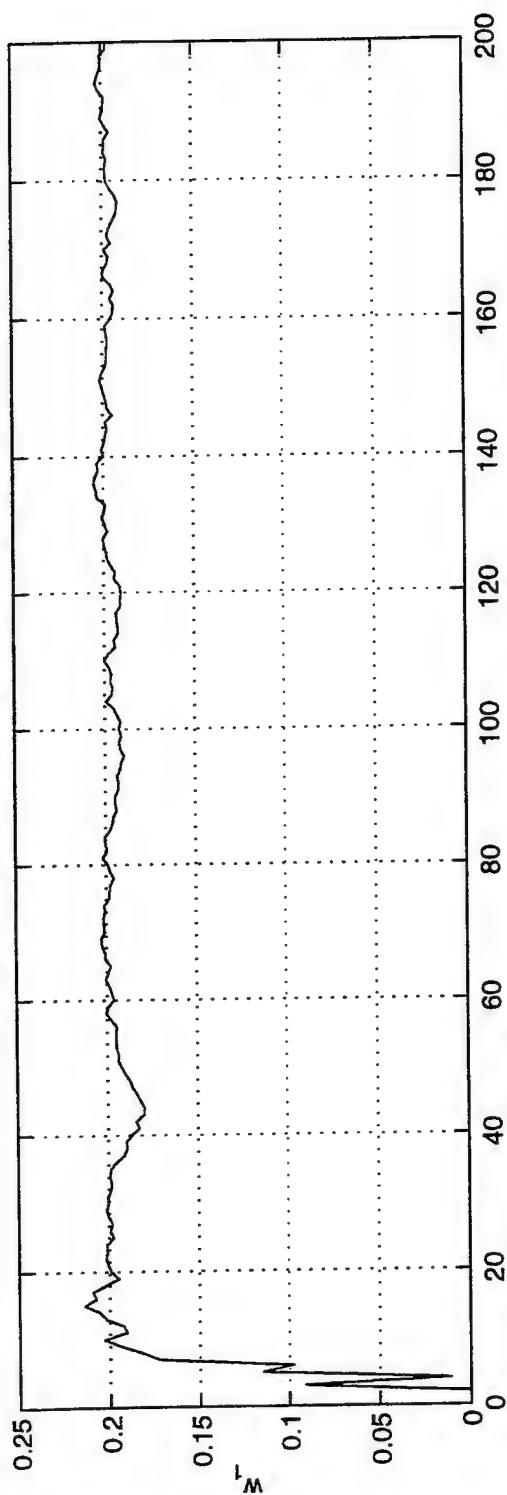
Simulation Example

- $N = 4, M = 2$.
- $\mathbf{U}_1 = \begin{bmatrix} \mathbf{I} \\ \mathbf{0} \end{bmatrix}$ $\mathbf{U}_3 = \begin{bmatrix} \mathbf{0} \\ \mathbf{I} \end{bmatrix}$ $\Omega = \begin{bmatrix} 0.2 & 0 \\ 0 & 0.3 \end{bmatrix}$
- At each time step k , data consists of two orthonormal vectors in $range(\mathbf{P}(k))$, plus 4×2 matrix of independent noise samples with standard deviation 0.2
- 200 iterations, with K_1 and K_2 sequence pre-computed
- For comparison purposes, we looked at 1st-order subspace tracker which computes principal components of $\mathbf{R}(k) = (1 - \mu)\mathbf{R}(k - 1) + \mu\mathbf{x}(k)\mathbf{x}^T(k)$ ($\mu = 0.3$)
- $\|\mathbf{P} - \hat{\mathbf{P}}\|_F$ used as error measure

ERROR IN SUBSPACE ESTIMATE



ESTIMATED VELOCITY PARAMETERS



References

P. Comon and G. Golub, "Tracking a few extreme singular values and vectors in signal processing", *Proc. IEEE*, vol. 78, no. 8, pp. 1327-1343, August 1990.

R. DeGroat, E. Dowling, and D. Linebarger, "Subspace Tracking", in V. Madisetti and D. Williams, eds., *The Digital Signal Processing Handbook* (ch. 66), CRC Press/IEEE Press, 1997.

D. Fuhrmann, "A Geometrical Approach to Subspace Tracking", in *Proc. 1997 Asilomar Conf. on Signals, Systems, and Computers* (Pacific Grove, CA), November 1997.

This work was supported in part by the Office of Naval Research under grant N00014-97-1-0567.

The author gratefully acknowledges many helpful interactions with Steve Smith of MIT Lincoln Laboratory and Anuj Srivastava of Florida State University.

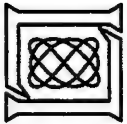
Mutual Coherence Parameter Estimation

Tim Barton

MIT Lincoln Laboratory
244 Wood Street, Room C-370
Lexington, MA 02173-9108
tel: (781) 981-3278
email: barton@ll.mit.edu

Abstract Combining data from multiple radar sensors with different operational bandwidths through ultra-wideband (UWB) signal processing has the potential to provide increased information about a target under track over the information provided by the radar sensors individually. All-pole models have been used to model the frequency domain radar return for multiple-scatterer targets for these radars with different operational bandwidths. This has lead to all-pole models, which not only model the frequencies for which observations have been made, but also provides a method for interpolation between, and extrapolation beyond, the observation frequency bands. This model then provides an UWB frequency response of the target scatterers which can be useful for many applications such as scatter characterization, UWB range profiling, UWB imaging, and other discrimination and intelligence applications.

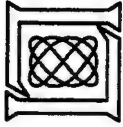
Combining data in different frequency bands from different radar sensors for use in UWB signal processing assumes that the data is mutually coherent with respect to phase and time delay (or range offset) for each target scatterer in each radar. However, data from multiple sensors is not, in general, mutually coherent due to such characteristics as hardware phase and time delay "synchronization" differences between the sensors, sensor deployment differences, target motion, observation time differences, and range offsets due to transmit waveform range-Doppler ambiguities. This presentation will show that mutually coherent data is essential for successful UWB signal processing through system analysis, simulation, and real data analysis. Specifically, the required mutual coherence is examined under a variety of different sensor-target scenarios. Given these considerations, data models are developed which are parameterized by the mutual coherence parameters as well as the other UWB signal processing parameters. Based on these data models, maximum likelihood methods for estimating the mutual coherence parameters are then derived. The process of maximum likelihood mutual coherence parameter estimation is then examined through simulation and data analysis. It will be shown that these techniques can potentially provide a robust method for mutually cohering data from multiple sensors and lead to successful UWB signal processing.



Mutual Coherence Parameter Estimation

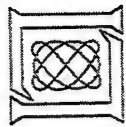
Tim Barton

1998 ASAP Workshop



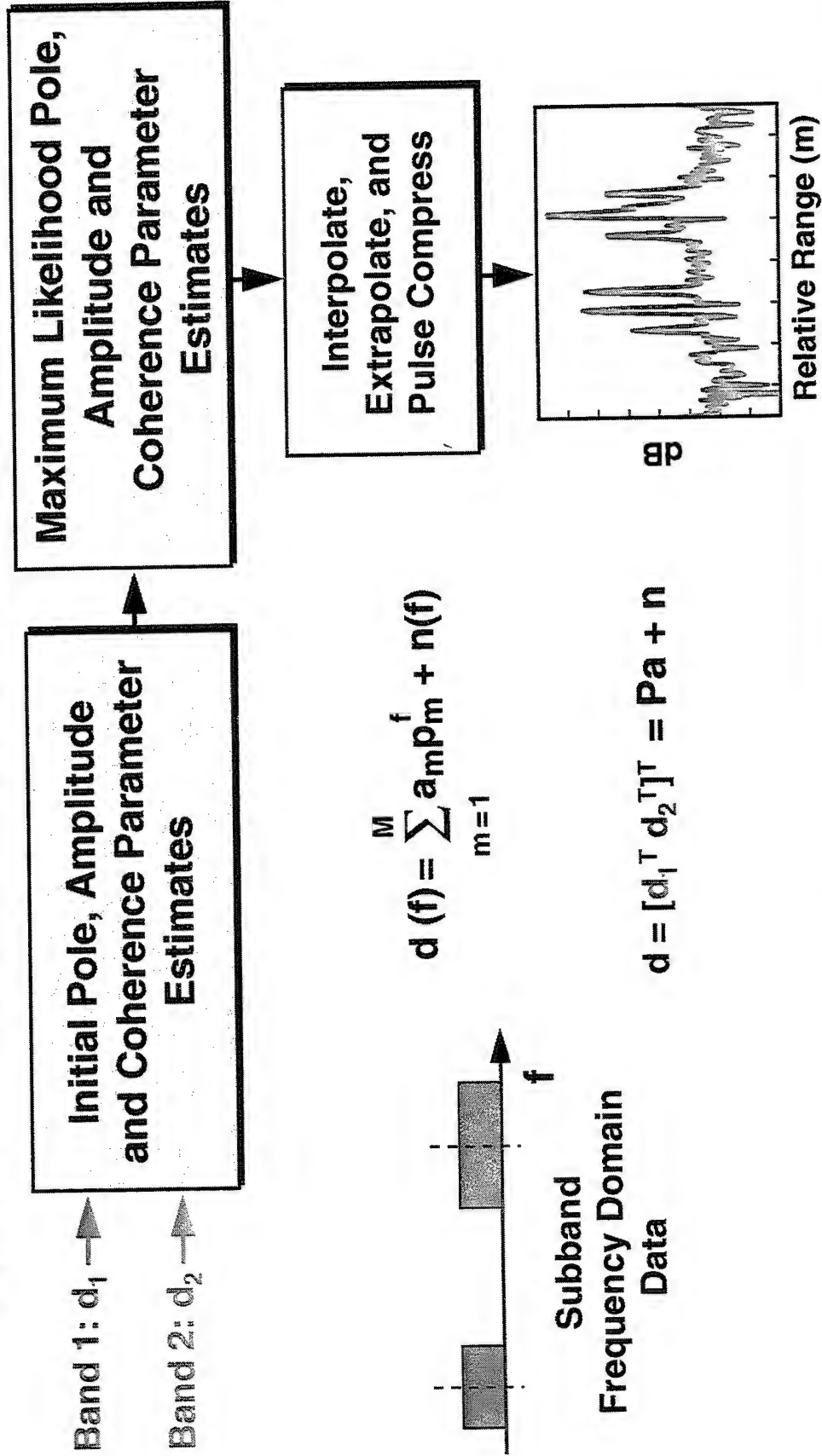
Outline

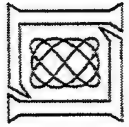
- **Introduction**
 - **Objectives**
 - **Real data set**
- **Estimation for constant range and phase offsets**
- **Estimation for different scatterer range and phase offsets**
- **Conclusions**



Nominal Ultra-Wideband Signal Processing Algorithm

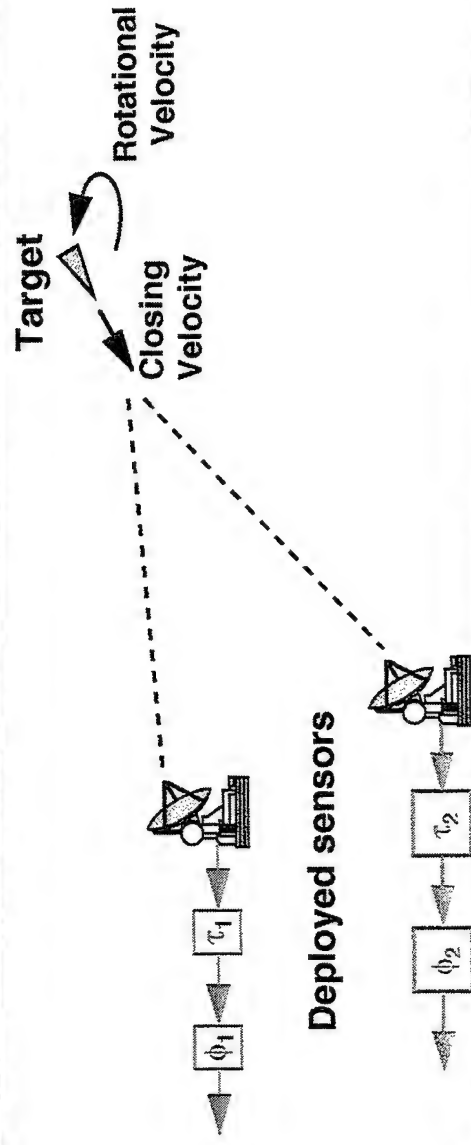
- In the 1997 ASAP Workshop, Kevin Cuomo proposed an ultra-wideband (UWB) signal processing algorithm ...

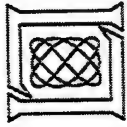




Mutual Coherence Parameter Estimation (MCPE)

- Mutual coherence parameter estimation accounts for phase and range offsets in data due to:
 - Hardware “synchronization” offsets
 - phase offsets
 - time delays (range offsets)
 - Sensor deployment
 - Target motion (Doppler shifts)
 - Observation time
 - Transmit waveform ambiguities

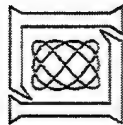




Objectives

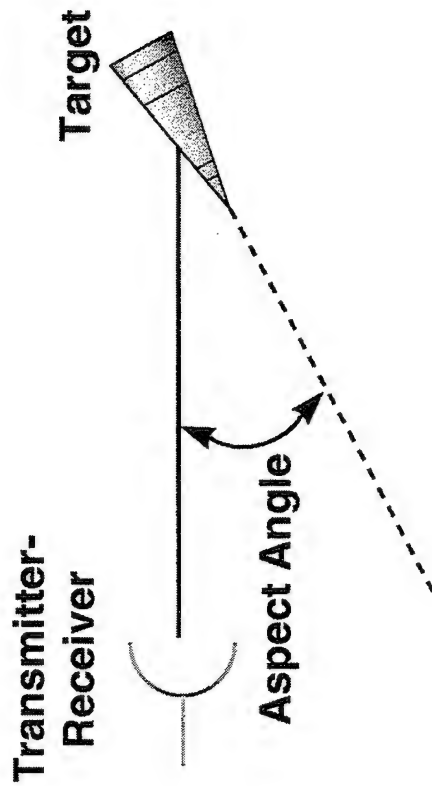
Establish the need for and feasibility of mutual coherence parameter estimation for:

- **Constant range and phase offsets**
 - Collocated radars tracking a constant velocity target
- **Constant phase offset and different scatterer range offsets**
 - Collocated radars tracking a rotating target at different observation times
 - Noncollocated radars tracking a constant velocity target
 - Noncollocated radars tracking a rotating target



Data Set Description

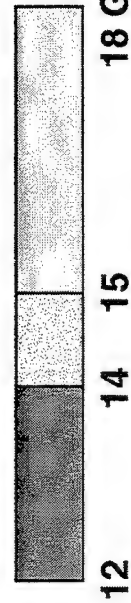
Experimental Setup



Fullband: 12–18 GHz

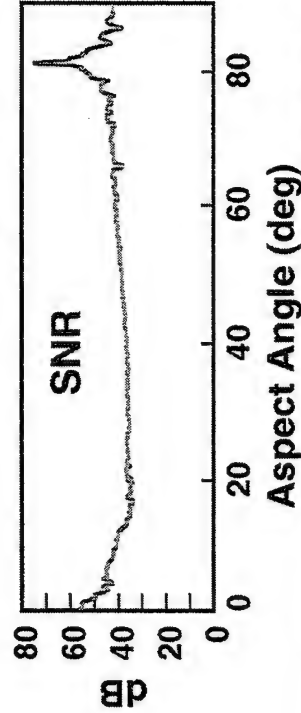
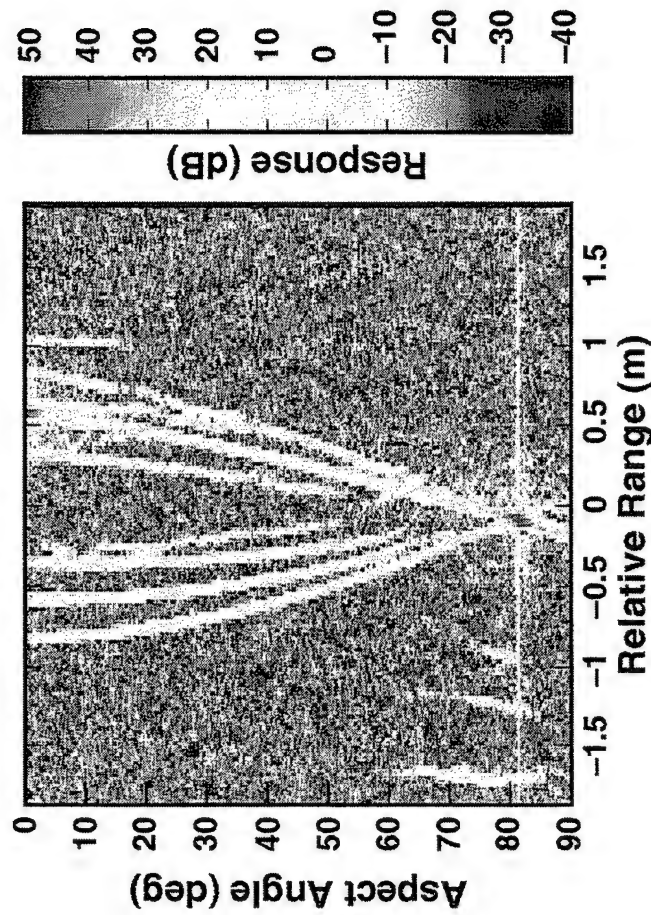
Band 1: 12–14 GHz

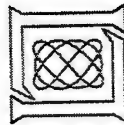
Band 2: 15–18 GHz



$\Delta f = 40 \text{ MHz}$

12–18 GHz Pulse Compressed Range Profiles



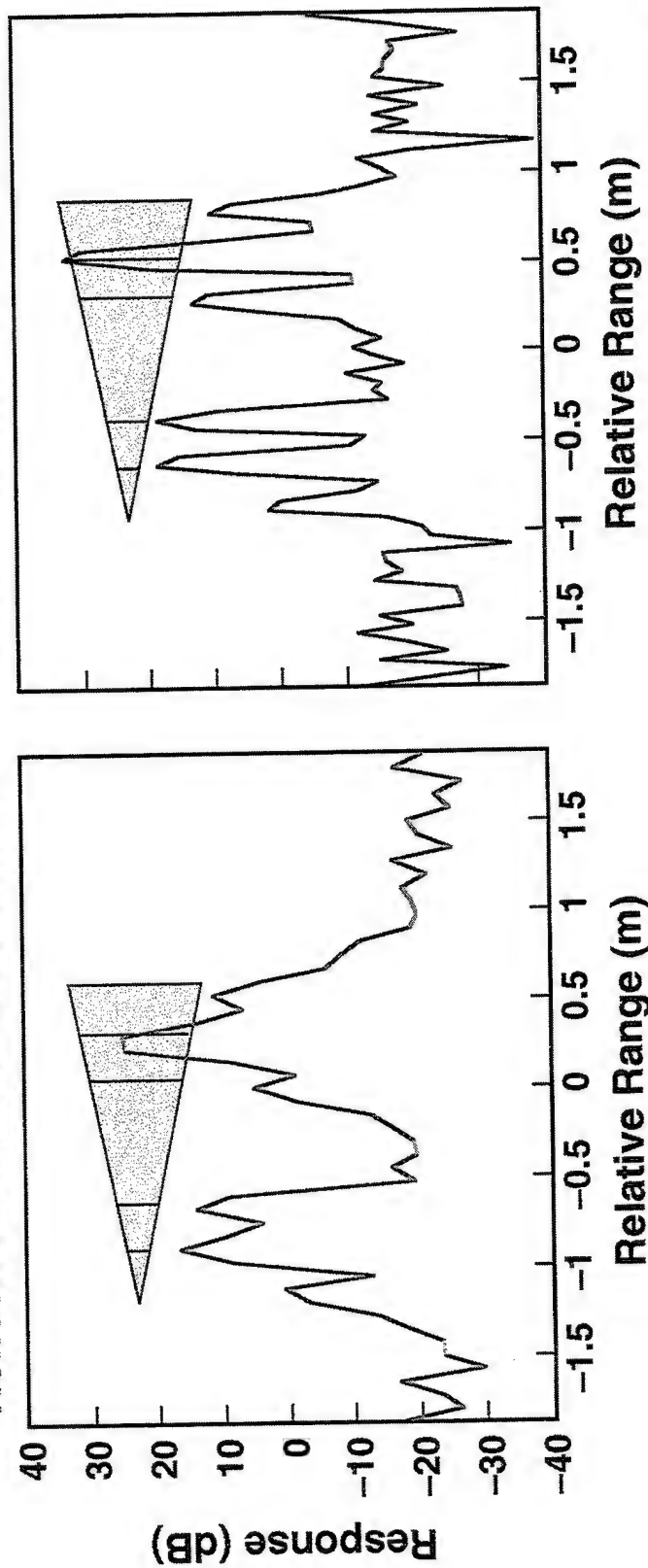


Data Set Description: Subband Data

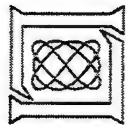
Pulse Compressed Range Profiles at 0 deg Aspect Angle

Reference Band 2: 15–18 GHz

Noncoherent Band 1: 12–14 GHz

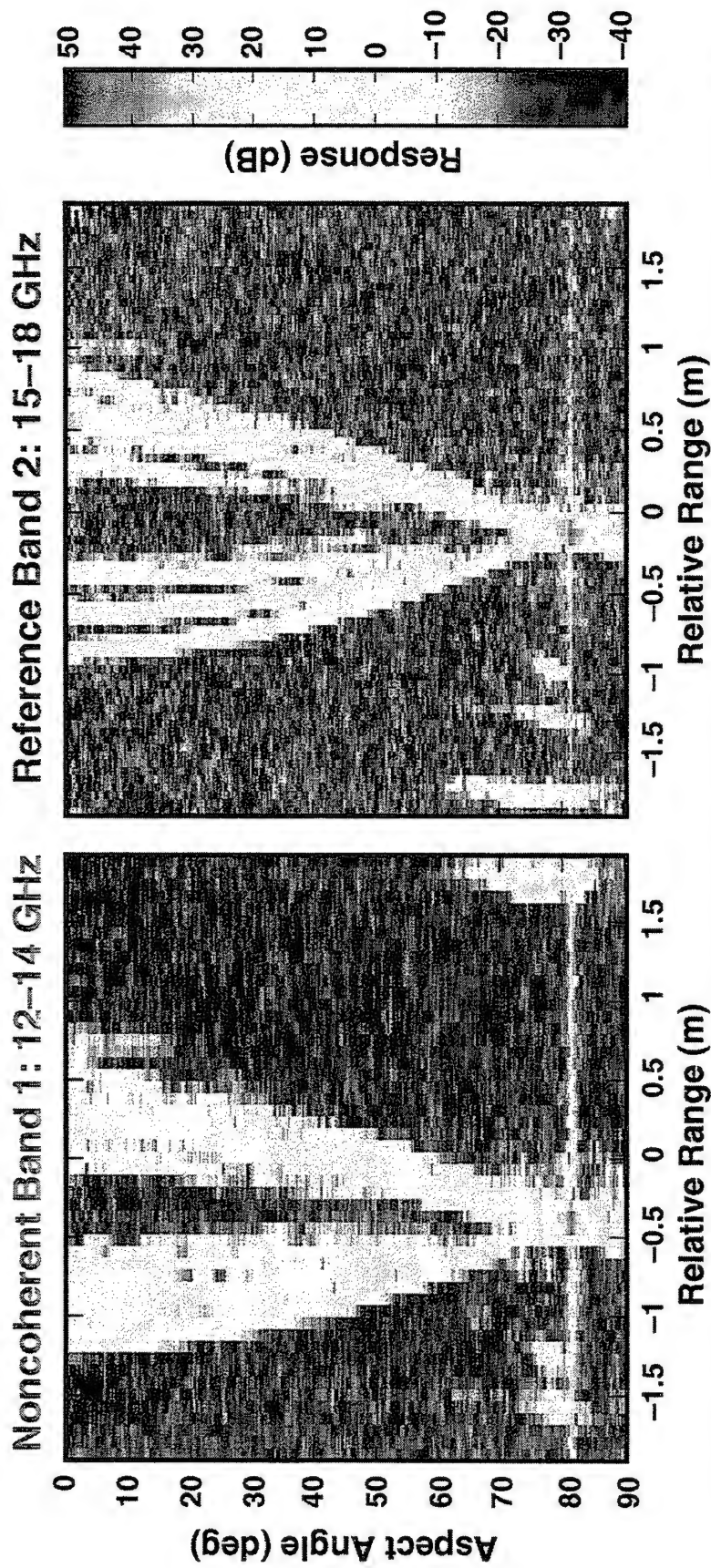


The Noncoherent Band 1 has a phase offset $\Delta\phi = 30$ deg and a range offset $\Delta r = -0.3$ m with respect to the Reference Band 2.

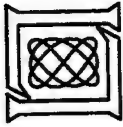


Data Set Description: Subband Data

Pulse Compressed Range Profiles vs Aspect Angle

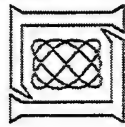


The Noncoherent Band 1 has a phase offset $\Delta\phi = 30$ deg and a range offset $\Delta r = -0.3$ m with respect to the Reference Band 2.



Outline

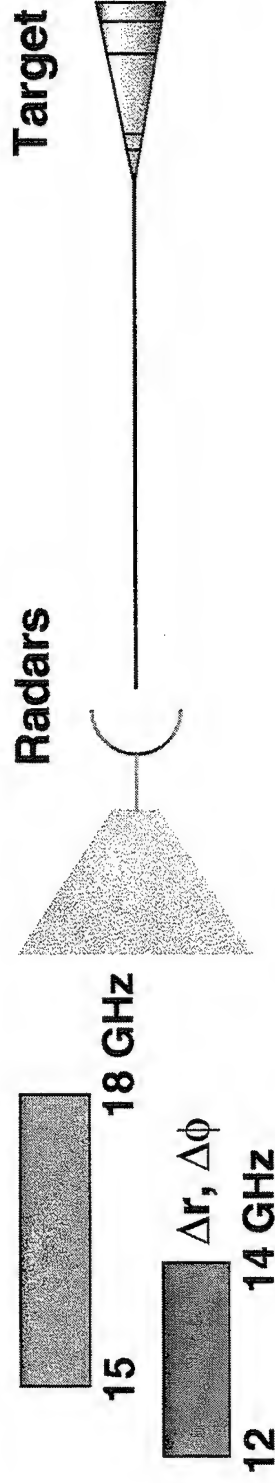
- Introduction
 - Objectives
 - Real data set
- Estimation for constant range and phase offsets
- Estimation for different scatterer range and phase offsets
- Conclusions



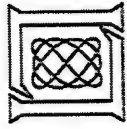
Mutual Coherence Parameter Estimation

Constant Range Offset Δr and Phase Offset $\Delta\phi$

- Problem description
 - Can data from different collocated radars with different operational bandwidths be mutually coerhered to allow robust UWB signal processing?



- Objective
 - Develop statistical data model that will allow ML estimation of Δr and $\Delta\phi$



Maximum Likelihood Coherence Parameter Estimation

Constant Range Offset Δr and Phase Offset $\Delta\phi$

- The statistical data model for $\mathbf{d} = [\mathbf{d}_1^T \mathbf{d}_2^T]^T$ is:

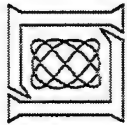
$$p(\mathbf{d}|\Delta\phi, \Delta r, \mathbf{P}, \mathbf{a}) = \frac{1}{\pi^{N|\mathbf{R}|}} \exp\left(-(\mathbf{d} - \mathbf{D}(\Delta\phi, \Delta r)\mathbf{P}\mathbf{a})^H \mathbf{R}^{-1}(\mathbf{d} - \mathbf{D}(\Delta\phi, \Delta r)\mathbf{P}\mathbf{a})\right)$$

$$\mathbf{D}(\Delta\phi, \Delta r) = \begin{bmatrix} \mathbf{D}_1(\Delta r) \mathbf{e}^{j\Delta\phi} \\ \vdots \\ \mathbf{D}_1(\Delta r) \mathbf{e}^{j\Delta\phi} \end{bmatrix} \mathbf{I}_2$$

$$\mathbf{D}_1(\Delta r) = \begin{bmatrix} \mathbf{e}^{jn_1\Delta\theta(\Delta r)} & & \\ & \ddots & \\ & & \mathbf{e}^{jn_{N_1}\Delta\theta(\Delta r)} \end{bmatrix} \quad \Delta\theta(\Delta r) = \left(\frac{4\pi(\Delta f)}{c} \right) \Delta r$$

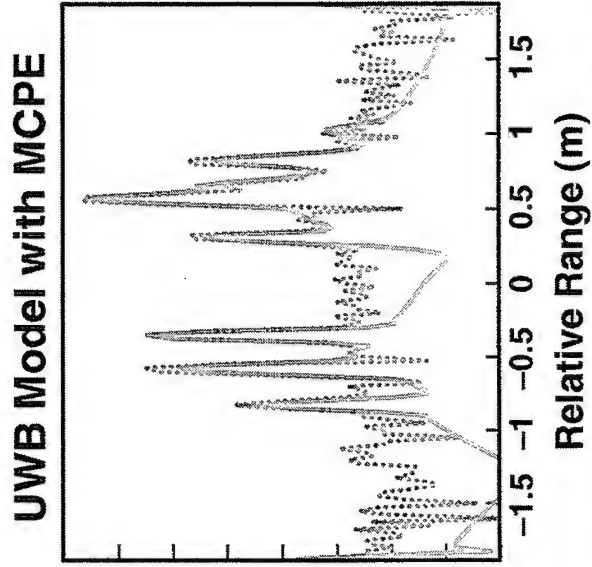
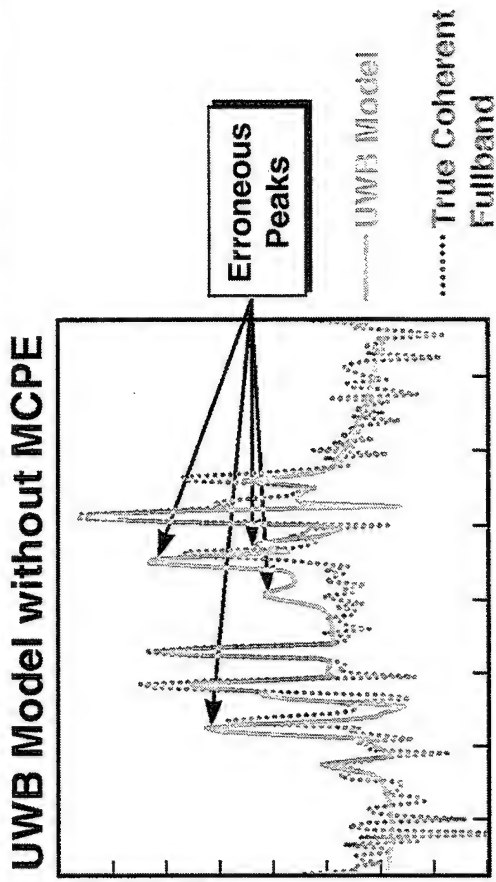
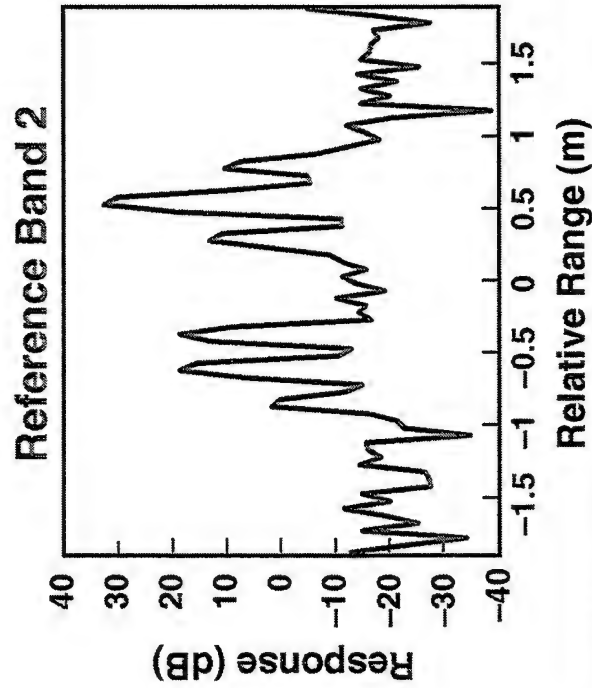
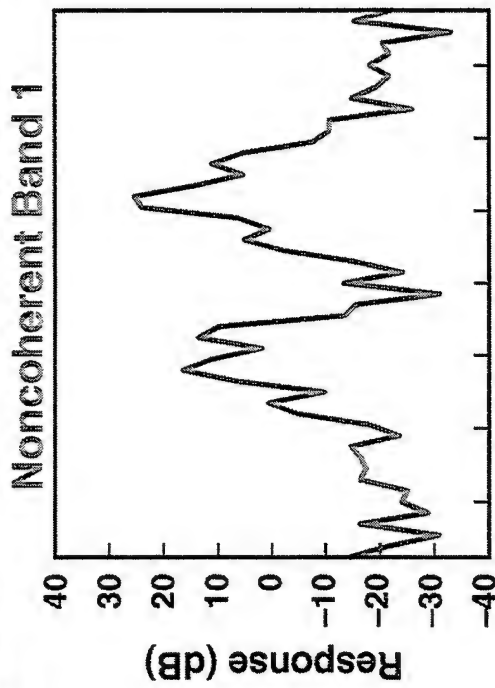
- Find the coherence parameters which maximize:

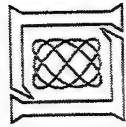
$$L(\mathbf{d}|\Delta\phi, \Delta r) = -(\mathbf{d} - \mathbf{D}(\Delta\phi, \Delta r)\mathbf{P}\mathbf{a})^H \mathbf{R}^{-1}(\mathbf{d} - \mathbf{D}(\Delta\phi, \Delta r)\mathbf{P}\mathbf{a})$$



UWB Signal Processing

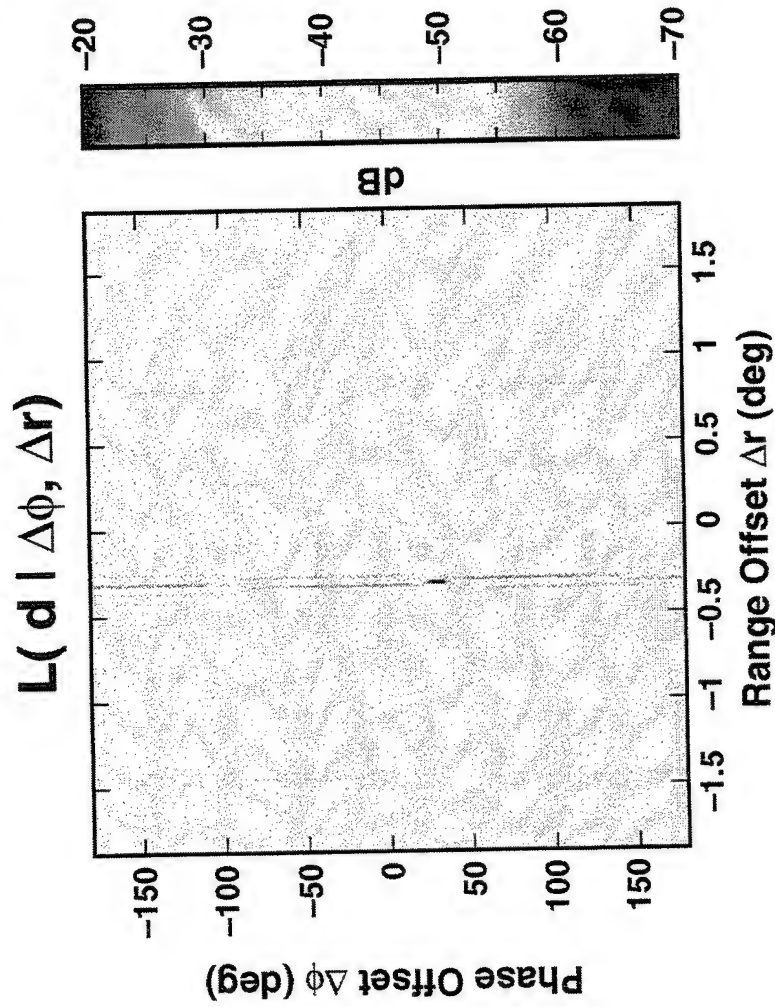
Pulse Compressed Range Profiles at 0 deg Aspect Angle





ML Surface for Mutual Coherence Parameter Estimation

0 deg Aspect Angle



- Assume poles and amplitudes P_a known

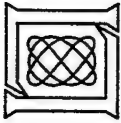
To mutually cohere
data from Band 1 with
data from Band 2
estimate:

$$\Delta\phi = 30 \text{ deg}$$

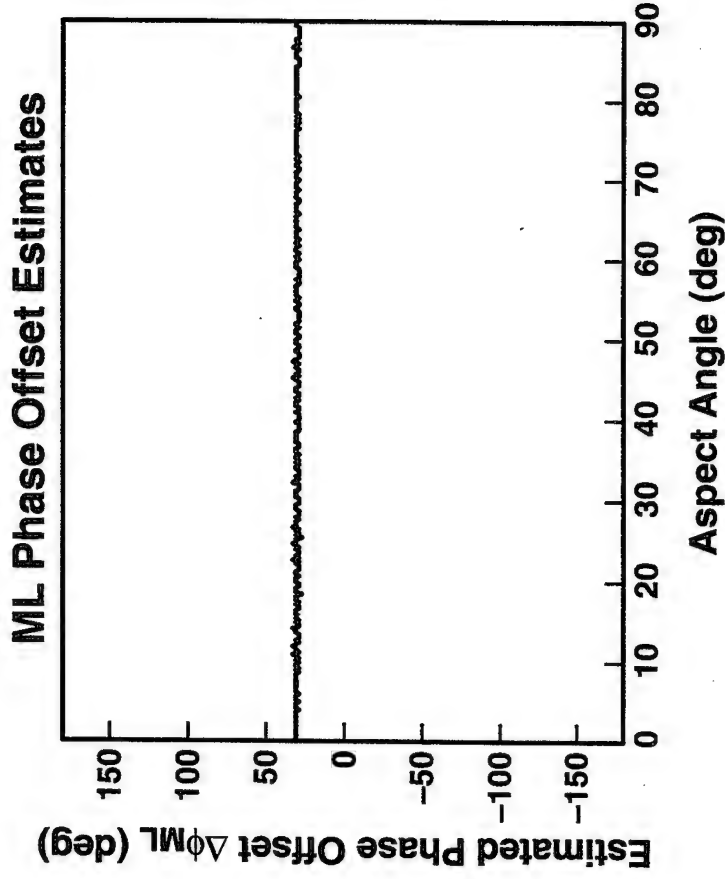
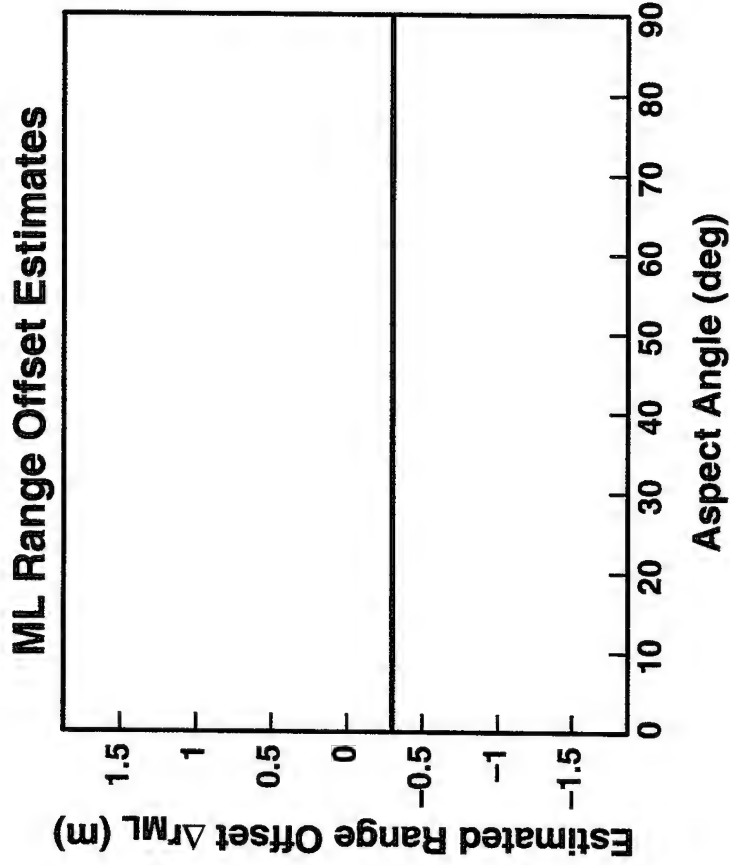
$$\Delta r = -0.3 \text{ deg}$$

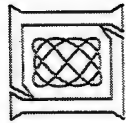
ML phase offset estimate $\Delta\phi_{ML} = 30.6 \text{ deg}$

ML range offset estimate $\Delta r_{ML} = -0.3 \text{ m}$

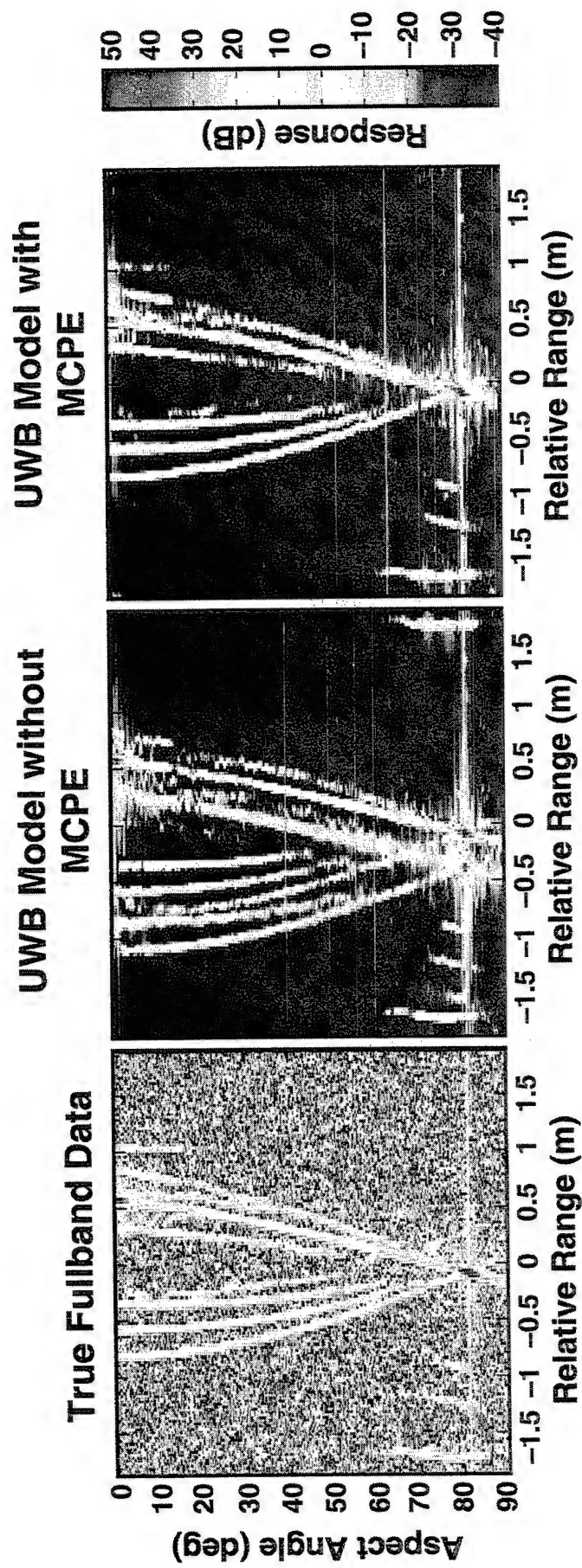


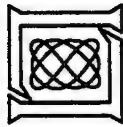
ML Coherence Parameter Estimates





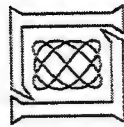
Pulse Compressed UWB Models vs Aspect Angle





Outline

- Introduction
 - Objectives
 - Real data set
- Estimation for constant range and phase offsets
- Estimation for different scatterer range and phase offsets
- Conclusions

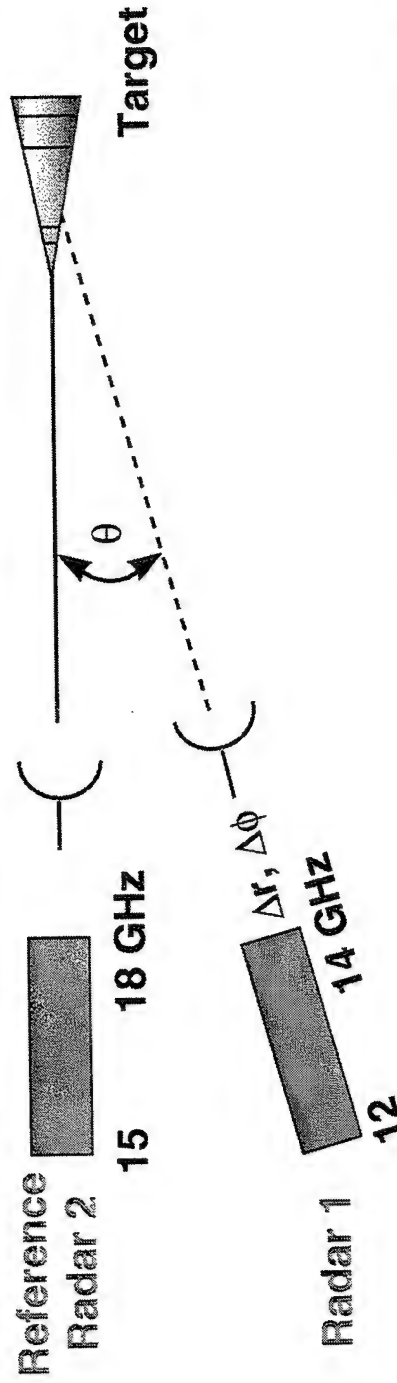


Mutual Coherence Parameter Estimation

Aspect Angle θ , Constant Range Offset Δr ,
and Phase Offset $\Delta\phi$

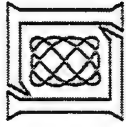
- Problem description

- Can data from different non-collocated radars with different operational bandwidths be mutually coerhered to allow robust UWB signal processing at the reference aspect angle?



- Objective

- Develop statistical data model that will allow ML estimation of Δr , $\Delta\phi$, and θ



Maximum Likelihood Coherence Parameter Estimation

Aspect Angle θ , Constant Range Offset Δr , and Phase Offset $\Delta\phi$

- The statistical data model for $\mathbf{d} = [\mathbf{d}_1^T \mathbf{d}_2^T]^T$ is:

$$p(\mathbf{d} \mid \Delta\phi, \Delta r, \theta, \mathbf{P}, \mathbf{a}) = \frac{1}{\pi^{N|\mathbf{R}|}} \exp\left(-(\mathbf{d} - [\mathbf{D}_a \circ \mathbf{P}]\mathbf{a})^H \mathbf{R}^{-1}(\mathbf{d} - [\mathbf{D}_a \circ \mathbf{P}]\mathbf{a})\right)$$

$$\mathbf{D}_a = \begin{bmatrix} \mathbf{D}_a e^{j\Delta\phi} \\ \mathbf{1}_2 \end{bmatrix}$$

$$\mathbf{D}_{a_1} = \begin{bmatrix} e^{jn_1\Delta\theta_1} & \dots & e^{jn_1\Delta\theta_M} \\ \vdots & \ddots & \vdots \\ e^{jn_{N_1}\Delta\theta_1} & \dots & e^{jn_{N_1}\Delta\theta_M} \end{bmatrix}$$

$$\Delta\theta_m = \theta_m(\cos(\theta) - 1) + \Delta\theta(\Delta r)$$

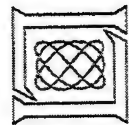
$$\theta_m = \left(\frac{4\pi\Delta f}{c}\right)r_m$$

r_m = scatterer "m" range

$$\Delta\theta(\Delta r) = \left(\frac{4\pi(\Delta f)}{c}\right)\Delta r$$

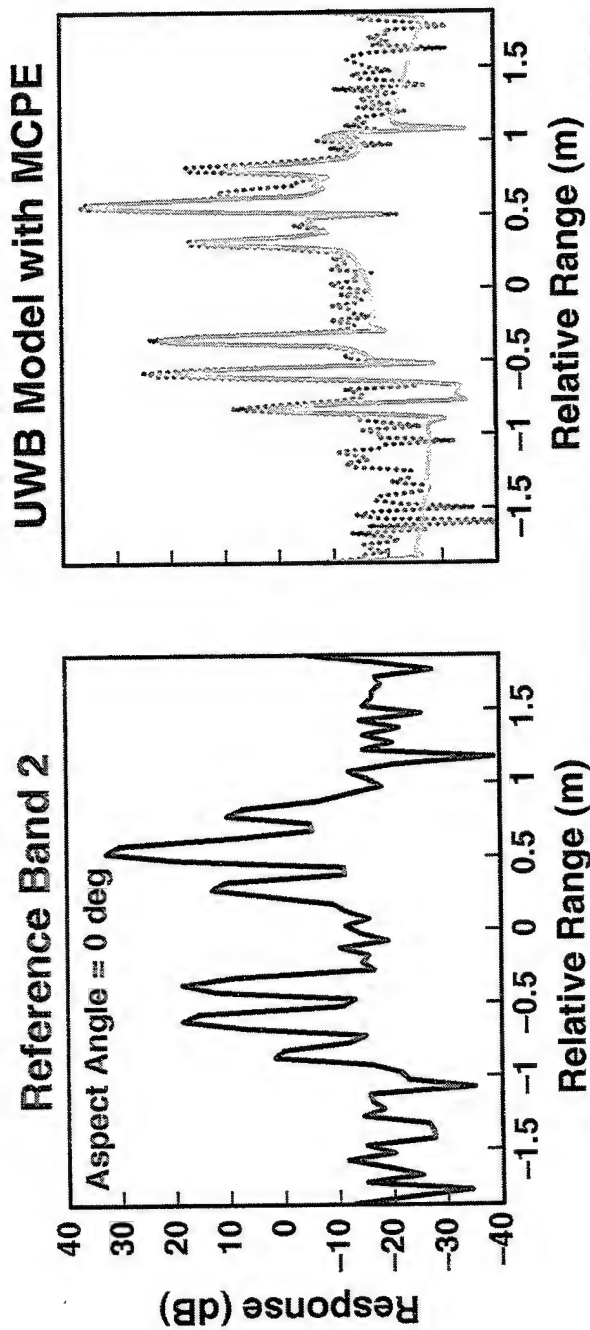
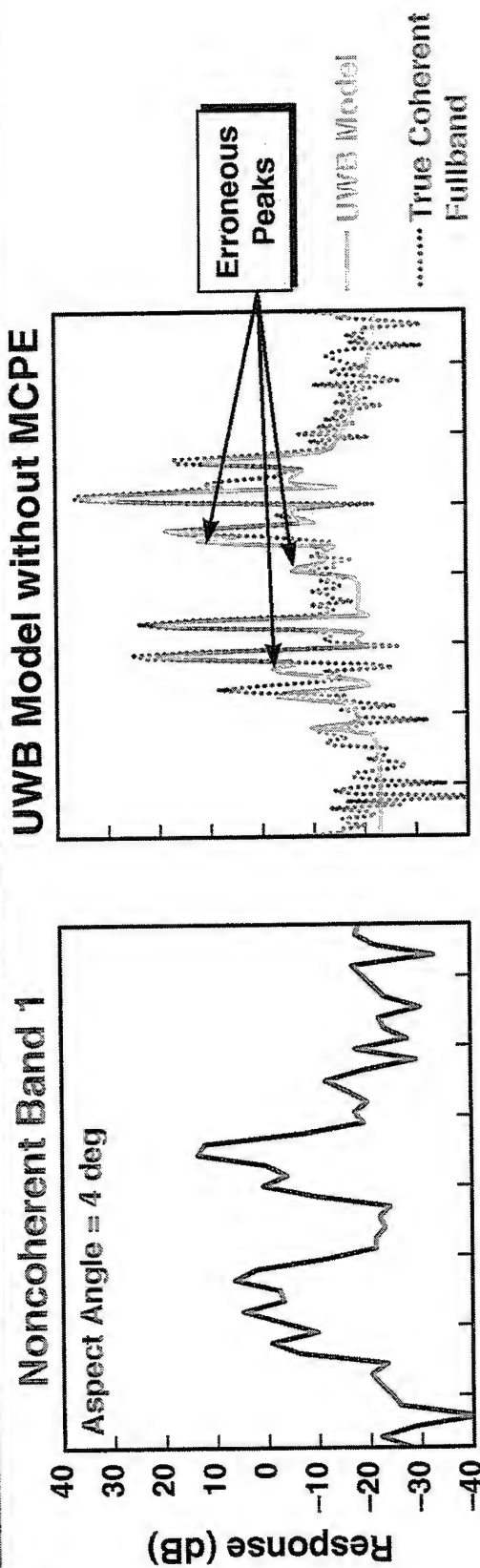
- Find the coherence parameters which maximize:

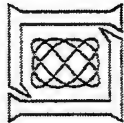
$$L(\mathbf{d} \mid \Delta\phi, \Delta r, \theta) = -(\mathbf{d} - [\mathbf{D}_a \circ \mathbf{P}]\mathbf{a})^H \mathbf{R}^{-1}(\mathbf{d} - [\mathbf{D}_a \circ \mathbf{P}]\mathbf{a})$$



UWB Signal Processing

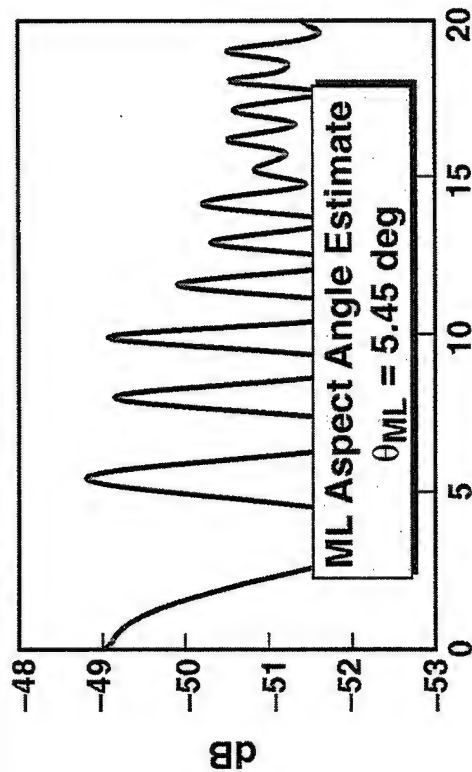
Pulse Compressed Range Profiles





ML Mutual Coherence Parameter Estimation

$L(d| \theta)$ at 4.0 deg Aspect Angle



To mutually cohere data from Band 1 with data from Band 2 estimate:

$$\theta = 4.0 \text{ deg}$$

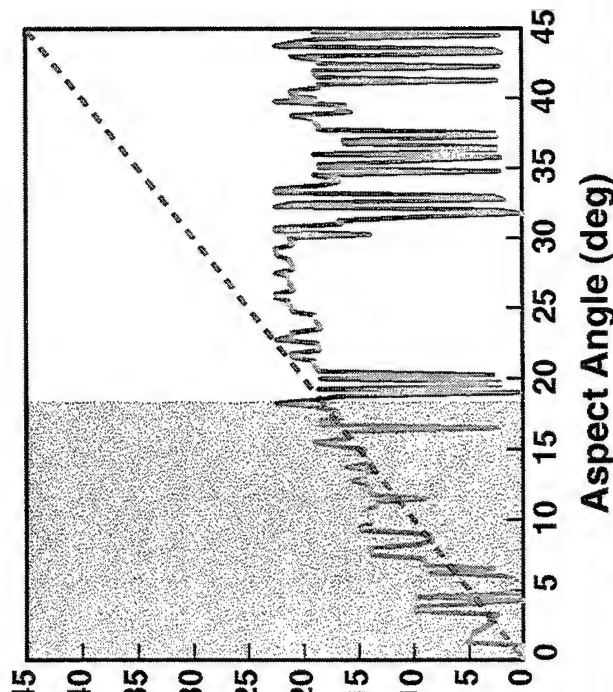
- Assumes poles and amplitudes P_a , $\Delta\phi$, and Δr known
- 0 deg aspect angle reference

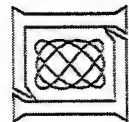
Aspect Angle Estimate θ_{ML}

True Aspect Angle θ

Agreement

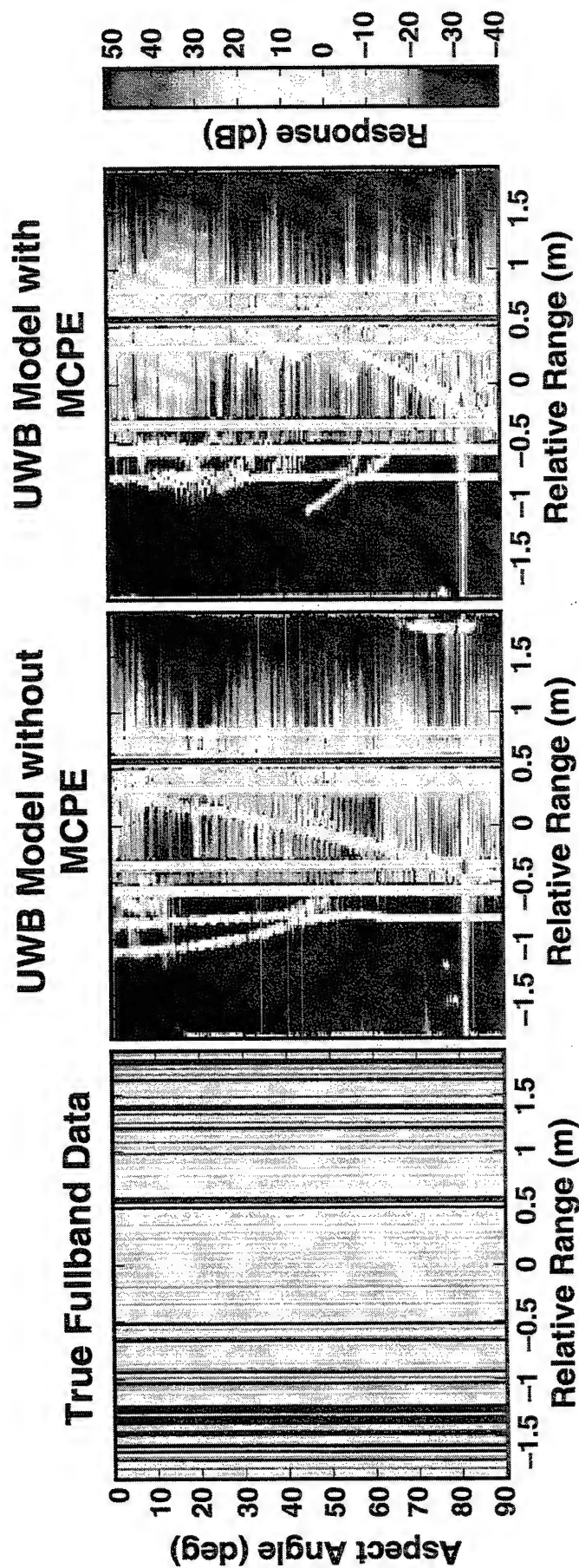
Estimated Aspect Angle θ_{ML} (deg)

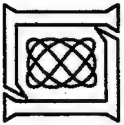




Pulse Compressed UWB Models vs Aspect Angle

0 deg Aspect Angle Reference





Conclusions

- Developed data models and ML estimation techniques for mutual coherence parameter estimation within the UWB signal processing context
 - Mutual coherence parameter estimation is essential for robust UWB signal processing
 - Mutual coherence requires applying phase ramps and a phase offset to the data
- Mutual coherence parameter estimation may allow sufficient sample support for further processing of the data
- Limitations
 - Target scatterer variation vs aspect, time, etc.
 - Model errors
 - Sample support

Adaptive Distributed Clutter Improvement Factor (ADDCIF)

John Hoffman, Louis Vasquez, Charles Farthing, and Clarence Ng

Systems Engineering Group, Inc.

Columbia, MD

tel: (410) 381-8740, ext. 131

email: sysenggrp@smtp806.crane.navy.mil

Kenneth Johnson

Naval Surface Warfare Center

Crane, Indiana

Abstract The system level clutter improvement factor (CIF) in heavy distributed clutter environments, such as the littoral environment, is limited by radar instabilities. In many radar systems the two largest instabilities are transmitter intrapulse noise and A-to-D converter quantization noise. A-to-D converter dynamic ranges are increasing at typical radar sampling rates leaving transmitter intrapulse noise (IPN) as the limiting factor for CIF performance. A pulse Doppler mode can be used to increase CIF through coherent integration gain, but the additional pulses required put a severe load on radar resources particularly for horizon search modes.

An alternative approach to improving radar system CIF performance is to employ MTI and cancel the transmitter IPN using advanced signal processing techniques. One approach is to measure the in-phase and quadrature components of the pulse compression coded transmit pulse on a chip-by-chip basis. The measured transmit pulse data is then applied to the radar return during signal processing to cancel the IPN.

A frequency domain de-convolution approach for transmitter noise cancellation is being developed. The time domain radar return from distributed clutter is the convolution of the coded transmit pulse and the distributed clutter field. By taking the Fast Fourier Transform (FFT) of the distributed clutter return, the IPN contribution of the noisy transmit waveform can be removed by dividing it by the frequency spectrum of the measured transmit waveform. An IFFT is used to return to the time domain for subsequent MTI processing.

The ADDCIF approach and its overall system performance capability will be summarized. Simulation results for coded waveforms will be presented which show the potential of the approach for canceling radar transmitter intrapulse noise. The results of MTI processing of measured radar return data from the AEGIS Combat System Center (ACSC) in Wallops Island, Virginia using the ADDCIF algorithm will be compared with simulation results.

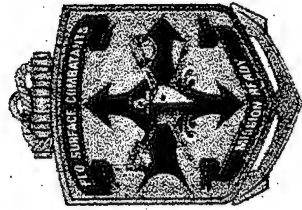
SEG

Systems Engineering Group, Inc.

ADAPTIVE
DISTRIBUTED CLUTTER IMPROVEMENT FACTOR
(ADDCIF)

Workshop On Adaptive Sensor Array Processing
MIT LINCOLN LABORATORY
11-12 March 1998

John Hoffman, Louis Vasquez, Charles Farthing, and
Clarence Ng.
SYSTEMS ENGINEERING GROUP, INC.
COLUMBIA, MD

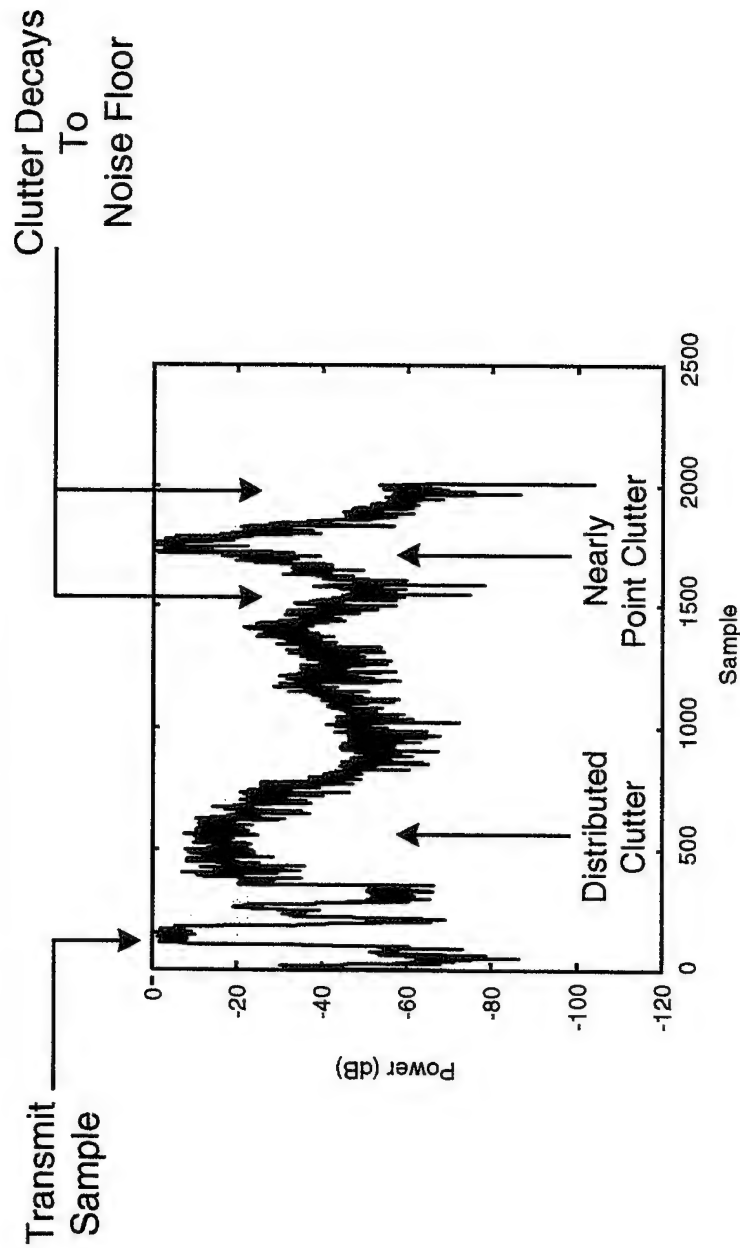


Kenneth Johnson
NAVAL SURFACE WARFARE CENTER
CRANE, INDIANA



SEG-05-377

MEASURED RADAR DATA PLOT



SPY-1B RADAR DATA
FROM ACSC, WALLOPS ISLAND, VA

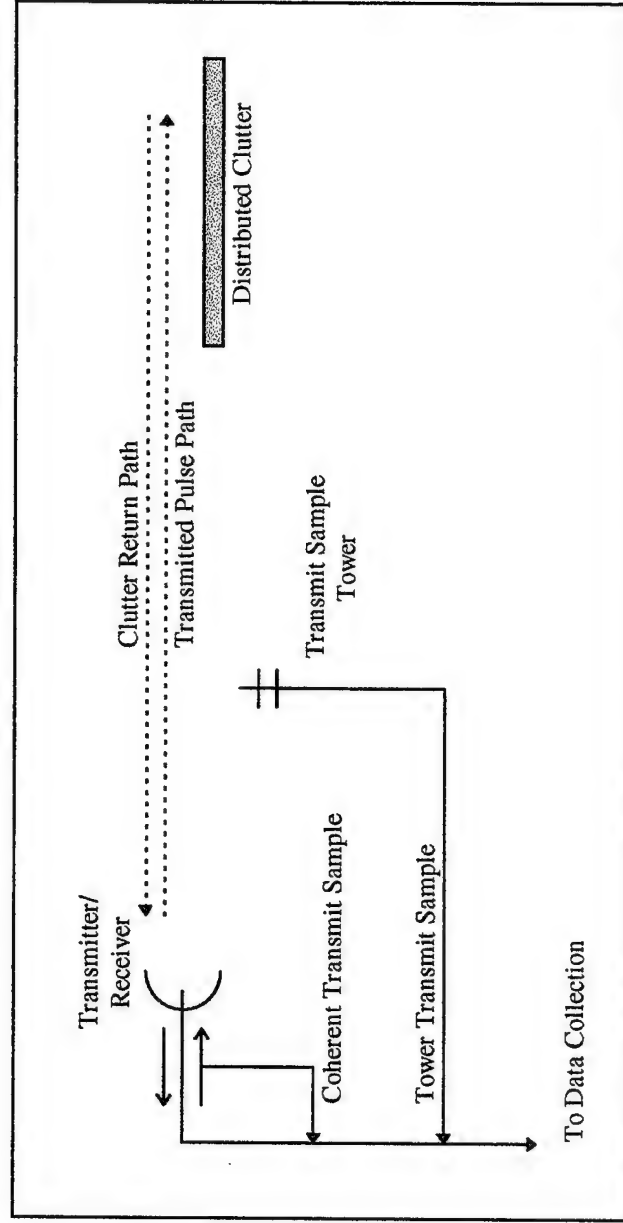
IPN MEASUREMENT ACCURACY

- DISTRIBUTED TRANSMITTER HAS 32 CFA CHANNELS IN FINAL POWER AMPLIFIERS
 - » EACH CHANNEL IS SAMPLED AND COMBINED TO DERIVE TRANSMIT SAMPLE
- PHASE AND AMPLITUDE IMBALANCES IN CHANNEL SAMPLE COMBINING NETWORK AFFECT TRANSMIT SAMPLE MEASUREMENT ACCURACY
- EFFECT OF RFM PHASE AND AMPLITUDE IMBALANCES ON TRANSMIT PULSE ACCURACY

	Error Level Relative to IPN
Worst Case Imbalances	-22.0 dB
Improved Imbalances (Upgrade)	-29.3 dB

- EXCEEDS NOTIONAL REQUIREMENTS FOR MEASUREMENT NOISE TO BE AT LEAST 10 dB BELOW IPN LEVEL
- TX SAMPLE NEEDS TO BE PROCESSED BY HIGH FIDELITY RECEIVER

TEST SETUP



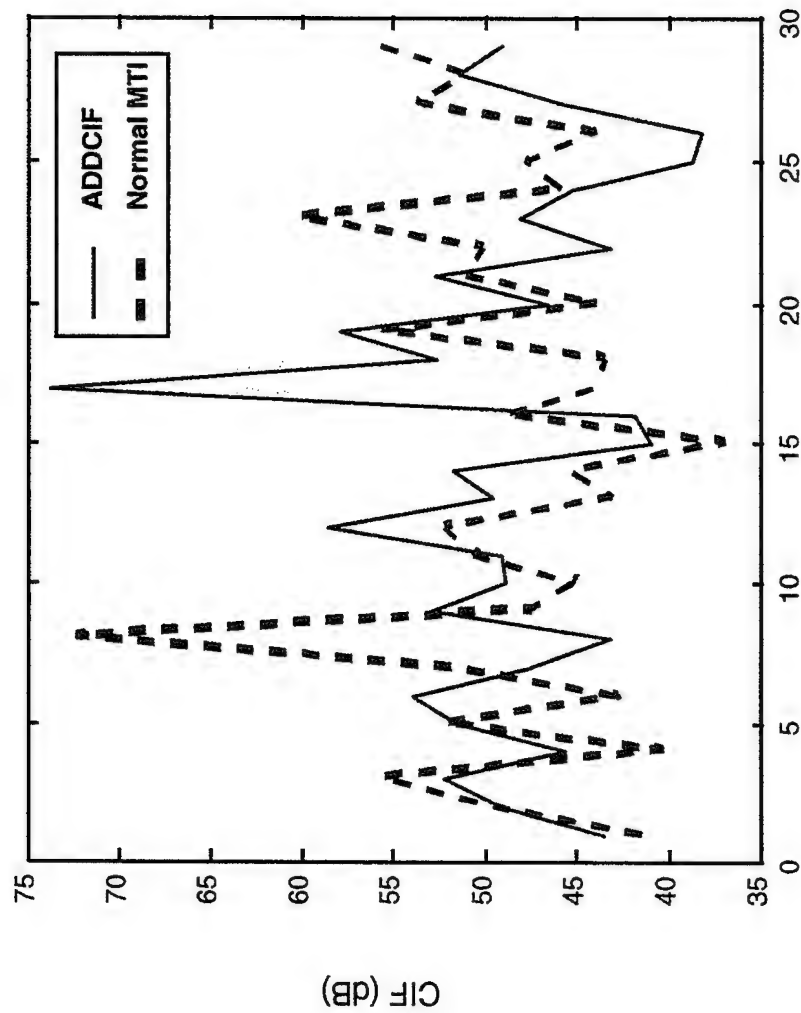
- TRANSMIT SAMPLE AND CLUTTER MEASURED WITH 12-BIT A-TO-D AT 40 MHZ SAMPLING RATE
 - » Special Combining Network Used To Minimize Imbalances
- 0° AZIMUTH BEAMSTEERING CASE EXAMINED

SEG-05-377

SYSTEM ISSUES

- ➔ ● TX IPN MEASUREMENT ACCURACY
- ➔ ● TX IPN DECORRELATION WITH BEAMSTEERING
 - ANTENNA TRANSFER FUNCTION
 - » Transmit Sample Equalization
 - CLUTTER RETURN TRUNCATION
 - FOLDED CLUTTER
- ➔ ● TWO SUBPULSE WAVEFORM USED IN SYSTEM DESIGN

MEASURED DATA CIF RESULTS



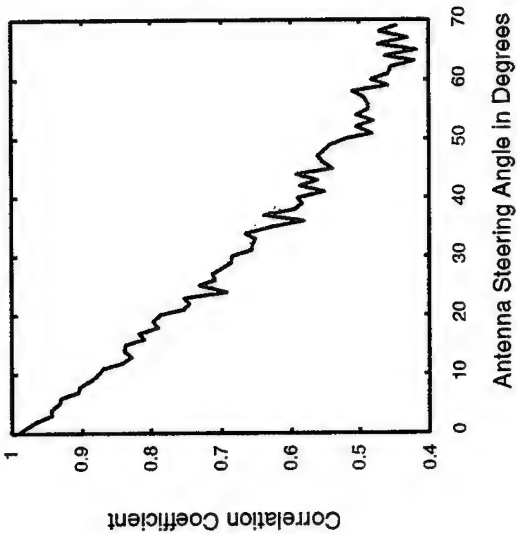
SLIDING WINDOW 2-PULSE MTI

SEG-05-377

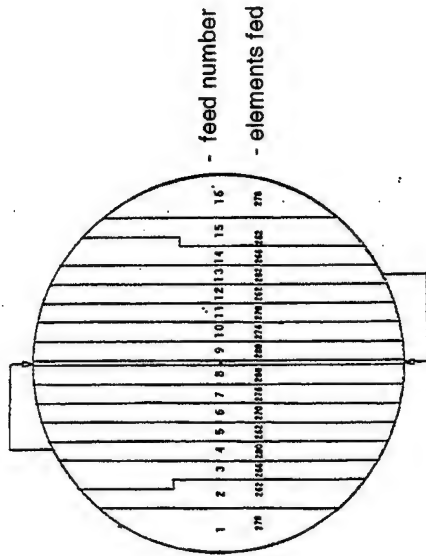
SEG

Systems Engineering Group, Inc.

IPN DECORRELATION WITH BEAM STEERING



**TWO-WAY IPN DECORRELATION
WITH AZIMUTH SCAN ANGLE**



**SPY-1B/D PHASED ARRAY
HAS 16 INDEPENDENT INPUTS**

- IPN IN TRANSMIT SAMPLE DECORRELATES WITH IPN IN RECEIVED RADAR RETURN DUE TO TIME DELAYS

OBJECTIVE

- INVESTIGATE FEASIBILITY OF CORRECTING FOR SPY-1B/D TRANSMITTER INTRAPULSE NOISE IN THE SIGNAL PROCESSOR TO IMPROVE SYSTEM CIF IN LITTORAL ENVIRONMENTS.
 - » SPY-1B/D TX IPN Limits System CIF
 - LNCFA Has Not Materialized
 - » SPY-1B/D Signal Processor 8-Bit A-To-D Also Limits System CIF
 - 12-Bit A-To-D Technology Is Mature
 - » ADDCIF Approach Also Compensates For Pulse-To-Pulse Disturbances Such As Clutter Doppler And Phase Droop

PROCESSING APPROACH (De-convolution In The Frequency Domain)

- DISTRIBUTED CLUTTER RETURN

$$s(t) = \int d(\tau)w'(t - \tau)d\tau$$

- » $d(t)$ = distributed clutter field
- » $w'(t)$ = transmitted waveform with errors (transmit sample)

- FREQUENCY DOMAIN PROCESSING

$$S(f) = D(f)W'(f)$$

$$D(f) = \frac{S(f)}{W'_m(f)}$$

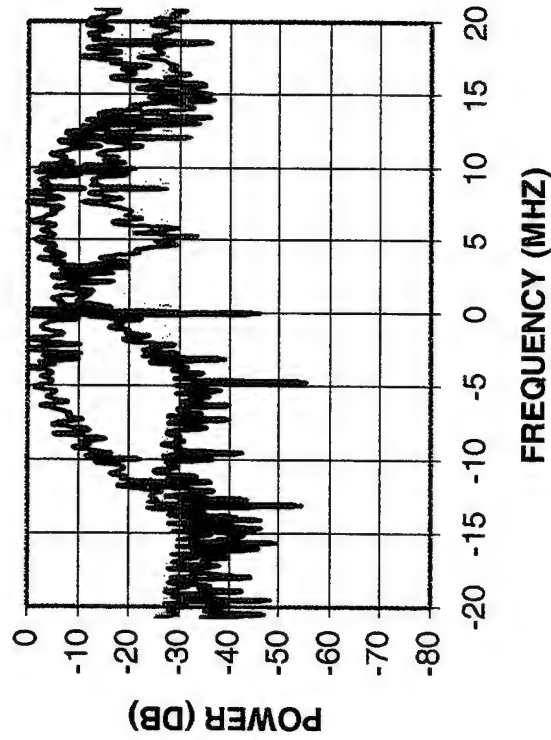
$$PC(f) = D(f)R_{ww}(f)$$

$$PC(t) = IFFT[PC(f)]$$

- » $R_{ww}(f)$ = unerrored waveform autocorrelation spectrum
- MTI PROCESS IPN COMPENSATED CLUTTER RETURNS

OVERLAP EXAMPLE FOR SUBPULSES F_A AND F_B

PHASE CODE 212/222



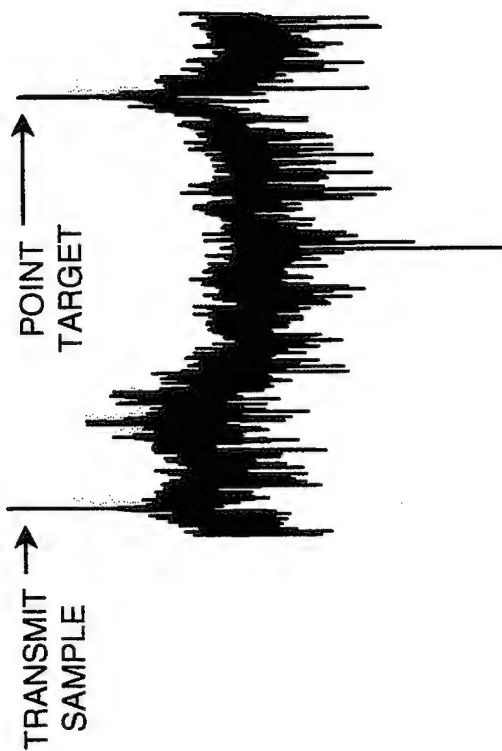
- WIDEBAND NOISE FROM BOTH SUBPULSES IS EQUAL IN BAND OF INTEREST
- IDEAL PHASE CODE SPECTRUMS SHOWN IN PLOT

SEG

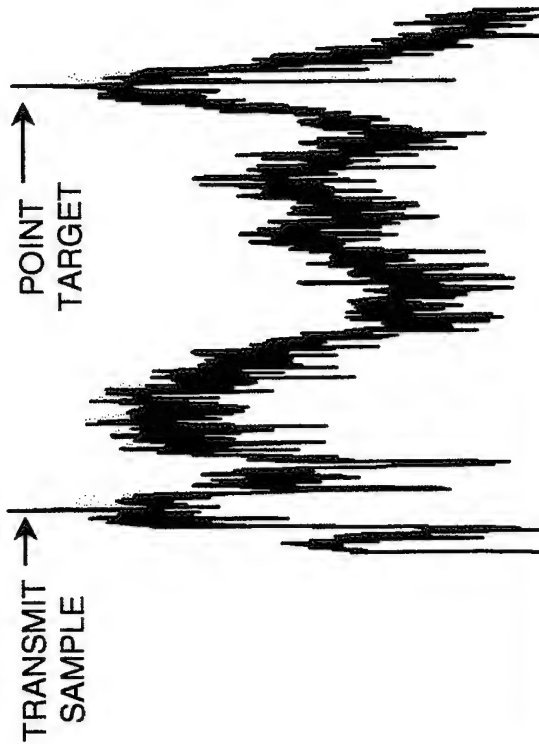
Systems Engineering Group, Inc.

MEASURED DATA TIME SIDELobe REDUCTION RESULTS - SINGLE PULSE

**ADDCIF
PULSE COMPRESSION**

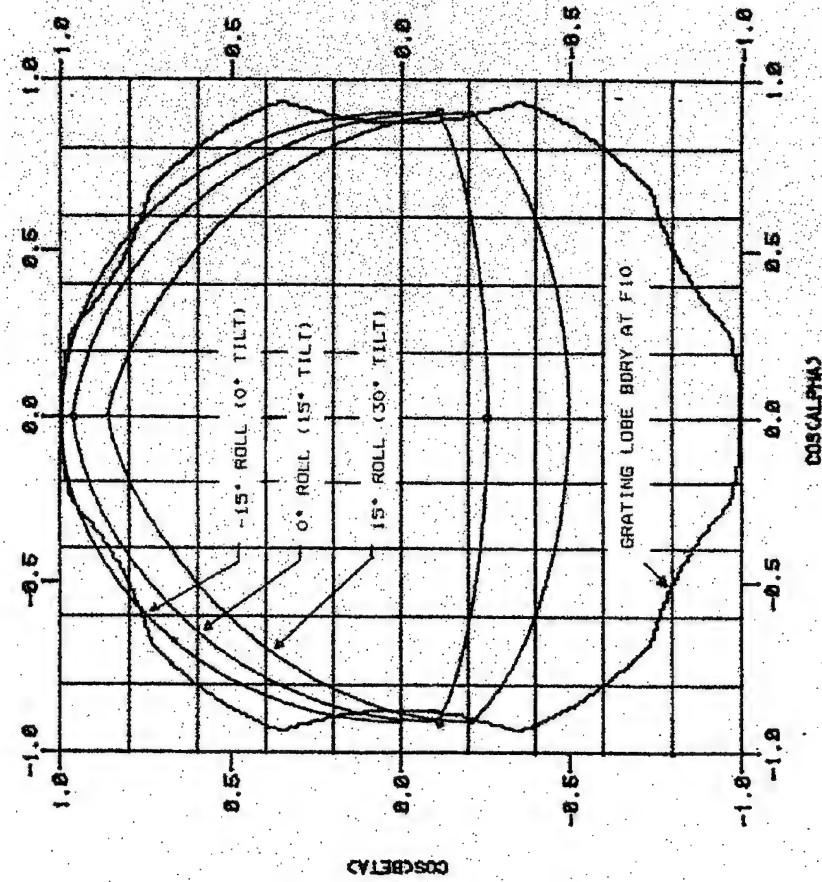


**NORMAL MTI
PULSE COMPRESSION**



TIME SIDELobe REDUCTION IMPROVES ABILITY TO
RESOLVE CLOSELY SPACED TARGETS WITH UNEQUAL RCS

NOTIONAL SHIPBOARD ARRAY COVERAGE REQUIREMENTS

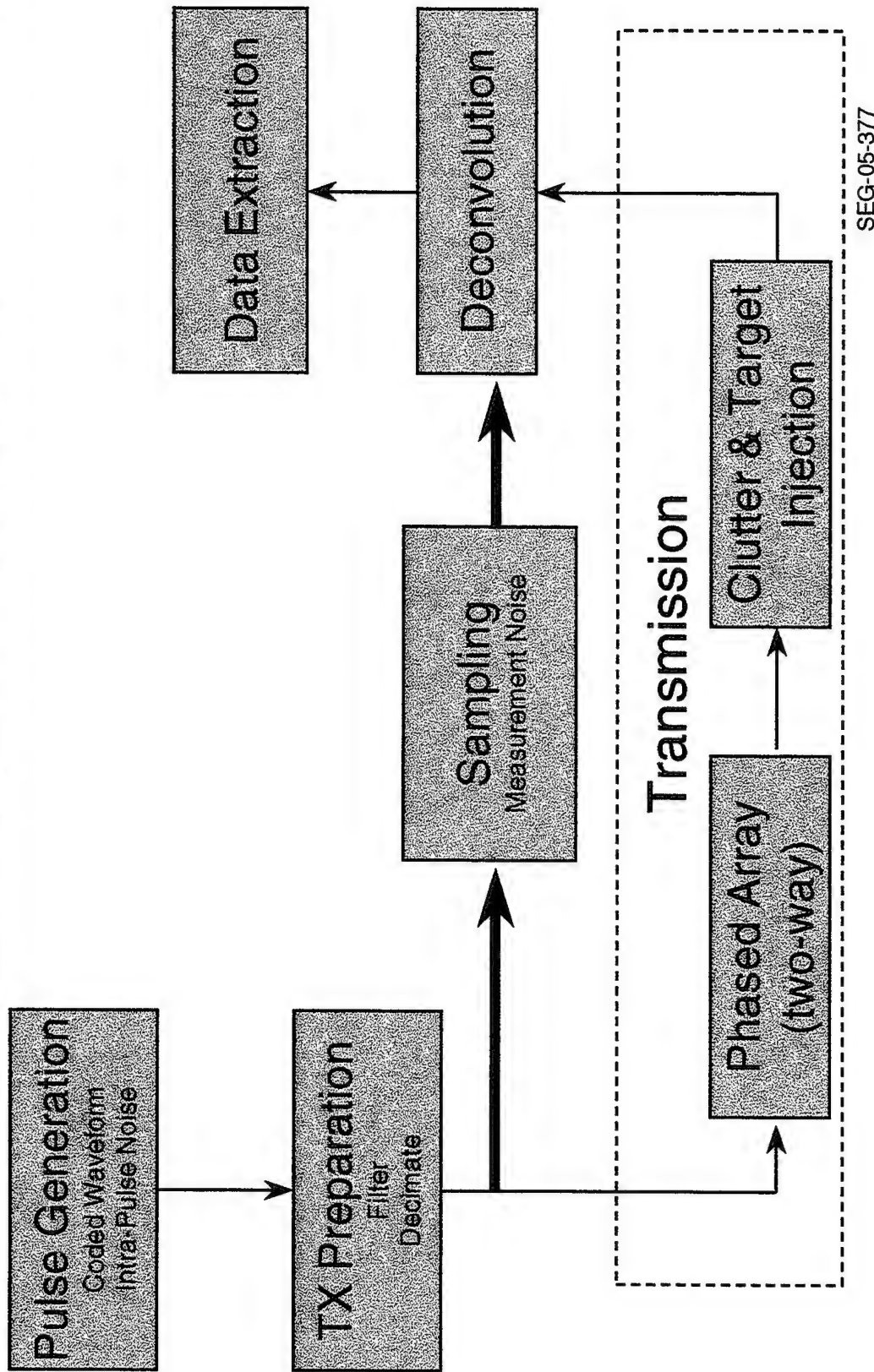


CONCLUSIONS/RECOMMENDATIONS

- CONTINUE TO ANALYZE MEASURED DATA
 - » UNDERSTAND SYSTEM ISSUES
 - » QUANTIFY EXPECTED SYSTEM PERFORMANCE

- INVESTIGATE THE POTENTIAL SYSTEM BENEFITS OF USING ADDCIF (FREQUENCY DOMAIN DECONVOLUTION) PROCESSING FOR TIME SIDELOBE REDUCTION
 - » IMPROVED PERFORMANCE IN CLOSELY SPACED OBJECT ENVIRONMENT

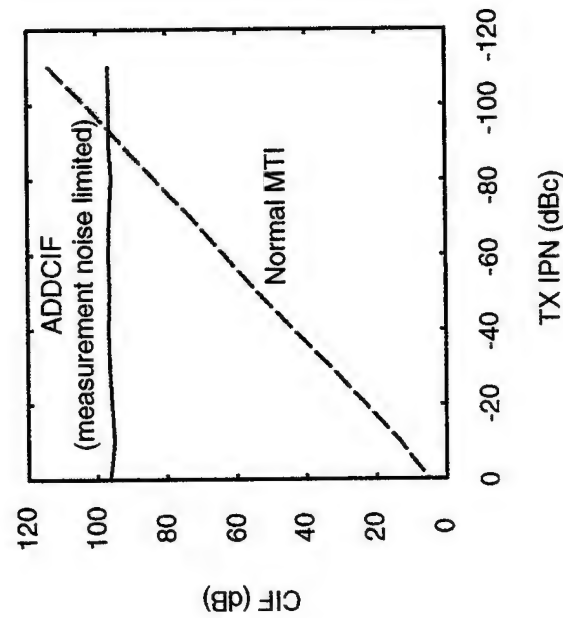
SYSTEM BLOCK DIAGRAM



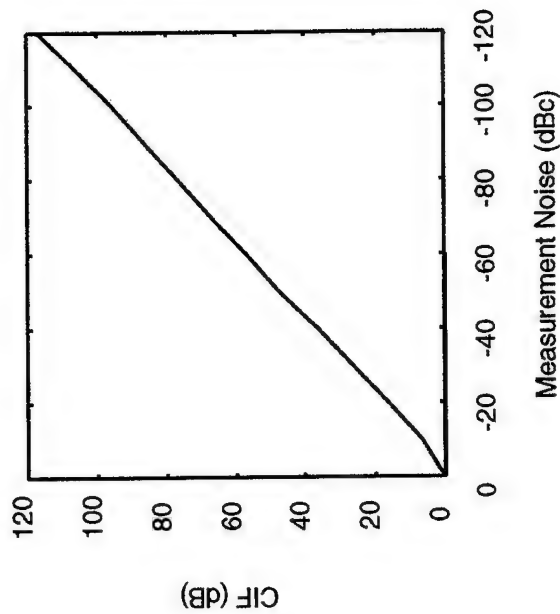
SEG-05-377

ADDCIF LIMITATIONS FOR TX IPN Single Subpulse Simulation

NO MEASUREMENT NOISE



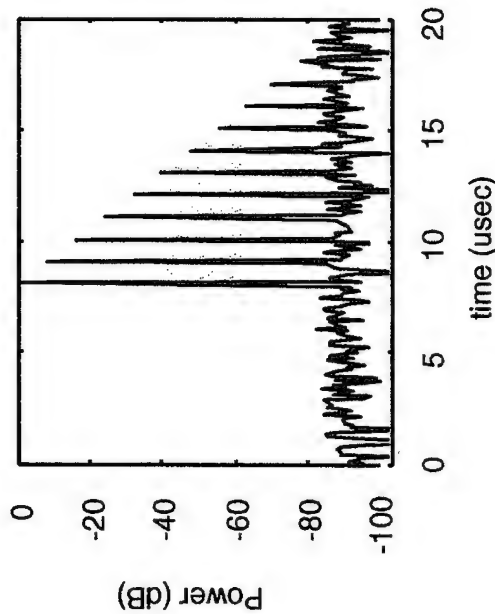
MEASUREMENT NOISE LIMIT



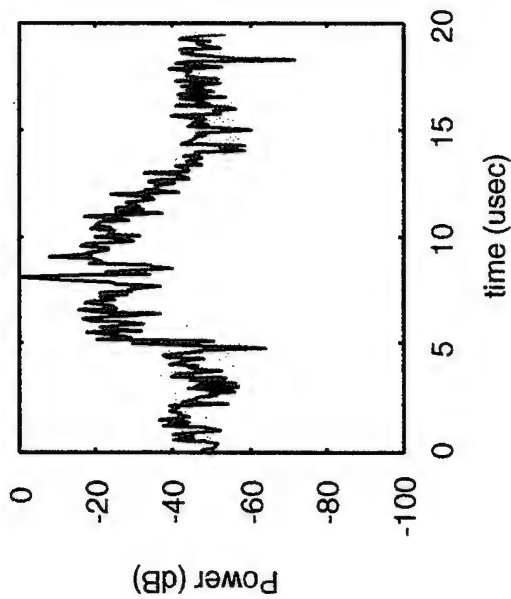
Measurement Noise Should Be At Least 10 dB Below Tx IPN

SIMULATION RESULTS MULTIPLE OVERLAPPED TARGETS

ADDCIF



NORMAL



IPN = -45 dBc
Measurement Noise = -100 dBc



ADDCIF Processing Potentially Removes Time Sidelobes

Adaptive Sidelobe Blanker: Threshold Setting and Performance in Inhomogeneous Clutter

Daniel E. Kreithen, Carl F. Pearson, and Christ D. Richmond

MIT Lincoln Laboratory
244 Wood Street, Room J-118D
Lexington, MA 02173-9108
tel: (781) 981-0144
email: kreithen@ll.mit.edu

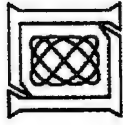
Abstract The homogeneous clutter assumption is often made when analyzing and designing post-adaptive nulling detection algorithms. In real-world scenarios, however, this assumption is invalid, and often leads to markedly elevated false alarm rates and generally poor target detection performance. A number of recent theoretical papers address the problem of target detection in post-adaptively nulled nonhomogeneous clutter [1,2], and demonstrate significant progress in this area. The present paper develops and analyzes criteria for setting thresholds in the two-dimensional adaptive sidelobe blanker (ASB) detection algorithm, which consists of a first stage adaptive matched filter (AMF) detector [3] followed by an adaptive coherence estimator (ACE) detector [4]. The ASB detector is theoretically analyzed in [2], where it is shown that there are infinite combinations of thresholds for the AMF and ACE which achieve the same false alarm rate. At one extreme it is possible to run the ASB as a strict AMF detector, which provides near optimum detection performance in homogeneous clutter with very little suppression of clutter discretely and sidelobe targets. At the other extreme, we can run the ASB as an ACE detector, which provides very good clutter discrete and sidelobe target suppression, but significantly degraded target detection performance. Clearly, it would be helpful to devise criteria that allow a sensible choice of thresholds somewhere between these two extremes. We propose two criteria for threshold setting for the ASB: (i) the "allowable loss" criterion and (ii) the "minimal loss" criterion. The allowable loss criterion, as the terminology implies, allows a given amount of target loss in exchange for clutter-discrete-induced false alarm and sidelobe target mitigation. The minimal loss criterion imposes a tolerable upper bound on false alarm rate given a minimum amplitude clutter discrete to arrive at a threshold combination. This paper formulates both criteria, and examines the behavior of the ASB in the presence of clutter discretely using an idealized model and simulation.

[1] D. E. Kreithen and A. O. Steinhardt, "Target Detection in Post-STAP Undermulled Clutter," 29th Annual Asilomar Conference on Signals, Systems, and Computers, Pacific Grove, CA, October 29–November 1, 1995.

[2] C. D. Richmond, "Statistical Performance Analysis of the Adaptive Sidelobe Blanker Detection Algorithm," to appear at 31st Annual Asilomar Conference on Signals, Systems, and Computers, Pacific Grove CA, November 2–5, 1997.

[3] F. C. Robey, D. R. Fuhrman, E. J. Kelly, R. A. Nitzberg, "A CFAR Adaptive Matched Filter Detector," IEEE Transactions on Aerospace and Electronic Systems, vol. 28, no. 1, 208–216 (1992).

[4] E. Conte, M. Longo, M. Lops, G. Ricci, "Asymptotically Optimum Radar Detection in Compound-Gaussian Clutter," IEEE Transactions on AES, vol. 31, no. 2, 617–625 (1995).



Adaptive Sidelobe Blanker: Threshold Setting and Performance in Inhomogeneous Clutter*

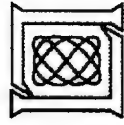
**Daniel E. Kreithen
C. Frederick Pearson
Christ D. Richmond**

**ASAP-98
11 March 1998**

KPR 3-11-98
Page 11 of 14

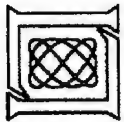
Preceding Page Blank

* This work was supported under Air Force contract F19628-95-C-0002.
Opinions, interpretations, conclusions, and recommendations are those of the author
and are not necessarily endorsed by the United States Air Force.

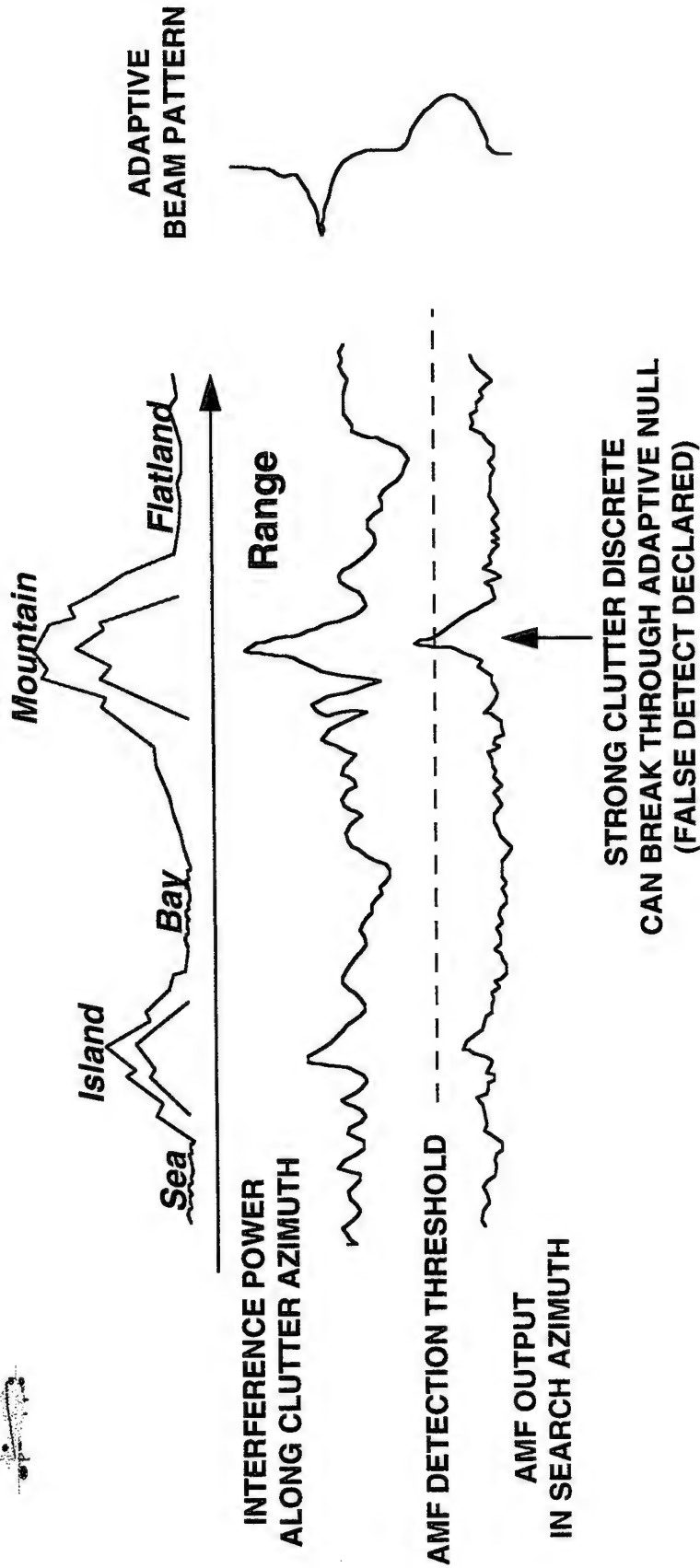


Outline

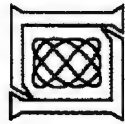
- ➔ • Goal and algorithm structure
- “Monte Carlo” method developed for study
- Detection threshold setting examples
 - “Allowable target desensitization” criterion
 - “Allowable increase in P_{FA} ” criterion
- Summary



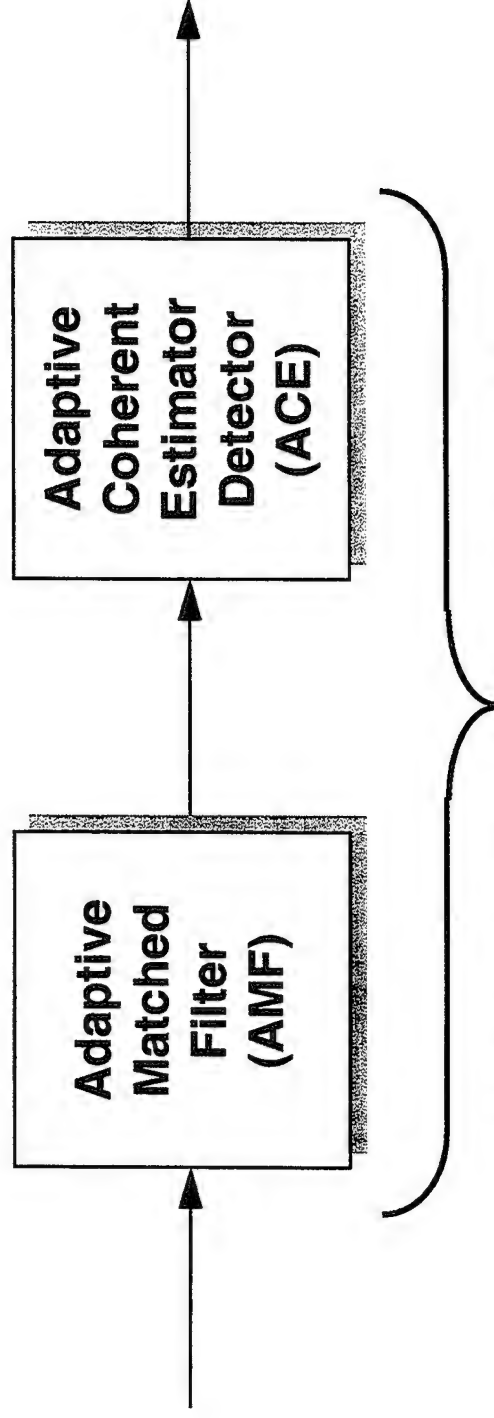
Overview



- Adaptive Sidelobe Blanking (ASB) designed to reject sidelobe detects (clutter breakthrough or sidelobe targets)



Adaptive Sidelobe Blanker Structure



Adaptive Sidelobe Blanker (ASB)

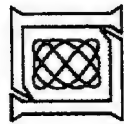
TRADITIONAL AMF TEST

$$T_{amf} \leq \frac{|v^H \hat{R}^{-1} x|^2}{v^H \hat{R}^{-1} v}$$

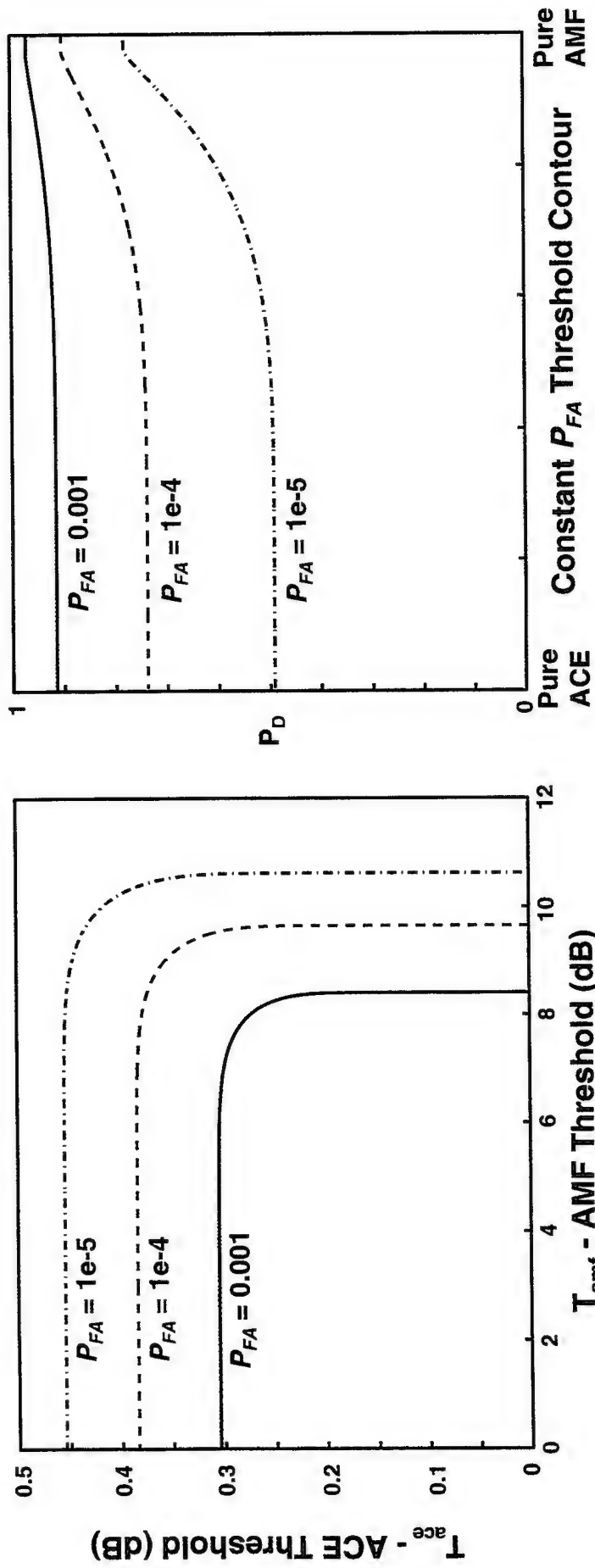
SIDELOBE REJECTION TEST

$$T_{ace} \leq \frac{|v^H \hat{R}^{-1} x|^2}{(v^H \hat{R}^{-1} v) (x^H \hat{R}^{-1} x)}$$

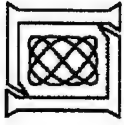
- How do we analyze P_D and P_{FA} for different (T_{amf}, T_{ace}) pairs?



P_{FA} Contours and P_D for ASB 20 Degrees-of-Freedom

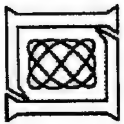


- P_D plotted for same target SNR P_T
- Known covariance (homogeneous interference)



Outline

- Goal and algorithm structure
- ➔ • “Monte Carlo” method developed for study
- Detection threshold setting examples
 - “Allowable target desensitization” criterion
 - “Allowable increase in P_{FA} ” criterion
- Summary



Monte Carlo Study of Threshold Parameters

- Generate: $z \sim CN^{(M)}(0, 1)$: $M = (\text{degrees-of-freedom})$

- Assume:

$$R_T = I + P_C v_C v_C^H \longrightarrow$$

$P_C = 0$ Homogeneous

$P_C \neq 0$ Non-homogeneous

- Set sidelobe leakage $\cos(a) = I v_t^H v_c /$

- Then:

$$x = R_T^{1/2} z + \sqrt{P_t} v_t$$

$$x = R_T^{1/2} z$$

Generate target realizations

Target power P_T

Generate clutter realizations

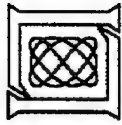
"Clutter discrete" power P_C

- Calculate AMF and ACE statistic for each x :

$$t_{AMF} = \frac{|v_t^H x|^2}{v_t^H v_t}$$

$$t_{ACE} = \frac{|v_t^H x|^2}{(v_t^H v_t)(x^H x)}$$

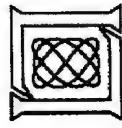
- Calculate P_D and P_{FA} for threshold pair (T_{AMF}, T_{ACE})



Efficient Implementation of Monte Carlo Simulation

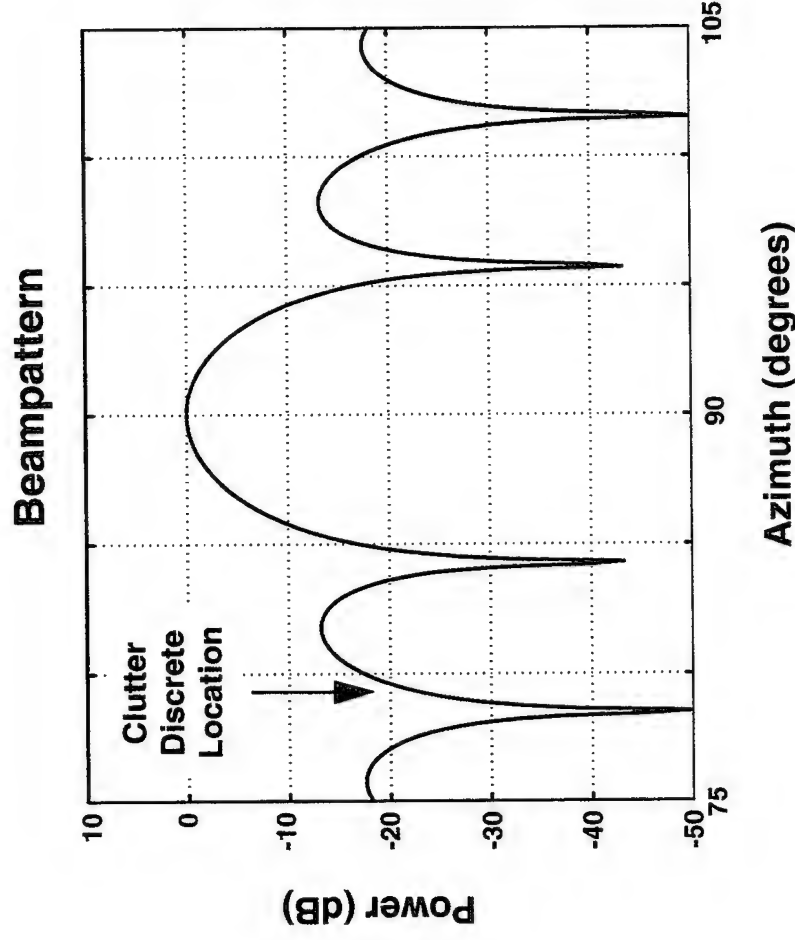
- Define: $\text{span}(v_c, v_t) = (e_1, e_2)$
- Write: $z^{(M)} = z_1 e_1 + z_2 e_2 + z^{(M-2)}$
 $v_t = \cos(a) \exp(j\phi) e_1 + \sin(a) e_2$
 $x_t = P_t^{1/2} v_t$
- For each (z_1, z_2) : ($\phi = 0$ does not change statistics)
$$x = (1 + P_c)^{1/2} z_1 e_1 + z_2 e_2 + x_t + z^{(M-2)} = y + z^{(M-2)}$$
- Evaluate $t_{\text{AMF}}(z_1, z_2) = |v_t^H y|^2$ (note $v_t^H z^{(M-2)} = 0$)
- If $t_{\text{AMF}} > T_{\text{AMF}}$: evaluate $P(t_{\text{ACE}} > T_{\text{ACE}} / t_{\text{AMF}} > T_{\text{AMF}})$
$$= P(t_{\text{AMF}} / (|y|^2 + |z^{(M-2)}|^2) > T_{\text{ACE}})$$

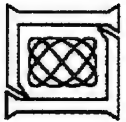
$$= P(|z^{(M-2)}|^2 < (t_{\text{AMF}} / T_{\text{ACE}}) - |y|^2): \text{Simple integral of } \chi^2_{(M-2)}(0)!$$
- Sum over all (z_1, z_2) to get ensemble average P_D or P_{FA}
- Much less computation required than for full M-dimensional Monte Carlo simulation



Operating Point for Monte Carlo Study

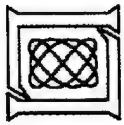
- 20 degrees-of-freedom ($M=20$)
- $P_{FA} = 10^{-4}$ for $P_C = 0$
- Set P_T to give $P_D = 0.9$
(with $T_{ACE} = 0$, $P_C = 0$)
- Set $\cos^2(a) = -20$ dB
(sidelobe level)
- Target at broadside
- Examine P_D and P_{FA} with
 $P_C = [-20 : 5 : 50]$ dB





Outline

- Goal and algorithm structure
- “Monte Carlo” method developed for study
- • Detection threshold setting examples
 - “Allowable target desensitization” criterion
 - “Allowable increase in P_{FA} ” criterion
- Summary



Design Criteria for Threshold Setting

- “Allowable target desensitization”

- Set (T_{AMF} , T_{ACE}) to give (in homogeneous interference):
Desired P_{FA} (same P_{FA} as with $T_{ACE} = 0$)
Same P_D with $P_T = P_T^{(0)} + L$ as with $T_{ACE} = 0$, $P_T = P_T^{(0)}$

Parameter L trades target sensitivity in *homogeneous* interference
for false alarm control in *inhomogeneous* interference

Example shown: $P_{FA} = 10^{-4}$, $P_D = 0.9$ (defines $P_T^{(0)}$), $L = 0.1$ dB

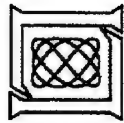
- “Allowable increase in P_{FA} ”

- Set (T_{AMF} , T_{ACE}) to limit P_{FA} in inhomogeneous interference
 $Max (P_{FA} / P_C > 0) = C \times (P_{FA} / P_C = 0)$

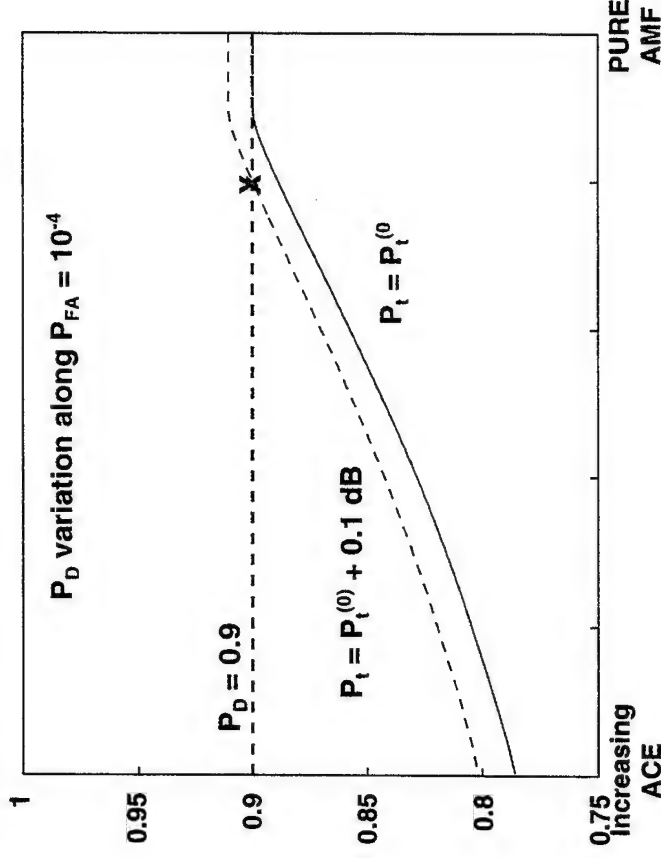
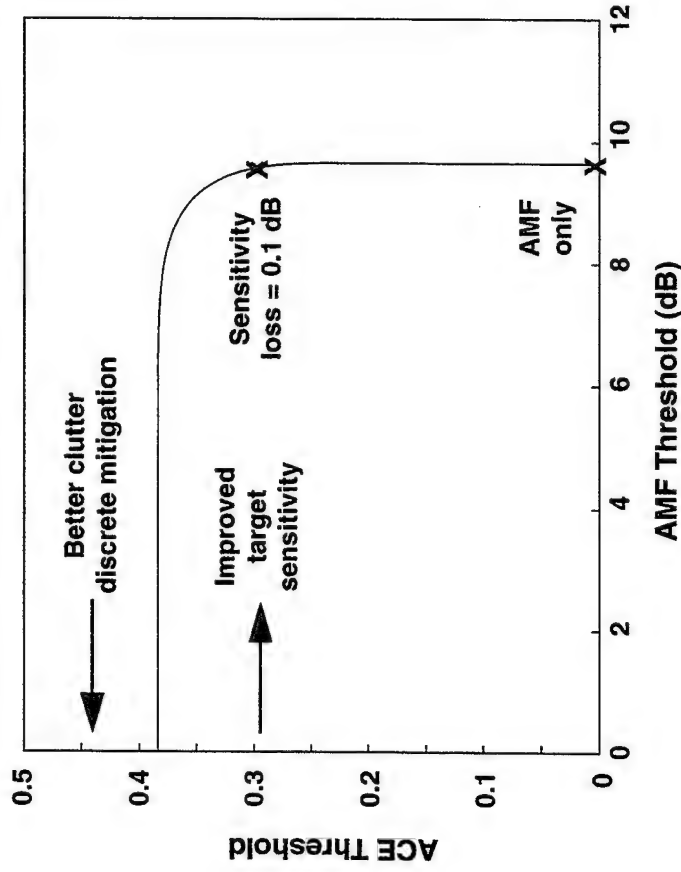
Example shown: $P_{FA} = 10^{-4}$, $C = 2$

- Criteria can not be set independently:

- Smaller C gives larger L , smaller L gives larger C

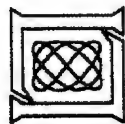


Allowable Target Desensitization



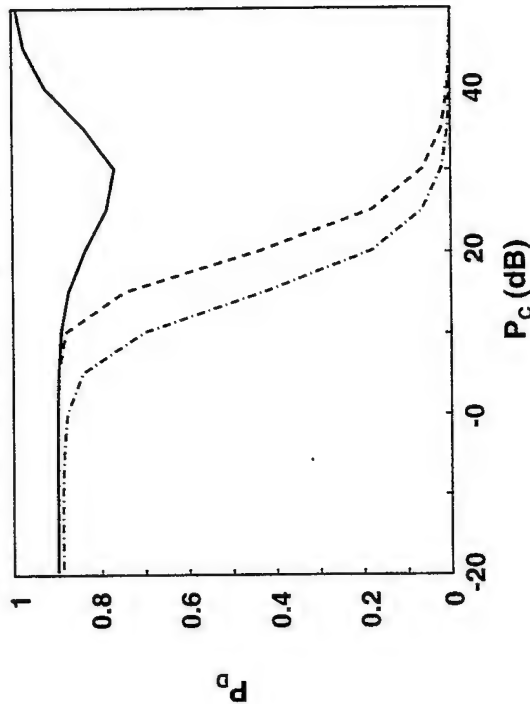
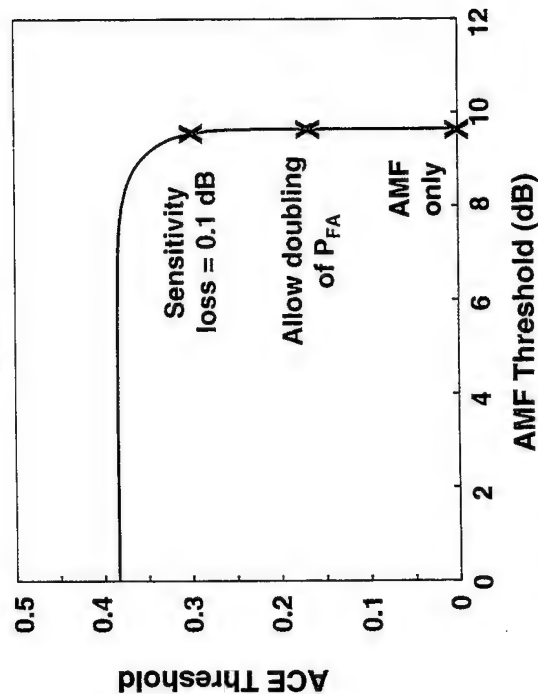
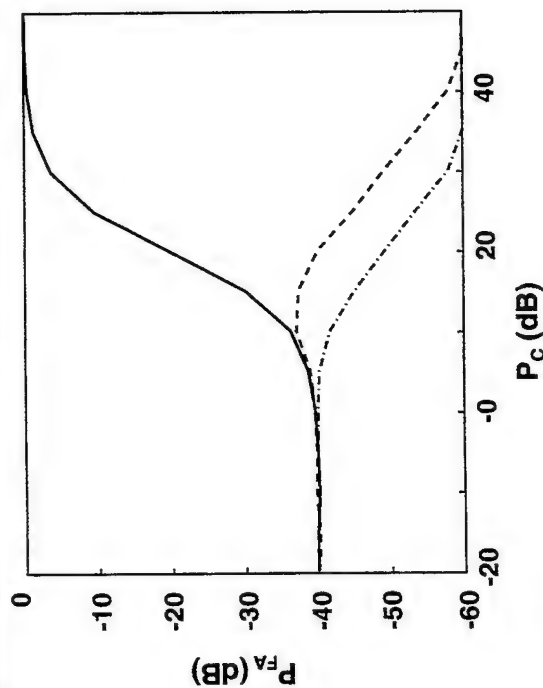
Specify allowed target desensitization in homogeneous interference
Small loss in sensitivity gives significant clutter discrete mitigation
Example: Choose $P_{FA} = 10^{-4}$ and set $P_t^{(0)}$ to give $P_D = 0.9$ for AMF-only
Accept 0.1 dB desensitization:

Choose (T_{AMF}, T_{ACE}) that gives same P_D for $P_t = P_t^{(0)} + 0.1$ dB



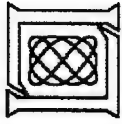
ASB Behavior in Non-Homogeneous Interference

20 degrees-of-freedom



— AMF Only
 - - Allow doubling of P_{FA} in presence of clutter discrete
 - . . Target desensitization = 0.1 dB

- Target desensitization example:
Allow desensitization $L = 0.1$ dB
- Allowable P_{FA} example:
Allow $(P_{FA} / P_C > 0) = 2 \times (P_{FA} / P_C = 0)$



Summary

- Reviewed Adaptive Sidelobe Blanker (ASB)
- Developed novel 2D Monte Carlo approach for analyzing ASB in *inhomogeneous* interference
 - Provides tool to understand system trades for ASB threshold settings
- Examples of two ASB threshold setting criteria:
 - Allowable target desensitization
 - Allowable increase in P_{FA}
- Examined ASB performance in presence of clutter discretes using both criteria
- Conclusion: Minor target desensitization provides significant clutter discrete mitigation

Adaptive Monopulse Processing in the Presence of TSI and Mainbeam Jamming

Yaron Seliktar, Douglas B. Williams, and E. Jeff Holder

School of Electrical and Computer Engineering

Georgia Institute of Technology

Atlanta, GA 30332-0250

tel: (404) 633-4737

email: yaron@ece.gatech.edu

Abstract Monopulse processing is used to provide high precision angle estimates for target tracking. Space-time processing in fast-time is necessary to reject terrain scattered interference (TSI) and has been applied to suppress mainbeam jamming. By judicious combination of the two techniques, we are able to attain high precision angle estimates in the presence of TSI and mainbeam jamming. The merit of the resulting processor is in the successful exploitation of what is typically a nuisance source of interference (i.e. TSI) to achieve target angle estimation performance far better than has previously been possible in a mainbeam jamming environment. Examples using Mountaintop datasets demonstrate the viability of the proposed space-time adaptive monopulse processor in real world TSI and mainbeam jamming scenarios. The examples further demonstrate a dramatic improvement in angle estimation performance over conventional and spatially adaptive monopulse techniques.

ADAPTIVE MONOPULSE PROCESSING
IN THE PRESENCE OF TSI AND
MAINBEAM JAMMING

YARON SELIKTAR

GEORGIA TECH, SCHOOL OF ECE
GEORGIA TECH RESEARCH INSTITUTE

DOUGLAS B. WILLIAMS

GEORGIA TECH, SCHOOL OF ECE

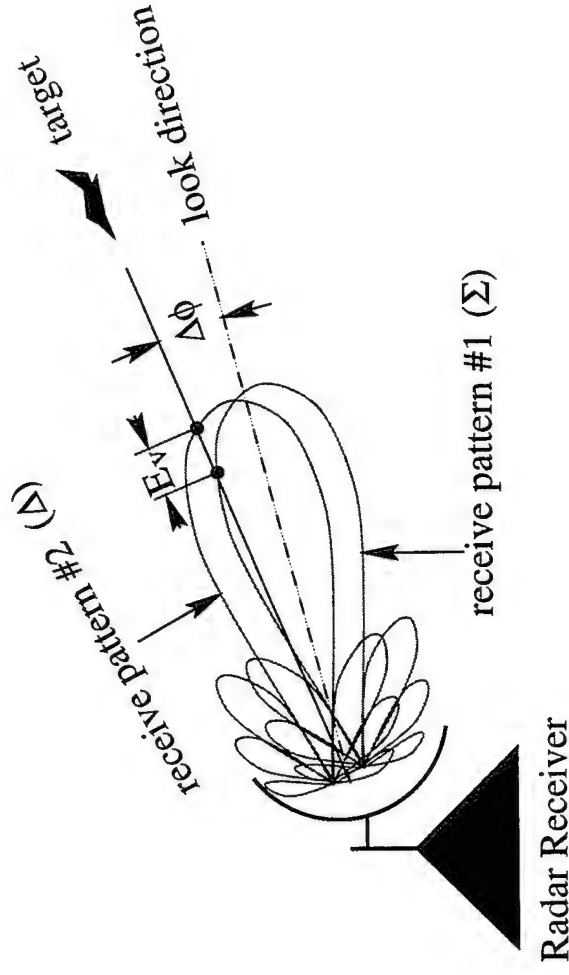
E. JEFF HOLDER

GEORGIA TECH RESEARCH INSTITUTE

Objectives

- Incorporate Space-Time Adaptive Processing into monopulse processing to attain high precision angle estimates of targets in the presence of terrain scattered interference (TSI) and main-beam jamming.
- Demonstrate results of new space-time monopulse processor on Mountaintop datasets.
- Develop an adaptive space-time mitigation algorithm for the combined effect of Monostatic Clutter (MSC), TSI, and main-beam jamming.
- Demonstrate improved mitigation and monopulse performance of new processor on Mountaintop dataset.

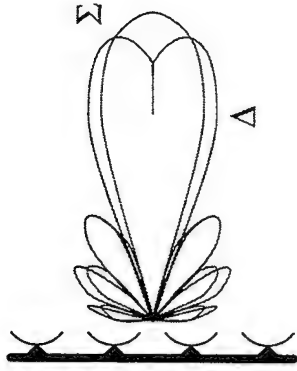
Classical Monopulse



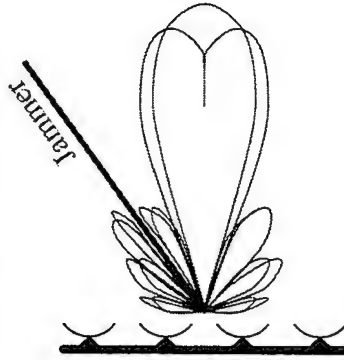
- Sum (Σ) and Difference (Δ) receive beams with corresponding output voltages, V_Σ and V_Δ .
- Ratio of voltages, E_v , corresponds to a given deviation of angle, $\Delta\phi$.
- $\phi_{target} = \phi_{look} + \Delta\phi$ gives us a better estimate of a target's angular location than possible with only one beam.

Phased Array Monopulse

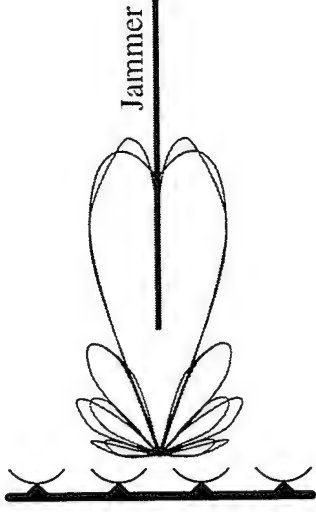
- Form receive beams electronically.



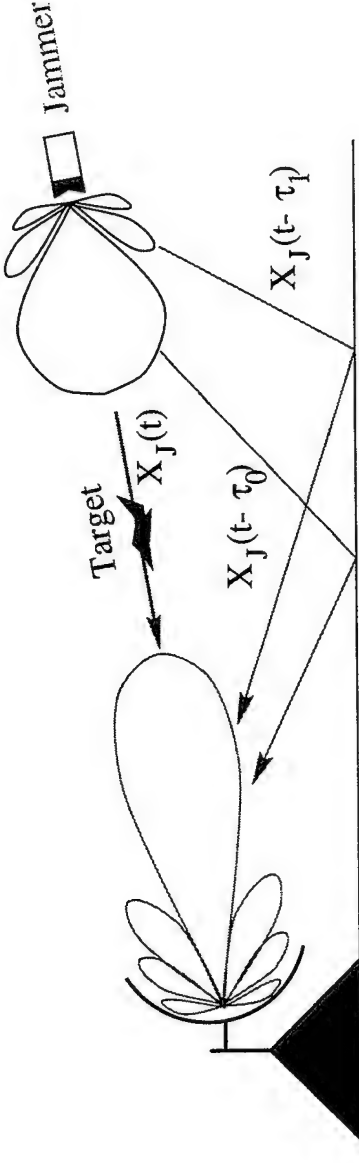
- When jammer interference is present, use adaptive beams to put a null in the jammer.



Mainbeam Jamming and TSI

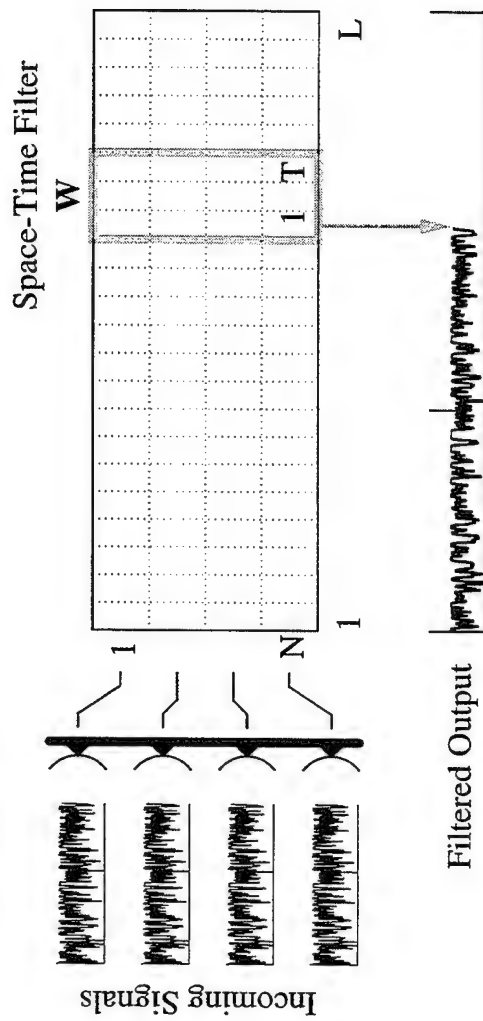


- If mainbeam Jamming is present beams become distorted – can't do monopulse.



- If ground reflections are present, we can use the delayed replicas to estimate and cancel the mainbeam jammer signal.
- Resulting TSI mitigation is achieved through space-time processing.

Space-Time Processing



- Adaptive weights are computed via constrained optimization.
- Constraint matrix (C) and constraint vector (c) are designed according to parameters and criteria that need to be met by the processor.

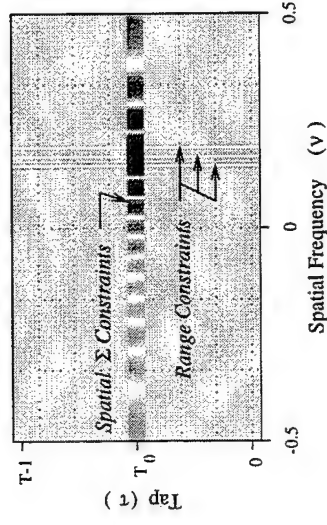
$$W = R_X^{-1} C^H (C R_X^{-1} C^H)^{-1} c.$$

Applying Space-Time Processing to Monopulse

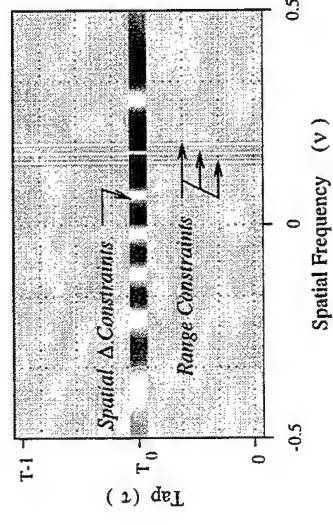
- Monopulse requires sum (Σ) and difference (Δ) processors.

$$W_{\Sigma}, W_{\Delta}$$

- Designing the sum processor –

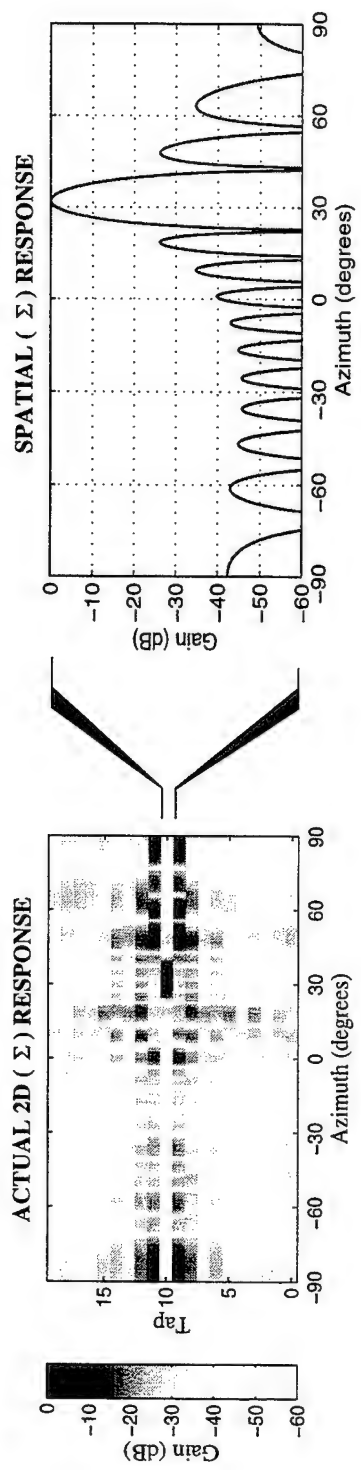


- Designing the difference processor –

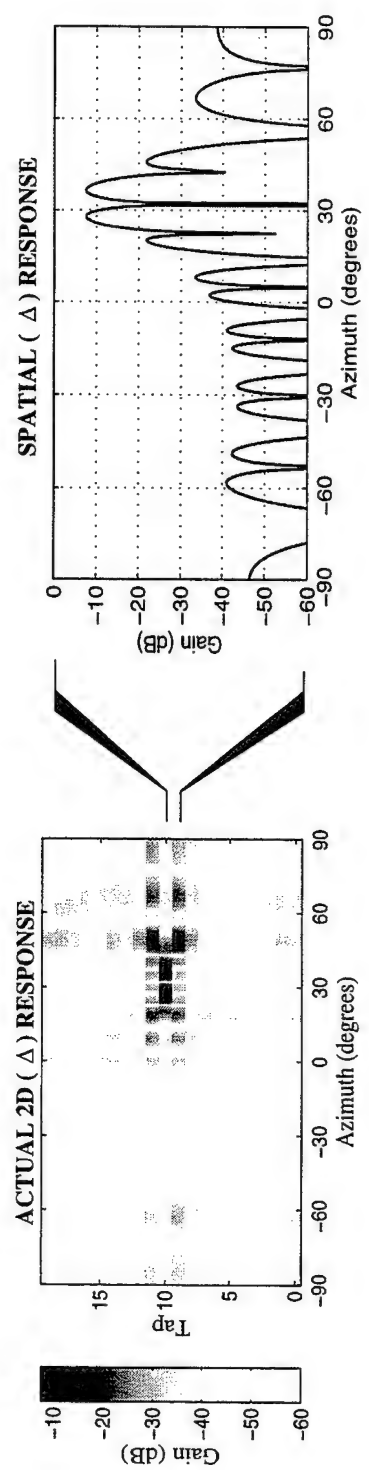


Actual Results for a 20-Tap Processor¹

• Actual sum (Σ) response²



• Actual difference (Δ) response²



¹Results are based on Mountaintop dataset mm1t004v1

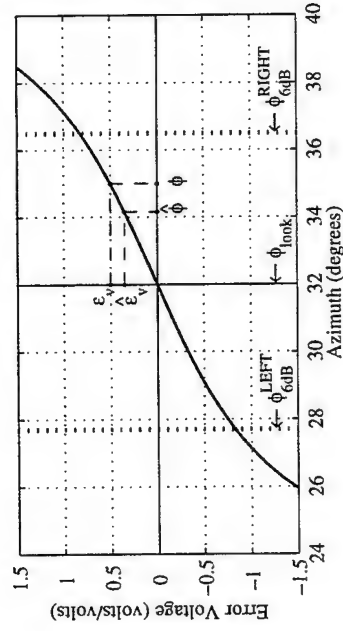
²Two-way response assumes a directional radar transmitter

Arriving at an Angle Estimate

- Error voltage is the measure obtained from the outputs of the sum and difference processors, $z_{\Sigma}(t)$ and $z_{\Delta}(t)$.

$$\epsilon_v(t) = \Im \left\{ \frac{z_{\Delta}(t)}{z_{\Sigma}(t)} \right\}.$$

- Monopulse Response Curve (MRC) maps a given error voltage to a corresponding azimuth angle.



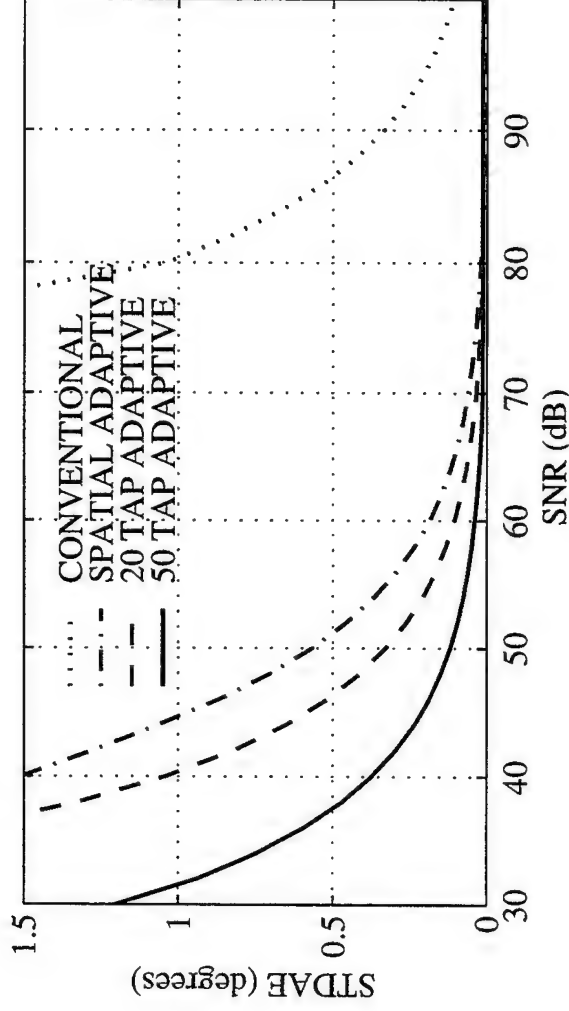
- In practice the processors are unable to completely reject interference. The residual interference in the outputs $z_{\Sigma}(t)$ and $z_{\Delta}(t)$ causes the error voltage to deviate from its ideal value, resulting in a corresponding error in the azimuth angle measurement, $\epsilon_{\phi} = \hat{\phi} - \phi$.

Performance

- The *Standard Deviation of Angle Error (STDAE)* gives us a useful measure of monopulse performance.

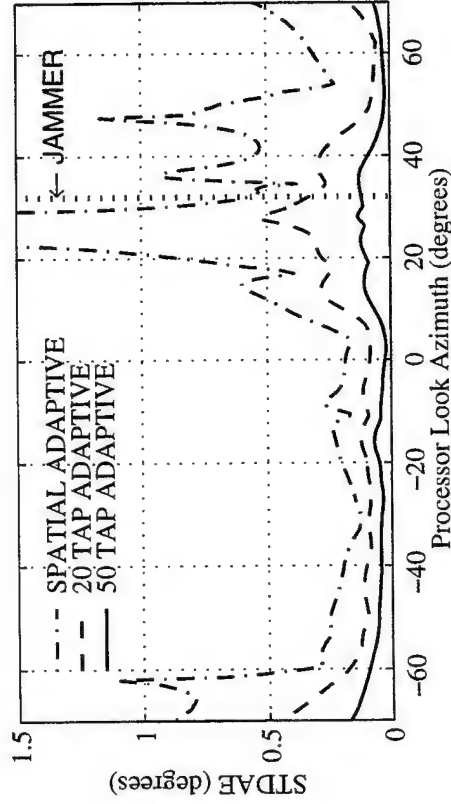
$$\sigma_{\epsilon_\phi} = \sqrt{E\{|\epsilon_\phi|^2\}}.$$

- Comparison of four processors in a mainbeam jamming scenario.



- Results for conventional processor indicate amount of burnthrough necessary to achieve performance of adaptive processors.

Other Performance Results



- Comparison of three processors when we vary the look direction.
- SNR is 50 dB.

- Other Mountaintop datasets.

- SNR is 50 dB.

- ϕ_{bw} is 6 dB beamwidth².

- σ_{ϵ_ϕ} is STDAE.

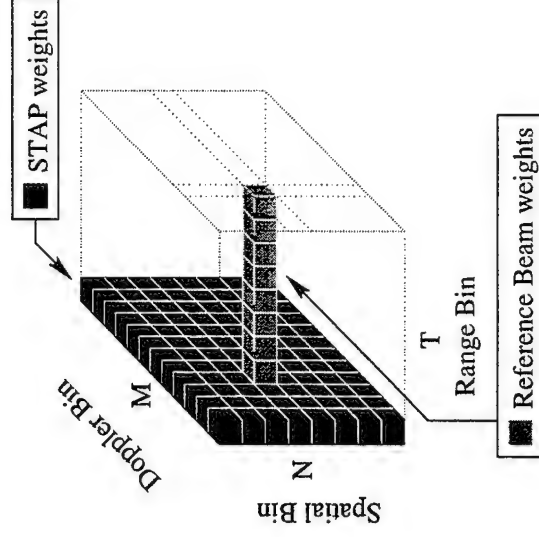
- OINR is output interference to noise ratio in dB.

¹Contain TSI without direct path jamming
²3 dB for transmission + 3 dB for receive

Name	1 Tap Processor			50 Tap Processor		
	ϕ_{bw}	OINR	σ_{ϵ_ϕ}	ϕ_{bw}	OINR	σ_{ϵ_ϕ}
mmit004v1	5.85	31.0	0.57	8.80	21.5	0.12
mmit013v1	12.3	33.2	1.96	15.5	22.4	0.21
mmit043v1	5.65	25.1	0.19	8.80	21.8	0.13
mmit044v1	5.90	25.7	0.19	8.80	22.0	0.14
mmit045v1	5.95	23.3	0.16	8.80	19.4	0.09
mmit048v1	5.75	25.1	0.18	8.80	22.2	0.14
mmit109v1 ¹	5.70	25.1	0.44	8.80	20.6	0.11
mmit112v1 ¹	5.70	25.0	0.44	8.80	20.6	0.11

Joint TSI/Monostatic Clutter Cancelation

- New algorithm, Beam-Augmented STAP, for the combined TSI/monostatic clutter cancelation problem.
- Methodology (Intuitive explanation)
 - Apply a 2D DFT at each range bin of the data cube, resulting in spatial/Doppler data.
 - Apply weights to all spatial/Doppler samples from the first tap as shown by the black filled cubes; these weights constitute the STAP portion of the processor.
 - Select a tapped reference beam as shown by the gray shaded cubes; these weights constitute the TSI canceler portion of the processor.
 - Optimize all weights simultaneously.



- Equivalent Implementation
 - Apply weights to all element/PRI samples from the first tap.
 - Apply weights to one or more tapped reference beams formed from the data cube.
 - Optimize all weights simultaneously.

Comparing Architectures

- Comparing three algorithms–
 - Beam-Augmented STAP (BASTAP) with 100 taps.
 - Factored Beamspace Approach (FBA) with 25 taps.
 - Space-Time Adaptive Processing (STAP).
- Computational complexity and sample support requirements.
 - In general.

NAME	BASTAP	FBA	STAP
Computational Complexity	$(MN+T-1)^3$	$M(NT)^3+(MN)^3$	$(MN)^3$
Sample Support (samples)	$MN+T-1$	$MN+NT$	MN
Convergence (samples)	T	T	1

- In example.

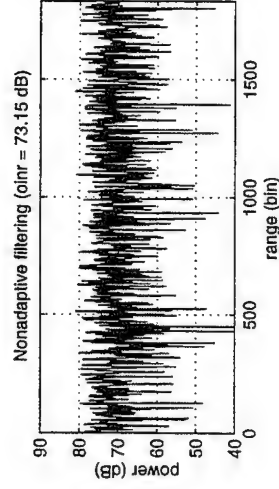
NAME	BASTAP	FBA	STAP
Computational Complexity	$3x$	$32.5x$	x
Sample Support (samples)	$1.44y$	$2.25y$	y
Convergence (samples)	100	25	1

- Other differences.
 - FBA requires “clutter free” training data (i.e., containing only TSI).

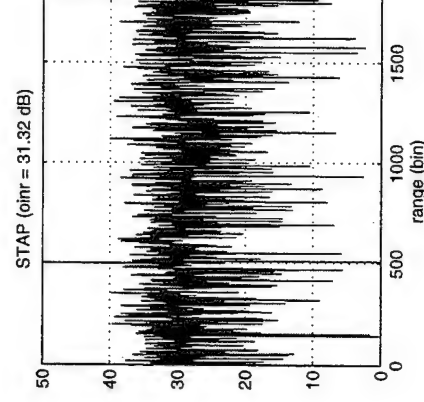
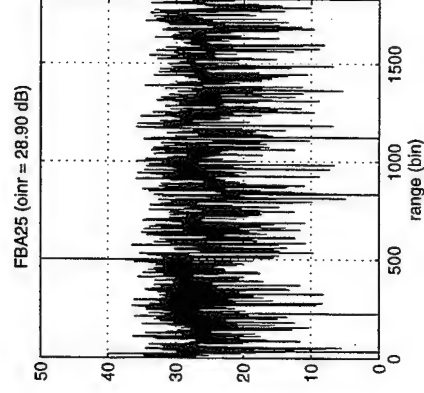
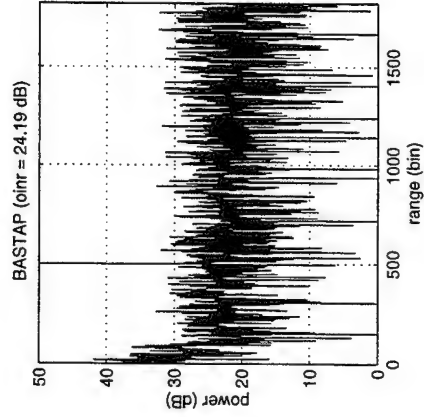
Performance Results I

- Mainbeam jamming and TSI from dataset mmit004v1 combined with 40 dB of synthetic monostatic clutter. Jammer and look direction are at 32° . A 50 dB synthetic target is injected in range bin 500.

- Nonadaptive filtering–

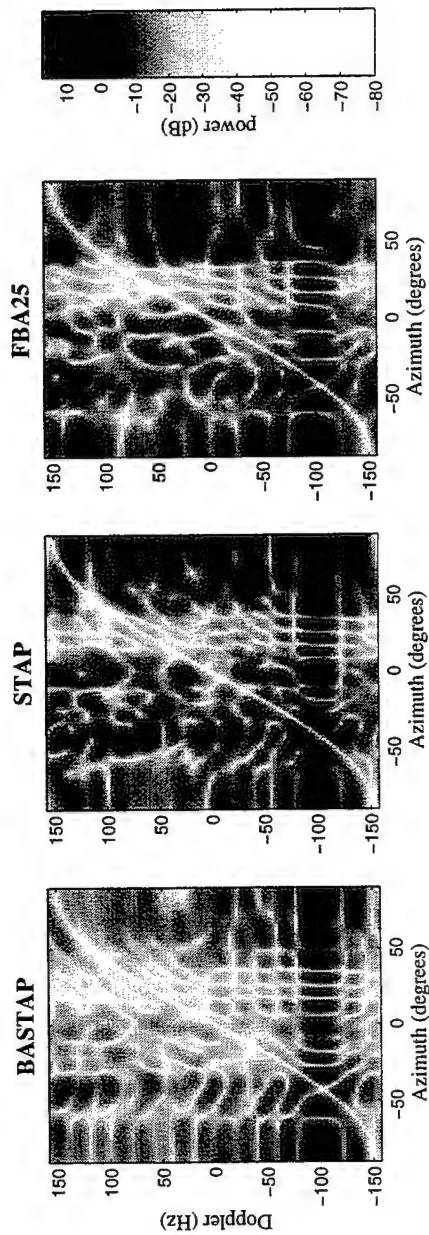


- Adaptive filtering–

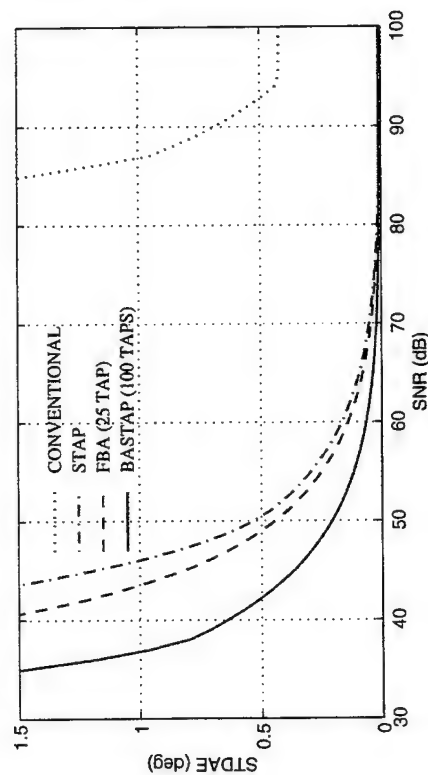


Performance Results II

- Sum (Σ) Responses (1-way) –



- Monopulse performance –



Summary of Main Results

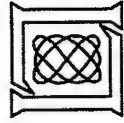
- Introduced a method by which a monopulse processor is combined with an adaptive space-time processor.
- Demonstrated the benefit of a tap-centered configuration with spatial constraints for improving the weight response and monopulse performance of such a processor.
- Developed new processor for combined TSI/monostatic clutter that offers improved mainbeam jamming cancellation and monopulse performance over existing algorithms.

Adaptive Wideband Interference Suppression for a Beamspace Application (AN/SPY-1)

Nicholas B. Pulsone and Edward J. Baranoski

MIT Lincoln Laboratory
244 Wood Street, Room S2-239
Lexington, MA 02173
tel: (781) 981-0268
email: pulsone@ll.mit.edu

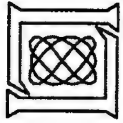
Abstract Adaptive array processing techniques are useful for rejecting coherent interference in applications such as radar, sonar, and communications. However, the performance of these techniques degrades with increasing bandwidth of the interference. Two methods for improving the bandwidth performance of an adaptive array processor include tapped delay-line processing and Discrete Fourier Transform (DFT) subband processing. This work analyzes the bandwidth performance of these methods for a beamspace application constrained to a limited number of beams. We relate the performance of these methods to the bandwidth, power, and bearing of the interference as well as to the antenna patterns of the beamspace application. Performance results are illustrated using both simulations and measurements made with AN/SPY-1.



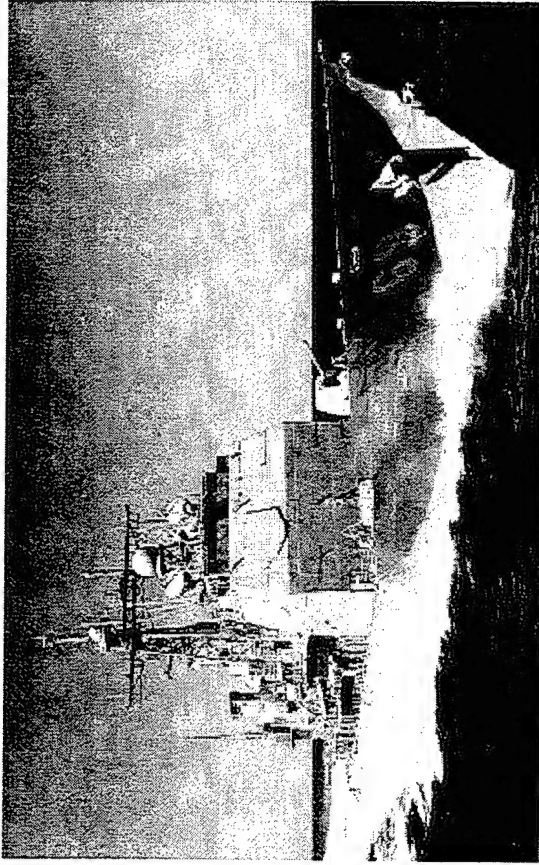
Adaptive Wideband Interference Suppression for a Beamspace Application (AN/SPY-1)

**Nicholas B. Pulsone
Edward J. Baranoski**

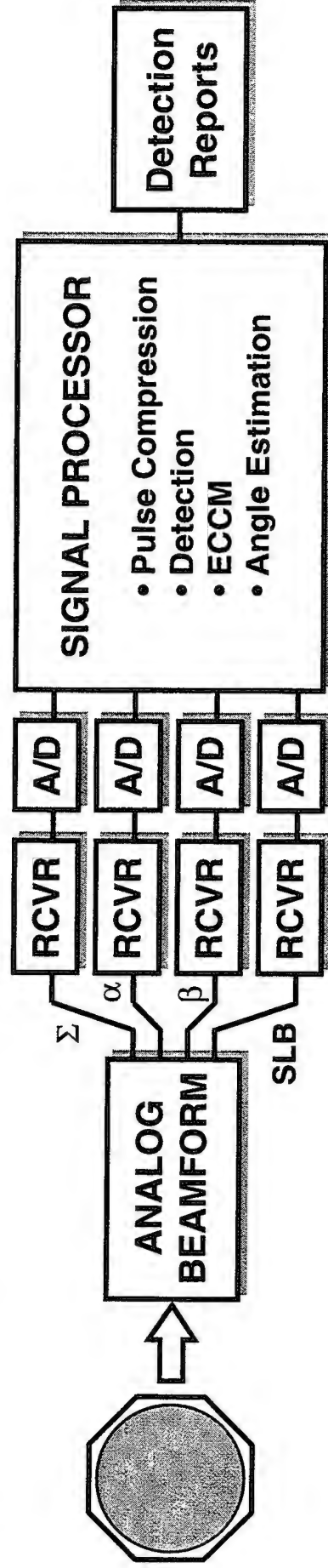
**Group 102
MIT Lincoln Laboratory
Lexington, MA**



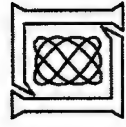
AEGIS System Overview



- AN/SPY-1 (Search & Track Radar)
 - Large Phased Array System
- Four Channel Monopulse
 - Σ Channel (Sum Beam)
 - α Channel (Azimuth Difference)
 - β Channel (Elevation Difference)
 - SLB Channel (Sidelobe Blanker)

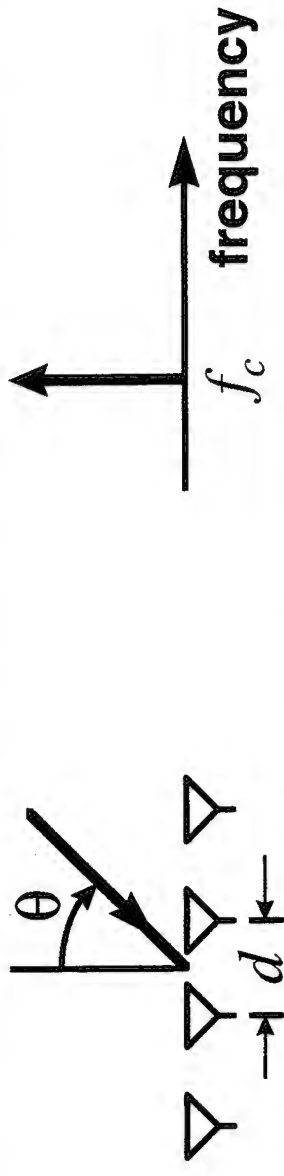


Objective: Investigate adaptive subband nulling for AEGIS AN/SPY-1 radar system

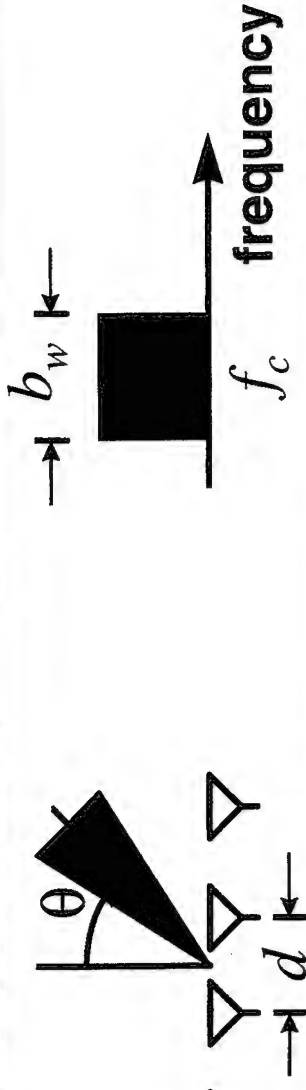


A Description of Wideband Interference

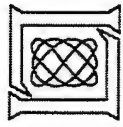
Narrowband Interference



Wideband Interference



- Narrowband interference appears to arrive from a single direction
- Wideband interference appears to arrive from an angular sector related to the bandwidth b_w and the center frequency f_c of the interfering signal

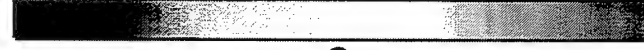


The Problem with Adaptive Processing in Wideband Interference

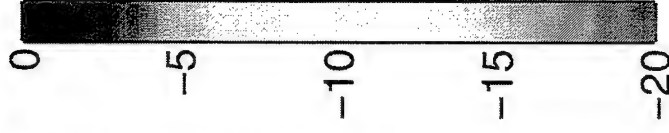
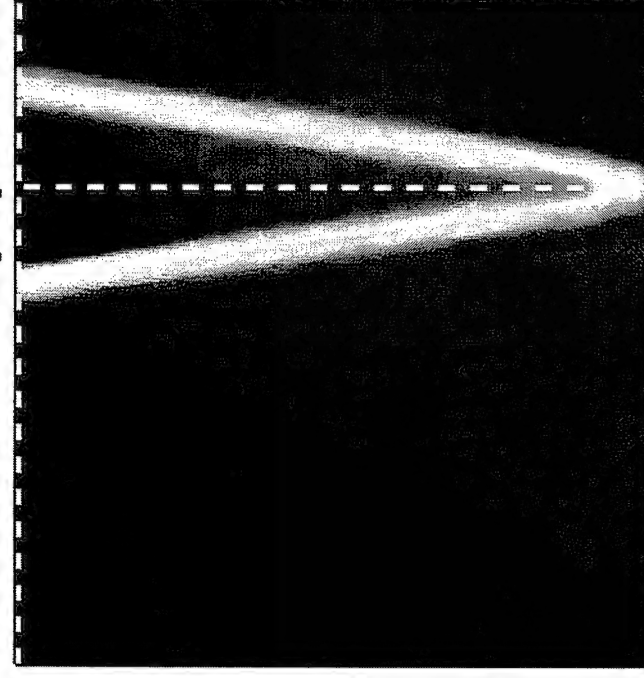
Beam Patterns after Adaptive Nulling



Increasing Power →



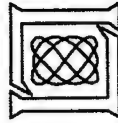
SINR Loss [dB]



Direction

Direction

- Conventional adaptive processing with wideband interference
 - Creates broad nulls
 - Requires multiple DOFs
- SINR Loss significantly degrades with increasing bandwidth



AEGIS Nulling Problem

PROBLEM STATEMENT

- Develop an approach for wideband interference nulling for the AN/SPY-1 radar system

CONSTRAINTS

- Solution must work with limited degrees of freedom (DOFs)
- Solution must support adaptive detection and estimation

SOLUTION

- Include adaptive subband nulling into processing [1-3]

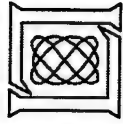
RESULTS

- Detection possible in the presence of a single jammer
- False alarm control is maintained
- Overcomes limited DOFs problem
- Supports adaptive detection and estimation

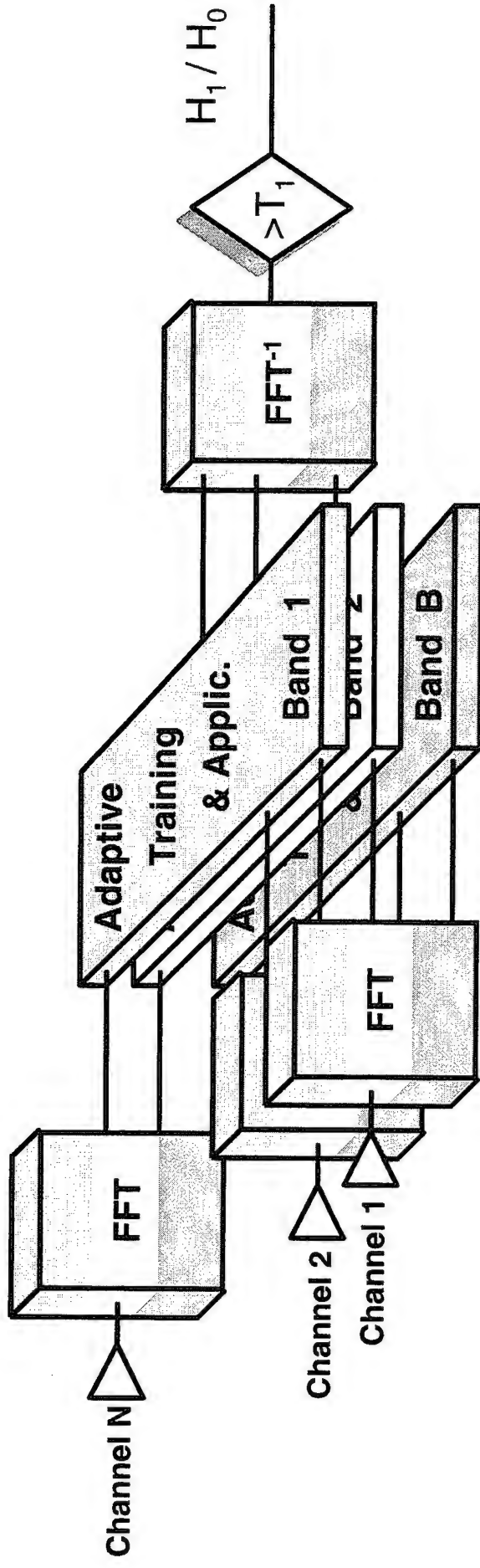
[1] Compton, *Adaptive Antennas*, 1988.

[2] Owsley, "Sonar array processing" in *Array Signal Processing*, Haykin (Editor), 1985.

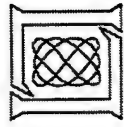
[3] Simanapalli and Kaveh, *Broadband focusing for partially adaptive beamforming*, T-AES, Jan. 1994.



Adaptive Processing using Frequency Subbanding



- For B subbands and for N channels, B problems of rank N
- Computationally less intensive than Tapped Delay-Line approach
 - Requires on the order of B (N^3) computations
 - Requires less sample support



Adaptive Processing with and without Frequency Subbanding

Null Pattern



Direction

- Adaptive processing without frequency subbanding
 - Creates broad nulls
 - Less usable free beam space
 - Requires more DOFs

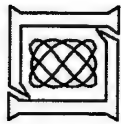
Null Pattern with Subbanding



Direction

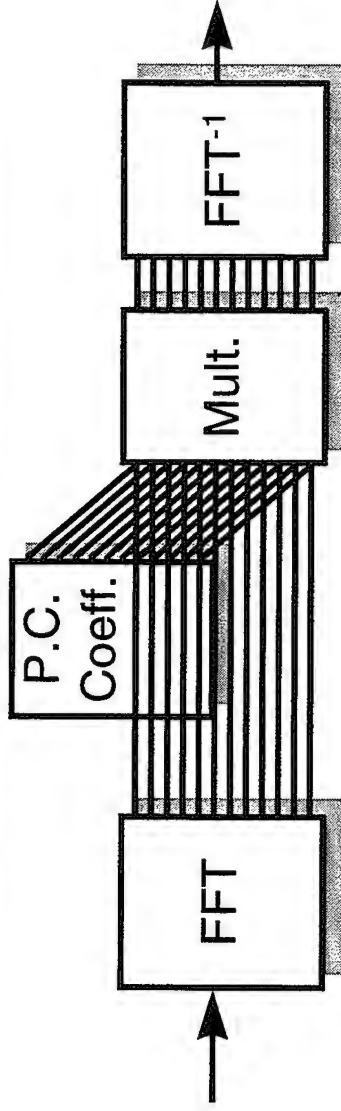
- Adaptive processing with frequency subbanding
 - Reduces null width down to narrowband interference null
 - More usable free beam space
 - Requires fewer DOFs/subband

Increasing Power →

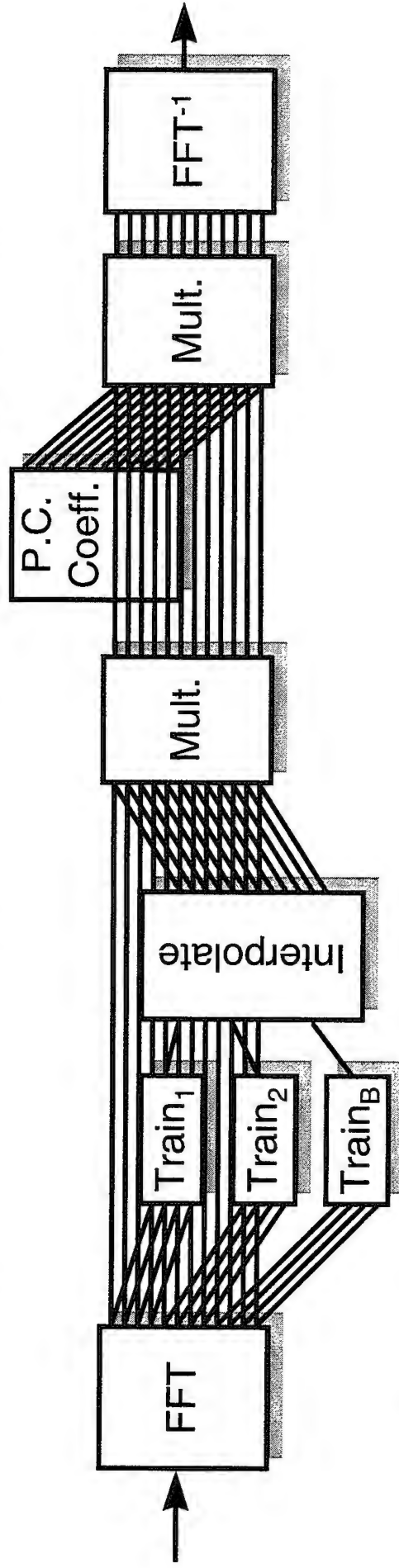


Frequency Subband Processing for AEGIS

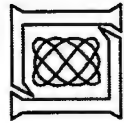
Pulse Compression (Frequency Domain)



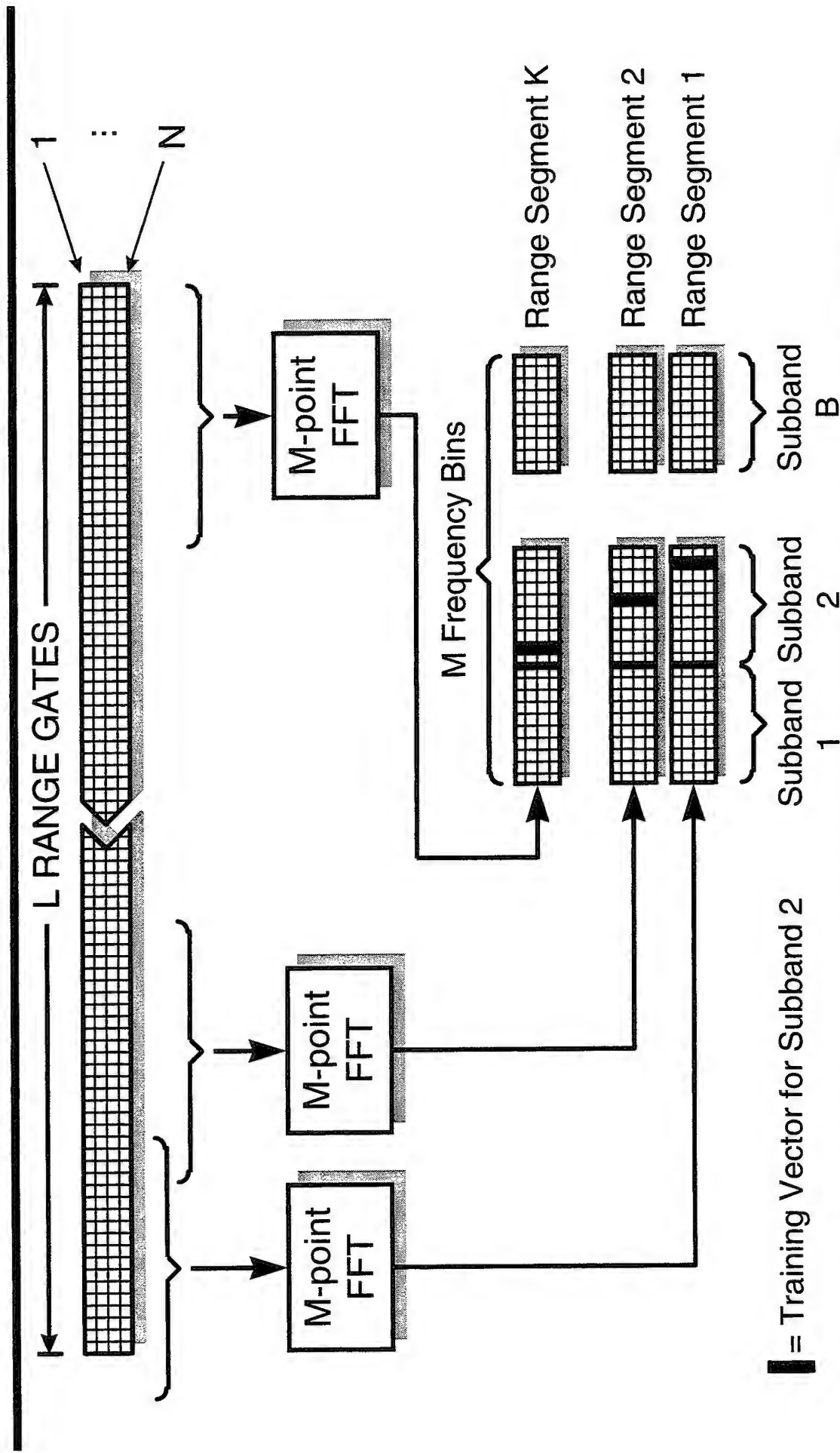
Pulse Compression with Subband Processing (Frequency Domain)



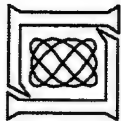
Frequency subbanding is easily incorporated as part of a frequency domain pulse compression operation



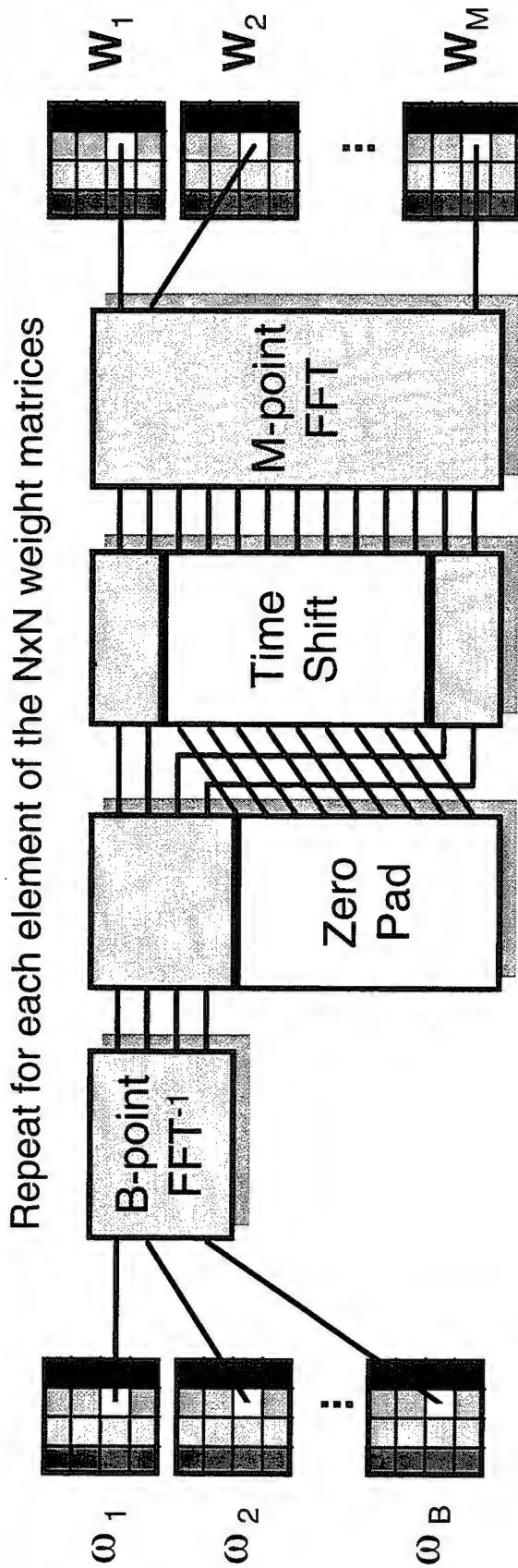
Details for Subband Adaptive Training



Sufficient sample support within each subband using AN/SPY-1 parameters

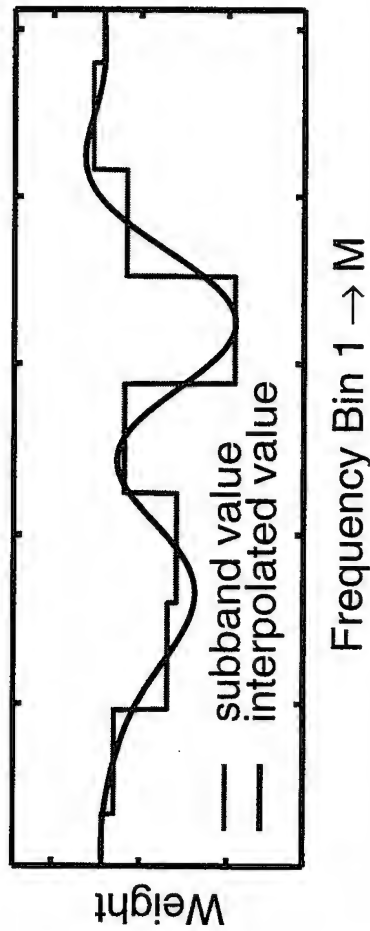


Details for Weight Interpolation

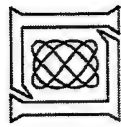


$$= [\underline{W}_{\Sigma} \quad \underline{W}_{\alpha} \quad \underline{W}_{\beta} \quad \underline{W}_{SLB}]$$

$$\underline{W}_x = \frac{\mathbf{R}^{-1} \underline{V}_x}{\underline{V}_x^H \mathbf{R}^{-1} \underline{V}_x} ; x = \Sigma, \alpha, \beta, SLB$$



Interpolate B subband weight matrices to M frequency bin weight matrices ($M \gg B$)



How to Choose the Number of Subbands, B

RESTRICTION:

- AEGIS monopulse has limited DOFs for adaptive nulling

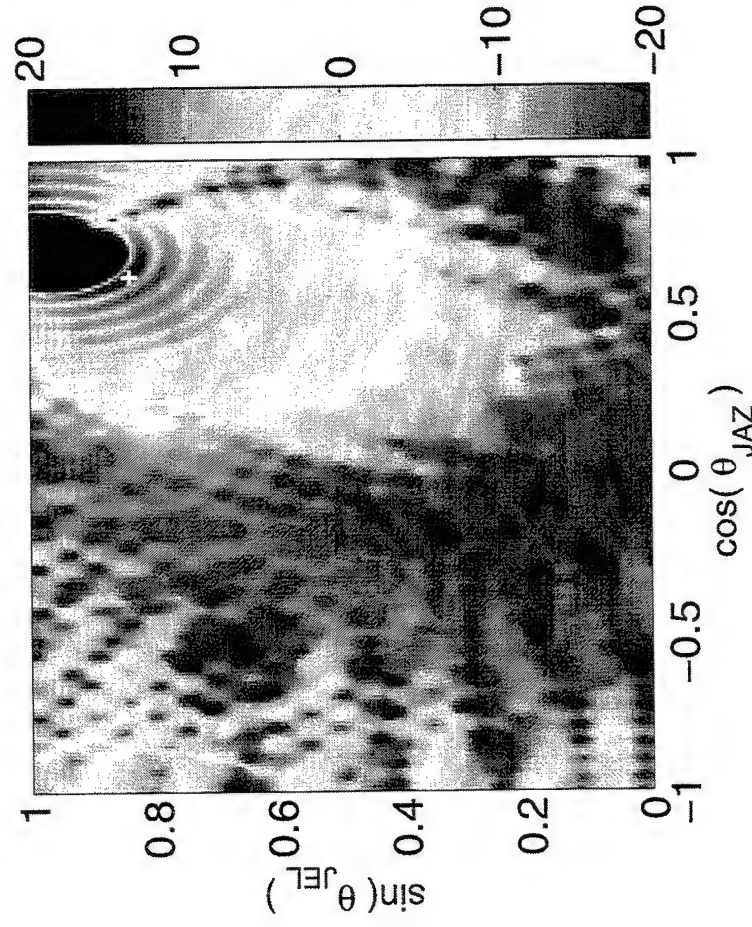
APPROACH:

- Keep the second covariance eigenvalue λ_2 below σ_{noise}^2
- Identify worst case dispersion scenario

Find highest λ_2 over all steering & jammer positions given relative bandwidth ($\beta = b_w / f_c$) & interference power ^[4]

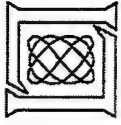
- Choose B so that subband bandwidth keeps $\lambda_2 < \sigma_{\text{noise}}^2$

[4] M. Zatman, *How Narrow is Narrowband?*, ASILOMAR 1997.



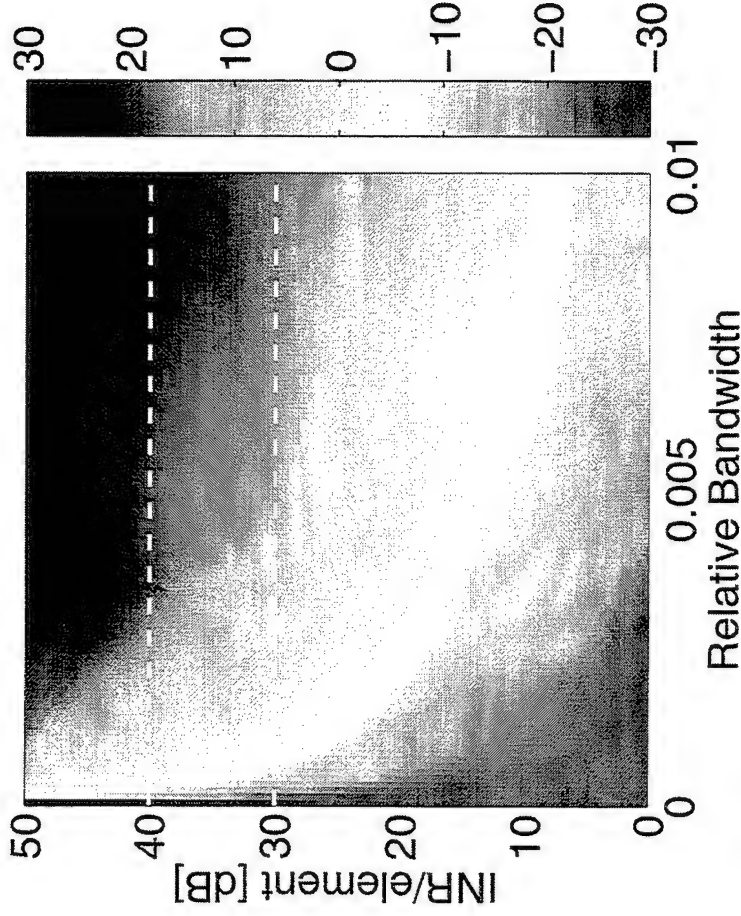
Identify worst case λ_2 value

- λ_2 versus $(\theta_{\text{JAZ}}, \theta_{\text{JEL}})$
- INR/element = 40 dB
- Relative bandwidth $\beta = 1/300$
- Steered direction: $\{\cos(\theta_{\text{AZ}}), \sin(\theta_{\text{EL}})\} = \{0.71, 0.97\}$
- dB scale relative to system noise
- + = worst case λ_2 outside of main beam

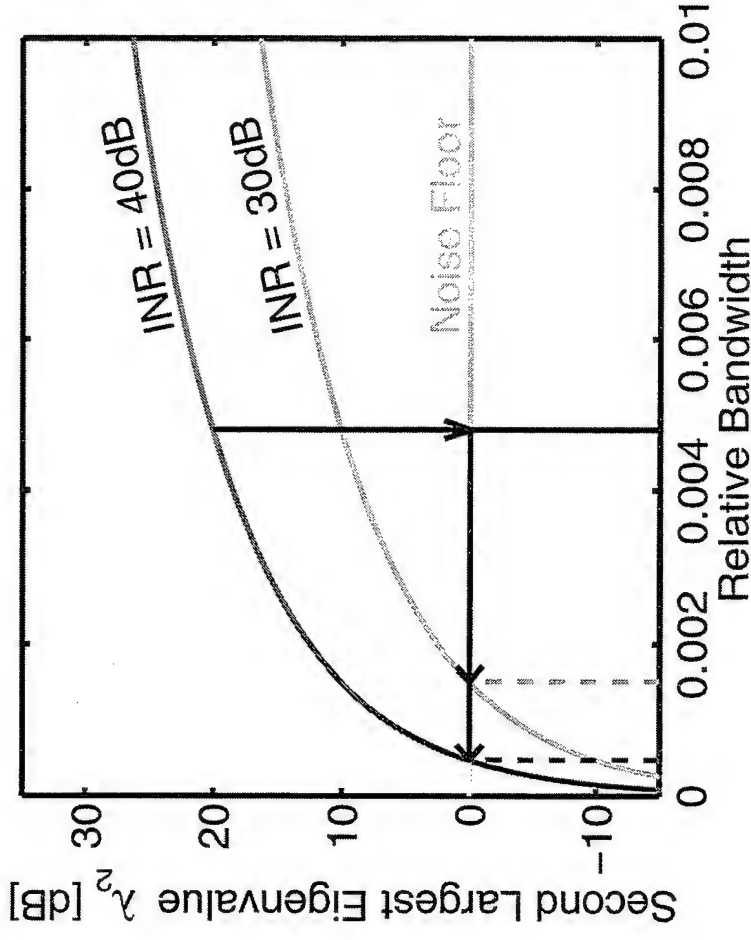


Calculating the number of subbands

λ_2 versus INR and β

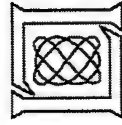


λ_2 versus β

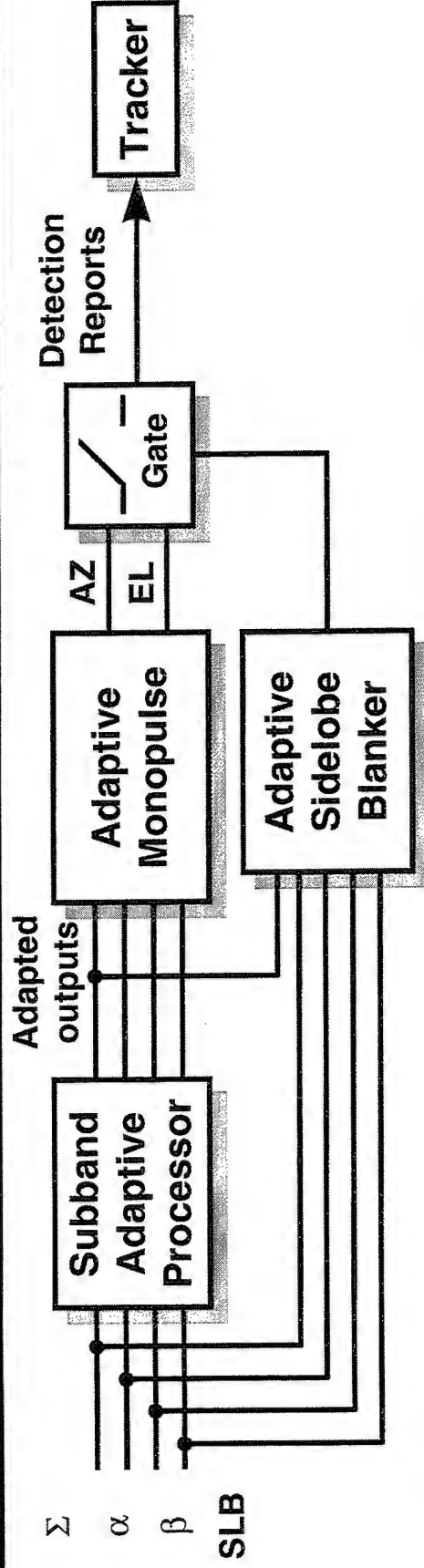


- dB scale relative to system noise
- Assumes worst case scenario
 - $\{\cos(\theta_{AZ}), \sin(\theta_{EL})\} = \{0.71, 0.97\}$
 - $\{\cos(\theta_{JAZ}), \sin(\theta_{JEL})\} = \{0.63, 0.84\}$

- Given: $\beta = 0.0048$ and
INR/element = 40dB (30dB)
- Worst case $\lambda_2 = 20$ dB (10 dB)
- For $\lambda_2 = 0$ dB then $\beta = 0.00048$ (.00152)
- Hence choose $B \geq 10$ (4) subbands



AN/SPY-1 Adaptive Processing Investigated



Adaptive Sidelobe Blanker [5]

- Two-stage detection algorithm
- Reduces false detects due to sidelobe targets

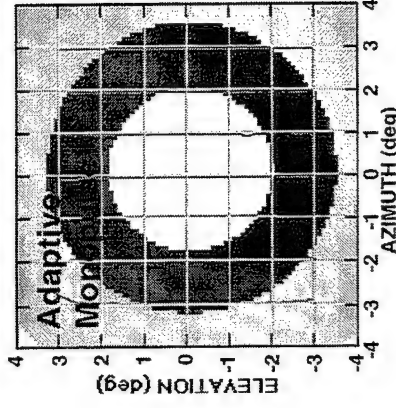
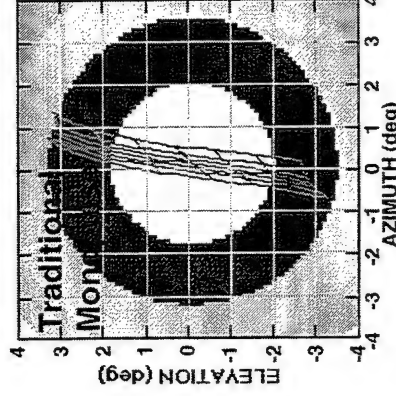


$$t_{AMF} = \frac{|\underline{V}^H \underline{R}^{-1} \underline{X}|^2}{\underline{V}^H \underline{R}^{-1} \underline{V}}$$

$$t_{ACE} = \frac{t_{AMF}}{\underline{X}^H \underline{R}^{-1} \underline{X}}$$

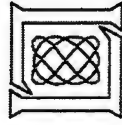
Adaptive Monopulse [6]

- Adaptation biases traditional monopulse
- Adaptive monopulse has negligible bias
- Implemented with all four channels



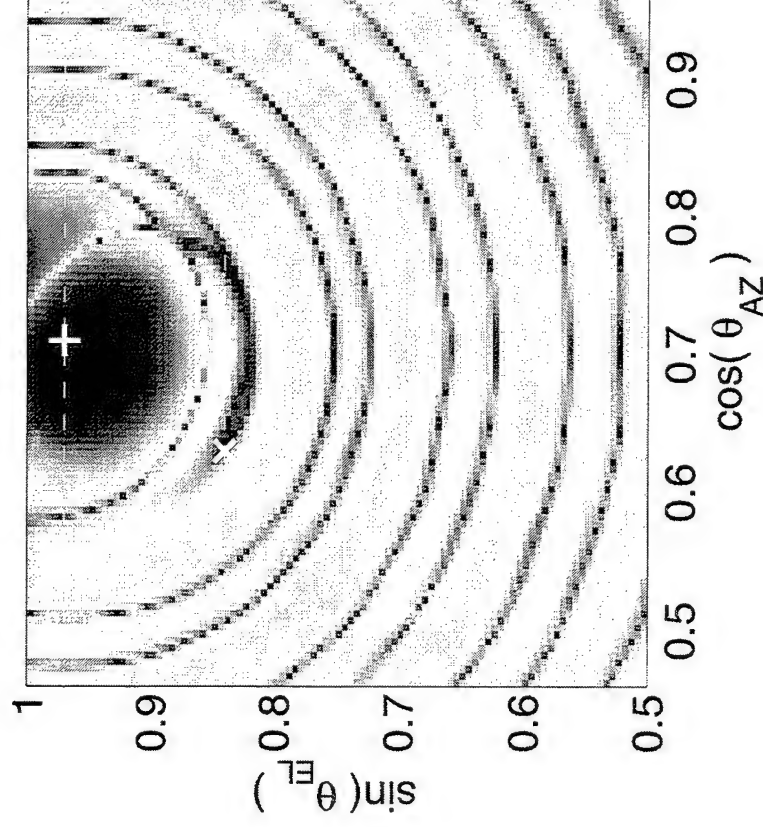
[5] Richmond, *Statistical Analysis of Clutter Editing Adaptive Detection Algorithm*, ASAP, 1997.

[6] Baranoski, *Modern Algorithm Upgrades for Existing Radar Systems*, ASAP, 1997.



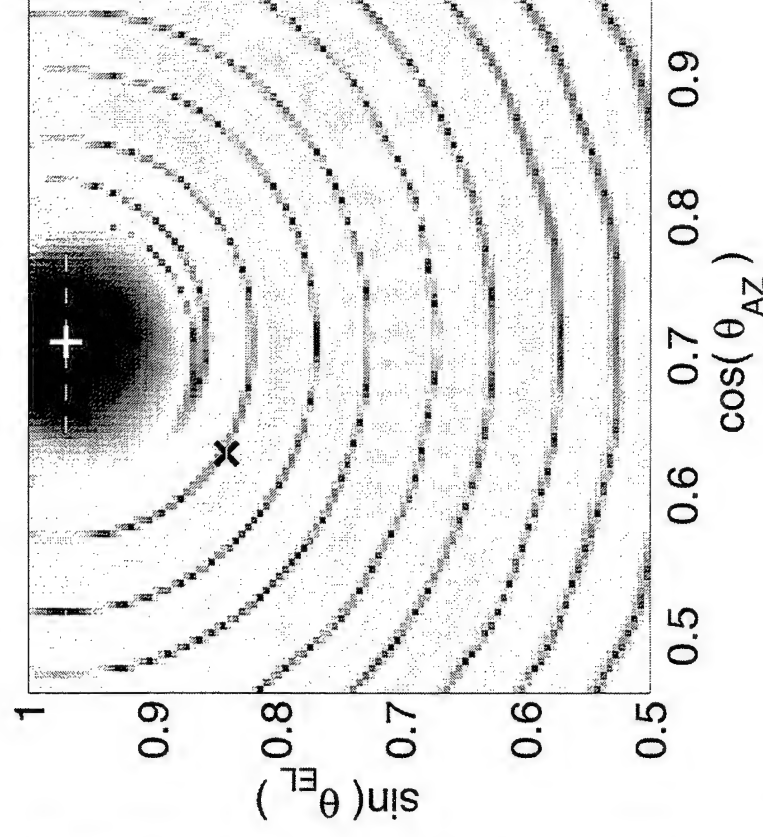
Adaptive Beam Patterns

Conventional AMF

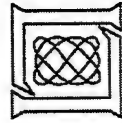


- Beam pattern maximum displaced from steered direction '+'
- Broad jammer null 'x'

AMF with subbanding

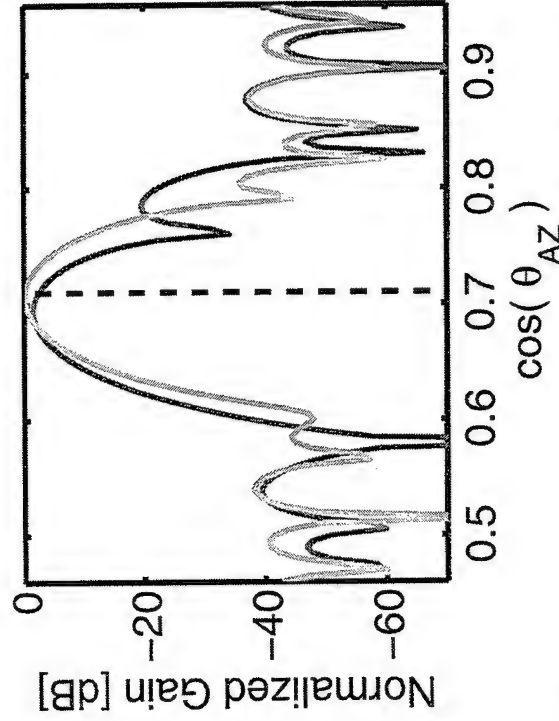


- Beam pattern maximum coincides with steered direction '+'
- Narrow jammer null 'x'

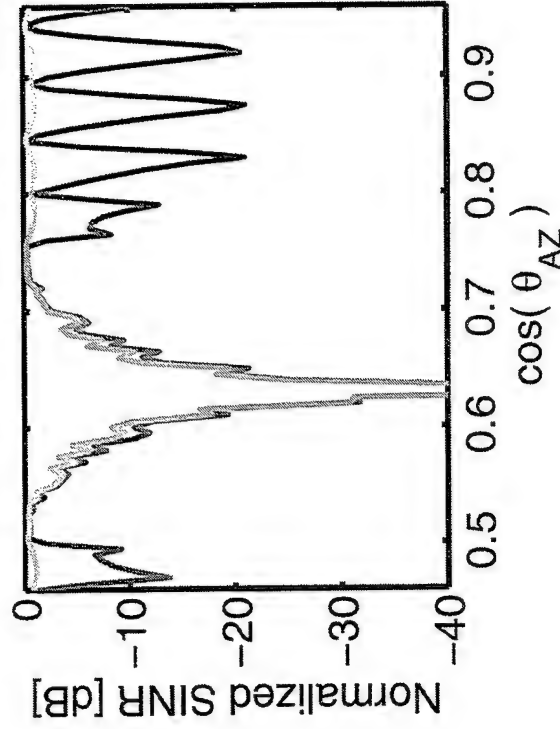


Slices of Adaptive Patterns

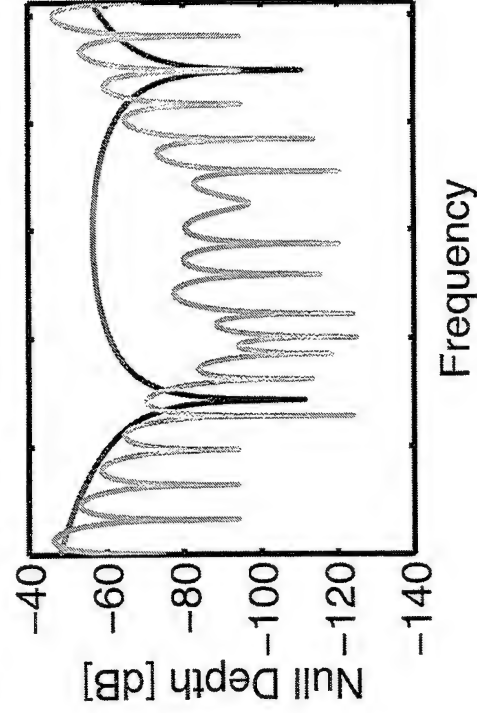
Azimuth slice at target elevation (θ_{EL})



Azimuth slice at jammer elevation (θ_{JEL})

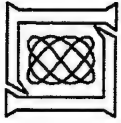


Frequency response of adaptive null



— AMF
— AMF with subbanding ($B = 16$)

- INR/element = 40dB and $\beta = 0.0048$
- Jammer at $\{\cos(\theta_{JAZ}), \sin(\theta_{JEL})\} = \{0.63, 0.84\}$



Summary

- Subband processing for the AN/SPY-1 radar system
 - Supports adaptive detection and adaptive monopulse
- Improved beam pattern in wideband interference
 - Maximum gain in steered direction
 - Narrow null in jammer direction
- Improved SINR performance in wideband interference

Open Issues

- Multipath jammer effects on performance
- Robustness with multiple jammers

Synthetic Aperture Sonar

Matthew Nelson and Ralph Chatham

Dynamics Technology, Inc.

1555 Wilson Blvd. Suite 320

Arlington, VA 22209

tel: (703) 841-0990

email: mnelson@dynatec.com, chatham@snap.org

Abstract The coherent combination of data from multiple transmissions in the form of synthetic aperture processing revolutionized radar imaging over the past 30 years. A key feature of the synthetic aperture approach is that cross range resolution becomes independent of range. During the past eight years Dynamics Technology, Inc. has been applying that revolution to sonar: first with medium stability measurements, the development of SAS emulators, adaptations of SAR imaging and autofocus algorithms to many-element real apertures, and more recently as the processing house for DARPA's Synthetic Aperture Sonar program. 50 KHz data from a spring 1987 experiment has been processed to produce images of mine shadows at 230 m and greater ranges with 10 cm cross range resolution, resolution which is only possible for current mine classification sonars at 30 meters range. We have also imaged the interior structure of a water-filled sunken airplane at 350 meters. Other images show the same cross range resolution out to a kilometer. This represents over an order of magnitude better resolution/range combination than ever achieved with sonar. A program to explore this concept further and to develop a hands-off real-time SAS processor for mine hunting applications is just starting under DARPA funding.

DARPA SYNTHETIC APERTURE SONAR

Dr. Matthew A. Nelson

Dynamics Technology, Inc.
Torrance, CA

(310) 543-5433

March 11, 1998



DYNAMICS TECHNOLOGY, INC.

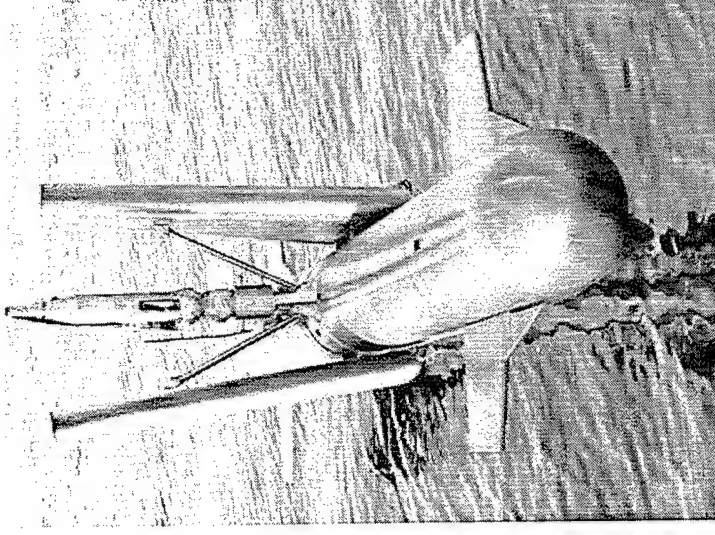
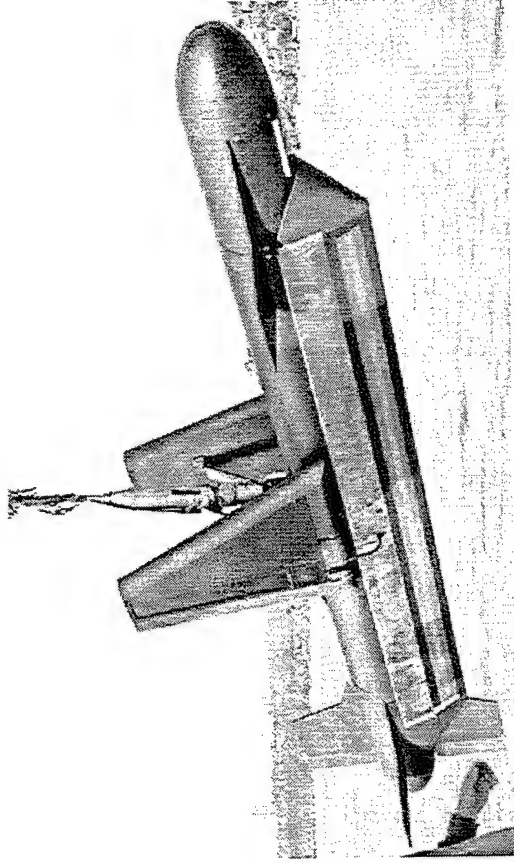
Raytheon

The DARPA SAS Program

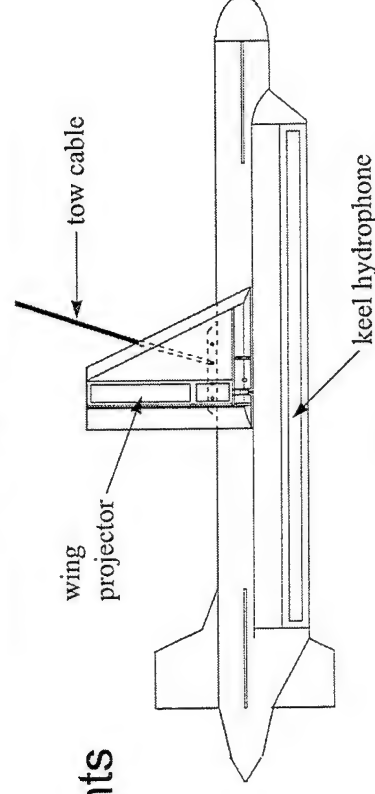
- ♦ DARPA Program Objectives:
 - *Develop SAS system suitable for detection and classification of mines*
 - *Resolution goal: 10 cm (azimuth) at 1000m range in shallow water*
- ♦ DTI's task:
 - *Develop high-performance image formation software for SAS*
 - » *Develop algorithms for precise motion compensation and receiver element location*
 - *Provide system design support through high-fidelity SAS system emulation*
- ♦ Raytheon's tasks:
 - *Develop a SAS test bed sonar and data acquisition system*
 - *Conduct at-sea tests, collecting SAS data at various sites using scientific targets, mine like objects, actual mines and naturally occurring objects*



DARPA SAS Towfish



- ◆ 50 kHz center frequency
- ◆ 10 kHz bandwidth
 - 7.5 cm range resolution
- ◆ Up to 50 ms long chirps
- ◆ 16 11- or 22-cm keel hydrophone elements (selectable)
 - 5.5 cm or 11 cm azimuth resolution
- ◆ Adjustable wing angle with narrow projector

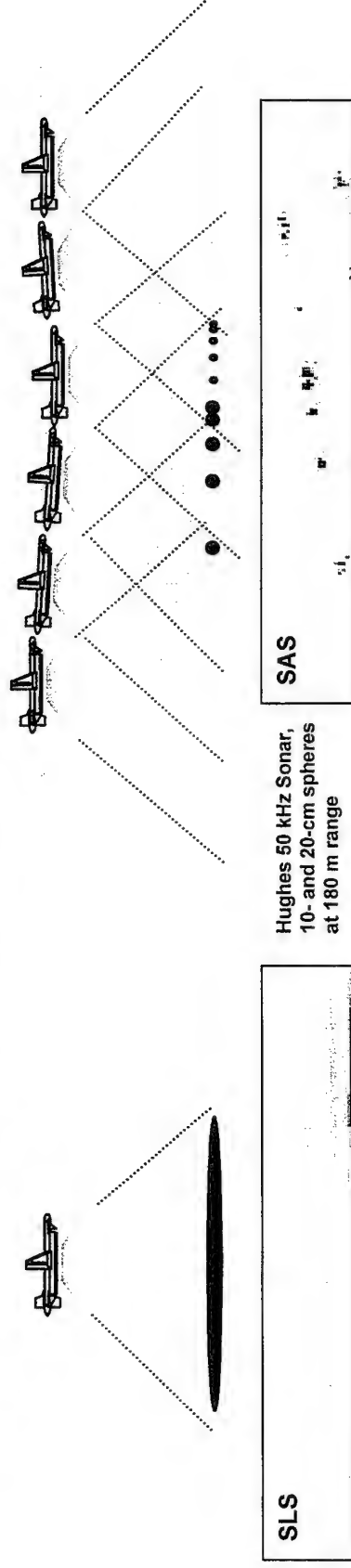


DYNAMICS TECHNOLOGY, INC.

Raytheon

What Is Synthetic Aperture Sonar (SAS)?

- ◆ Coherent combination of data from many pings allows synthesis of larger aperture (= better resolution)



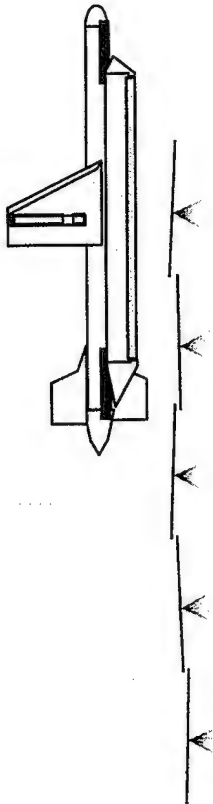
- ◆ SAS gives high cross-range resolution that is *independent of range and frequency*
- ◆ Technical Challenges
 - Phase errors from vehicle motion and medium fluctuations
 - » MOCOMP and autofocus provide solutions
 - Shallow water phenomena (multipath, reverberation)
- ◆ Processing technique, algorithms and optimizations are key
 - 30 years of SAR research provide appropriate tools



DYNAMICS TECHNOLOGY, INC.

Raytheon

Overview of SAS Processor



Calculate synthetic aperture using multiple returns; requires that platform advance less than 1/2 of RX array length each ping



Compensate motion using data from both MOCOMP hardware and motion estimates derived from scene content (RPC); correct multi-beam artifacts



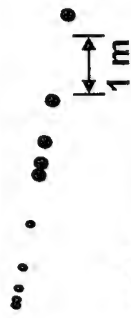
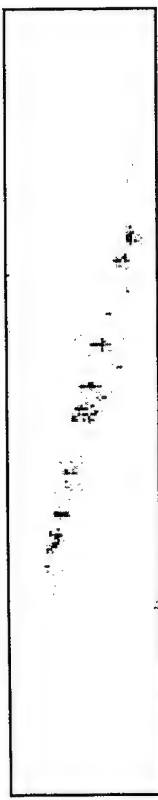
Generate image with Range Migration Algorithm (RMA), a FFT-based image formation algorithm adapted from SAR community



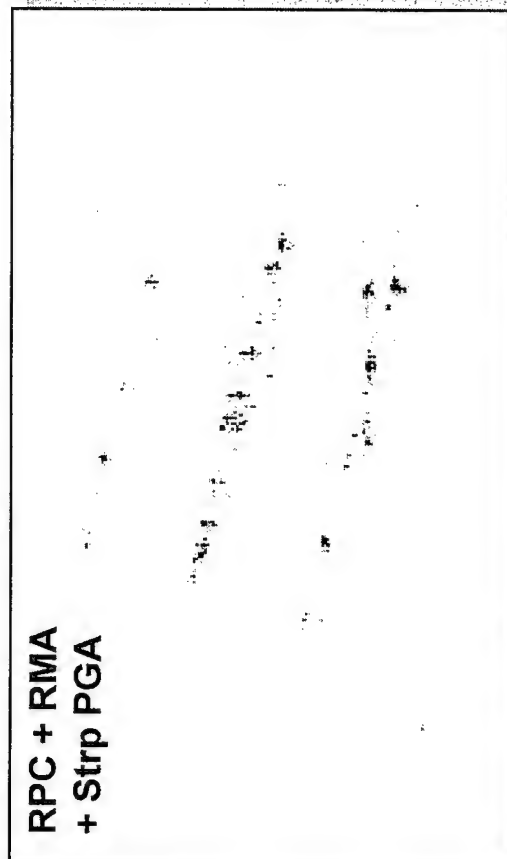
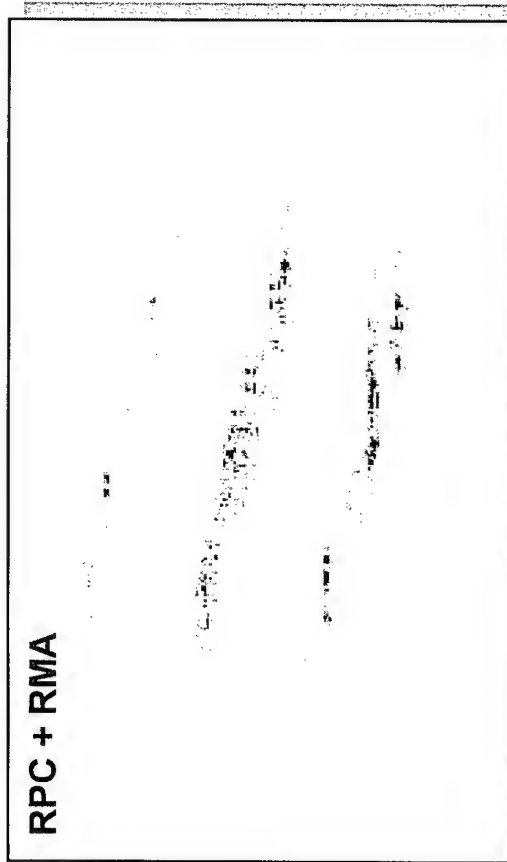
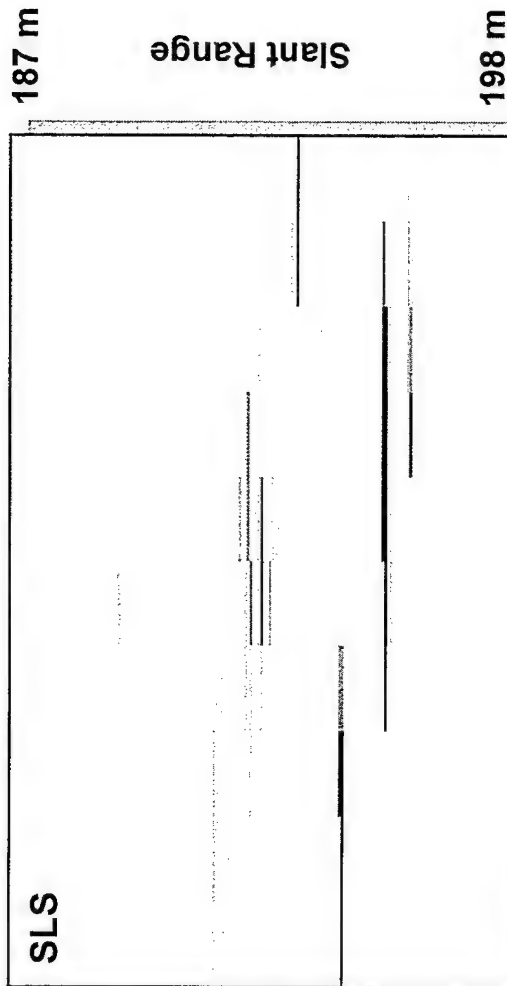
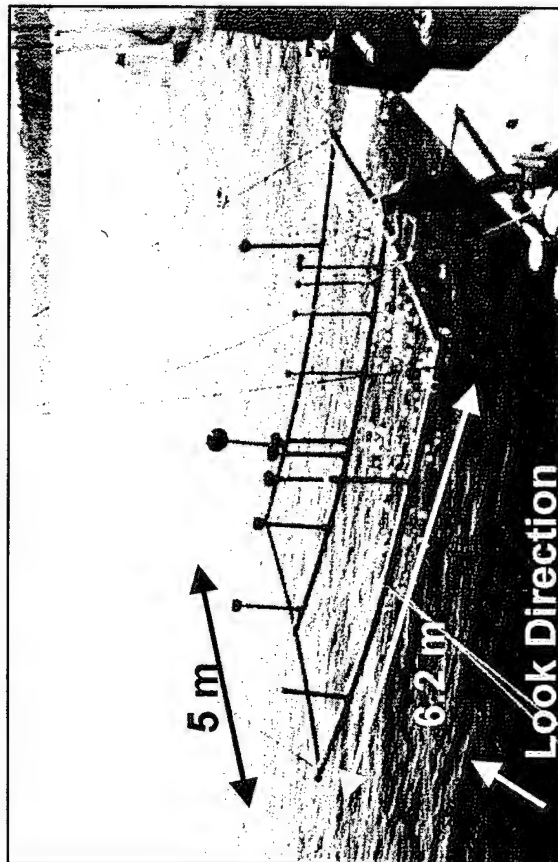
Auto-focus image with Phase Gradient Autofocus (PGA) or Sub-Aperture Correlation (Mapdrift), adapted from SAR community



Display and record

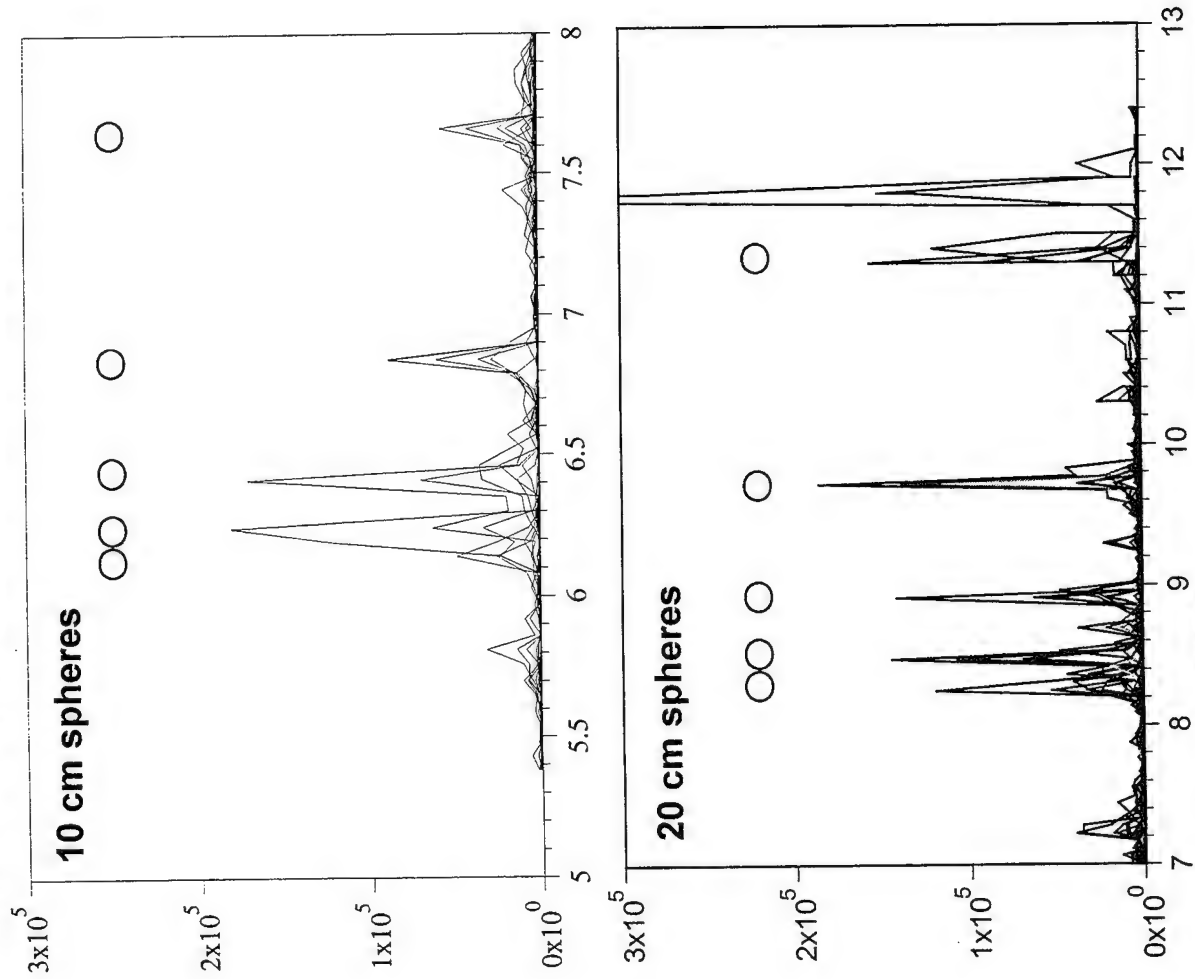


Imaging Improvements Through SAS Processing



DYNAMICS TECHNOLOGY, INC.

Intensity Cuts: Target Frame Spheres (Run L2A)



- ◆ Processed with RPC mocomp, RMA image formation and PGA autofocus
- ◆ 16 11-cm RX elements, realizing 5-10 cm azimuthal resolution at ~200 m range

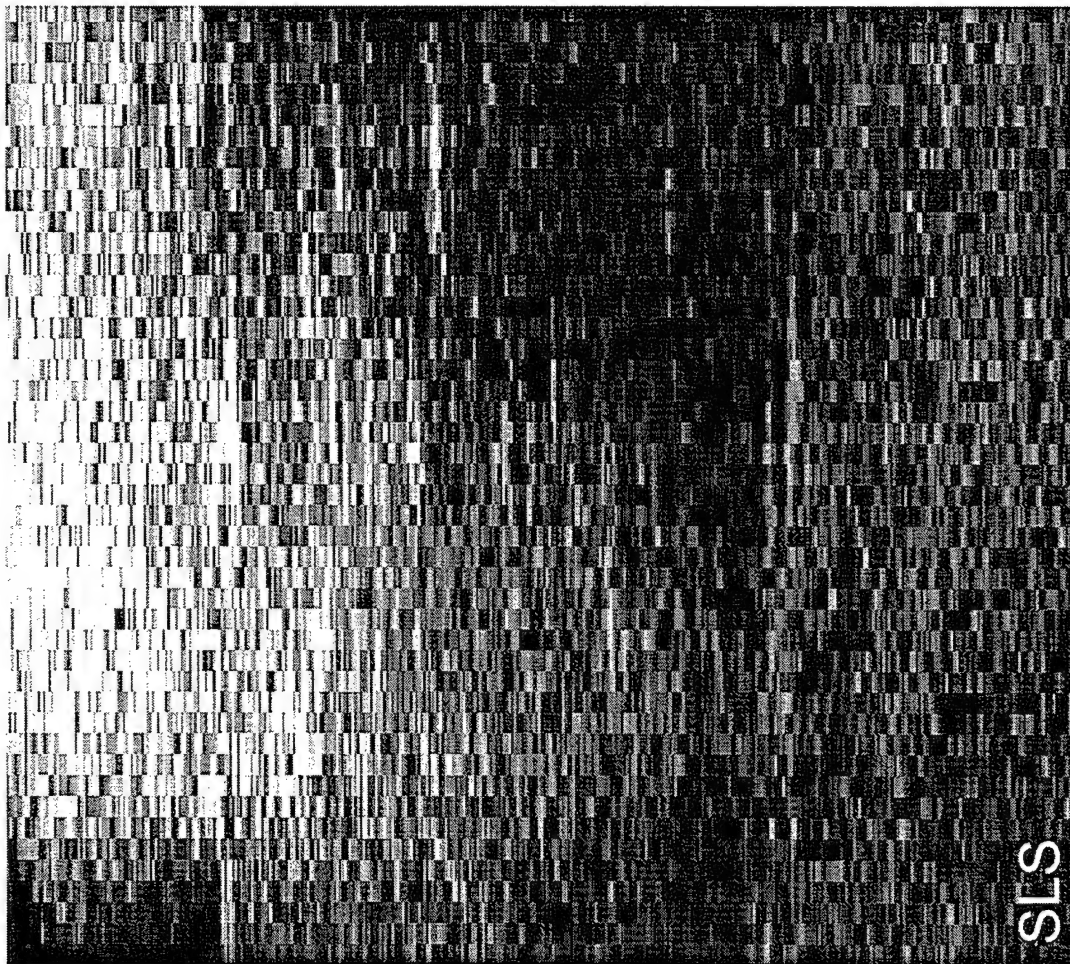


DYNAMICS TECHNOLOGY, INC.

Raytheon

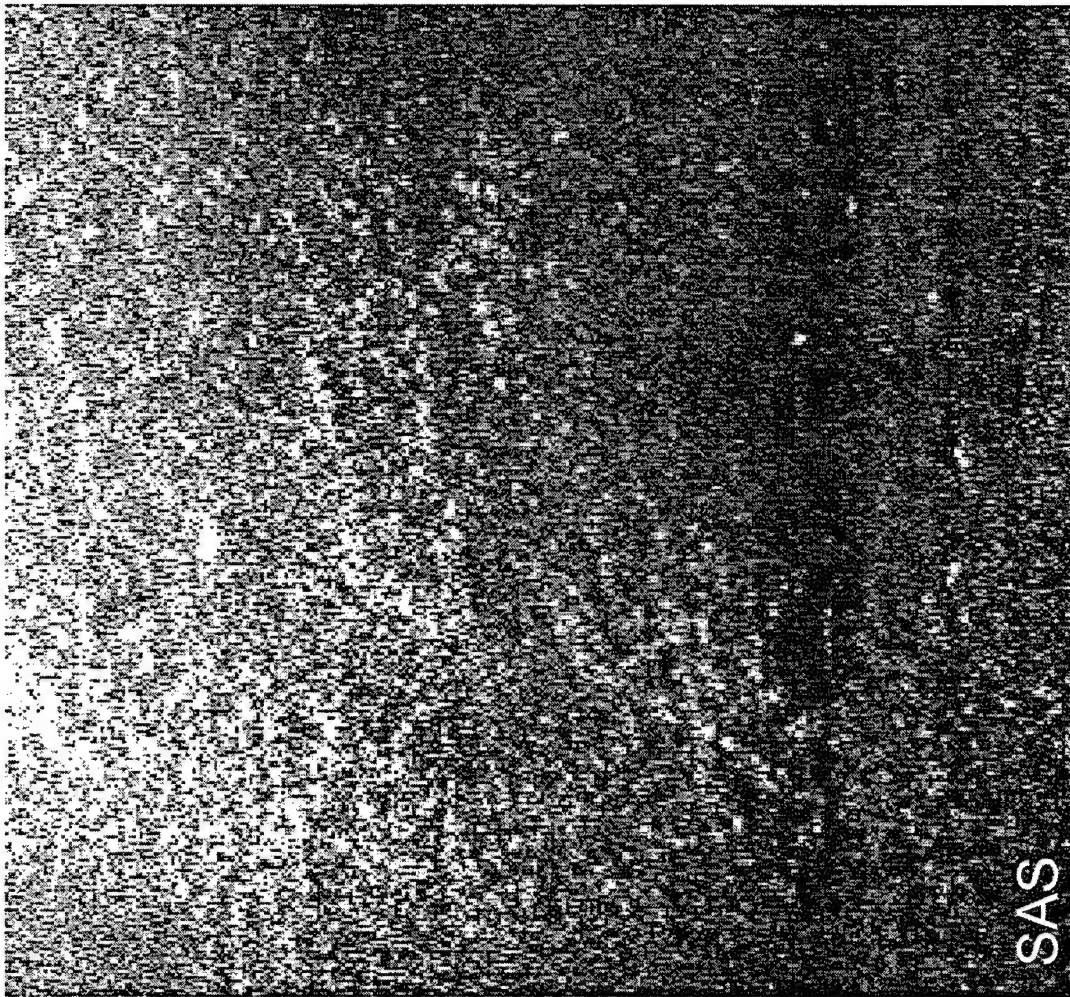
SAS Imagery of Bottom Clutter (Run L5E)

|1m|



SLS image: bottom clutter field 80 to 100 m range. 33 cm cross-range resolution; 6 cm range resolution

|1m|



DTI processed SAS image: 5cm cross-range resolution; 6 cm range resolution

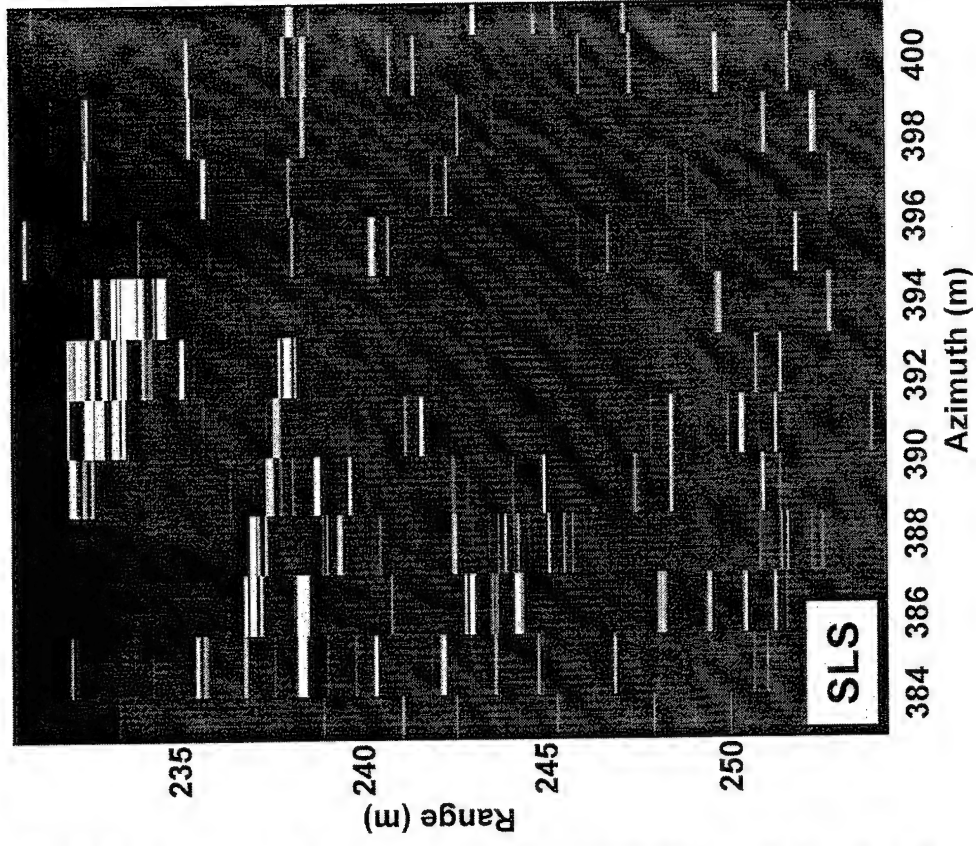
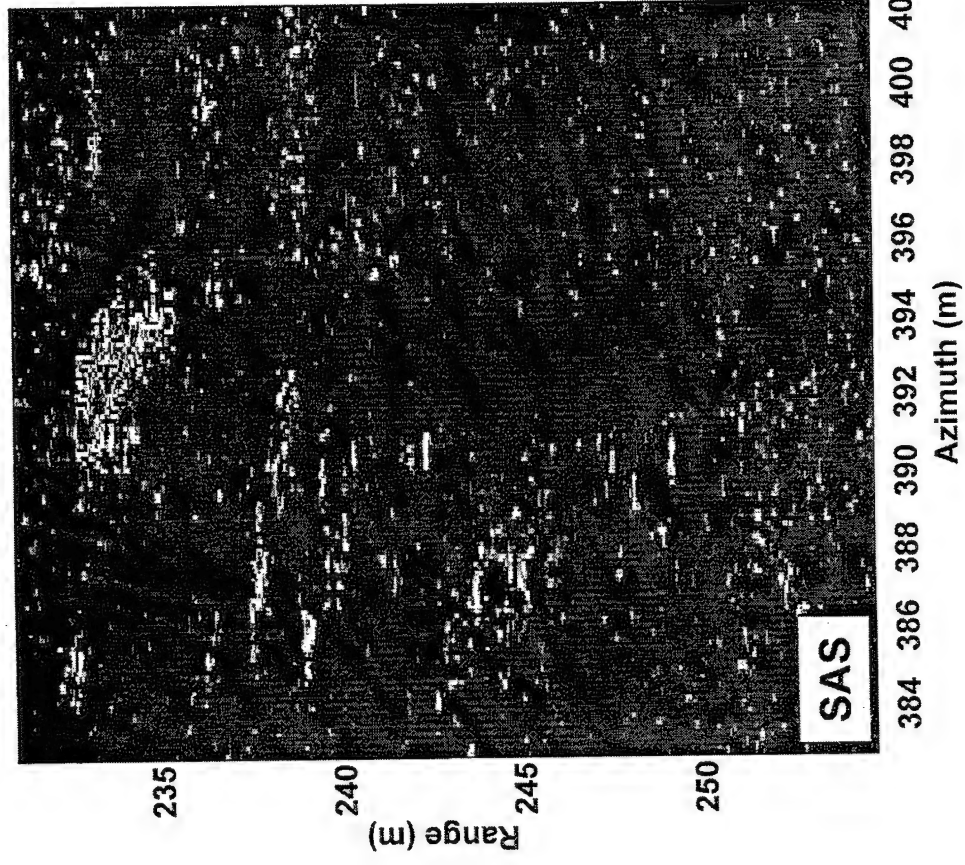


DYNAMICS TECHNOLOGY, INC.

Raytheon

Bottom Mine and Shadow: SAS vs SLS

- ◆ Resolution: 10 cm (SAS) versus 2.2 m (SLS)
 - SLS image is oversampled, with 1.5 m pixel size

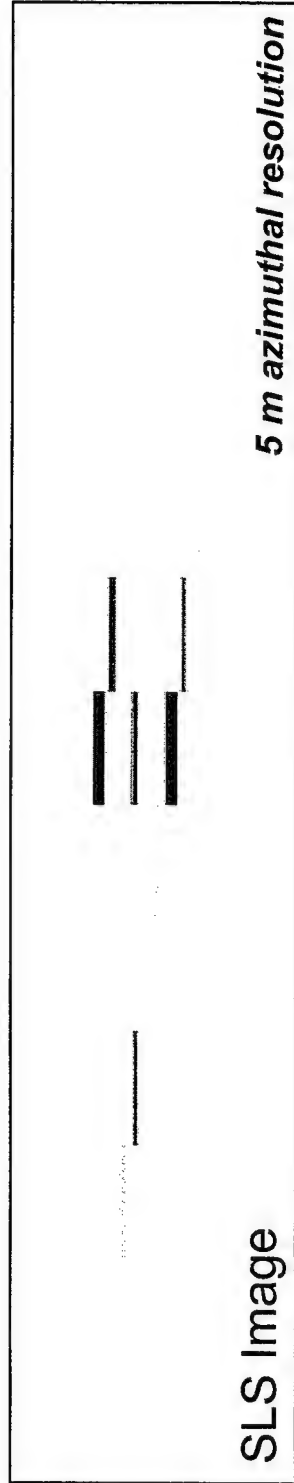
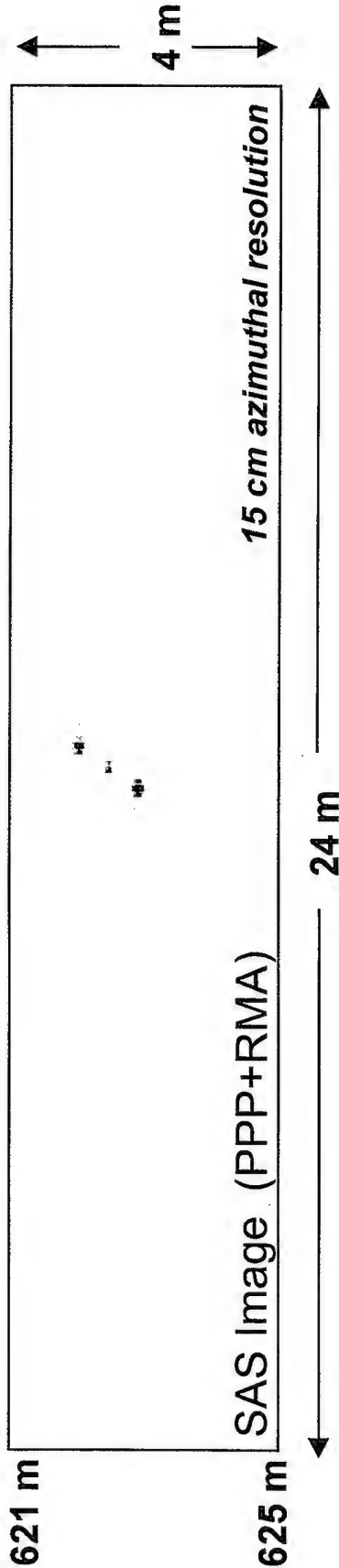
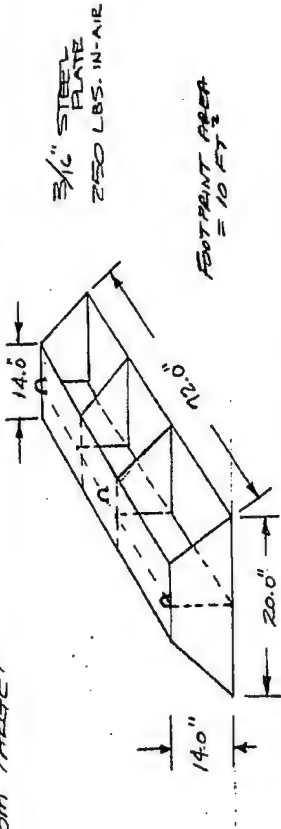


DYNAMICS TECHNOLOGY, INC.

Raytheon

SAS/SLS Images of Mine-Like Target at 625 m (Run C1C)

BOTTOM TARGET



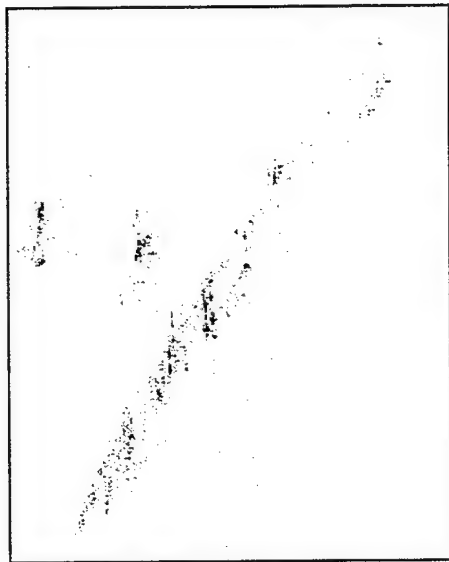
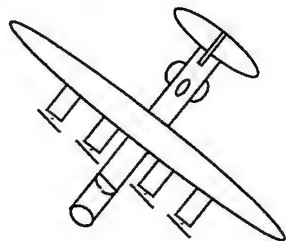
DYNAMICS TECHNOLOGY, INC.

Raytheon

SAS Resolution is Independent of Range



Magnitude
400
0



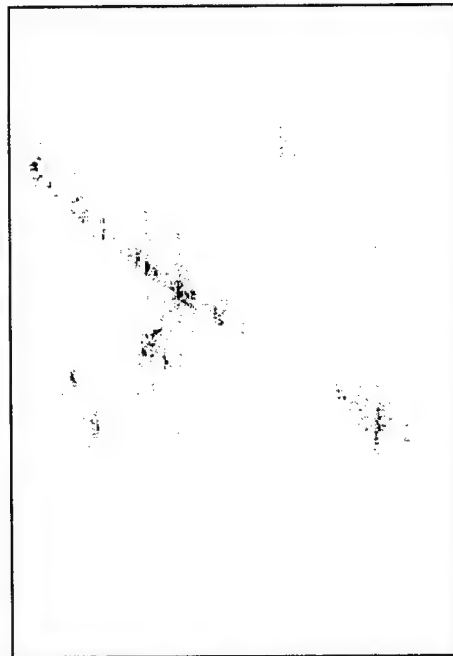
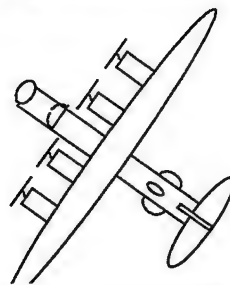
Slant Range (m)
109 128

100 m
Range

SAS

SLS

Magnitude
20
0



Slant Range (m)
980 1001

1000 m
Range

~10 cm resolution

1-10 m resolution (range-dependent)



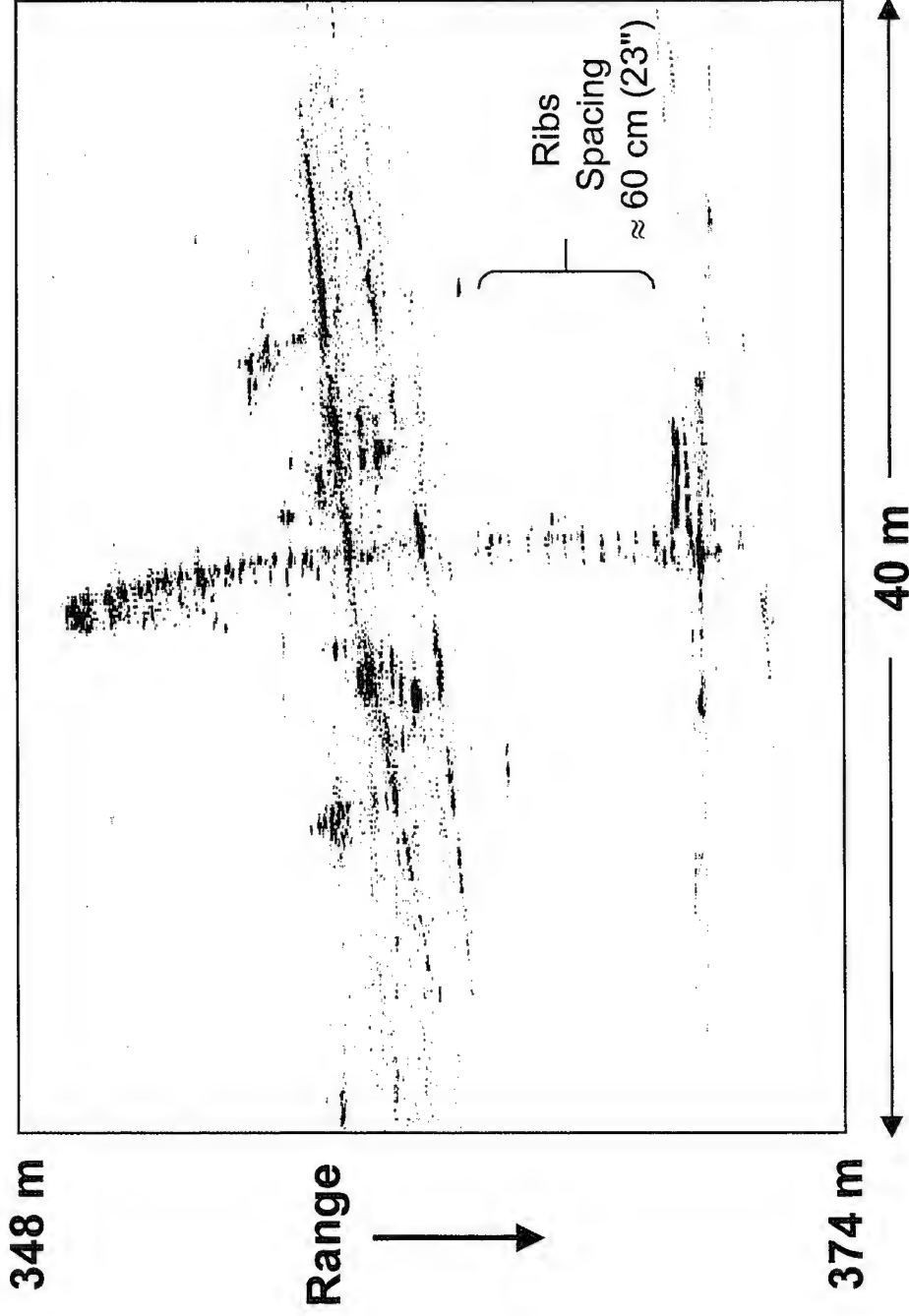
DYNAMICS TECHNOLOGY, INC.

Raytheon

SAS Image of PB4Y-2 in Lake Washington (April 1997)

Navy patrol aircraft based upon B-24 design modified to have a single tail and a pair of AA blisters on aft quarter of fuselage. Wrecked near Seattle in 1956. Attempts at salvage tore off port inboard engine and damaged starboard inboard engine. Resting in 163 feet of water. Starboard wing tip is 16 feet above the bottom.

This data taken with DARPA-Hughes 3 m array and processed as a synthetic aperture image by DTL with 10 cm cross-range resolution, and 3 cm in-range resolution. Vertical angle was about 2° from grazing.

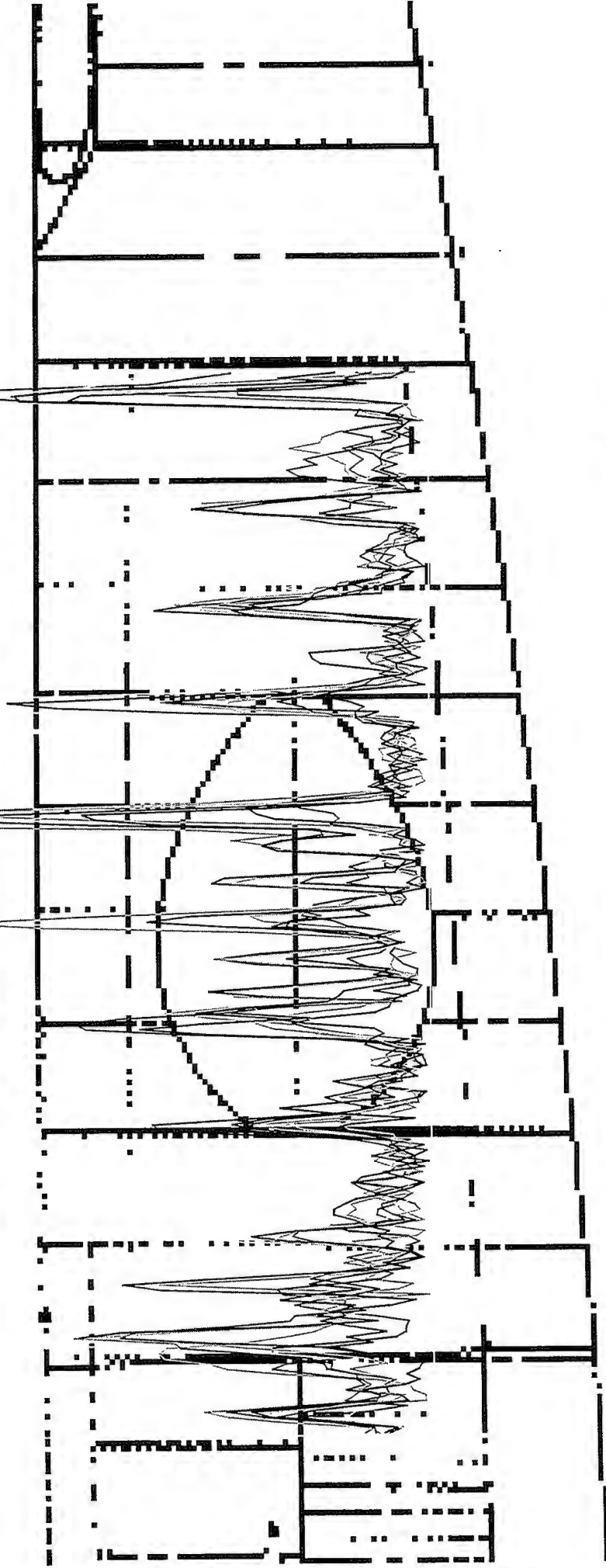


The 50 kHz SAS is seeing through the skin into the water-filled interior of the aircraft.



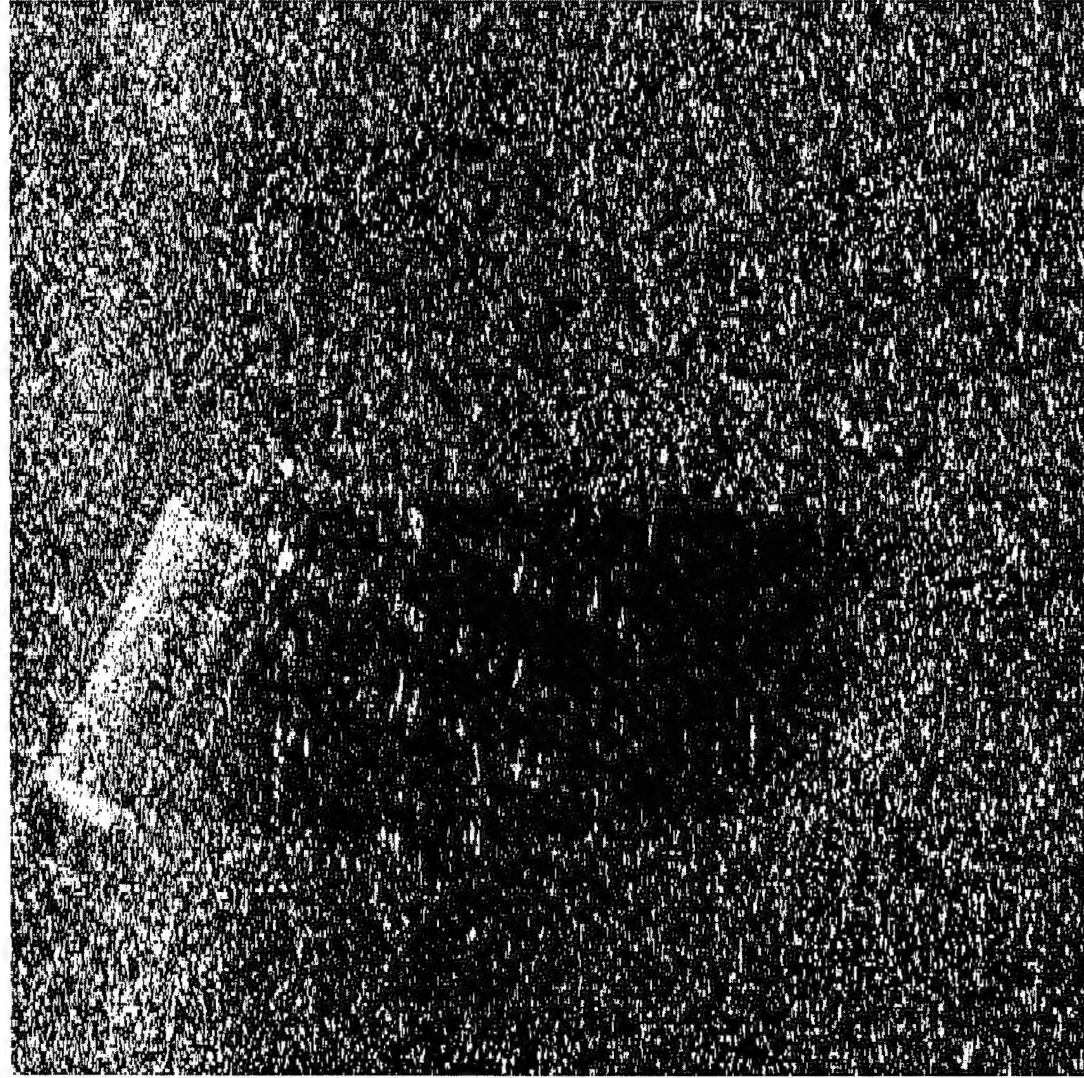
DYNAMICS TECHNOLOGY, INC.

Raytheon

[illegible]

SAS Image of Submarine-Like Target

107 m



143 m

Range



33.6 m

Water-filled steel tank, approx. 5m in diameter, resting at the bottom of Dabob Bay, WA.

Image generated by DTI SAS processor, azimuthal resolution ~10 cm.

Notice distinct shadow and resonant returns.



DYNAMICS TECHNOLOGY, INC.

Raytheon

Summary

- ◆ SAS has been demonstrated at ranges up to 1000 meters in shallow water
- ◆ Near-theoretical azimuthal resolutions have been achieved
- ◆ Towfish motion was the most limiting factor
 - *Most processing time is spent compensating for platform motion*
 - *Yaw of 0.2 degrees can visibly raise grating lobes*
 - *Small uncompensated sway dramatically broadens main lobe*
- ◆ Medium fluctuations have not been a problem in current data sets
- ◆ Multipath has not been a problem in current data sets



1998 Adaptive Sensor Array Processing Workshop

Radar Array Processing

Session Chairman

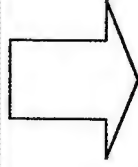
Travis Slocumb

SAIC

Adaptive Array Algorithm Design

Ideal Covariance Analysis

- Match algorithm to antenna architecture and waveforms
- Evaluate order reduction options
- Establish tight performance bound



**Make the hardware
and algorithm really
work together!**

- High fidelity sample simulations
- Field data collection and reduction
- Evaluate/understand anomalies and adjust algorithm design

Algorithm Performance Limiting Factors vs. ASAP Radar Session '98

Hardware

- Antenna Near Field Effects
- Array Mutual Coupling
- Channel Mismatch

Environment

- Clutter Statistical Properties
- Terrain Scattered Jamming

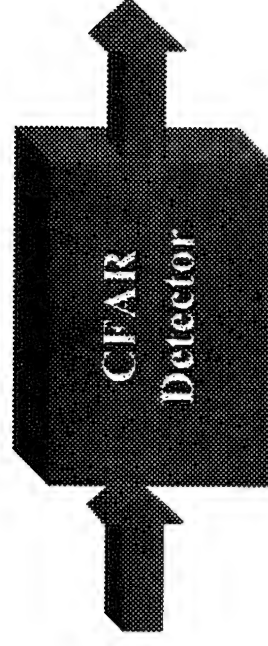
Algorithm

- Weights Training Techniques
- Segregation of Training and Test Data
- Algorithm Computational Complexity

Session Papers

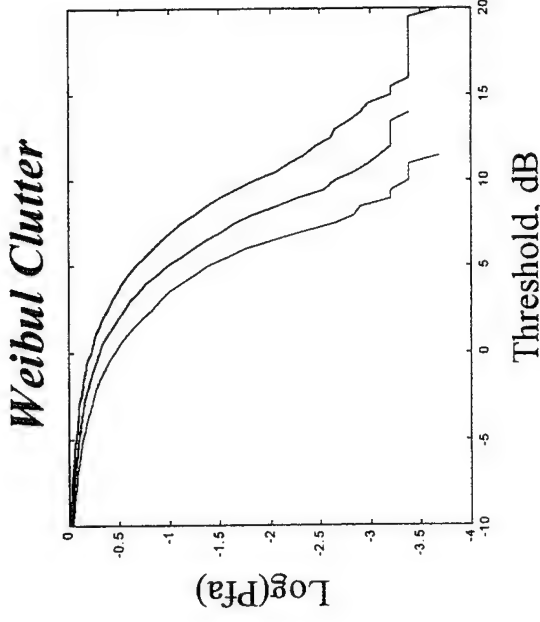
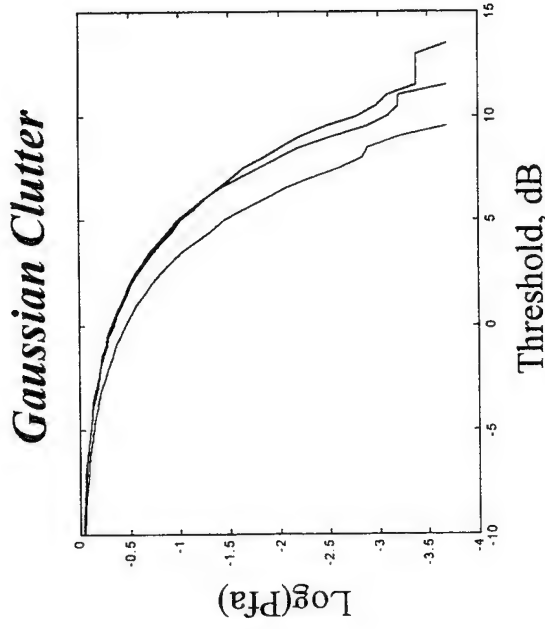
- "Adaptive Array Processing for Wideband Nulling in GPS Systems"
G. Hatke
- "Covariance Matrix Tapers: A Unifying Theory for Robust Adaptive Beamforming"
J. Guerci
- "Wavelet Based Optimization of Space-time Adaptive Processing"
D. Braunreiter
- "A New Interpretation of the Weiner Filter and its Implications"
S. Goldstein
- "Strategies for Minimal Sample Support STAP"
S. U. Pillai
- "Advanced STAP for TSI Modulated Clutter"
D. Rabideau

Performance Metrics



- | | |
|---|--|
| <ul style="list-style-type: none">• Residue Statistical Analysis<ul style="list-style-type: none">– Histogram Analysis– Undernullled clutter ("$\log P_{fa}$")• SINR (MDV)• Multitarget Performance<ul style="list-style-type: none">– Target Masking• Ops Count | <ul style="list-style-type: none">• Residue Statistical Analysis<ul style="list-style-type: none">– Histogram Analysis– $\log P_{fa}$• Pre-Threshold SINR (MDV)• Multitarget Performance<ul style="list-style-type: none">– Target Masking• Ops Count |
|---|--|

Beamformer Residual Statistical Analysis

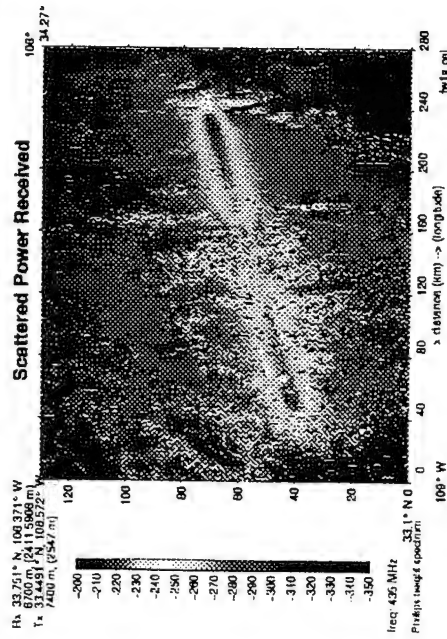


- Noise Normalized Weights, $w w' = 1$
- AMF Normalized Weights, $w w' = 1/(w R w')$
- Both normalizations for training and test data identical

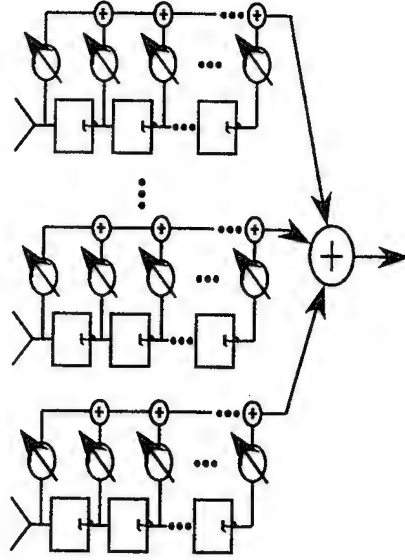
- AMF normalized weights do not accurately indicate clutter leakage relative to receiver noise
- When clutter is cancelled to the receiver noise limit, both normalizations give the same result

Site Specific TSJ Cancellation Analysis

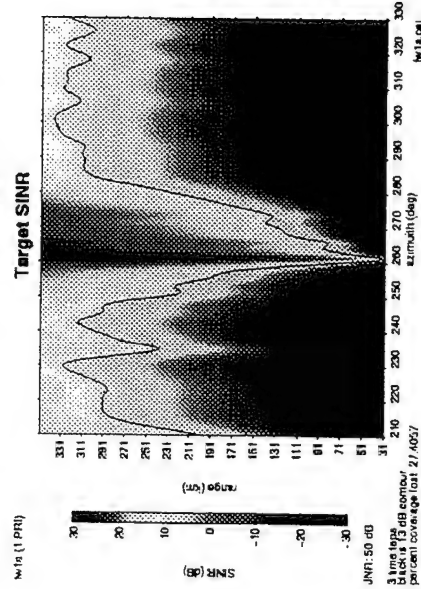
Bistatic Coefficient Calculation



Ideal Covariance Analysis of Filter



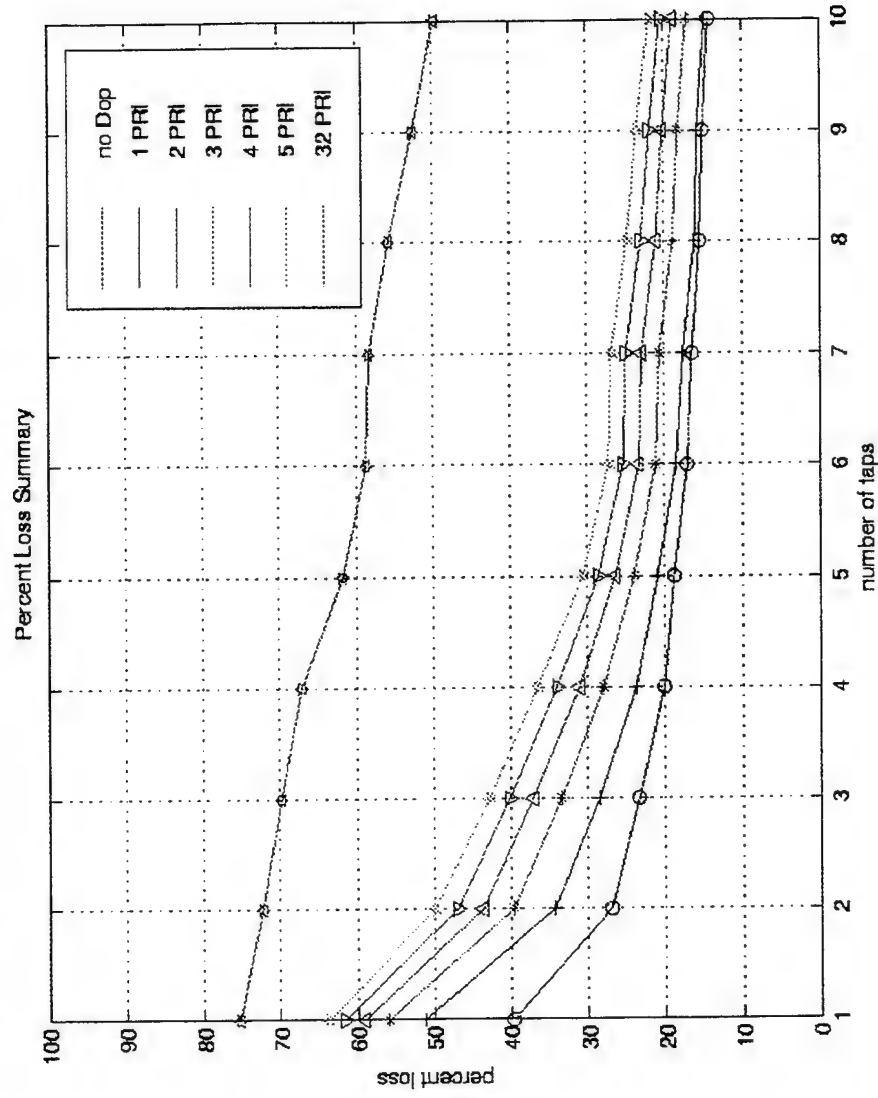
Radar Coverage Summary



**% Coverage vs.
Jammer Location
& ERP for Various
Filter Designs**

Fast-time STAP Performance Summary

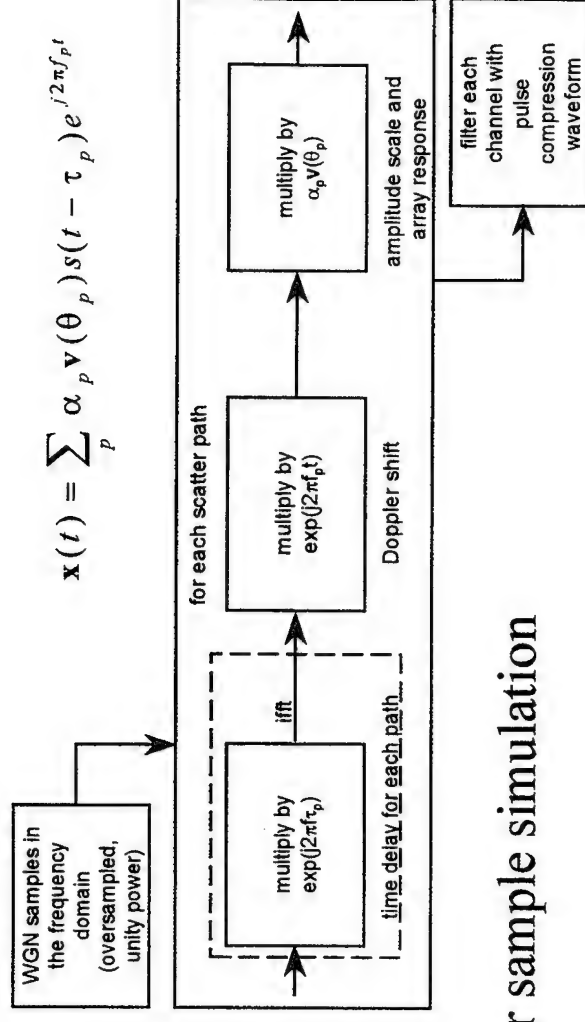
- Doppler effects impact performance for filter update intervals greater than a couple of PRI's
- Minimal improvement beyond 10 fast-time DOFs



What about Cold Clutter ?

Sample Simulations Are Used to Evaluate Joint Interference Canceller Architectures

- Convert site-specific Ideal Covariance simulation to a sample-based simulation



- Sum TSJ signals with cold clutter sample simulation
- Evaluate Joint Canceller Performance

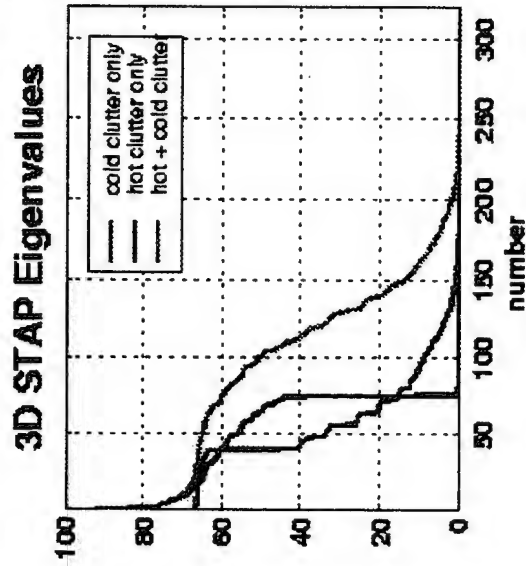
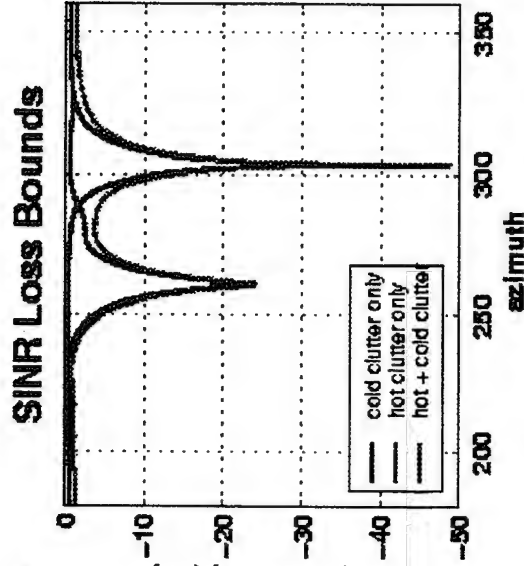
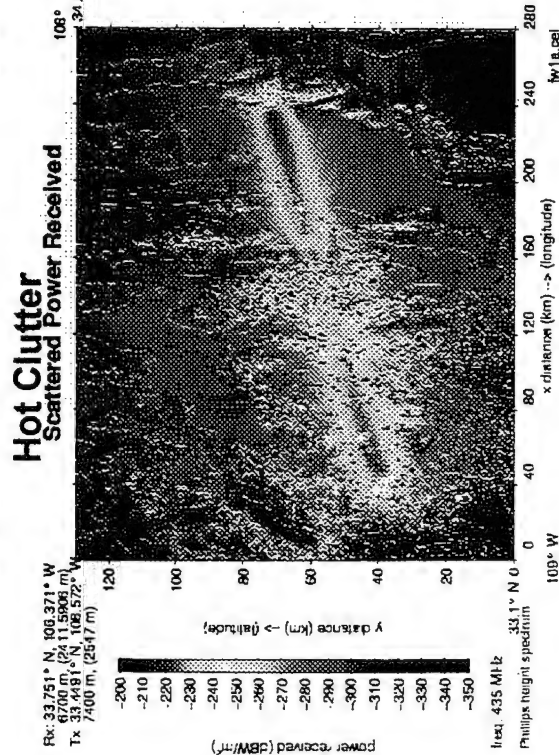
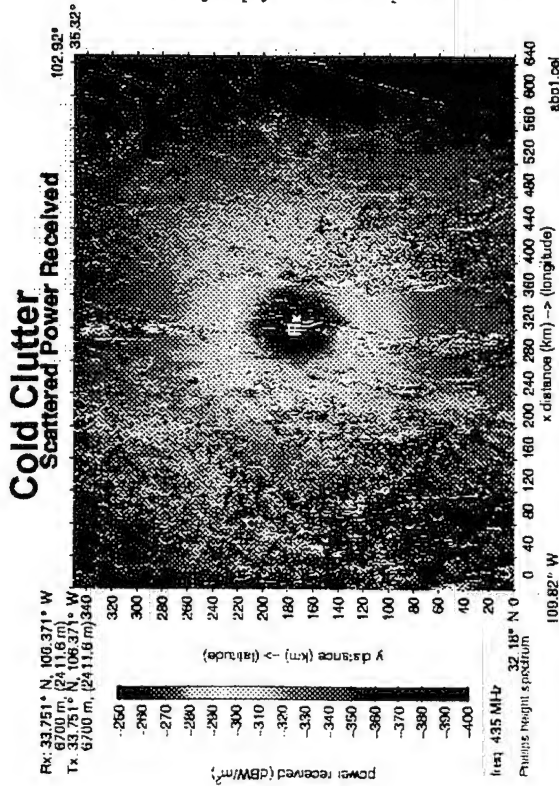
Problem: What are the performance bounds of the canceller being evaluated?

Performance Bounds for Hot and Cold Clutter Mitigation in Airborne Radar Systems

P. M. Techau, J. R. Guerci, T. H. Slocumb, and L. J. Griffiths

- Methodology for establishing bounds on joint hot and cold clutter mitigation performance
- Hybrid deterministic-stochastic optimization based on knowledge of individual hot and cold clutter scatterers
- Uses the instantaneous 3D STAP covariance matrix of interference sources
- Much tighter bound on performance than the thermal noise floor limit
- Potentially lends insight into mitigation factorization process

Joint Ideal Covariance Analysis of Clutter and TSJ



- Terrain-specific phenomenology using SCATS
- Scatter maps generated assuming 1 W ERP - results then scaled as desired
- 8 elements
- 8 pulses
- 5 fast time taps
- 100 kHz bandwidth
- 725 kHz PRF
- Range bin of 150 km
- Doppler frequency of 200 Hz
- CNR = 60 dB per element and pulse in middle range bin/fast time tap
- JNR = 50 dB per element

ASAP '98 Radar Array Processing Session

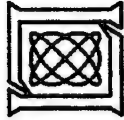
- "Adaptive Array Processing for Wideband Nulling in GPS Systems"
G. Hatke
- "Covariance Matrix Tapers: A Unifying Theory for Robust Adaptive Beamforming"
J. Guerci
- "Wavelet Based Optimization of Space-time Adaptive Processing"
D. Braunreiter
- "A New Interpretation of the Weiner Filter and its Implications"
S. Goldstein
- "Strategies for Minimal Sample Support STAP"
S. U. Pillai
- "Advanced STAP for TSI Modulated Clutter"
D. Rabideau

Space-Time Adaptive Processing Applied to GPS Adaptive Arrays

Gary F. Hatke

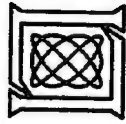
MIT Lincoln Laboratory
244 Wood Street, Room S3-413
Lexington, MA 02173-9108
tel: (781) 981-3364
email: hatke@ll.mit.edu

Abstract Military GPS systems must operate in the presence of hostile jamming. The spread spectrum nature of the GPS signal allows some anti-jamming (A/J) capability, but the vast power differences between a nearby jammer and distant low-power satellite signals can quickly overwhelm the receiver. Adaptive array processing has been applied to this problem in an attempt to give an adaptive spatial nulling A/J capability. Arrays of seven elements (a controlled radiation pattern antenna, or CRPA) has been used for spatial nulling along with a sidelobe canceller array processor. Past analysis of this system has ignored local multipath generated by the platform on which the array is mounted (typically an aircraft). This multipath can greatly increase the effective aperture of the array system. For wideband systems like GPS, this large effective aperture can lead to decorrelation of the jamming wavefront at the array, thus limiting the null depths achievable by a standard spatial only adaptive processor. We propose using a space-time adaptive processor to increase the nulling capability of the adaptive array. Special care must be taken when using a space-time processor for the GPS problem, however, since the nulling operation may distort the desired GPS signal and degrade the time delay estimates which are necessary for accurate position estimation. The optimal method for time delay estimation in the presence of wideband interference is derived. In addition, a novel technique of using soft constraints to limit signal distortion while allowing sufficient null depths on the interference is proposed which can dramatically decrease computational cost relative to the optimal processing method. The performance of the two techniques is compared in simulation.



Space-Time Adaptive Processing Applied to GPS Adaptive Arrays

Gary F. Hatke
MIT Lincoln Laboratory
ASAP 98

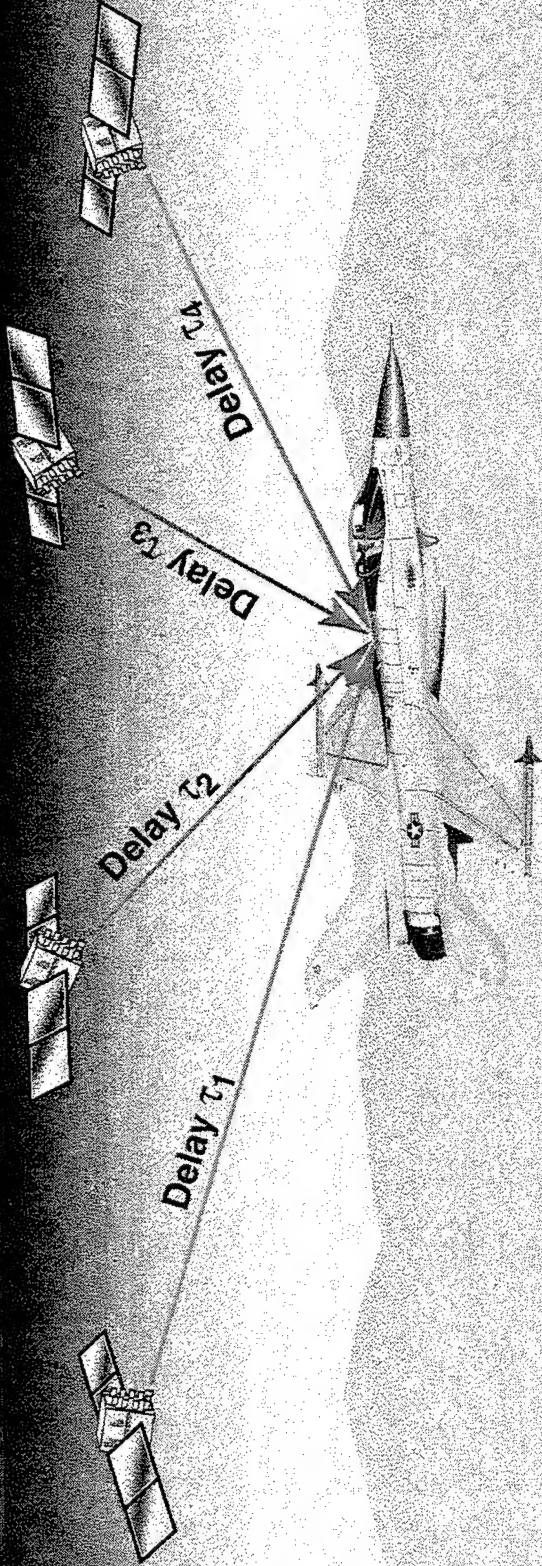


Outline

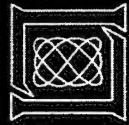
- Introduction
- Space-Time Adaptive Processing (STAP) for broadband nulling
- Compensating for STAP effects on GPS positioning
- Conclusions



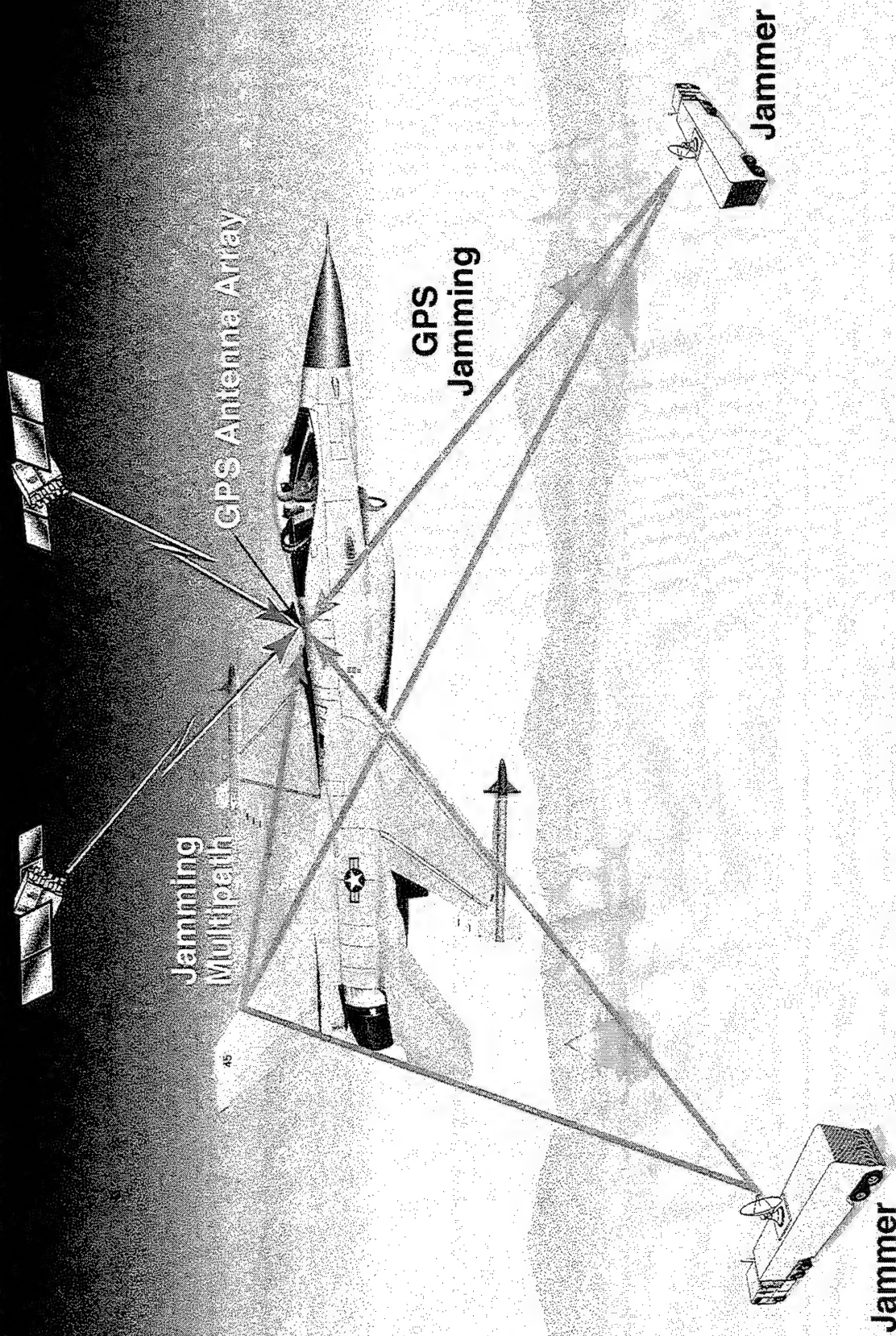
GPS Positioning



- GPS receiver estimates time delays of spread-spectrum CDMA signals from multiple satellites
- User position can be uniquely determined if pseudo-ranging available to 4 or more satellites
- Satellites appearing both low in the horizon and directly overhead desirable for good positioning accuracy

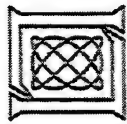


Utilizing GPS in a Jamming Environment



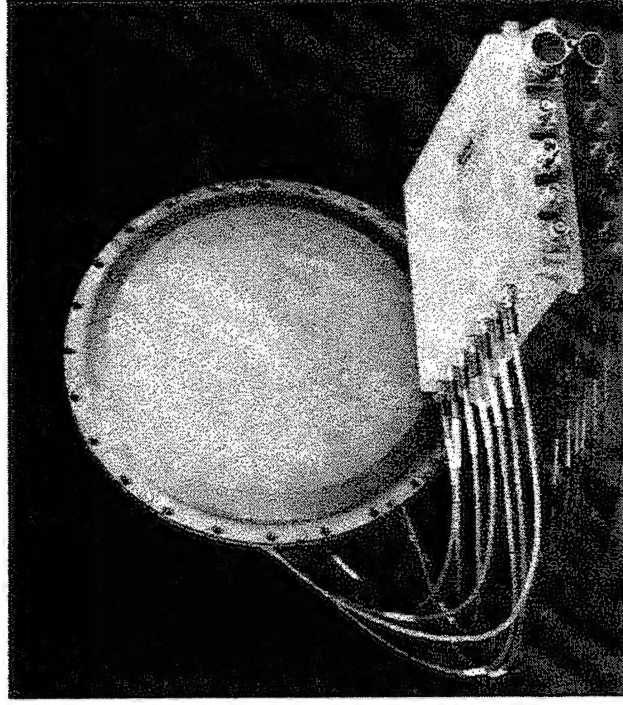
310561-1B
GFH

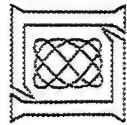
MIT Lincoln Laboratory



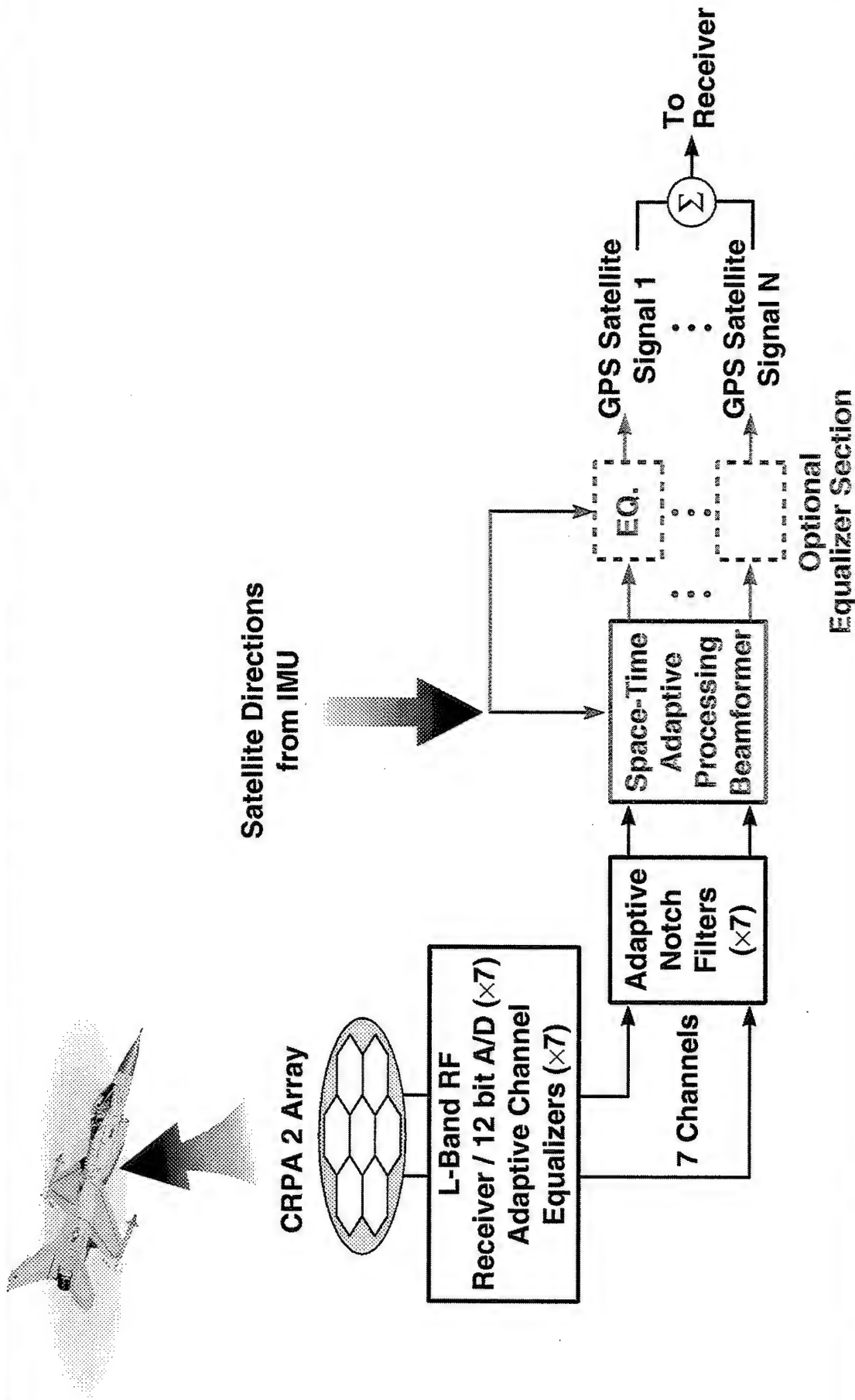
GPS Adaptive Array Hardware

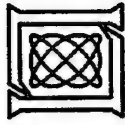
- Controlled Radiation Pattern Antenna (CRPA)
- Seven element hexagonally-configured array
- Roughly 1ft diameter
- Mounts on top surface of US aircraft





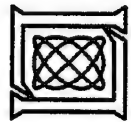
GPS Adaptive Processing Architecture





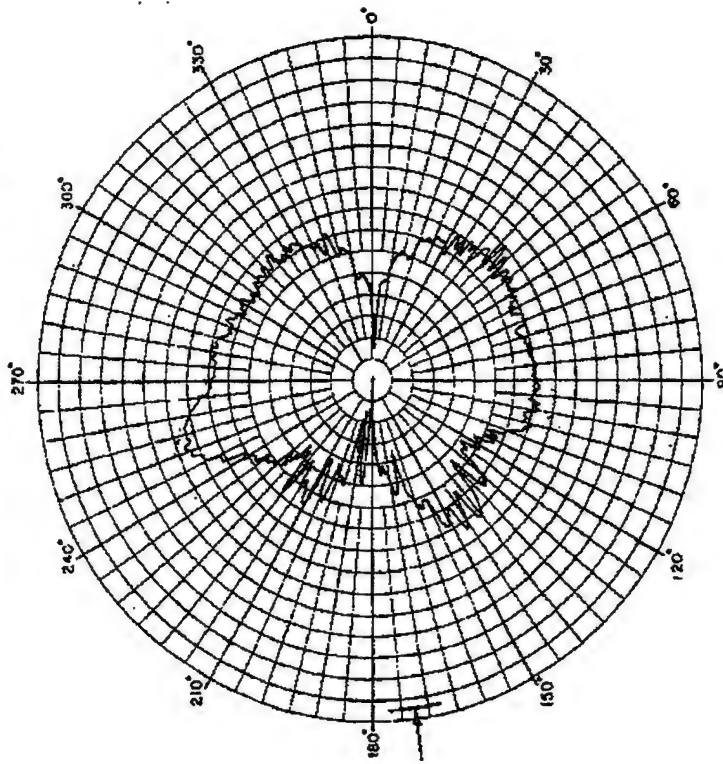
Outline

- Introduction
 - ⇒ Space-Time Adaptive Processing (STAP) for broadband nulling
- Compensating for STAP effects on GPS positioning
- Conclusions

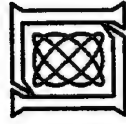


Multipath Scattering on Platform-Mounted GPS Antennas

F-16 GPS Microstrip Antenna Azimuth Pattern 10° Depression Angle

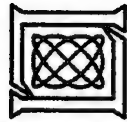


- Antenna pattern features on 1°- 2° scale
- Effective antenna aperture of 30-60 λ
- Implies scatterer radius of up to 40ft

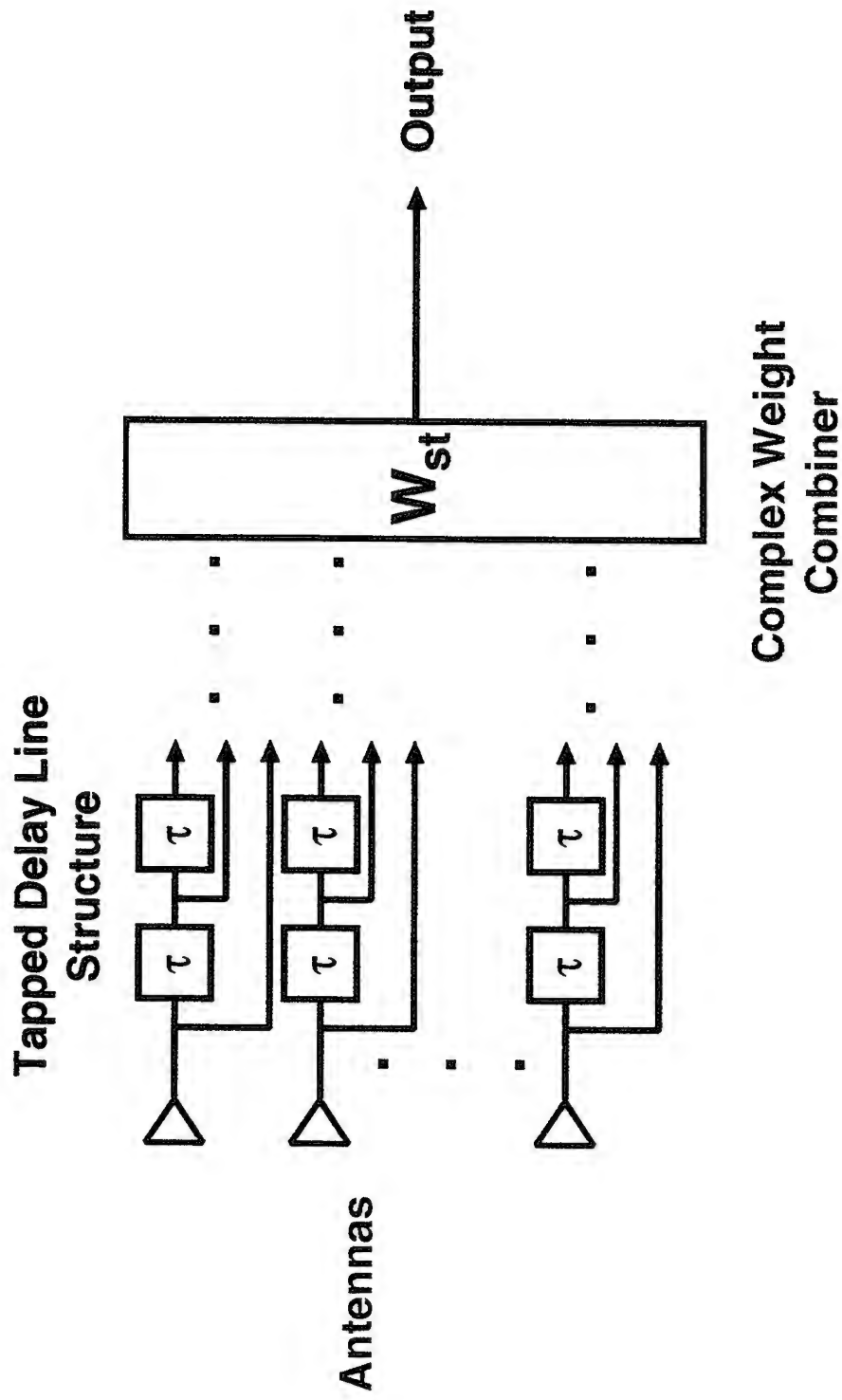


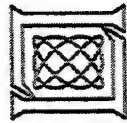
Near-Field Multipath Scattering

- Near-field multipath causes multiple paths to array antenna elements
 - Different paths have (in general) different path length delays, τ_i
- If $(\tau_i - \tau_j) \cdot \text{BW}$ is not small, path i and path j will begin to decorrelate
- Spatially nulling decorrelated sources requires more degrees of freedom than nulling completely correlated sources



Space-Time Adaptive Processor

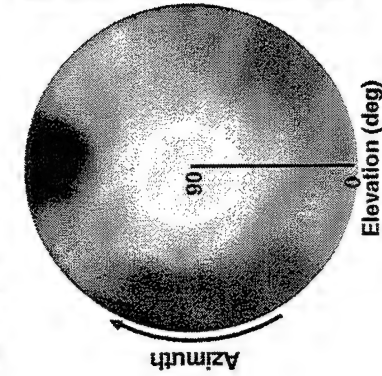
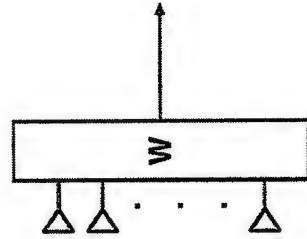




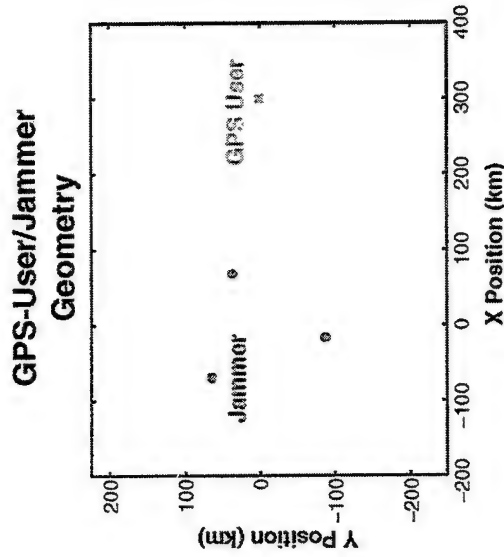
GPS Adaptive Beamforming Performance

Performance vs. Satellite Location

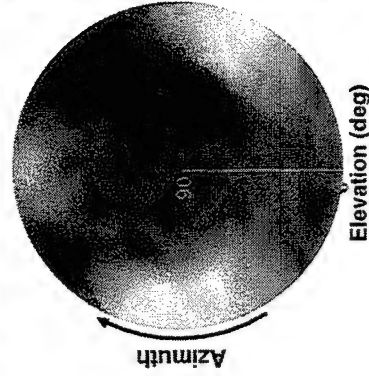
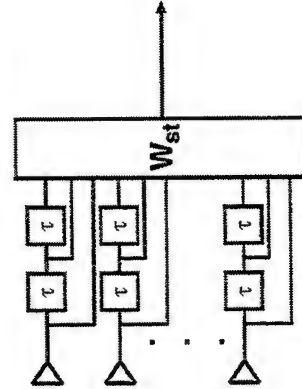
Standard Adaptive Beamformer



SINR loss (dB)
vs. no jamming (dB)

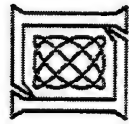


3 Tap Space-Time Adaptive Beamformer

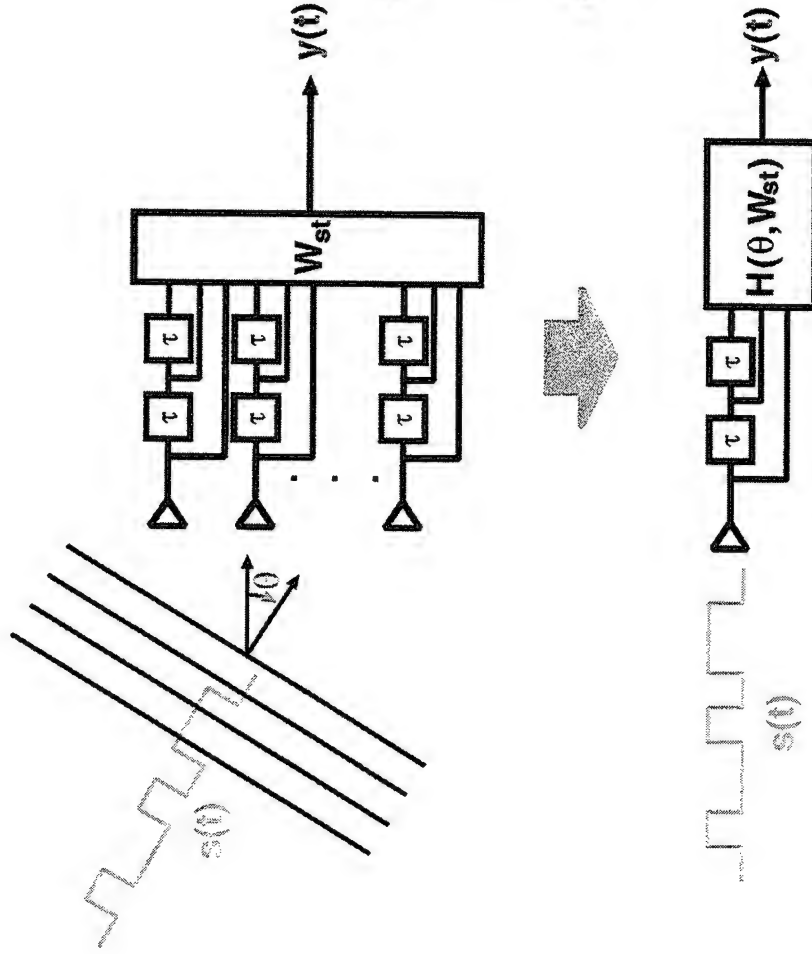


SINR loss (dB)
vs. no jamming (dB)

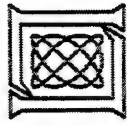
- 70dBw EIRP jammers
- Seventeen -30dB, three -10dB scatterers distributed within 25 ft of CRPA
- 10ft vertical scatterer range
- 50dB null depth processor
- 1/4 P-code-chip tap spacing



STAP Processing Effects on Plane-wave Signals

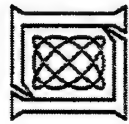


- STAP beamformer appears as a directionally-dependent FIR filter to individual plane-wave signals
- Number of taps in equivalent filter equal to depth of taps in STAP processor

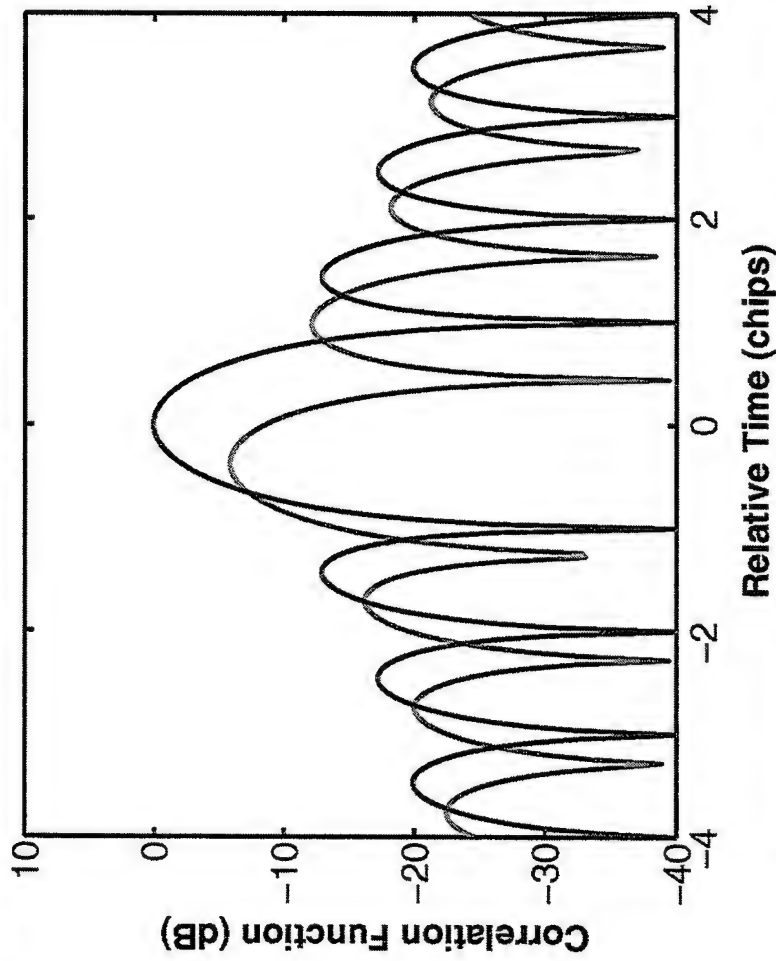


STAP Beamforming Effects on GPS Signals

- STAP beamforming acts as a directionally-dependent FIR filter to GPS satellite signals
 - Different directions will have different equivalent filters
- Filtered GPS signal will have altered correlation function
 - Correlation peaks may be shifted in time, dependent on interference and signal direction
 - Differential time-correlation peak shifts will bias GPS pseudoranging estimates
- Steps must be taken to keep STAP beamforming from biasing GPS solution



Effects of STAP Nulling on Satellite Correlation Functions

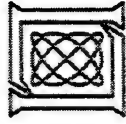


Unequalized 3 tap STAP
Correlation Function

Interference-Free
Single Antenna Element
Correlation Function

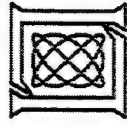
- STAP processor tap spacing of 1/4 chip

- Unconstrained, unequalized STAP beamforming can increase correlation sidelobes, bias correlation peak



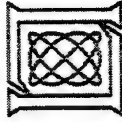
Outline

- Introduction
- Space-Time Adaptive Processing (STAP) for broadband nulling
 - ⇧ Compensating for STAP effects on GPS positioning
- Conclusions

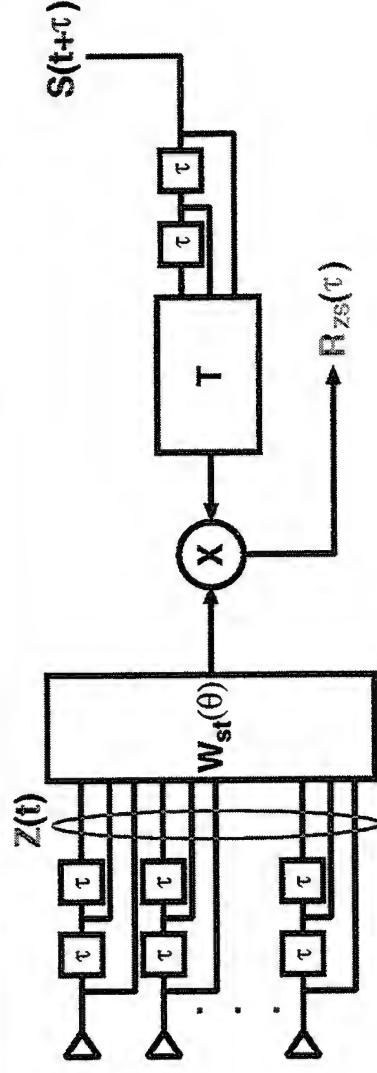


Practical Constraints on STAP Compensation

- Position estimation bias due to STAP beamforming is unacceptable
- GPS receivers are procured in quantity to be used with adaptive arrays as well as non-adaptive antenna systems
 - Proposed STAP system should not modify GPS receiver topology
- Computational complexity of solution should be minimized
 - Processing load must be supportable by near-term available hardware
- Solutions should be optimized to maximize SINR subject to previously mentioned constraints

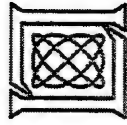


Distorting Correlation Signal



- If GPS receiver is allowed to correlate with a distorted signal waveform, optimization problem can be re-formulated as:

$$\arg \min_{W_{st}, T} ||W_{st}^H Z - T^H S||^2$$
- T, the distorting filter, has an optimal solution of $H(\theta, W_{st}(\theta))$
- This solution requires 'breaking in' to the GPS receiver, which may be infeasible



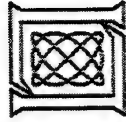
Weight Constraints on STAP Beamformer

- Constraints can be placed on $W_{st}(\theta)$ such that $H(\theta, W_{st}(\theta))$ has benign response in satellite directions
 - Constrain $H(\theta, W_{st}(\theta))$ to be a pure delay in satellite directions
- Soft constraints can be used to force $H(\theta, W_{st}(\theta)) \approx \delta(t - \tau)$ for θ corresponding to satellite directions

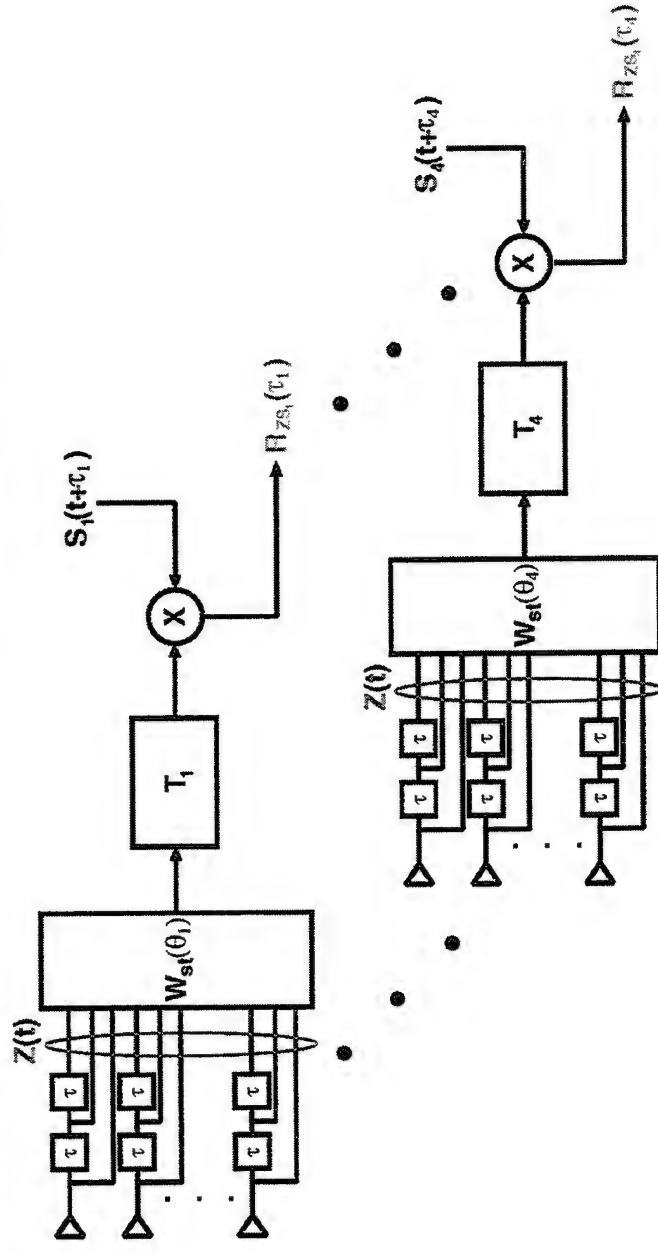
$$H(\theta, W_{st}(\theta)) = (R_I + \alpha C)^{-1} V_{st}(\theta_s, \tau)$$

$$C = P_{\bar{\tau}} R_s(\theta_s) P_{\bar{\tau}}$$

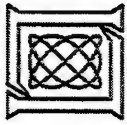
- Satellite direction, satellite signal PSD must be known for $V_{st}(\theta_s, \tau)$ and $R_s(\theta_s)$
- Constrained weight vector may yield lower output signal-to-interference-plus-noise ratio (SINR) than unconstrained beamformer



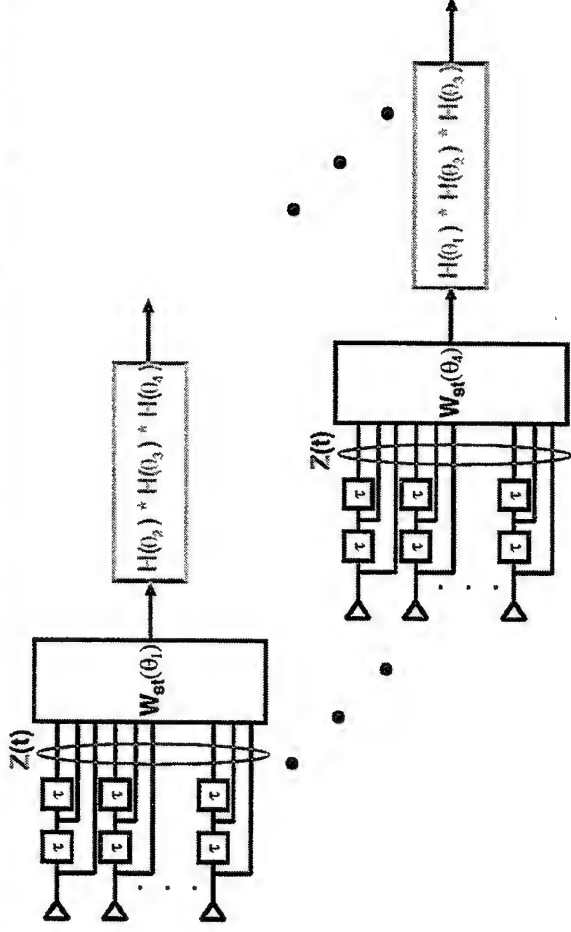
Equalizing STAP-Filtered Signals



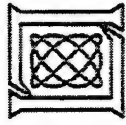
- STAP-induced signal distortion may be compensated by equalization
- Direct channel inversion may yield unstable equalizers
- If all channels equalized to have *same* distortion, unbiased positioning is retained



Satellite-Independent Channel Distortions



- Forcing all satellite signals to undergo identical distortions eliminates positioning bias
- Equalizer for each satellite signal is the convolution of all other satellites' equivalent STAP filters
- For N satellite tracking using a STAP processor of depth M , equalizer length is $NM - N - M + 2$

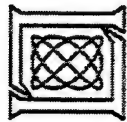


Equalizer Effects on Correlator Performance

- STAP processor combined with equalizer will alter correlator output performance
 - Correlation 'beamwidth' will be widened
- Cascading of N equivalent STAP filters yields a Gaussian-like filter
- Assuming STAP equivalent filter coefficients are i.i.d., standard deviation of Gaussian profile (in units of tap spacing) is:

$$\frac{\sqrt{NM}}{2\sqrt{3}}$$

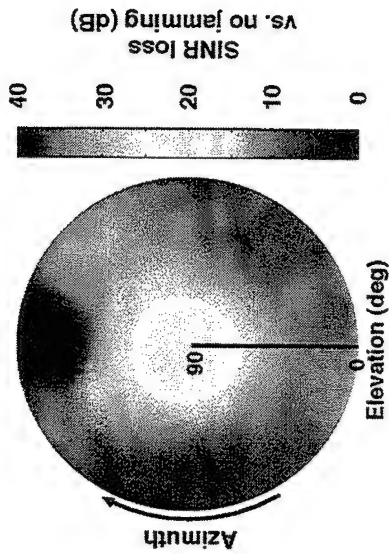
- For 4 satellite channels and STAP processor depth of 3, this is predicts a 3dB correlation peak spread of no more than 3 taps



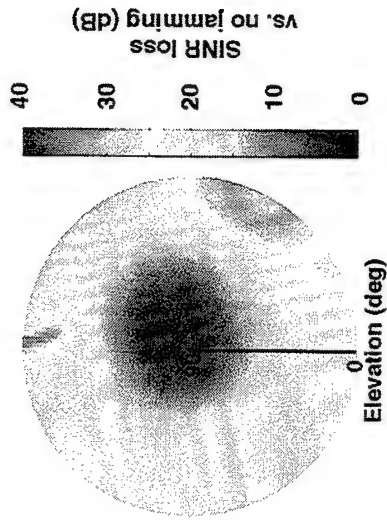
Constraint Method Performance Comparison

Beamformer Performance vs. Satellite Location

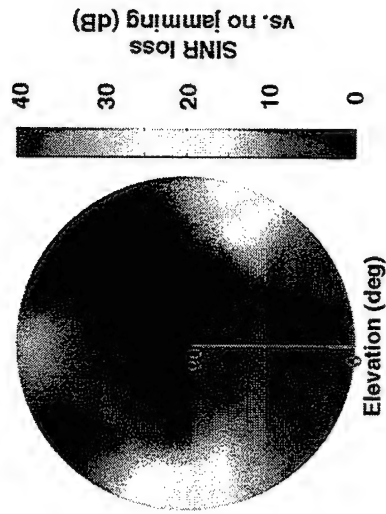
Spatial-only Adaptive Beamformer



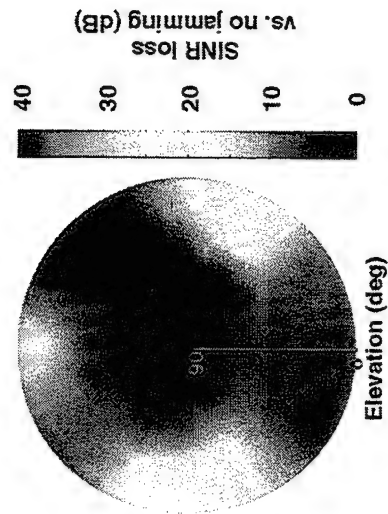
**Space-Time Adaptive Beamformer
With Weight Constraints**

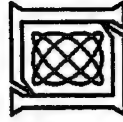


**Space-Time Adaptive Beamformer
Optimal Performance**



**Space-Time Adaptive Beamformer
With Equalizer**





Conclusions

- Mitigation of GPS jamming via adaptive beamforming benefits from STAP architecture
 - Near-field multipath scattering coupled with broadband interference drives STAP architecture
- Uncompensated STAP beamforming can bias GPS position estimates
 - STAP beamformer acts as a directionally dependent FIR filter, distorting each satellite signal differently
- Weight constraints, channel equalization can eliminate positioning bias
 - Differential equalization provides best performance

Covariance Matrix Tapers: A Unifying Theory for Robust Adaptive Beamforming

Joseph R. Guerci

Science Applications International Corp.
Air Defense Technology Division
4001 N. Fairfax Drive, Suite 400
Arlington, VA 22201
tel: (703) 243-9830
email: jguerci@trg1.saic.com

Abstract In this paper, we unify several seemingly disparate approaches to robust adaptive beamforming through the introduction of the concept of a "covariance matrix taper (CMT)." This is accomplished by recognizing that an important class of adapted pattern modification techniques [1]-[3], are realized by the application of a conformal matrix "taper" to the original sample covariance matrix. From the Schur Product Theorem for positive (semi) definite matrices, and Kolmogorov's existence theorem, we further establish that CMTs are in fact the solution to a minimum variance optimum beamformer associated with an auxiliary stochastic process which is related to the original by a Hadamard (Schur) product. This allows us to gain deeper insight into the design of both existing pattern modification techniques and new CMTs that can, for example, simultaneously address several different design constraints such as pattern distortion due to insufficient sample support, and weights mismatch due to nonstationary interference. Also introduced is a new 2D CMT for space-time adaptive radar applications designed to provide more robust clutter cancellation. Since the CMT approach only involves a single matrix Hadamard product, it is also inherently low complexity. The practical utility of the CMT approach is illustrated through its application to both spatial and spatio-temporal adaptive beamforming examples.

- [1] B.D. Carlson, "Covariance Matrix Estimation Errors and Diagonal Loading in Adaptive Arrays," IEEE Transactions on Aerospace and Electronic Systems, vol. 24, no. 4, pp. 397-401, July 1988.
- [2] R.J. Mailloux, "Receive Array Pattern Modification Using Covariance Matrix Augmentation," Electronics Letters, vol. 31, no. 10, pp. 771-772, 1995.
- [3] M. Zatman, "Production of Adaptive Array Troughs by Dispersion Synthesis," Electronics Letters, vol. 31, no. 25, pp. 2141-2142, 1995.

Covariance Matrix Tapers (CMTs) A Unifying Framework for Robust Adaptive Array Beamforming

J. R. Guerci

Air Defense Technology Division
Science Applications International Corp.
4001 N. Fairfax Drive, Suite 400
Arlington, VA 22201
(703) 243-9830
jguerci@trg1.saic.com



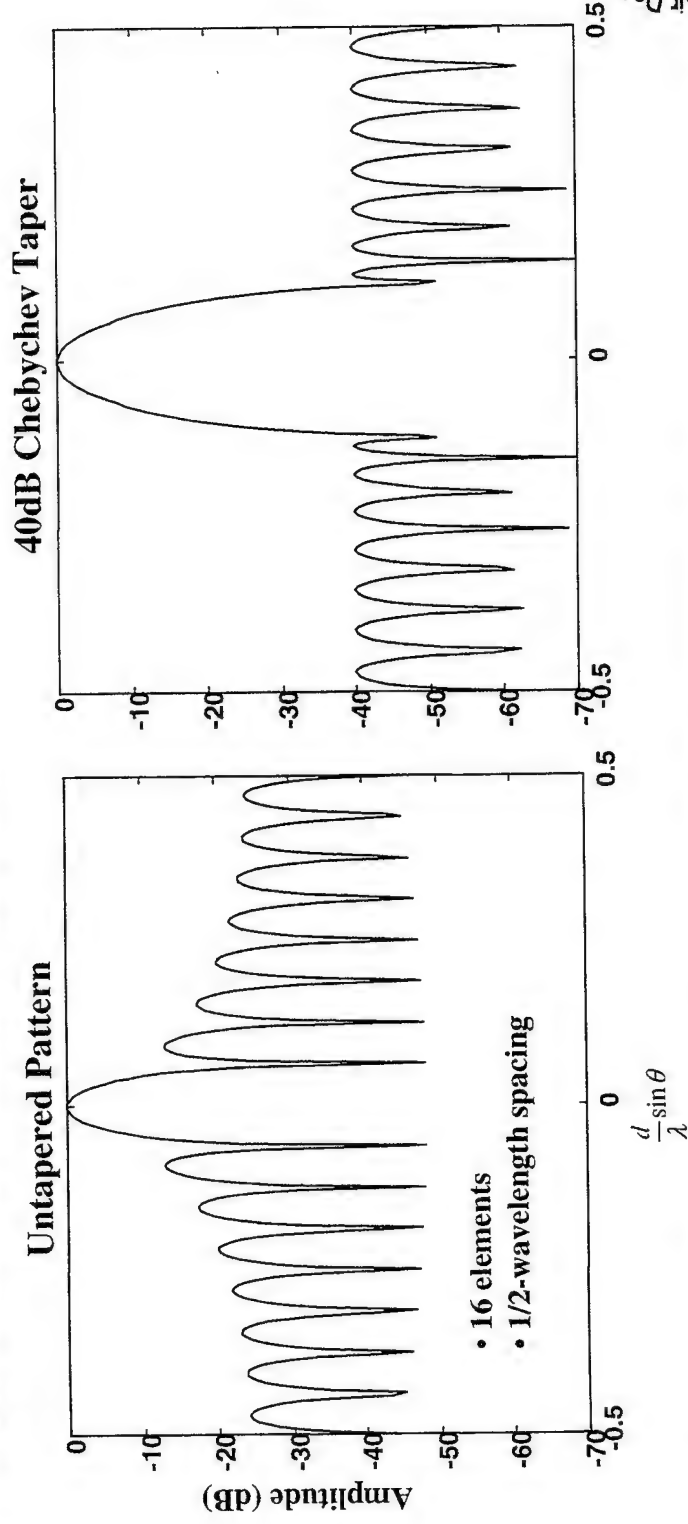
Outline

- Conventional tapers for non-adaptive “robust” beamforming
 - Properties
- Adapted pattern “robustification” and covariance matrix tapers (CMTs)
- Definition and properties of CMTs
- Design examples
 - Robust Jammer nulling
 - Robust clutter nulling (STAP)
- Summary and areas for future investigation



Conventional Tapers

- Conventional tapers (or window functions) for sidelobe control are virtually universally implemented in practice
 - Sidelobe target masking problem
 - Better jammer suppression
 - Better sidelobe clutter mitigation
 - Overall better “robustness” in real-world applications
- Well worth the small SNR cost!



The Hadamard (Schur) Product

- Conventional tapers are effected via a Hadamard product:

$$C = A \circ B = \begin{bmatrix} a_{11} & a_{12} & \cdots & a_{1n} \\ a_{21} & a_{22} & & \vdots \\ \vdots & & \ddots & \\ a_{m1} & a_{m2} & & a_{mn} \end{bmatrix} \circ \begin{bmatrix} b_{11} & b_{12} & \cdots & b_{1n} \\ b_{21} & b_{22} & & \vdots \\ \vdots & & \ddots & \\ b_{m1} & b_{m2} & & b_{mn} \end{bmatrix} = \begin{bmatrix} a_{11}b_{11} & a_{12}b_{12} & \cdots & a_{1n}b_{1n} \\ a_{21}b_{21} & a_{22}b_{22} & & \vdots \\ \vdots & & \ddots & \\ a_{m1}b_{m1} & a_{m2}b_{m2} & & a_{mn}b_{mn} \end{bmatrix}$$

Thus, the Hadamard identity matrix is given by

$$A \circ \mathbf{1}_{M \times N} = A$$

Identity

and the Hadamard inverse A^{-1} is given by

$$\{A^{-1}\}_j = \frac{1}{a_{ij}}$$

Inverse

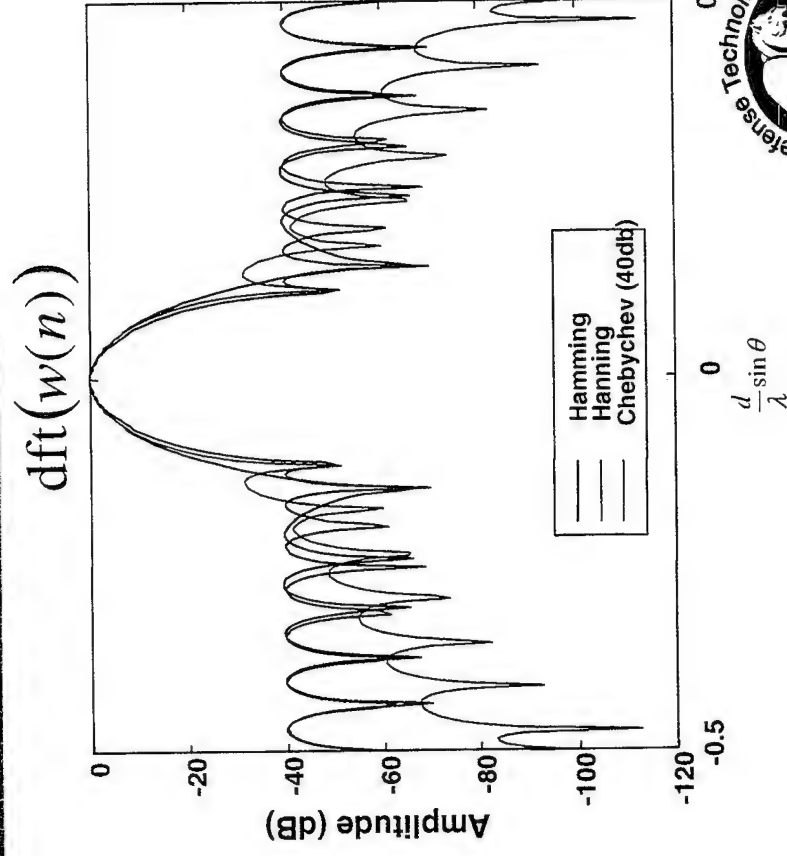
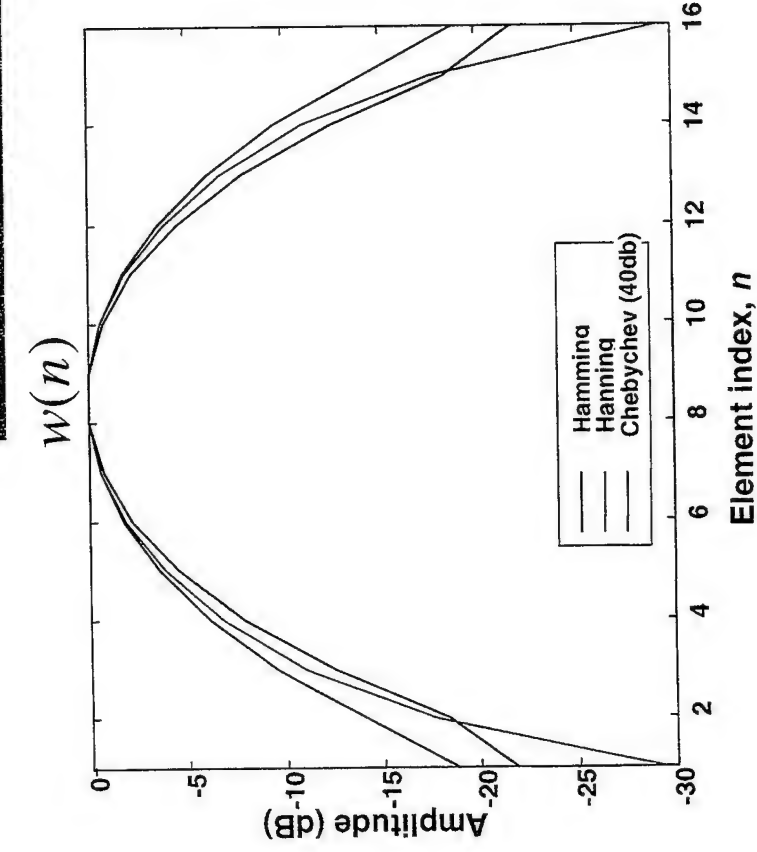
thus A^{-1} exists iff. $a_{ij} \neq 0, \forall i, j$



Properties of Conventional Tapers

- In conventional “narrowband” applications, the taper function $w(k)$ is a *positive semidefinite* and *symmetric* sequence, i.e.,

- $w(n) \geq 0$ (positive semidefinite)
- $w(n + \frac{N+1}{2})$ is an *even* function (symmetric)

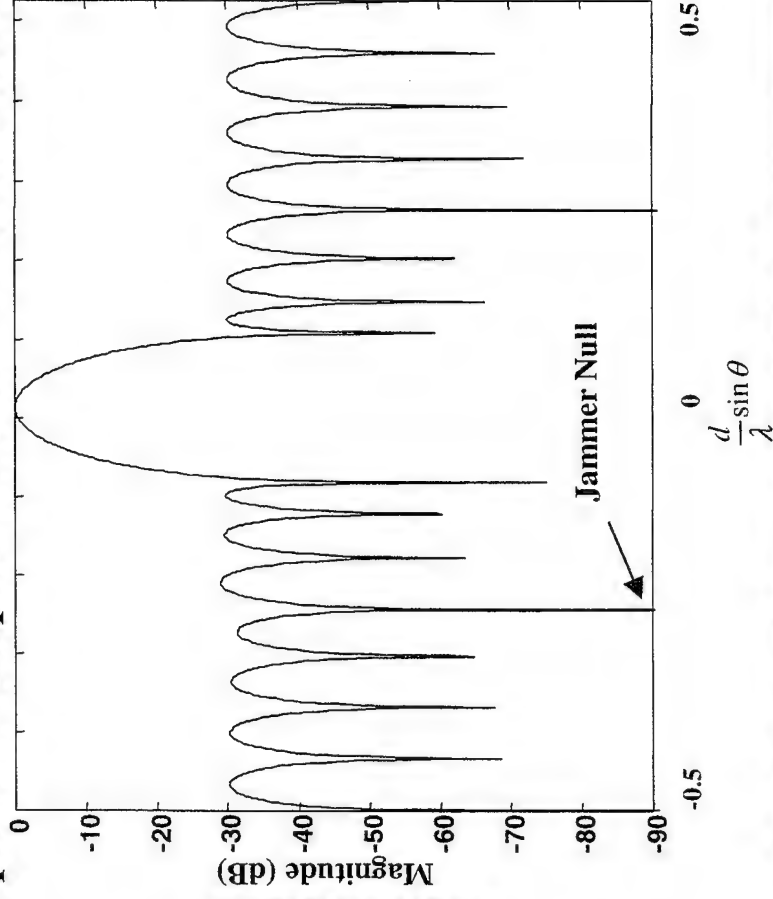


Adaptive Pattern Synthesis

- Given *exact* knowledge of the interference statistics (covariance matrix), an optimal adapted pattern can be synthesized

$$\mathbf{w} = \mathbf{R}^{-1}(\mathbf{s} \circ \mathbf{t})$$

Optimum Adapted Pattern w/Conventional Taper



- 16 elements
- 1/2-wavelength
- JNR = 60 dB
- 30 dB Chebychev

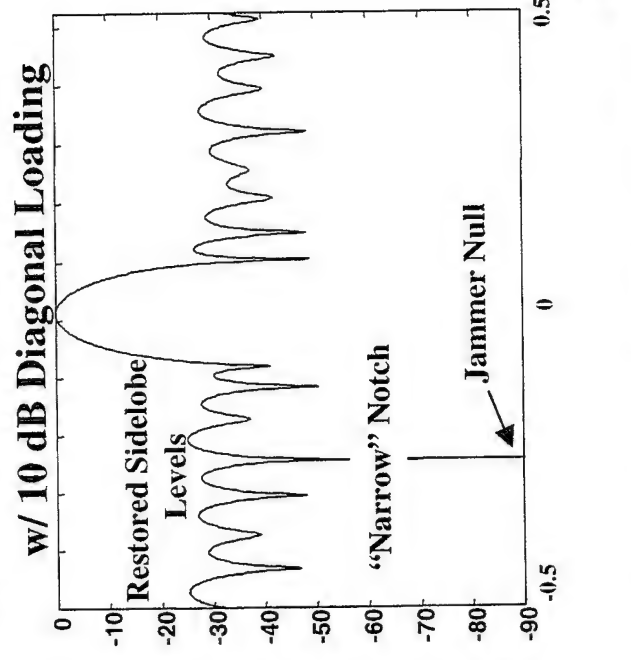
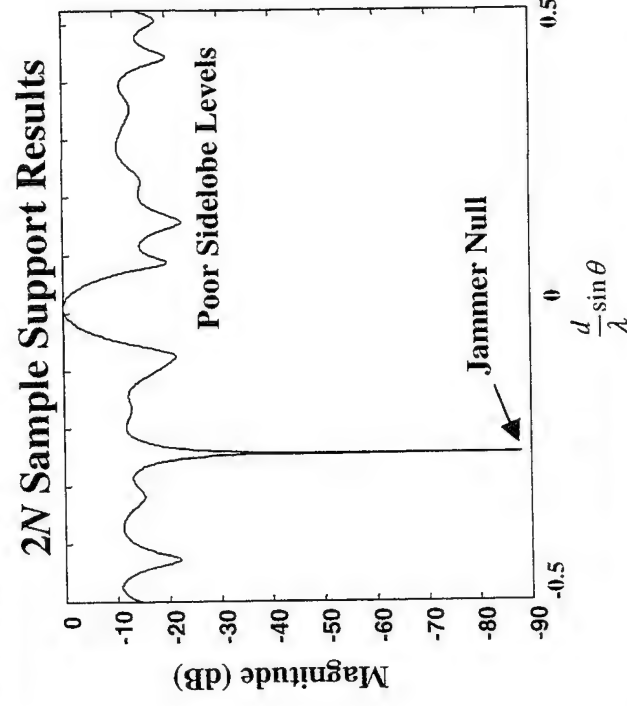
- \mathbf{w} = linear combiner weights
- \mathbf{R} = interference - only covariance matrix
- \mathbf{s} = target steering vector
- \mathbf{t} = conventional taper
- \circ = Hadamard (Schur) product



Practical Implementation Issues

- Some practical considerations effecting performance:
 - Finite sample support effects
 - Interference nonstationarity
 - Adaptive weight update rates (“stale” weights)
 - Unresolved/undetected array motion
 - Computational burden, etc.

- Simplest and most ubiquitous remedy: Diagonal Loading



Diagonal Loading is a “Covariance Matrix Taper” (CMT)

- Diagonal loading is mathematically equivalent to applying a CMT to the interference covariance matrix:

$$\begin{aligned} R_{DL} &= R + \delta I \\ &= R \circ (1 + \varepsilon I) \\ &\triangleq R \circ T_{DL} \end{aligned}$$

- What properties must a CMT possess to be both mathematically meaningful and useful?
- What does a CMT do to the pattern? SINR? Etc.
- How does one design a CMT?

[†] Assumes that the diagonal entries of R are equal. Otherwise the solution is $1 + D$, where D is diagonal.

Definition and Properties of CMTs

- To be physically meaningful, the tapered covariance matrix must be at least positive semidefinite (preferably pos. def.)
- Schur Product Theorem (SPT) provides sufficient conditions:

† **Theorem 1 (Schur Product Theorem)** If A and B are $p.s.d.$ matrices, so is $A \circ B$. Moreover, if A is $p.d.$ and B is $p.s.d.$, then $A \circ B$ is $p.d.$

- Thus the SPT provides a minimal definitional requirement for a CMT, viz.,

CMT : $T \in$ Positive Semidefinite Matrices

(with no zero diagonal entries)

† *Topics in Matrix Analysis*, R. A. Horn and C. R. Johnson, Cambridge University Press, 1991.

Definition and Properties of CMTs

- Eigenvalue Majorization Theorem (EMT) helps narrow the definition of a useful class of CMTs:

Theorem 2 (Eigenvalue Majorization) If A is p.d., and B is a correlation matrix, then $\text{cond}(A \circ B) \leq \text{cond}(A)$.

where

$$\text{cond}(A) = \frac{\lambda_{\max}}{\lambda_{\min}}$$

and

$$B = \text{p.d. matrix with } \text{diag}(B) = [1 \ 1 \ 1 \dots 1]'$$

- Thus a CMT which is proportional to a correlation matrix will tend to improve the condition number of the original matrix
 - Diagonal loading is (proportional to) a correlation matrix CMT!



Interpreting CMTs

- The introduction of a CMT is tantamount to solving an auxiliary optimum beamforming problem:

Theorem 3 If given a *p.d.* covariance matrix R , and a *p.d.* or *p.s.d.* CMT T (with no zero diagonal entries), then the beamformer

$$w = \kappa(R \circ T)^{-1} s$$

is an **optimum minimum variance** beamformer associated with the auxiliary additive stochastic interference

$$\begin{aligned} \tilde{v} &= \tilde{\mathbf{n}} \circ \tilde{\eta} \\ \text{cov}(\tilde{\mathbf{n}}) &= R \text{ and } \text{cov}(\tilde{\eta}) = T \end{aligned}$$

From Kolmogorov's
Existence Theorem



A New (“Almost”) CMT for Robust Beamforming

- From Theorem 3 and Kolmogorov’s existence theorem, we can associate an auxiliary stochastic process with T_{DL} (Diagonal Loading):

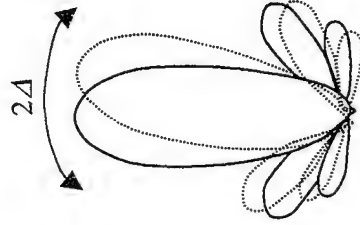
Associated with $\text{cov}(\tilde{\eta}) = T_{DL} = \mathbf{e}\mathbf{e}' + \varepsilon I$ is

$$\tilde{\eta} = \mathbf{e} + \tilde{\mathbf{w}}$$

white noise

$$\mathbf{e} = \begin{bmatrix} 1 \\ \vdots \\ 1 \\ \vdots \\ 1 \end{bmatrix} \quad \text{Boresight-aligned steering vector}$$

- The “e” term provides a mechanism for providing directional robustness against jammers.



$$\tilde{\mathbf{e}} = \begin{bmatrix} 1 \\ \vdots \\ e^{j2\pi\frac{d}{\lambda}(n-1)\sin\tilde{\theta}} \\ \vdots \\ e^{j2\pi\frac{d}{\lambda}(N-1)\sin\tilde{\theta}} \end{bmatrix} = \begin{bmatrix} 1 \\ \vdots \\ e^{j(n-1)\tilde{\omega}} \\ \vdots \\ e^{j(N-1)\tilde{\omega}} \end{bmatrix}$$

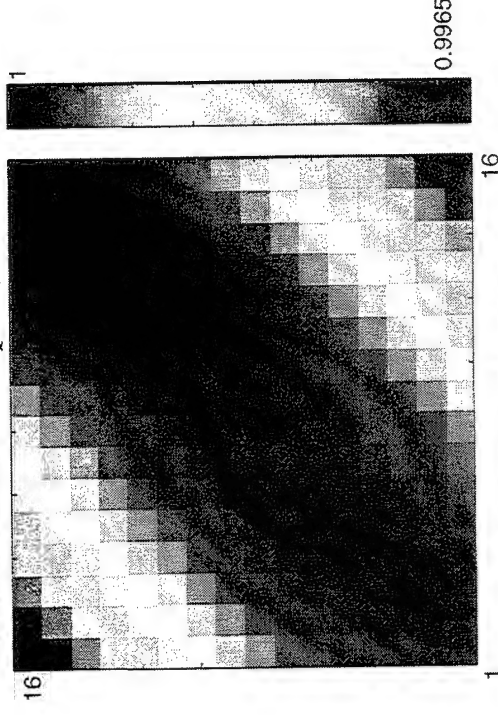
$$-\Delta \leq \tilde{\omega} \leq \Delta, \text{ Uniform R. V.}$$

A New ("Almost") CMT for Robust Beamforming

- For which the associated covariance is:

$$\begin{aligned} \text{cov}(\tilde{\eta}) &= \text{cov}(\tilde{\mathbf{e}} + \tilde{\mathbf{w}}) = T_{DLMZ}^{\Delta} \\ &= \left[\text{sinc} \left(\frac{(i-j)\Delta}{\pi} \right) \right]_{i,j} + \epsilon I \end{aligned}$$

Mailloux-Zatman Taper ($\Delta=0.01$)



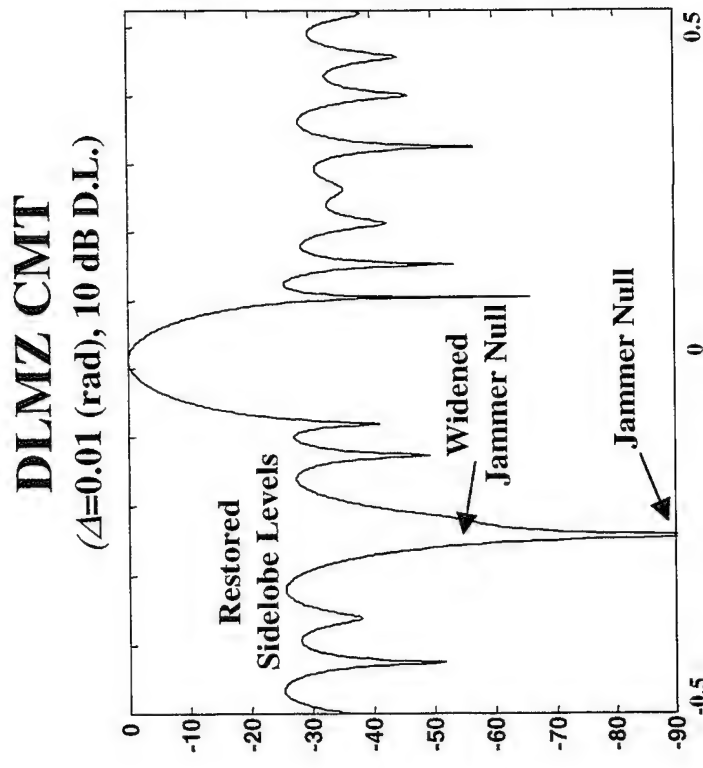
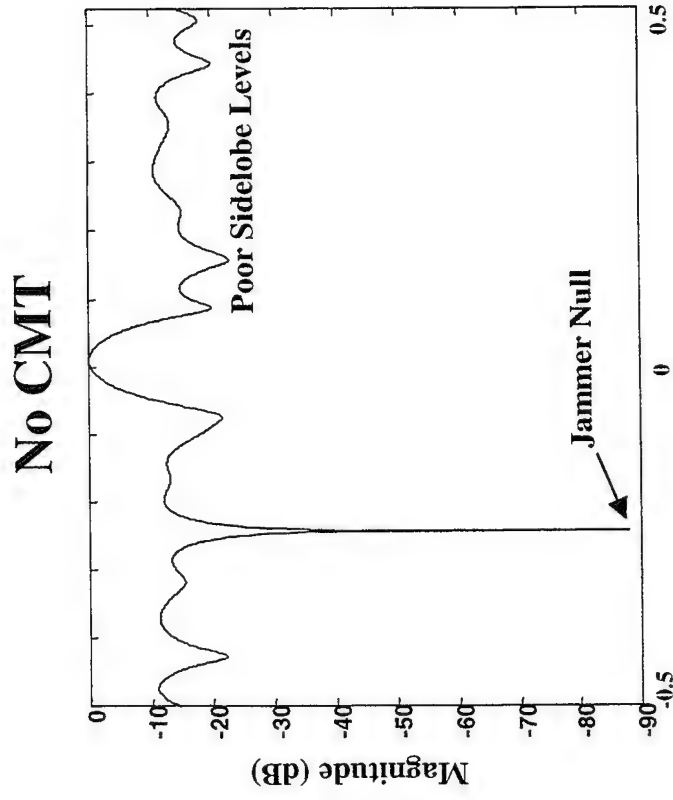
Diagonally Loaded "Mailloux-Zatman" (DLMZ) CMT

- R. Mailloux and M. Zatman independently introduced the "sinc" CMT form:
 - R. Mailloux, "Covariance Augmentation to Produce Adaptive Pattern Troughs," Electronic Letters, Vol. 31, No. 10, 1995.
 - M. Zatman, "Production of Adaptive Pattern Troughs by Dispersion Synthesis," Electronic Letters, Vol. 31, No. 25, 1995.



Application of the Diagonally Loaded Maillox-Zatman CMT

- Simultaneous sidelobe control AND jammer null robustness



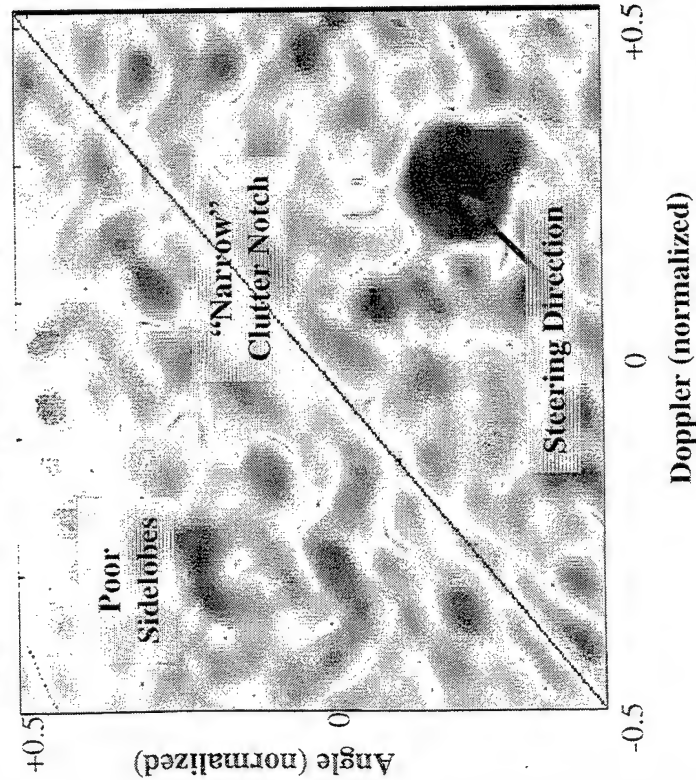
- Additional SINR loss < 0.06 dB



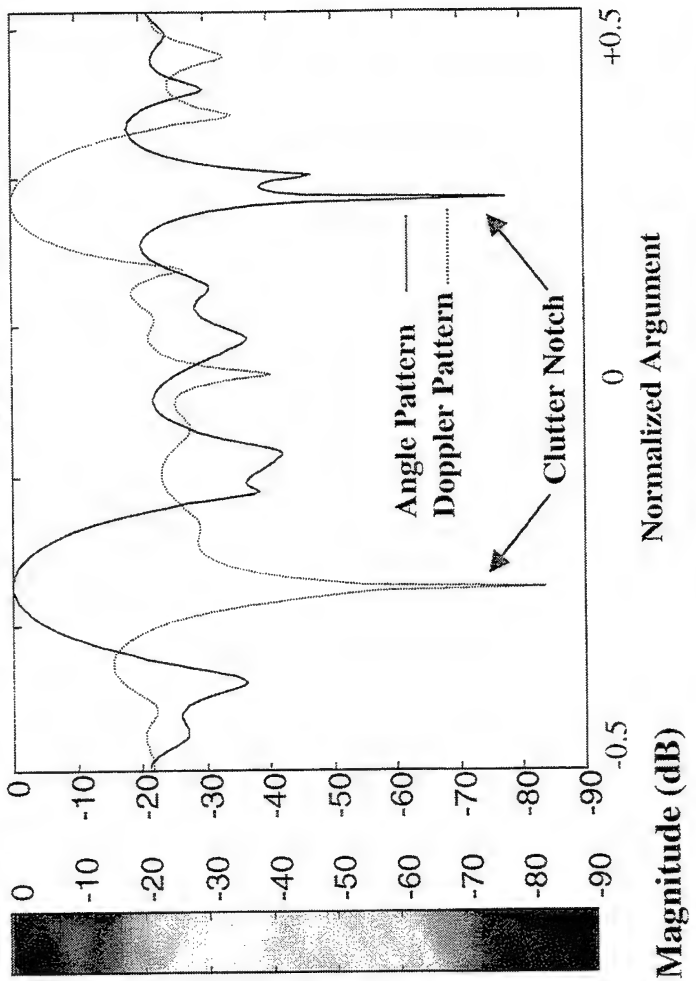
Application to STAP for Airborne MTI Radar

- 2D SMI (2N samples) adapted pattern distortion:
 - Can result in undernulled clutter

SMI (2N samples) Adapted Pattern



Angle & Doppler Patterns



- 16 Elements ($\lambda/2$)
- 16 Pulses ($\beta=1$)
- CNR = 60 dB (per element)
- 40 dB Angle & Doppler Sidelobes

2D Diagonally Loaded Mailloux-Zatman CMT for STAP

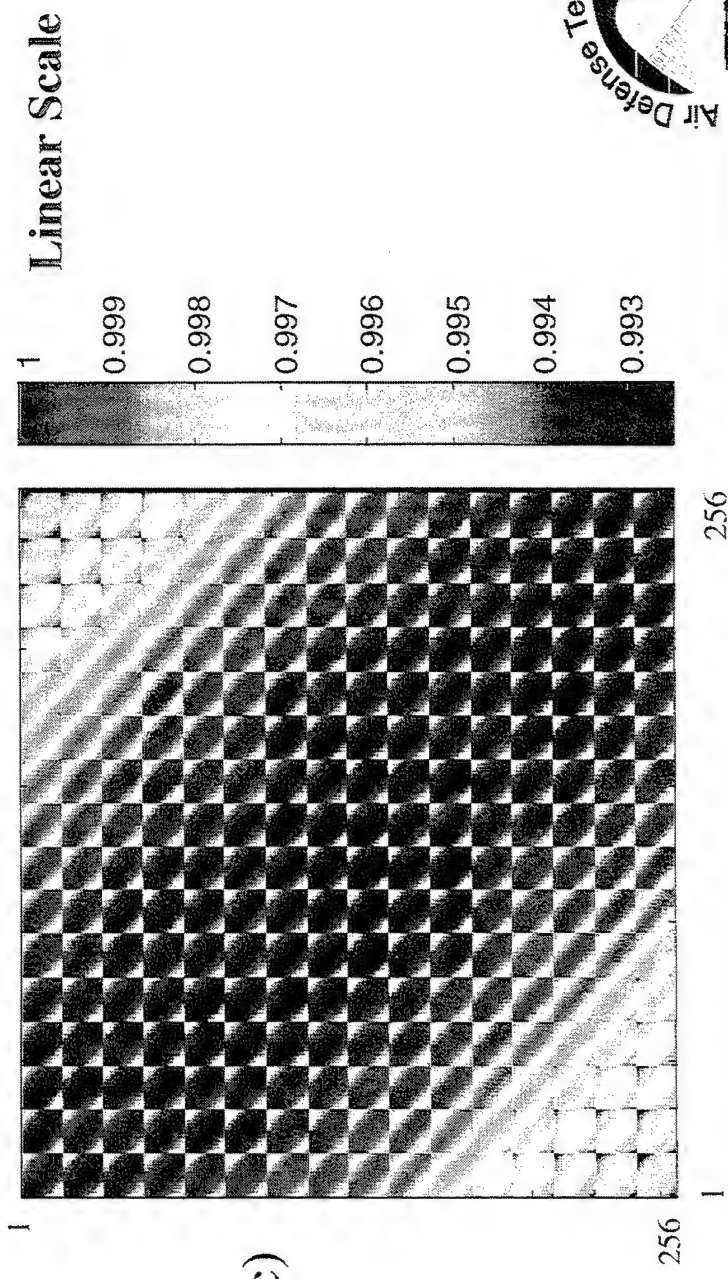
- 1D DLMZ CMT is extensible to 2D STAP case:

$$T_{DLMZ_{2D}} = (T_{MZ_\omega} \otimes I_{N \times N}) \circ (I_{M \times M} \otimes T_{MZ_\theta}) + \epsilon I$$

where

$$T_{MZ_\omega} = \left[\text{sinc}\left(\frac{(i-j)\Delta_\omega}{\pi}\right) \right]_{i,j} \quad (\text{Doppler MZ CMT})$$

$$T_{MZ_\theta} = \left[\text{sinc}\left(\frac{(i-j)\Delta_\theta}{\pi}\right) \right]_{i,j} \quad (\text{Angle MZ CMT})$$



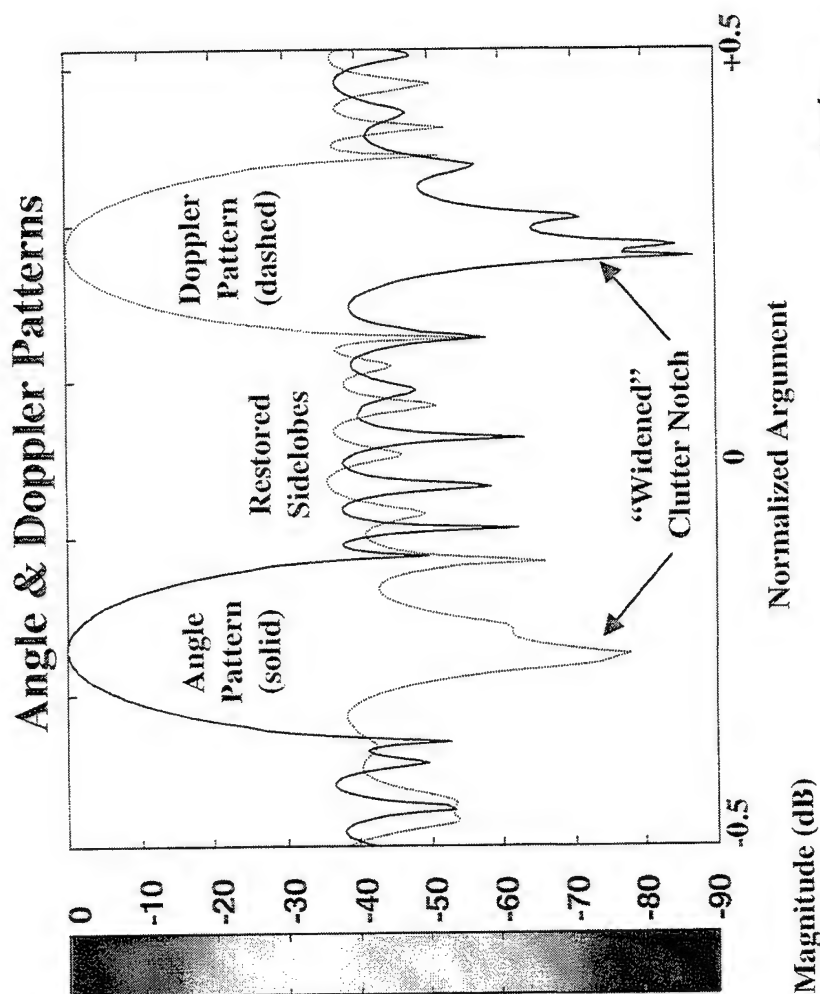
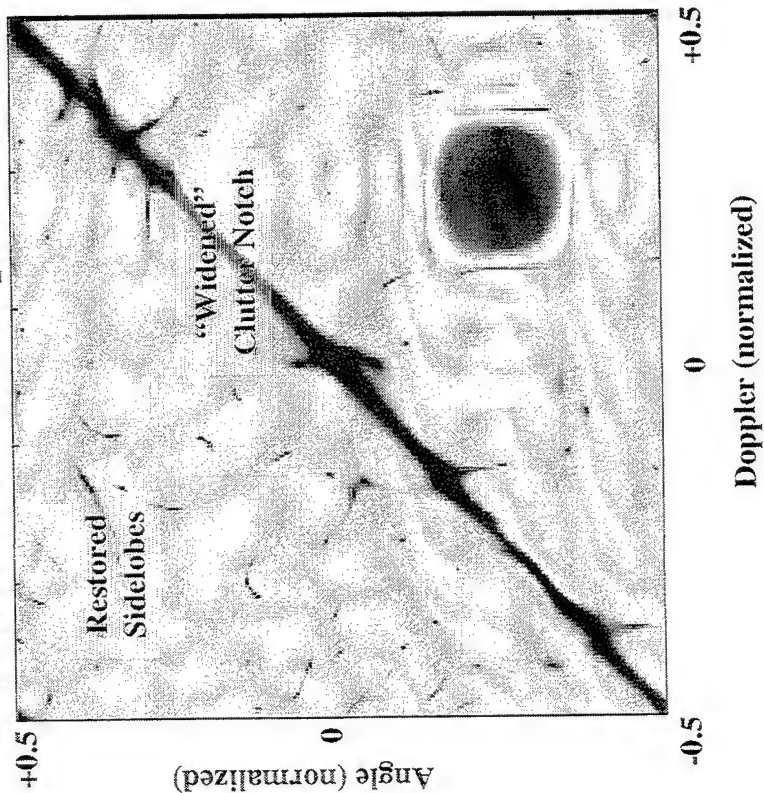
$$\Delta_\omega = 0.01 \text{ (rad/sec)}$$

$$\Delta_\theta = 0.01 \text{ (rad)}$$

Application of 2D DLMZ CMT to STAP

- Robust adapted angle-doppler pattern

2D DLMZ CMT Adapted Pattern



- Additional SINR loss < 0.06 dB

Summary & Areas for Future Investigation

- CMTs provide a unifying mathematical framework for an important class of adapted pattern “robustification” techniques
 - Diagonal loading & Mailloux-Zatman “trough” techniques are CMTs
- Fundamental mathematical properties established
 - Minimal defining requirements (*p.s.d.*, *p.d.*, “correlation” matrix)
 - “Theorem 3” (Auxiliary minimum variance beamformer)
- Application to 1D and 2D (STAP) adaptive pattern synthesis
 - Improved jammer null and clutter notch robustness
- Trivial to implement!
- Many other CMTs are possible:
 - Other “dither” functions than Mailloux-Zatman
 - Notch “shaping”
 - Tapers that minimize SINR loss penalty
 - Tapers that minimize DOFs utilized by CMT (compact)



J. Scott Goldstein

MIT Lincoln Laboratory
244 Wood Street
Lexington, MA 02173-9108
tel: (781) 981-0459
email: scott@ll.mit.edu

I.S. Reed

University of Southern California

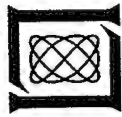
L.L. Scharf

University of Colorado

Abstract A new interpretation of the Wiener filter is introduced which demonstrates a low complexity and motivates a different method of reduced-rank Wiener filtering. The vector process observed by the Wiener filter is first decomposed by a sequence of transformations which project the data onto the cross-correlation vector and its orthogonal complement, in a stage-by-stage manner. The resulting data vector, at the output of this decomposition, is then processed by a nested chain of scalar Wiener filters to provide the minimum-mean square error solution.

The implementation of this Wiener filter is efficient, and can be realized in the voltage domain by a data matrix bidiagonalization technique or in the power domain using the Householder tridiagonalization. Rank reduction is obtained by simply pruning the tree-structure of the decomposition and does not require any eigen-analysis of the covariance matrix.

This new multistage Wiener filter provides the diagonalization of the covariance matrix in a different basis representation. This technique represents an extension of the cross-spectral metric in that the cross-spectral energy is compactly represented in few coefficients. A narrowband array processing example is presented to compare the performance of the multistage Wiener filter, the cross-spectral metric Wiener filter and the principal-components Wiener filter as a function of rank.



A New Interpretation of the Wiener Filter

J.S. Goldstein, I.S. Reed and L.L. Scharf

ASAP 98

11 March 1998

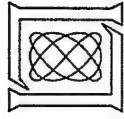
217

980311-0
ASAP98

This work was sponsored by DSPO under Air Force Contract F19628-95-C-0002. Opinions, interpretations, conclusions and recommendations are those of the author and are not necessarily endorsed by the United States Air Force.

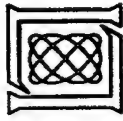
MIT Lincoln Laboratory

Preceding Page Blank



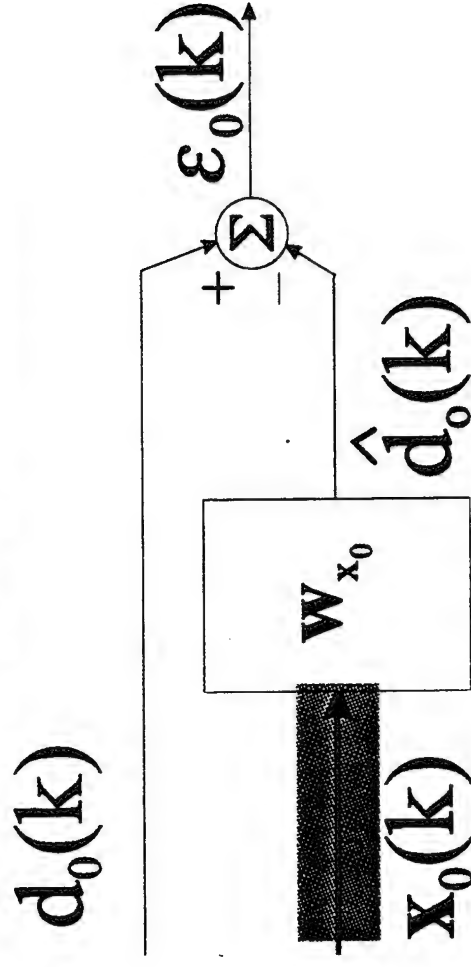
Outline

- Introduction
- The multistage Wiener filter
- Rank reduction
- Example
- Conclusions

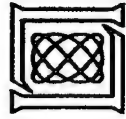


Introduction

Previous Approach

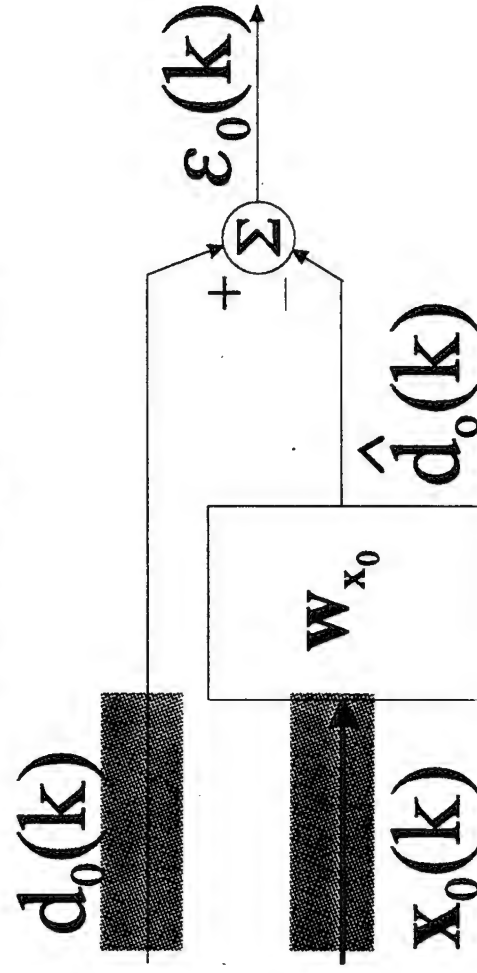


- Find $\mathbf{w}_{x_0} = \mathbf{R}_{x_0}^{-1} \mathbf{r}_{x_0 d_0}$ as a single-port problem:
 - $\mathbf{x}_0 \rightarrow \mathbf{R}_{x_0}$
 - Solve Wiener filter by projections in \mathbf{R}_{x_0} space:
Gram-Schmidt, SVD, etc.
- Single-port problem doesn't use information about d_0 for basis selection



Introduction

New Approach



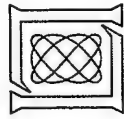
- Find $w_{x_0} = R_{x_0}^{-1} r_{x_0 d_0}$ as a dual-port problem:

$$- \kappa = \begin{bmatrix} d_0 \\ x_0 \end{bmatrix} \longrightarrow R_\kappa = \begin{bmatrix} \sigma_{d_0}^2 & r_{x_0 d_0}^H \\ r_{x_0 d_0} & R_{x_0} \end{bmatrix}$$

- Solve Wiener filter by projections in R_κ space:

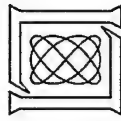
Gram-Schmidt, SVD, etc.

- Dual-port problem uses all available information

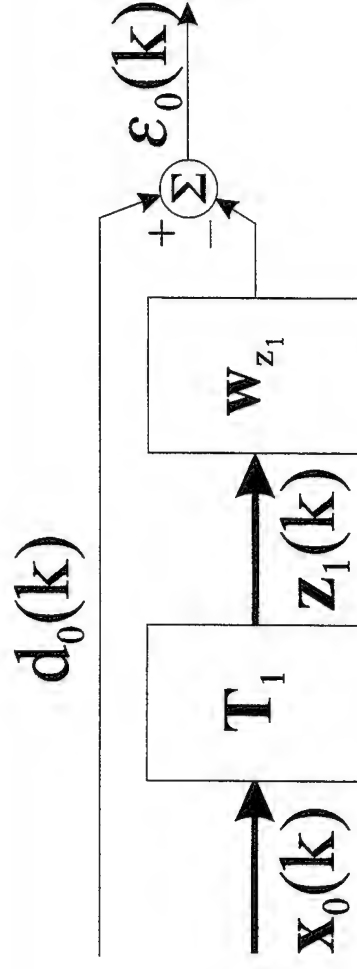


Outline

- Introduction
- The multistage Wiener filter
- Rank reduction
- Example
- Conclusions



An Equivalent Wiener Filter

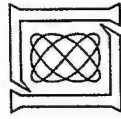


- An equivalent, transformed data vector is formed by T_1 operating on the observed data vector where

$$T_1 = \begin{bmatrix} h_1^H \\ B_1 \end{bmatrix}, \quad h_1 = \frac{r_{x_0 d_0}}{\sqrt{r_{x_0 d_0}^H r_{x_0 d_0}}}$$

- The Wiener filter for the transformed process is computed now to have the form:

$$w_{z_1} = R_{z_1}^{-1} r_{z_1 d_0}$$



An Equivalent Wiener Filter

- The covariance matrix R_{z_1} , its inverse $R_{z_1}^{-1}$ and the cross-correlation vector $r_{z_1 d_0}$ are given by:

$$R_{z_1} = \begin{bmatrix} \sigma_{d_1}^2 & r_{x_1 d_1}^H \\ r_{x_1 d_1} & R_{x_1} \end{bmatrix}$$

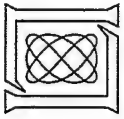
$$R_{z_1}^{-1} = \xi_1^{-1} \begin{bmatrix} 1 & -r_{x_1 d_1}^H R_{x_1}^{-1} \\ -R_{x_1}^{-1} r_{x_1 d_1} & R_{x_1}^{-1} (\xi_1 I + r_{x_1 d_1}^H r_{x_1 d_1} R_{x_1}^{-1}) \end{bmatrix}$$

$$r_{z_1 d_0} = E [z_1(k) d_0^*(k)] = T_1 r_{x_0 d_0} = \begin{bmatrix} \delta_1 & 0 & \dots & 0 \end{bmatrix}^T.$$

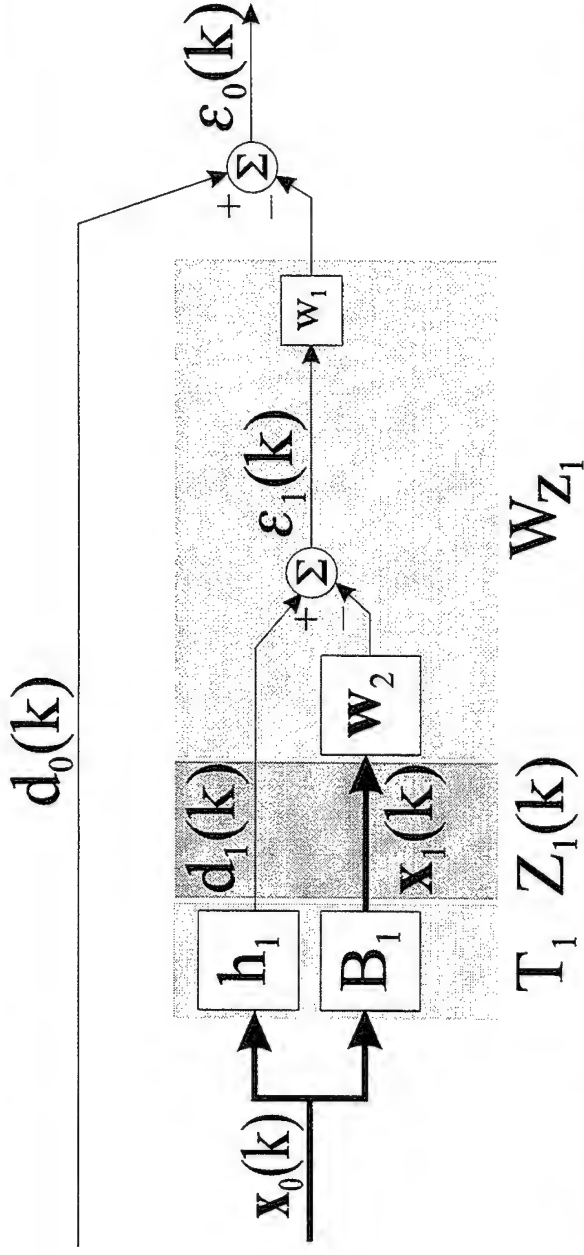
- The Wiener filter for the transformed process is now expressed as

$$w_{z_1} = R_{z_1}^{-1} r_{z_1 d_0} = \xi_1^{-1} \delta_1 \begin{bmatrix} 1 \\ -R_{x_1}^{-1} r_{x_1 d_1} \end{bmatrix}$$

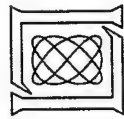
which yields the identical MMSE as the original Wiener filter



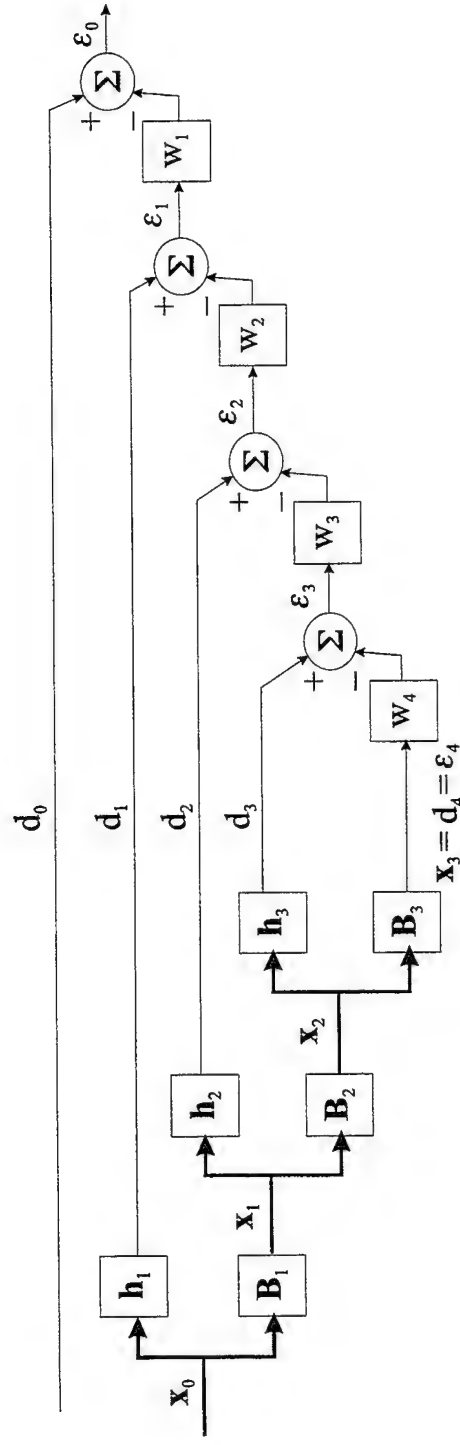
An Equivalent Wiener Filter



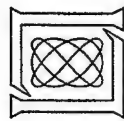
- This structure suggests that a new $(N - 1)$ -dimensional “weight” vector $w_2 = R_{x_1}^{-1} r_{x_1 d_1}$ be defined, which is the Wiener filter for estimating the scalar $d_1(k)$ from the vector $x_1(k)$
- The scalar “weight” vector $w_1 = \xi_1^{-1} \delta_1$ is the Wiener filter for estimating $d_0(k)$ from the error signal $\varepsilon_1(k) = d_1(k) - w_2^H x_1(k)$



The Multistage Wiener Filter

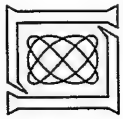


- Continue the recursion until the dimension of both the data and the corresponding Wiener filter is reduced to one at level $(N - 1)$ in the tree



The Decomposition of the Matrix R_K for $N=4$:

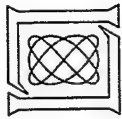
$$\begin{aligned}
& \begin{bmatrix} \sigma_{d_0}^2 & r_{x_0 d_0}^H \\ r_{x_0 d_0} & R_{x_0} \end{bmatrix} \Rightarrow \begin{bmatrix} \sigma_{d_0}^2 & \delta_1^* & 0 & 0 & 0 \\ \delta_1 & \sigma_{d_1}^2 & r_{x_1 d_1}^*(1) & r_{x_1 d_1}^*(2) & r_{x_1 d_1}^*(3) \\ 0 & r_{x_1 d_1}(1) & R_{x_1}(1,1) & R_{x_1}^*(2,1) & R_{x_1}^*(3,1) \\ 0 & r_{x_1 d_1}(2) & R_{x_1}(2,1) & R_{x_1}(2,2) & R_{x_1}^*(3,2) \\ 0 & r_{x_1 d_1}(3) & R_{x_1}(3,1) & R_{x_1}(3,2) & R_{x_1}(3,3) \end{bmatrix} \\
& \Rightarrow \begin{bmatrix} \sigma_{d_0}^2 & \delta_1^* & 0 & 0 & 0 \\ \delta_1 & \sigma_{d_1}^2 & \delta_2^* & 0 & 0 \\ 0 & \delta_2 & \sigma_{d_2}^2 & r_{x_2 d_2}^*(1) & r_{x_2 d_2}^*(2) \\ 0 & 0 & r_{x_2 d_2}(1) & R_{x_2}(1,1) & R_{x_2}^*(2,1) \\ 0 & 0 & r_{x_2 d_2}(2) & R_{x_2}(2,1) & R_{x_2}(2,2) \end{bmatrix} \\
& \Rightarrow \begin{bmatrix} \sigma_{d_0}^2 & \delta_1^* & 0 & 0 & 0 \\ \delta_1 & \sigma_{d_1}^2 & \delta_2^* & 0 & 0 \\ 0 & \delta_2 & \sigma_{d_2}^2 & \delta_3^* & 0 \\ 0 & 0 & \delta_3 & \sigma_{d_3}^2 & \delta_4^* \\ 0 & 0 & 0 & \delta_4 & \sigma_{d_4}^2 \end{bmatrix}
\end{aligned}$$



Outline

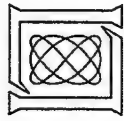
- Introduction
- The multistage Wiener filter
- Rank reduction
- Example
- Conclusions





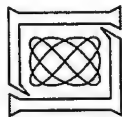
Taxonomy of Data-Dependent Reduced-Rank Methods

METHOD	BASIS	CRITERION
PC	eigenvectors	largest eigenvalues
CSM	eigenvectors	largest contribution to MMSE
MWF	normalized cross-correlation vectors	largest contribution to MMSE

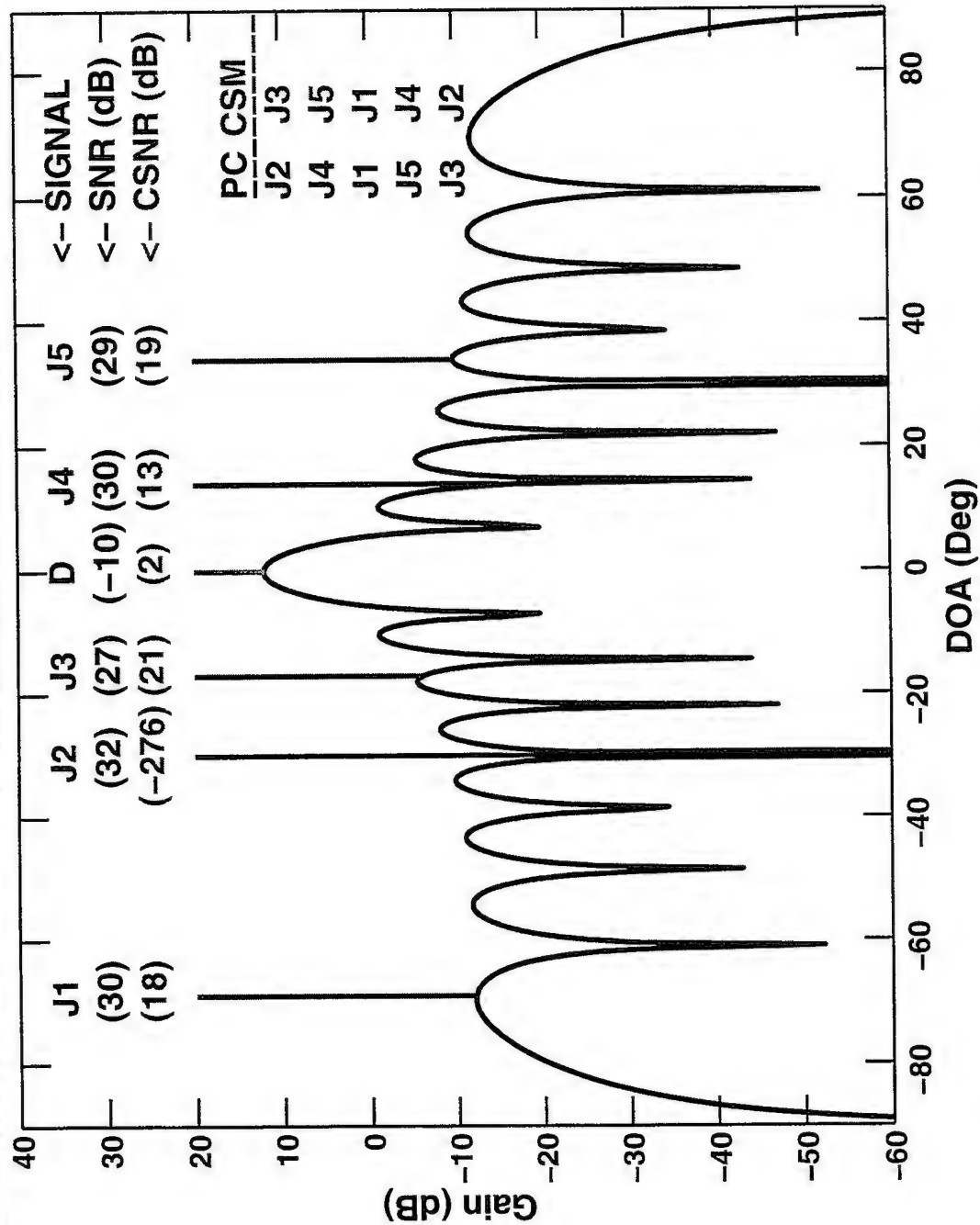


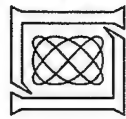
Outline

- Introduction
- The multistage Wiener filter
- Rank reduction
- Example
- Conclusions

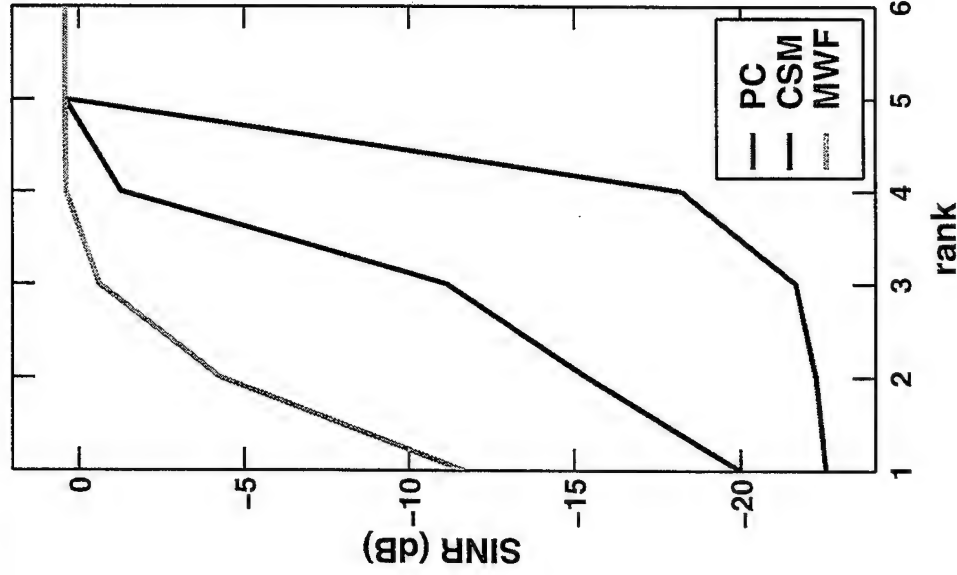


Signal Geometry





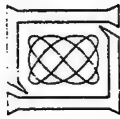
SINR Performance as a Function of Rank



- MWF CHOOSES BASES TO MAX ENERGY
IN CONSTRAINT SUBSPACE

- YIELDS RAPID CONVERGENCE

- CSM ONLY OPTIMIZES EIGENVECTOR
BASIS



Conclusions

- Introduced a new decomposition of the Wiener filter
 - Based on two-port analysis of the Wiener filter
 - Incorporates information about the desired signal
- The multistage Wiener filter represents an efficient structure in terms of its implementation
 - The Householder tridiagonalization technique can be used in the power domain
- Rank reduction can be achieved by truncating the multistage Wiener filter
 - Does not require any eigen-analysis
- Convergence is possible with fewer weights
- Sample-data case is under investigation

S. Unnikrishna Pillai, Y.L. Kim, and Joseph R. Guerci

Polytechnic University
Five Metrotech Center
Brooklyn, New York 11201
tel: (718) 260-3732
email: pillai@arma.poly.edu

Abstract This paper provides a comprehensive strategy for maintaining effective STAP performance while utilizing a parsimonious sample support for adaptive weight training. The need for such minimal sample support techniques is particularly acute in overland operations, where the usual wide sense stationarity assumption with down range is rarely satisfied, often leading to the so-called undernullled clutter problem [1]. The mitigation approach described herein is two pronged: The first element consists of a new closed form expression for the optimal loading factor for generally rank deficient sample covariance matrices. The expression also yields as special cases both the traditional SML covariance estimate when the sample support is very large relative to the number of adaptive degrees-of-freedom (DOFs), and the Hung-Turner projection when the sample support is small [2]-[4]. A new computationally efficient inversion procedure is established for the small sample support case, which can yield up to an order of magnitude reduction in complexity as compared to a direct matrix inversion (DMI) of a diagonally loaded sample covariance matrix. This approach is then combined with new forward-backward smoothing techniques resulting in STAP interference cancellation performance equivalent to SML with a sample support many times greater than the DOFs employed. All results are based on both synthetic and real data sets, the latter originating from the DARPA Mountaintop radar.

- [1] J.R. Guerci, S.U. Pillai and Y.L. Kim, "Empirical Findings of Post-STAP Clutter Cancellation Residual Statistics: A Case for Adaptive Sub-CPI Processing," Post-STAP Detection Technical Interchange Meeting, MIT Lincoln Laboratory, November 8, 1995.
- [2] S.U. Pillai, Y.L. Kim and J.R. Guerci, "An Efficient Implicit Interference Removal Technique for STAP," Proceedings of the Adaptive Sensor Array Processing (ASAP) Workshop, 12-14 March, MIT Lincoln Laboratory, Lexington, MA 1997.
- [3] M. Zatman, "Properties of Hung-Turner Projections and their Relationship to the Eigencanceler," Proceedings of the Thirtieth Annual Asilomar Conference on Signals, Systems and Computers, Monterey, CA, October 29-November 1, 1996.
- [4] C.H. Gierul, "Performance Analysis of Fast Projections of the Hung-Turner Type for Adaptive Beamforming," Signal Processing, vol. 50, 1996.

Strategies for Minimal Sample Support STAP[†]

S. U. Pillai, Y. L. Kim and J. Guerci

Dept. of Electrical Engineering

Polytechnic University

Brooklyn, New York

e-mail: pillai@arma.poly.edu

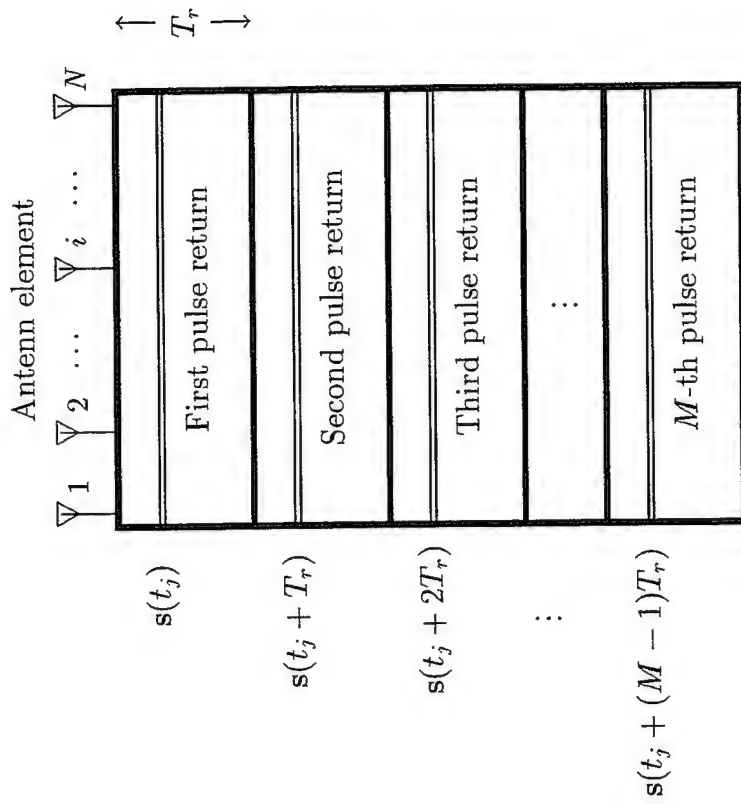
[†]This research was partially supported by the Office of Naval Research under contract N-00014-89-J-1512P-5.

Introduction and Motivation

- Heterogeneous terrain can lead to insufficient sample support for adaptive weight training
 - Severe undernulled clutter
 - Lower Pd (desensitization)
 - Clutter discretes
 - High false alarms
- Techniques for “boosting” available sample support
 - Principal components
 - Optimized loading strategies
 - Implicit interference subspace removal (e.g., Hung-Turner)
 - Generalized F/B “smoothing”

STAP Problem

N sensors; M pulses



j -th range bin Return Signal:

$$\mathbf{x}_j = [\mathbf{s}(t_j), \mathbf{s}(t_j + T_r), \dots, \mathbf{s}(t_j + (M-1)T_r)]^T ; \quad MN \times 1 \text{ vector}$$

Desired Target + (Clutter + Noise)

$$\mathbf{x}_j = \alpha \mathbf{a}_t + \mathbf{x}_c \quad : H_1$$

$$\mathbf{x}_j = \mathbf{x}_c \quad : H_0$$

Target steering vector : $\mathbf{a}_t = \mathbf{a}(\theta, \omega_d) = \mathbf{a}_2(\omega_d) \otimes \mathbf{a}_1(\theta)$

$$\mathbf{a}_1(\theta) = \begin{bmatrix} 1 \\ e^{-j\pi \sin \theta} \\ \vdots \\ e^{-j\pi(N-1) \sin \theta} \end{bmatrix}, \quad \mathbf{a}_2(\omega_d) = \begin{bmatrix} 1 \\ e^{j2\pi\omega_d} \\ \vdots \\ e^{j2\pi(M-1)\omega_d} \end{bmatrix}$$

- Find weight vector \mathbf{w} so that

$$z = \mathbf{w}^* \mathbf{x}_j$$

can be used for threshold detection optimally.

Maximize output signal to interference plus noise ratio (SINR).

- The total output power under H_1 :

$$P_{\text{out}} = E\{|z_j|^2\} = P_t |\mathbf{w}^* \mathbf{a}_t|^2 + \mathbf{w}^* R_c \mathbf{w}.$$

where

$$R_c = E\{\mathbf{x}_c \mathbf{x}_c^*\}$$

represents the interference (clutter + noise) covariance matrix.

$$\text{SINR}_{\text{out}} = \frac{P_t |\mathbf{w}^* \mathbf{a}_t|^2}{\mathbf{w}^* R_c \mathbf{w}}$$

- Optimum weight vector:

$$\boxed{\mathbf{w}_o = R_c^{-1} \mathbf{a}_t}$$

R_c is $MN \times MN$; Usually unknown.

- Sample Matrix Inversion (SMI) Method

$$\hat{R}_c = \frac{1}{k} \sum_{i=1}^k \mathbf{x}_i \mathbf{x}_i^* .$$

Problems

- High Computational Complexity:
 - ◊ We need $k > MN$ to invert \hat{R}_c .
 - ◊ Matrix inversion of size MN . (BAM inversion method etc.)
- Sample Data Support Problem:
 - ◊ Nonstationarity of the neighboring range bin data.
 - ◊ \hat{R}_c is not an optimal estimate when the samples are not stationary.

Eigencanceller Method

- Clutter subspace dimension $r \ll MN$

$$r \approx N(M-1)\beta.$$

$$R_c = U \text{diag}[\lambda_1, \lambda_2, \dots, \lambda_r, \sigma^2, \dots, \sigma^2] U^*$$

$$U = [\mathbf{u}_1, \mathbf{u}_2, \dots, \mathbf{u}_r, \mathbf{u}_{r+1}, \dots, \mathbf{u}_{MN}]$$

Optimal Solution

$$\mathbf{w}_o = R_c^{-1} \mathbf{a}_t = \mathbf{a}_t - \sum_{i=1}^r p_i \mathbf{u}_i \quad ; \quad p_i = \left(1 - \frac{\sigma^2}{\lambda_i}\right) \mathbf{u}_i^* \mathbf{a}_t \quad (1)$$

- Use (1) directly to compute \mathbf{w}_o (Eigencanceller method).
- Needs less number of samples in this case.
- Need to evaluate the clutter subspace eigenvectors $\mathbf{u}_1, \mathbf{u}_2, \dots, \mathbf{u}_r$. Should know r . Somewhat messy.

Implicit Subspace Removal (ISR) method

- Can achieve the same performance, without performing an eigen-decomposition of \hat{R}_c !

$$\hat{R}_k = \frac{1}{k} \sum_{i=1}^k \mathbf{x}_i \mathbf{x}_i^* = \frac{1}{k} Y_k Y_k^*, \quad k < MN$$

$$Y_k = [\mathbf{x}_1, \mathbf{x}_2, \dots, \mathbf{x}_k] \text{ is } MN \times k$$

$$k < MN \Rightarrow \hat{R}_k + \epsilon I = \frac{1}{k} Y_k Y_k^* + \epsilon I \triangleq \hat{R}_\epsilon$$

$$(P^{-1} + MQ^{-1}M^*)^{-1} = P - PM(M^*PM + Q)^{-1}M^*P$$

$$\hat{R}_\epsilon^{-1} = \frac{1}{\epsilon} [I - Y_k(Y_k^*Y_k + \epsilon kI)^{-1}Y_k^*] \quad (2)$$

$$\hat{\mathbf{w}}_k = \lim_{\epsilon \rightarrow 0} \epsilon \hat{R}_\epsilon^{-1} \mathbf{a}_t = \mathbf{a}_t - Y_k(Y_k^*Y_k)^{-1}Y_k^* \mathbf{a}_t = \mathbf{a}_t - \sum_{i=1}^r p'_i \mathbf{u}_i \quad (3)$$

- (3) has the same form as the Eigencanceller method (1).

- Inversion of a $k \times k$ ($k \ll MN$) matrix $Y_k Y_k^*$ only is required. Same as Hung-Turner (HT) projection method ($\epsilon = 0$).
- What if $\epsilon \neq 0$? What is the optimal ϵ ?
- $\epsilon \neq 0$ case can also be realized with same computations! (use (2))

$$\mathbf{w}_\epsilon = \hat{R}^{-1} \mathbf{a}_t - \sum_{i=1}^{MN-1} p''_i \mathbf{u}_i \quad (4)$$

$$p''_i = \frac{\lambda_i - \lambda_\nu}{\lambda_i - \epsilon} \mathbf{u}_i^* \mathbf{a}_t$$

- For optimum ϵ -case, weight vector \mathbf{w}_ϵ should look like (1) and (3).
- Thus $p''_{r+1}, p''_{r+2}, \dots, p''_{MN-1}$ should be minimized. Thus

$$\epsilon_{\text{opt}} = -\lambda_\nu + \sqrt{(\lambda_r - \lambda_\nu)(\lambda_{r+1} - \lambda_\nu)}, \quad \nu = MN.$$

- Case 1 : $k > MN \Rightarrow \lambda_{r+1} = \lambda_{r+2} = \dots = \lambda_\nu = \sigma^2$

$$\epsilon_{\text{opt}} = 0$$

- Case 2 : $r < k < MN \Rightarrow \lambda_\nu = 0$

$$\epsilon_{\text{opt}} = \sqrt{\lambda_r \lambda_{r+1}}$$

- Case 3 : $k < r \Rightarrow \lambda_r = \lambda_{r+1} = \dots = \lambda_\nu = 0$

$$\epsilon_{\text{opt}} = 0$$

\Rightarrow For too many samples as well as for too few samples, use no diagonal loading for optimum performance; otherwise use optimal loading (Implicit Subspace Removal).

Further improvement by forward/backward averaging. (reverse and complex conjugate each data sample vector.)

Backward Data

- Let \mathbf{x}^b represent complex conjugated and reversed form of \mathbf{x} .

$$\mathbf{x}^b \triangleq J\bar{\mathbf{x}} : \text{“Backward” data} = \sum_{k=1}^L \alpha_k^* e^{j\psi_o} \mathbf{a}_k$$

$$\psi_o = \pi\{(N-1)d \sin \theta + 2(M-1)\omega_d\}$$

- Backward data has the same covariance matrix as the forward data in an uncorrelated scene.

$$E\{\mathbf{x}^b \mathbf{x}^{b*}\} = \sum_{k=1}^L p_k \mathbf{a}_k \mathbf{a}_k^* = E\{\mathbf{x} \mathbf{x}^*\},$$

$$\text{where } p_k = E\{|\alpha_k|^2\}.$$

- Backward data is uncorrelated with forward data and acts as new samples.

$$E\{\mathbf{x}^b \mathbf{x}^*\} = 0.$$

- Hence available data samples :

$$Y_k^{f/b} = [\mathbf{x}_1, \mathbf{x}_2, \dots, \mathbf{x}_k, \mathbf{x}_1^b, \mathbf{x}_2^b, \dots, \mathbf{x}_k^b]$$

$2k$ samples are available!

Figure 1. SINR improvement factors vs. Number of samples.

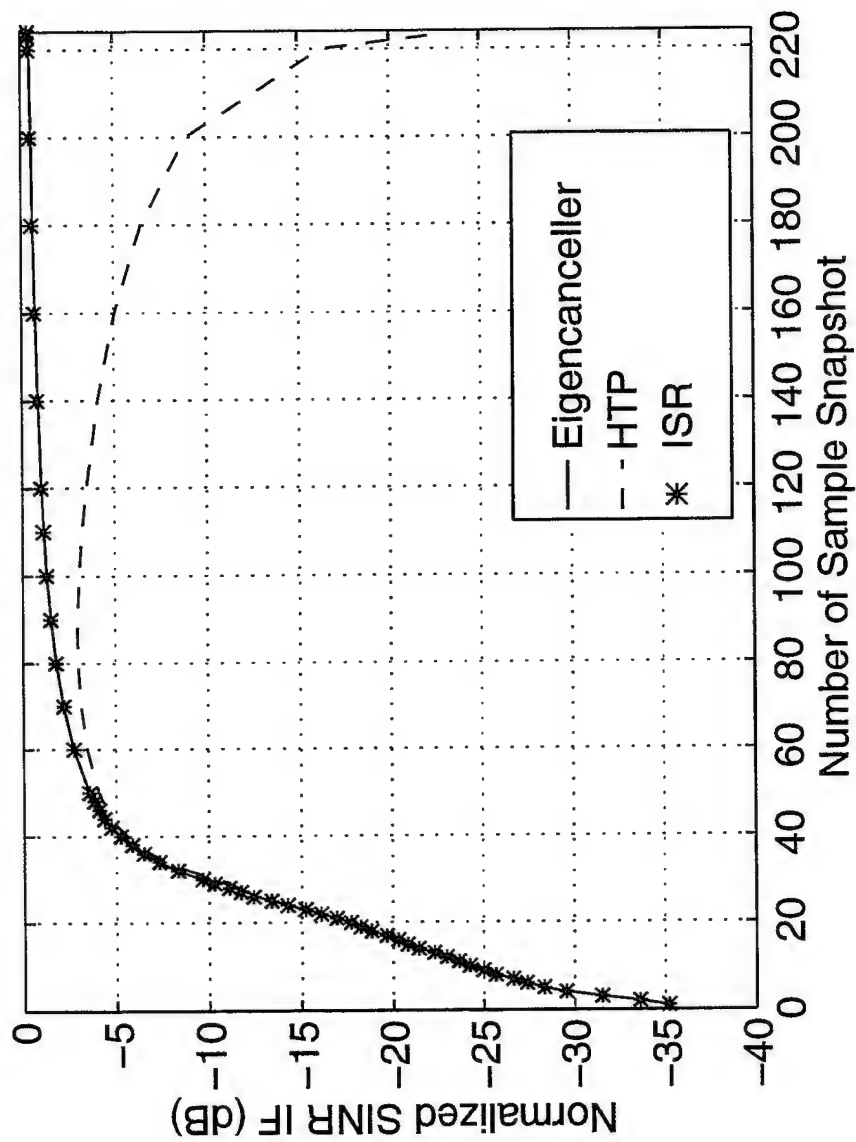


Figure 2. SINR vs. Loading Factor.
 With $k = 300$ ($k > MN$),

$$\delta_o = \frac{-\lambda_{MN} + \sqrt{(\lambda_{32} - \lambda_{MN})(\lambda_{33} - \lambda_{MN})}}{\lambda_{32} - \lambda_{MN}}.$$

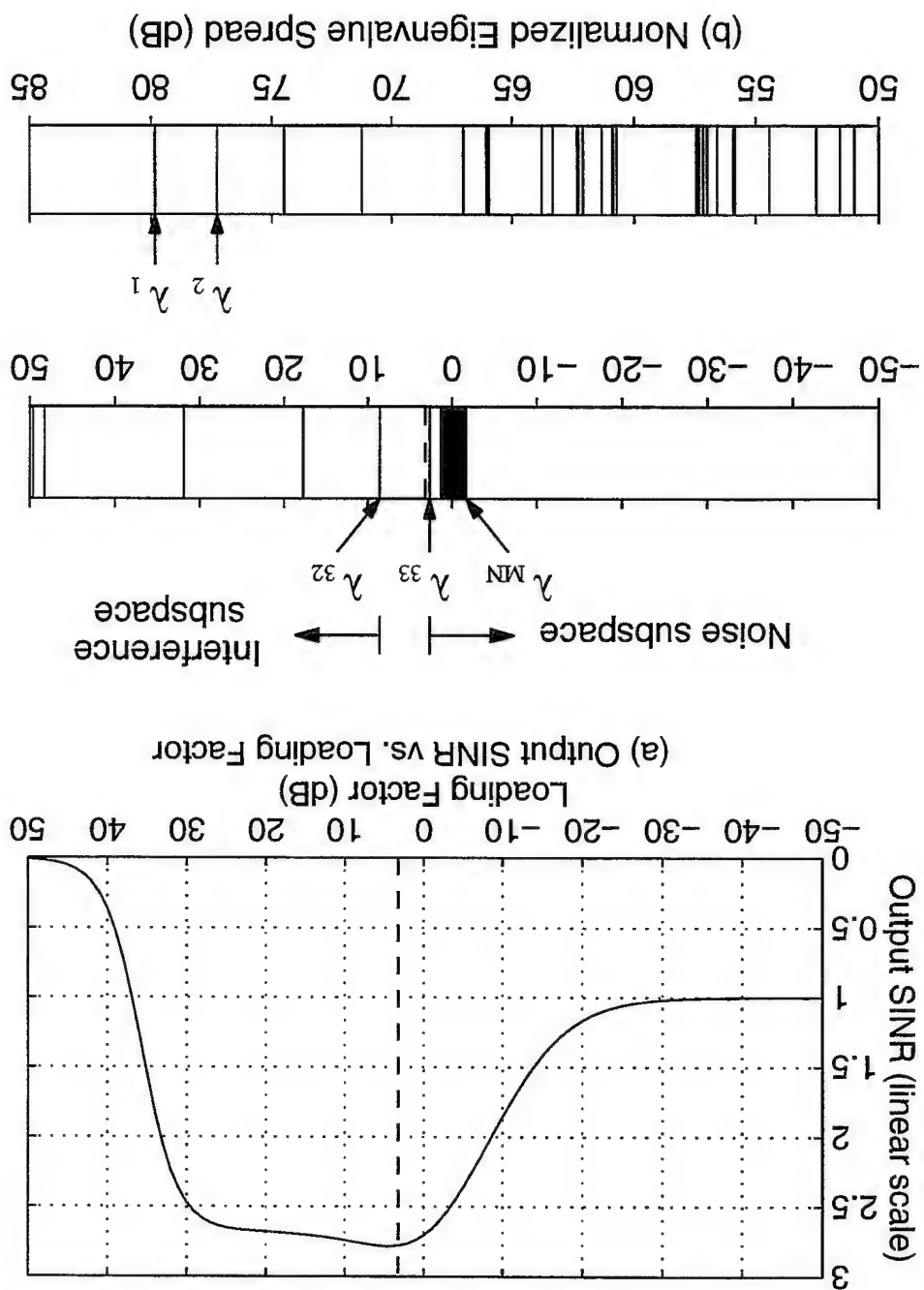
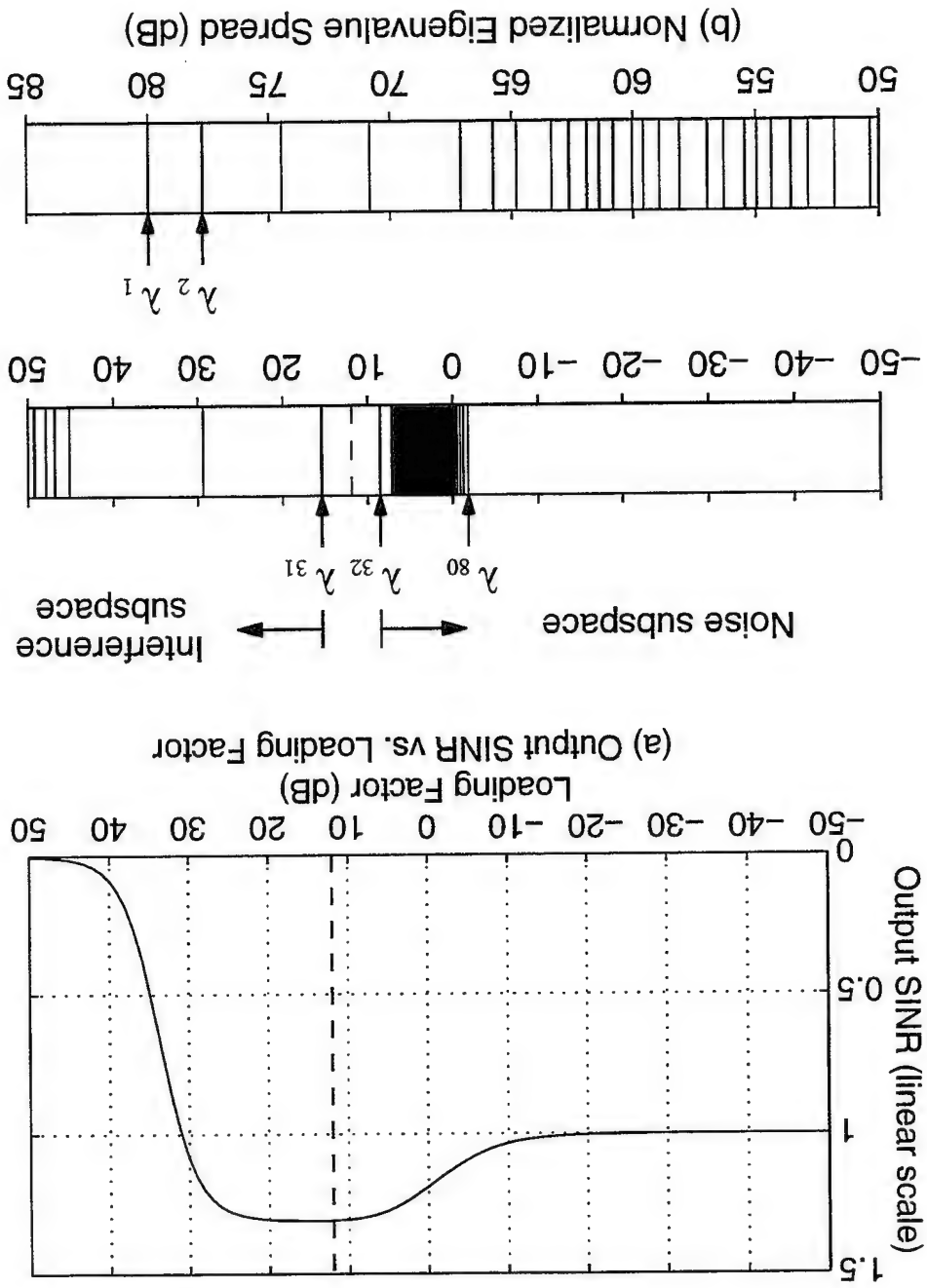


Figure 3. SINR vs. Loading Factor.
 With $k = 80$ ($r < k < MN$), $\delta_o = \sqrt{\lambda_{31}\lambda_{32}}$.



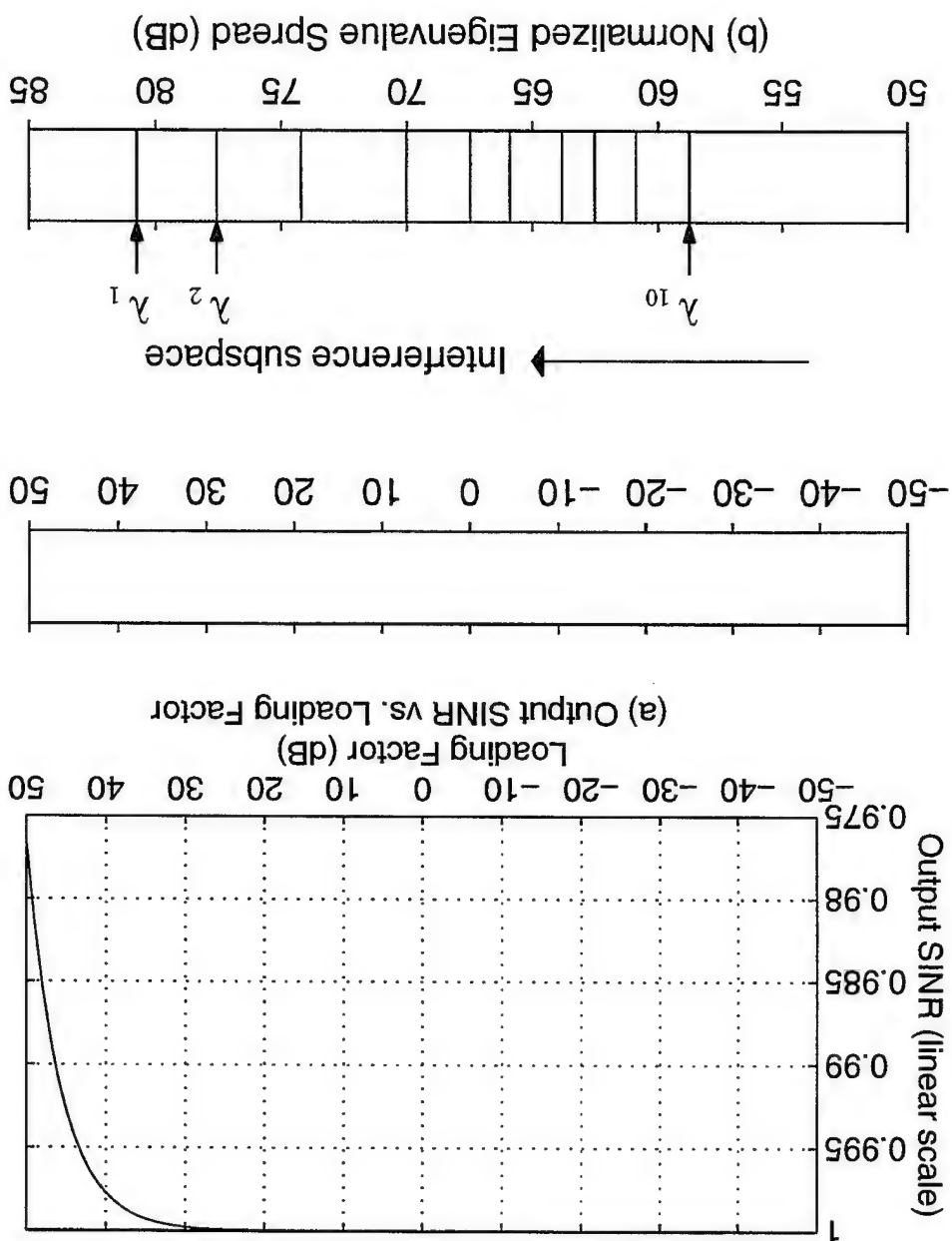
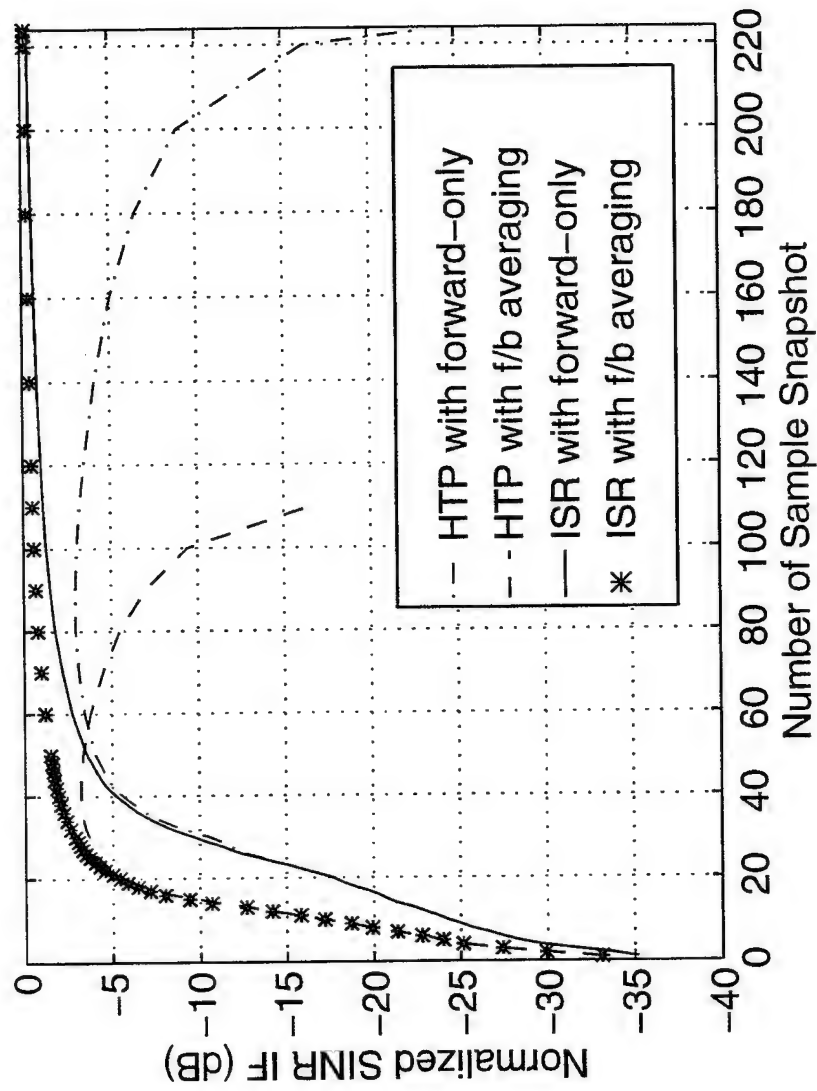


Figure 4. SINR vs. Loading Factor.
With $k = 10$ ($k < r$), $\delta_o = 0$.

Figure 5. SINR improvement factors vs. Number of samples.



Generalized Forward/Backward Subaperture Techniques

A new approach to “boost up” the sample data support.

STAP Data Structure

- Array output : $\mathbf{s}(t_i) = [x_1(t_i), x_2(t_i), \dots, x_N(t_i)]^T$
- MN -dimensional data vector that contains M pulse returns from L independent scatterers :

$$\mathbf{x}_i = \begin{bmatrix} \mathbf{s}(t_i) \\ \mathbf{s}(t_i + T) \\ \vdots \\ \mathbf{s}(t_i + (M-1)T) \end{bmatrix} = \sum_{k=1}^L \alpha_k \mathbf{a}_k$$

- $MN \times k$ data matrix with k available samples

$$Y_k = [\mathbf{x}_1, \mathbf{x}_2, \dots, \mathbf{x}_k] : \text{“Forward” data}$$

Subpulse Approach

Use only M_s pulse returns at a time

$$\mathbf{x}_i = \begin{bmatrix} \mathbf{s}(t_i) \\ \mathbf{s}(t_i + T) \\ \vdots \\ \mathbf{s}(t_i + (M_s - 1)T) \\ \vdots \\ \mathbf{s}(t_i + (M - 1)T) \end{bmatrix} \quad \begin{matrix} \mathbf{x}_{i,1}^f & \cdots & \mathbf{x}_{i,M-M_s+1}^f \end{matrix}$$

- $M - M_s + 1$ forward samples each of size $M_s N \times 1$.

$$[\mathbf{x}_{i,1}^f, \mathbf{x}_{i,2}^f, \cdots, \mathbf{x}_{i,M-M_s+1}^f]$$

- Also an equal number of backward samples $\mathbf{x}_{i,1}^b, \mathbf{x}_{i,2}^b, \dots, \mathbf{x}_{i,M-M_s+1}^b$ are available.
- All of these samples have the same covariance matrices.
- Forward/backward subpulse data matrix

$$Z_k = [W_1, W_2, \dots, W_k]$$

of size $M_s N \times 2(M - M_s + 1)$ matrix, where

$$W_i = [\mathbf{x}_{i,1}^f, \mathbf{x}_{i,2}^f, \dots, \mathbf{x}_{i,M-M_s+1}^f, \mathbf{x}_{i,1}^b, \mathbf{x}_{i,2}^b, \dots].$$

- $2k(M - M_s + 1)$ samples are available!
- Aperture size is $M_s N$.
- Ex: If $M_s = M - 1$, then $4k$ samples are available!

Subarray Approach

Use only N_s elements at a time.

$$\mathbf{s}(t_i) = \begin{bmatrix} x_1(t_i) \\ x_2(t_i) \\ \vdots \\ x_{N_s}(t_i) \\ \vdots \\ x_N(t_i) \end{bmatrix} \quad \begin{matrix} \mathbf{z}_1^f(t_i) & \dots & \mathbf{z}_{N-N_s+1}^f(t_i) \end{matrix}$$

- Effective sample size is $2k(N - N_s + 1)$.
- Aperture size is MN_s .

Subarray-Subpulse Approach

Use M_s pulses and subarrays of size N_s simultaneously.

- Total number of forward/backward subarray-subpulse samples is $2k(M - M_s + 1)(N - N_s + 1)$.
- Aperture dimension is $M_s N_s$ instead of MN .
- Let $M_s = M - 1$, $N_s = N - 1$. This gives $8k$ samples for somewhat slightly reduced aperture.
- Perform ISR on these data samples.

Figure 6. SINR improvement factors vs. Number of samples.

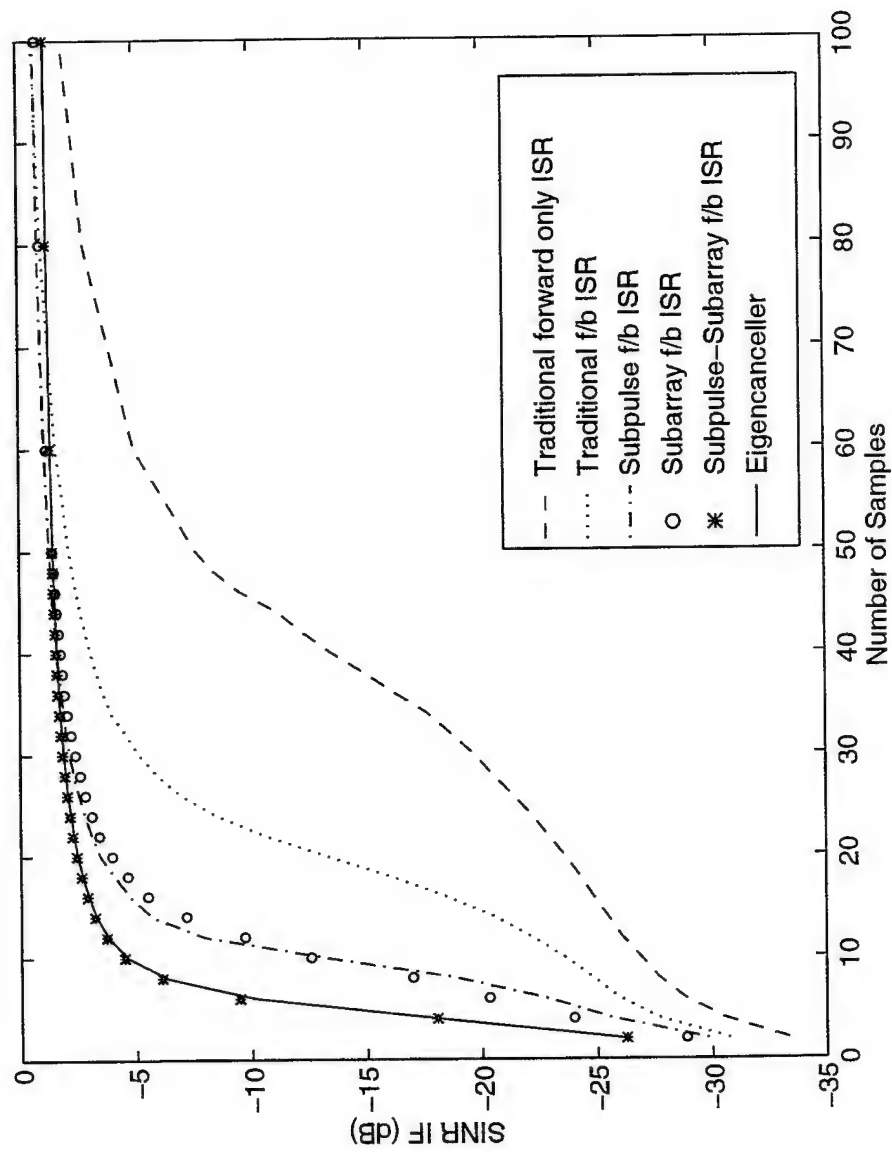


Figure 7. Adaptive Gain Patterns with $k = 10$.

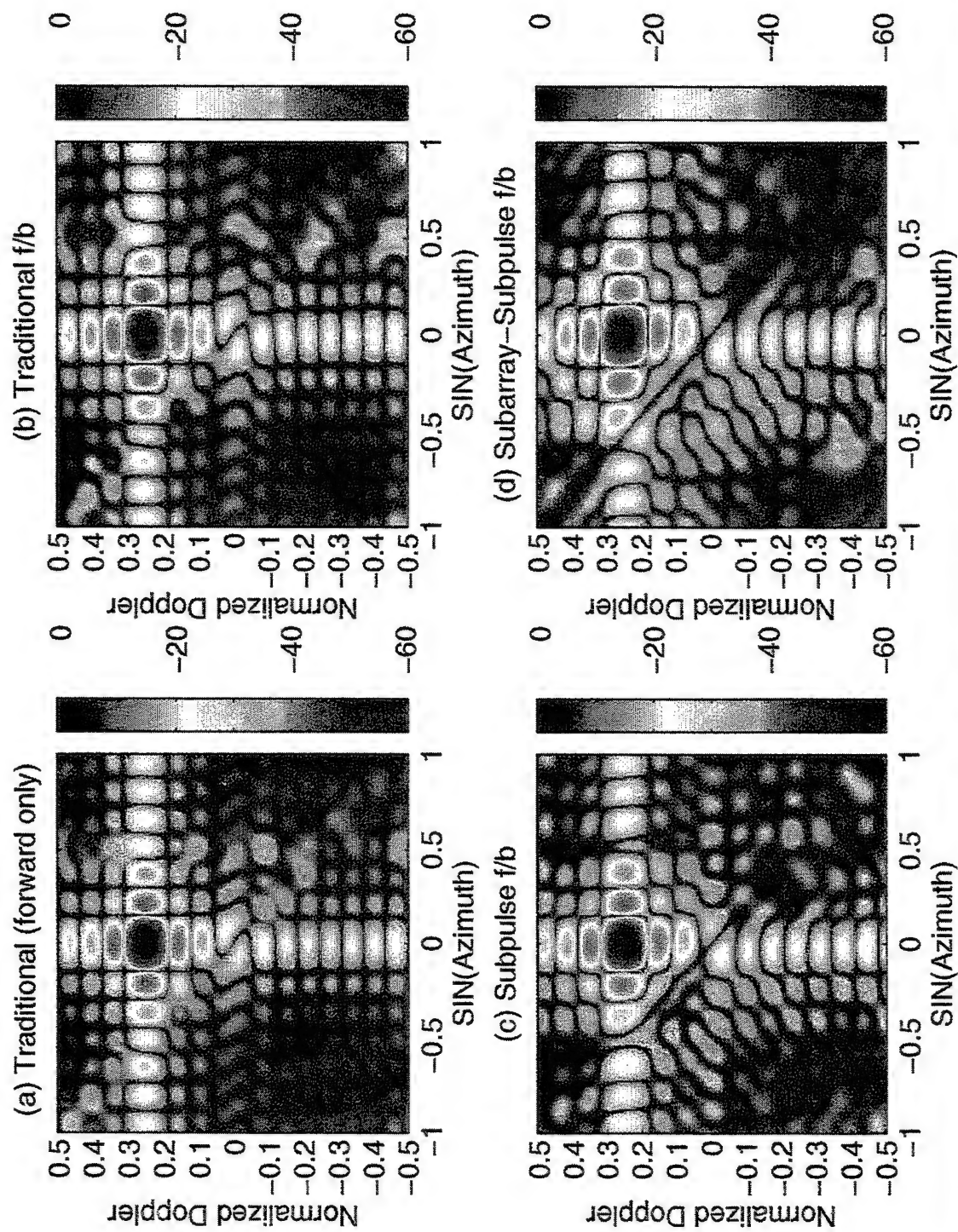
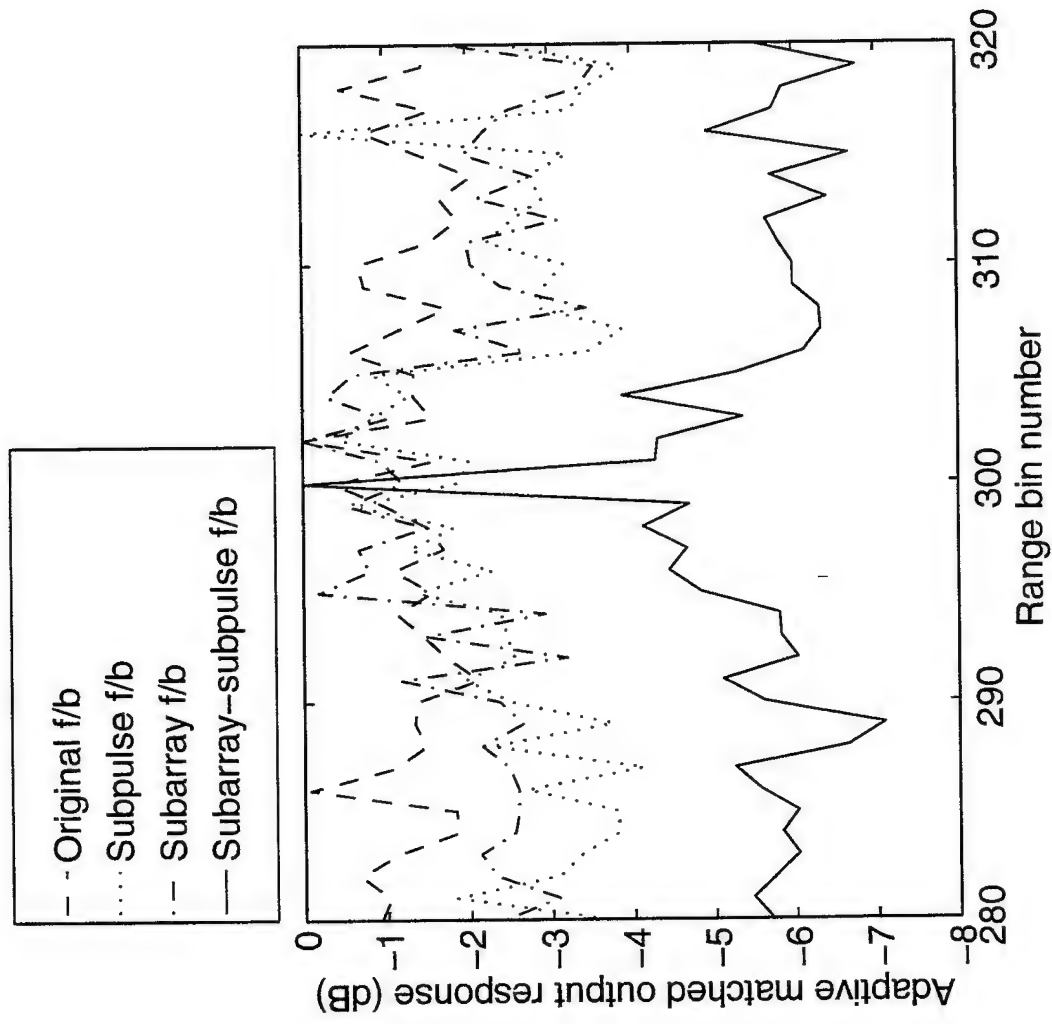


Figure 8. Adaptive Matched Filter Output with $k = 10$.



Daniel J. Rabideau

MIT Lincoln Laboratory
244 Wood Street, Room J-118D
Lexington, MA 02173-9108
tel: (781) 981-2892
email: danr@ll.mit.edu

Abstract This paper addresses the problem of adaptively canceling both conventional clutter and terrain-scattered jamming (TSJ) in airborne radar systems. Many traditional algorithms for this problem have involved first adapting in space/fast-time to cancel TSJ, then adapting in space/slow-time to cancel conventional clutter. Unfortunately, the rapid updating required to cancel the nonstationary TSJ will modulate the clutter and targets, making the cancellation of conventional clutter extremely difficult and reducing the metric accuracy of the reported target locations. In this paper, we build on the foundation laid in [1] to give detailed descriptions of several novel algorithms for handling modulated clutter and targets. First a multi-stage beamformer is described which prevents the modulated clutter from degrading system performance. Second, a reduced DOF 3 dimensional STAP algorithm is employed to cancel TSJ and clutter together. Third, we compare conventional pre and post-Doppler STAP algorithms and show that pre-Doppler STAP is better suited to modulated clutter, but that a modified post-Doppler STAP algorithm employing detached bins can also perform well. Finally, we propose a multidimensional sidelobe target editing algorithm which can be used to find the correct target location from many modulated target echoes. In each case, a formulation of the processor is presented and its properties are described. Examples showing the application of these proposed structures to site-specific simulated data sets are used to illustrate their performance.

[1] D. Rabideau, "Signal Modulation in Pulse-By-Pulse Adaptive Nulling Systems," Proc. Adaptive Sensor Array Proc. Workshop, 1997.



Advanced STAP for TSI Modulated Clutter

Daniel J. Rabideau
Lincoln Laboratory
Massachusetts Institute of Technology

1998 Adaptive Sensor Array Processing Workshop

This work was sponsored by DARPA under Air Force Contract #F19628-95-C-0002. Opinions, interpretations, conclusions and recommendations are those of the author and are not necessarily endorsed by the United States Air Force.

MIT Lincoln Laboratory

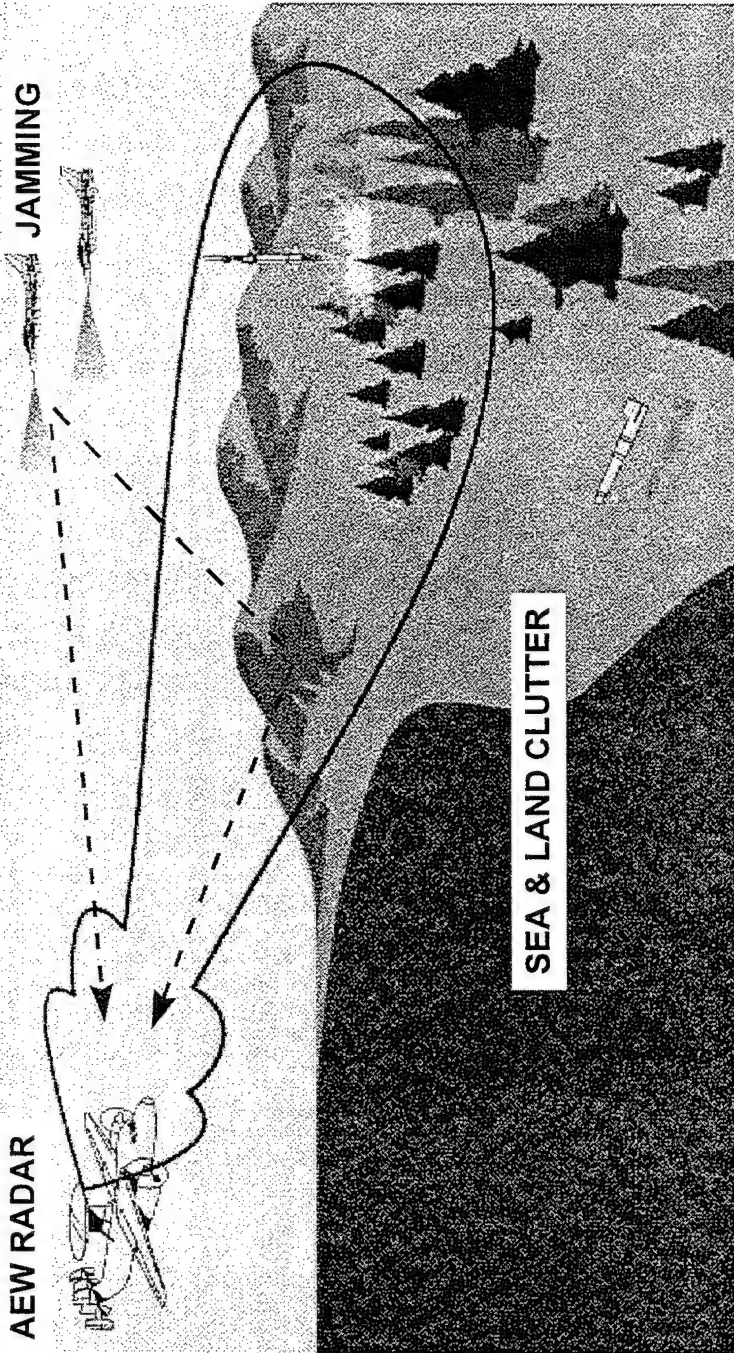
/Documents/ASAP'98/charts.ppt
2/11/98

1

In this paper, I will present new results on the cancellation of TSI and conventional radar clutter. The new algorithms that will be presented are specially constructed to deal with the problem of TSI-induced signal modulation, which we analyzed at last year's workshop.



AEW Interference Environment



- Radar receives combined TSI and monostatic clutter

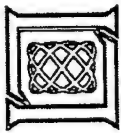
/documents/ASAP'96/charts.ppt
2/11/98

MIT Lincoln Laboratory

2

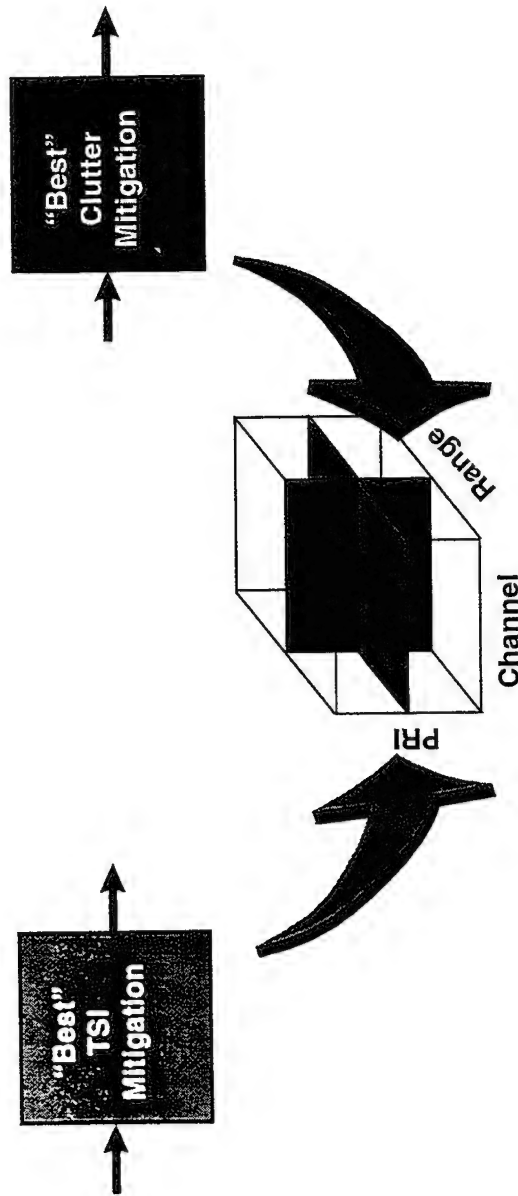
In airborne radar, the receiver is confronted with 2 very different types of interference. First, because the radar transmits a large amount of energy toward the ground to see small, low-flying targets, it must contend with a fraction of that energy which is reflected off the ground and back into the receiver. This is what we call clutter. It is correlated spatially and in PRI-time, and we can use conventional Space-Time Adaptive Processing (STAP) techniques to remove this interference.

Second, other signal sources may be operating in the same band. Often, these jamming signals are received in the sidelobes of the receiver. They can then be canceled using spatial-only adaptive processing. However, some of the jammer's energy may also be reflected from multiple points on the ground -- covering a wide angular sector -- and back into the receiver. This is called Terrain Scattered Interference (TSI). When TSI is present, spatial-only processing is of limited utility. However, since the reflected paths are time-delayed and phase shifted versions of the direct-path signal, Space-Time Adaptive Processing can still be used to remove this interference. In this case, "time" refers to delays on the order of the difference in path delays. One important thing to notice is that (due to platform motion) the TSI is will be nonstationary over long periods of time. Because of this, the STAP weights used to cancel the TSI must be updated frequently.



TSI & Clutter Cancellation

One View of the World ...



- Question: Best TSI/Clutter Mitigation = Best TSI + Best Clutter?

/Documents/ASAP'98/cherita.ppt
2/11/98

MIT Lincoln Laboratory

3

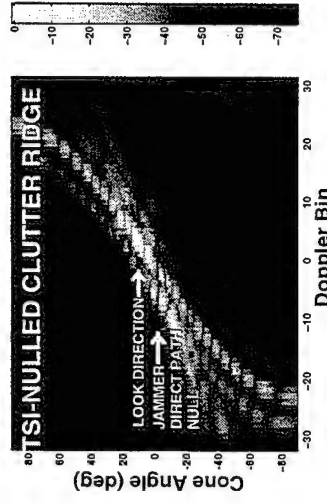
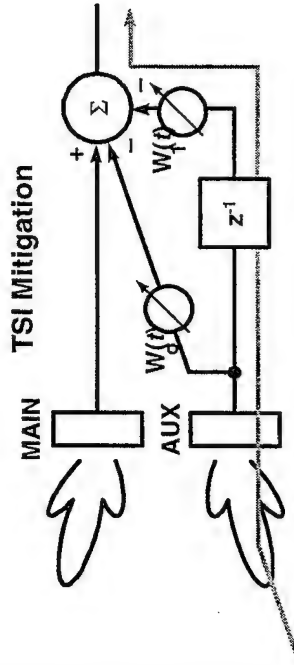
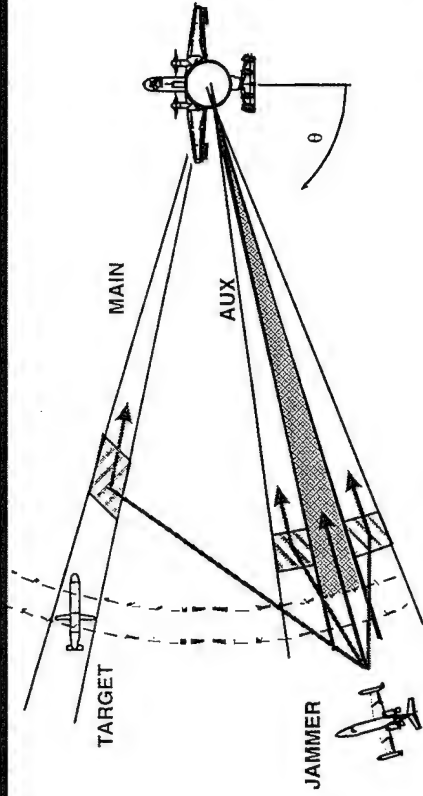
There has been a great deal of work focused on the cancellation of TSI only (and on the cancellation of clutter only). We have seen that the TSI can be canceled using STAP in the space/fast-time subspace of the radar data cube; clutter, on the other hand, can be canceled by using STAP in the space/slow-time subspace.

It is tempting, then, to try approaching the problem of combined TSI and clutter by using a factored architecture as shown: first cancel the TSI, then the clutter. But, is this really the best way to proceed?

The answer is no! This is because the TSI canceller modulates the clutter, making its subsequent cancellation very difficult.



TSI-Induced Clutter Modulation



- TSI weights must modulate to cancel TSI, but this modulates all other signals too! (including clutter & targets)

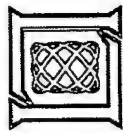
/Documents/ASAP98/charte.ppt
2/11/98

MIT Lincoln Laboratory

4

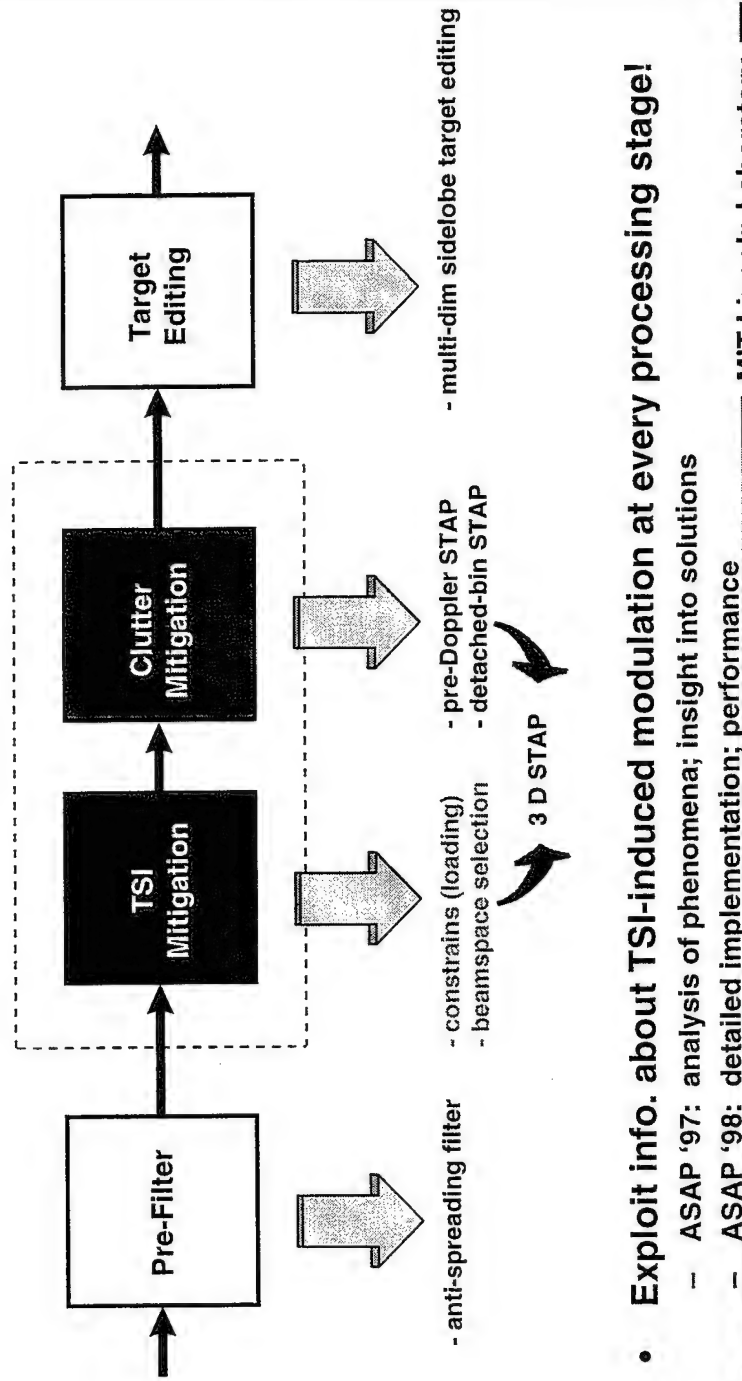
What is "TSI-induced modulation"? Simply put, the TSI-canceling adaptive beamformer collects jammer energy from the sidelobes, phase-shifting and time-delaying it to cancel the correlated energy received in the mainlobe. Recall that these weights must change over time because the TSI is nonstationary.

Also note that the clutter and targets must pass through the *same* adaptive filter. As a result, they will experience the same time-varying phase shifts. This process can take a relatively benign clutter "ridge" and modulate it in Doppler, spreading it over a much broader region in the angle-Doppler plane. The spread pattern will differ from beam to beam. It is this modulated clutter which needs to be canceled by the subsequent clutter-canceling STAP processor.



TSL & Clutter Cancellation

Another View of the World ...



- **Exploit info. about TSL-induced modulation at every processing stage!**

- ASAP '97: analysis of phenomena; insight into solutions
- ASAP '98: detailed implementation; performance

/Documents/ASAP'98/charts.ppt
2/11/98

MIT Lincoln Laboratory

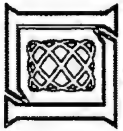
5

So, in our enlightened view of the world, we see that we must CAREFULLY consider how TSL-induced modulations will effect the performance of EACH processing stage, and thus the end-to-end system performance.

More to the point, we would like to exploit our knowledge of how modulation is introduced at each processing stage to compensate for this effect.

At the most basic level, this means constructing TSL and clutter canceling processors which work together, as a team, to minimize modulated clutter. Beyond that, it means pre-conditioning the data to minimize the ill-effects of modulated clutter, as well as post-processing the data to clean-up the modulated targets. The bottom line is: at each stage of processing, exploit what we know about the modulation to improve overall performance.

At last years workshop, we introduced this basic philosophy. We also identified some basic approaches that could be used. This paper expands on this foundation, giving detailed algorithm descriptions and performance evaluations.

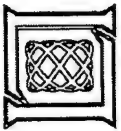


Outline

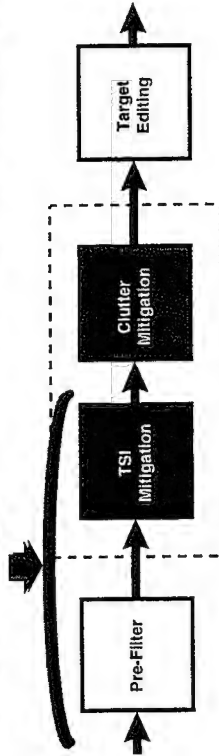
"Exploit info. about TSI-induced modulation at every processing stage ..."

- Introduction
- ➡ • **Strategies for TSI-Induced Modulation**
- Summary

The last chart listed a number of techniques -- at each stage of processing -- for dealing with TSI-induced modulation. Conceptually, ALL of these techniques utilize one of perhaps two very basic and intuitively appealing strategies.

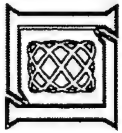


Strategy #1: Prevention



- Objective: Prevent clutter from modulating
- Methods:
 - Pre-Filters
 - 3D STAP
 - TSI beamformer constraints, Beamspace selection

I call the first of these strategies "prevention." Techniques that utilize this strategy attempt to prevent clutter from modulating *from the start*. Because the modulation is introduced by the TSI-canceller, these strategies are associated with the left side of the flow diagram above. There are several techniques which use this strategy (grayed-out topics were discussed at length during last years workshop and will not be dealt with here).



Pre-Filtering Concept

Objective: Prevent clutter modulation

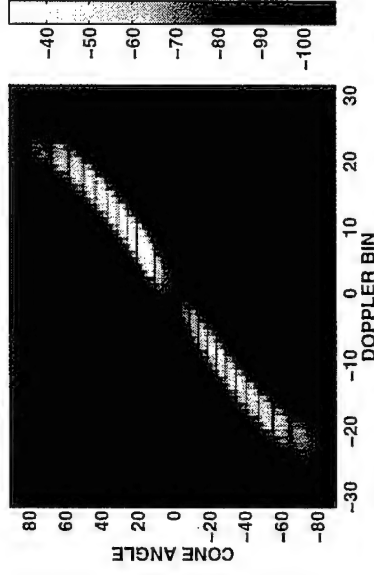
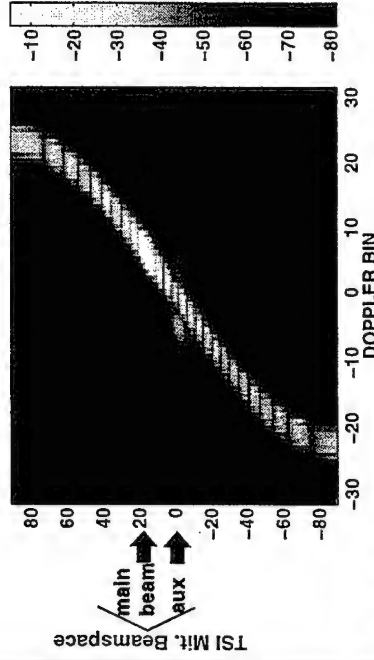
Approach: 1. Identify "which" clutter will be modulated
2. Design a filter to mitigate this clutter
(100% cancellation not required)

the filter's structure depends on the TSI cancellation architecture

Clutter at Sel. Aux. TSI beamformer output

without pre-filtering

with pre-filtering



MIT Lincoln Laboratory

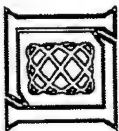
/documents/ASAP-98/charte.ppt
2/11/96

8

The first of our prevention strategies is "pre-filtering". Pre-filters approach the problem of preventing clutter modulation by:

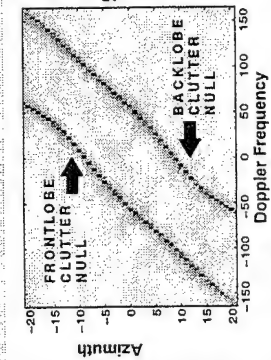
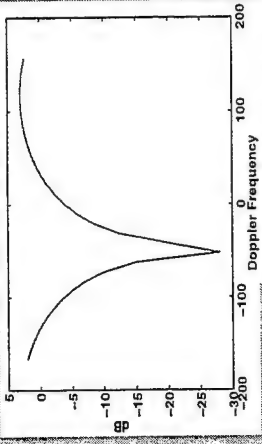
1st) identifying which parts of the clutter ellipse will be modulated

2nd) designing a pre-filter which reduces this clutter. The clutter does not need to be removed completely. It just needs to be attenuated to the point where, after modulation, it is below the noise. Thus, both adaptive and nonadaptive strategies may be useful.



Pre-Filtering Algorithms

- Filter Choice Depends on subsequent TSI algorithm

TSI Algorithm	Beamspace 2D STAP (i.e., extended Beamspace)	Selected Aux.
Which clutter will modulate?	Broad region of clutter ridge	Selected "spots" along the clutter ridge.
Example Pre-Filter	<p>"Elliptic" filter (McClellan et. al.)</p>  <p> $a_{n_1, n_2} \leftrightarrow A(e^{j\omega_1}, e^{j\omega_2}), n_1 = 0 \dots 2$ $\Rightarrow [1 + a_{0,1}]k^2 - 2[a_{0,0} - a_{0,2}]k + a_{1,0} = -1$ where $k = \text{slope of clutter ridge}$. Choose clutter points (w_1, w_2) & solve weighted LS (weighted by Tx pattern) </p>	<p>Optimized 1D notch filter (strong clutter)</p>  <p> Data matrix: $X = \text{hankel}(x_{1,p}^p, x_{2,p}^p)$ (... p tap filter, range gatep) Covar. Est: $R = \frac{1}{R} \sum_p X X^H$ Weights: $w = \arg \max_w (w^H R w)$ </p>



/Documents/ASAP'98/charts.ppt
2/11/98

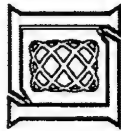
MIT Lincoln Laboratory

9

Because the pre-filter only needs to filter-out select clutter regions, the architecture of this pre-filter must be well-matched to the architecture of the subsequent TSI canceller. At last year's workshop, we saw that the beamspace used to cancel the TSI plays a dominant role in determining the location of the clutter which will be modulated. I have chosen two extreme examples (above) to high-light how pre-filters might be designed here.

On the left, we consider pre-filters which would be appropriate for use with TSI cancellers that process data in an extended beamspace (or, element space). These cancellers modulate clutter over an extended region of the clutter ridge. Our pre-filter must cancel this clutter... so we want to place nulls along an extended region of the clutter ridge. Many filter techniques are available. One that I like is the 2D FIR filter technique based on Power Series expansions, presented by McClellan at ASAP 96.

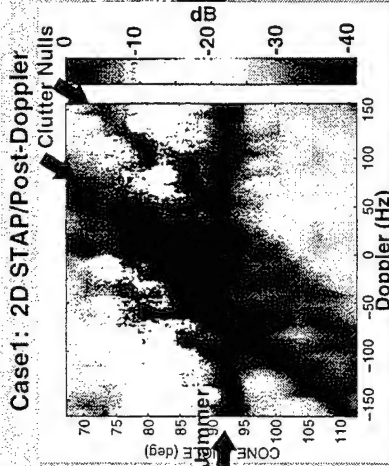
On the right, we consider pre-filters which would be appropriate for use with TSI cancellers that process data from a small number of selected beams. These architectures modulate clutter only in selected spots along the clutter ridge. Our pre-filter must cancel this clutter. One way to do this is to use a PRI-domain adaptive filter trained on the strongest clutter ($CNR > INR$) to place a notch on clutter.



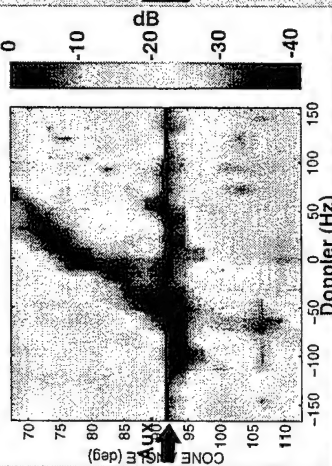
Pre-Filtering Performance

SINR Loss Comparison

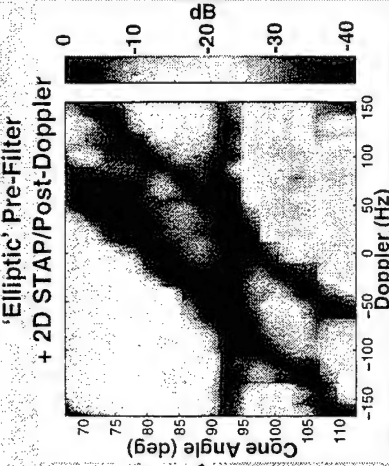
BEFORE



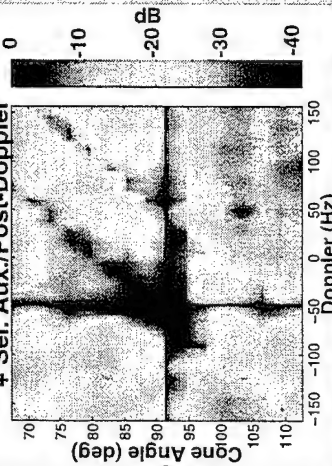
Case 2: Sel. Aux./Post-Doppler



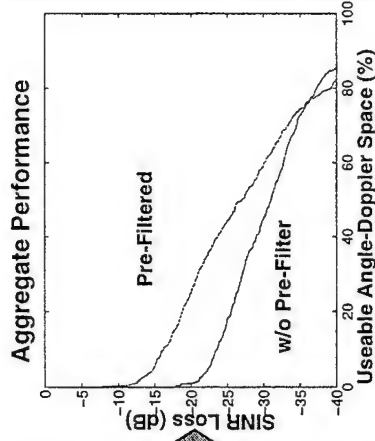
AFTER



Optimal 1D Pre-Filter
+ Sel. Aux./Post-Doppler



COMPARISON



Small improvements away
from clutter and jamming
... exchanged for notched-out
Doppler bins

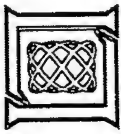
MIT Lincoln Laboratory

/documents/ASAP/sigcharlie.ppt
2/11/98

cube: HCTIM_1, 100 km
10

How do these techniques perform? To answer this, Scott Coutts, Sigrd Close and Pam Kove at Lincoln Lab created a simulation tool which can synthesize a TSI and clutter data cube. I then processed this cube using a factored architecture consisting of (top left) extended beamspace TSI canceller followed by Adjacent-bin post-Doppler STAP and (bottom left) selected-auxiliary TSI canceller followed by the same post-Doppler STAP. In both cases, you see the (expected) large SINR losses near the clutter ridge and in the jammer direction. In addition, you can also see rather large losses in regions of the angle-Doppler plane which are far from these interference sources. These losses are due to modulated clutter.

Next, we pre-processed the data using the pre-filters from the previous chart (above middle). Note the improvement in performance in the regions that were previously dominated by modulated clutter. We can use these SINR loss plots to make quantitative comparisons by plotting a "cumulative distribution" for the measured SINR (above right). We see a 5 to 10dB improvement from the pre-filtering.

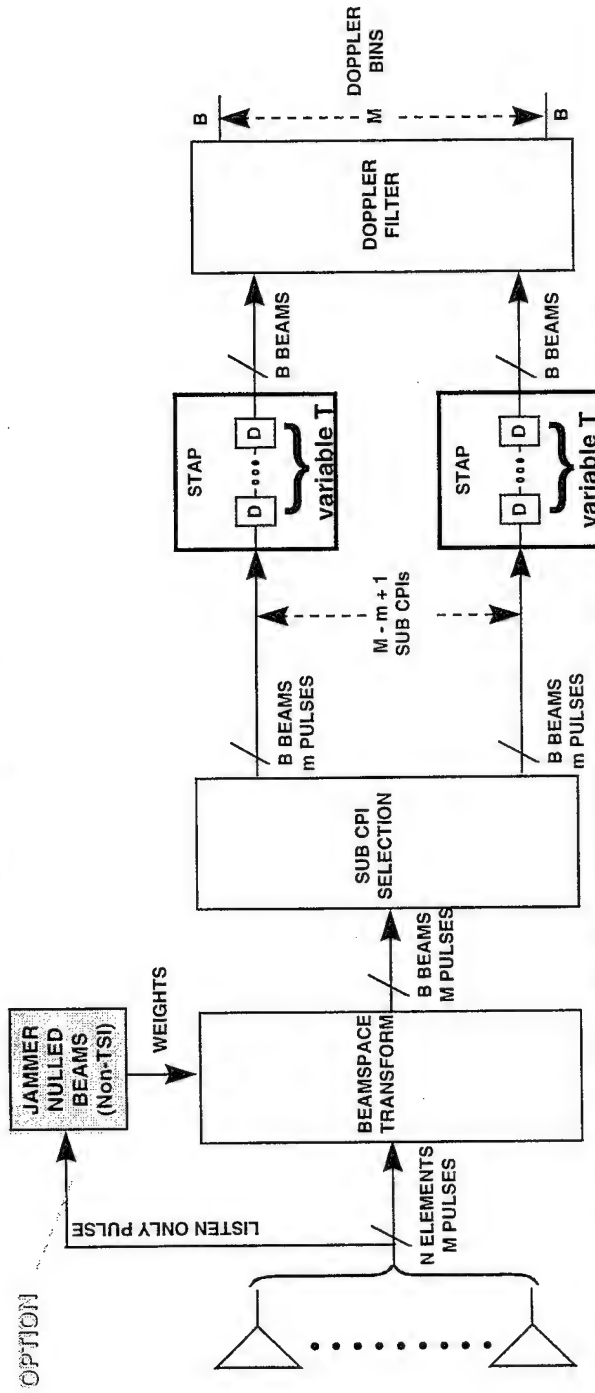


3D-STAP Concept

Objective: Prevent clutter modulation

Approach: Simultaneously cancel TSI & clutter

- Similar algorithms in this class initially proposed by Fante/Torres (not motivated by clutter modulation)



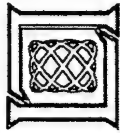
/Documents/ASAP'98/charts.ppt
2/11/98

MIT Lincoln Laboratory

11

Pre-filtering is just the first of our strategies for preventing clutter modulation. 3D-STAP is our second. 3D-STAP accomplishes the desired objective by simultaneously canceling both the TSI and the clutter. The basic idea is to cancel the clutter before it can be modulated (N.b. undernullled clutter and targets may still be a problem).

In doing this, 3D-STAP uses adaptive DOFs in both the fast-time domain (for TSI) and slow-time domain (for clutter), as well as the spatial domain. Because of the large number of adaptive DOFs that can result, practical 3D-STAP algorithms process data in a reduced dimension beamspace, and in sub-CPIs. Within sub-CPIs, we also want to use the smallest number of fast-time taps that we can get away with.

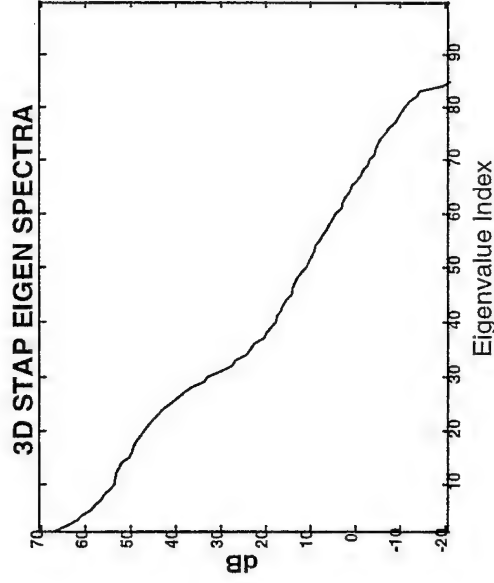
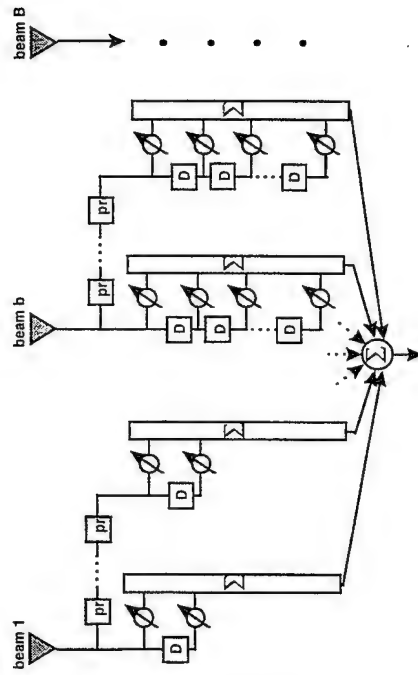


3D STAP Algorithms (1)

Issue: lots of FLOPs & huge training sets required due to large # DOFs

➔ Must reduce DOFs ➔ Weight Thinning; Eigen-beamforming

WEIGHT THINNING



- DOF reduction trades performance for lower cost /training ...

/documents/ASAP99/charts.ppt
2/11/98

MIT Lincoln Laboratory

12

Even then, the number of DOFs may be large, resulting in algorithms with very large computation counts and requiring huge training sets. To reduce the number of DOFs further, we can extend the techniques of "weight-thinning" and "eigenbeamforming" into three dimensions for use with 3D-STAP. Note, however, that the eigenvalues for combined TSI/clutter drop-off much more slowly than those from clutter alone. Thus, selecting the dominant subspace is more difficult; but the technique still helps you pick the best subspace of a given size.

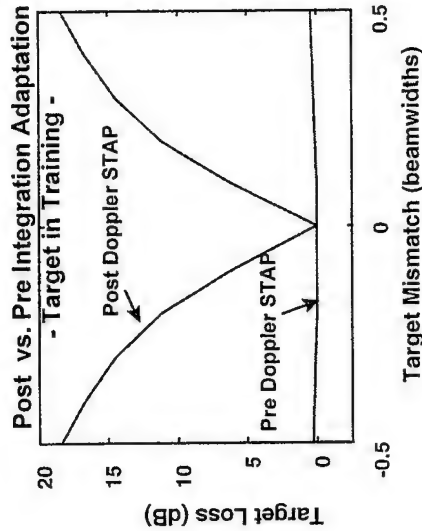
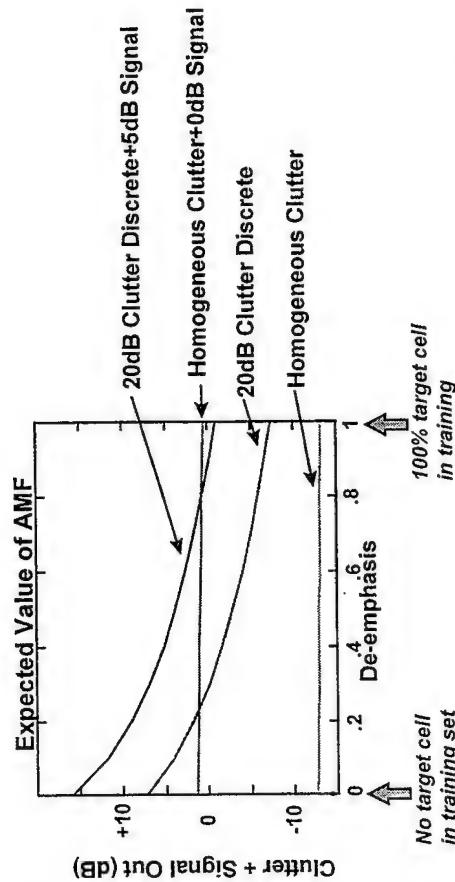


3D STAP Algorithms (2)

- 3D-STAP can train in combined interference.
- 3D STAP can train on targets (cheaper)
 - By exploiting low pre-integration target SNR to avoid target losses

Factored methods need mutually exclusive training sets

3D STAP can use all range gates



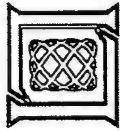
Attributes desired to prevent target loss: weak targets, large training sets, homogeneous clutter [see ASAP96]

/Documents/ASAP96/charts.ppt
2/11/98

Left: 8 channel beamformer, clutter at 40dB; Right: 100 PRI's, 2dB pre-Doppler SNR

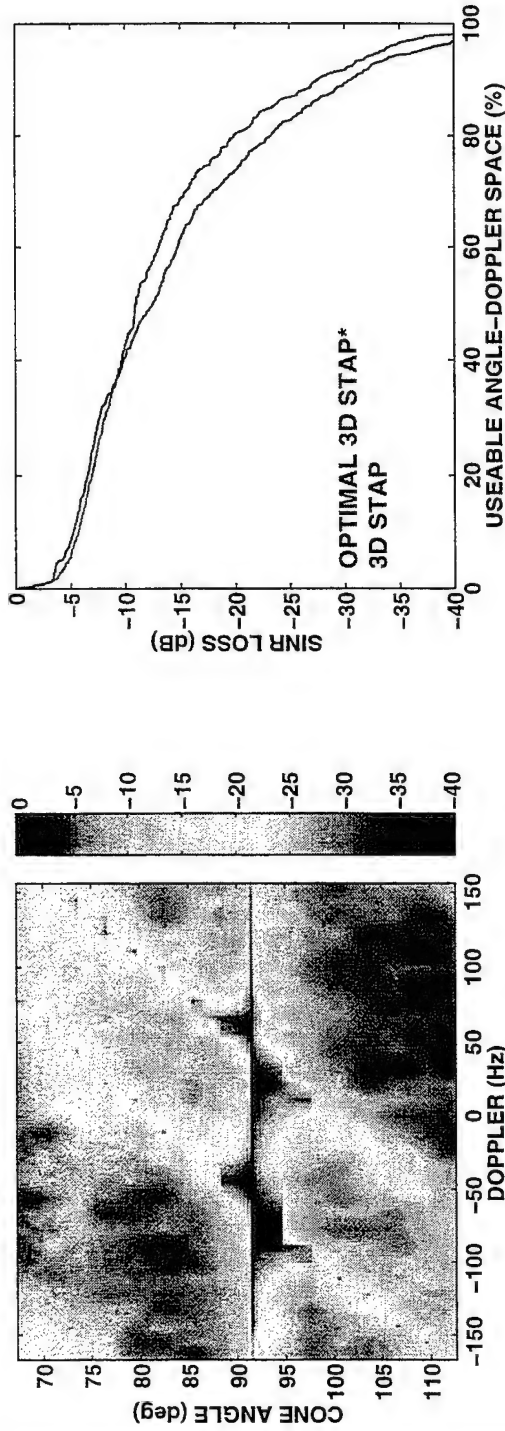
As for finding enough training data for 3D-STAP, we note that because we are adapting on TSI and clutter together, we can use a much bigger pool of samples for training. By comparison, the factored algorithms require training data which is exclusive (i.e., the TSI canceller needs data that is free of clutter for training -- forcing you to use over-the-horizon samples, or listen-only data).

Furthermore, because the adaptive processing is done prior to Doppler integration (and possibly pulse compression), target SNR's will be low and may permit training "through" targets. That is, we can leave the target cell in the training set. This is a big advantage computationally! On the left, we plot the expected value for the output of an AMF beamformer. We see that when the target is weak, little target energy is lost by leaving the target in the training set. However, if the target is strong (or the test cell contains a strong clutter discrete) there is a much larger loss. On the right, we see measured target losses for pre- and post-Doppler STAP processing of the same target. With pre-Doppler STAP, the target's eigenvalue is small and it will not be nulled. After adaptive beamforming, the target energy is integrated in Doppler. Compare this to post-Doppler STAP. With post-Doppler STAP, the target's eigenvalue is big and it will be canceled if there is any steering vector mismatch.



3D STAP PERFORMANCE

SINR Loss



- Aggregate performance largely driven by Pre-Doppler's ability to cancel monostatic clutter

* using taper optimization --extension of Baranoski ASAP 96 technique

MIT Lincoln Laboratory

/documents/ASAP96/charts.ppt
2/11/98

14

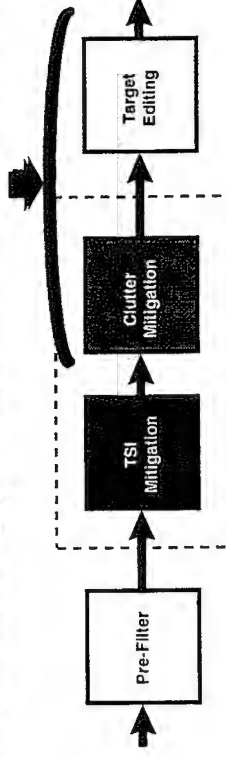
cube: HCTIM_1 100 km

This chart illustrates the performance of 3D-STAP. Note the large regions of relatively low SINR loss away from the clutter and jammer.

Also note that since 3D-STAP is just a fancy extension of conventional pre-Doppler STAP, we are able to extend the optimized taper work of Baranoski (ASAP 96) to 3 dimensions, giving us sharper clutter notches.



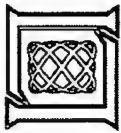
Strategy #2: Treatment



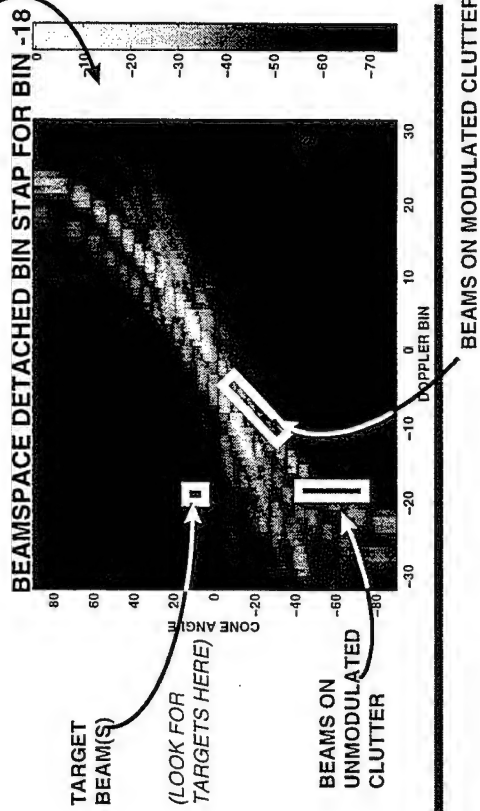
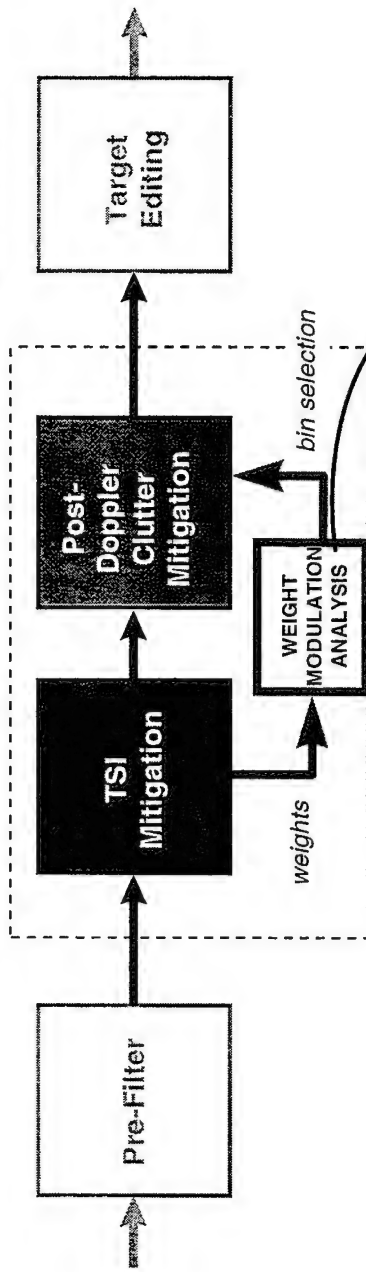
- **Objective: Remove modulated clutter and targets**
- **Methods:**
 - Detached Bin STAP
 - Pre-Doppler clutter cancellation
 - Multi-dimensional Sidelobe Target Editing

Pre-filters and 3D-STAP make up our core “prevention” techniques. Next, I’d like to move on to our second strategy for dealing with TSI-induced modulation. I call this second strategy “treatment.” As the name implies, treatment techniques are used in the processing chain after modulation occurs (right side above) to remove the modulated signals.

There are 3 core techniques that I will discuss in this category...



Detached Bin STAP Concept

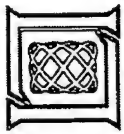


/Documents/ASAP98/charts.ppt
2/11/98

Two of these techniques deal with our choice of clutter canceling STAP algorithm. The first of these treatment techniques is a modified version of post-Doppler STAP called "Detached-Bin STAP".

The basic idea of detached bin STAP is to allow the clutter to pass through the TSI canceller, where it is modulated (of course, we would like to minimize the modulation if possible). On output, we send this modulated clutter through our post-Doppler STAP box. Conventional post-Doppler STAP algorithms can not cancel all of this clutter, though, because they are restricted in where they place their adaptive nulls (in the angle-Doppler plane). We need to modify post-Doppler STAP so that it has the freedom to place nulls in locations which will cancel the modulated clutter too.

To do this, we can analyze the adaptive weights applied in the TSI canceller. This will tell us "where" and "how" clutter will be modulated.



Detached-Bin STAP Algorithm

- Clutter DOF Selection:
 - Main Beam (TSI-nulled) weights: $W = [w_1 \dots w_M]$
 $\mathbf{v}_{f_{look}} =$ Doppler of look
 - Expected clutter ridge: $\sigma_c \mathbf{v}_{clutter} = \sigma_c \mathbf{v}_{\theta_c} \otimes \mathbf{v}_{f_c}$
where $\langle \theta_c, f_c \rangle \in$ clutter ridge and $\sigma_c^2 =$ expected power at $\langle \theta_c, f_c \rangle$
 - Compute: $\gamma_{\theta_c, f_c} = \sigma_c^2 \left| \text{vec} \left(W \cdot \text{diag}(\mathbf{v}_{f_{look}})^H \right) \mathbf{v}_{clutter} \right|^2$
 - Sort γ_{θ_c, f_c} and point beams at $\langle \theta_c, f_c \rangle$ corresponding to largest expected modulated clutter
- Nulling:
 - Project data into beamspace & perform SMI

... Many Variants Possible

MIT Lincoln Laboratory

/Documents/ASAP/gcharts.ppt
2/11/98

17

These equations describe specifics of how this could be done.

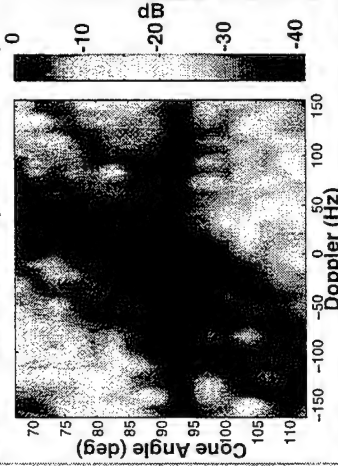


Detached Bin STAP Performance

SINR Loss Comparison

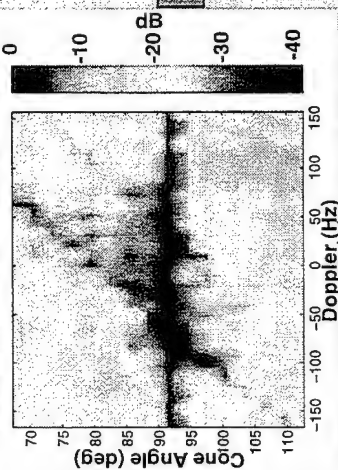
BEFORE

Case 1: 2D STAP/Adj. Bin Post-Dop



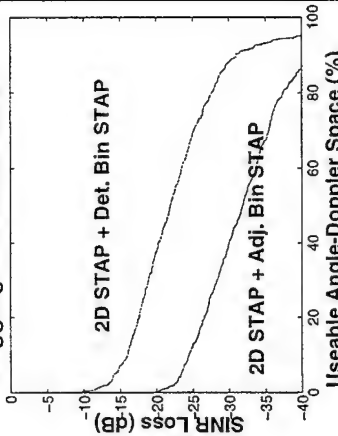
AFTER

2D STAP/Detached Bin Post-Dop

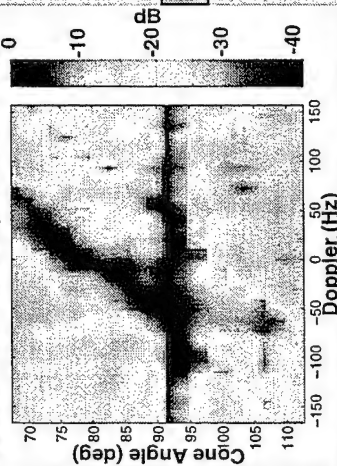


COMPARISON

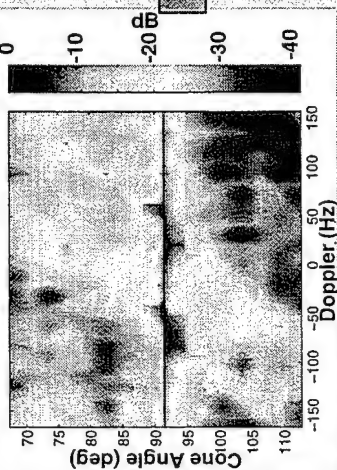
Aggregate Performance



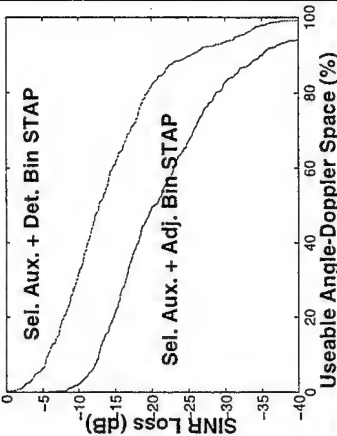
Case 2: Sel. Aux/Adj. Bin Post-Dop



Sel. Aux/Detached Bin Post-Dop



Aggregate Performance



/Documents/SAP'98/chata.ppt
2/11/98

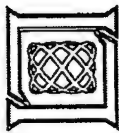
HCTIM_1, Top: 50km, Bottom: 100km

Here, we illustrate the performance of Detached-Bin STAP when preceded by the two TSI cancellers we looked at earlier.

LEFT: TSI cancellation followed by conventional (adjacent bin) post-Doppler STAP. Note that regions which are well-separated from the clutter and jammer still have poor performance due to modulated clutter.

MIDDLE: TSI cancellation followed by Detached-Bin STAP. Note that performance improves.

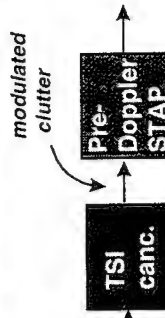
RIGHT: Useable angle-Doppler space.



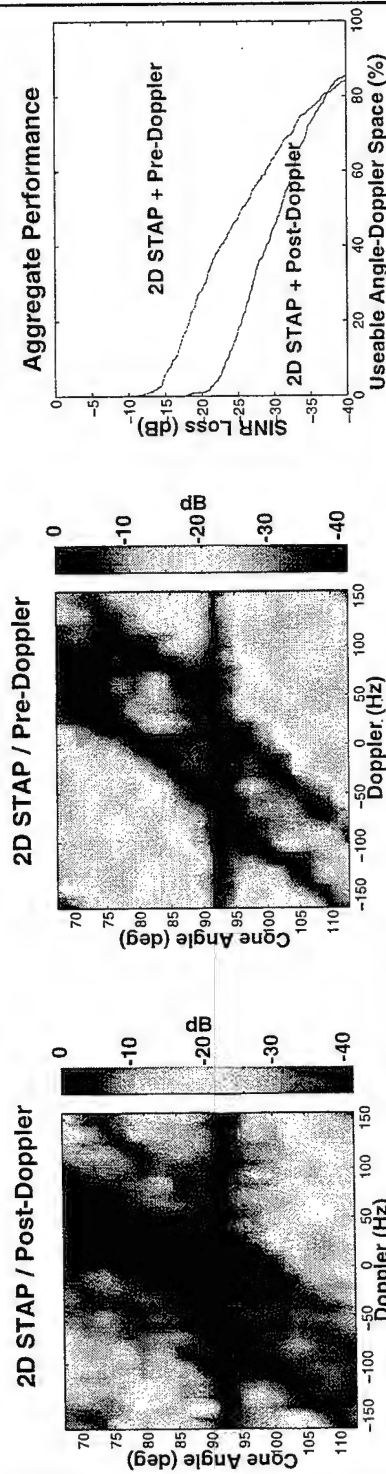
Pre-Doppler Concept/Performance

Objective: Reduce modulated clutter

Approach: 1. Cancel TSI (modulating clutter)
2. Use clutter STAP algorithm which can place nulls anywhere in angle-Doppler space



Pre-Doppler STAP uses minimal a priori info about the clutter when the subspace is chosen for adapting



MIT Lincoln Laboratory

/Documents/ASAP'98/charlie.ppt
2/11/98

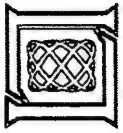
19

cube: HCTIM_1 100 km

Detached-bin STAP is only one of two techniques for canceling modulated clutter. The key to making it work was permitting the adaptive canceller to place nulls over a wide region of the angle-Doppler Space.

Our second technique for canceling modulated clutter is pre-Doppler STAP. I won't say a lot about the details of this algorithm because it is the same old pre-Doppler STAP algorithm we all know and love. What's different here is "why" we are using it. Specifically, pre-Doppler STAP processes "subCPI's" of data. Beyond that, it is free to place nulls in virtually all of the angle-Doppler space. This is exactly the kind of thing we need for canceling modulated clutter!

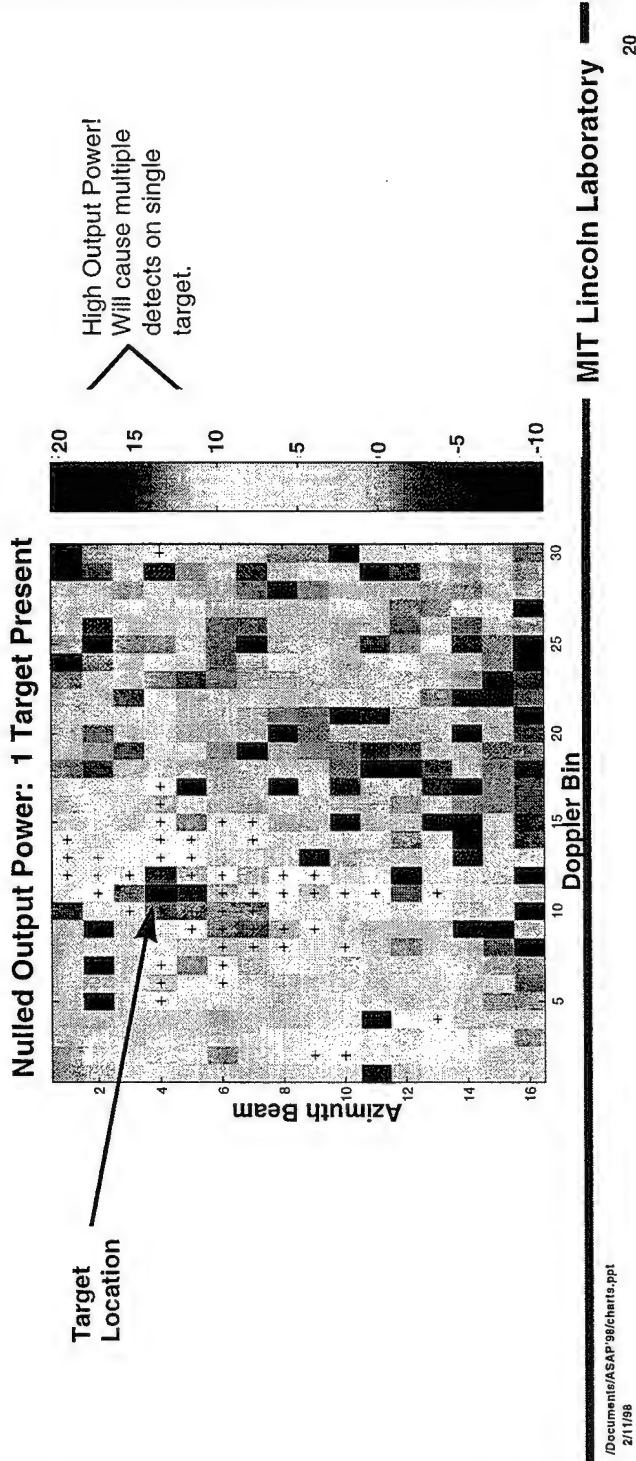
Examining the performance of this approach, we again see that we can achieve a large improvement the regions of the space where performance was previously limited by the modulated clutter.



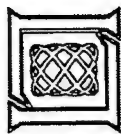
Modulated Sidelobe Target Editing Concept

Objective: Remove detections on modulated target

Approach: For each pair of detects, test the hypothesis that one is due to a modulated target in the location of the other

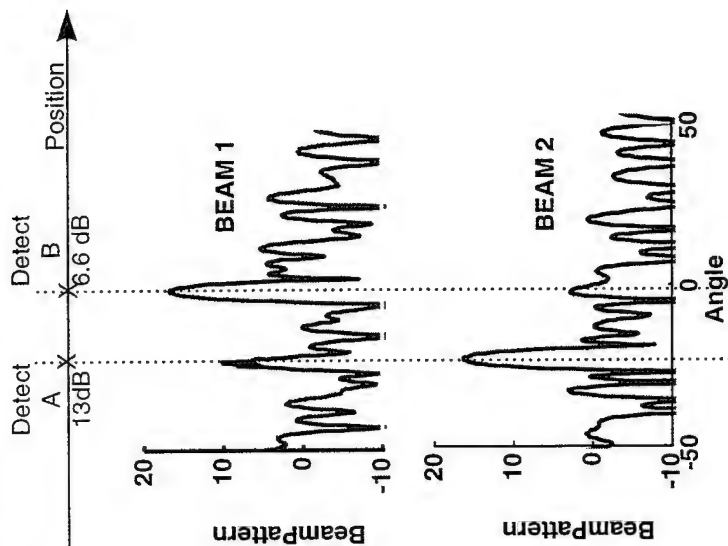


Our final "treatment" technique differs from the others in that it is designed to deal with modulated targets, not clutter. Due to TSI weight updating, recall that both targets and clutter are modulated. For targets this means that if we look at the beamformers output for a single target in noise (here), we will see the expected strong return in the true direction of the target, but also large returns widely space throughout the angle-Doppler plane. Putting these nulls outputs through a range-CFAR, we would get many false target reports, spread-out across the angle-Doppler plane.



Modulated Sidelobe Target Editing Algorithm

1-Dimensional Example:



Detect A power: 13 dB
-Gain of Beam 2 on A: -16.5 dB
+Gain of Beam 1 on A: 10 dB
- Detect B power: -6.6 dB

Within tolerance? .1 dB -- Yes

2-Dimensions (or more): Same algorithm using "composite" weights

/Documents/ASAP98/charlie.ppt
2/11/98

MIT Lincoln Laboratory

21

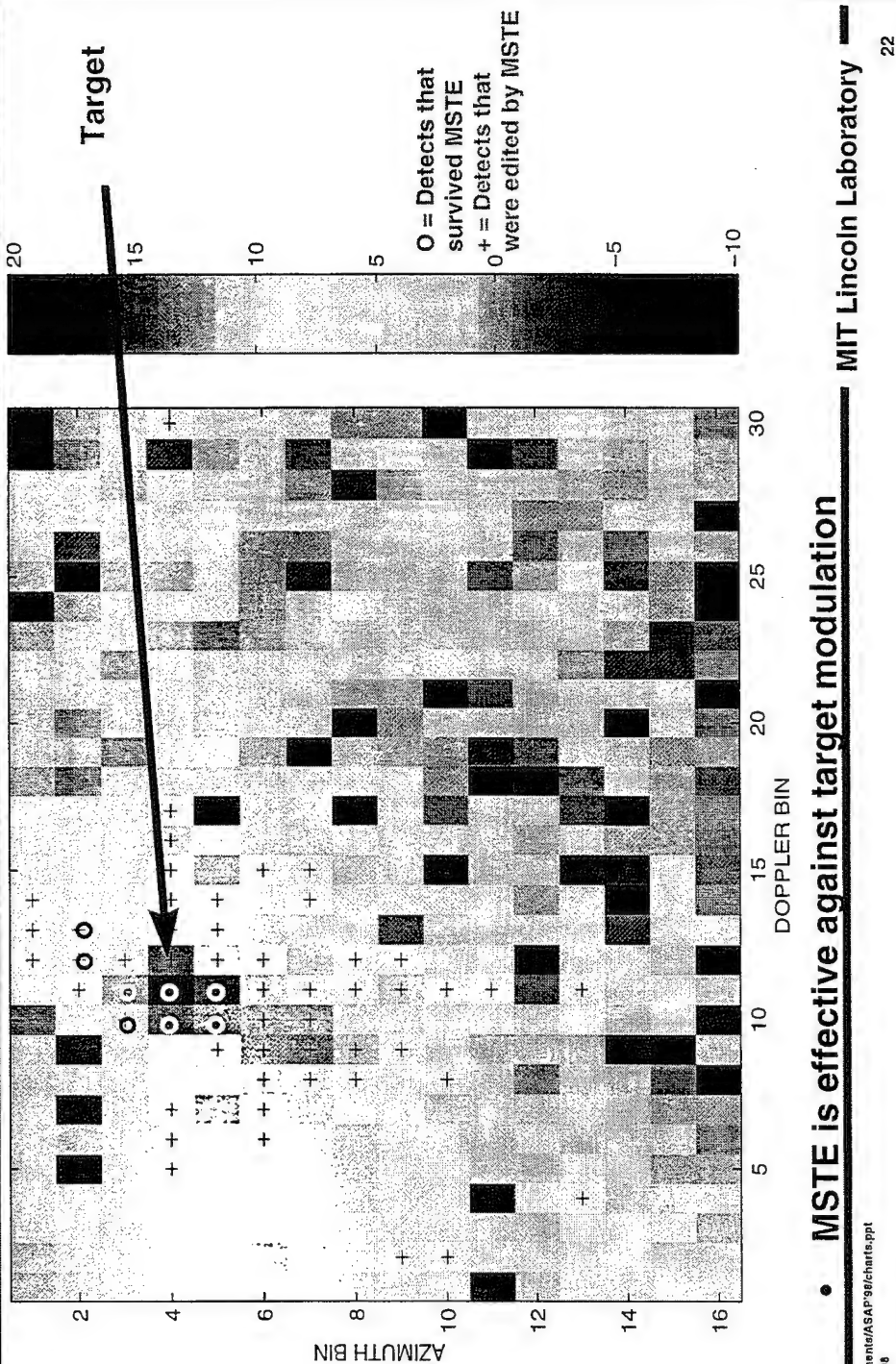
Our basic algorithm for treating this is one that, for every pair of detects differing by more than a beamwidth, tests the hypothesis that one of those detects is due to a modulated sidelobe in the direction of the other. (this requires computing beam patterns at a few select points, and is thus attractive from a real-time perspective; we note that other more ML-like approaches are possible but will be costlier).

This is easy to visualize in 1-D, and can be extended to 2 or more dimensions in a straightforward manner.

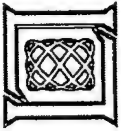
Here, suppose there are two detects at "A" and "B." Each has a measured SNR. Can we tell if "B" is due to a "A"? First, take the measured power on "A" and subtract the gain that the beam in that direction has on "A." Next, add the sidelobe gain that the beam on "B" has in the direction of "A". If the result is close to the measured SNR of "B", then the detect is probably due to a sidelobe --- throw it away.



Modulated STE Performance



How does this work? Here, the plusses denote raw detects coming out of our range-CFAR (single target in noise). The circles denote detects which are passed by the MSTE box. Note that MSTE kept the detects which are within a beamwidth of the true target, and tossed-out the false target reports. (in all, there were 55 detects at the input, but only 8 at the output).



Summary

- TSI-induces modulation in both clutter and targets
 - Modulated clutter lowers visibility
 - Modulated targets “flood” the tracker
- We can/should exploit info. about TSI-induced modulation at every stage of processing
 - Multiple techniques investigated
- Combining techniques can often lead to even better performance

SINR improvements of 5 to 15 dB observed
False target reductions of 85% observed

So, in summary we have seen that TSI cancellation induces modulation in both clutter and targets. In the case of clutter, this modulation limits visibility over an extended region of the angle-Doppler plane. In the case of targets, it results in many false targets reports. However, we have also seen that if we understand the mechanisms behind the modulation, we can exploit that understanding at one or more stages of the processing chain to improve our end-to-end system performance. We saw improvements of 5 to 15dB in SINR loss when exploiting this info. in a *single* stage of processing, and would probably gain more by *combining* techniques. We also saw that we can reduce false targets by 85%!

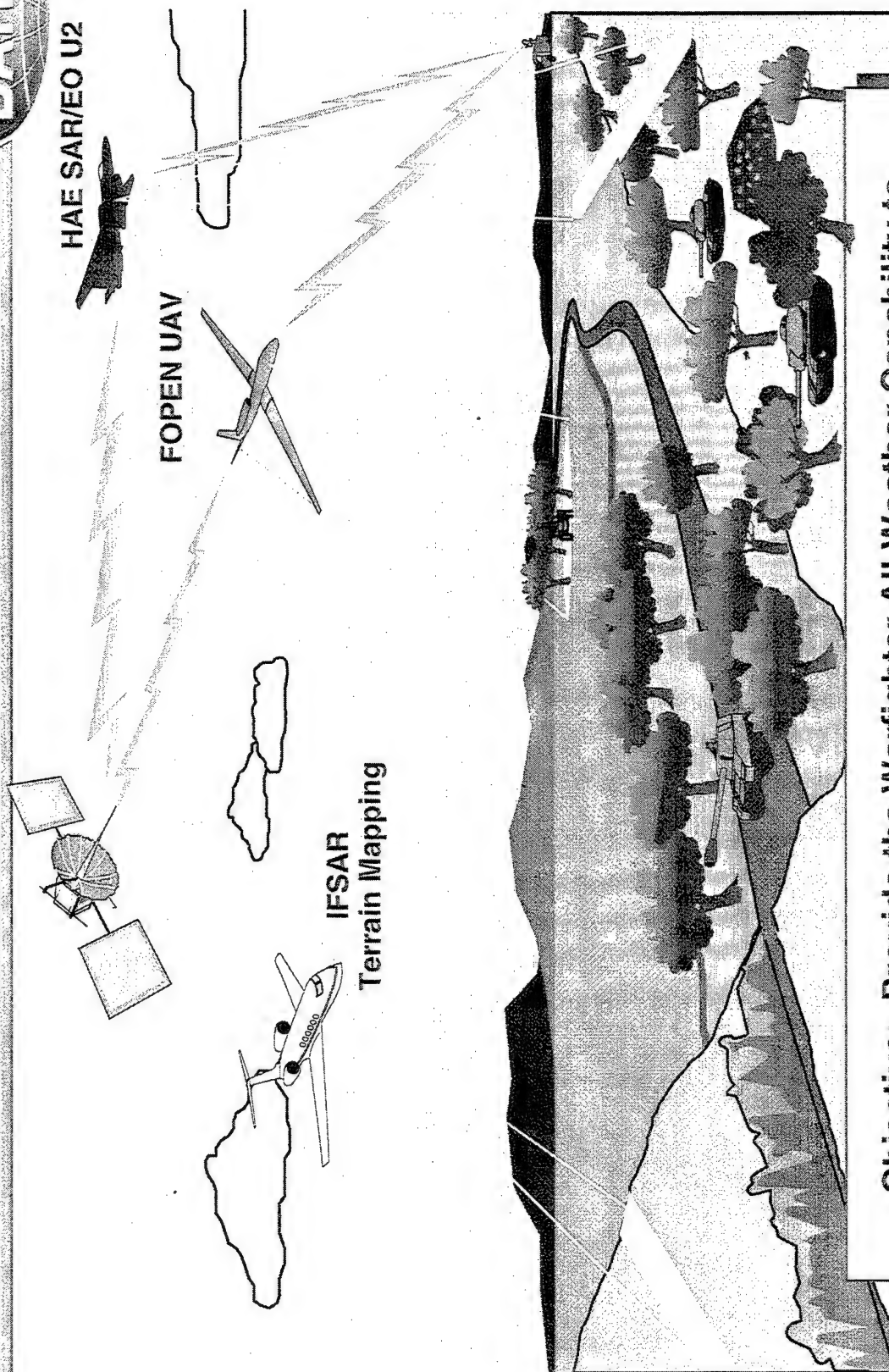
ASAP 98
Session II Synthetic Aperture Radar

Chair:

Mark E. Davis

**Defense Advanced Research Projects Agency
Sensor Technology Office**

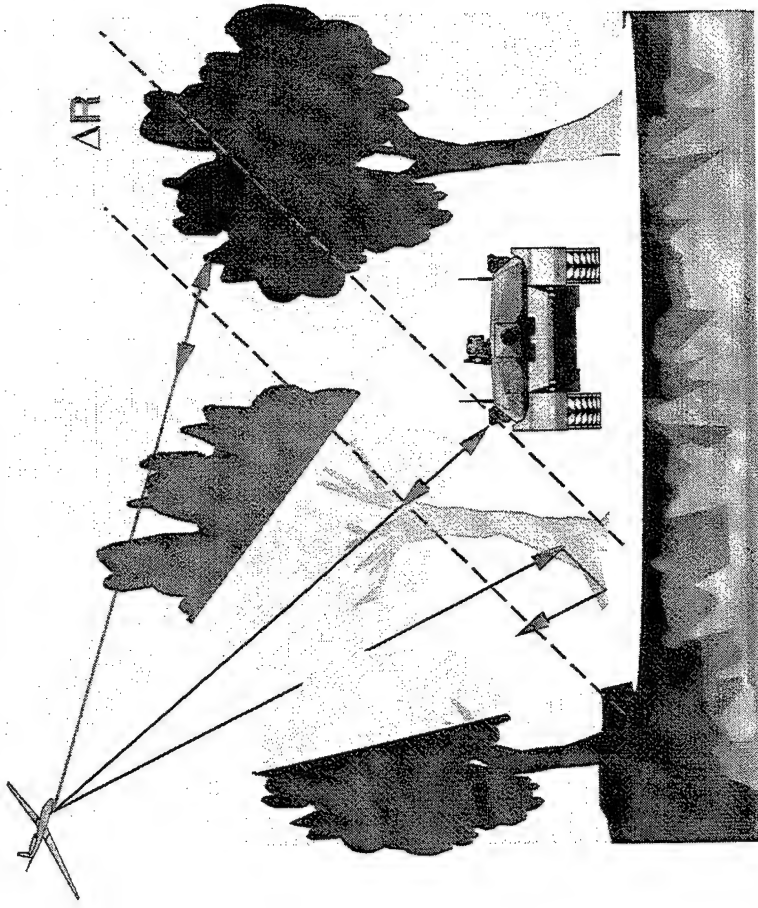
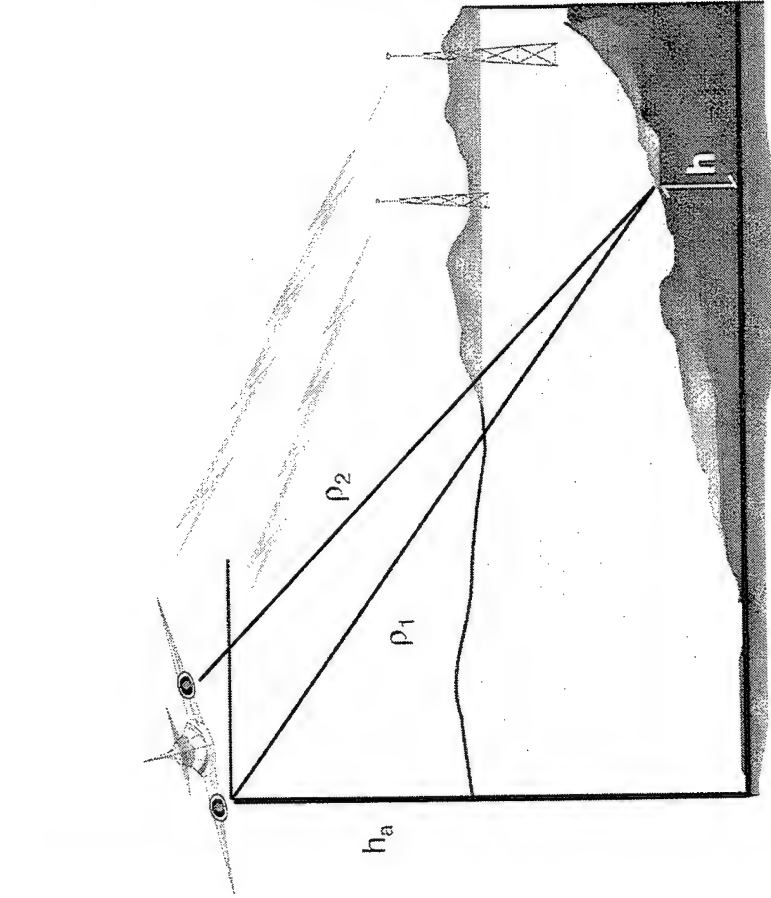
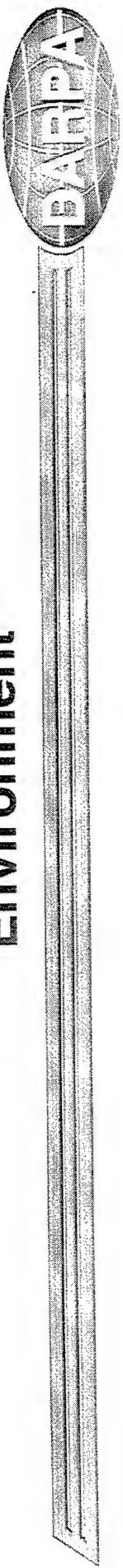
Dominant Battlefield Awareness



Objective: Provide the Warfighter All Weather Capability to Map Terrain, and Detect Targets Under Foliage and Camouflage

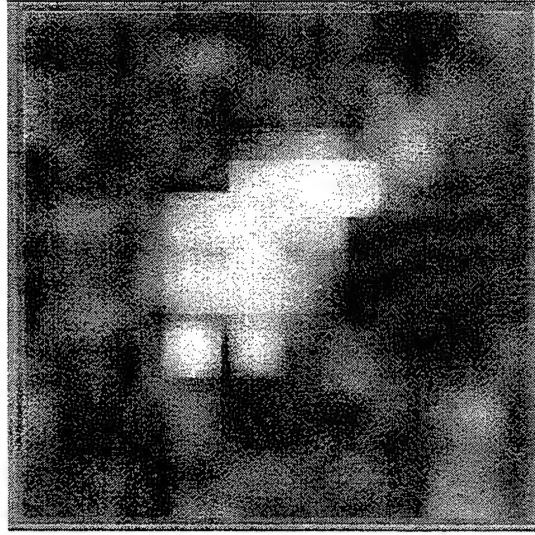
lap/mrsmk_b/990302v1/2

SAR Measurements In Real Environment



- Operational Systems Must Remove Effects of Environment:
 - Scattering by Volumetric Clutter or Cultural Overlays
 - Clutter Caused by Radio Frequency Interference
 - Effects of Moving Target or Uncompensated Platform Motion

Super Resolution Image Enhancement



Conventional 1 m Image

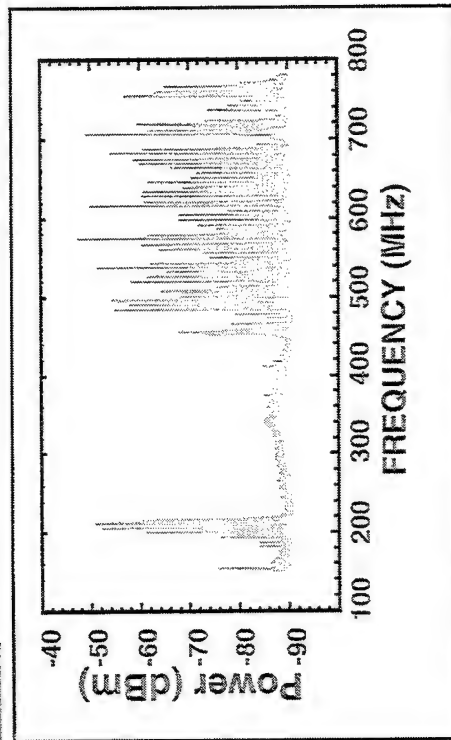
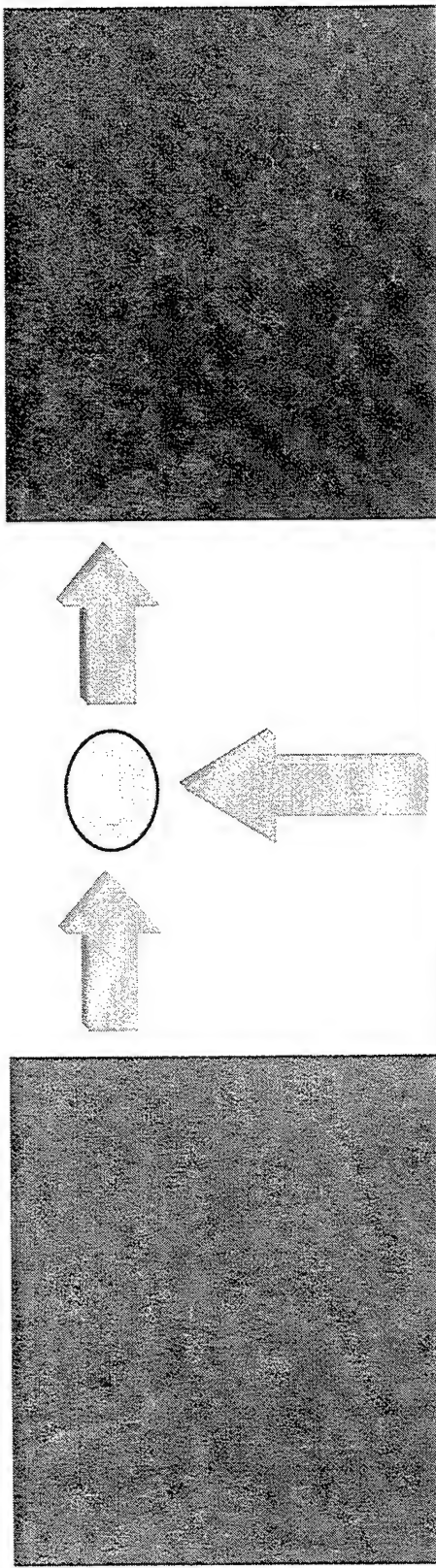
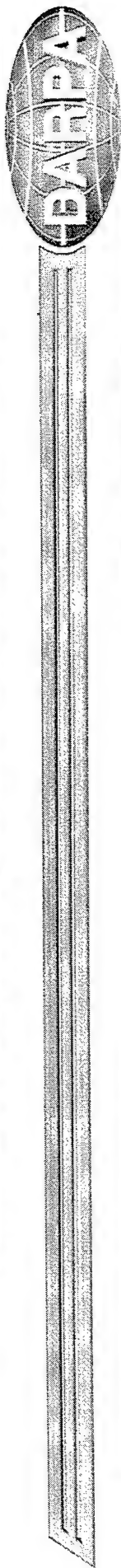


HDI Processed to 0.5 m

**“ High Definition Vector Imaging for FOPEN SAR” ,
Keith Forsythe, MIT Lincoln Laboratory**

**“Adaptive SAR Imaging and its Impact on
ATD/R and Image Exploitation”
Stuart R. DeFraaf, Northrop Grumman**

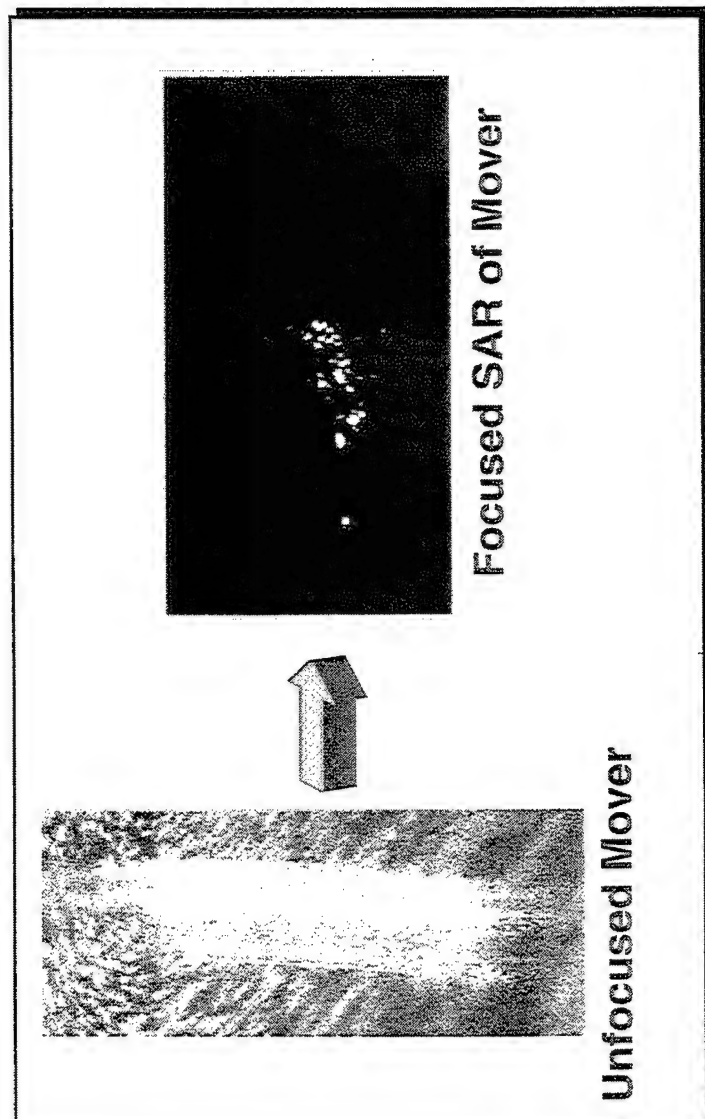
Radio Frequency Interference Removal



**"RFI Rejection in Wideband SAR Signals Using LMS Adaptive Filters",
Charles Le, Scott Hensley, Elaine Chapin, Jet Propulsion Laboratory**

800asap/mismk_b980302v1/5

Moving Target Imaging



**" Adaptive Dual Aperture Clutter Cancellation",
Mitchell I. Mirkin, MIT Lincoln Laboratory**

RFI Rejection in Wideband SAR Signals Using LMS Adaptive Filters

Charles T.C. Le and Scott Hensley

Jet Propulsion Laboratory
4800 Oak Grove Drive
Pasadena, CA 91109
tel: (818) 354-3322
email: sh@kailak.jpl.nasa.gov

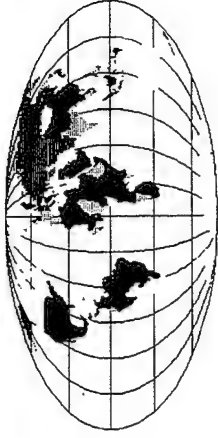
Abstract We present the approach of least-mean-square (LMS) adaptive filter for the removal of narrowband radio frequency interference (RFI) from wideband synthetic aperture radar (SAR) signals. Three variations of the LMS adaptive filter are considered: the time-domain (TDLMS), the frequency-domain (FDLMS), and the filter-bank (FBLMS) LMS adaptive filters. The filters are tested with simulation and real SAR data. The simulator produces the range-Doppler image of a point target. It consists of a radar signal generator, thermal random noise and RFI generator, and an 8-bit (or BFPQ) A/D converter. The radar signal is characterized by its bandwidth, chirp slope, pulse length, caltone frequency, and notching parameters. RFI sources include tones and communication signals of different modulation schemes (AM, FM, QAM, PM, communication satellite modulations, etc). Real SAR data are taken from existing data collected by the JPL P-band TopSAR/AirSAR programs. The filter performance, with respect to the filter parameters and input signal characteristics, is analyzed in terms of the radar performance parameters, such as the ISLR, PRSL, phase history, resolution, etc. Finally, we compare the performance and throughput requirements of the three proposed adaptive filters.

[1] M. Braunstein, J. Ralston, and D. Sparrow, "Signal processing approaches to radio frequency interference suppression," in *Algorithms for Synthetic Aperture Radar Imaging*, SPIE vol. 2230, pp. 190-208, 1994.

[2] Session 3: Radio frequency interference rejection, in *Algorithms for Synthetic Aperture Radar Imaging*, SPIE vol. 2487, pp. 72-129, 1995.



GeoSAR



RFI Rejection in Wideband SAR Signals Using LMS Adaptive Filters

Charles Le and Scott Hensley

Jet Propulsion Laboratory
Pasadena, California

OUTLINE

- GeoSAR project overview.
- Statement of radio-frequency-interference (**RFI**) problem.
- Simulator block diagram and waveforms.
- Introduction to the least-mean-square (**LMS**) adaptive filter.
- **TDLMS**: the time-domain LMS adaptive filter.
 - Algorithm description and simulator results.
 - Cleaned image from P-band TopSAR data.
- **FDLMS**: the frequency-domain LMS adaptive filter.
 - Algorithm description and simulator results.
 - Cleaned image from P-band TopSAR data.
- **FBLMS**: the filter-bank LMS adaptive filter
 - Block diagram and working principles.
- Throughput requirements.
- Conclusion.



Project Overview

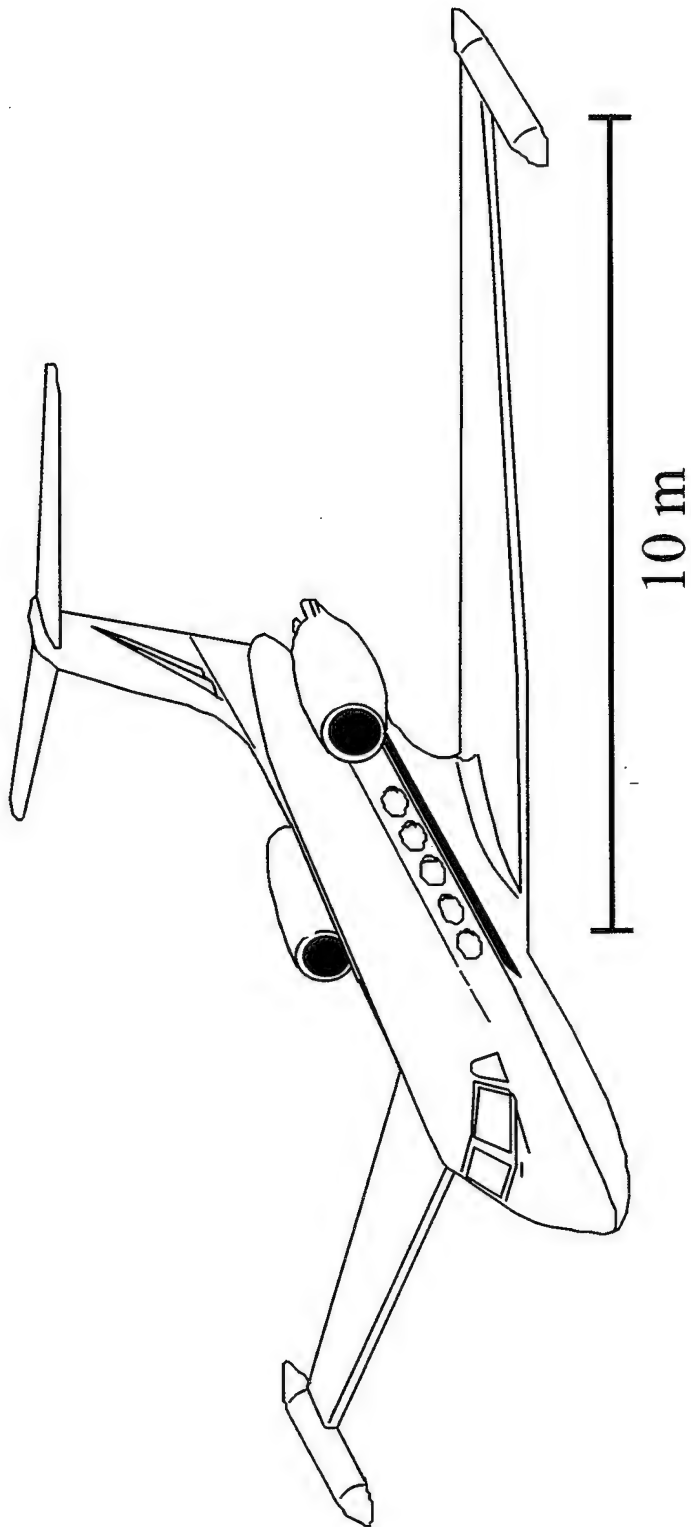
- GeoSAR is a DARPA funded project to develop a dual frequency airborne interferometric mapping radar.
- The Overall Goals for the Project Are to:
 - Develop precision foliage penetration mapping technology based upon dual frequency interferometric radar
 - Provide military and civilian users with significant increase in mapping technology
 - Produce true ground surface digital elevation models suitable for military and civilian applications
- Total Project Duration Is 3 Years Starting November 1, 1996
- GeoSAR expected to be operational in November of 1999



Mapping System

- Mapping System Will Consist of:
 - Aircraft platform to host data collection hardware (Gulfstream II)
 - Flight planning software
 - Dual frequency (X-band/UHF) interferometric SARs
 - Single polarization @ X-band
 - Dual polarization @ UHF
 - Automated radar control
 - Laser interferometric baseline measurement system augmented with embedded GPS/INU systems and differential GPS for precision reconstruction of aircraft flight trajectory and attitude history
 - SAR processors capable of producing DEMs @ X-band and UHF and a true ground surface DEM from combined X-band/UHF analysis
 - A GIS system to analyze digital data

Gulf Stream-II Aircraft With Wing-Tip Pods





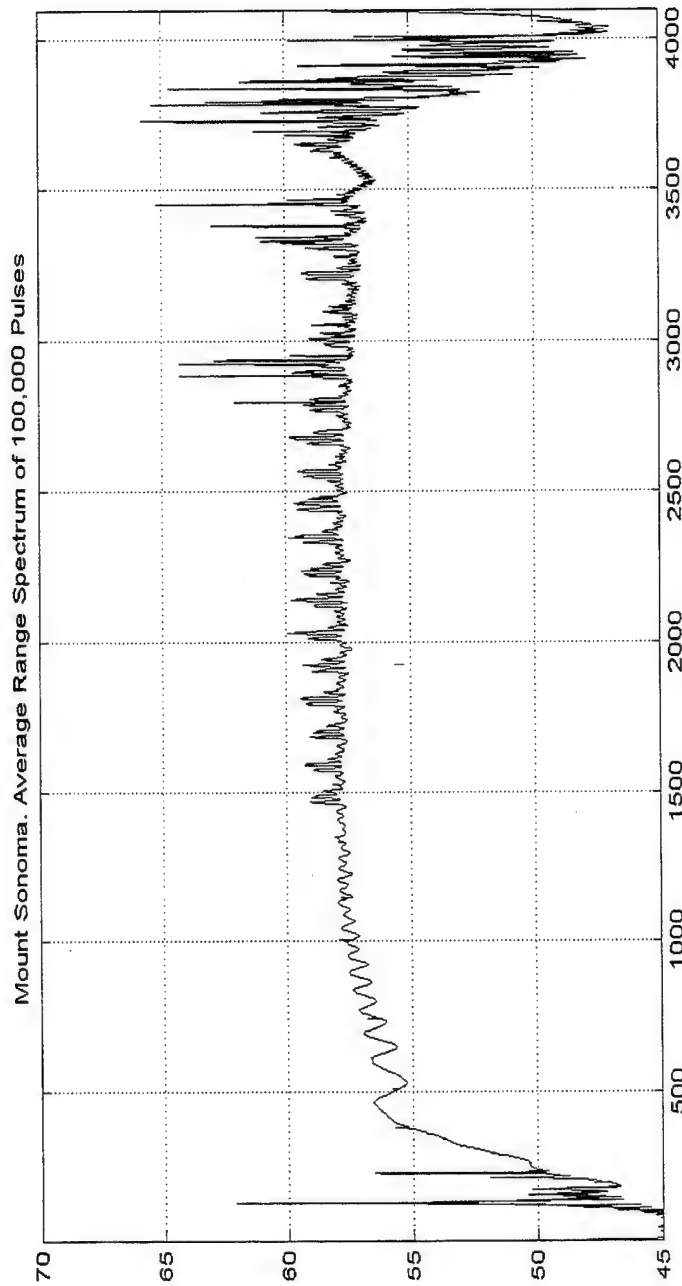
GeoSAR System Overview

Parameter	UHF System	X-Band System
Peak Transmitting Power	4 KW	8 KW
Bandwidth	80/160 Mhz	80/160 Mhz
Pulse Length	40 μ sec	40 μ sec
Sampling Rate	8/4 BFPQ @ 160MHz 8 bit for 80 MHz	8/4 BFPQ @ 160MHz 8 bit for 80 MHz
Antenna Size	1.524 m x 0.381 m	1.5 m x 0.035 m
Antenna Gain at Boresight	11 dBi	26.5 dBi
Antenna Look Angle	27 - 60 Deg	27 - 60 Deg
Antenna Boresight	60 Deg	60 Deg
Wavelength @ Center Frequency	0.86 m for 160 MHz 0.97 m for 80 MHz	0.031 m for 160 MHz 0.031 m for 80 MHz
Baseline Length	20/40 m	2.5/5 or 1.3/2.6 m
Baseline Tilt Angle	0 Deg	0/45 Deg
Platform Altitude	5000 - 10000 m	5000 - 10000 m



Problem Statement

- The dual requirements of a low radar frequency for foliage penetration and a wide bandwidth for high resolution in ultra-wideband radar lead to frequency bands occupied by other RF systems, such as in communications, navigation, police, emergency rescue, ...





Mount Sonoma, California. P-band TopSAR. RFI Contaminated Image

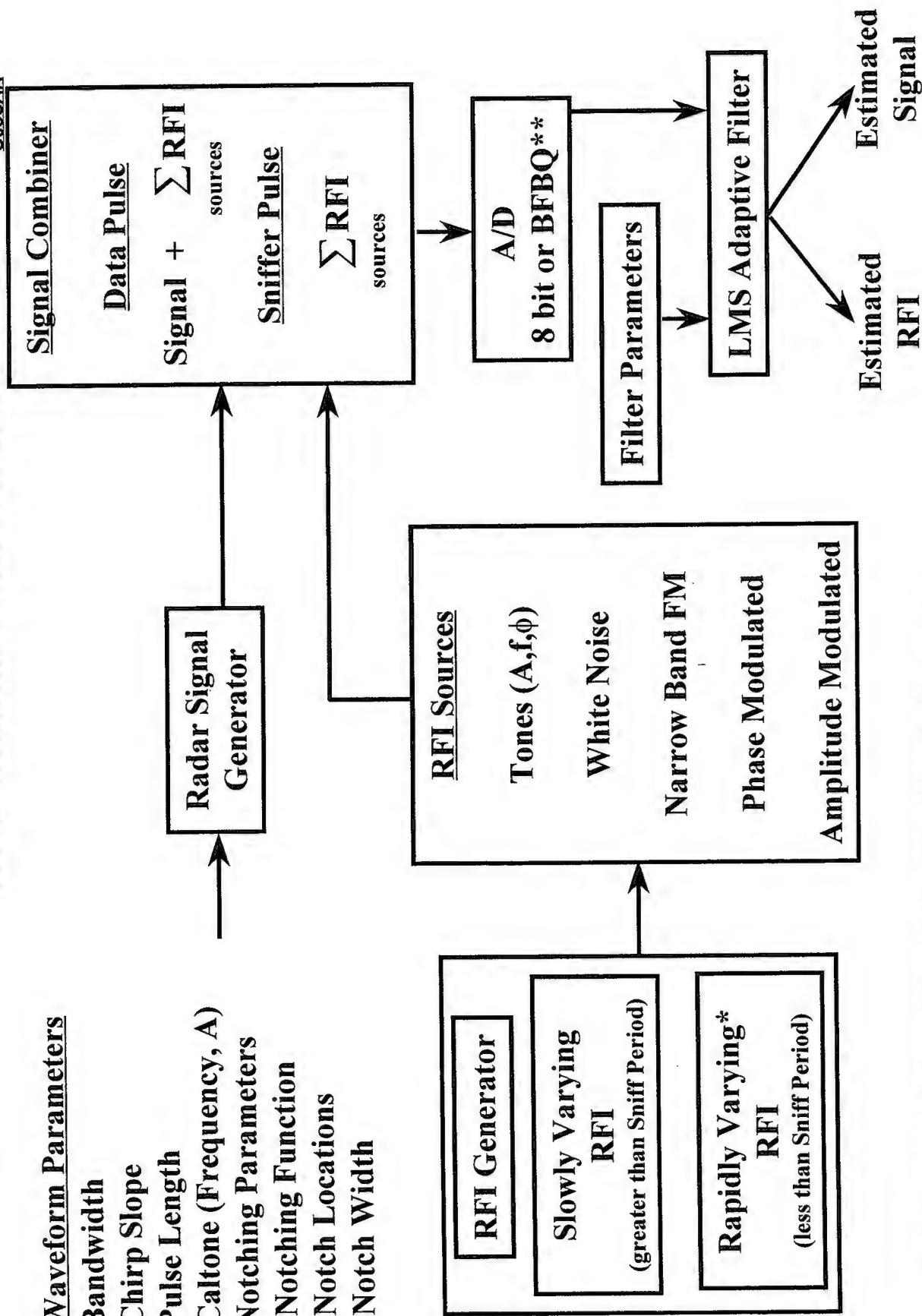




RFI Simulator Block Diagram

Waveform Parameters

Bandwidth
 Chirp Slope
 Pulse Length
 Caltone (Frequency, A)
 Notching Parameters
 -Notching Function
 -Notch Locations
 -Notch Width



* RFI values and time changes chosen from a random distribution

** not yet implemented



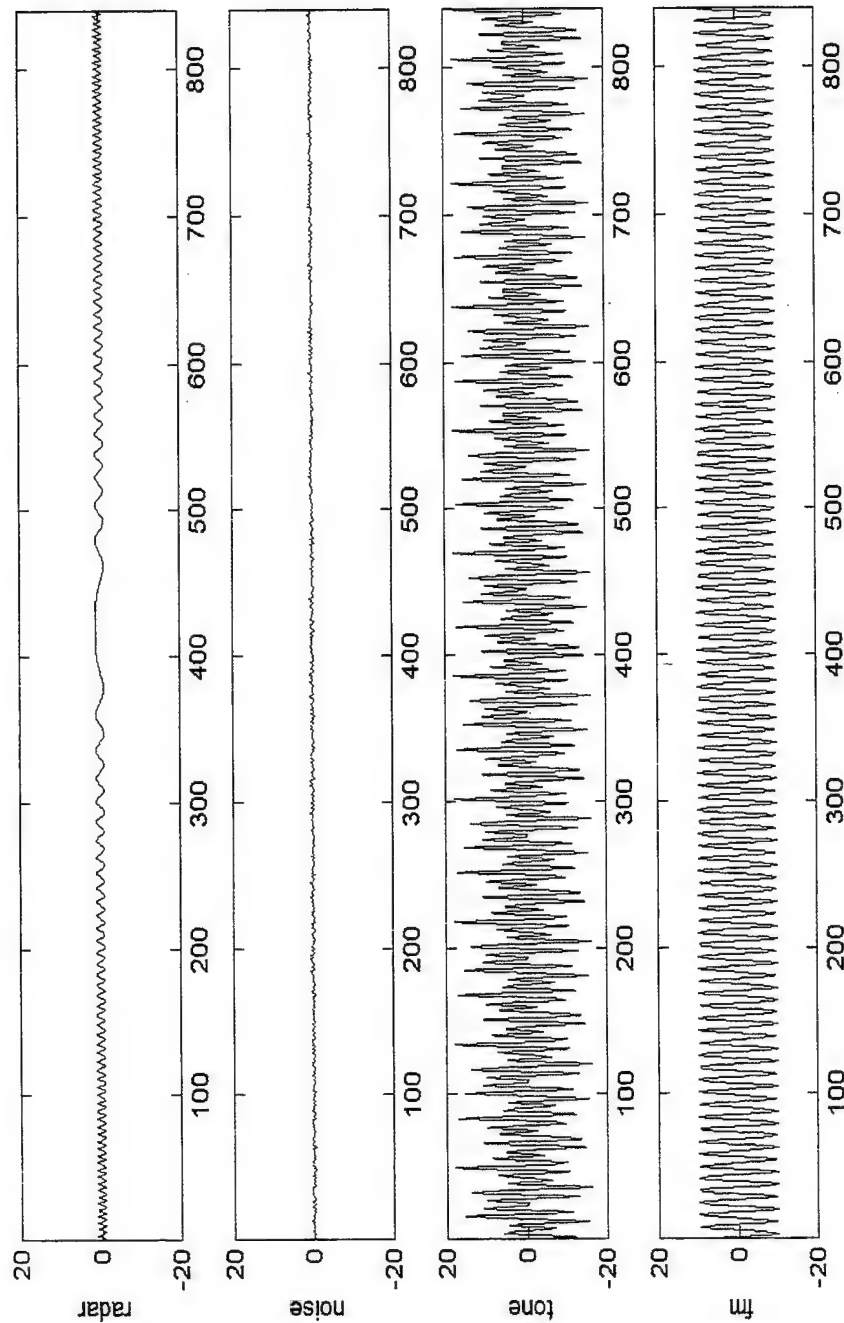
Noise Descriptions

- 8-bit A/D converter
 - quantization types: rounding, 2's-complement truncation, magnitude truncation.
 - overflow handling modes: saturation limiter, 2's-complement overflow, triangle limiter.
- Gaussian random thermal noise.
- Tones (sinusoidal signals).
- Communication modulation signals:
 - AM-DSB-TC (Amplitude modulation, double sideband with transmission carrier).
 - AM-DSB-SC (Amplitude modulation, double sideband suppressed carrier).
 - AM-SSB (Amplitude modulation, single side band suppressed carrier).
 - QAM (Quadrature amplitude modulation).
 - FM (Frequency modulation).
 - PM (Phase modulation).
 - satellite modulation signals: ASK, PSK, QASK, FSK, MSK ...

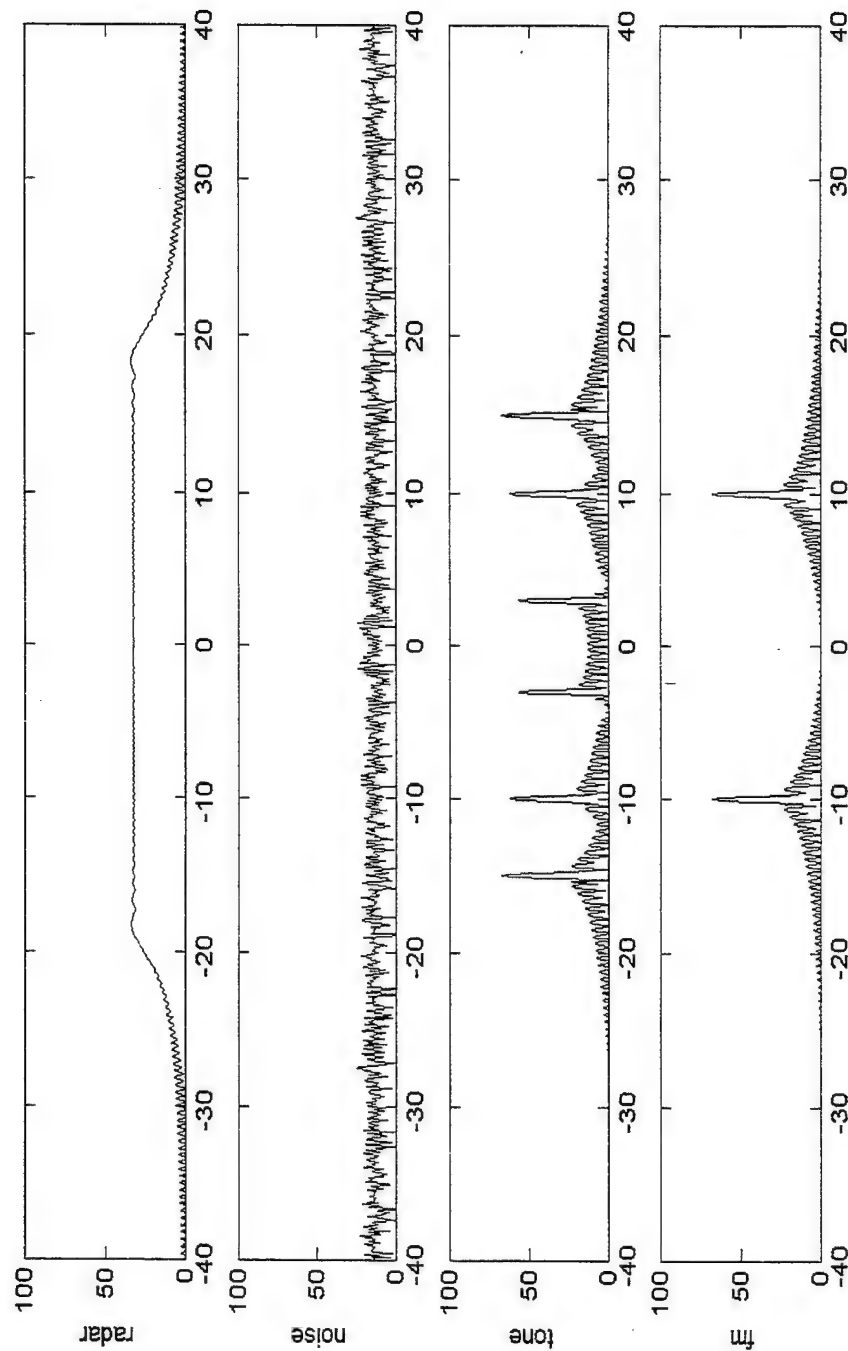


Time-Domain Components of the Total Signal

BW = 40 MHz; SNR = 10 dB; ISR = 10 dB; 6 tones and 2 FM's



Frequency-Domain Components of the Total Signal

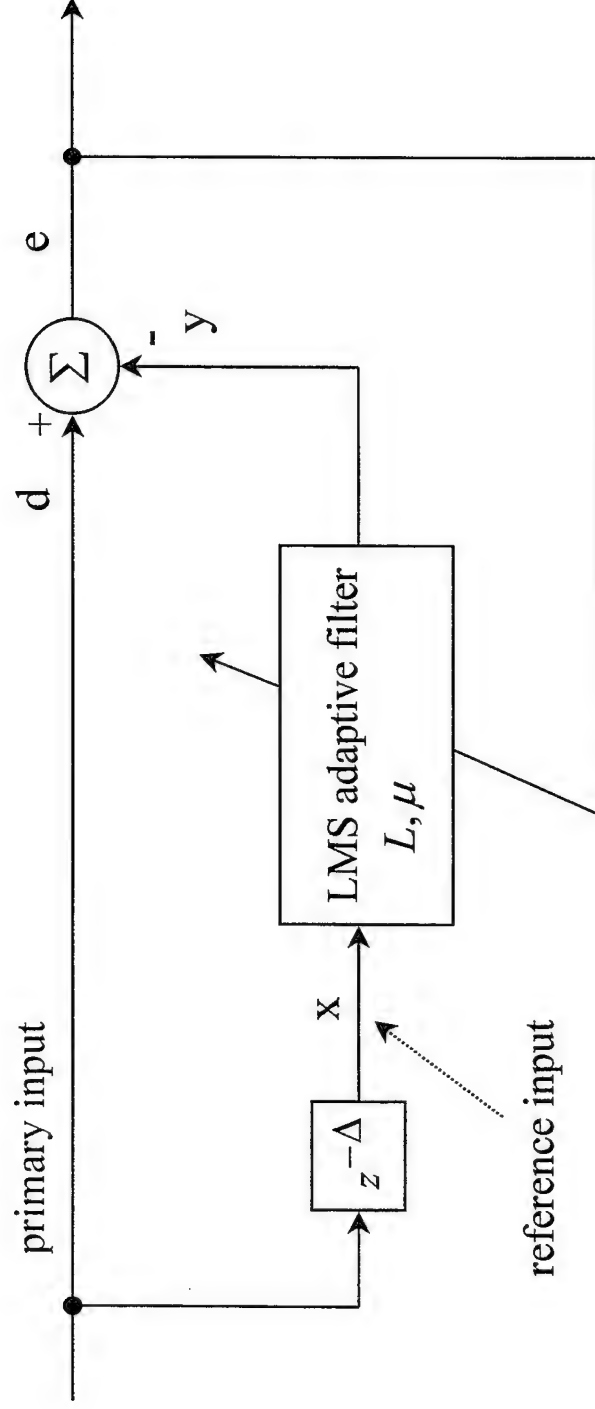




Introduction to the LMS Adaptive Filter

- Factors which affect RFI notch filter design
 - convergence speed and final misadjustment.
 - stability and complexity.
 - throughput requirement and coding simplicity.
 - adaptability.
- The LMS adaptive technique is one of the most popular algorithms due to good compromise for the above performance factors
 - when first introduced, the concept was simple but effective.
 - over the years, it has been extensively refined to give both good performance and fast implementation.
 - its many different versions provide a choice depending on applications.
 - it is readily to be used (in cascade) with other current DSP techniques (wavelets, subbands, ...).
 - FDLMS: blocking in the **time-domain**.
 - FBLMS: blocking in the **frequency-domain** (and **time-domain**).

The Time-Domain LMS Adaptive Filter



The LMS algorithm

Reference signal:

$$x = d(n - \Delta)$$

Filter Output:

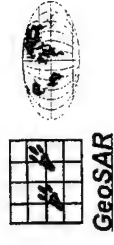
$$y(n) = \bar{w}^T \cdot \bar{x}$$

Estimation Error:

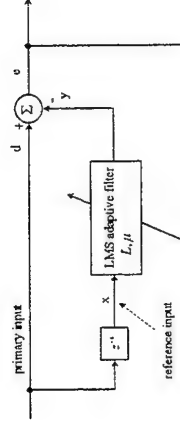
$$e(n) = d(n) - y(n)$$

Tap-weight adaptation:

$$\bar{w}(n+1) = \bar{w}(n) + \mu \bar{x} e^*(n)$$



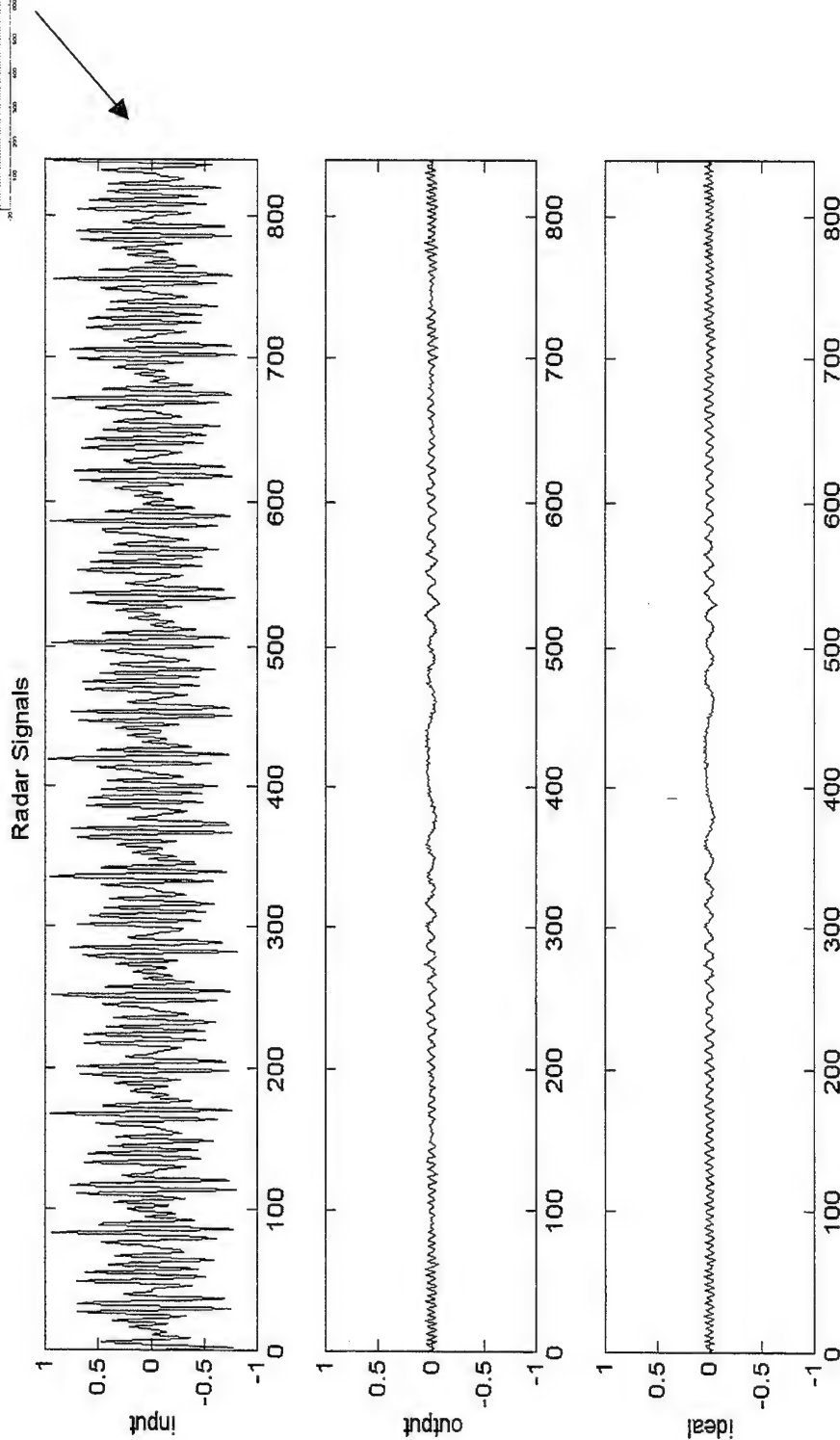
Working principles of the Time-Domain LMS adaptive filter

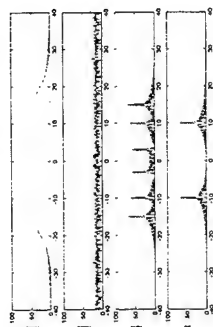


- Principles
 - Radar signal is WIDEBAND ---> low correlation between samples.
 - RFI is NARROW BAND ---> high correlation between samples.
- How it works
 - The delay causes decorrelation between the wideband component in the primary and reference input.
 - The adaptive filter tries to predict the RFI, and thus forms an equivalent transfer function to that of a narrow-band filter centered at the frequencies of the RFI.
- Computational issues
 - No matrix solving or correlation coefficient calculations required.
- Limitations and Solutions
 - Speed and eigenvalue spread
 - frequency-domain LMS and filter-bank LMS.
 - Non-stationary
 - wavelets.

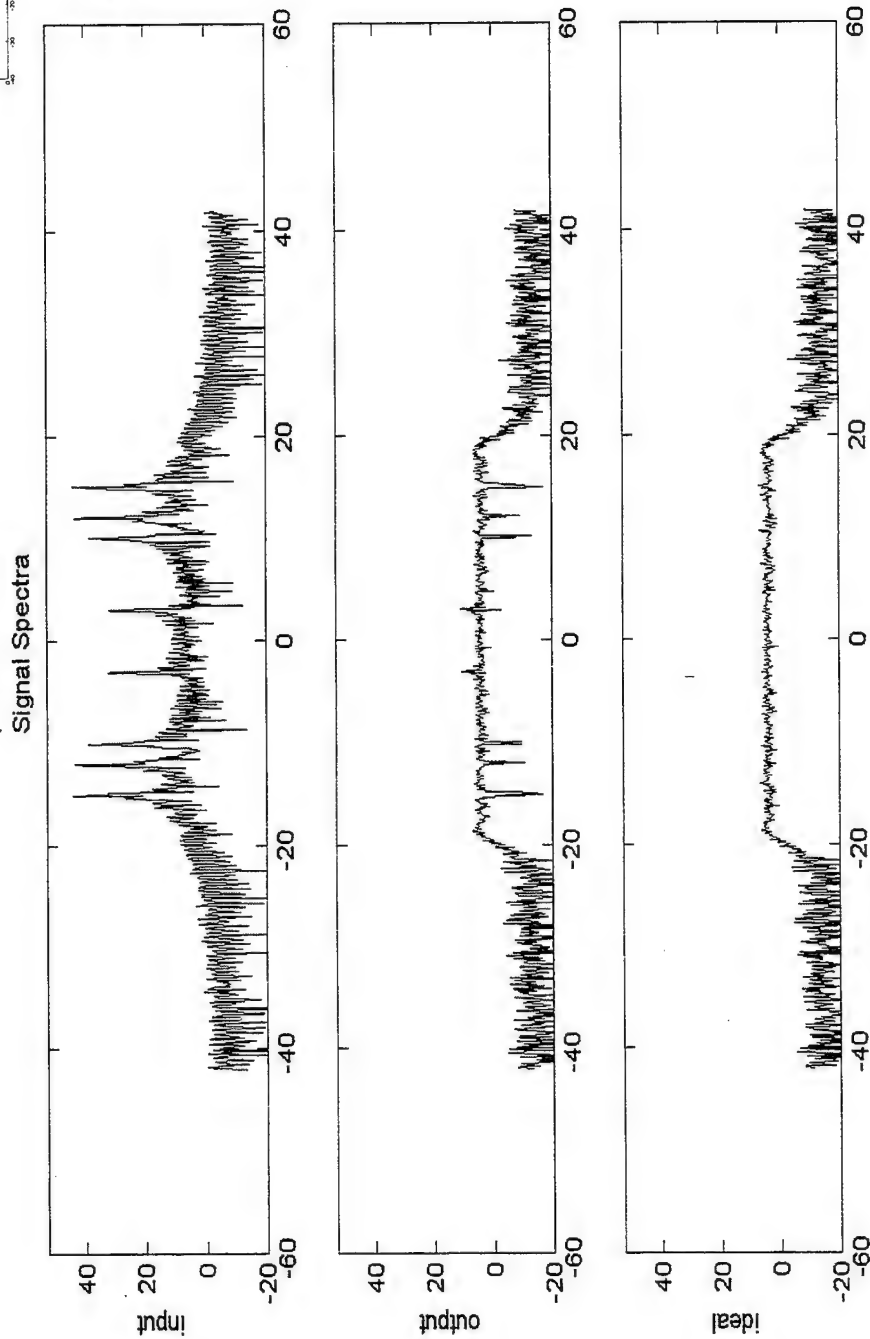


TDLMS: Comparison of waveforms

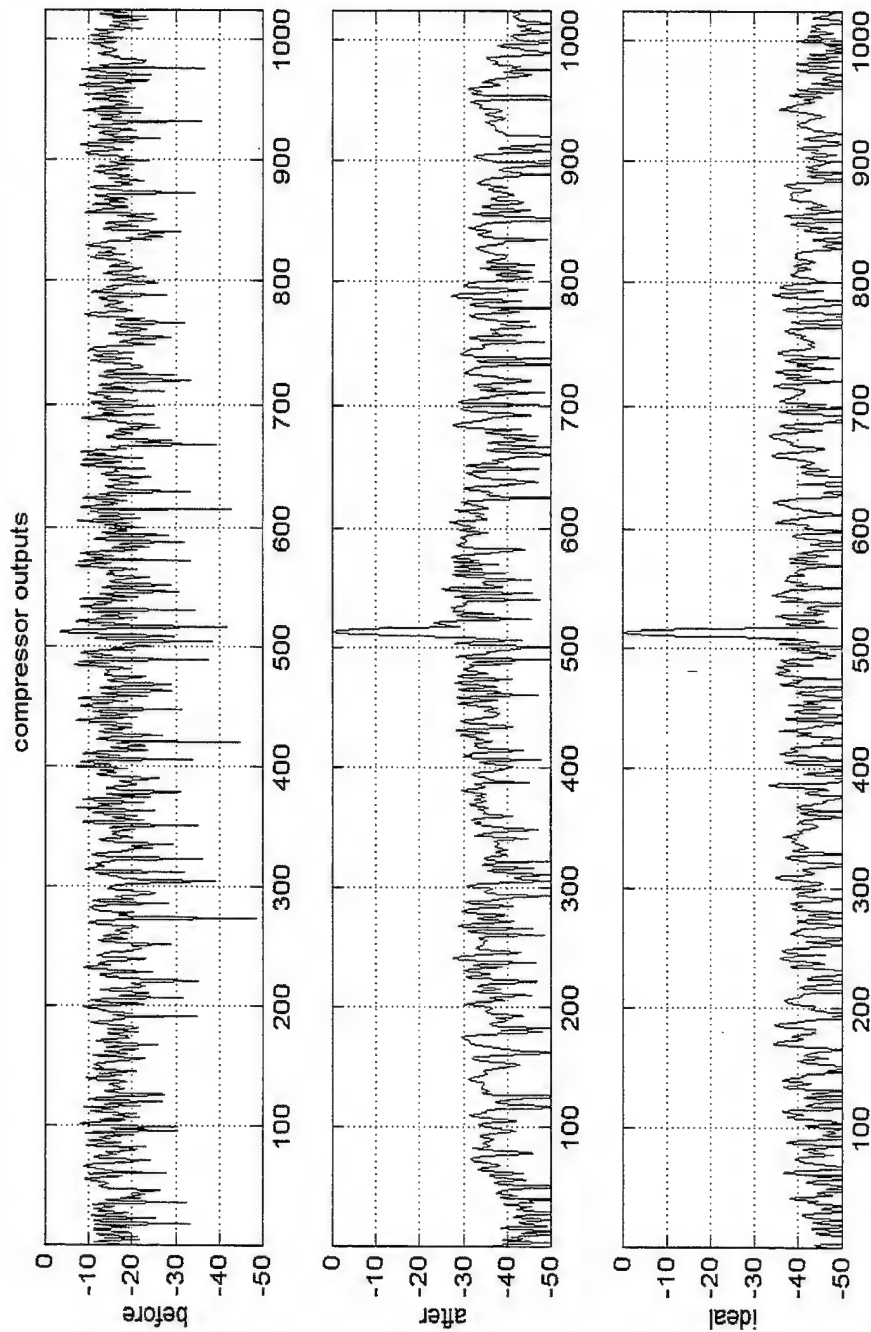




TDLMS: Comparison of spectra



TDLMS: Comparison of compressor outputs



Performance Evaluation

- **Filter parameters**
 - Filter Length (L): frequency resolution of the filter.
 - Stepsize (μ): convergence speed and final misadjustment.
 - Delay (Δ): decorrelation of primary and reference signals.
- **Performance parameters**
 - ISLR: integrated sidelobe ratio

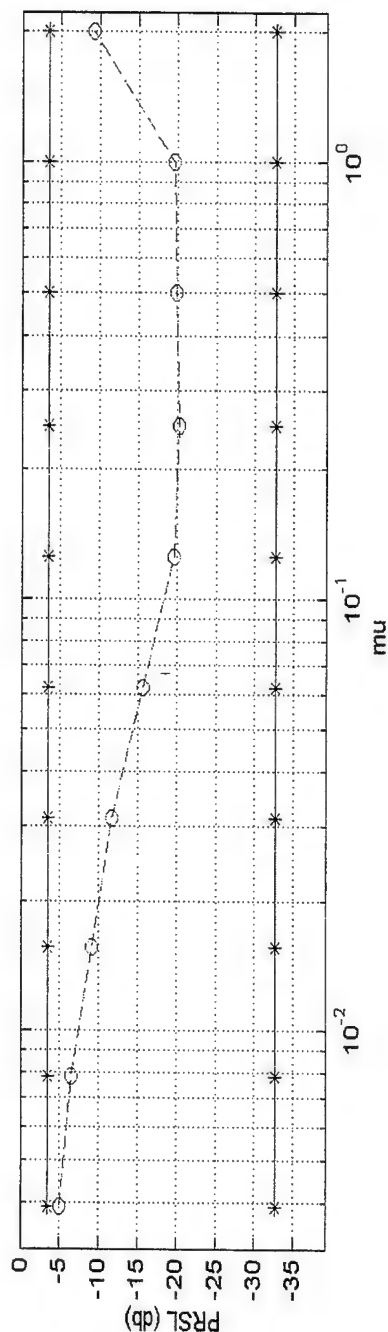
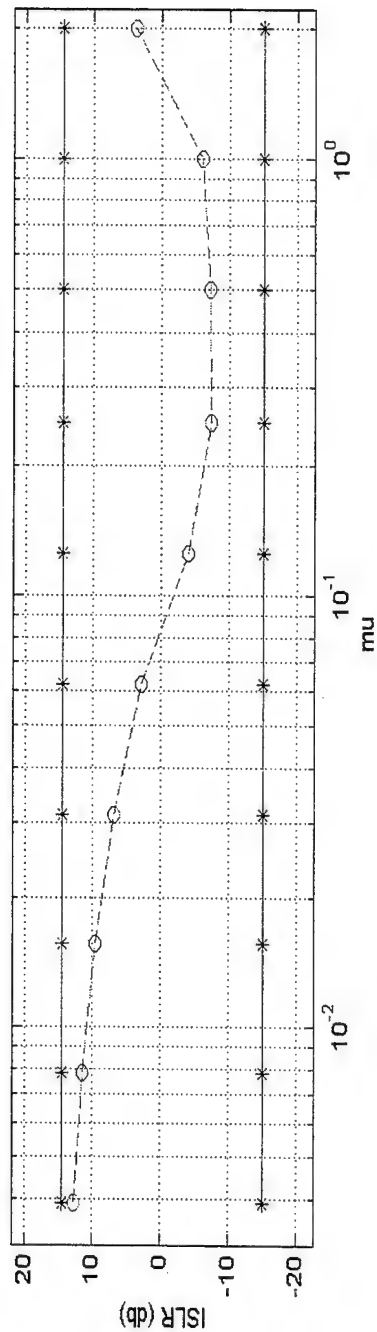
$$ISLR = \frac{\int |x(r)|^2 dr}{\int_{ML} |x(r)|^2 dr}$$
 - PRSL: peak range sidelobe level

$$PRSL = \frac{\max_{SL} \{x(r)\}}{\max_{ML} \{x(r)\}}$$
- **Other metrics will later be defined and calculated.**

TDLMS: Performance Curves

($L=128$; $\Delta=1$)

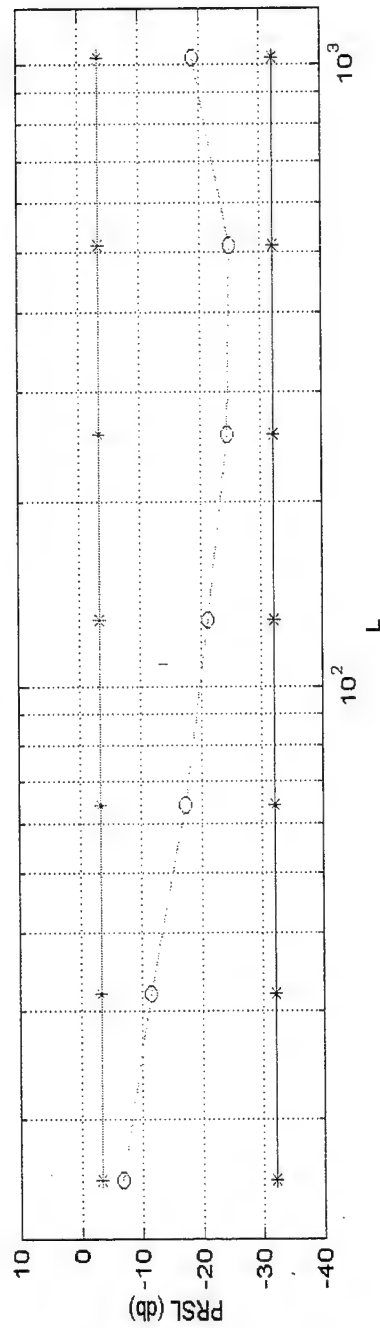
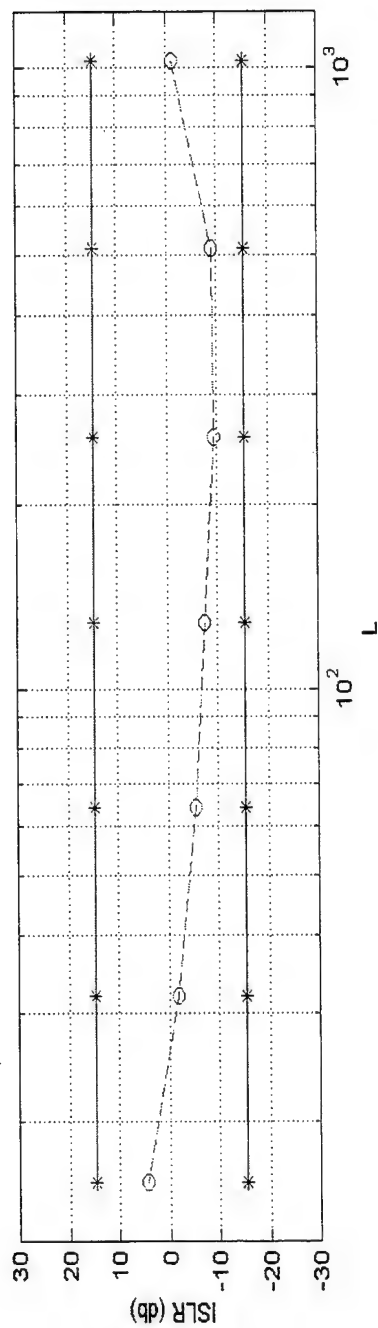
* filter off (upper), ideal (lower)
 o filter on



TDLMS: Performance Curves

($\mu=0.35$; $\Delta=1$)

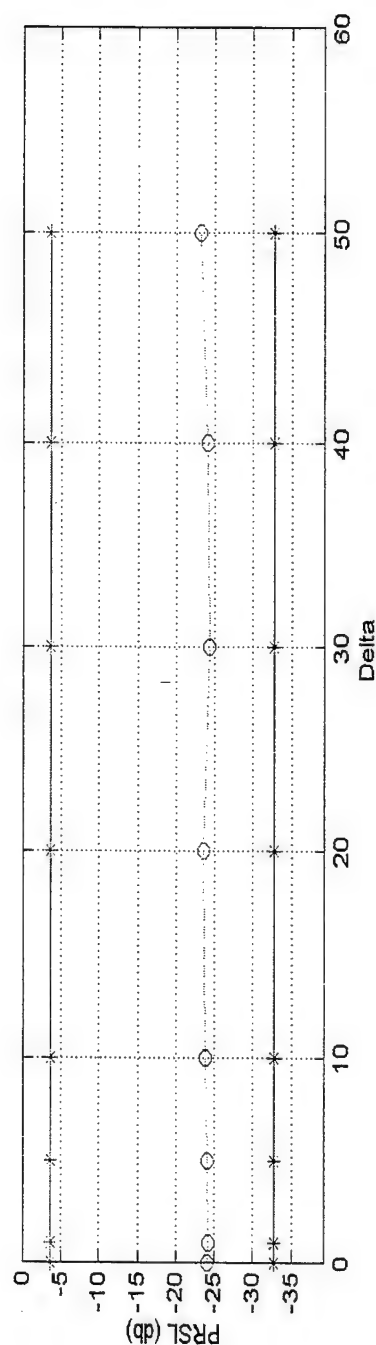
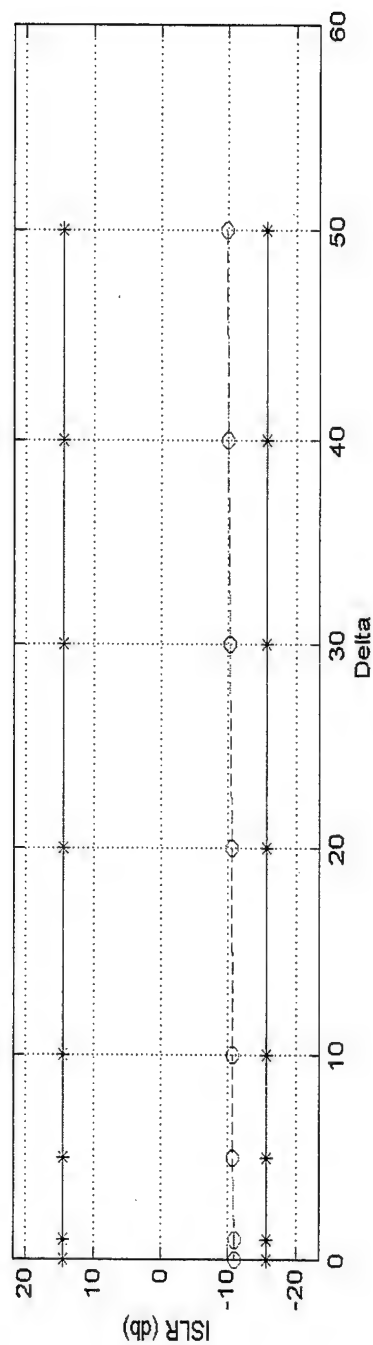
- * filter off (upper), ideal (lower)
- o filter on



TDLMS: Performance Curves

($L=512$, $\mu=0.35$)

- * filter off (upper), ideal (lower)
- o filter on



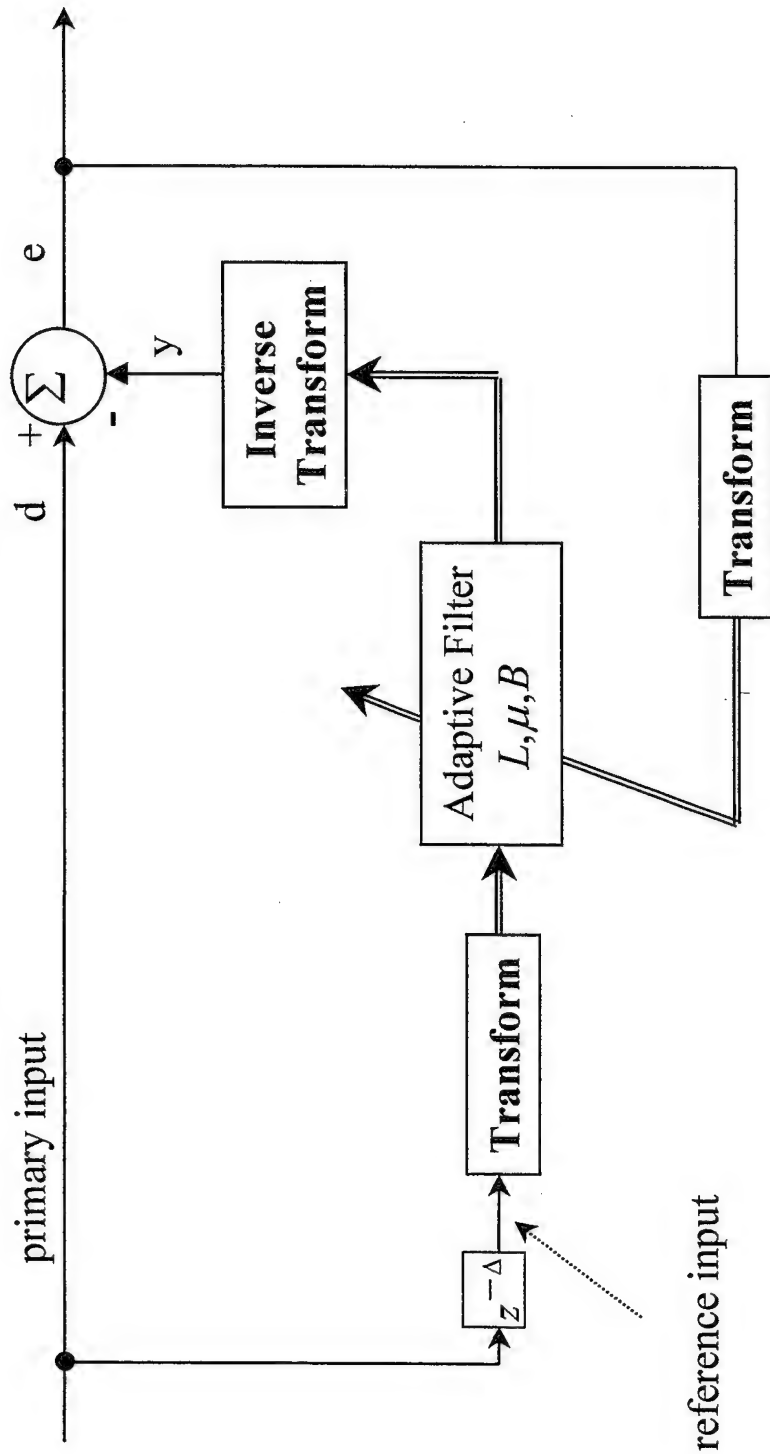
JPL RFI Adaptive Filtering

Mount Sonoma, California. P-band TopSAR.

Cleaned with TDLMS Filter



FDLMS Adaptive Filter. Simple Block Diagram



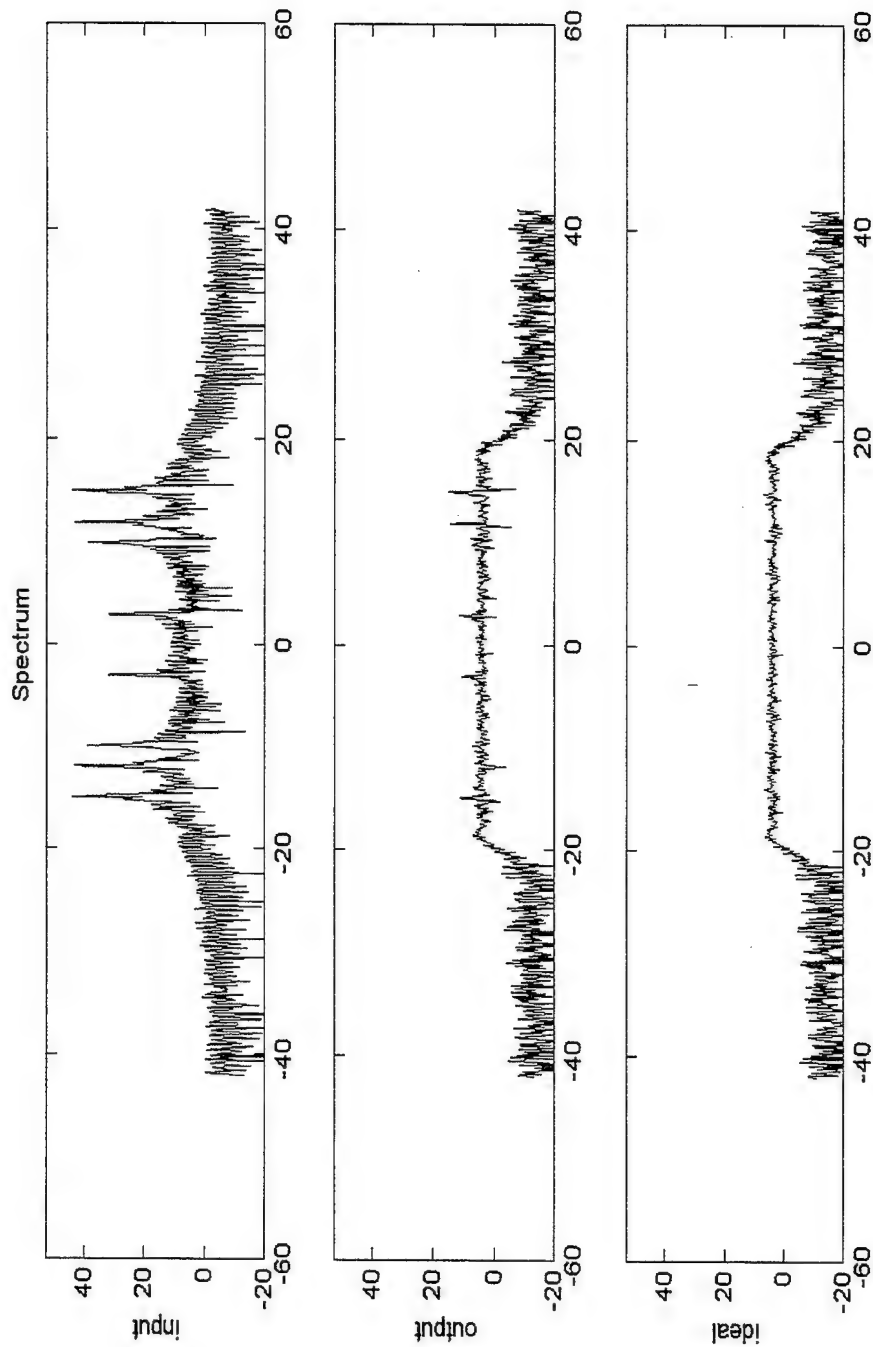
Main idea: keeping the filter weights fixed for a block of samples (time-domain blocking). And use the average error over this block to update the tap weights



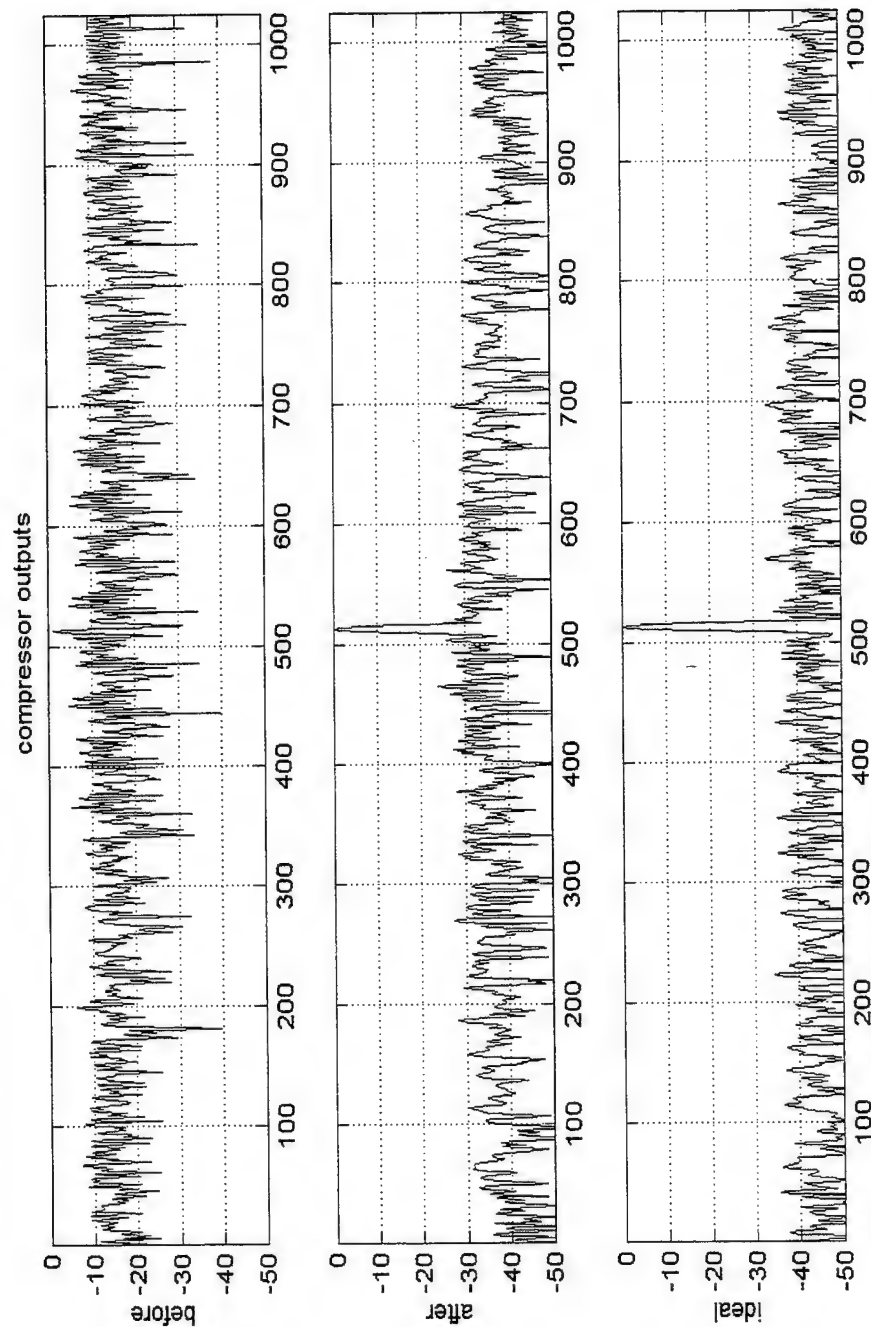
Advantages of Frequency-Domain Adaptive Filter

- Allowing block adaptive filtering (of time-domain samples)
 - large saving in computational complexity.
 - **efficient implementation** with FFT.
- Generating (approximately) uncorrelated signals in the frequency domain
 - Different step size in each frequency bin.
 - Reduce eigenvalue spread by normalization .
 - **Faster convergence.**
- Warning: for nonstationary signals, the tracking performance of the block algorithm may become worse, and it is better to use other “**transform domain**” adaptive techniques, such as DCT, filter banks, wavelet, ...
- However, this situation has not yet been encountered in the TOPSAR data (so far).

FDLMS: Comparison of spectra



FDLMS: Comparison of compressor outputs

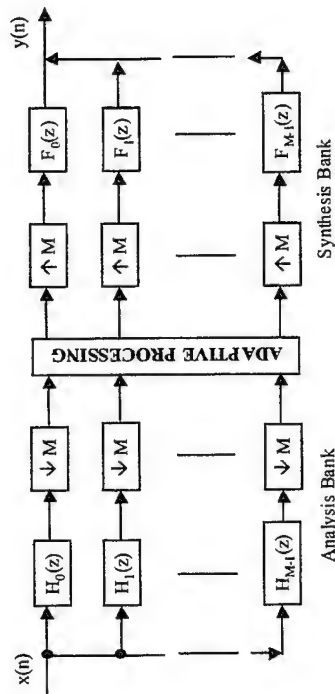




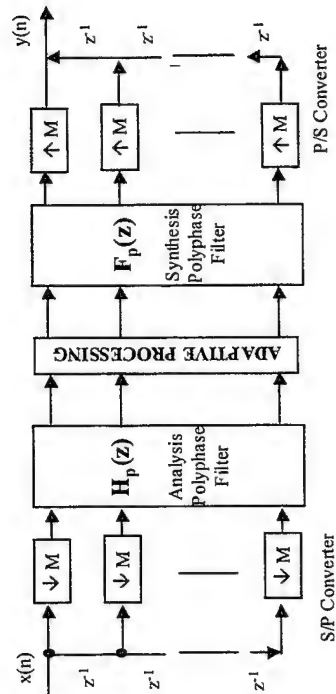
Mount Sonoma, California. P-band TopSAR.
Cleaned with FDLMS Filter



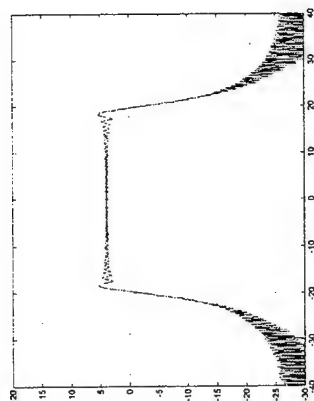
The Filter-Bank LMS Adaptive Filter



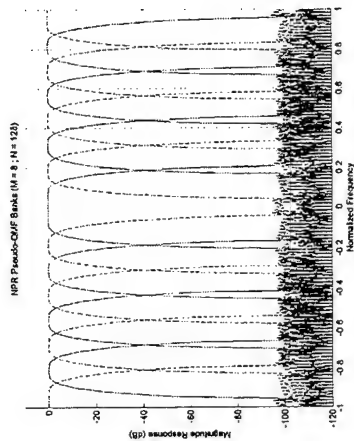
Direct Implementation



Efficient Polyphase Implementation



Radar Spectrum

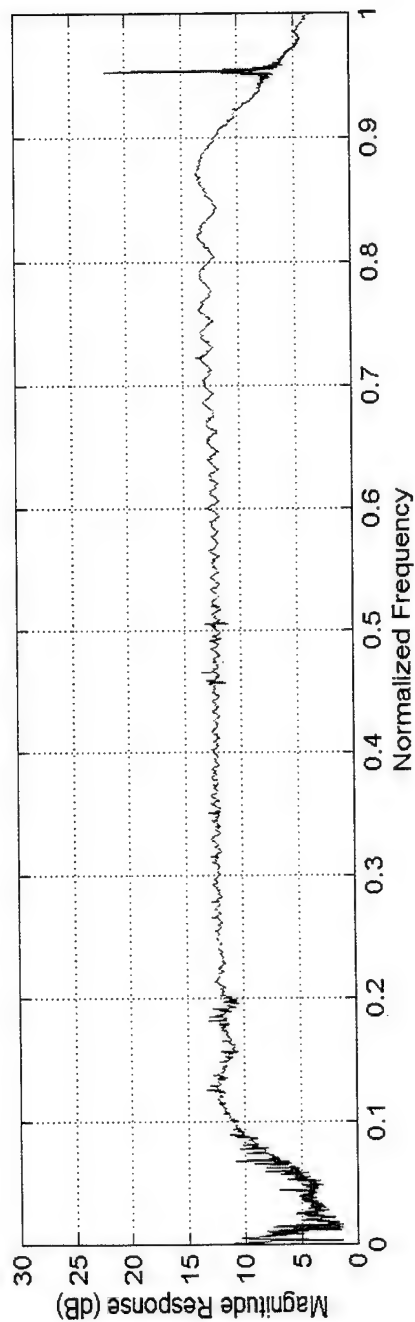
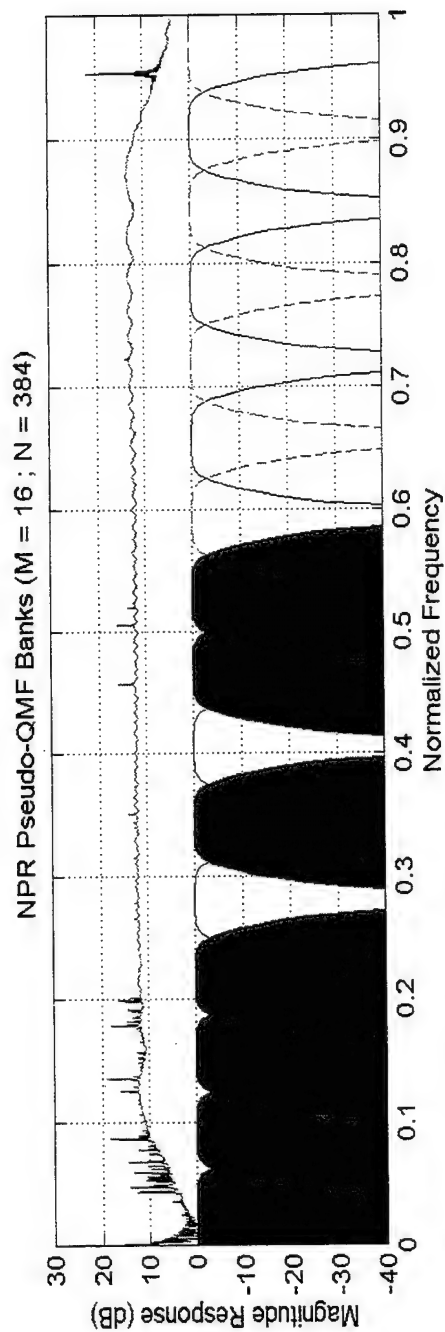


Filter Banks

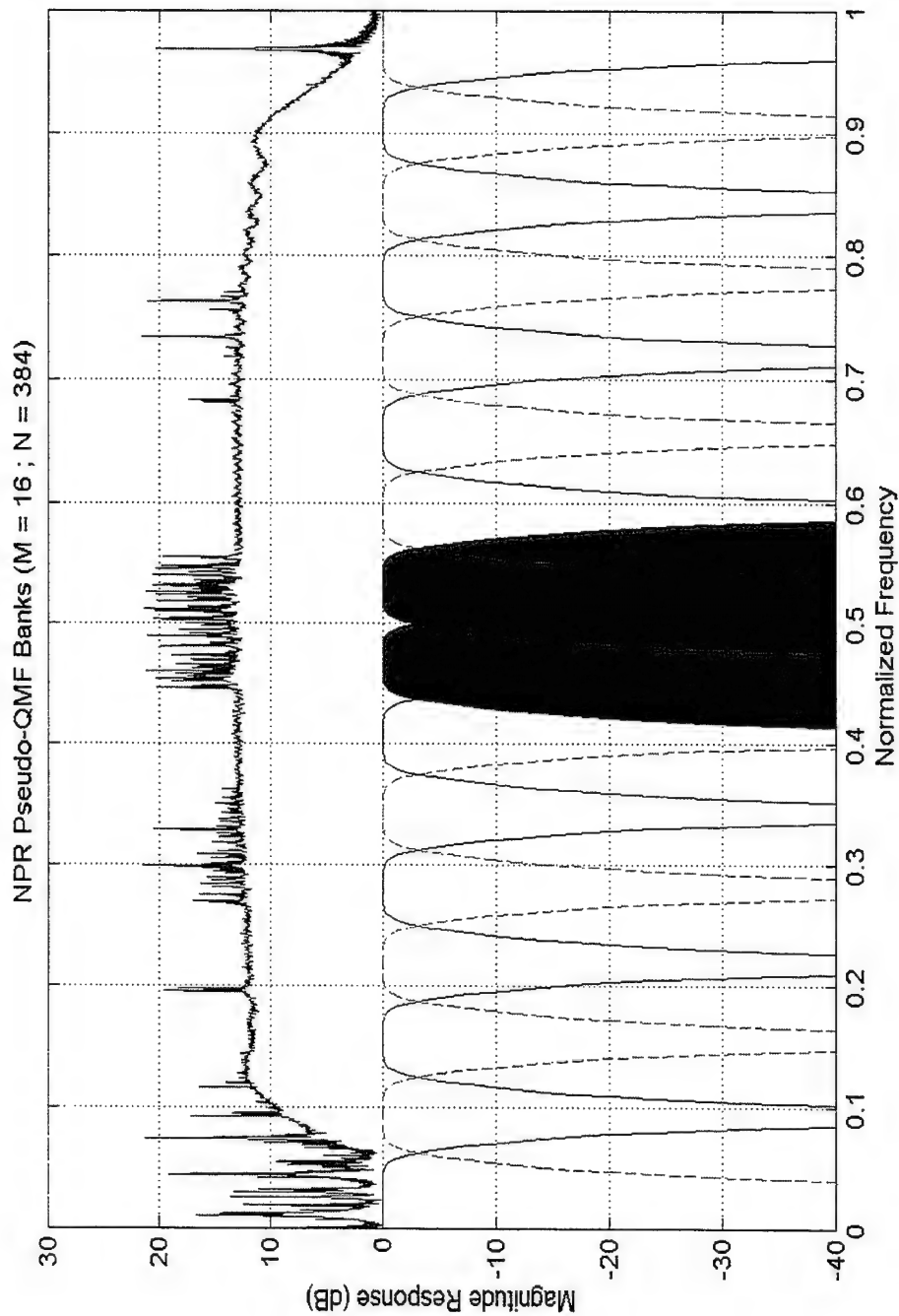
Introduction to the Filter Bank LMS Adaptive Filter

- Intuitive idea: blocking in the **frequency domain**.
- Advantages:
 - through subband
 - parallel processing, each subband is adapted independently of each other.
 - reducing eigenvalue spread, faster convergence speed.
 - through decimation
 - in each subband, processing signals at lower rate.
 - reducing the computational load.
- Disadvantages:
 - Decimation leads to spectral overlaps (aliases).
 - Interpolation leads to spectral images.
 - Solutions
 - cross filters.
 - auxiliary subbands.
 - wavelets.
 - **perfect-reconstruction filter banks.**

FBLMS Advantage: Reduction of Computational Load

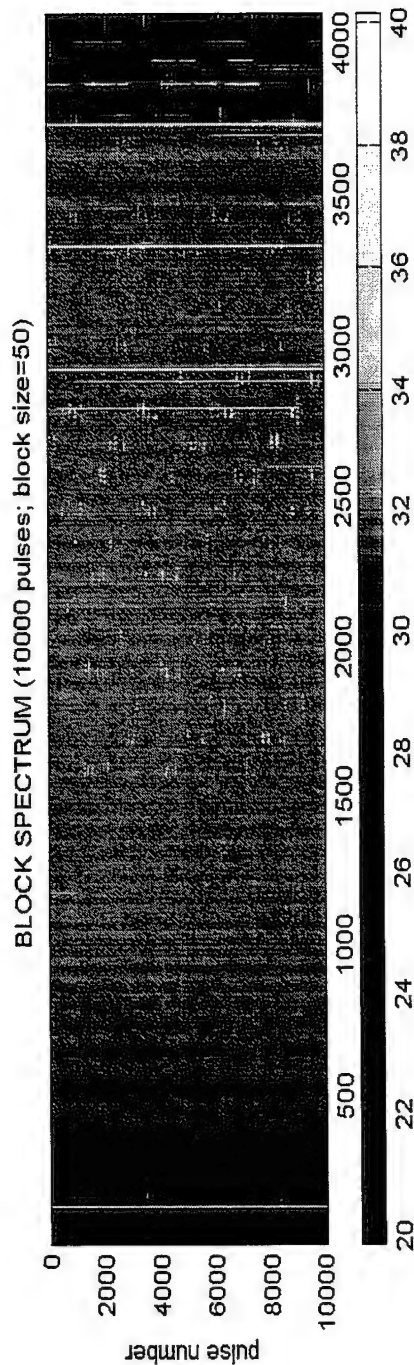
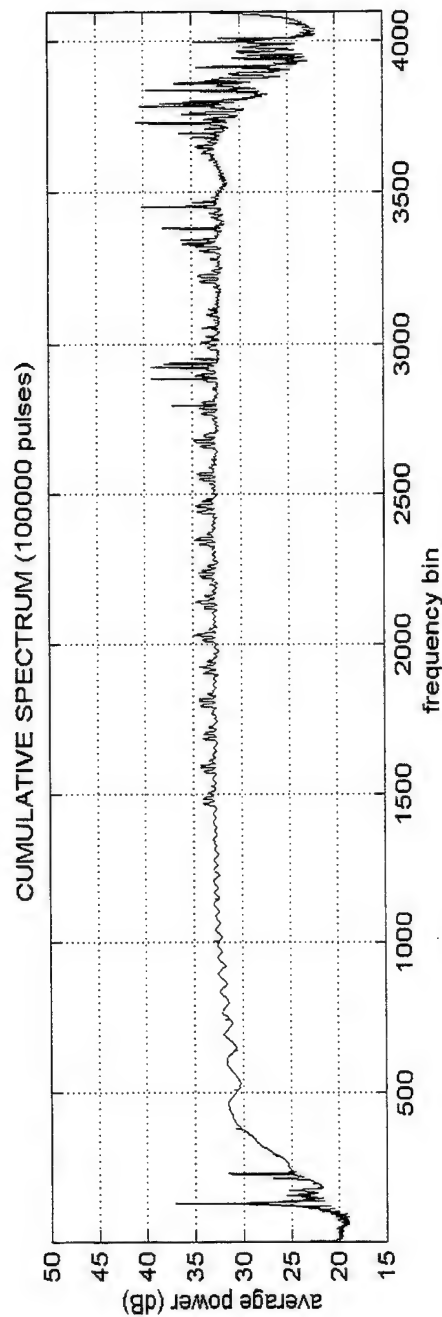


FBLMS Advantage: Reduction of Eigenvalue Spread





Mount Sonoma, CA. P-Band TopSAR. Block Spectra. (Used to study the filter's refreshing rate)



Throughput Requirements

(with current SGI Challenge workstation for 100,000 pulses)

	TopSAR (40MHz)	GeoSAR P-band (80 MHz)	GeoSAR P-band (160 MHz)
Number of range samples	6144	19,000	38,000
Worst case (without parallelization, weight update for every pulse)			
TDLMS	4 days	12 days	24 days
FDLMS (~10)	10 hrs	30 hrs	2.5 days
FBLMS (~4)	2.5 hrs *	7.5 hrs *	15 hrs *
Parallelization with 8 processors (~8)			
TDLMS	0.5 days	1.5 days	3 days
FDLMS	1.25 hrs	4 hrs	7.5 hrs
FBLMS	0.3 hrs *	1 hrs *	2 hrs *
Weight update at every N=50 pulses (~N^{1/2} ~ 7)			
TDLMS	1.7 hrs	5 hrs	10 hrs
FDLMS	10 min	30 min	1 hrs
FBLMS	2.5 min *	8.5 min *	17 min *

* projected



Conclusion and Current Activities

Conclusion:

- **TDLMS:** except for long running time, provides excellent performance when applied to both simulation and real TOPSAR data.
- **FDLMS:** provides great saving (by an order of magnitude) in computational complexity with similar performance.
- **FBLMS:** targeted algorithm to further reduce the computation by an order of magnitude and to increase the performance (at the same time) .

Current Activities:

- Overlapping filter banks to avoid spectral gaps.
- Azimuth ISLR and PSLR measures.
- Filtering effects on radiometric calibration and polarimetric calibration.
- Ability of the adaptive filters to recover the phases needed for interferometry.
- Optimal incorporation of sniffer pulse data into the algorithm.
- Intensive testing of the algorithms with real data in different noisy environments.

Adaptive Dual Aperture Clutter Cancellation

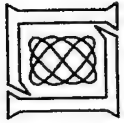
Mitchell I. Mirkin

MIT Lincoln Laboratory
244 Wood Street, Room S4-453
Lexington, MA 02173-9108
tel: (781) 981-3453
email: mirkin@ll.mit.edu

Abstract The DARPA Moving Target Exploitation (MTE) Program seeks to develop the technology to classify moving ground vehicles from an aircraft using a microwave radar with high range resolution. An MTE X-band radar data collection with moving vehicles occurred at China Lake, CA, in September 1995. The (ERIM DCS) airborne radar used in this collection is a 600 MHz instantaneous bandwidth, linear FM system with two along-track antennas to enable clutter cancellation, an obvious requirement for boosting the contrast of slow movers in competing ground clutter. The nominal data collection mode was synthetic aperture radar (SAR) with simultaneous receive beams as well as alternating transmit pulses from each aperture. Stationary clutter could be imaged with 0.3-m resolution in both range and cross-range.

This paper discusses a method for adaptively canceling clutter by using SAR clutter data from each of the simultaneous receive beams. One SAR image is equalized to the other by amplitude and phase compensation both in range and in cross-range (Doppler). Then, the images are subtracted for clutter cancellation. Vehicles moving with respect to the clutter are then easily detected and passed to a high-resolution classifier, which is outside the scope of this paper.

This paper concentrates on the shapes of the amplitude and phase compensation curves, their physical causes (such as post-deramping amplifier mismatches, range and cross-range distance between antenna horns, and antenna boresight error), the day-to-day and pass-to-pass variations that were encountered, and the estimation and clutter cancellation accuracy.



Adaptive Dual Aperture Clutter Cancellation*

Mitch Mirkin

MIT Lincoln Laboratory

ASAP Workshop

11 March 1998

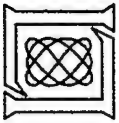
* Sponsored by DARPA / STO

ASAP.1-1
MIM 1/28/98

Preceding Page Blank

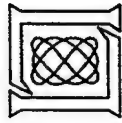
335

MIT Lincoln Laboratory



Outline

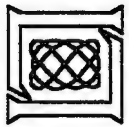
- Background
 - STAP and generalized DPCA (arrested SAR)
 - Adaptive calibration and adaptive nulling
- Dual aperture radar data processing for clutter cancellation
- Summary



Overview

- **Moving Target Exploitation Program sponsors clutter cancellation work**
 - Needed for high-resolution range profiles and images of moving ground vehicles for ATR
 - First used ERIM DCS radar data (600 MHz bandwidth)
 - Currently using Enhanced Joint STARS data
 - Future use with DARPA Sensor Emulation Platform (SEP/GH)
- **Talk objectives**
 - Bridge STAP and SAR communities
 - Link adaptive clutter cancellation weights to physical parameters

Understanding aids in accurate and efficient processing design

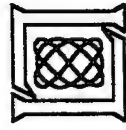


ERIM International DCS Radar



● Parameters

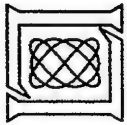
- 9.66 GHz center frequency
- 600 MHz RF bandwidth
- 5.2 deg azimuth beam width
- 977 Hz PRF
- 10 km nominal range
- 0.47 m between antenna effective phase centers
- 100 m/s nominal aircraft speed
- -45 dB noise equivalent σ_0



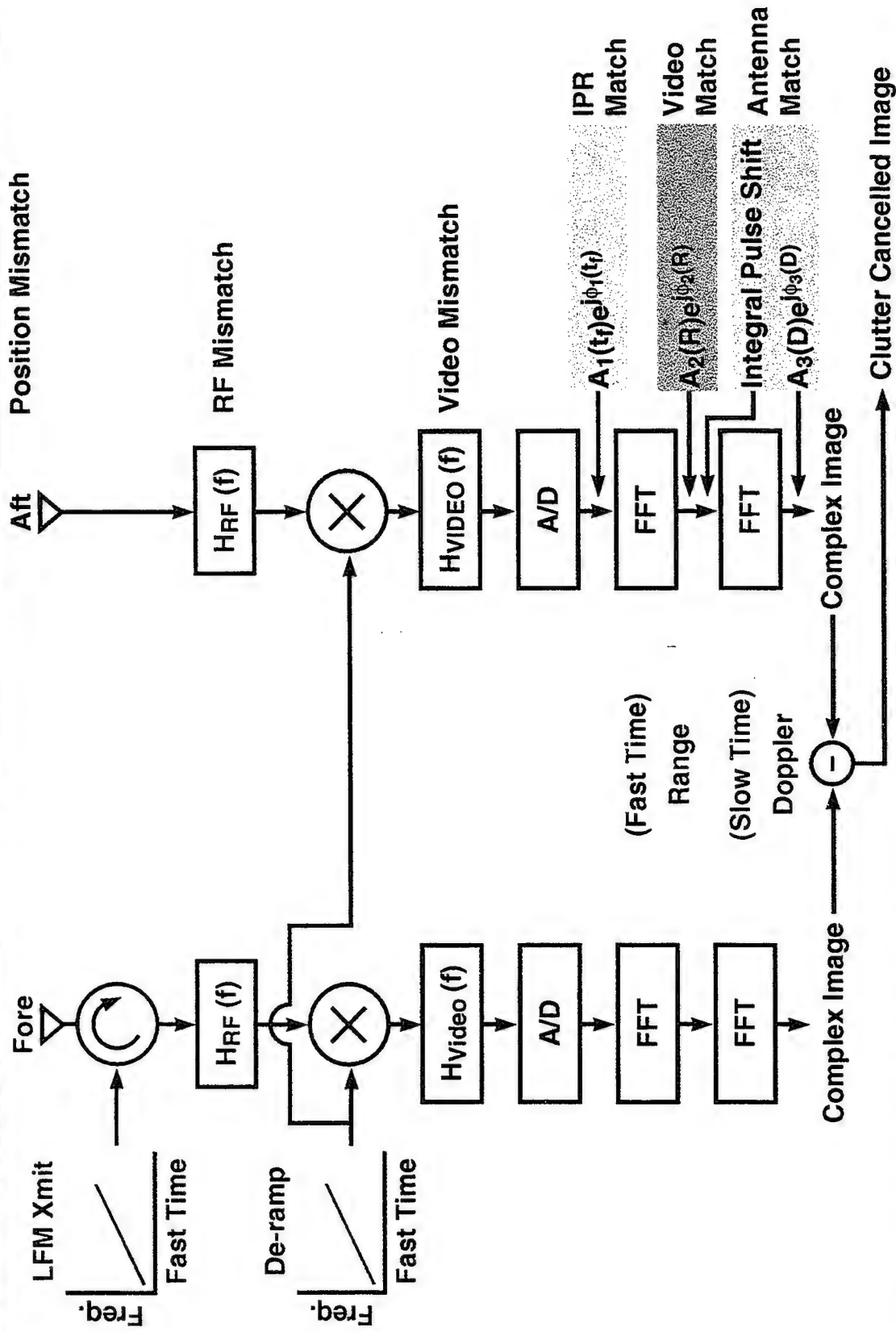
Displaced Phase Center Antenna (DPCA)

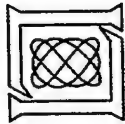
- “Strict sense” DPCA clutter cancellation
 - Two identical subapertures
 - Variable PRF dependent on aircraft velocity
 - Two pulse canceller when subapertures spatially coincide
 - Coherent integration (Doppler filter bank)
- Generalized DPCA (arrested SAR) clutter cancellation
 - Two similar antennas
 - Fixed PRF (above Nyquist sampling rate for interpolation)
 - Doppler filter banks (2 SAR images)
 - Equalize or compensate one image
 - Subtract images

In general, weight depends on target and clutter Dopplers and CNR

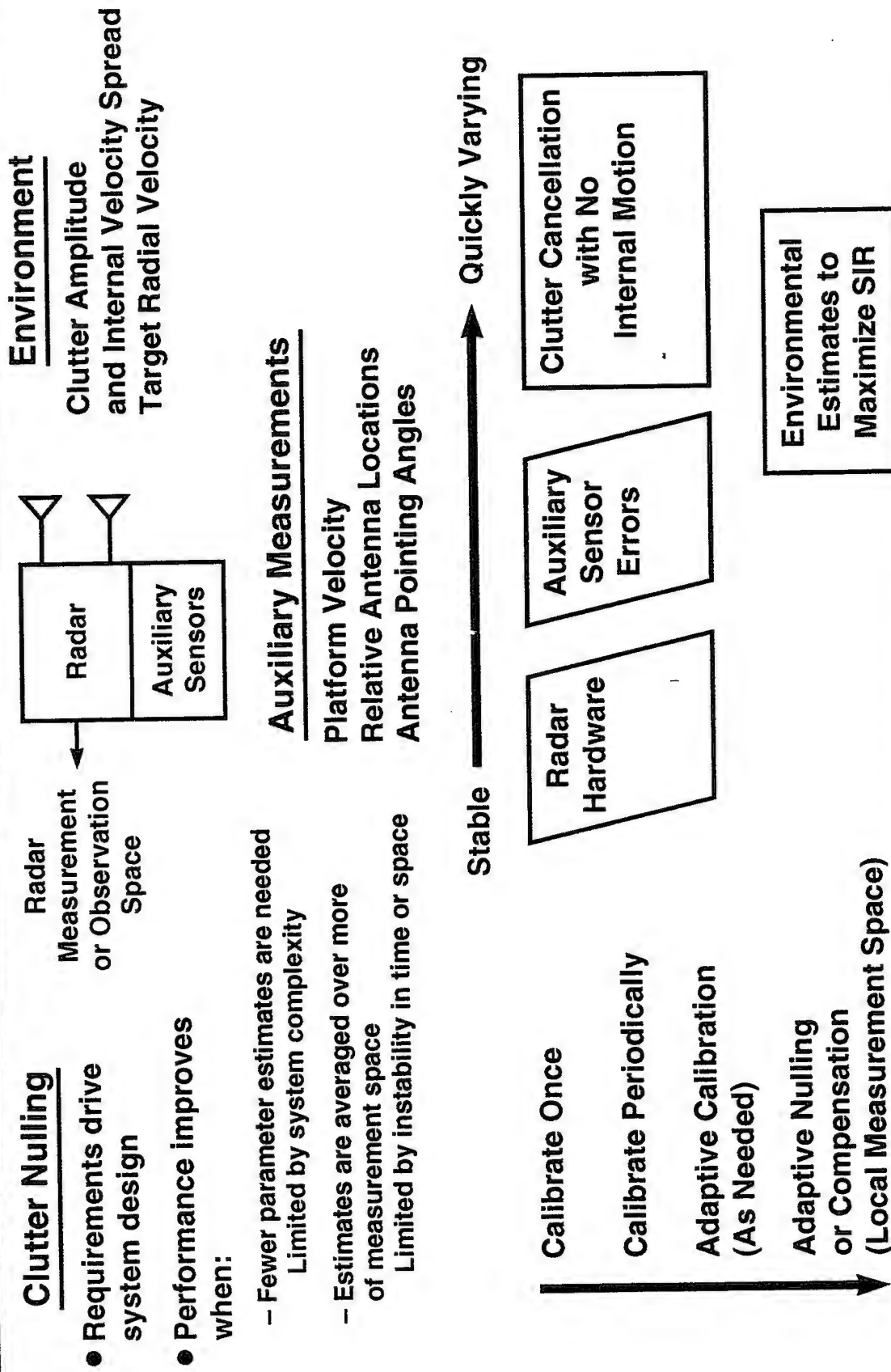


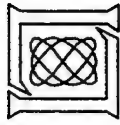
Mismatch Sources and Correction Locations





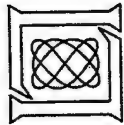
Roles for Adaptive Processing in Two Antenna SAR System





Outline

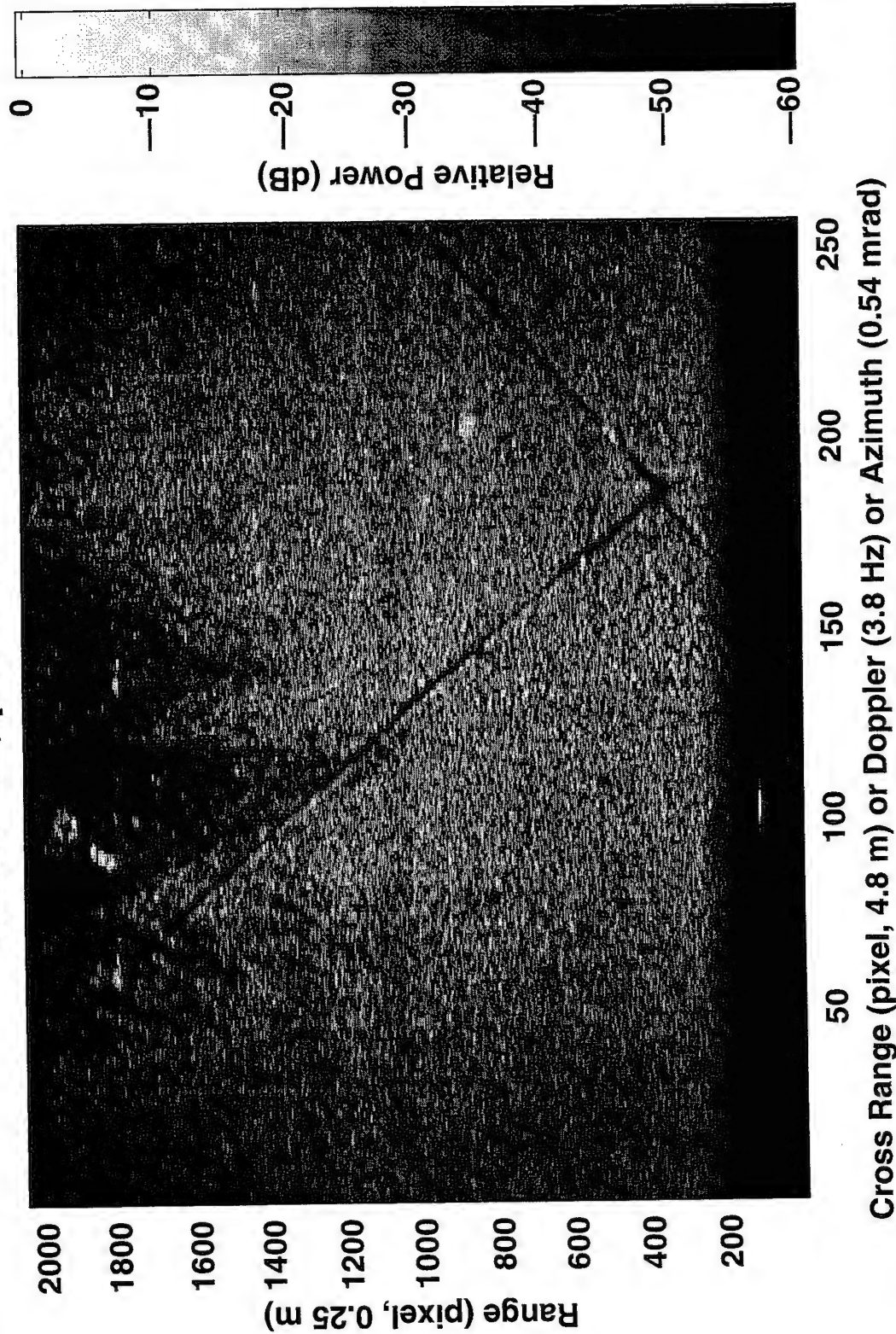
- Background
- Dual aperture radar data processing for clutter cancellation
 - Amplitude and phase corrections in Doppler
 - Amplitude and phase corrections in range
 - Measured cancellation effectiveness
- Summary



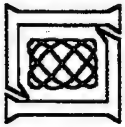
Single Antenna SAR Image

Full FFTs Are Shown

dra216d2, pulses 1—256

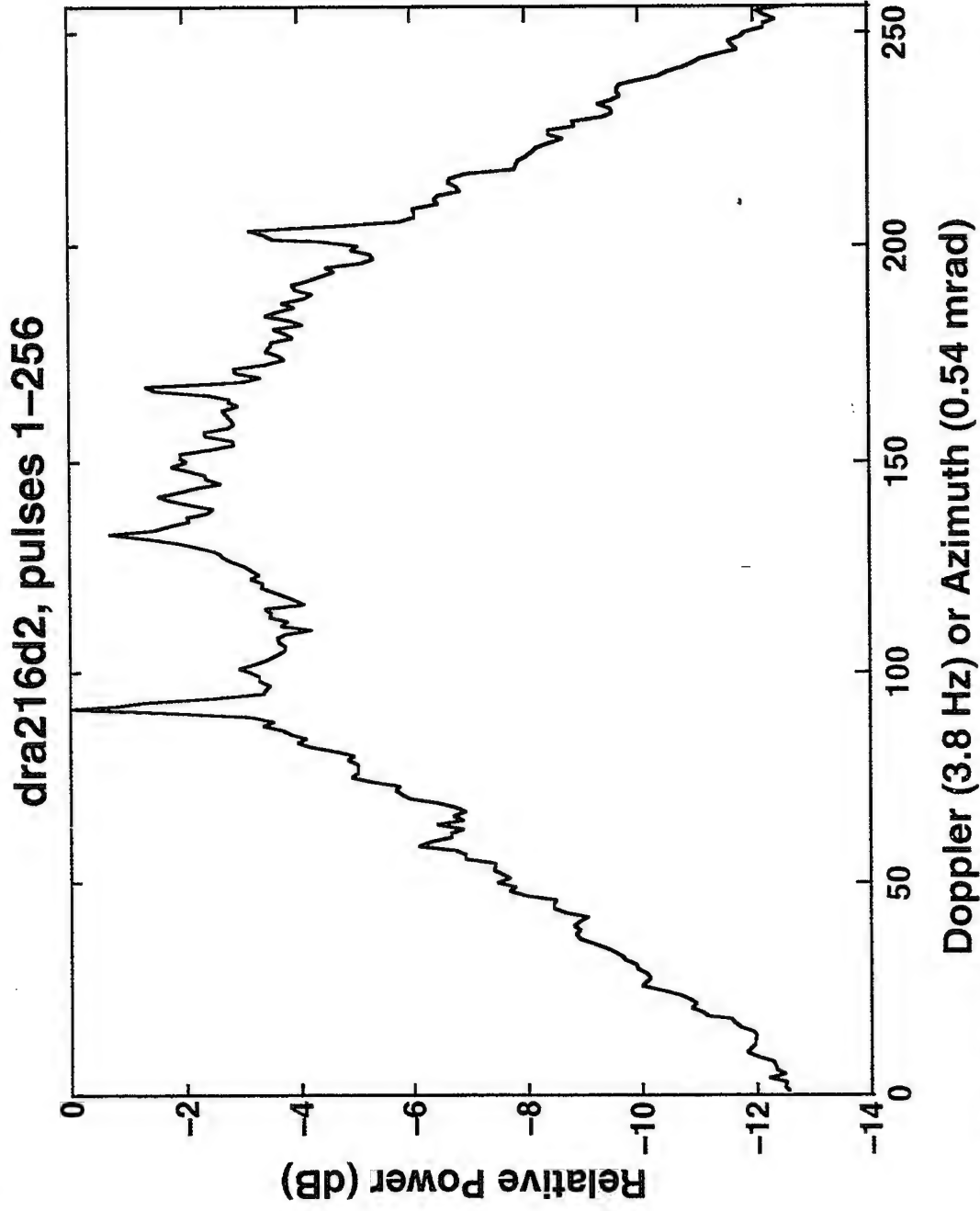


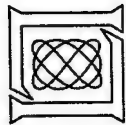
MIT Lincoln Laboratory



Estimate of Antenna Beam Shape

$$\bar{P}(D) = \int P(R,D) dR$$

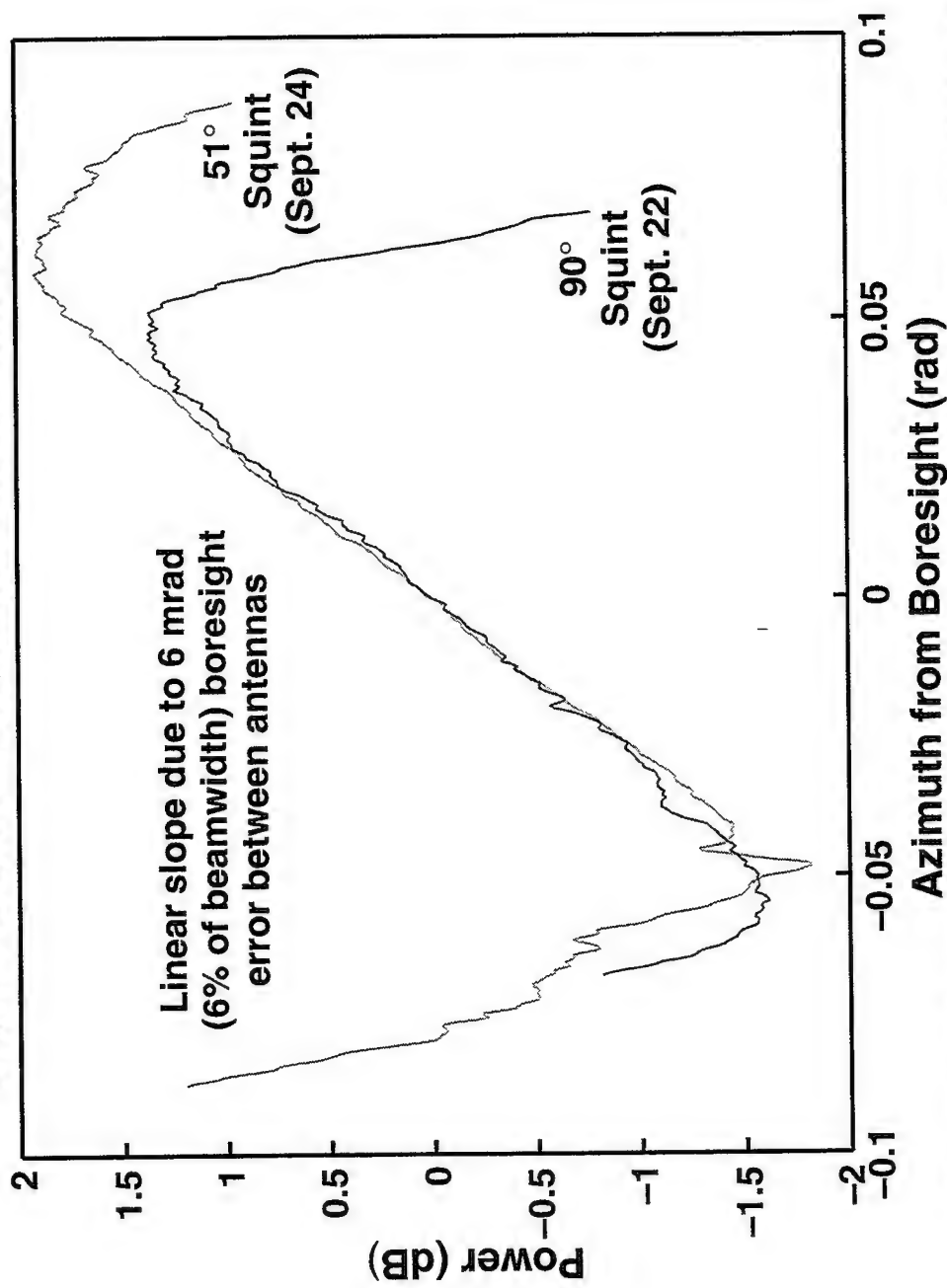




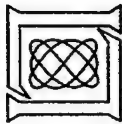
Power Differential in Doppler

$\bar{P}_F(D) / \bar{P}_A(D)$

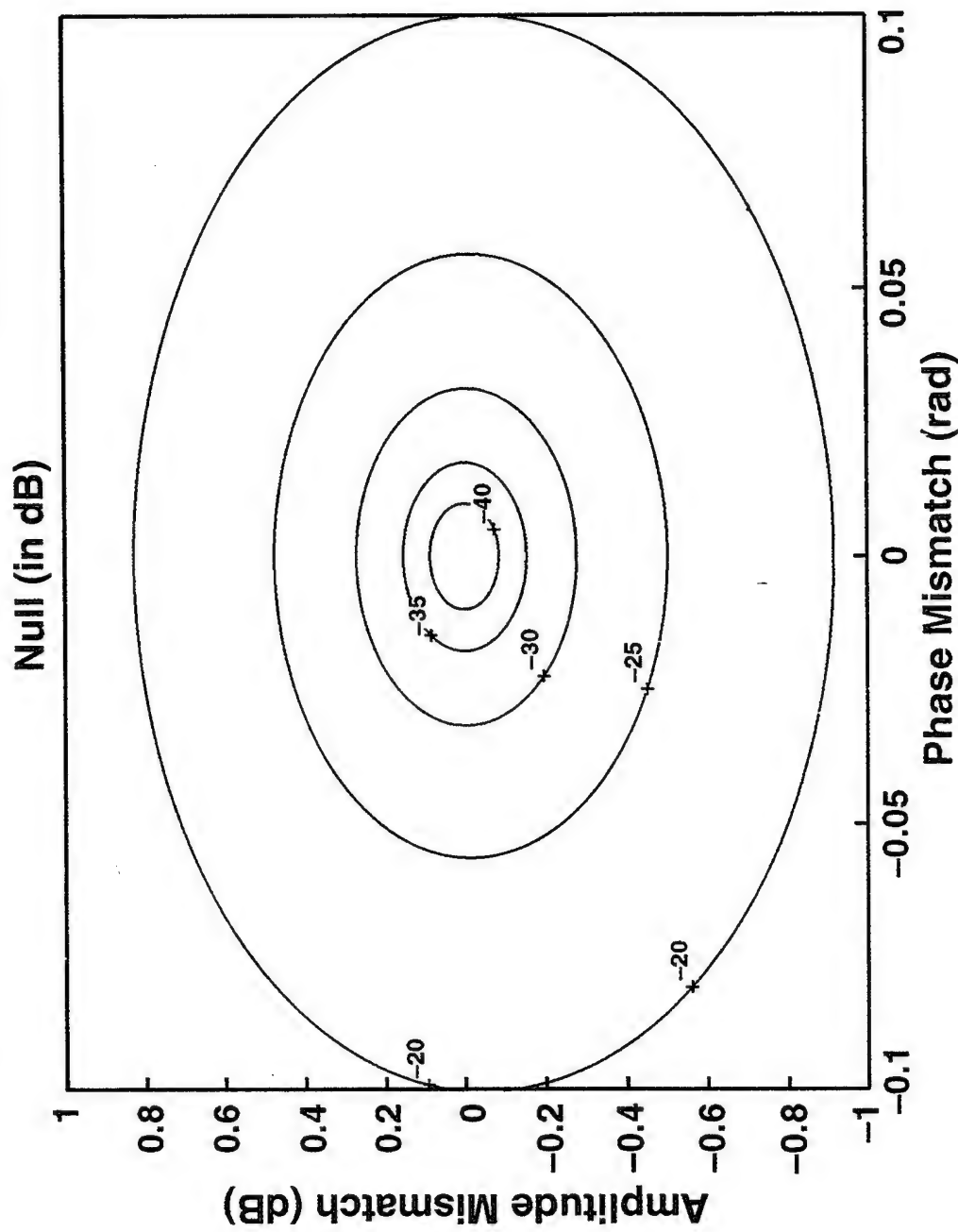
Clutter Calibration, dra216d2 vs dra305a29

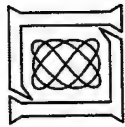


Boresight error = Slope (dB/rad) \times (3 dB Beamwidth)² / 48 dB



Dual Channel Matching Requirements to Null

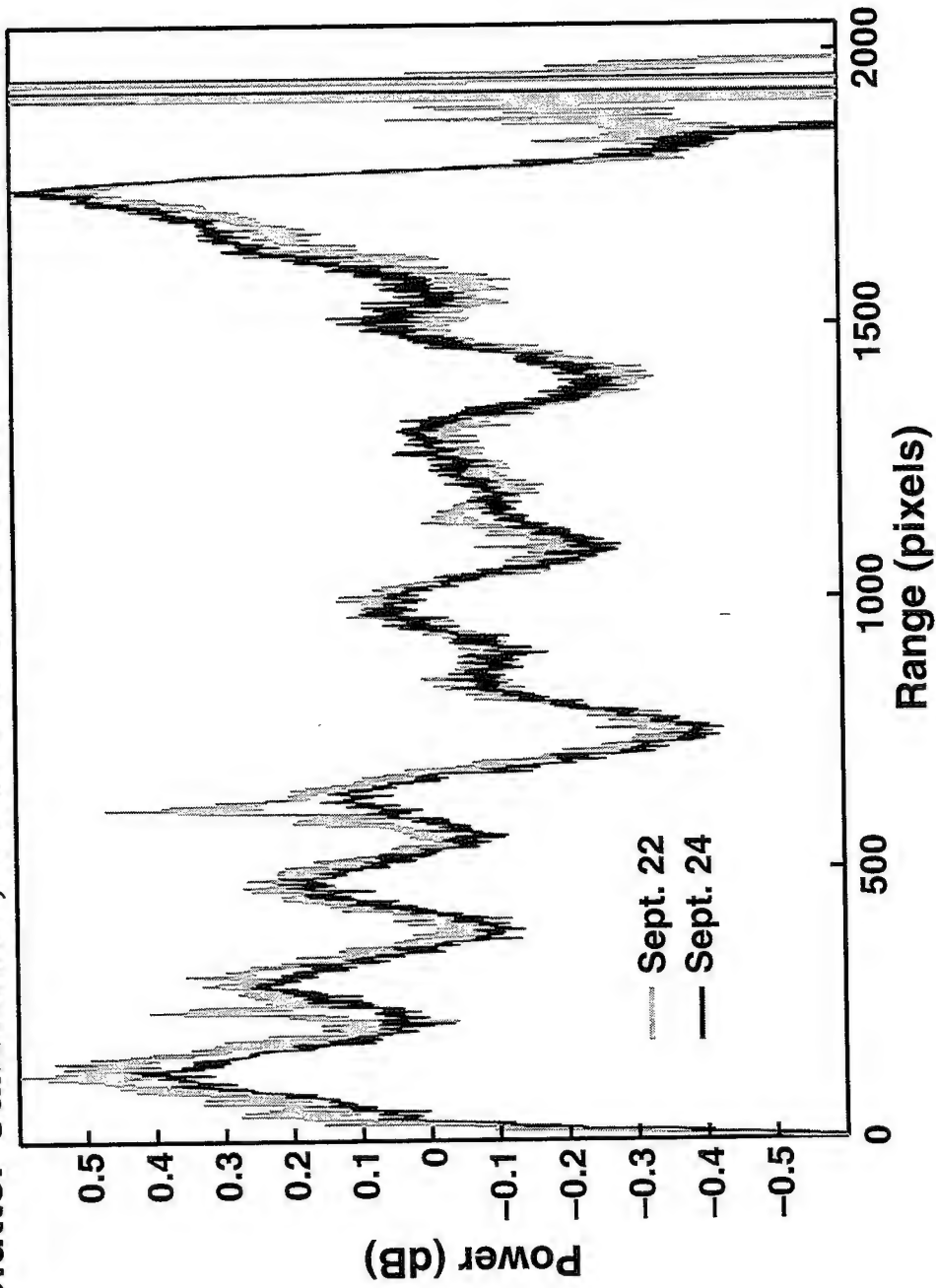


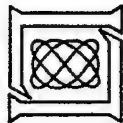


Power Differential in Range

$$\bar{P}_F(R) / \bar{P}_A(R)$$

Clutter Calibration, dra216d2 vs dra305a29, rms diff = 0.08 dB

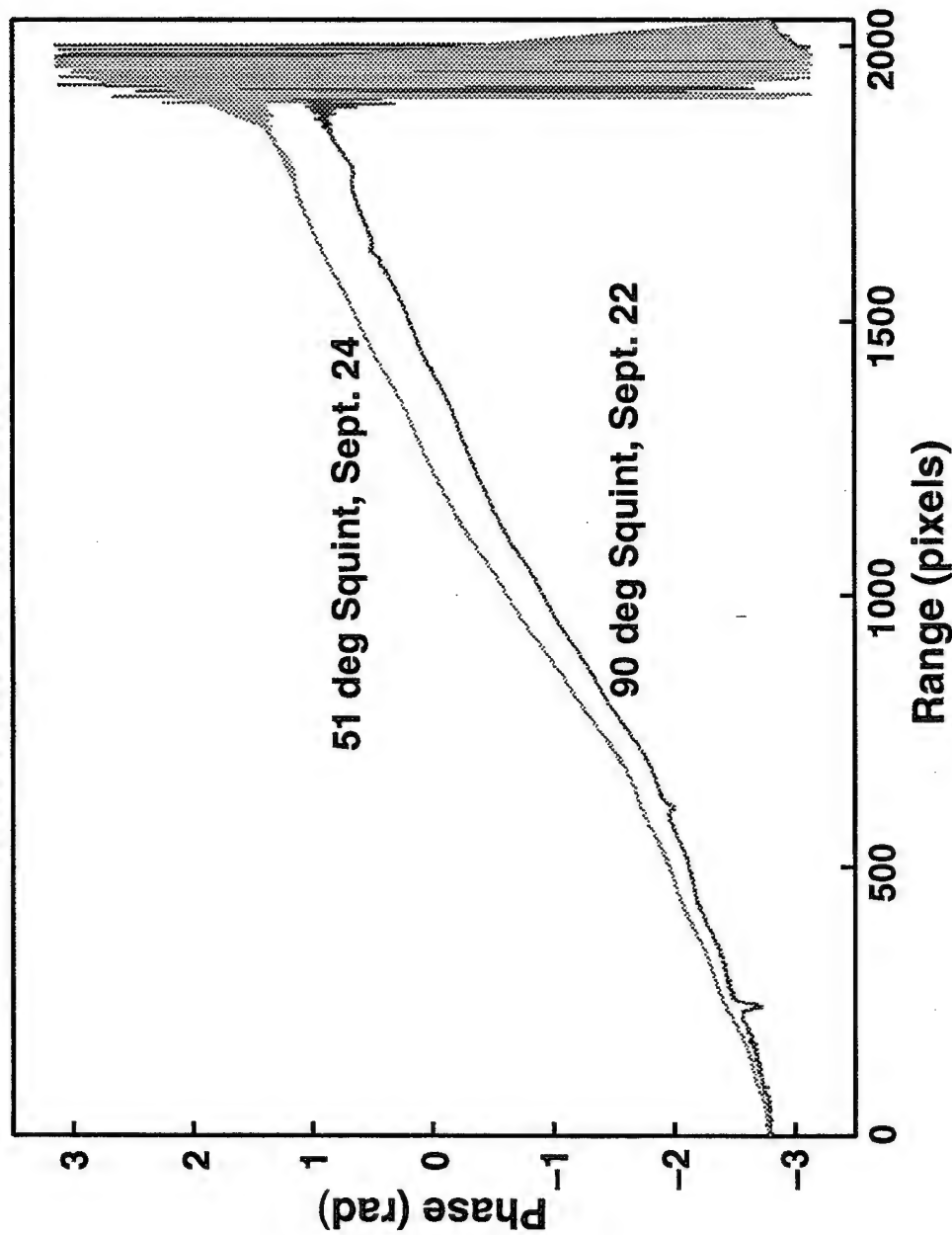


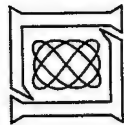


Phase Differential in Range

Angle $[\int X_F(R,D) X_A^*(R,D) dD]$

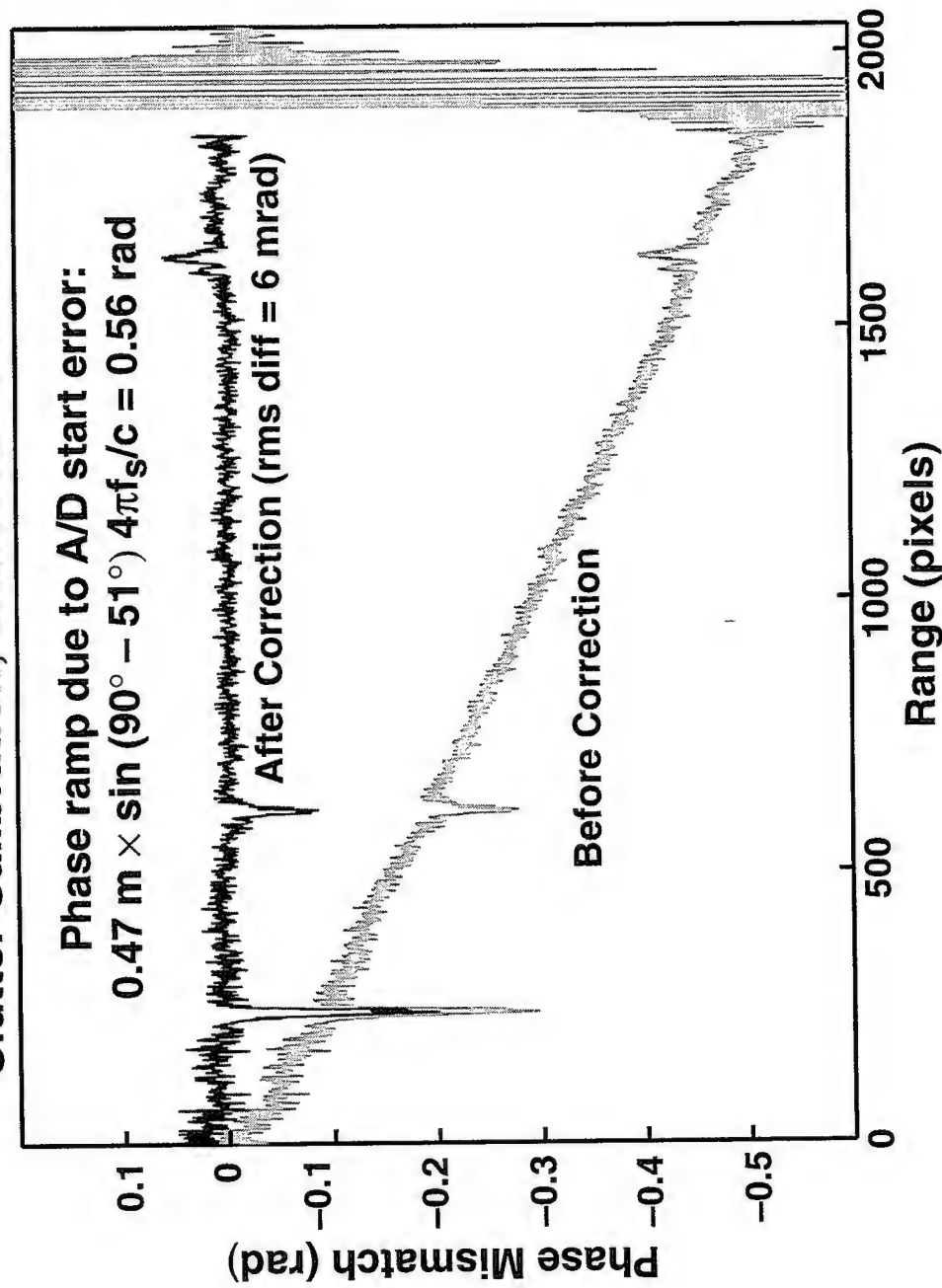
dra216d2 vs dra305a29

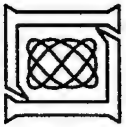




Phase Mismatch in Range Due to Squint Angle Difference

Clutter Calibration, dra216d2 vs dra305a29





Signal Processing

- **To adaptively calibrate with clutter images**

Create fore image, $X_F(R, D)$

Create aft image after integral pulse delay based on auxiliary measurements (aux) or cross correlation

$a(D) = dB [\bar{P}_F(D) / \bar{P}_A(D)]$, fit straight line (non-aliased region, LPF rest)

$D \Rightarrow az$ (using aux) $\Rightarrow az$ boresight error of antennas (fixed)

$a(R) = dB [\bar{P}_F(R) / \bar{P}_A(R)]$, low pass filter \Rightarrow video mismatch (fixed)

$\phi(D) = \text{angle} [X_F X_A^* dR]$, fit straight line \Rightarrow fractional pulse slip (compare to aux)

$\phi(R) = \text{angle} [X_F X_A^* dD]$, LPF \Rightarrow video mismatch (fixed) + linear (squint, compare to aux)

- **Methods to clutter cancel fore and aft images**

(1) Use aux and previous cal to generate aft compensation, $a(D)a(R)e^{j[\phi(D)+\phi(R)]}$, then subtract aft compensated image from fore image

(2) Adaptively calibrate these 2 images, apply compensation, subtract

(3) Hybrid: use whichever cal functions are very stable, adaptively estimate the rest for this pair, apply full compensation, subtract

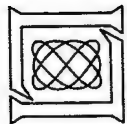
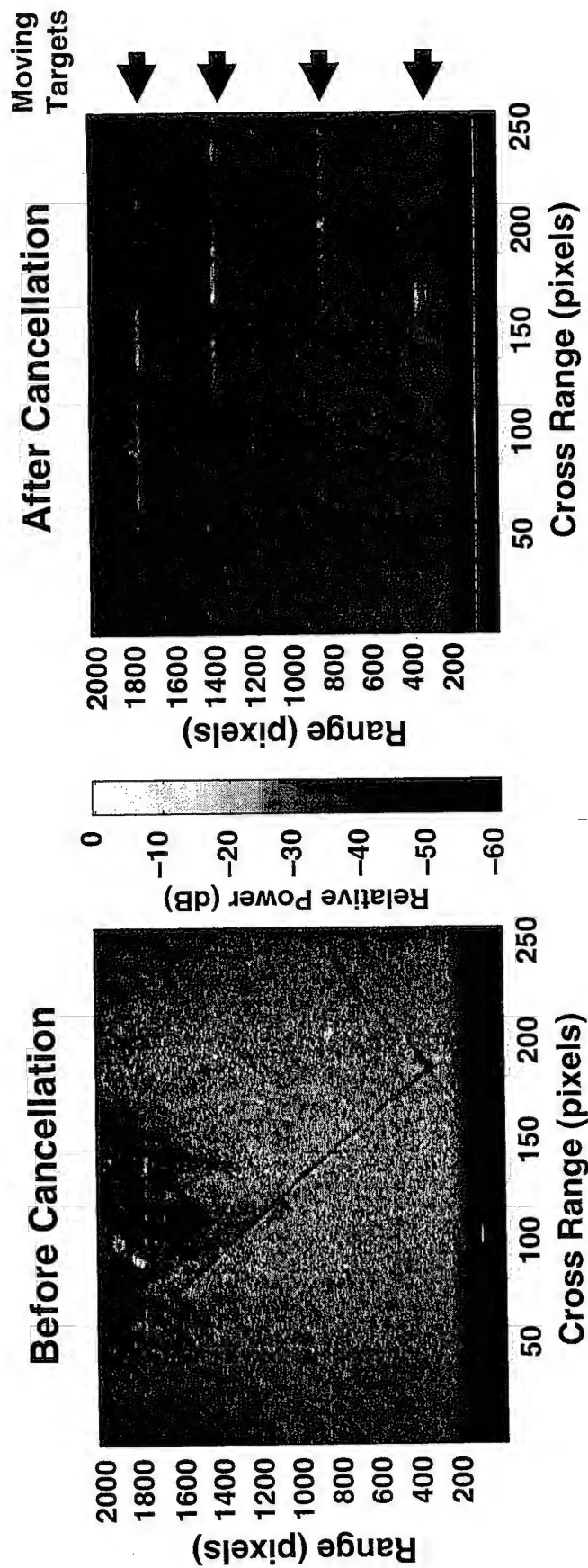
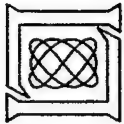


Image Comparisons

dra216d2, pulses 1-256

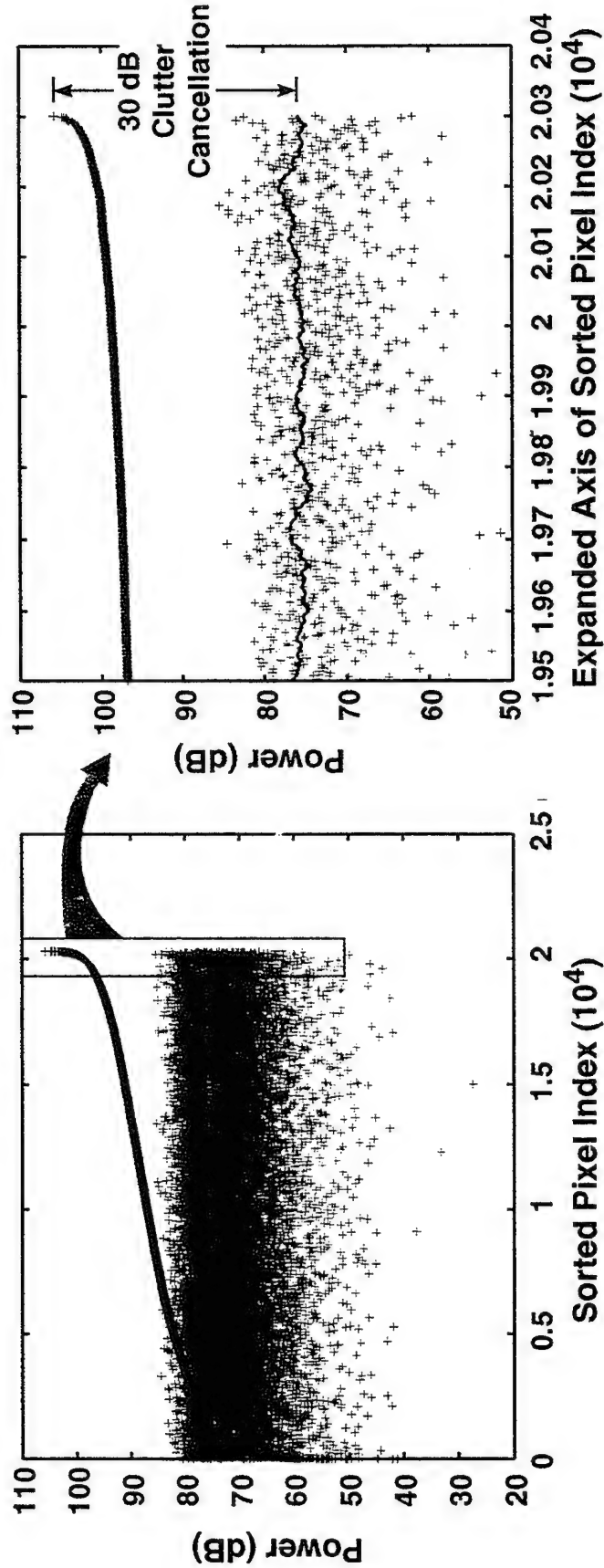


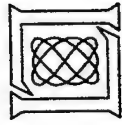


Clutter Canceller Effectiveness

dra0216d2, Pixels 1000:1200, 75:175

- Power from single antenna image
- Average power from clutter cancelled image





Summary

- DPCA processing was reviewed for dual apertures
 - “Strict sense”
 - Generalized or arrested SAR or STAP
- Adaptive calibration provided at least 30 dB clutter cancellation that was stable for at least 2 days
- Calibration and nulling strategy was described
 - Calibrate over full measurement space when possible
 - Average as long as stable
 - Fit straight line functions when correct
 - Low pass filter slow variations
 - Adaptively null or compensate over local space when needed

Adaptive SAR Imaging and Its Impact on ATD/R and Image Exploitation

Stuart R. DeGraaf

Northrop Grumman Corporation
Electronic Sensors and Systems Division
P.O. Box 746, MS 1155
Baltimore, MD 21203
email: srd@cestua.md.essd.northgrum.com

Abstract Conventional spotlight SAR imaging exploits the Fourier transform pair relationship between signal history and scene reflectivity, and therefore employs a weighted 2-D FFT to form a SAR image. Since SAR collection apertures are of finite size in wavenumber space, the spatial resolution afforded by Fourier imaging is inherently limited. Finite resolution leads to speckle or scintillation, which is caused by random constructive and destructive interference of independent unresolved scatterers. Modern spectral estimation (super resolution) techniques offer improved image resolution and contrast, and more importantly, reduced clutter speckle and target scintillation. Ongoing research at Northrop Grumman has shown that two methods offer enormous benefits for SAR imaging and automatic target detection and recognition. The minimum variance method (MVM) and Pisarenko's method reduce target scintillation and clutter speckle through the signal history domain forward-backward subaperture averaging for covariance matrix estimation. MVM (and Pisarenko) make homogeneous clutter distributions appear more log-normal. As a result, MVM reduces the false alarm rate of a standard two-parameter CFAR screener by more than an order-of-magnitude and MVM imagery takes on a more "optical" appearance. Classical image processing tools, such as Laplacian sharpening filters, work better on MVM and Pisarenko imagery than on Fourier. Pisarenko's method reduces misclassification of military vehicles by roughly a factor of three, and may reduce the number of target templates required for target recognition. MVM improves image compressibility by an order-of-magnitude. MVM improves Bayesian SAR scene segmentation performance. Modern spectral estimation methods promise to improve dramatically all facets of SAR imaging and exploitation.

The presentation will review the rationale for MVM and Pisarenko imaging methods, show examples of adaptive SAR imagery, and illustrate our ATR results.

ADAPTIVE SAR IMAGING AND ITS IMPACT ON ATD/R AND IMAGE EXPLOITATION

Dr. Stuart R. DeGraaf

Northrop Grumman Corporation
Electronic Sensors & Systems Division
PO Box 746 - MS 1155
Baltimore, MD 21203
(410) 765-4560

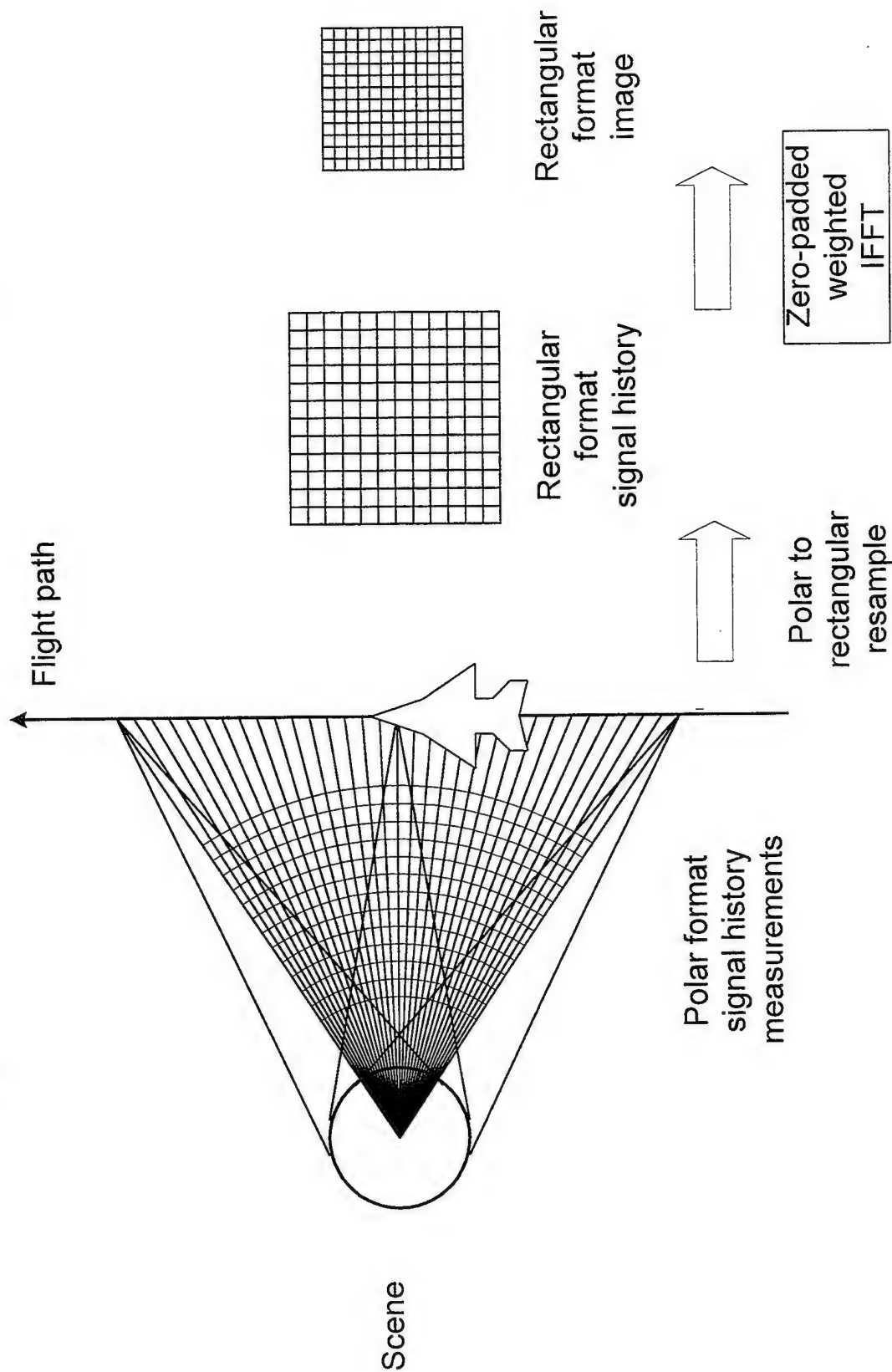
srd@cestua.md.essd.northgrum.com (preferred)
degraaf.s.r-@postal.essd.northgrum.com

“Superresolution” SAR Image Formation

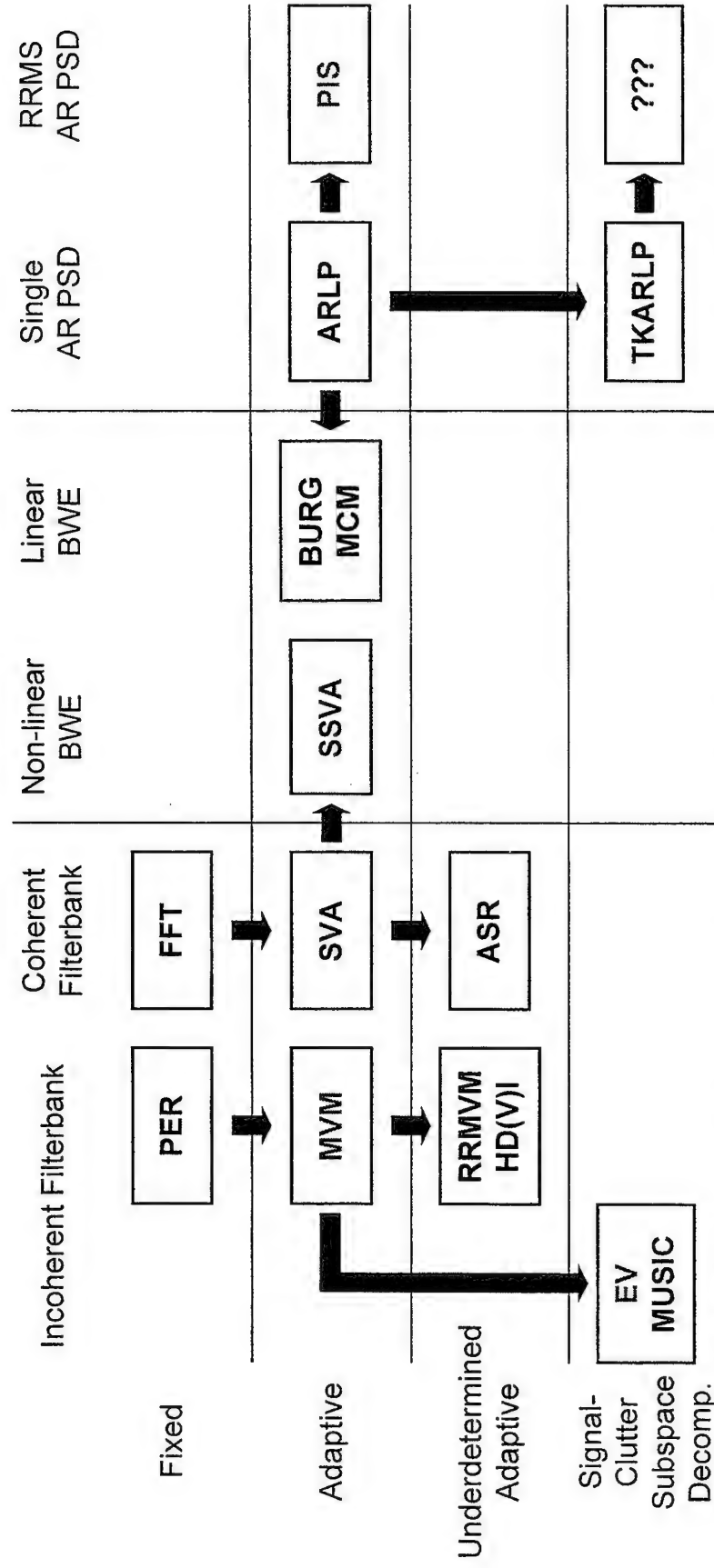
Processing

- ☐ Role of spectral estimation algorithms in spotlight SAR imaging
- ☐ Relationships of 2-D spectral estimation algorithms
- ☐ Impact of SAR image formation methods
 - examples and quantitative results
- ☐ Conclusions

Spotlight SAR Processing



Relationships Between Algorithms



RED: good for ATR BLUE: computationally simple BLACK: also ran

What Can Spectral Estimation Methods

Do for SAR Imagery?

- Improve full-scene SAR image quality
 - for human
 - MVM makes radar imagery resemble IR/optical imagery
 - for ATD/R
 - MVM reduces detection FAR by more than 10X
 - PIS reduces target misclassification by 3X
 - PIS reduces template azimuth sensitivity roughly 4X
 - for exploitation
 - MVM improves Bayesian scene segmentation
 - for compression
 - MVM imagery roughly 10X more compressible than Fourier

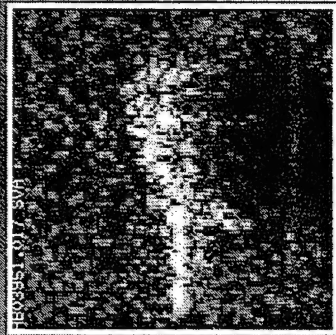
□ Why/How?

- reduce target scintillation, improve target support definition
- reduce clutter speckle, enhance contextual information
- improve resolution/definition, isolate prominent scatterers

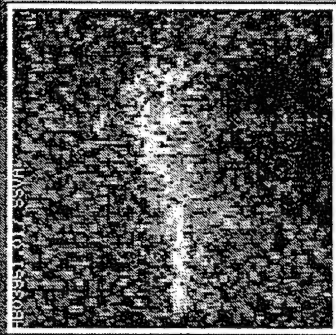
MVM, Pisarenko & EV Improve T72 Imagery Dramatically



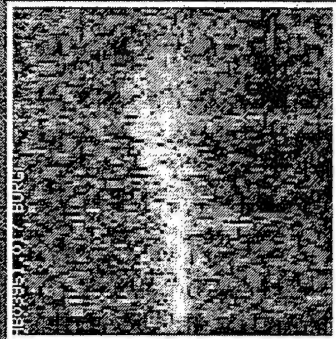
Fourier (Taylor)



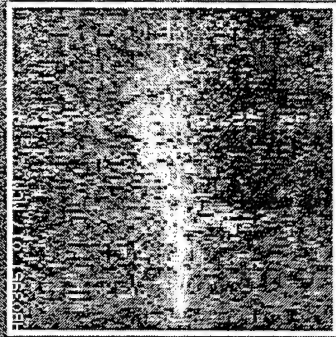
SVA



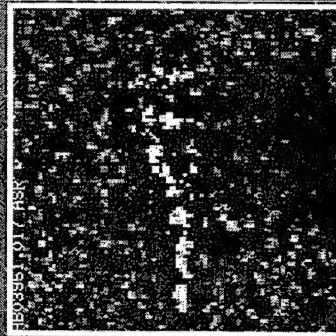
Super SVA X2



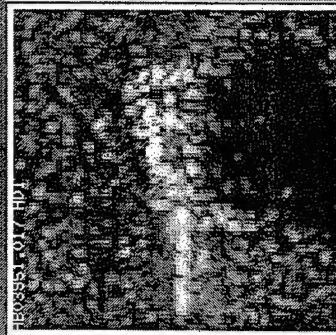
Burg X2



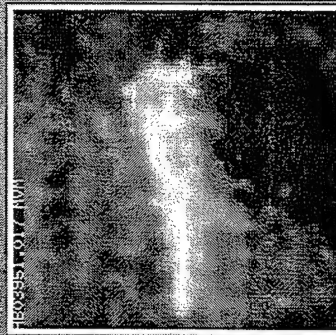
MCM ARLP X2



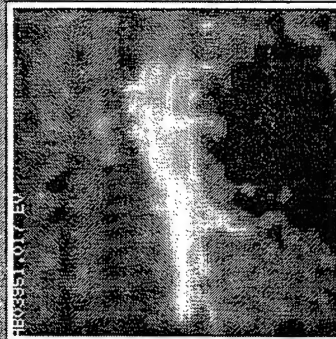
ASR



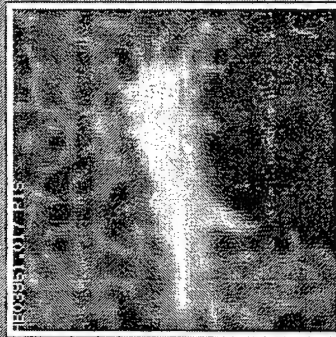
HDI



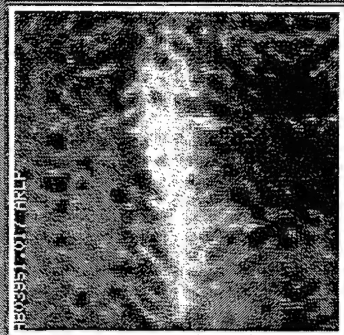
MVM



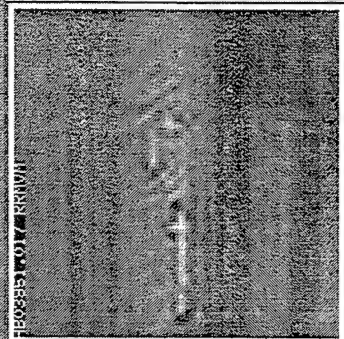
EV



Pisarenko



ARLP

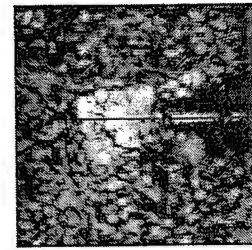


TKARLP

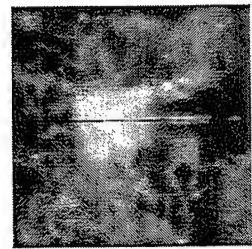
NORTHROP GRUMMAN

Electronic Sensors & Systems

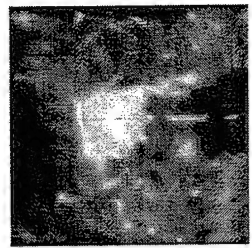
PSDs and BWEs Both Sharpen, But Only PSDs Reduce Scintillation



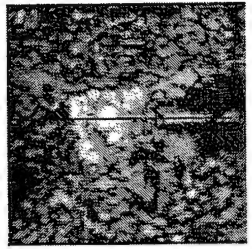
Taylor



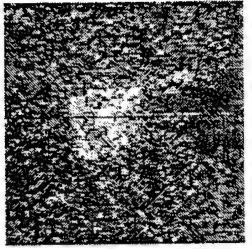
MVM



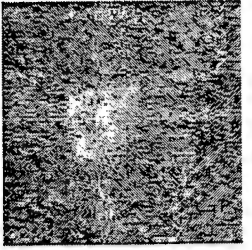
EV



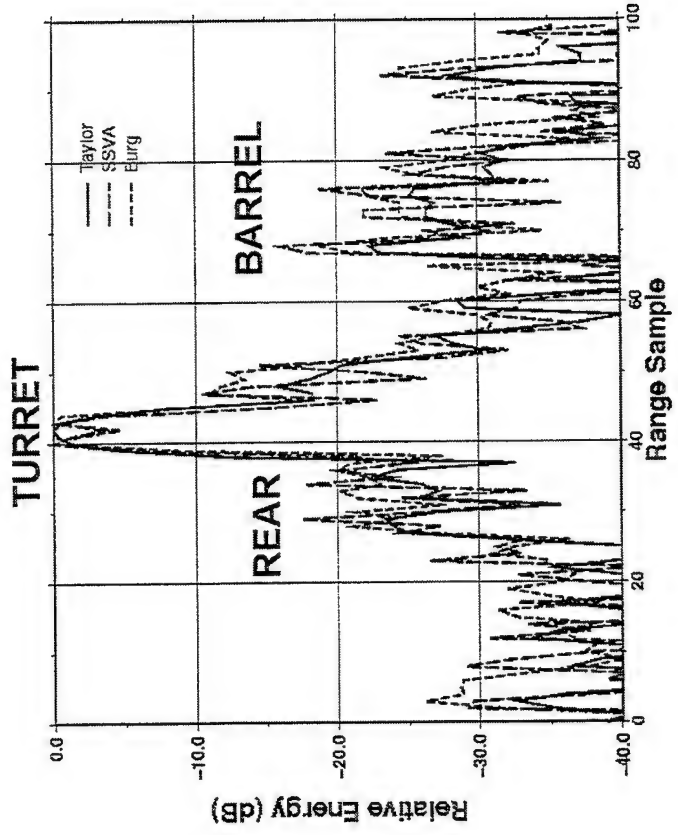
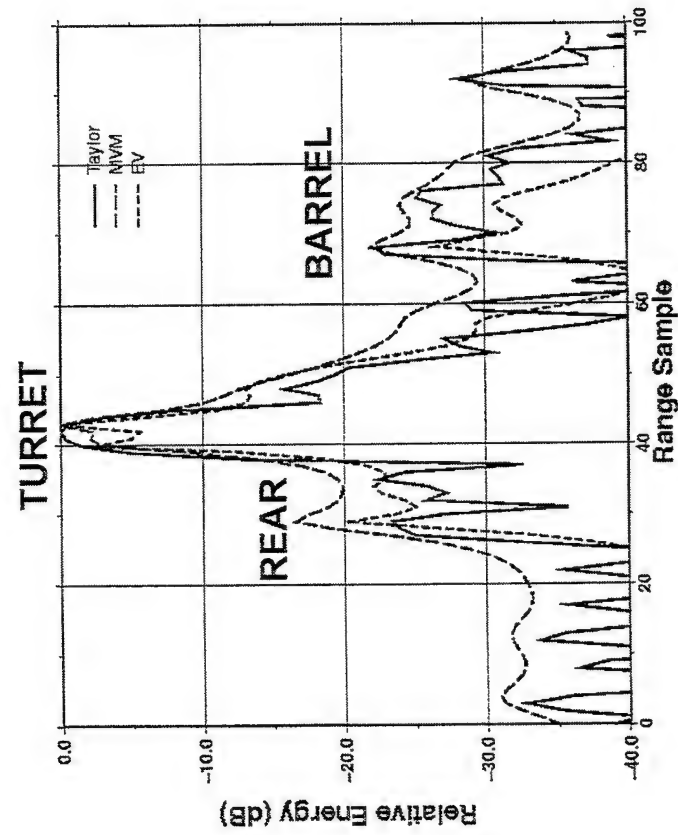
Taylor



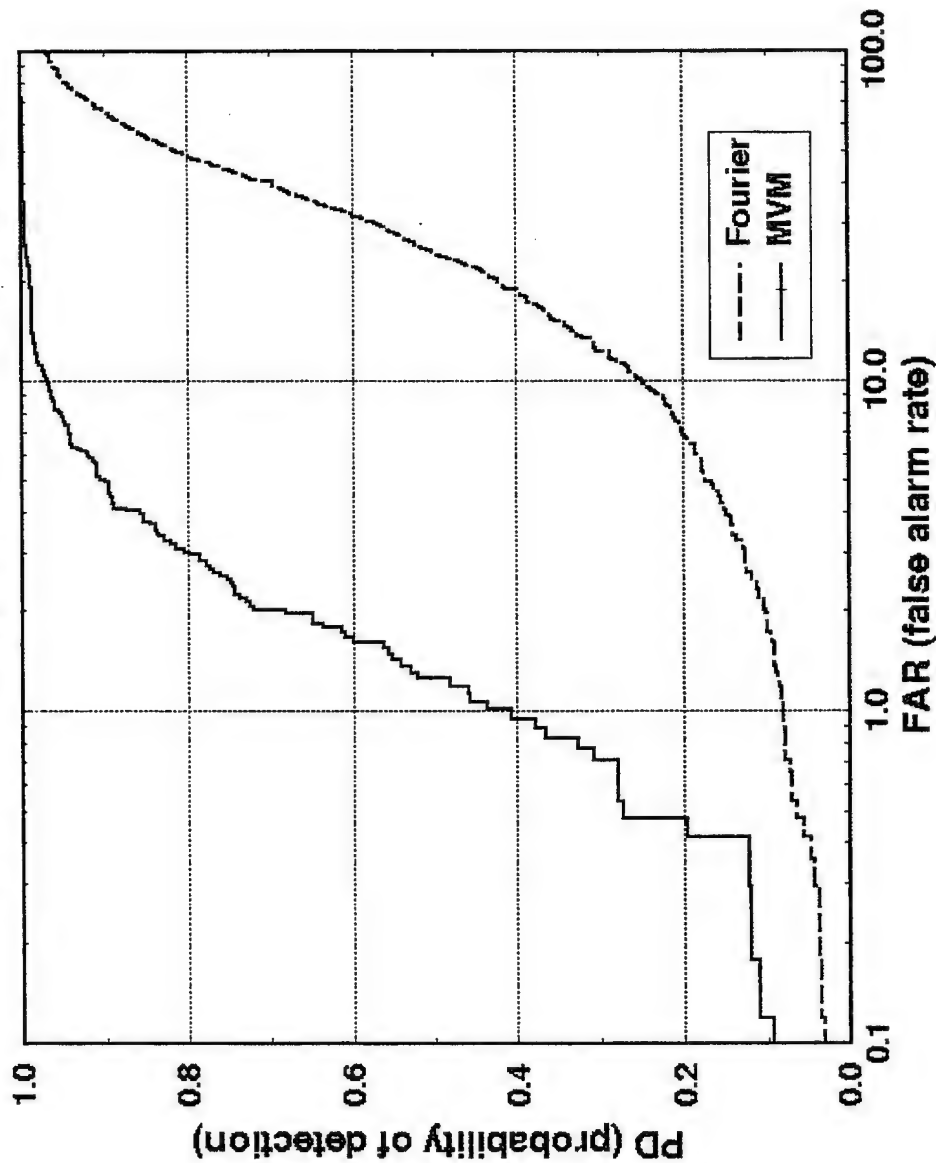
SSVA



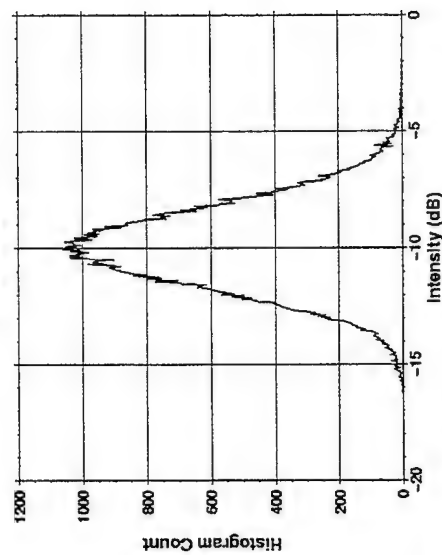
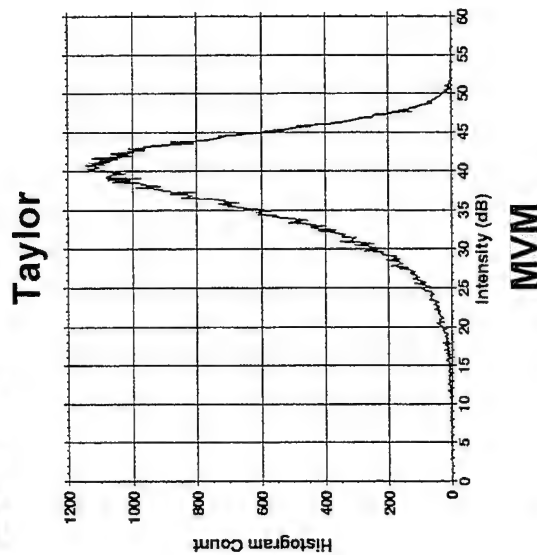
Burg



MVM Reduces Two-Parameter CFAR FAR By An Order-of-Magnitude



MSTAR public clutter 15° depression

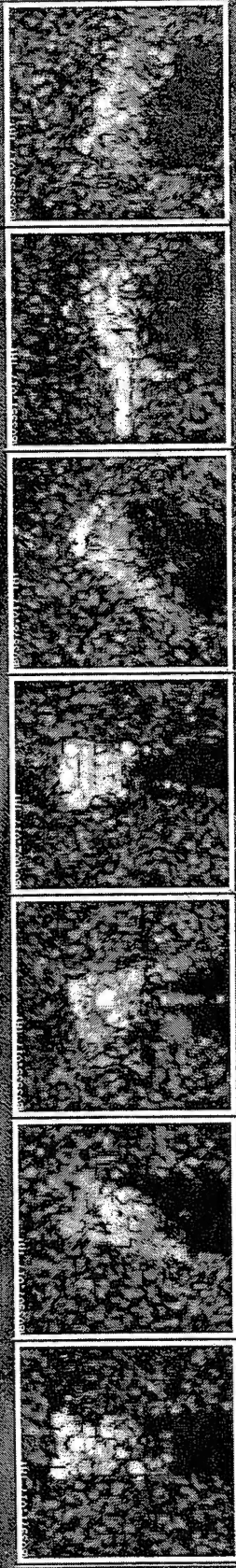


MVM improves log-normality & reduces speckle roughly 3dB

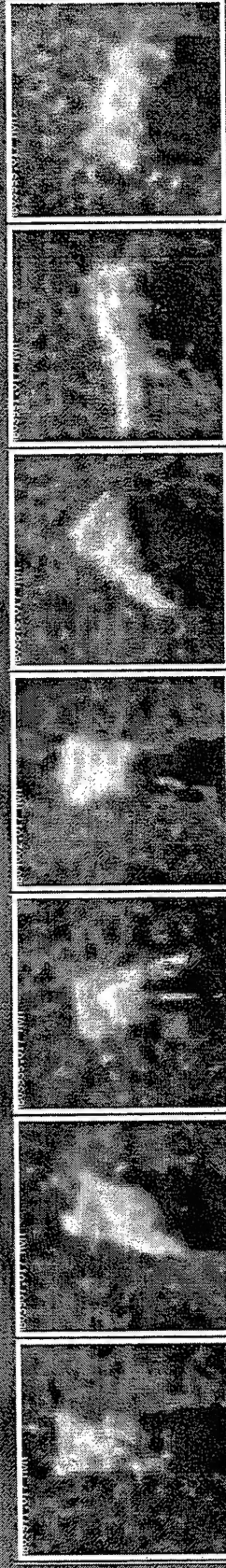
NORTHROP GRUMMAN

Electronic Sensors & Systems

MVM and Pisarenko Improve Quality of T72 Tank Signatures



Fourier



MVM

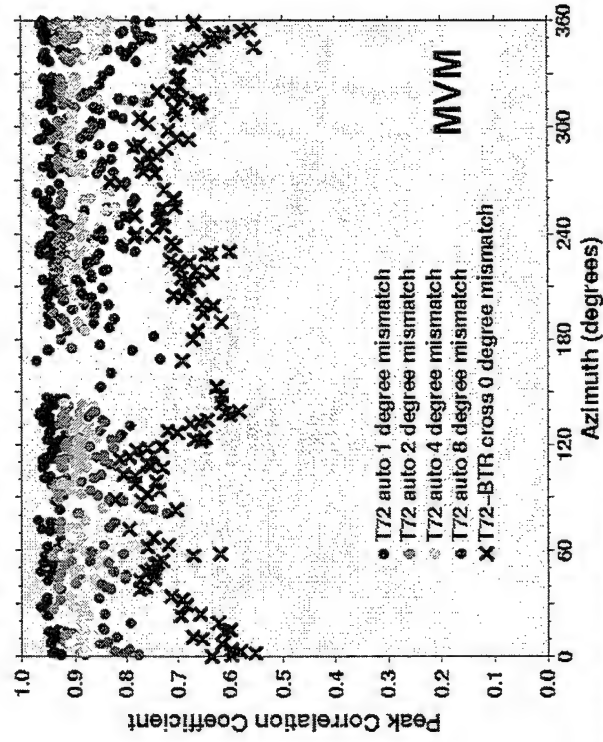
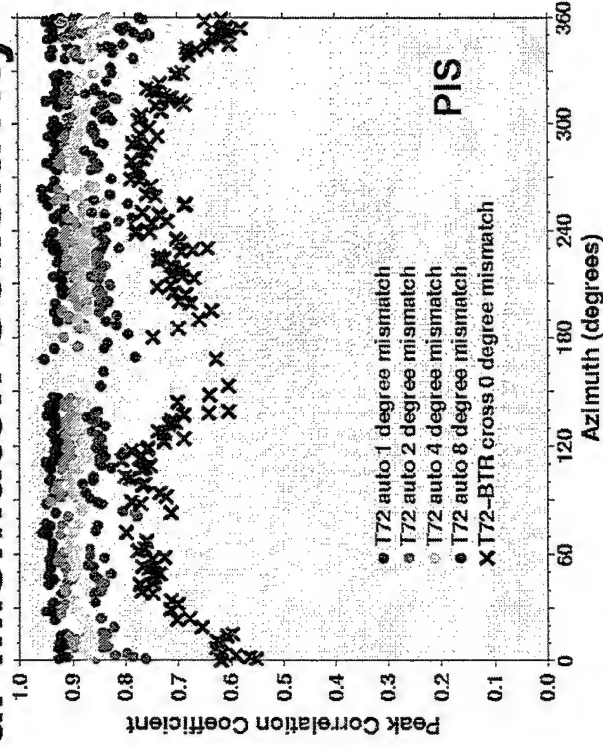
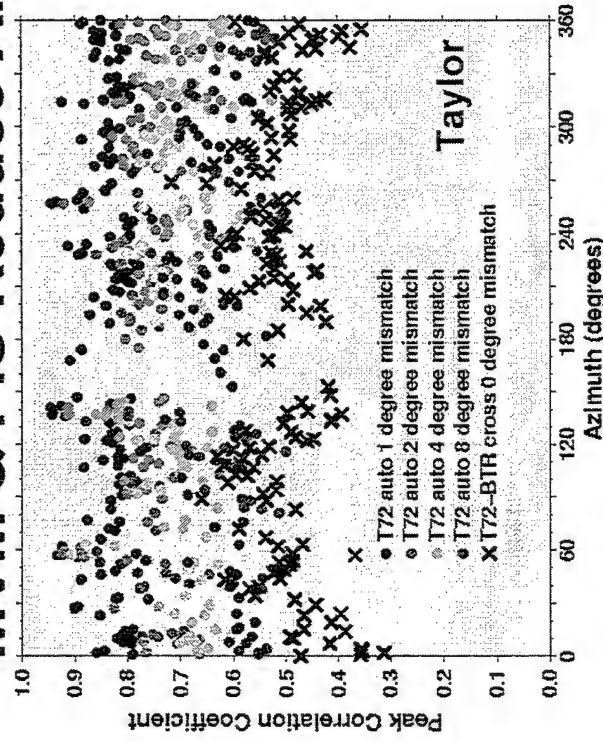


Pisarenko

NORTHROP GRUMMAN

Electronic Sensors & Systems

MVM & PIS Reduce Angular Mismatch Sensitivity



□ MVM & PIS improve 3-way target ID (T72, M2, BMP)

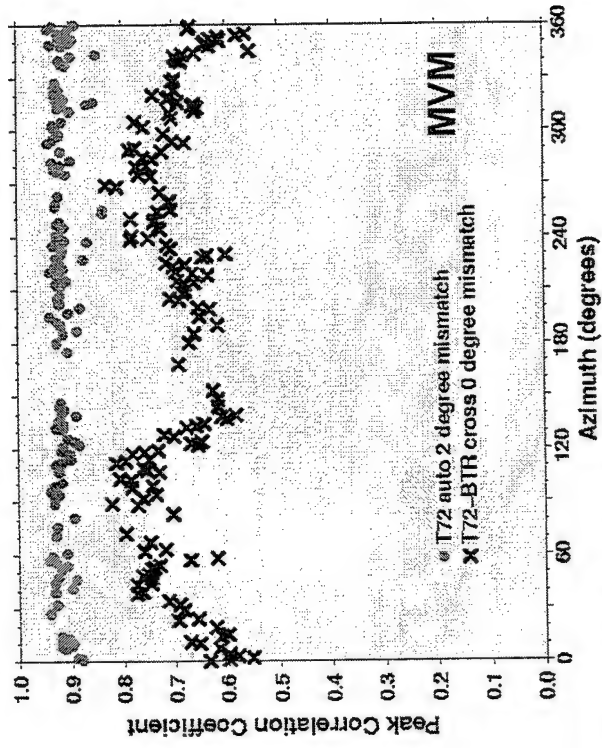
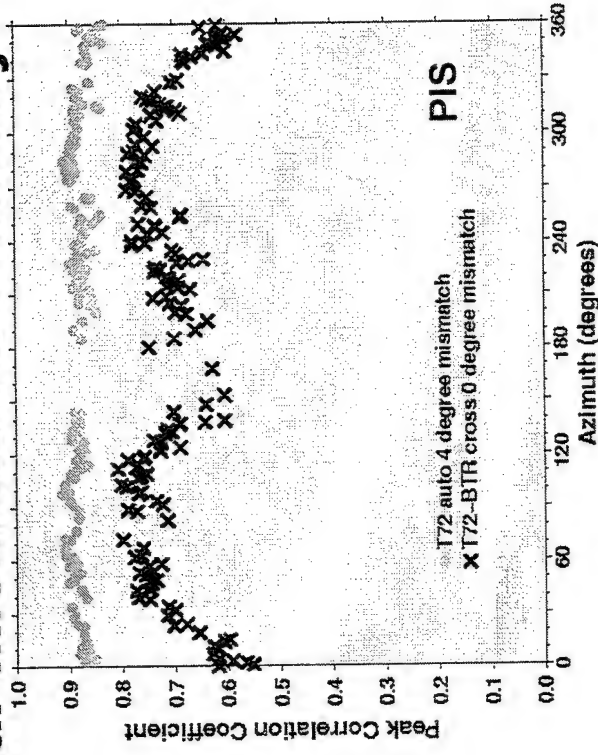
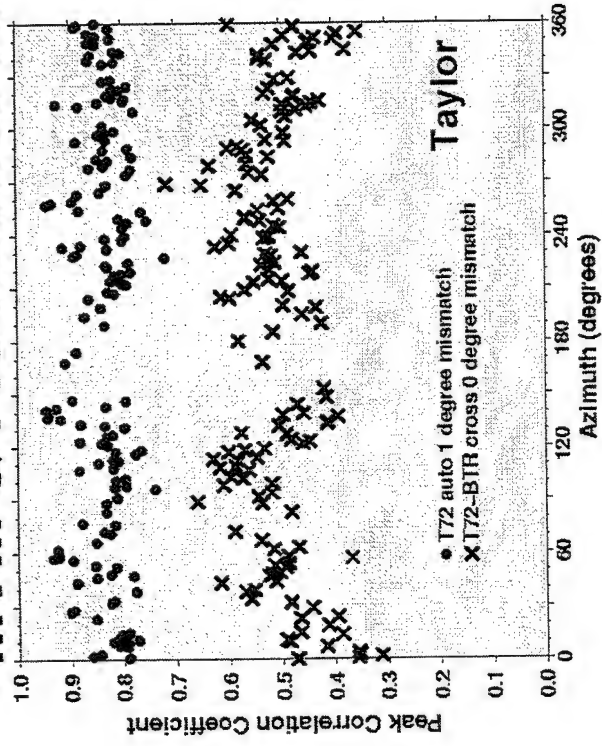
• $P_{ID}^{Tay} = .86$

• $P_{ID}^{MVM} = .91$

• $P_{ID}^{PIS} = .96$

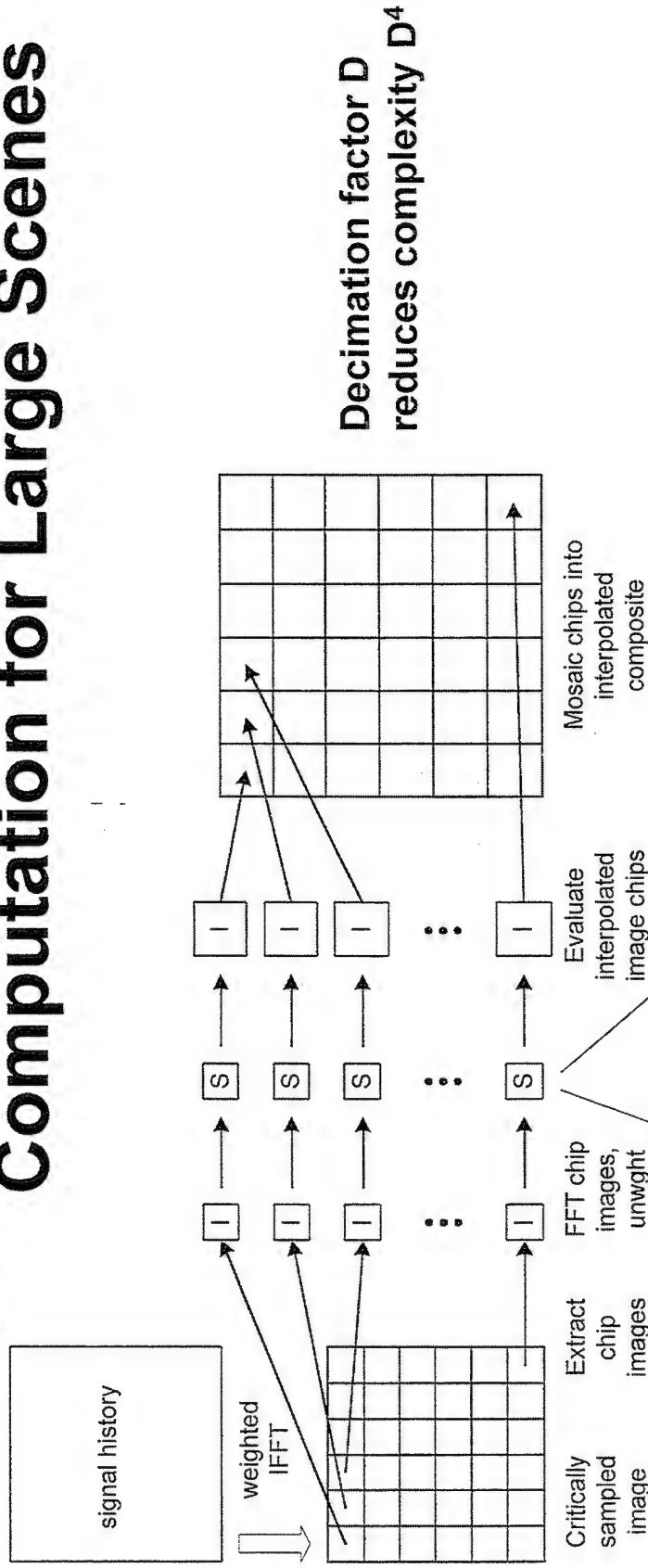
□ MSTAR public test target chips

MVM & PIS Reduce Angular Mismatch Sensitivity



- ☐ MVM & PIS reduce requirements on angular spacing of templates or training data
- ☐ 2° MVM = 1° Fourier mismatch
- ☐ 4° PIS = 1° Fourier mismatch

Decimation & Mosaicking Reduces Computation for Large Scenes



Decimation factor D
reduces complexity D^4

Forward-backward
subaperture average
for each decimated
signal history

full aperture size
subaperture size
no. of subapertures

$$K_x \times K_y$$

$$\hat{K}_x \times \hat{K}_y$$

$$A = (K_x - \hat{K}_x + 1)(K_y - \hat{K}_y - 1)$$

$$\mathbf{R} = \frac{1}{2A_{i,j}} \sum (\bar{X}_{i,j} \bar{X}_{i,j}^H + \mathbf{J} \bar{X}_{i,j}^* \bar{X}_{i,j}^T \mathbf{J})$$

forward-backward
subaperture avg.

invert or decompose
evaluate quadratic form

$$\frac{1}{\bar{\mathbf{W}}^H(\vec{r}) \mathbf{R}^{-1} \bar{\mathbf{W}}(\vec{r})}$$

MSTAR/Sandia One Foot Resolution Taylor Weighted Fourier



NORTHROP GRUMMAN

Electronic Sensors & Systems

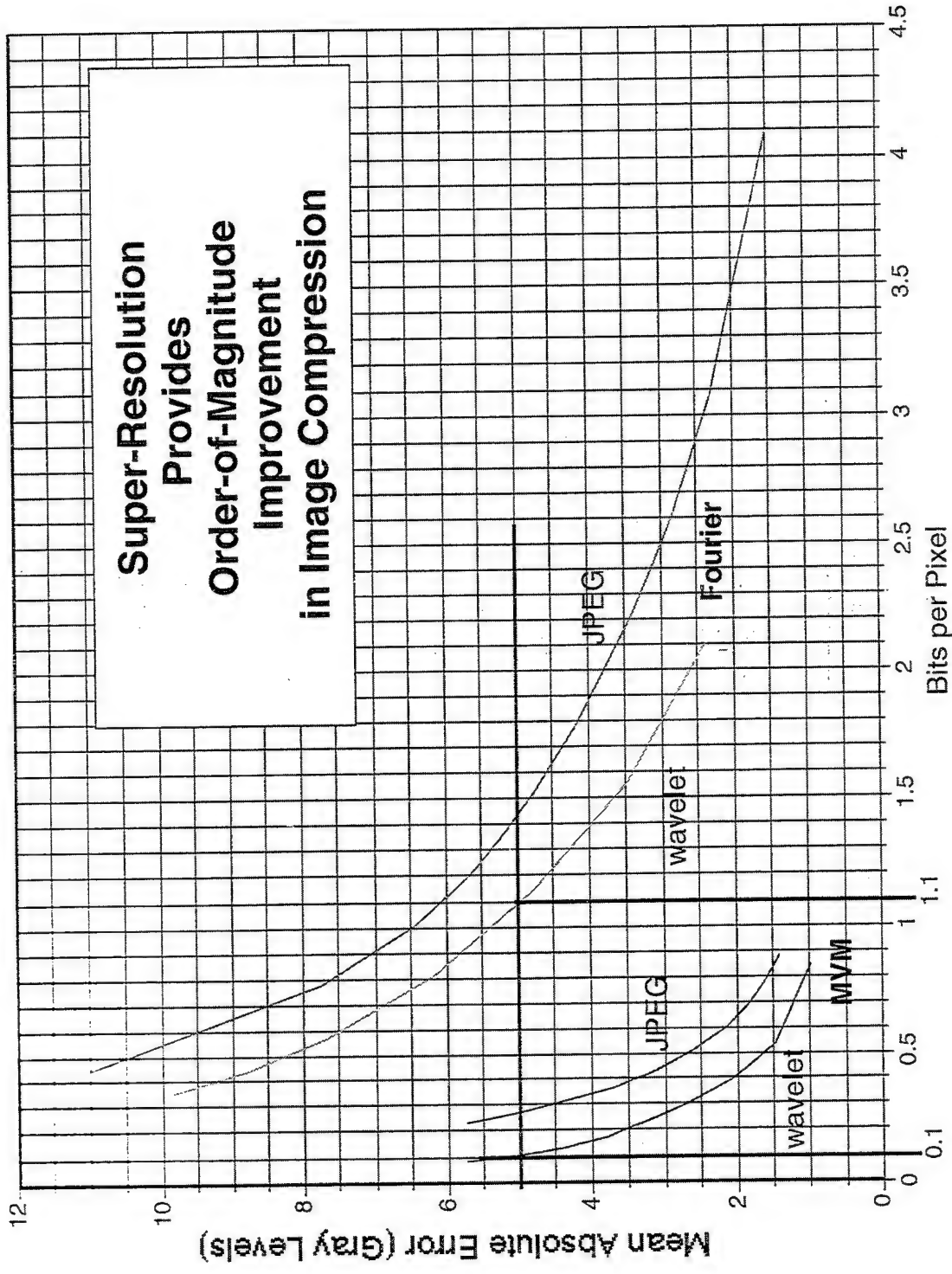
MSTAR/Sandia One Foot Resolution MVM Improves Image Quality



NORTHROP GRUMMAN

Electronic Sensors & Systems

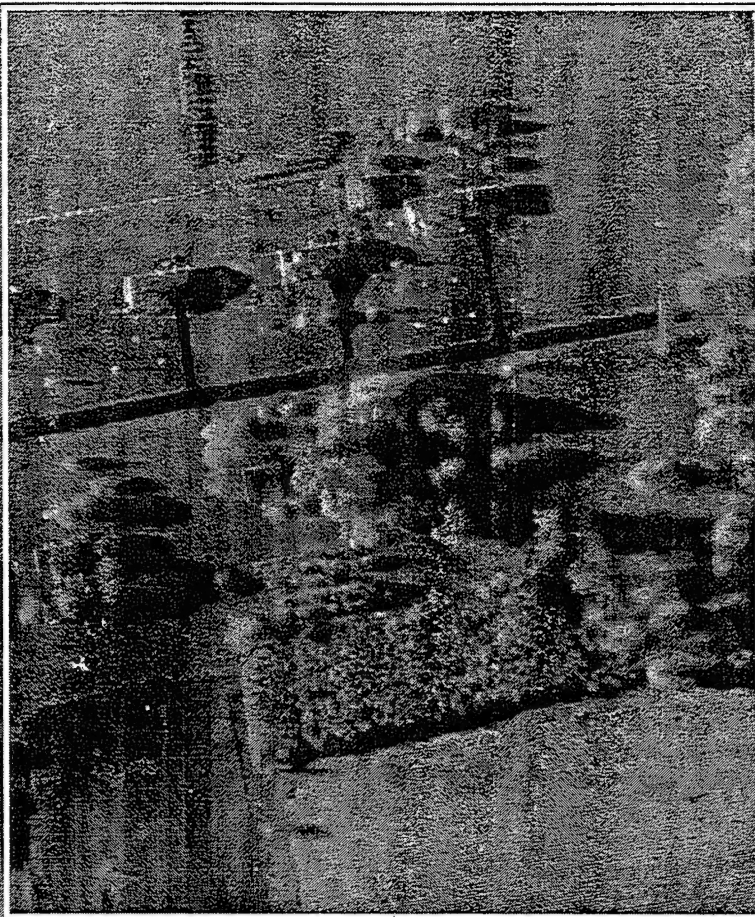
MVM Facilitates Image Compression



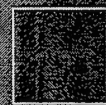
MVM Improves Performance of Bayesian SAR Image Segmentation



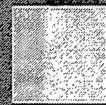
Fourier



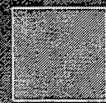
MVM



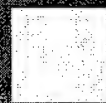
shadow



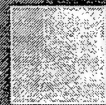
grass



crops H



crops V



trees



CFAR



intensity modulated hue

NORTHROP GRUMMAN

Electronic Sensors & Systems

Conclusions and Recommendations

- ☐ Modern spectral estimation methods offer enormous benefits for SAR imaging, ATD/R and exploitation
 - MVM makes radar imagery resemble IR/optical imagery
 - MVM reduces detection FAR more than 10X
 - PIS reduces target misclassification by 3X
 - PIS reduces template azimuth sensitivity roughly 4X
 - MVM improves Bayesian scene segmentation
 - MVM imagery roughly 10X more compressible than Fourier
- ☐ Apply techniques to full scene data, not just target chips
- ☐ Integrate modern spectral estimation methods into SAR ATD/R and exploitation systems
- ☐ Establish radar system requirements to insure that potential of methods is realized



School of Information Technology & Engineering

Session III Detection & Estimation I

Session Chair: Lloyd J. Griffiths
George Mason University
Fairfax, VA



Detection & Estimation I

1. "On the use of unstructured array models for radar space-time adaptive processing".
A. Lee Swindlehurst (BYU)
Petre Stoica (Uppsala University)
2. "Performance of the adaptive sidelobe blanker detection algorithm in the presence of signal mismatch".
Christ D. Richmond (MIT Lincoln Labs)
3. "Estimation methods and bounds for synthetic wideband processing".
Steve Smith (MIT Lincoln Labs)



Detection & Estimation in Adaptive Arrays

Issues:

- Array Calibration Errors
 - signal cancellation (SNR loss)
- Covariance Matrix Estimation Errors
 - relationship to calibration errors
- Wideband Processing From Narrowband Measurements
 - synthetic reconstruction



School of Information Technology & Engineering

On the Use of Unstructured Array Models for Radar Space-Time Adaptive Processing

A. Lee Swindlehurst & Petre Stoica

Self Calibration Approach

- Unstructured signal spatial waveform models
- Optimal ML methods based on the use of “blind” adaptive algorithms



School of Information Technology & Engineering

Performance of the Adaptive Sidelobe Blanker Detection Algorithm in the Presence of Signal Mismatch

Christ D. Richmond

Adaptive Sidelobe Blanker Algorithm

- Mitigation of undernullled clutter, clutter discretely, and sidelobe targets
- Performance in the presence of steering vector errors



School of Information Technology & Engineering

Estimation Methods and Bounds for Synthetic Wideband Processing

Steve Smith

Synthetic Wideband Processing

- Parametric estimation approach
- All-pole signal parameter model
- ESPRIT, Root-MUSIC comparison

On the Use of Unstructured Array Models for Space-Time Adaptive Processing

A. Lee Swindlehurst

Brigham Young University
Department of Electrical and Computer Engineering
Provo, UT 84602
tel: (801) 378-4343
email: swindle@ee.byu.edu

Petre Stoica

Uppsala University
Systems and Control Group
Uppsala, Sweden
tel: +46 18 183074
email: ps@syscon.uu.se

Abstract Most algorithms for space-time adaptive processing (STAP) in radar applications rely on the availability of array calibration data in order to detect the presence of point targets and estimate their azimuthal position. If calibration errors or multipath is present, standard STAP approaches may suffer from signal cancellation and even strong targets may be missed. Recently, in signal processing research conducted for wireless communications applications, so-called "blind" algorithms have been developed for such situations that employ an unstructured spatial signature model for the array response rather than one parameterized in terms of directions of arrival (DOAs). In this talk, we demonstrate how similar ideas may be applied to the STAP problem to render target detection and parameter estimation algorithms robust to array imperfections and multipath. Despite the fact that such models require more parameters than those using DOAs, the parameter dependence is linear, and simpler estimation procedures may be used. As a result, it becomes possible to consider optimal maximum likelihood (ML) approaches to the problem, which are not typically used for DOA-parameterized models due to the need for a complicated non-linear search. Depending on what assumptions are made about the additive clutter and jammer signals, different ML solutions result, and these are described in the talk. The extended invariance principle of ML estimation is used to show that, in situations where the DOA model holds exactly, the unstructured approach can still achieve asymptotically the same estimation accuracy as the standard approach using a weighted least-squares fit. We also derive a generalized likelihood ratio detection test (GLRT) for the unstructured case, and compare it with the one that results from a DOA-based model. When no array errors or multipath is present, the unstructured GLRT has a slightly higher detection threshold (1-2 dB) than the corresponding DOA-based detector. With calibration errors, however, the unstructured GLRT shows a significant performance advantage.



On the Use of Unstructured Array Models for Space Time Adaptive Processing¹

A. Swindlehurst

Dept. of Electrical & Computer Eng.

Brigham Young University

Provo, Utah

¹Financial support for this work provided by the Office of Naval Research
under contract N00014-96-1-0934.



Coherent Data Model

For each CPI (xmit direction), coherently record echoes from N pulses with an m -element antenna array. If target is present in some range bin:

$$\mathbf{x}(t) = b_0 \mathbf{a}(\theta_0) e^{j\omega_0 t} + \mathbf{e}(t)$$

where

b_0 = target signal amplitude

θ_0 = target DOA

ω_0 = target doppler

$\mathbf{e}(t)$ = clutter, jamming, noise, etc.

Problem statement: Using $\mathbf{X} = [\mathbf{x}(1), \dots, \mathbf{x}(N)]$, detect presence of target and estimate b_0, θ_0, ω_0 .



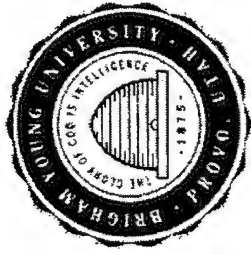
Standard Solution

- *Max SINR ("fully adaptive")*

1. Vectorize data: $\chi = \text{vec} \mathbf{X}$
2. Estimate $mN \times mN$ clutter covariance \mathbf{C} from secondary data
3. Compute space-time signature $\mathbf{v}(\theta, \omega) = \text{vec}(\mathbf{a}(\theta)[e^{j\omega} \cdots e^{jN\omega}])$
4. Apply space time filter $\mathbf{w}(\theta, \omega) = \mathbf{C}^{-1} \mathbf{v}$ to data:

$$P(\theta, \omega) = \mathbf{w}^* \chi$$

5. Search for peak in $P(\theta, \omega)$



Some Observations

- Unstructured clutter/jammer model, structured array model
- If $e(t)$ is Gaussian, solution essentially equivalent to ML
- 2-D search for θ, ω required in general
- Large amount of data necessary to reliably estimate C
- Computation of C^{-1} prohibitive
- Not clear how to reduce sensitivity to calibration errors



An Alternative Approach

- Motivation: Computational simplicity, sacrificing as little performance as possible.
- Key Idea: Use an unstructured array model, and a structured (parametric) clutter/jammer model
- Exploit extended invariance principle (EXIP) for ML estimation
- Promising results with simulated and Mountain Top data – at least an order of magnitude less computation



Unstructured Array Model

Consider a model parameterized by the target “spatial signature” rather than b and θ :

$$\mathbf{x}(t) = \boldsymbol{\alpha}_0 e^{j\omega_0 t} + \mathbf{e}(t)$$

- $\boldsymbol{\alpha}_0$ treated as vector of unknown complex constants
- Approach often used in blind source separation problems
- Model is linear in target’s spatial parameters



Structured Clutter Model

- Assume vector AR (VAR) filter

$$\mathcal{H}(z^{-1}) = \mathbf{I} + \sum_{l=1}^L \mathbf{H}_l z^{-l}$$

exists such that $\mathcal{H}(z^{-1})\mathbf{e}(t) = \boldsymbol{\epsilon}(t)$ is (approx.) white.

- Pre-whiten array data

$$\mathbf{x}_f(t) = \mathcal{H}(z^{-1})\mathbf{x}(t) = b_0 \mathcal{H}(e^{-j\omega_0})\mathbf{a}(\theta_0)e^{j\omega_0 t} + \boldsymbol{\epsilon}(t)$$

- Form of unstructured array model is unchanged:

$$\boxed{\mathbf{x}_f(t) = \boldsymbol{\alpha}_f e^{j\omega_0 t} + \boldsymbol{\epsilon}(t)} \quad \boldsymbol{\alpha}_f = b_0 \mathcal{H}(e^{-j\omega_0})\mathbf{a}(\theta_0)$$



Maximum Likelihood Estimator

Suppose initial pre-whitening renders $\epsilon(t)$ temporally but not spatially white, with $\mathcal{E}\{\epsilon(t)\epsilon^*(t)\} = \mathbf{Q}$. ML estimates of model parameters easily found:

$$\hat{\mathbf{Q}}_f = \frac{1}{N} \sum_{t=1}^N (\mathbf{x}_f(t) - \hat{\boldsymbol{\alpha}}_f e^{j\hat{\omega}_f t}) (\mathbf{x}_f(t) - \hat{\boldsymbol{\alpha}}_f e^{j\hat{\omega}_f t})^*$$

$$\hat{\boldsymbol{\alpha}}_f = \frac{1}{N} \sum_{t=1}^N \mathbf{x}_f(t) e^{-j\hat{\omega}_f t} = \mathbf{y}(\hat{\omega}_f)$$

$$\hat{\omega}_f = \arg \max_{\omega} \mathbf{y}^*(\omega) \hat{\mathbf{R}}_f^{-1} \mathbf{y}(\omega)$$

where $\hat{\mathbf{R}}_f$ is $m \times m$ sample covariance of $\mathbf{x}_f(t)$.



Questions

- If target is detected, DOA θ is needed. How do we get $\hat{\theta}$ from $\hat{\alpha}_f$?
- How will accuracy of $\hat{\theta}$ compare with standard solution which uses full model from the beginning?
- What is the relative computational cost?
- Does VAR approach successfully render real clutter temporally white?



Extended Invariance Principle (EXIP)

Accuracy of structured & unstructured ML estimates can be related by means of the EXIP (Stoica & Söderström, 1989). The following are asymptotically efficient estimates of the target parameters:

$$\hat{\mathbf{Q}}_e = \hat{\mathbf{Q}}_f$$

$$\hat{\omega}_e = \hat{\omega}_f$$

$$\hat{b}_f = \frac{\mathbf{a}^*(\hat{\theta}_f)\mathcal{H}^*(e^{-j\hat{\omega}_f})\hat{\mathbf{Q}}_f^{-1}\hat{\boldsymbol{\alpha}}_f}{\mathbf{a}^*(\hat{\theta}_f)\mathcal{H}^*(e^{-j\hat{\omega}_f})\hat{\mathbf{Q}}_f^{-1}\mathcal{H}(e^{-j\hat{\omega}_f})\mathbf{a}(\hat{\theta}_f)}$$

$$\hat{\theta}_f = \arg \max_{\theta} \frac{\left| \mathbf{a}^*(\theta)\mathcal{H}^*(e^{-j\hat{\omega}_f})\hat{\mathbf{Q}}_f^{-1}\hat{\boldsymbol{\alpha}}_f \right|^2}{\mathbf{a}^*(\theta)\mathcal{H}^*(e^{-j\hat{\omega}_f})\hat{\mathbf{Q}}_f^{-1}\mathcal{H}(e^{-j\hat{\omega}_f})\mathbf{a}(\theta)}$$



Summary of Proposed Approach

1. Use secondary data to estimate initial pre-whitening filter $\mathcal{H}(z^{-1})$.
2. Apply filter to data: $\mathbf{x}_f(t) = \mathcal{H}(z^{-1})\mathbf{x}(t)$.
3. Estimate $\hat{\alpha}$, $\hat{\omega}$, $\hat{\mathbf{Q}}$ from filtered data via ML.
4. Apply GLRT to determine presence/absence of target.
5. If target is detected, use EXIP to get $\hat{\theta}$, \hat{b} .



Some Observations

- Much easier to compute $\mathcal{H}(z^{-1})$ from secondary data than full space-time covariance \mathbf{C} ; much less secondary data required.
- For L tap VAR filter ($N \gg L$), must estimate $m^2 L$ parameters instead of $m^2 N^2 / 2$ for \mathbf{C} .
- Only inverse of $m \times m$ matrix $\hat{\mathbf{R}}_f$ required, not that of $mN \times mN$ matrix \mathbf{C} .



Observations (cont.)

- Unstructured parameters estimated with a single 1-D search over ω – fast implementation using FFTs.
- For ULA, EXIP search for θ can be eliminated using rooting techniques.
- Estimation of θ can be made insensitive to calibration errors by regularization; not clear how to do this with 2-D search.



An Unstructured GLRT

Unstructured model can be used to develop GLRT that is insensitive to calibration errors:

1. Find threshold λ_T by solving

$$F(\lambda_T) = (1 - P_f)^{\frac{1}{N}}$$

$$F(\lambda) = P \{ \rho \leq \lambda \mid \rho \sim \chi^2(2m) \}$$

2. Compute sample covariance $\hat{\mathbf{R}}_f$ and DFT $\mathbf{y}(\omega_k)$.
3. Maximize vector periodogram $\mathbf{y}^*(\omega) \hat{\mathbf{R}}_f^{-1} \mathbf{y}(\omega)$ over ω_k . Call this frequency $\hat{\omega}_f$.



Unstructured GLRT, (cont)

4. Decide that H_1 is true if

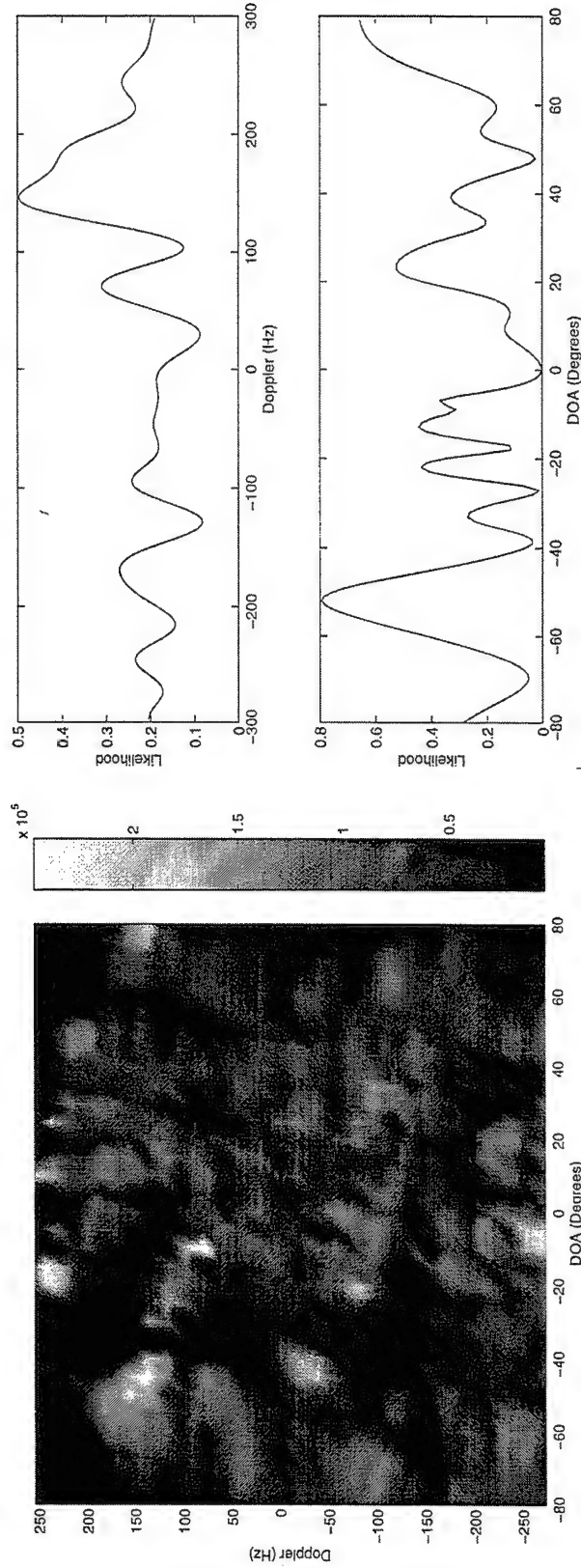
$$\lambda_u = -2N \log \left(1 - \mathbf{y}^*(\hat{\hat{\omega}}_f) \hat{\mathbf{R}}_f^{-1} \mathbf{y}(\hat{\hat{\omega}}_f) \right) > \lambda_T,$$

otherwise assume that H_0 holds.



Detection in Real Data

-25 dB SCNR, 12 Element Array, 16 Pulses per CPI
Target DOA: -50 Degrees, Target Doppler: 140 Hz



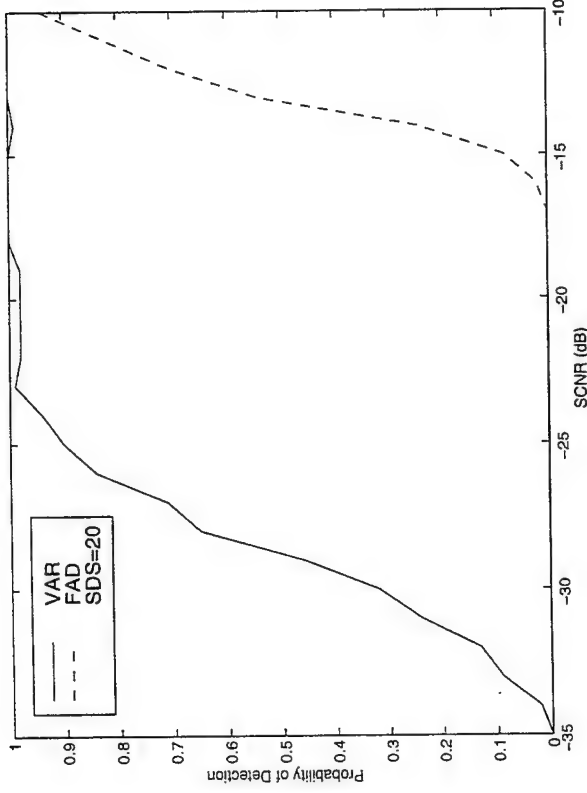
Fully Adaptive Detection
50 Secondary Data Sets
DOA = -45°
Doppler = 136 Hz

VAR + EXIP Detection
2 Secondary Data Sets
DOA = -52°
Doppler = 146 Hz

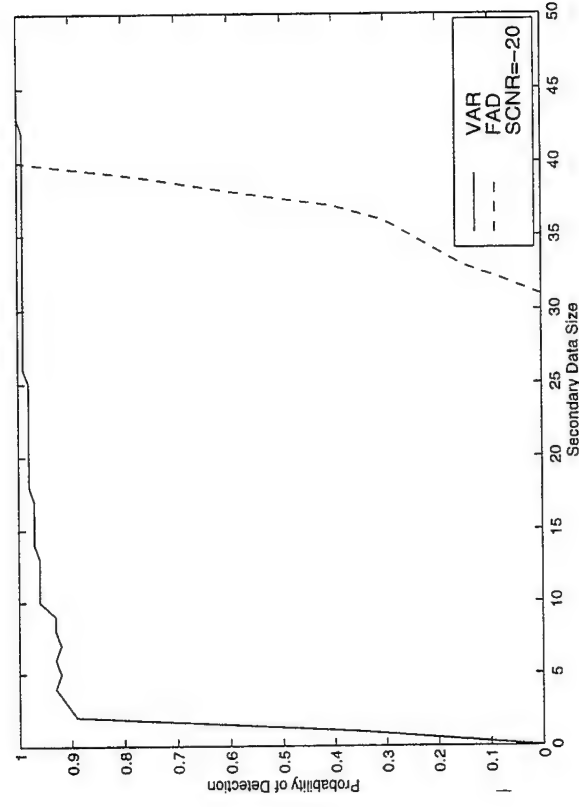


Detection Performance

Performance vs.
SCNR



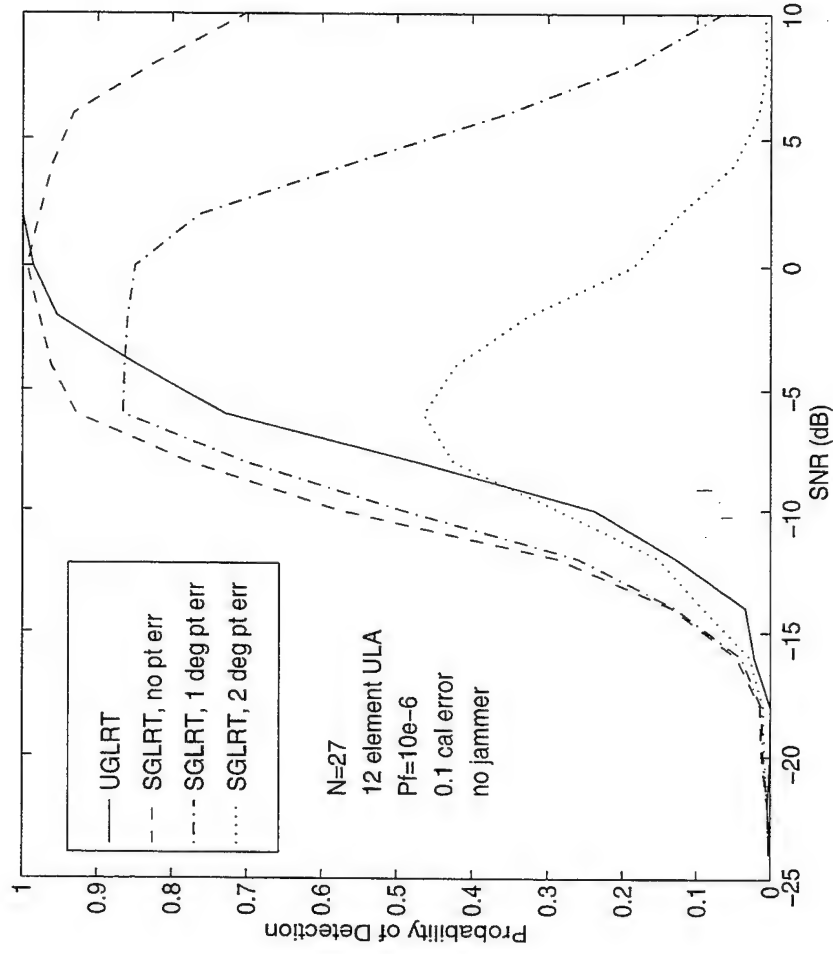
Performance vs.
Secondary Data Size



Even for poor SCNR levels, the VAR method requires fewer secondary data samples for successful noise cancellation.



Simulation Example 1

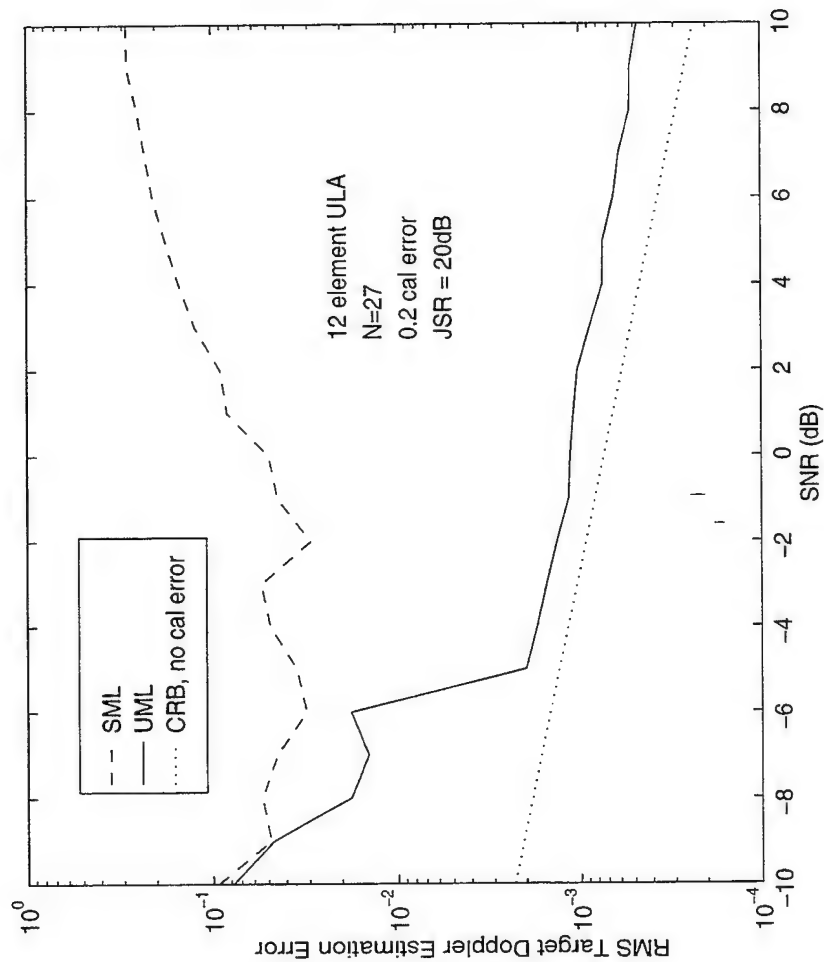


Independent gaussian calibration errors, std=0.1

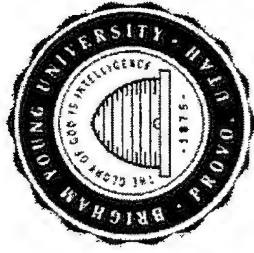
random Q , 500 trials/SNR



Simulation Example 2



Strong jammer at 5°
random Q , 1000 trials/SNR



Concluding Remarks

- Standard solution assumes

Structured array, unstructured clutter/jammer model

- Target detection and estimation algorithms developed here for

Unstructured array, structured clutter/jammer model

- New approach provides order of magnitude reduction in computation (no inverse of full space-time covariance needed)
- Much less secondary data needed for structured (parametric) clutter model



Concluding Remarks (cont.)

- “Fast” detection for unstructured array model, robust to calibration and pointing errors
- Accuracy of doppler and clutter covariance estimates unaffected by use of unstructured model
- Use EXIP to obtain asymptotically accurate target DOA and amplitude estimates with no calibration errors
- Real and simulated data show promising results

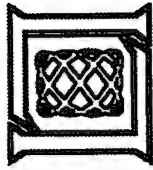
Performance of the Adaptive Sidelobe Blanker Detection Algorithm in the Presence of Signal Mismatch

Christ D. Richmond

MIT Lincoln Laboratory
244 Wood Street, Room J-118D
Lexington, MA 02173-9108
tel: (781) 981-5954
email: christ@ll.mit.edu

Abstract Recently a two-dimensional (2-D) adaptive detection algorithm known as the adaptive sidelobe blanker (ASB) was introduced as a means of mitigating the effects of undernullled clutter, clutter discreties, and sidelobe targets in 1-D adaptive matched filter (AMF) detection [1]. A previous study [2] of the 2-D ASB provided closed form expressions for the probabilities of false alarm (PFA) and detection (PD) under both homogeneous and non-homogeneous conditions. Heterogeneous conditions were modeled via a mismatch between the covariance of the training set samples and that of the test cell in an attempt to analyze the algorithm's ability to reject sidelobe breakthroughs. The study, however, presumed perfect knowledge of the target array response vector (signal steering vector). In this presentation we consider the effects of steering vector mismatch under homogeneous complex Gaussian data conditions. Closed form expressions for the PD and PFA in the presence of steering vector mismatch are provided for the 2-D ASB algorithm. It is observed that the adaptive cosine estimator (ACE) [3] has the best sidelobe rejection capability and the worst target sensitivity, whereas the AMF has the worst sidelobe rejection capability and the best target sensitivity. The generalized likelihood ratio test (GLRT) has performance falling between the two. The ASB algorithm provides a systematic way of trading off target gain for sidelobe rejection via the appropriate choice of threshold pairs. We likewise compare a 1-D tapered AMF to the untapered 2-D ASB. Both are designed to handle sidelobe breakthroughs, so the comparison is of practical interest.

- [1] D.E. Kreithen, A.O. Steinhardt, "Target Detection in Post-STAP Undernullled Clutter," 29th Annual Asilomar Conference on Signals, Systems, and Computers, Pacific Grove, CA, October 29–November 1, 1995.
- [2] C.D. Richmond, "Statistical Performance Analysis of the Adaptive Sidelobe Blanker Detection Algorithm," to appear at 31st Annual Asilomar Conference on Signals, Systems, and Computers, Pacific Grove, CA, November 2–5, 1997.
- [3] L.T. McWhorter, L.L. Scharf, L.J. Griffiths, "Adaptive Coherence Estimation for Radar Signal Processing," 30th Annual Asilomar Conference on Signals, Systems, and Computers, Pacific Grove, CA, November 3–6, 1996.



Performance of the Adaptive Sidelobe Blanker Detection Algorithm in the Presence of Signal Mismatch

Christ D. Richmond

ASAP Workshop 1998 March 12

•This work was sponsored by DARPA under Air Force contract F19628-95-C-0002.
Opinions, interpretations, conclusions, and recommendations are those of the author
and are not necessarily endorsed by the USAF.

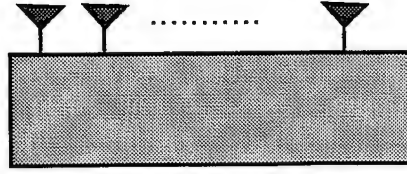


Outline

- ➔ •Adaptive Detection
- Adaptive Sidelobe Blanker
- Signal Mismatch Performance
- Closing Remarks



Adaptive Detection Problem



Test Cell:

$$H_0 : \mathbf{x}_T = \mathbf{n}$$

$$H_1 : \mathbf{x}_T = \mathbf{S} \mathbf{v}_T + \mathbf{n}$$

$$\text{COV}(\mathbf{x}_T) = \mathbf{R}_T$$

•Two Unknowns \mathbf{R} & \mathbf{S}

•Use Noise Only Training Set

$$\mathbf{x}_1, \mathbf{x}_2, \dots, \mathbf{x}_L$$

$$\text{COV}(\mathbf{x}_i) = \mathbf{R}$$

Classical Assumptions:

•All Data Complex Gaussian

•Training Samples Homogeneous with Test Cell
($\mathbf{R}_T = \mathbf{R}$)



Adaptive Detection Algorithms

• Adaptive Matched Filter
(AMF) Robey, Reed, Chen

$$t_{AMF} = \frac{|v^H \hat{R}^{-1} x_T|^2}{v^H \hat{R}^{-1} v}$$

• Generalized Likelihood Ratio
Test (GLRT) Kelly, Khatri

$$t_{GLRT} = \frac{t_{AMF}}{1 + x_T^H \hat{R}^{-1} x_T}$$

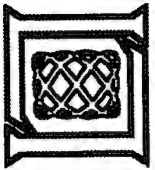
• Adaptive Cosine Estimator
(ACE) Conte, Scharf (NEW)

$$t_{ACE} = \frac{t_{AMF}}{x_T^H \hat{R}^{-1} x_T}$$

• Adaptive Sidelobe Blanker

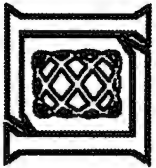
(ASB) Kreithen, Baranoski, Richmond (NEW) $f(t_{AMF}, t_{ACE})$

Sample Covariance: $\hat{R} = x_1 x_1^H + x_2 x_2^H + \dots + x_L x_L^H$

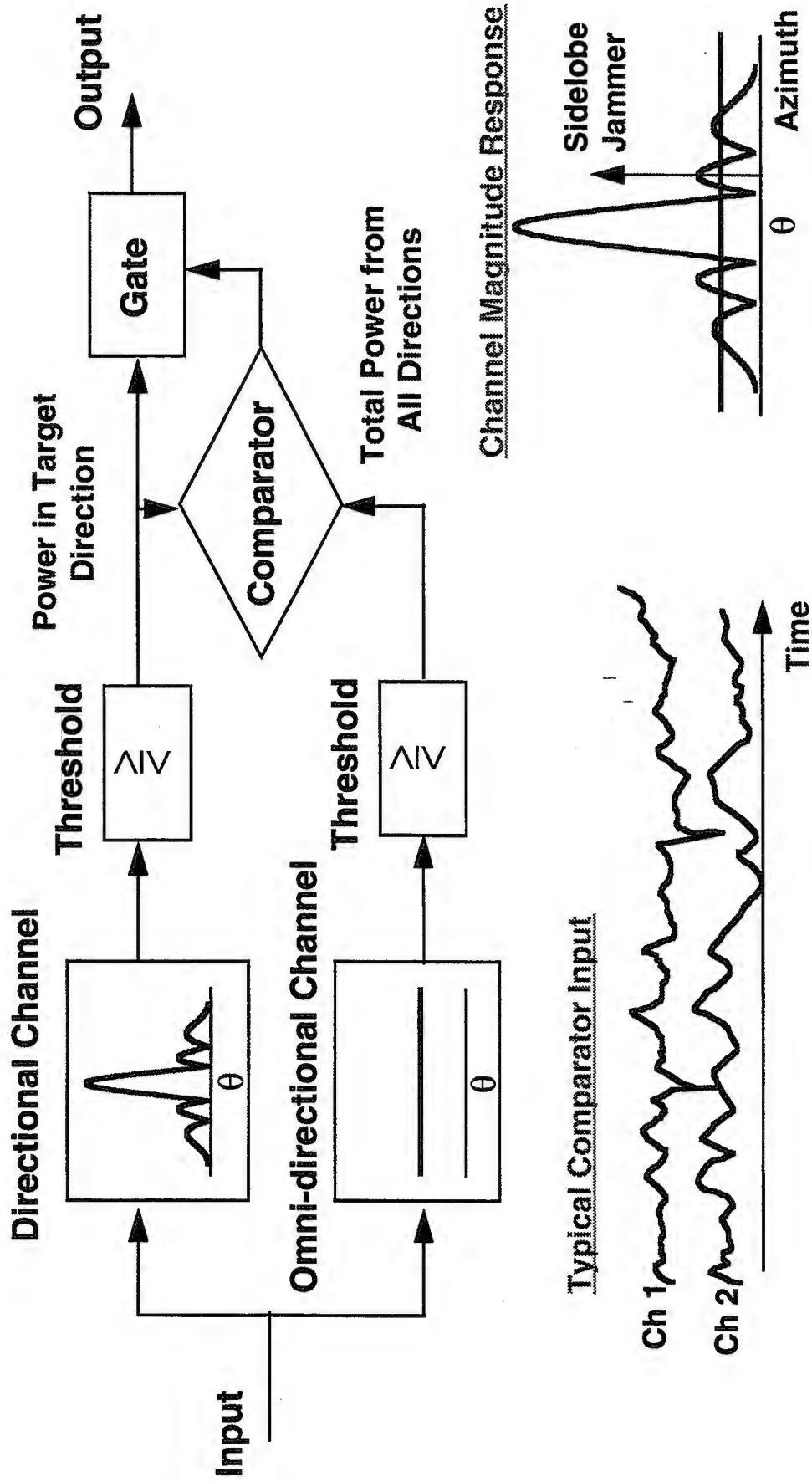


Outline

- Adaptive Detection
- ➔ • Adaptive Sidelobe Blanker
- Signal Mismatch Performance
- Closing Remarks

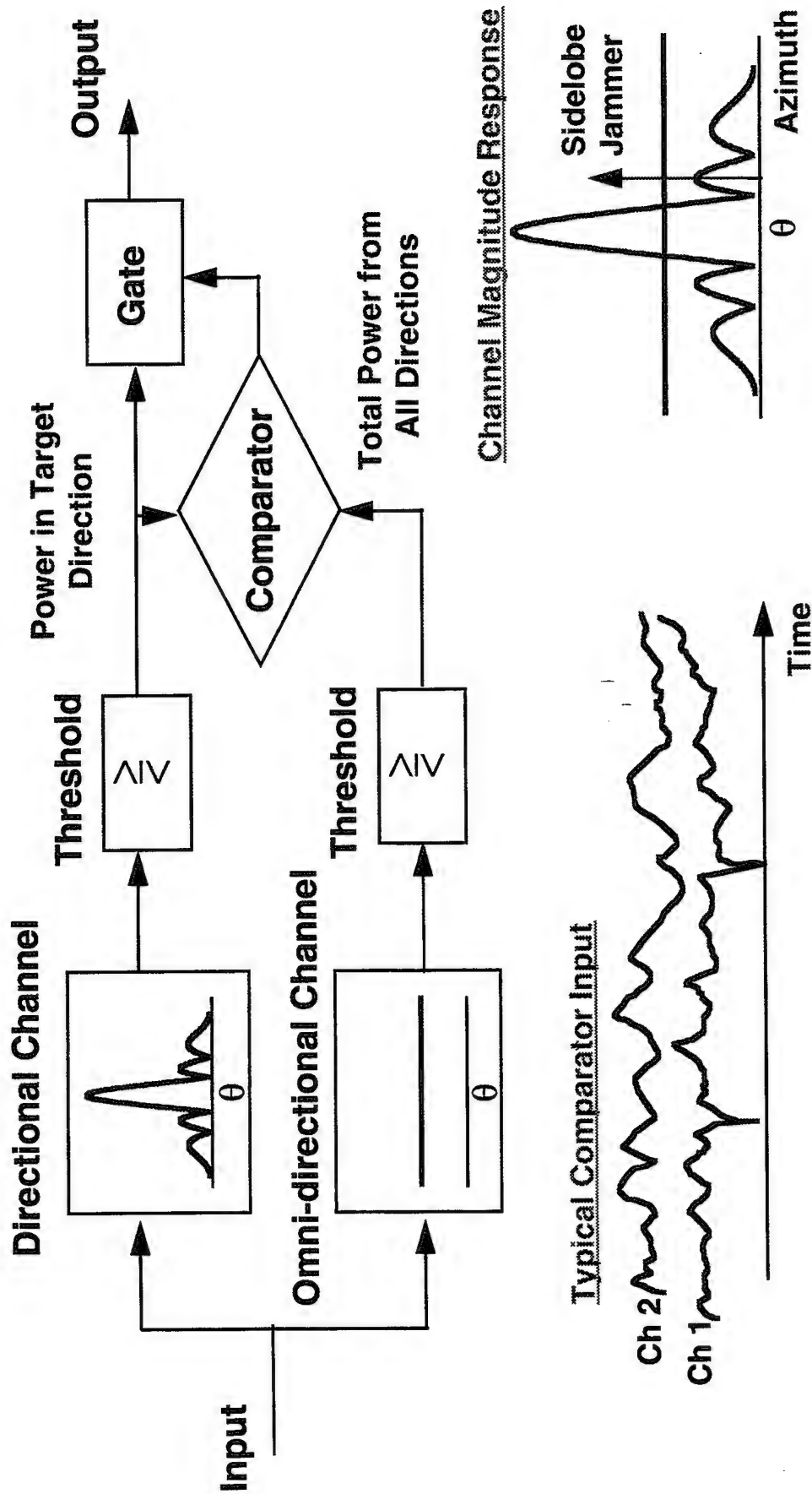


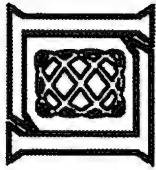
Classical Sidelobe Blanking





Classical Sidelobe Blanking





2-D ASB Detection Algorithm

Step 1: Beamforming

$$t_{AMF} > \eta_{amf}$$

Power in Target
Direction

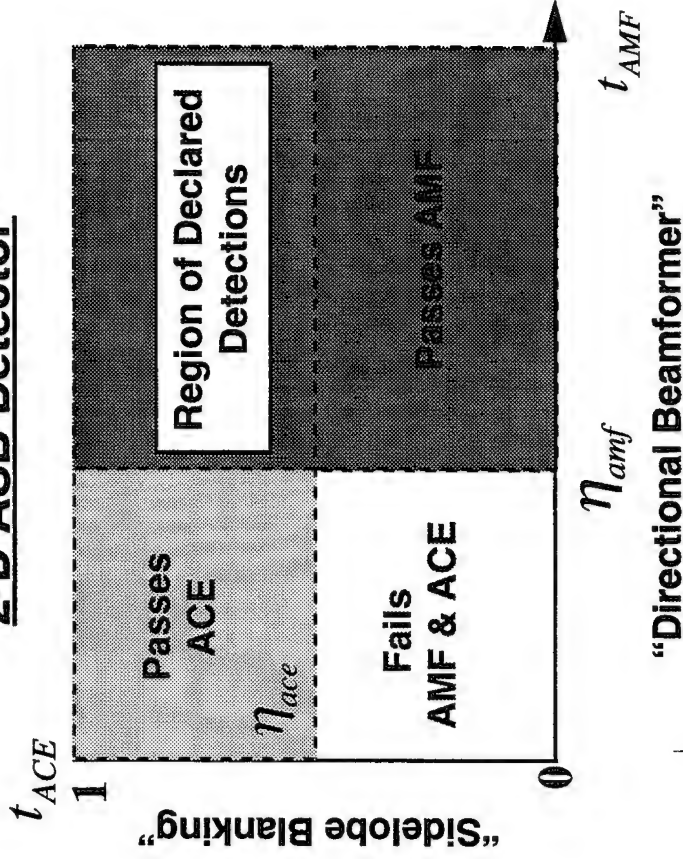
Step 2 : "Sidelobe Blanking"

$$t_{AMF} > \eta_{ace} \bullet \mathbf{x}_T^H \hat{\mathbf{R}}^{-1} \mathbf{x}_T$$

Power in Target
Direction

Total Power From
All Directions

2-D ASB Detector





Overview of Analysis

	<u>Homogeneous</u> $R_T = R$	<u>Inhomogeneous</u> $R_T \neq R$
<u>Perfect Look</u> $V_T = V$	AMF, GLRT, ACE, ASB	Generalized Eigen- Relation (GER): ALL Detectors < Open Problem >
<u>Signal Mismatch</u> $V_T \neq V$	AMF, GLRT Open Problem: ACE, ASB	< Open Problem >

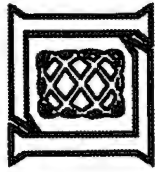
Today's Talk

- R_T - covariance of test cell x_T
 R - covariance of training samples x_i
 v_T - true target array response
 v - assumed target array response



Outline

- Adaptive Detection
- Adaptive Sidelobe Blanker
- ➔ • Signal Mismatch Performance
 - Theoretical Probabilities
 - Signal Mismatch Performance
 - Sidelobe Targets
- Closing Remarks



Distributions of 1-D Detectors

- Recall that PD of ASB is

$$PD_{ASB} = \Pr(t_{ACE} > \eta_{ace}, t_{AMF} > \eta_{amf})$$

- Define the following

$$\tilde{t}_{GLRT} \equiv t_{GLRT} / (1 - t_{GLRT}) \quad \tilde{t}_{ACE} \equiv t_{ACE} / (1 - t_{ACE}) \quad K = L - N + 2$$

$$\delta_\beta^2 \equiv |S|^2 \cdot \mathbf{v}_T^H \mathbf{R}^{-1} \mathbf{v}_T \cdot \cos^2(\mathbf{v}, \mathbf{v}_T) \cdot \beta_{K,N-1}(c) \quad c^2 \equiv |S|^2 \cdot \mathbf{v}_T^H \mathbf{R}^{-1} \mathbf{v}_T \cdot \sin^2(\mathbf{v}, \mathbf{v}_T)$$

- It can be shown that

$$\cos^2(\mathbf{v}, \mathbf{v}_T) \equiv \frac{|\mathbf{v}_T^H \mathbf{R}^{-1} \mathbf{v}_T|^2}{\mathbf{v}_T^H \mathbf{R}^{-1} \mathbf{v} \cdot \mathbf{v}_T^H \mathbf{R}^{-1} \mathbf{v}_T}$$

Distributions of Adaptive Detectors

$$\tilde{t}_{GLRT}^d = F_{1,K-1}(\delta_\beta)$$

$$t_{AMF}^d = F_{1,K-1}(\delta_\beta) / \beta_{K,N-1}(c)$$

$$\tilde{t}_{ACE}^d = F_{1,K-1}(\delta_\beta) / [1 - \beta_{K,N-1}(c)]$$



Distributions of 1-D Detectors

• Recall that PD of ASB is

$$PD_{ASB} = \Pr(t_{ACE} > \eta_{ace}, t_{AMF} > \eta_{amf})$$

Requires knowledge
of Dependence!

• Define the following

$$\tilde{t}_{GLRT} \equiv t_{GLRT} / (1 - t_{GLRT}) \quad \tilde{t}_{ACE} \equiv t_{ACE} / (1 - t_{ACE}) \quad K = L - N + 2$$

$$\delta_\beta^2 \equiv |S|^2 \cdot \mathbf{v}_T^H \mathbf{R}^{-1} \mathbf{v}_T \cdot \cos^2(\mathbf{v}, \mathbf{v}_T) \cdot \beta_{K, N-1}(c) \quad c^2 \equiv |S|^2 \cdot \mathbf{v}_T^H \mathbf{R}^{-1} \mathbf{v}_T \cdot \sin^2(\mathbf{v}, \mathbf{v}_T)$$

• It can be shown that

$$\cos^2(\mathbf{v}, \mathbf{v}_T) \equiv \frac{|\mathbf{v}^H \mathbf{R}^{-1} \mathbf{v}_T|^2}{\mathbf{v}^H \mathbf{R}^{-1} \mathbf{v} \cdot \mathbf{v}_T^H \mathbf{R}^{-1} \mathbf{v}_T}$$

Distributions of Adaptive Detectors

$$\tilde{t}_{GLRT}^d = F_{1, K-1}(\delta_\beta)$$

$$t_{AMF}^d = F_{1, K-1}(\delta_\beta) / \beta_{K, N-1}(c)$$

$$\tilde{t}_{ACE}^d = F_{1, K-1}(\delta_\beta) / [1 - \beta_{K, N-1}(c)]$$

Found in this
Summary!



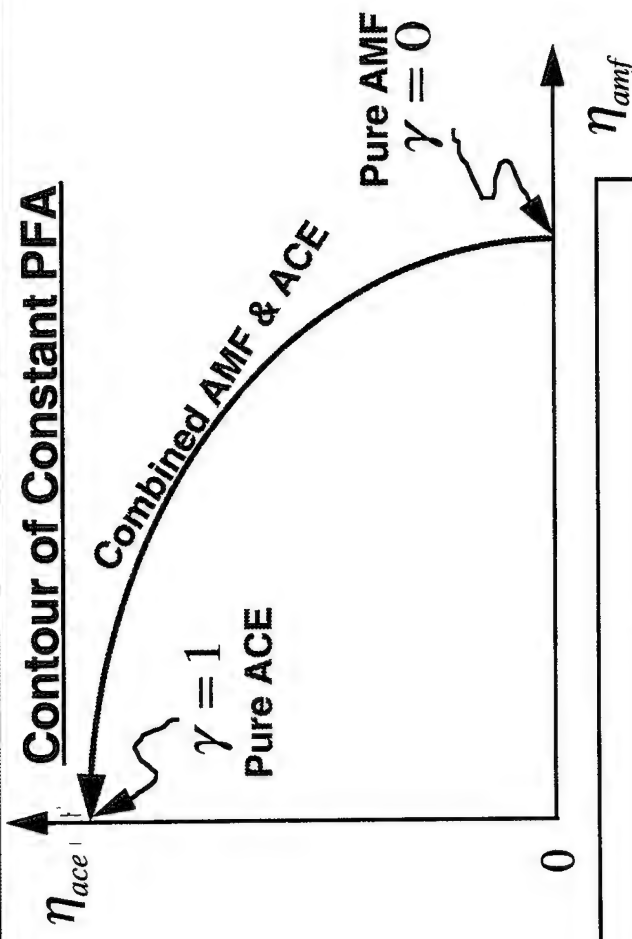
Probabilities for ASB Algorithm

- Define the quantity

$$\gamma(\eta_{ace}, \eta_{amf}) \equiv \frac{\eta_{ace}}{\eta_{ace} + \eta_{amf}(1 - \eta_{ace})}$$

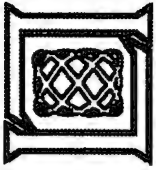
$$0 \leq \gamma(\eta_{ace}, \eta_{amf}) \leq 1$$

- It can be shown that



$$PD_{ASB} = \int_0^{\gamma(\eta_{ace}, \eta_{amf})} P_{\beta} d\beta \cdot PD_{ACE|\beta} + \int_{\gamma(\eta_{ace}, \eta_{amf})}^1 P_{\beta} d\beta \cdot PD_{AMF|\beta}$$

$$PFA_{ASB} = \int_0^{\gamma(\eta_{ace}, \eta_{amf})} P_{\beta} d\beta \cdot PFA_{ACE|\beta} + \int_{\gamma(\eta_{ace}, \eta_{amf})}^1 P_{\beta} d\beta \cdot PFA_{AMF|\beta}$$



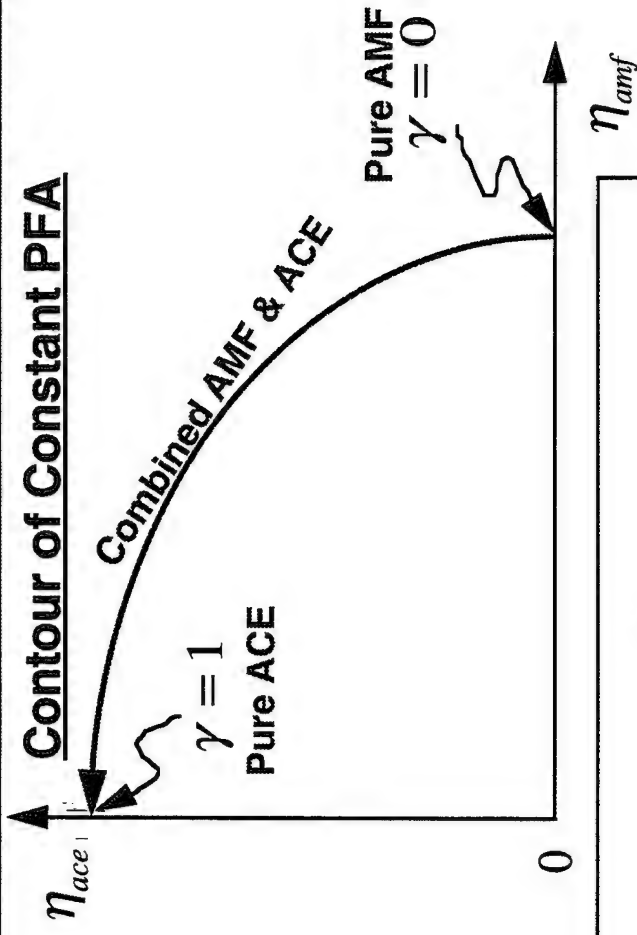
Probabilities for ASB Algorithm

- Define the quantity

$$\gamma(\eta_{ace}, \eta_{amf}) \equiv \frac{\eta_{ace}}{\eta_{ace} + \eta_{amf}(1 - \eta_{ace})}$$

$$0 \leq \gamma(\eta_{ace}, \eta_{amf}) \leq 1$$

- It can be shown that

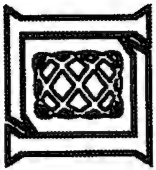


$$PD_{ASB} = \int_0^{\gamma(\eta_{ace}, \eta_{amf})} P_{\beta} d\beta \cdot PD_{ACE|\beta} + \int_{\gamma(\eta_{ace}, \eta_{amf})}^1 P_{\beta} d\beta \cdot PD_{AMF|\beta}$$

ACE AMF

$$PFA_{ASB} = \int_0^{\gamma(\eta_{ace}, \eta_{amf})} P_{\beta} d\beta \cdot PFA_{ACE|\beta} + \int_{\gamma(\eta_{ace}, \eta_{amf})}^1 P_{\beta} d\beta \cdot PFA_{AMF|\beta}$$

ACE AMF



Probabilities for ASB Algorithm

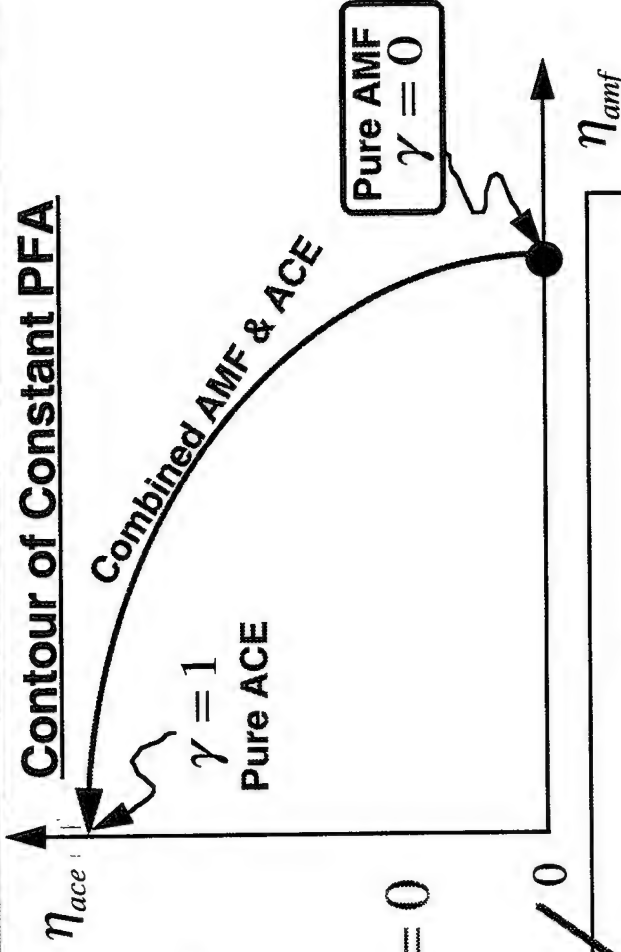
- Define the quantity

$$\gamma(\eta_{ace}, \eta_{amf}) \equiv \frac{\eta_{ace}}{\eta_{ace} + \eta_{amf}(1 - \eta_{ace})} = 0$$

$$0 \leq \gamma(\eta_{ace}, \eta_{amf}) \leq 1$$

$$\eta_{ace} = 0$$

- It can be shown that



$$\gamma(\eta_{ace}, \eta_{amf})$$

$$PD_{ASB} = \int_0^1 P_{\beta} d\beta \cdot PD_{ACE|\beta} + \int_{\gamma(\eta_{ace}, \eta_{amf})}^1 P_{\beta} d\beta \cdot PD_{AMF|\beta}$$

$$\gamma(\eta_{ace}, \eta_{amf}) \quad AMF$$

$$\gamma(\eta_{ace}, \eta_{amf})$$

$$PFA_{ASB} = \int_0^1 P_{\beta} d\beta \cdot PFA_{ACE|\beta} + \int_{\gamma(\eta_{ace}, \eta_{amf})}^1 P_{\beta} d\beta \cdot PFA_{AMF|\beta}$$

$$\gamma(\eta_{ace}, \eta_{amf}) \quad AMF$$



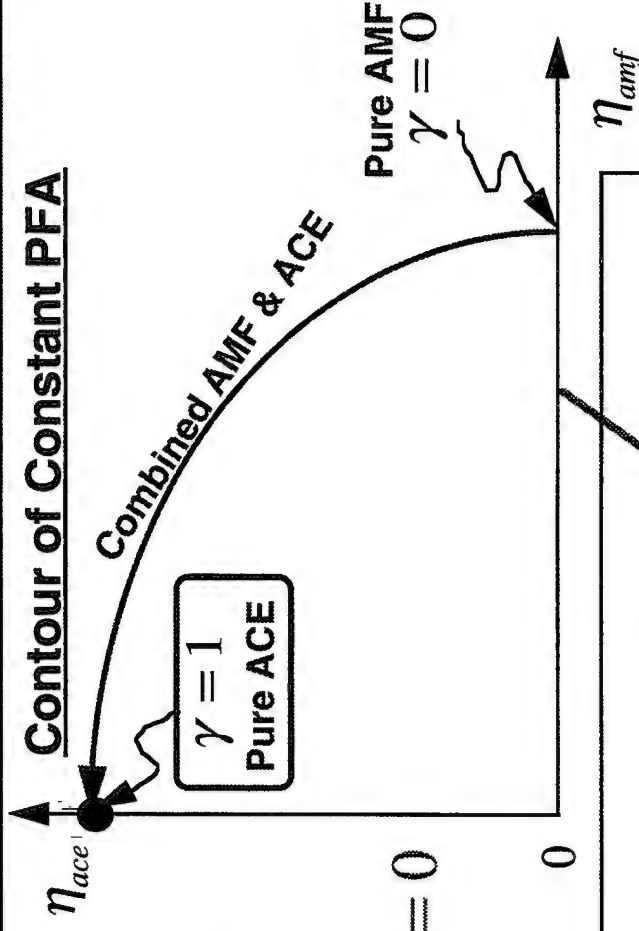
Probabilities for ASB Algorithm

- Define the quantity

$$\gamma(\eta_{ace}, \eta_{amf}) \equiv \frac{\eta_{ace}}{\eta_{ace} + \eta_{amf}(1 - \eta_{ace})} = 1$$

$$0 \leq \gamma(\eta_{ace}, \eta_{amf}) \leq 1$$

- It can be shown that



$$\gamma(\eta_{ace}, \eta_{amf})$$

$$PD_{ASB} = \int_0^1 P_{\beta} d\beta \cdot PD_{ACE|\beta} + \int_0^1 P_{\beta} d\beta \cdot PD_{AMF|\beta}$$

AMF

$$\gamma(\eta_{ace}, \eta_{amf})$$

$$PFA_{ASB} = \int_0^1 P_{\beta} d\beta \cdot PFA_{ACE|\beta} + \int_0^1 P_{\beta} d\beta \cdot PFA_{AMF|\beta}$$

AMF

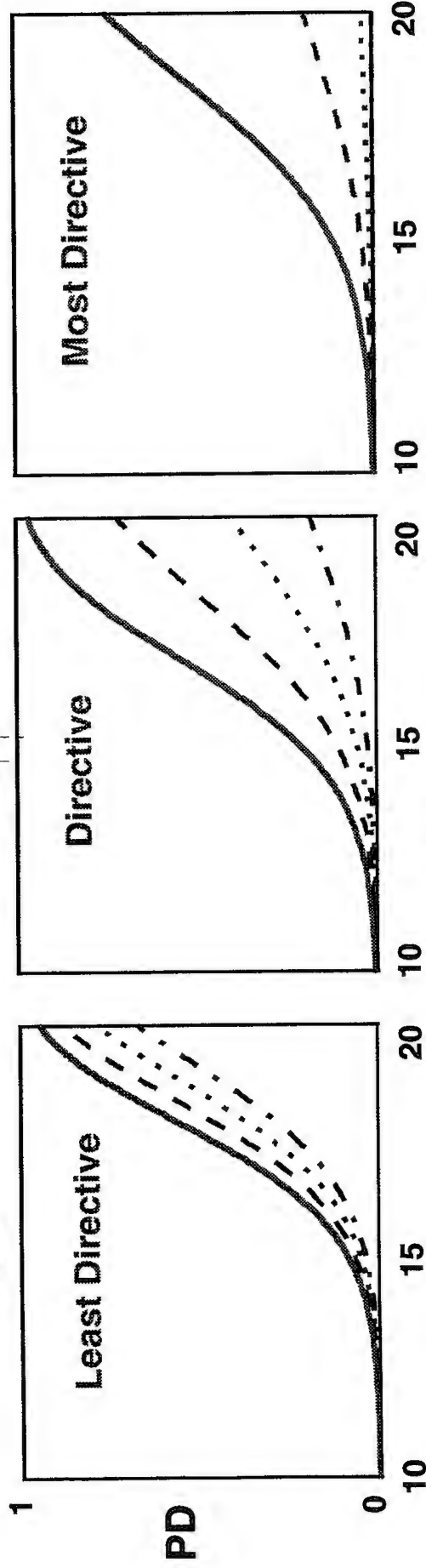


Signal Mismatch: AMF, GLRT, & ACE

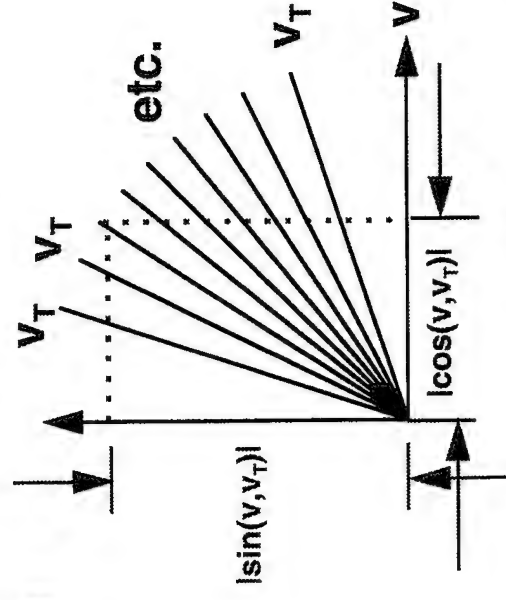
AMF

GLRT

ACE



SNR (dB)



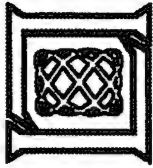
•Parameters: $N = 10, L = 2N, PFA = 1e-6$

$\cos^2(v, v_T) = 1$ ———

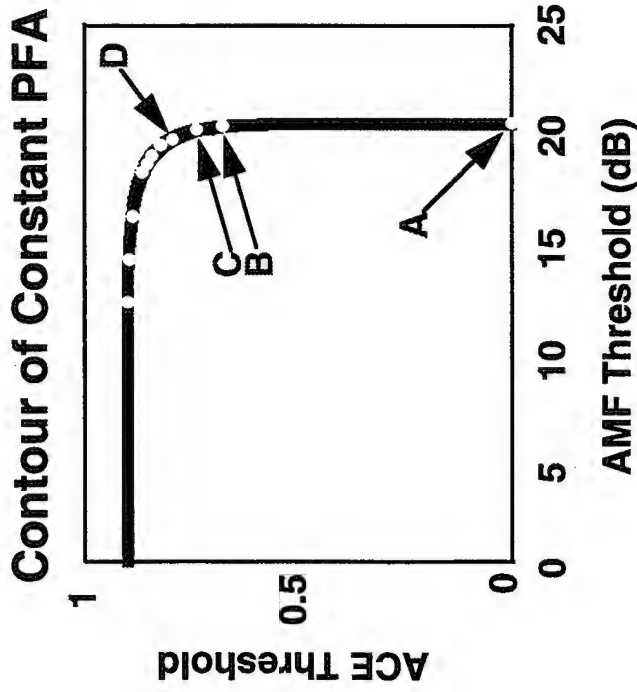
$\cos^2(v, v_T) = 0.9$ - - -

$\cos^2(v, v_T) = 0.8$ ·····

$\cos^2(v, v_T) = 0.7$ - ··· -



Signal Mismatch and the 2-D ASB



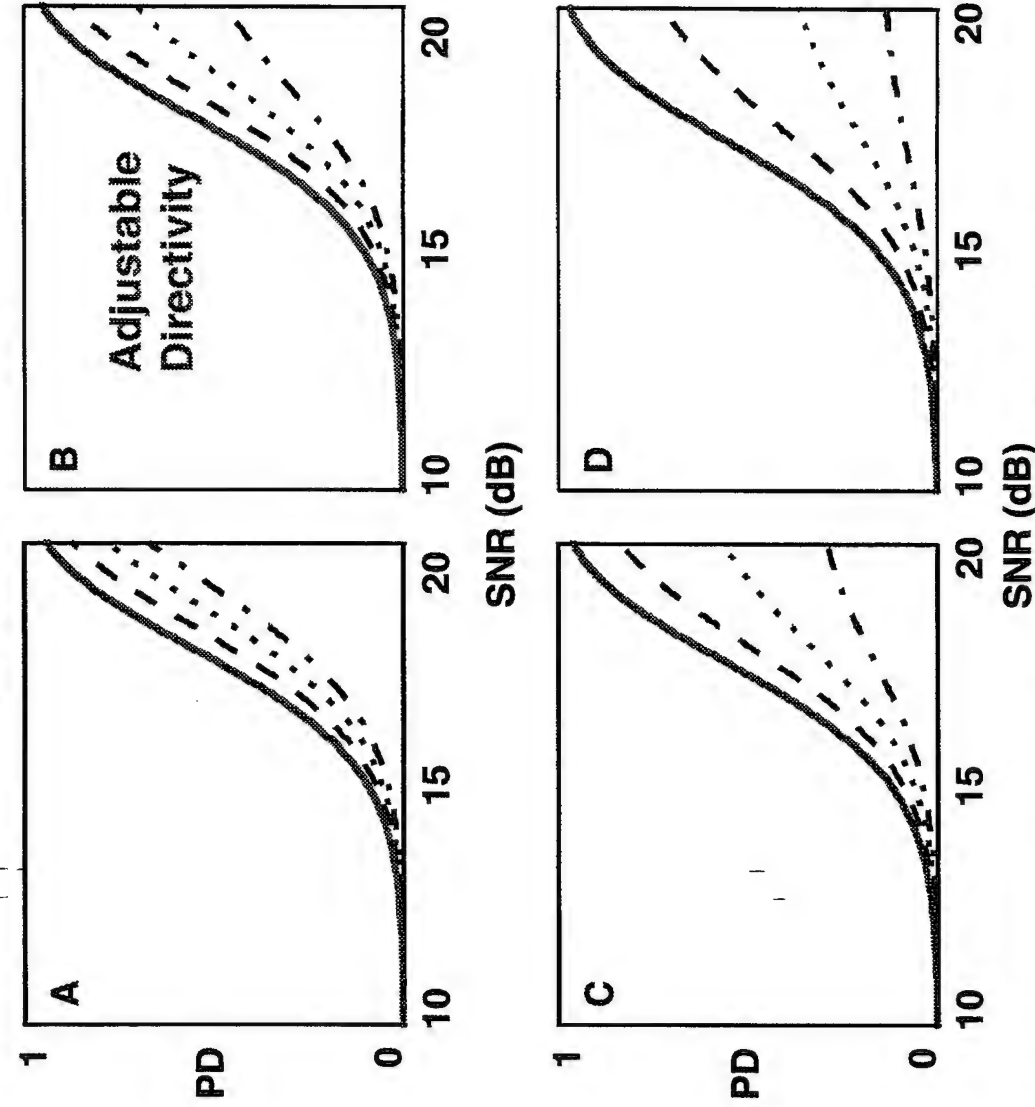
Parameter Choice of

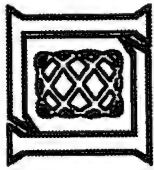
$N = 10, L = 2N, PFA = 1e-6$

$\cos^2(v, v_T) = 1, \cos^2(v, v_T) = 0.9$

$\cos^2(v, v_T) = 0.8, \cos^2(v, v_T) = 0.7$

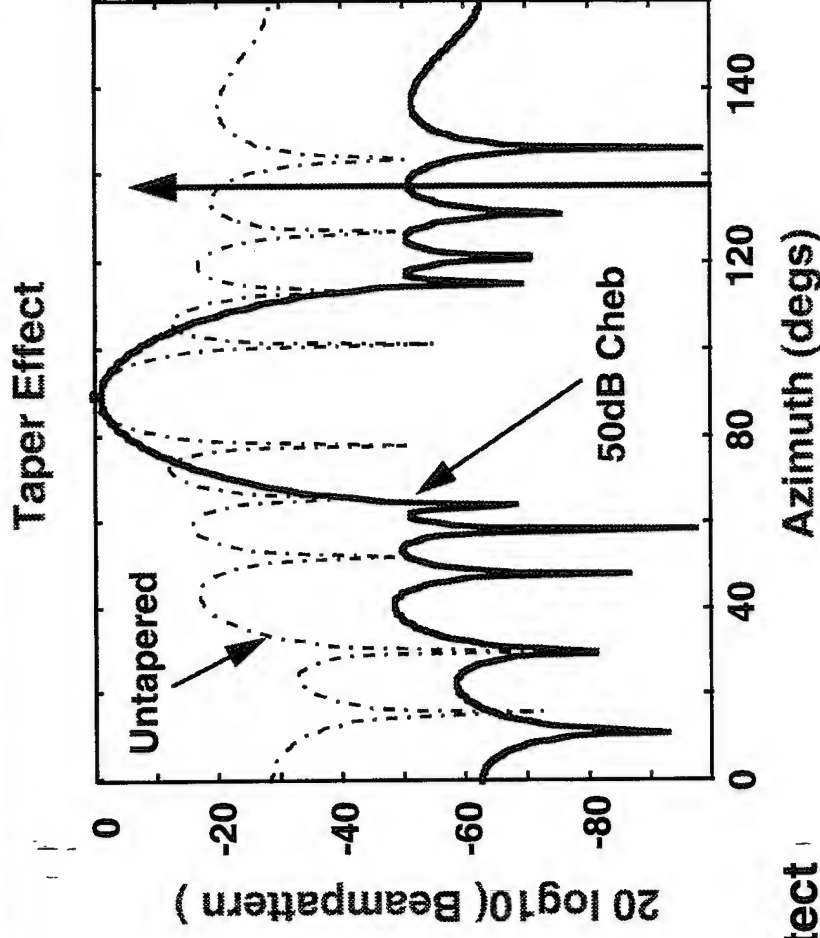
2-D ASB Detector





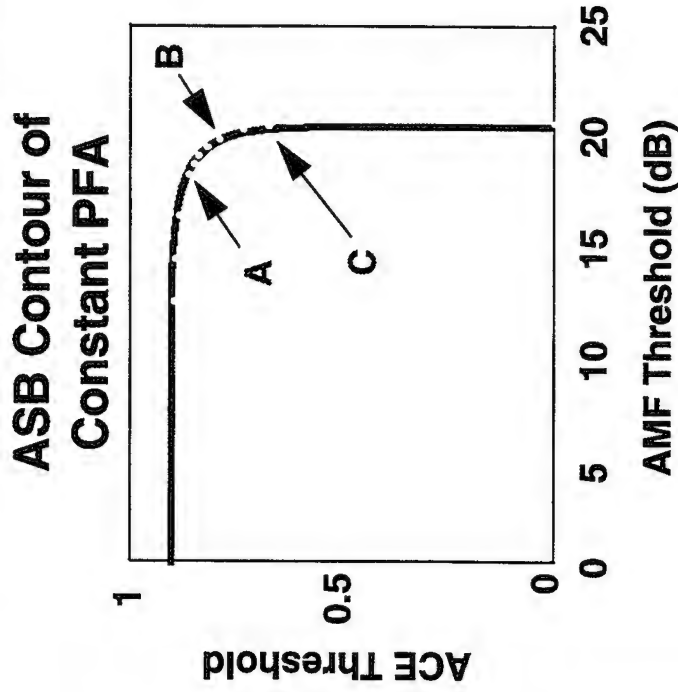
Chebyshev Tapered AMF

- Tapers reduce sidelobe levels but widen the mainlobe
- Reduces likelihood of sidelobe detects
- Also reduces likelihood of mainlobe detects!
- No mechanism to distinguish a sidelobe detect from a mainlobe detect

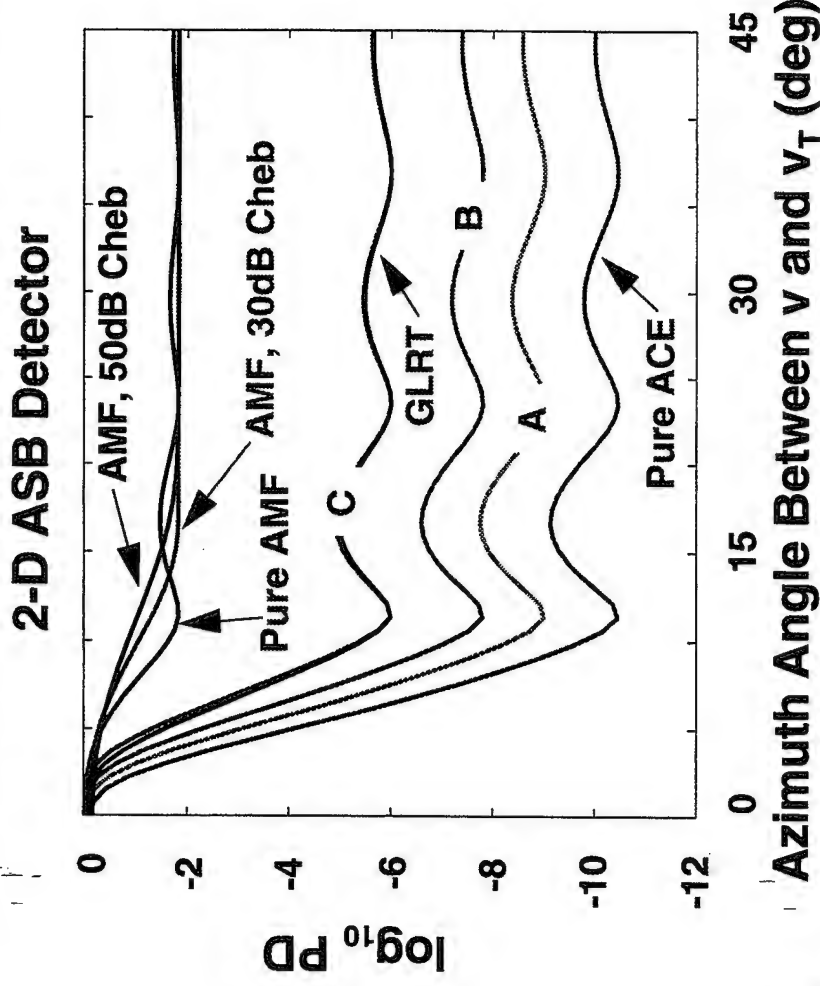




Sidelobe Detection Performance



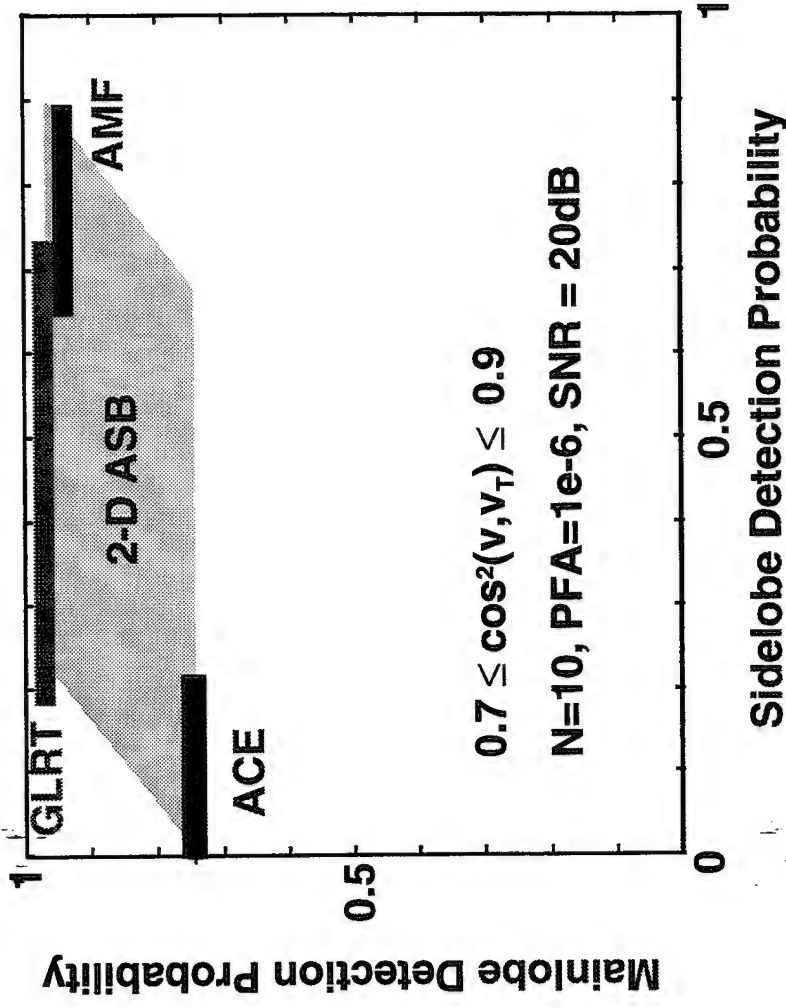
- Parameter Choice of
 $N = 10$, $L = 2N$, $PFA = 1e-6$, $SNR = 20dB$
- ULA, 0.5 Wavelength Spacing





Remarks on Mismatch Performance

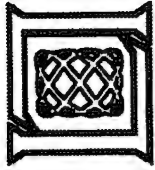
- Each 1-D Detector has a characteristic directivity
- The 2-D ASB allows one to adjust directivity via thresholds



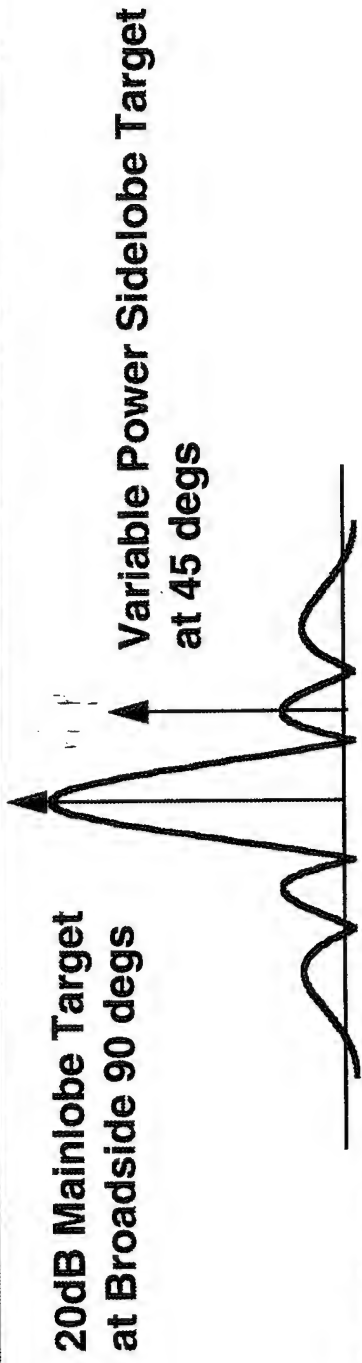


Outline

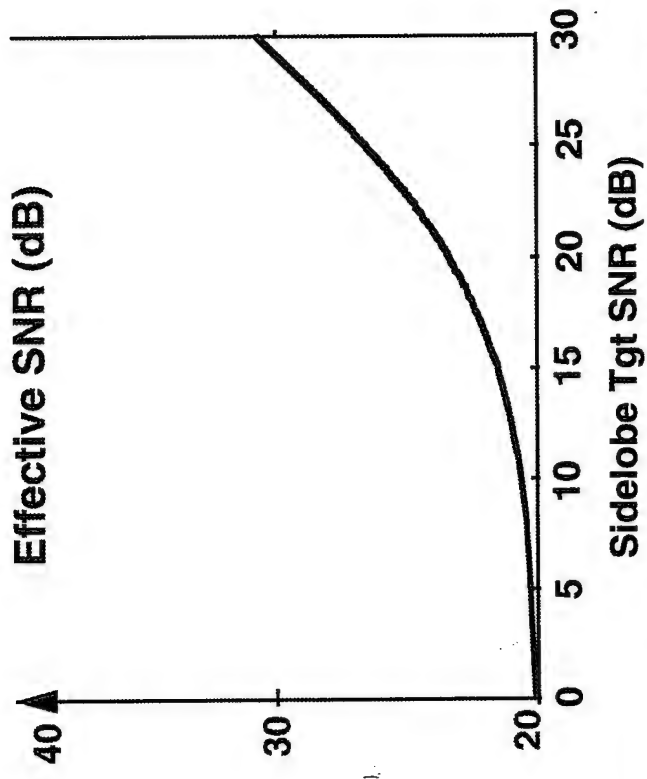
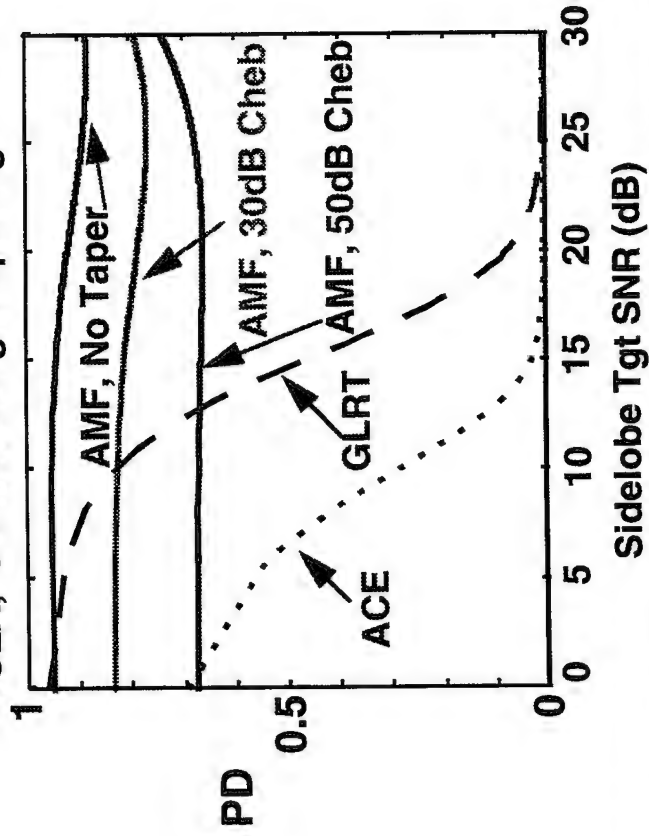
- Adaptive Detection
- Adaptive Sidelobe Blanker
- Signal Mismatch Performance
 - Theoretical Probabilities
 - Signal Mismatch Performance
 - ➔** - Sidelobe Targets
- Closing Remarks



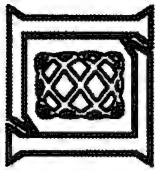
Sidelobe Targets and 1-D Detectors



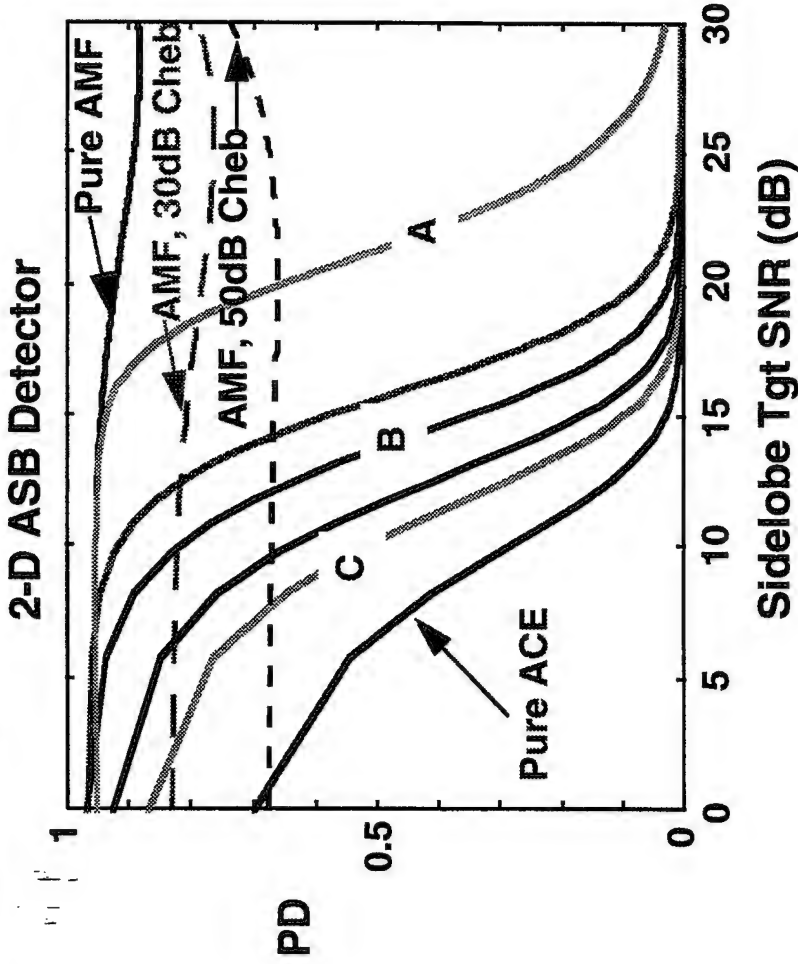
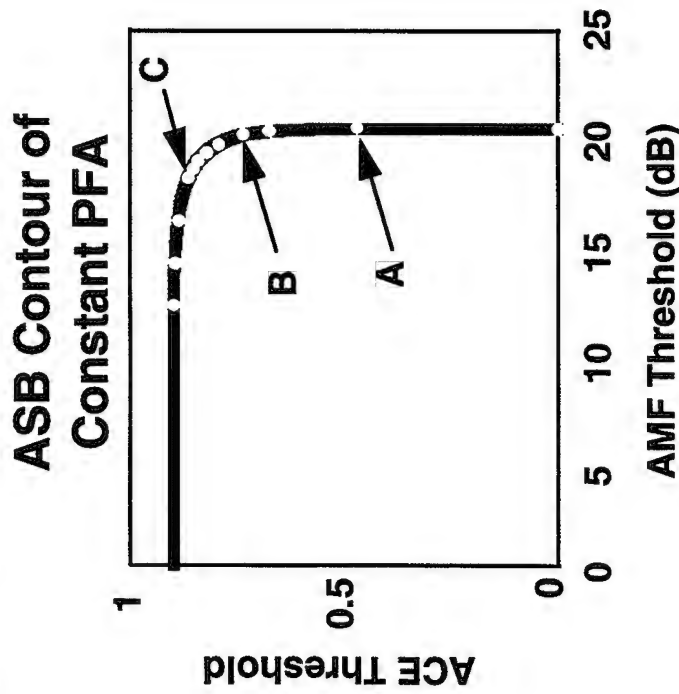
- Parameter: $N = 10$, $L = 2N$, $PFA = 1e-6$
- ULA, 0.5 Wavelength Spacing



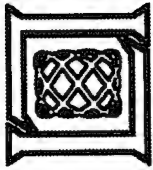
MIT Lincoln Laboratory



Sidelobe Targets and the 2-D ASB



- Parameter: $N = 10$, $L = 2N$, $PFA = 1e-6$
- ULA, 0.5 Wavelength Spacing
- 20dB Mainlobe Target



Closing Remarks

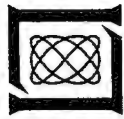
- AMF Least Directive with Highest PD per SNR
- ACE Most Directive with Lowest PD per SNR
- GLRT Between AMF and ACE
- 2-D ASB has Adjustable Directivity
- Tapered AMF has no mechanism to delineate sidelobe detects from mainlobe detects

Estimation for Synthetic Bandwidth Processing

Steven T. Smith

MIT Lincoln Laboratory
244 Wood Street, Room J-149M
Lexington, MA 02173-9108
tel: (781) 981-3106
email: stsmith@ll.mit.edu

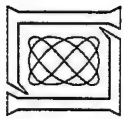
Abstract Synthetic wideband processing as proposed by Cuomo, Plou, and Mayhan employs parametric estimation methods to construct wideband data from widely separated subbands. The goal is to obtain ultrawideband resolution from two or more sensors operating at different frequencies greater than that achievable using conventional methods. The key is accurate estimation of the target return's signal parameters, which in this talk are assumed to be those of an all-pole model. The estimation algorithm consists of an initialization step to compute rough estimates of the pole parameters, followed by a maximum likelihood estimation step to compute ML estimates of poles and their associated amplitudes. In this talk we describe the fundamental accuracy and resolution bounds associated with this estimation problem, compare the performance of different superresolution algorithms (ESPRIT versus root-MUSIC) for the initialization stage, and compare different optimization algorithms (Newton-Raphson versus various quasi-Newton methods) for ML estimation. One interesting question addressed is the true resolution achieved by widely separated subbands; it is shown, for example, that by separating two subbands each of width B Hz by a bandgap of MHz, one achieves a resolution improvement of about \sqrt{B} (M/B). Experimental data provided by Lincoln Laboratory's Divisions 3 and 9, as well as simulated data, is used to compare different algorithms.



Estimation for Synthetic Bandwidth Processing

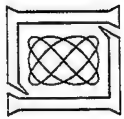
Steven T. Smith
1998 ASAP WORKSHOP

This work was sponsored by DARPA under Air Force contract F19628-95-C-0002. Opinions, interpretations, conclusions, and recommendations are those of the author and are not necessarily endorsed by the United States Air Force.

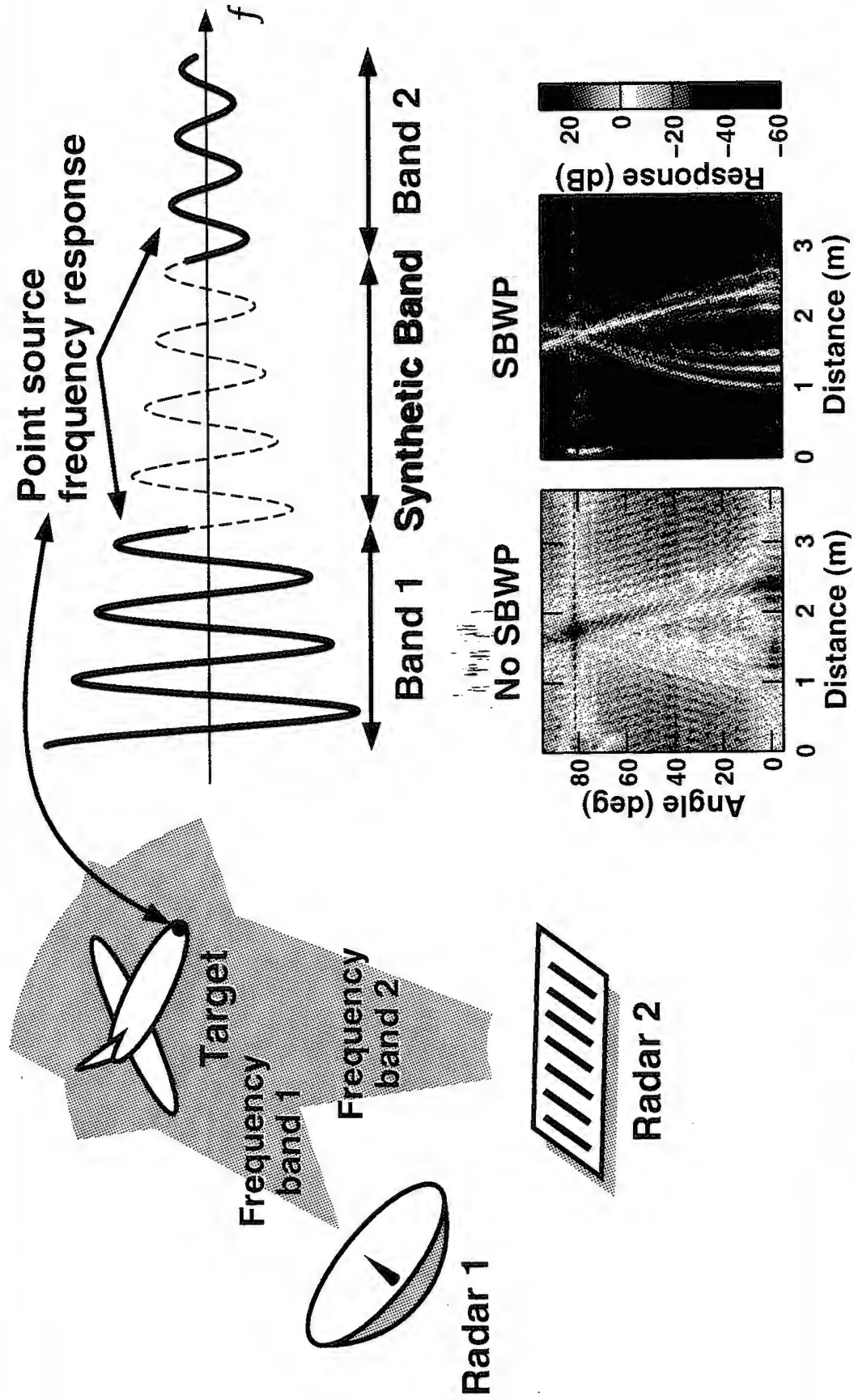


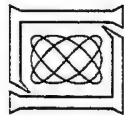
Outline

- Introduction
- Split-band ESPRIT
- Synthetic bandwidth resolution
- Conclusions



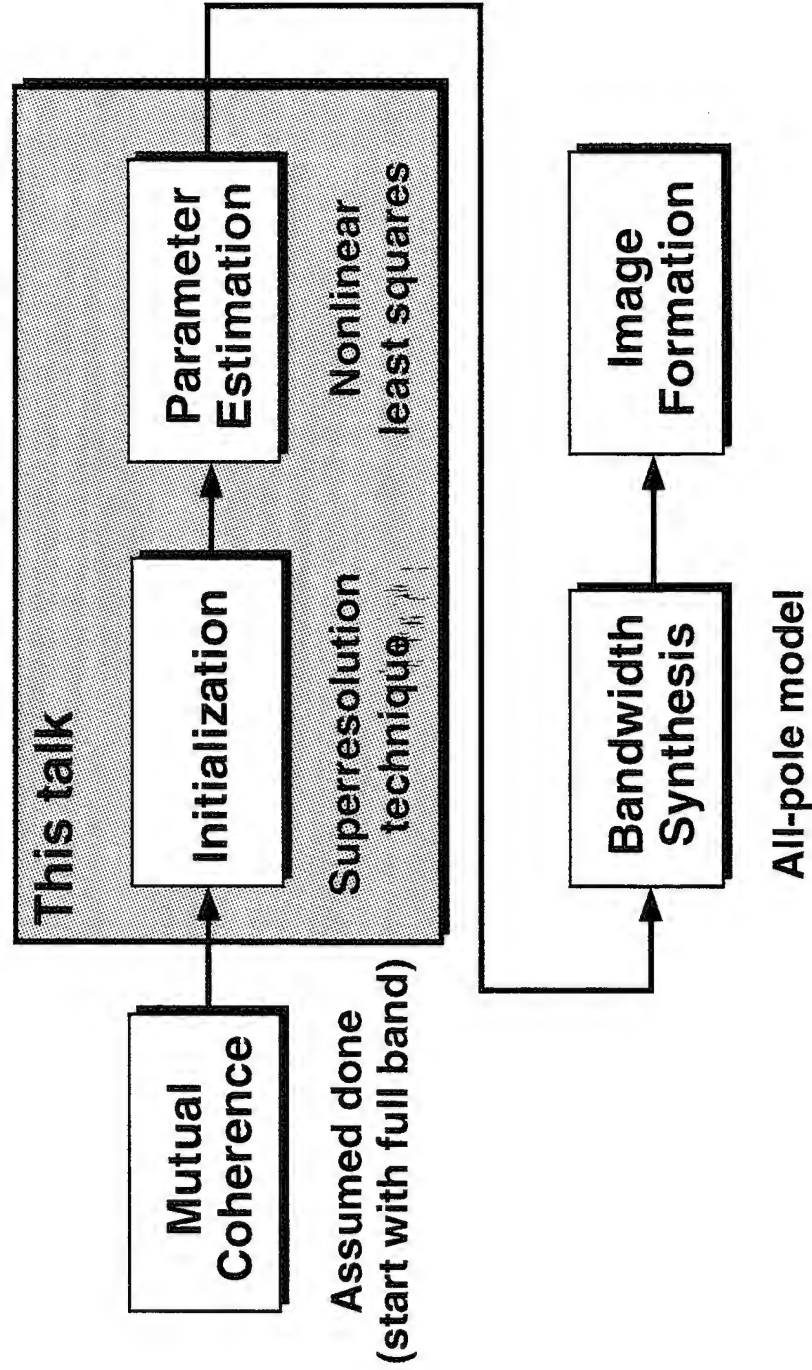
Synthetic Bandwidth Processing

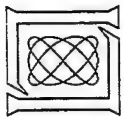




Synthetic Bandwidth Processing Architecture

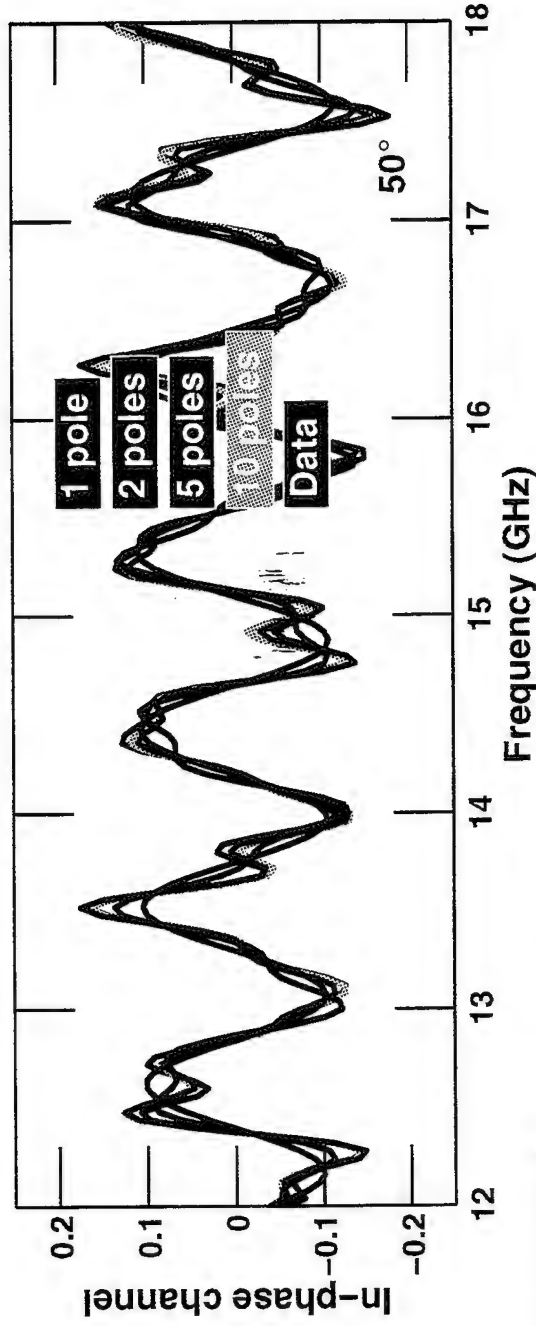
Synthetic Bandwidth Processing



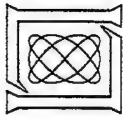


All-Pole Signal Model

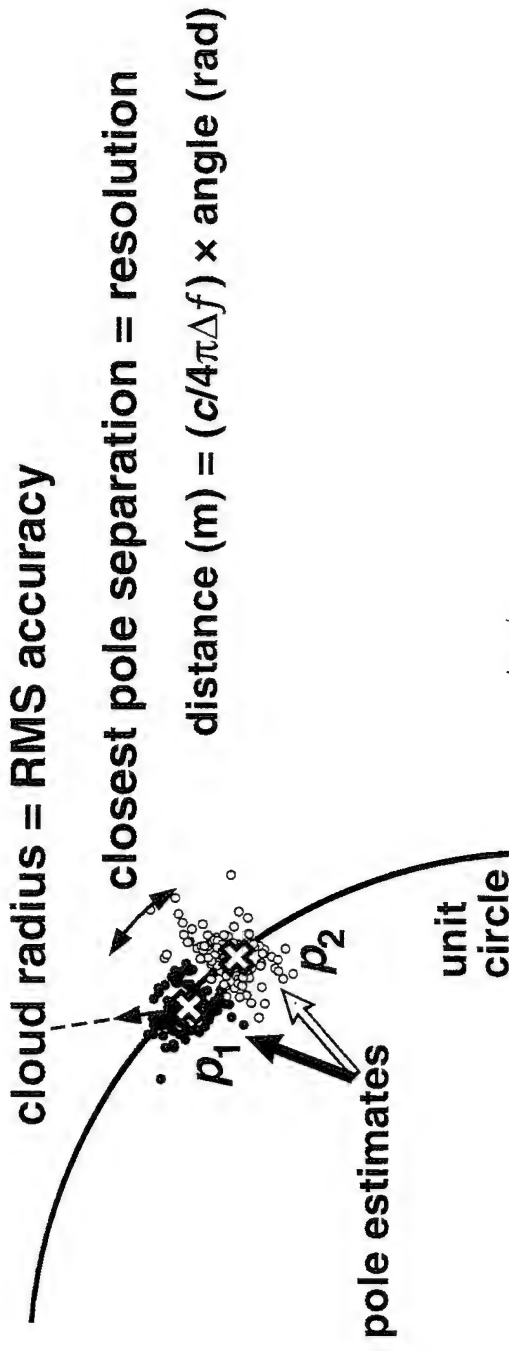
$$\text{signal} = a_1 \begin{pmatrix} p_1^{f_1} \\ p_1^{f_2} \\ \vdots \\ p_1^{f_N} \end{pmatrix} + a_2 \begin{pmatrix} p_2^{f_1} \\ p_2^{f_2} \\ \vdots \\ p_2^{f_N} \end{pmatrix} + \dots + a_K \begin{pmatrix} p_K^{f_1} \\ p_K^{f_2} \\ \vdots \\ p_K^{f_N} \end{pmatrix} + \text{noise}$$



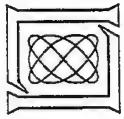
- Estimation problem**
- Poles p_k are unknown
 - Amplitudes a_k are also unknown



Accuracy vs Resolution



- How accurately can we describe the data?
 - Related to estimation accuracy
- What is the resolution of synthetic bandwidth processing?
 - At what distance are two point sources not resolved?



Maximum Likelihood Formulation

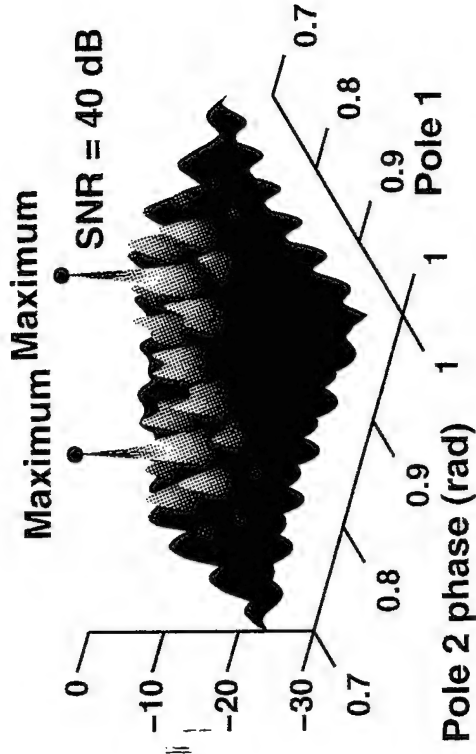
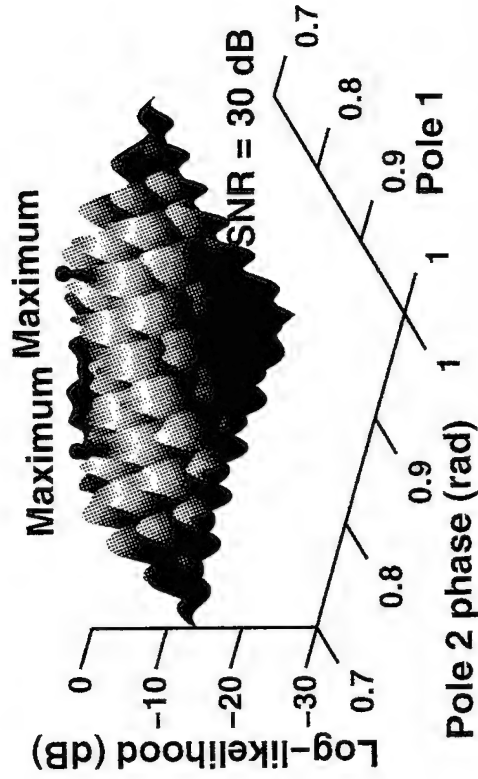
- Statistical model for synthetic bandwidth processing

$$P_{kn} = p_k^{f_n} \quad (\text{pole matrix})$$

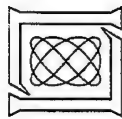
a = vector of amplitudes

R = covariance matrix

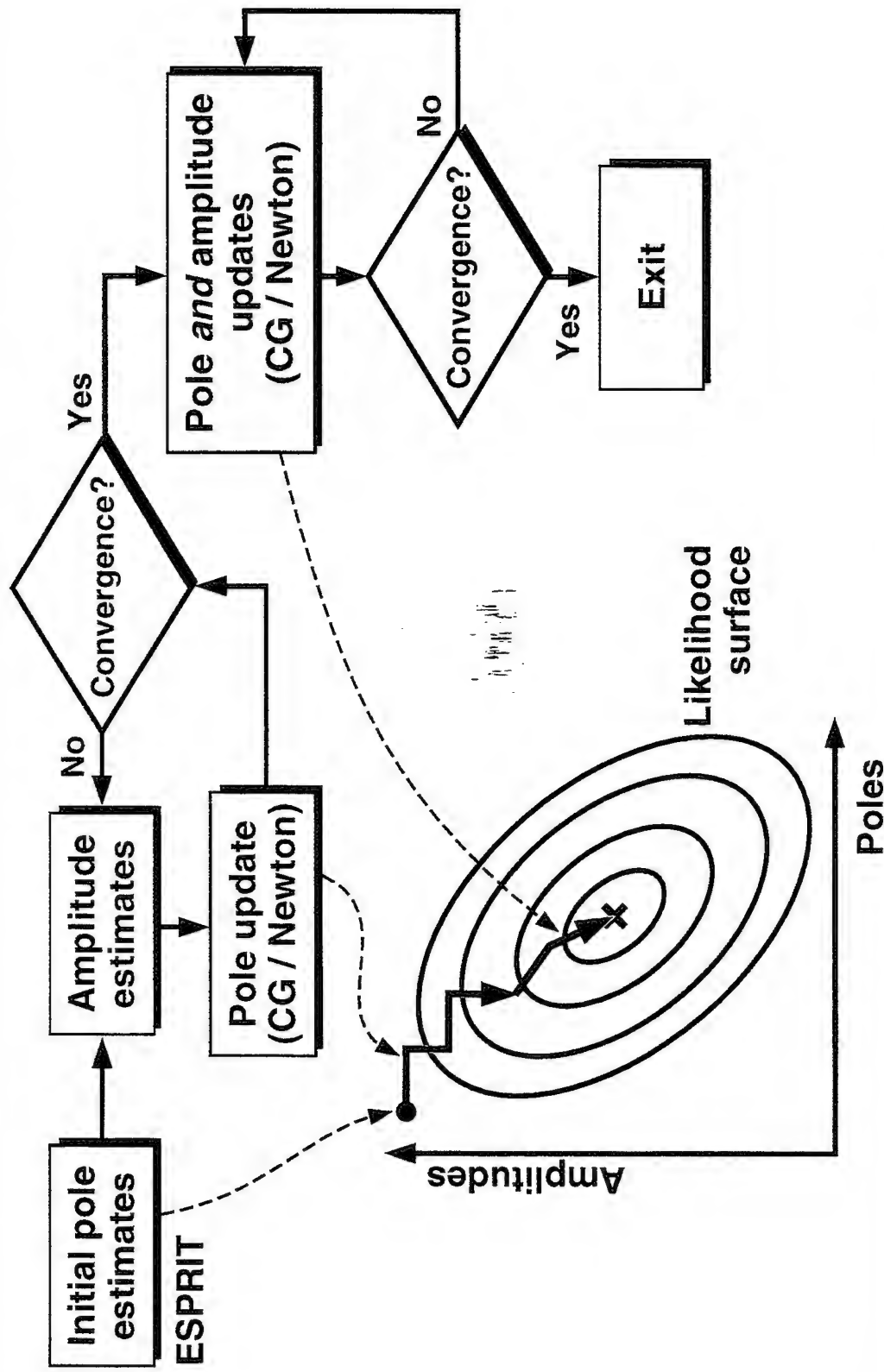
$$f(z) = \frac{1}{\pi^N \det R} e^{-(z - Pa)^H R^{-1} (z - Pa)}$$

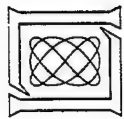


Optimize nonlinear function with $2 \times \# \text{poles complex dof}$



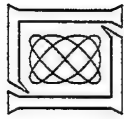
All-Pole Maximum Likelihood Algorithm





Outline

- Introduction
- Split-band ESPRIT
- Synthetic bandwidth resolution
- Conclusions



ESPRIT—What Is It?

A Superresolution Method That Exploits Shift Invariance

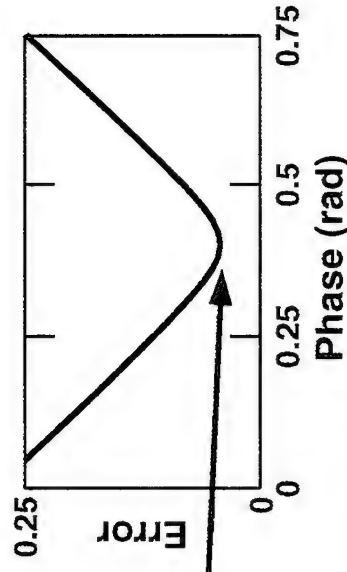
$$\text{Unshifted} = \begin{bmatrix} p^0 & p^1 & p^2 & p^3 \end{bmatrix} + \text{noise}$$

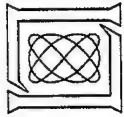
$$\text{Shifted} = \begin{bmatrix} p^1 & p^2 & p^3 & p^4 \end{bmatrix} + \text{noise} \approx p \times \text{Unshifted}$$

- Problem: Transform model to look like data

$$\min_{P, \Phi, T} \left\| \begin{pmatrix} \text{Unshifted} \\ \text{Shifted} \end{pmatrix} - \begin{pmatrix} P \\ P\Phi \end{pmatrix} T \right\|^2$$

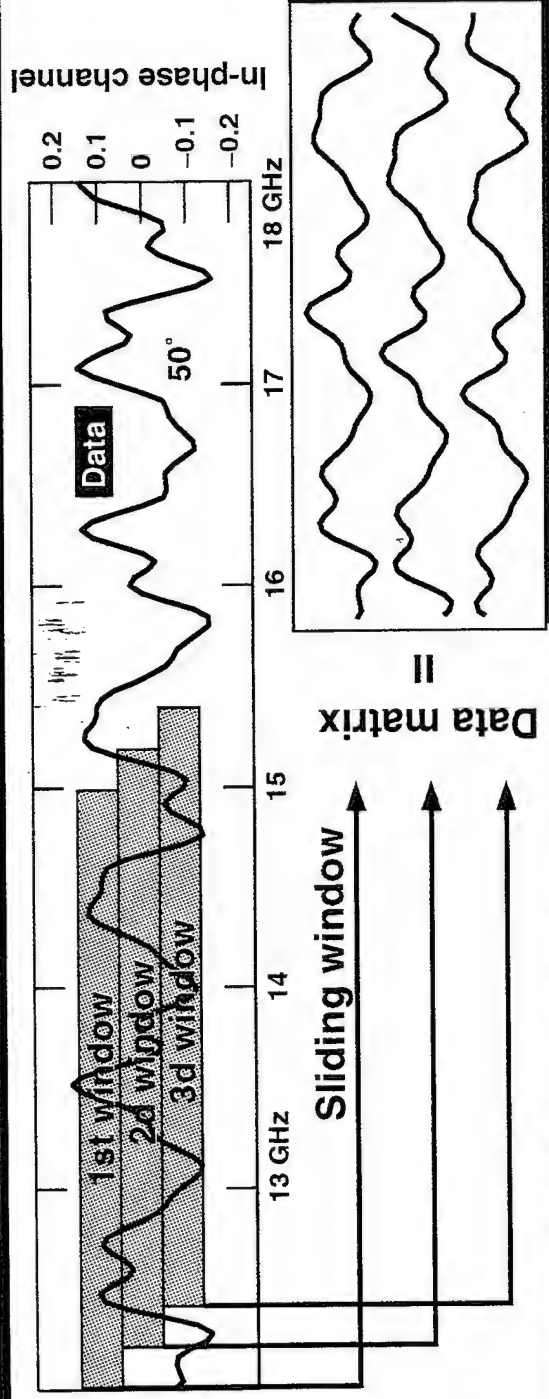
ESPRIT determines the best model efficiently

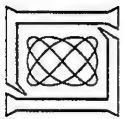




Signal Subspace Estimation

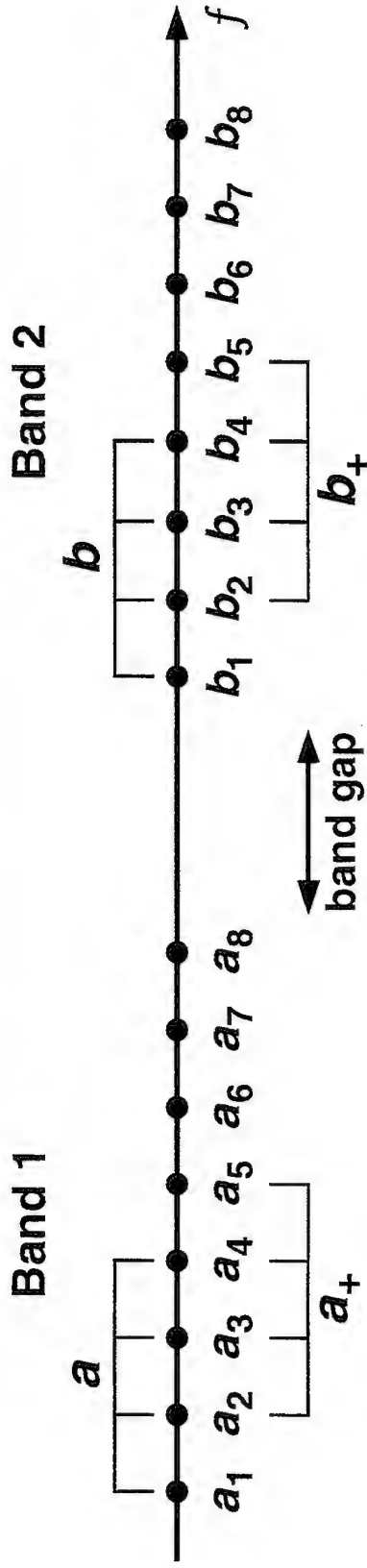
- **Fact:** Require at least K data vectors to estimate K -dimensional subspace
- **Problem:** Only have a “single snapshot”
- **Solution:** Sliding window across data
- **Issues:** Window size affects accuracy and resolution
 - Long window \Rightarrow poor accuracy / good resolution
 - Short window \Rightarrow good accuracy / poor resolution





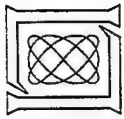
Split-band ESPRIT

Coherent Data from Widely Separated Bands



$$\text{Unshifted window} = \begin{pmatrix} a \\ b \end{pmatrix} \quad \text{Shifted window} = \begin{pmatrix} a_+ \\ b_+ \end{pmatrix}$$

- ESPRIT window spans both bands
- Bands may have different widths
- Different sampling rates an issue
- Window size affects accuracy and resolution



Split-band ESPRIT Data Matrix and Algorithm

$$\begin{array}{c}
 \text{Unshifted} \\
 \text{data}
 \end{array}
 \begin{pmatrix}
 a_1 & a_2 & a_3 & a_4 & \cdot & \cdot & \cdot & \cdot \\
 a_2 & a_3 & a_4 & a_5 & a_6 & a_7 & \cdot & \cdot \\
 a_3 & a_4 & a_5 & a_6 & a_7 & b_4 & b_5 & b_6 \\
 a_4 & a_5 & a_6 & a_7 & b_3 & b_4 & b_5 & b_6 \\
 b_1 & b_2 & b_3 & b_4 & b_5 & b_6 & b_7 & \cdot \\
 b_2 & b_3 & b_4 & b_5 & b_6 & b_7 & \cdot & \cdot \\
 b_3 & b_4 & b_5 & b_6 & b_7 & \cdot & \cdot & \cdot \\
 b_4 & b_5 & b_6 & b_7 & \cdot & \cdot & \cdot & \cdot
 \end{pmatrix}$$

$$\begin{array}{c}
 D = \\
 \\
 \text{Shifted} \\
 \text{data}
 \end{array}
 \begin{pmatrix}
 a_2 & a_3 & a_4 & a_5 & a_6 & a_7 & a_8 & \cdot & \cdot & \cdot & \cdot \\
 a_3 & a_4 & a_5 & a_6 & a_7 & a_8 & b_5 & b_6 & b_7 & b_8 & \cdot \\
 a_4 & a_5 & a_6 & a_7 & a_8 & b_4 & b_5 & b_6 & b_7 & b_8 & \cdot \\
 a_5 & a_6 & a_7 & a_8 & b_3 & b_4 & b_5 & b_6 & b_7 & b_8 & \cdot \\
 b_2 & b_3 & b_4 & b_5 & b_6 & b_7 & b_8 & \cdot & \cdot & \cdot & \cdot \\
 b_3 & b_4 & b_5 & b_6 & b_7 & b_8 & \cdot & \cdot & \cdot & \cdot & \cdot \\
 b_4 & b_5 & b_6 & b_7 & b_8 & \cdot & \cdot & \cdot & \cdot & \cdot & \cdot \\
 b_5 & b_6 & b_7 & b_8 & \cdot & \cdot & \cdot & \cdot & \cdot & \cdot & \cdot
 \end{pmatrix}$$

ESPRIT (Matlab code):

```

[U,S,V] = svd(D,0);

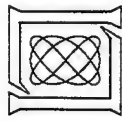
E = U(:,1:dim); % signal subspace
Ex = E(1:size(D,1)/2,:);
Ey = E(size(D,1)/2+1:size(D,1),:);

if 1 % TLS-ESPRIT
    [U,S,V] = svd([Ex,Ey],0);
    i1 = 1:dim; i2 = dim+1:2*dim;
    Psi = -V(i1,i2)/V(i2,i2);
else % LS-ESPRIT
    Psi = Ex\Ey;
end

Phi = eig(Psi); % pole estimates

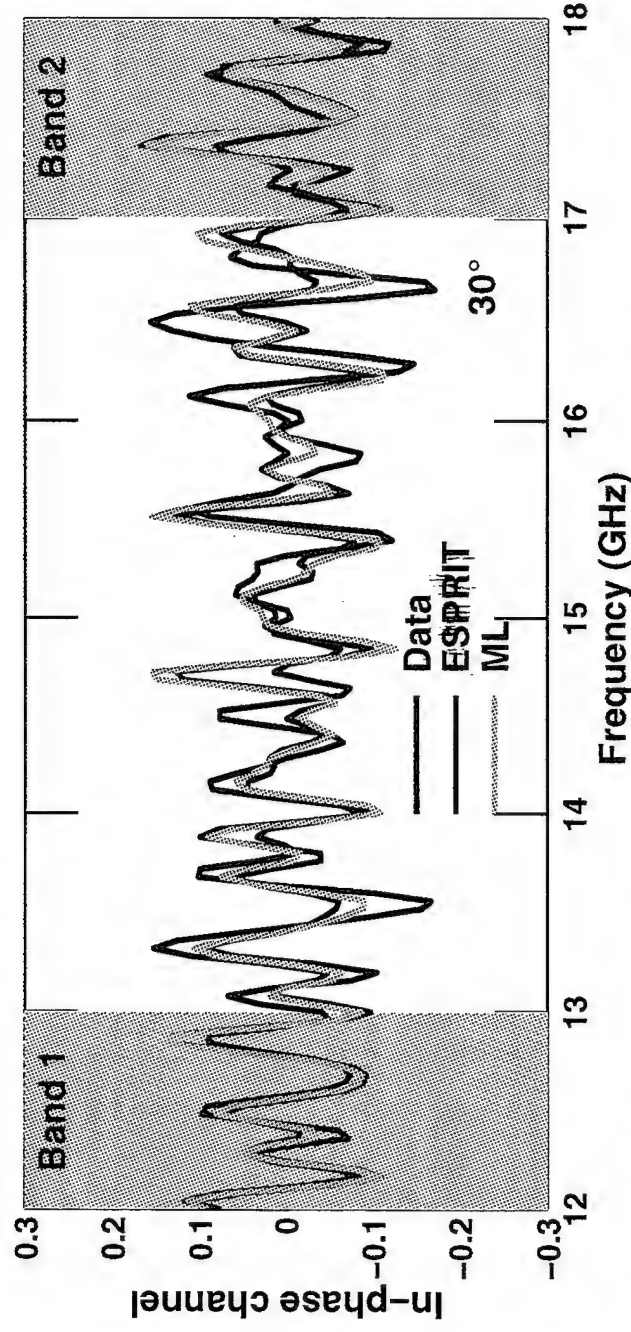
```

ESPRIT is simple and efficient

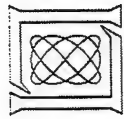


Split-band ESPRIT and ML Performance

Synthetic Bandwidth Using 12–13 and 17–18 GHz

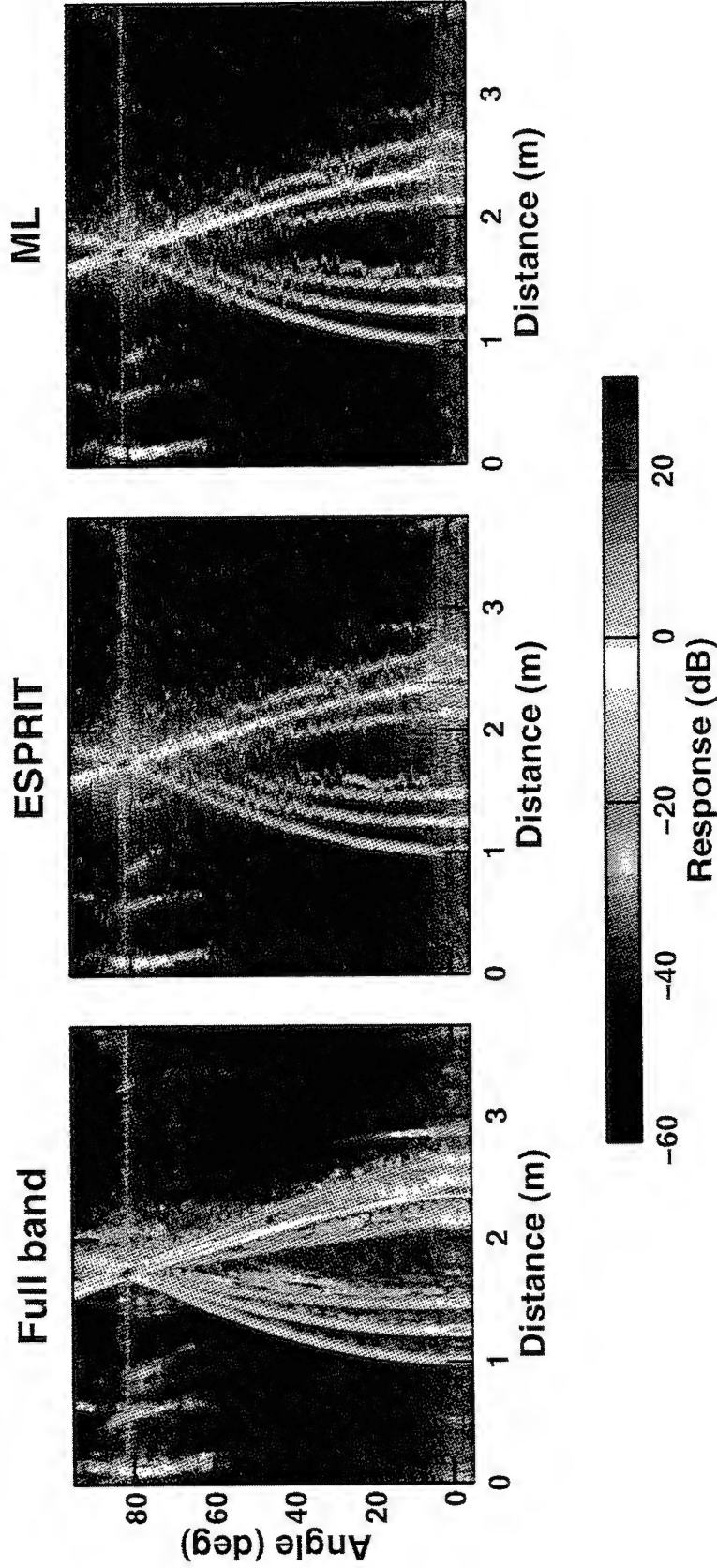


- ESPRIT and ML match data between 12–13 and 17–18 GHz
- Overall trends matched faithfully elsewhere
- ML matches data better than ESPRIT

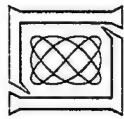


Split-band ESPRIT and ML Performance

Pulse Compressed Data and Synthetic Data (12–13, 17–18 GHz)

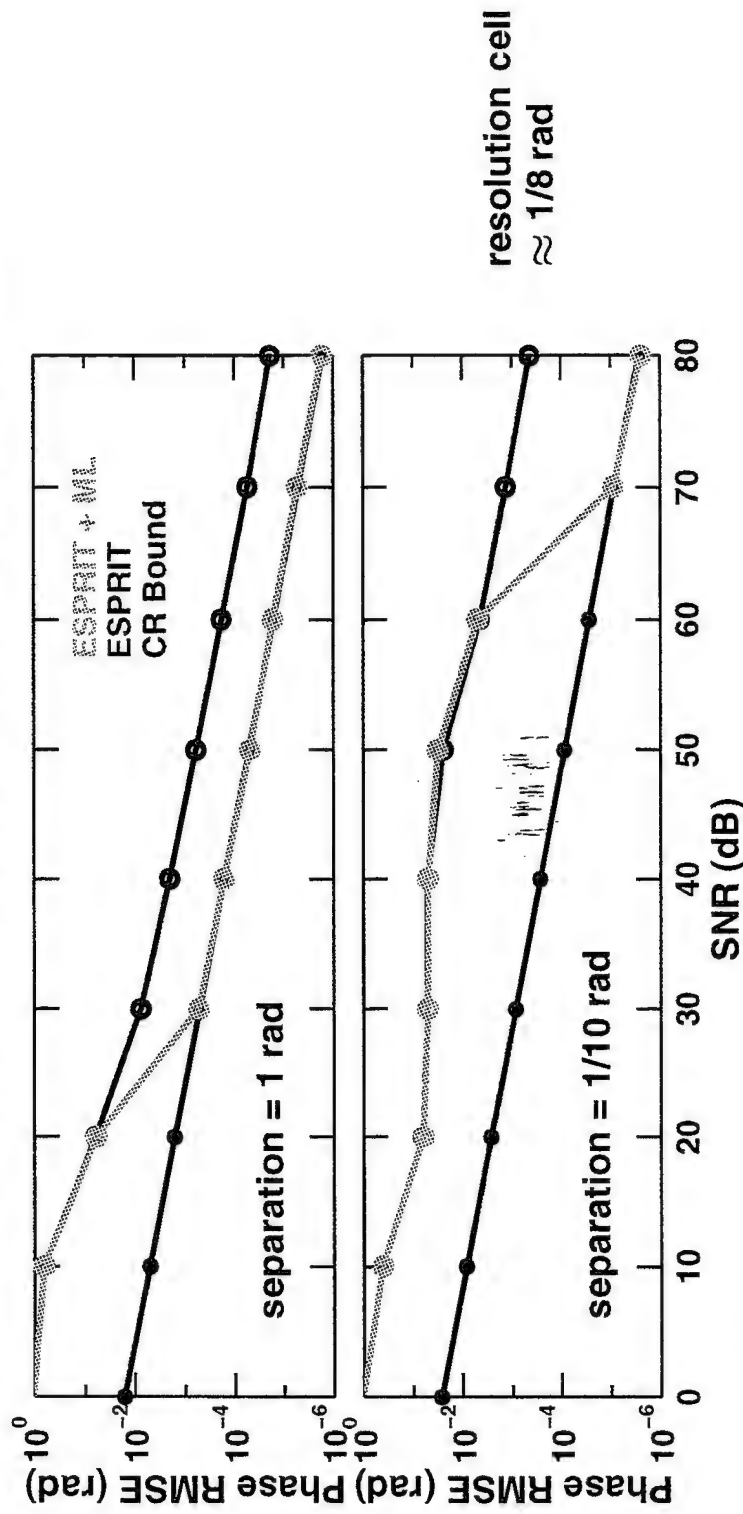


- Small difference between ESPRIT and ML



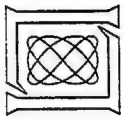
ESPRIT vs ML Accuracy

Monte Carlo Simulation with Two Poles



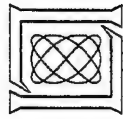
- ESPRIT loss due to window size
- High SNR required for high resolution

Comparable parameters to measurement data



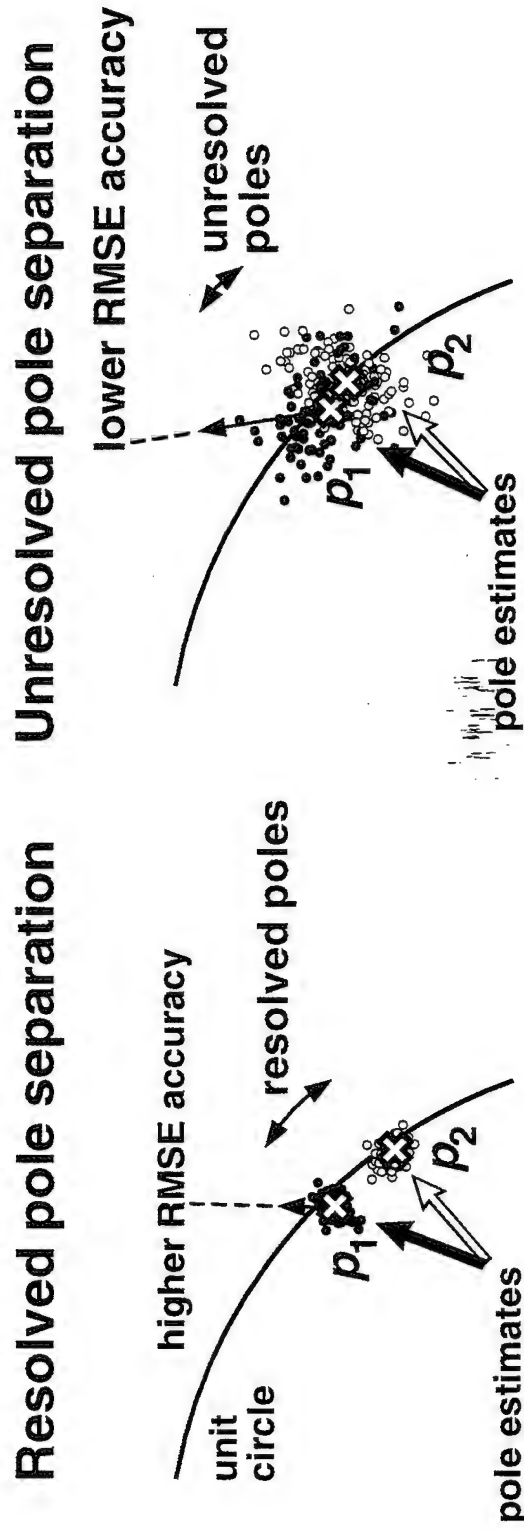
Outline

- Introduction
- Split-band ESPRIT
- Synthetic bandwidth resolution
 - What's the resolution improvement?
- Conclusions



Analysis Method

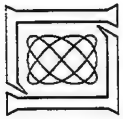
Cramér-Rao Accuracy Bounds



Fact: accuracy $\propto 1/\text{separation}$

Resolution criterion:

RMSE accuracy \leq pole separation



Cramér-Rao Bounds for Multiple Pole Estimation

Unknown Amplitudes / Gaussian Noise

- Bounds for estimating $p_k = r_k e^{j\theta_k}$ ($k = 1, 2, \dots, K$):

$$\text{covariance of estimates} \geq \frac{1}{2}(\Delta - M)^{-1}$$

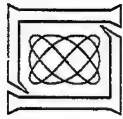
$$\mathbf{p}_i = \begin{bmatrix} p_i^{f_1} \\ p_i^{f_2} \\ \vdots \\ p_i^{f_N} \end{bmatrix}$$

$$- \Delta_{ij} = \text{Re}(\mathbf{a}_i^* \mathbf{a}_j \mathbf{V}_i^H \mathbf{R}^{-1} \mathbf{V}_j), \quad \mathbf{V}_i = \frac{\partial}{\partial(r_i \text{ or } \theta_i)} \begin{pmatrix} p_i^{f_1} \\ p_i^{f_2} \\ \vdots \\ p_i^{f_N} \end{pmatrix}$$

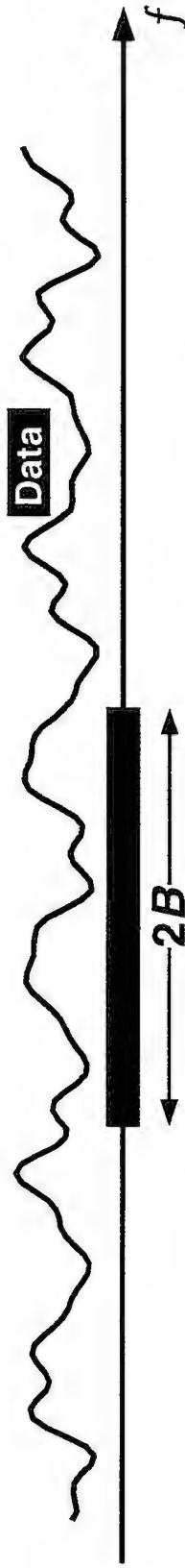
Matrix of “cross difference SNR” terms

$$- M_{ij} = \text{Re}(\Lambda(\mathbf{P}^H \mathbf{R}^{-1} \mathbf{P})^{-1} \Lambda^H), \quad \Lambda(i, :) = \mathbf{a}_i^* \mathbf{V}_i^H \mathbf{R}^{-1} \mathbf{P} \text{ (} i\text{-th row)}$$

Extra loss for estimation of amplitudes



Does Synthetic Bandwidth Improve Resolution?



$$\text{standard resolution} \approx \frac{3.6 \text{ rad}}{\text{SNR}^{1/4} \times B}$$

(B not too small, high SNR)

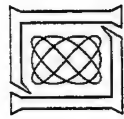
versus



$$\text{synthetic bandwidth resolution} \approx \frac{3.7 \text{ rad}}{\text{SNR}^{1/4} \times M^{1/2} \times B^{1/2}}$$

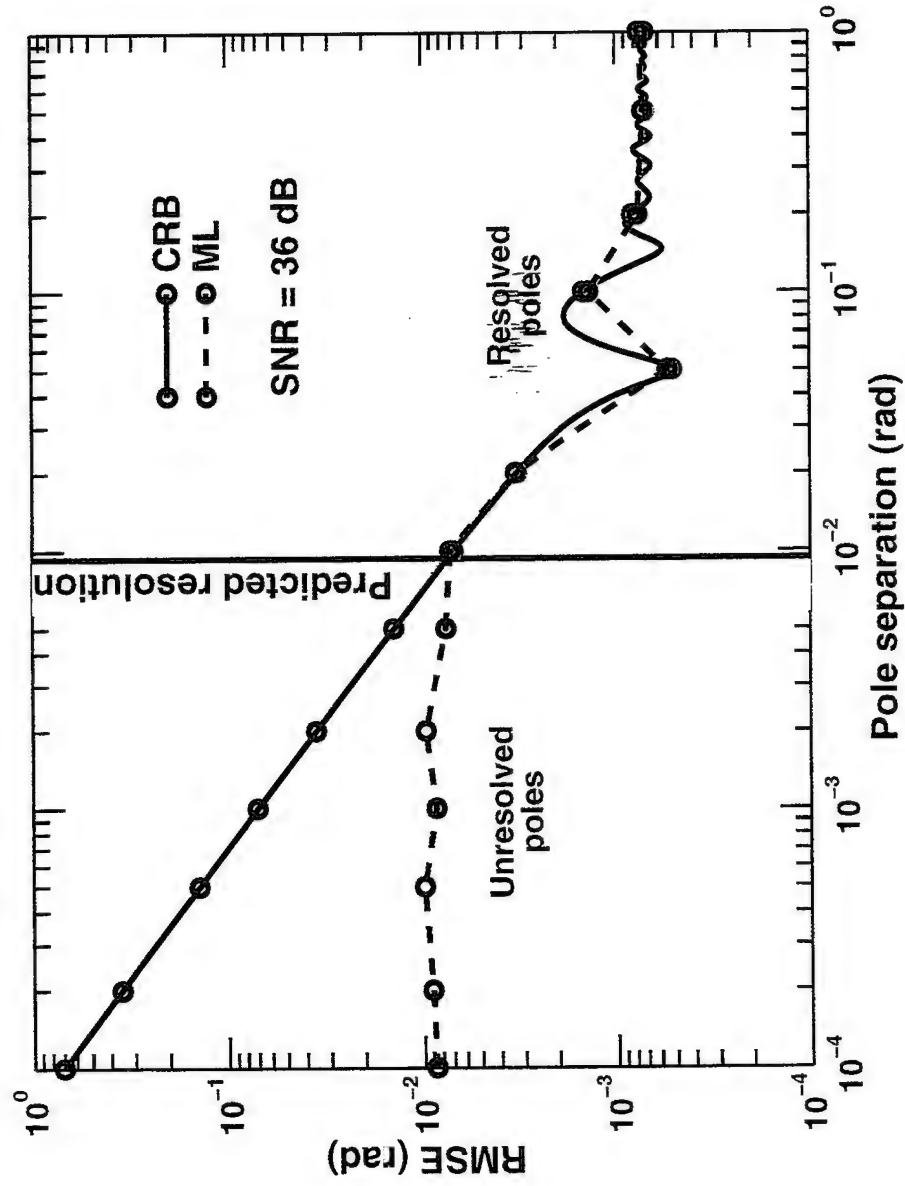
(B not too small, M larger than B , high SNR)

$$\text{synthetic bandwidth resolution improvement} \approx \sqrt{\frac{M}{B}}$$



Predicted vs Measured Resolution

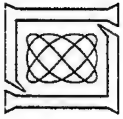
Monte Carlo Simulation with Two Poles



• $B = 25, M = 100$

resolution cell
 $= 2\pi/50 \approx 1/8 \text{ rad}$

Comparable parameters to measurement data



Conclusions

- Split-band ESPRIT algorithm proposed for synthetic bandwidth processing
- ESPRIT comparable to ML performance for real data
- Accuracy and resolution bounds derived for synthetic bandwidth processing
- Synthetic bandwidth processing improves resolution by

$$\text{resolution improvement} = \sqrt{\frac{\text{band gap}}{\text{bandwidth}}}$$

– High SNR required

1998 Adaptive Sensor Array Processing Workshop

Session IV: Sonar 1

Session Chairman
Gregory Duckworth
BBN Technologies

Target Tracking Using Fuzzy Logic Association Techniques

Howard Lazoff

BBN Technologies

7966 Brightmeadow Court

Ellicott City, MD 21043

tel: (410) 796-0312

email: hlazoff@bbn.com

Abstract Tracking a target in the presence of a large amount of clutter is a difficult task. A common technique that is used to accomplish this is the Kalman filter, which predicts the state of the target at the next time period, and chooses the detection that best matches this predicted state. This is called the nearest neighbor approach. However, nearest neighbor association is not always successful, especially when there are other detections from which to choose. One such case where this is true is in a shallow water environment. In this type of application, multistatic active sonar systems are used to try to ensnify quiet targets, and detect the returned signal. Unfortunately, many other returns are received as well, especially from bathymetric features. Therefore, it is critical that the system can distinguish the real target from the clutter, and associate the correct detection with the correct track. Equally important is the ability to suppress the tracks formed by the clutter, while at the same time allowing the true target track to be promoted through the system. To accomplish this, additional information will be used which is not used in the nearest neighbor association technique. The Kalman filter only uses kinematic information on which to base its decision, but this is just a small subset of the information that is available to the tracker. Additionally, there is information about the SNR of each detection, the location of the source and the receiver, the quality of the detection, and the history of detections from this particular location. An effective way of combining all this information to make a decision is to use an association technique which employs fuzzy logic. By using fuzzy logic, the target of interest will be tracked correctly, and at the same time, clutter tracks will be substantially reduced.



TARGET TRACKING USING FUZZY LOGIC
ASSOCIATION TECHNIQUES

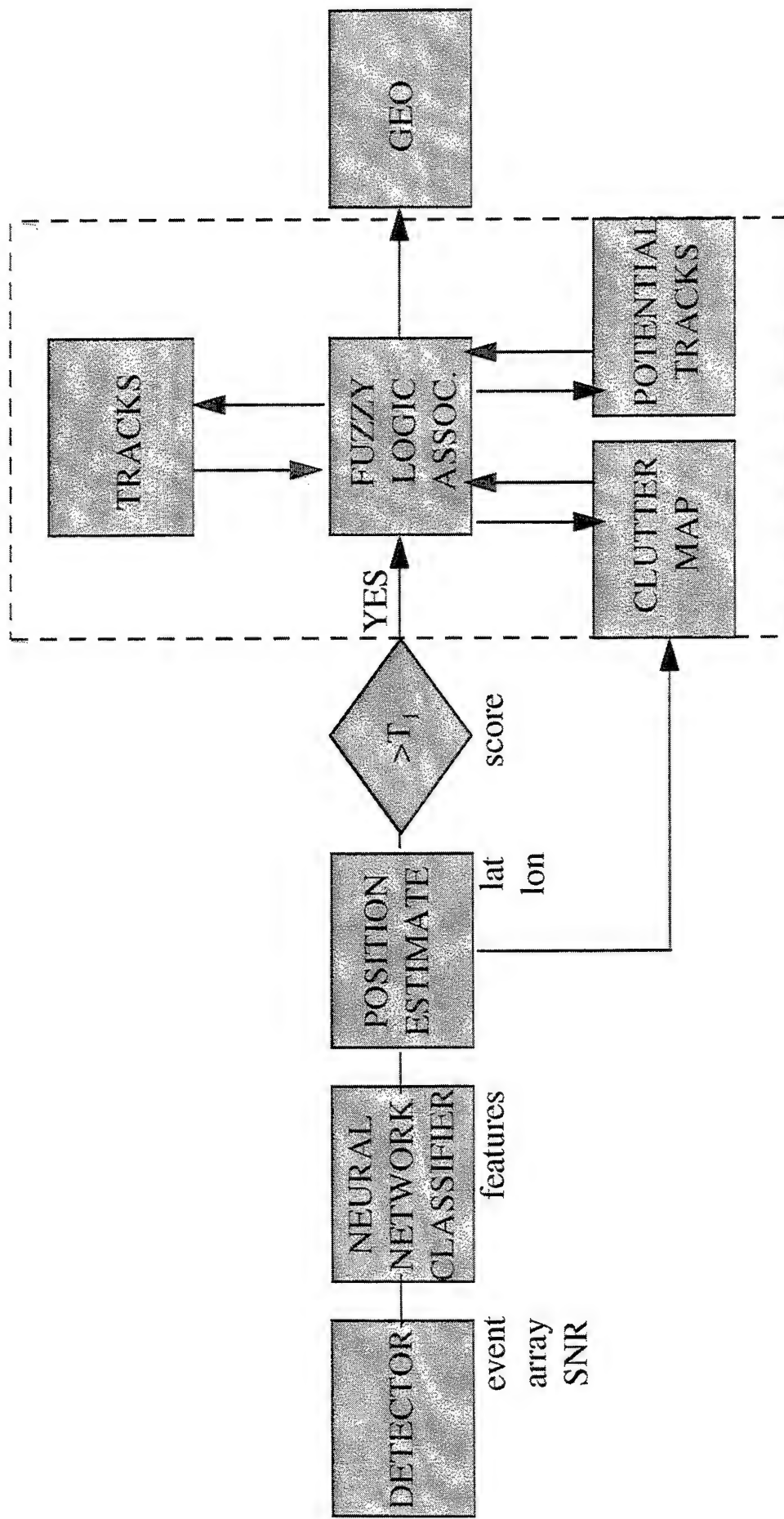
Howard Lazoff
BBN Technologies
March 12, 1998



Significantly reduce the number of false
tracks while continuing to accurately
track the target in a shallow water
environment



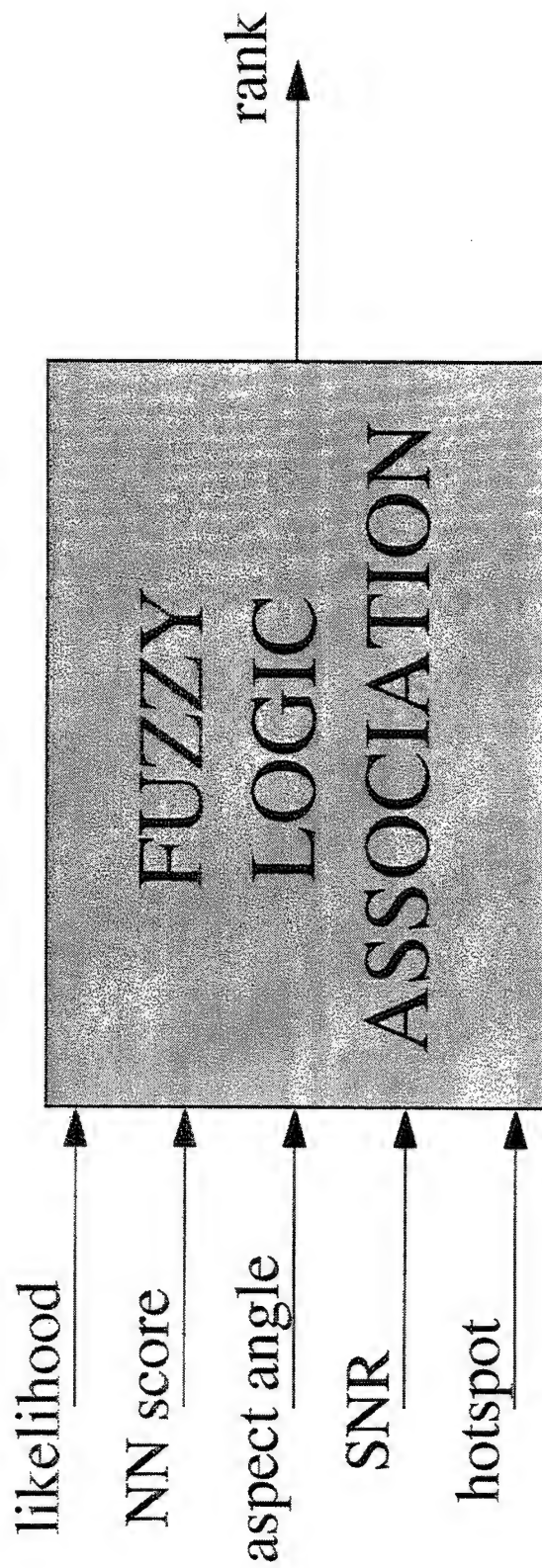
SYSTEM BLOCK DIAGRAM



TRACKER
BBN Technologies



BLACK BOX DIAGRAM

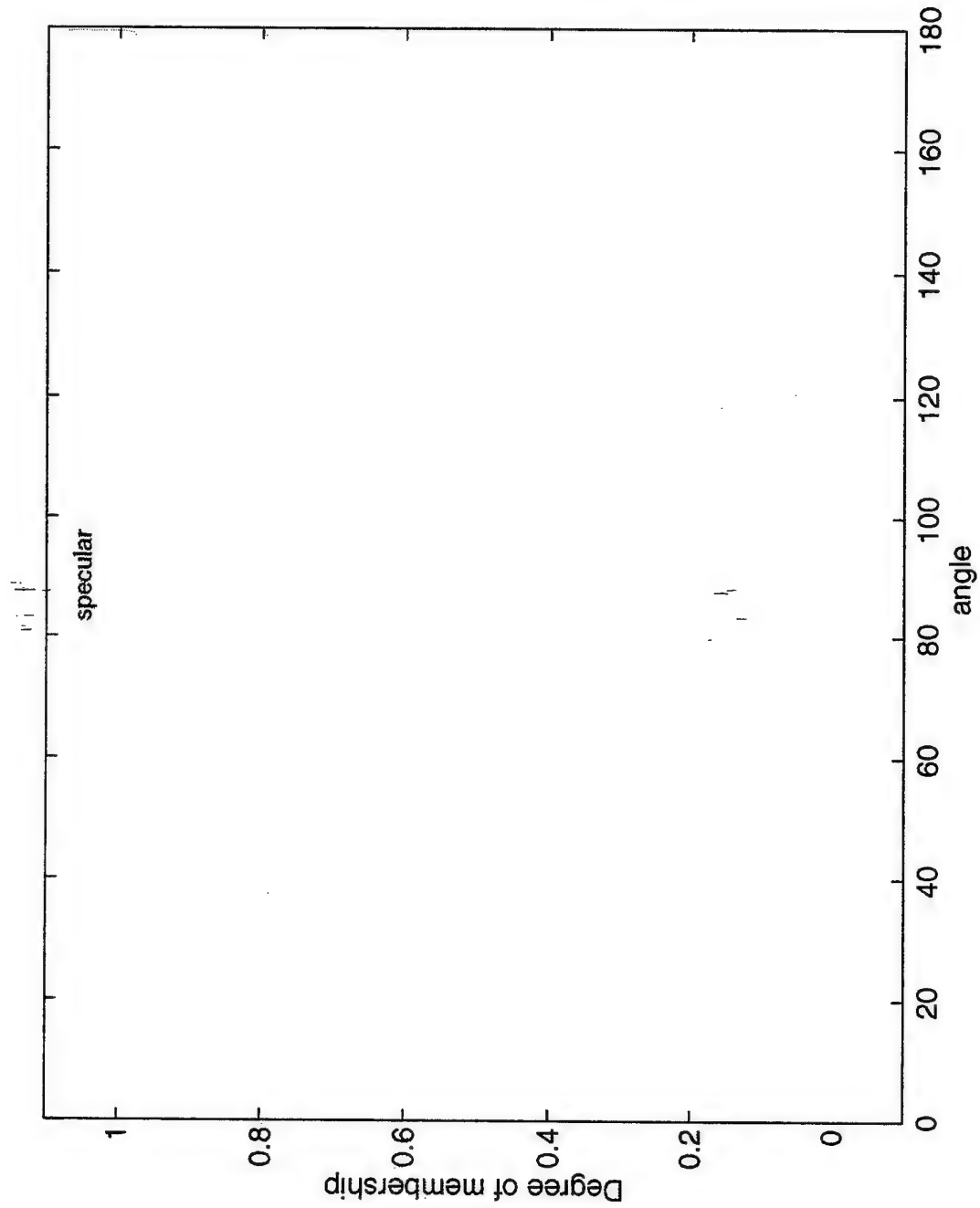




- IF L is likely THEN rank is high
- IF L is unlikely THEN rank is low
- IF L is somewhat likely THEN rank is medium
- IF angle is not specular AND SNR is high THEN rank is low
- IF hotspot is near THEN rank is low
- IF angle is specular THEN rank is high
- IF NN is good AND SNR is high THEN rank is high



ADAPTIVE INTERFERING NETWORKS

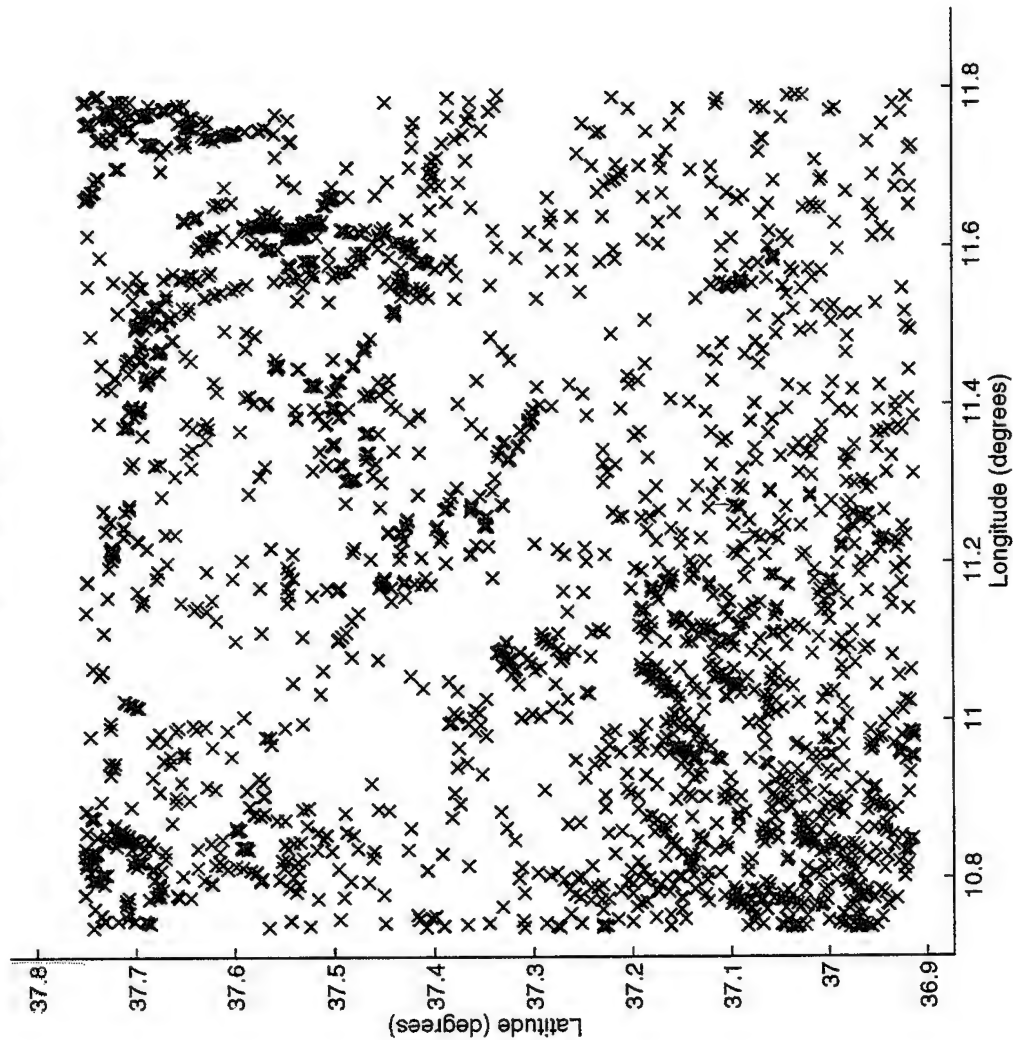




RAW DETECTIONS

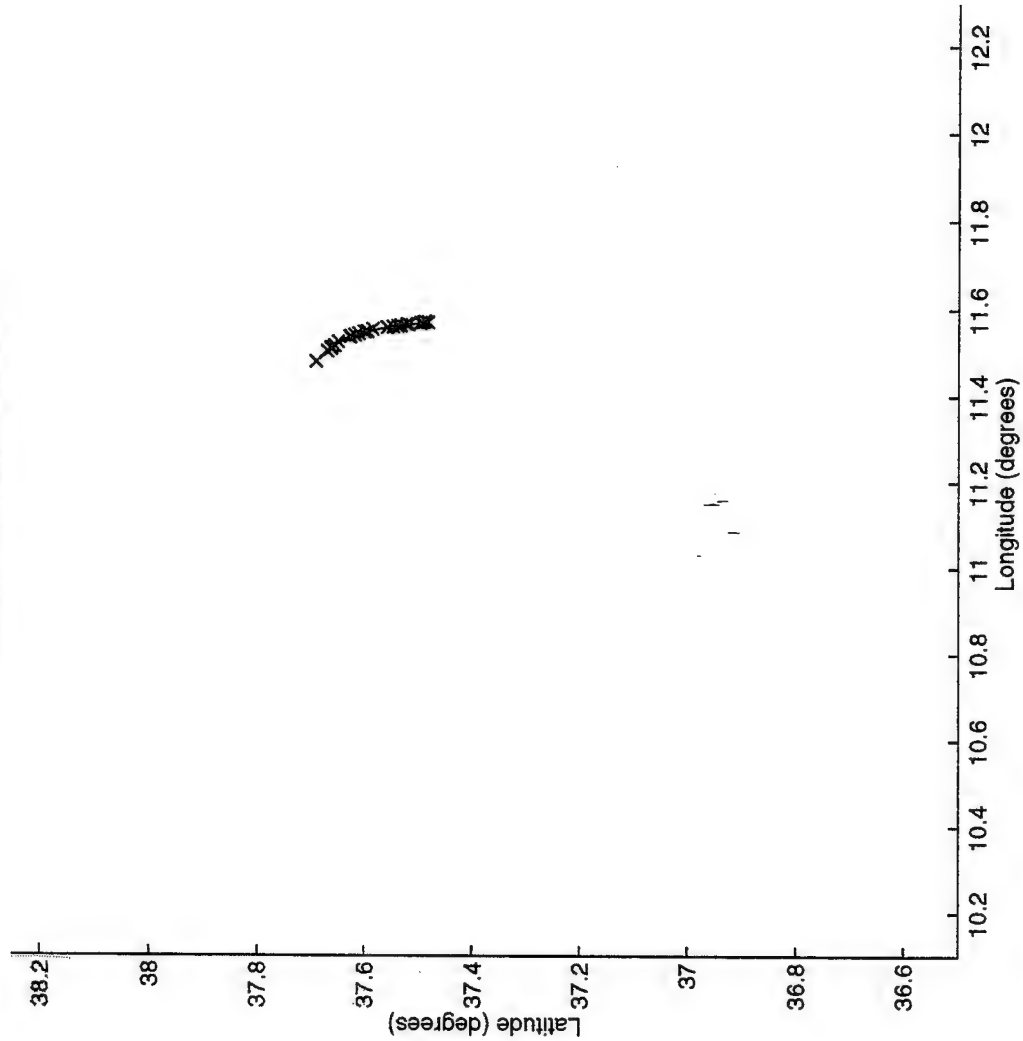


Run 2B Raw Detections





Run 2B Echo Tracks: 3/5, MS= 25

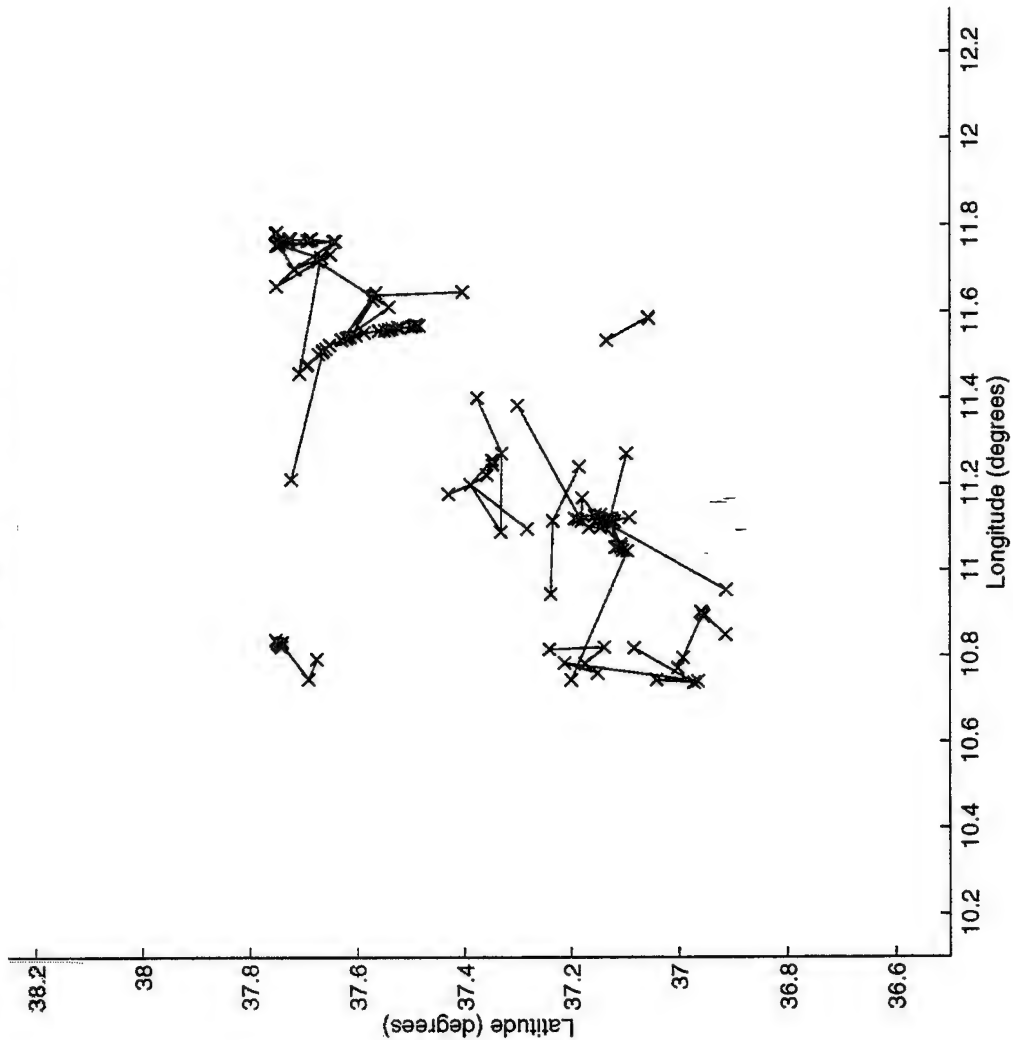




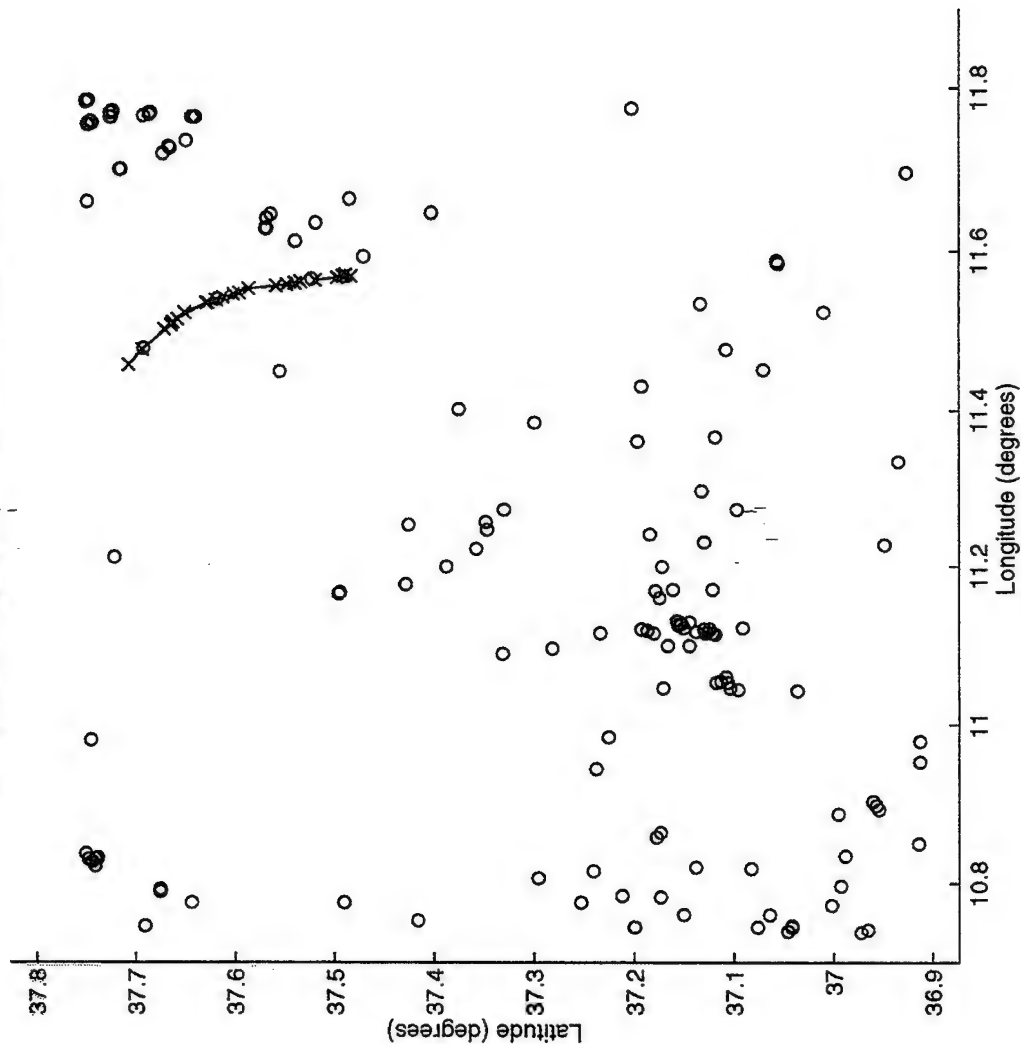
NEAREST NEIGHBOR TRACKS



Run 2B Kalman Filter Tracks: 3/5, MS= 25



Run 2B Fuzzy Logic Tracks And Detections: 3/5, MS= 10



Some Improvements to Dominant Mode Rejection Adaptive Beamforming

Henry Cox

Orincon Corp.

9363 Towne Centre Drive

San Diego, CA 92121

tel: (619) 455-5530

email: hcox@east.orincon.com

Abstract Dominant mode rejection DMR is an approach to adaptive beamforming in which only the large eigenvalues are used. It has the advantage of requiring fewer snapshots due to the reduced degrees of freedom. Starting with DMR a modification is developed to improve robustness to signal mismatch. An approach to controlling the quiescent beam pattern that works for acoustic noise is also presented. The standard approaches fail because source array elements are usually spaced closer than one-half wavelength so that the noise is correlated.

These new approaches are illustrated with examples.



Some Improvements to Dominant Mode Rejection Adaptive Beamforming

**Henry Cox
ORINCON Corporation**

**ASAP Workshop
March 11, 12, 1998**



ADAPTIVE BEAMFORMING CONCERNS

- **REQUIRED NUMBER OF SNAPSHOTS
ESPECIALLY FOR LARGE ARRAYS AND CHANGING ENVIRONMENTS.**
- **MISMATCH BETWEEN SIGNAL MODEL AND SIGNAL
ESPECIALLY IN MULTIPATH PROPAGATION CONDITIONS,
"MATCHED FIELD" SITUATIONS AND DYNAMIC ARRAYS.**
- **SPEED OF ALGORITHM CONVERGENCE
ESPECIALLY IN ACTIVE SYSTEMS AND DYNAMIC SITUATIONS.**
- **COMPUTATIONALLY COMPLEXITY.**
- **PERFORMANCE OF VARIOUS APPROACHES TO OVERCOMING
THE CONCERNS.**



SOME APPROACHES

- **MULTIPLE LINEAR CONSTRAINTS**
- **WHITE NOISE GAIN CONSTRAINT (QUADRATIC)**
- **DIAGONAL LOADING**
- **PENALTY FUNCTION**
- **REDUCED DEGREES OF FREEDOM**
 - **DMR, PCI**
 - **BEAM-BASED**
 - **SIDE LOBE CANCELLERS**
- **FREQUENCY DOMAIN**
- **TIME DOMAIN**
- **RECURSIVE**
- **SAMPLE MATRIX**
- **RANK-ONE UPDATE**



DESIRED PROPERTIES

- SINGLE MATRIX INVERSION - GOOD FOR ALL DIRECTIONS
- ROBUST TO MISMATCH
- ADJUST WHITE NOISE GAIN AS NEEDED ON A BEAM-BY-BEAM BASIS
- REDUCED DEGREES OF FREEDOM
- FEW SNAPSHOTS REQUIRED
- RAPID CONVERGENCE
- REDUCED COMPUTATION



MATRIX APPROXIMATION

$$\mathbf{R} = \underbrace{\sum_{i=1}^k \lambda_i \mathbf{v}_i \mathbf{v}_i^*}_{\text{large}} + \underbrace{\sum_{i=k+1}^N \lambda_i \mathbf{v}_i \mathbf{v}_i^*}_{\text{small}}$$

FIND APPROXIMATION $\tilde{\mathbf{R}}$ SUCH THAT

- (1) $\tilde{\mathbf{R}}$ and \mathbf{R} have identical k -largest eigenvalues and corresponding eigenvectors.
- (2) $\text{trace}(\tilde{\mathbf{R}}) = \text{trace}(\mathbf{R})$, power is preserved
- (3) $\tilde{\mathbf{R}}$ is the best conditioned matrix satisfying (1) and (2).

SOLUTION: HOMOGENIZED APPROXIMATION

$$\tilde{\mathbf{R}} = \alpha \mathbf{I} + \sum_{i=1}^k (\lambda_i - \alpha) \mathbf{v}_i \mathbf{v}_i^* = \alpha \left[\mathbf{I} + \sum_{i=1}^k \left(\frac{\lambda_i - \alpha}{\alpha} \right) \mathbf{v}_i \mathbf{v}_i^* \right]$$

WHERE α IS THE AVERAGE OF THE SMALL EIGENVALUES

$$\alpha = \frac{1}{N - k} \sum_{i=k+1}^N \lambda_i$$



$\tilde{\mathbf{R}}$ PROPERTIES

- REDUCED DEGREES OF FREEDOM
- LESS AVERAGING REQUIRED - RAPID ADAPTATION
- REDUCED COMPUTATION
- EXPLICIT INVERSION FORMULA

$$\tilde{\mathbf{R}}^{-1} = \alpha^{-1} \left[\mathbf{I} - \sum_{i=1}^k \left(\frac{\lambda_i - \alpha}{\lambda_i} \right) \mathbf{v}_i \mathbf{v}_i^* \right] \rightarrow \alpha^{-1} \left[\mathbf{I} - \sum_{i=1}^k \mathbf{v}_i \mathbf{v}_i^* \right] \text{ as } \frac{\alpha}{\lambda_i} \rightarrow 0$$

$$[\tilde{\mathbf{R}} + \epsilon \mathbf{I}]^{-1} = (\alpha + \epsilon)^{-1} \left[\mathbf{I} - \sum_{i=1}^k \left(\frac{\lambda_i - \alpha}{\lambda_i + \epsilon} \right) \mathbf{v}_i \mathbf{v}_i^* \right]$$

- STEERS NULLS IN DIRECTION OF LARGEST EIGENVALUES
- SIMPLY RELATED DMR, EMVDR, PCI, ETC.



MVDR WITH $\tilde{\mathbf{R}}$ (DMR)

$$\mathbf{w} = \frac{\tilde{\mathbf{R}}^{-1} \mathbf{s}}{\mathbf{s}^* \tilde{\mathbf{R}}^{-1} \mathbf{s}} = \frac{\mathbf{s} - \sum_{i=1}^k \beta_i (\mathbf{v}_i^* \mathbf{s}) \mathbf{v}_i}{|\mathbf{s}|^2 - \sum_{i=1}^k \beta_i (\mathbf{v}_i^* \mathbf{s})^2}$$

$$\beta = (\lambda_i - \alpha) / \lambda_i$$

NULLS "EIGEN-BEAMS"

MAINLOBE PROTECTION (THRESHOLD TEST)

$$\mathbf{w} = \frac{\mathbf{s} - \sum_{i=1}^k \delta_i \beta_i (\mathbf{v}_i^* \mathbf{s}) \mathbf{v}_i}{|\mathbf{s}|^2 - \sum_{i=1}^k \delta_i \beta_i |\mathbf{v}_i^* \mathbf{s}|^2}$$

$$\delta_i = \begin{cases} 1 & \text{for } |\mathbf{v}_i^* \mathbf{s}|^2 \leq \gamma |\mathbf{s}|^2 \\ 0 & \text{for } |\mathbf{v}_i^* \mathbf{s}|^2 \geq \gamma |\mathbf{s}|^2 \end{cases}$$

PREVENTS MAINLOBE
NULLING

WHITE NOISE GAIN CONSTRAINT

$$\mathbf{w}^* \mathbf{w} = \frac{|\mathbf{s}|^2 + \sum_{i=1}^k \delta_i (\beta_i^2 - 2\beta_i) |\mathbf{v}_i^* \mathbf{s}|^2}{\left[|\mathbf{s}|^2 - \sum_{i=1}^k \delta_i \beta_i |\mathbf{v}_i^* \mathbf{s}|^2 \right]^2}$$

$$\mathbf{w}^* \mathbf{w} \leq a^2$$

$$\beta_i = (\lambda_i - \alpha) / (\lambda_i + \varepsilon)$$

SCALAR ADJUSTMENT

NOTES: 1) VECTOR MULTIPLES $|\mathbf{s}|^2$ AND $|\mathbf{v}^* \mathbf{s}|^2$ ARE NOT EXTRA
2) ADJUST δ_i AND β_i BEAM-BY-BEAM



MAINLOBE PROTECTION

- CLOSENESS TEST PROTECTS MAINLOBE TO SPECIFIED "J DB DOWN POINT" (E.G. 2.0 DB)
- THIS PERMITS TRADEOFF BETWEEN RESOLUTION AND TOLERANCE TO MISMATCH
- OTHER TRADEOFFS INCLUDE:
 - NUMBER OF BEAMS
 - WHITE NOISE GAIN
 - UNLIKE DIAGONAL LOADING, SIDELOBE NULLING IS NOT IMPAIRED



THRESHOLD TESTS FOR LARGE EIGENVALUES

$$tr(\mathbf{R}) = \sum \lambda_i$$

$$(1) \quad \frac{\lambda_j}{tr(\mathbf{R})} \geq n_1$$

TOTAL POWER

$$(2) \quad \frac{\lambda_j}{tr(\mathbf{R}) - \sum_{i=1}^{j-1} \lambda_i} \geq n_2$$

REMAINING POWER

$$(3) \quad \lambda_j / \lambda_{j+1} \geq n_3$$

PREVIOUS LARGE EIGENVALUE

SELECTION OF THRESHOLDS PROVIDES GREAT FLEXIBILITY IN
ACCOMPLISHING OBJECTIVES



ADAPTIVE BEAMFORMING

ABF GAINS COME FROM:

- A) EXPLOITING SMALL EIGENVALUES (NOISE VALLEY)
 - SUPERGAIN
 - HIGHLY SENSITIVE
 - LONG AVERAGING TIMES REQUIRED
- B) NULLING NOISE PEAKS (LARGE EIGENVALUES)
 - EASY TO ESTIMATE
 - DMR APPLIES

CAN WE COMBINE THESE WITHOUT BRUTE FORCE?

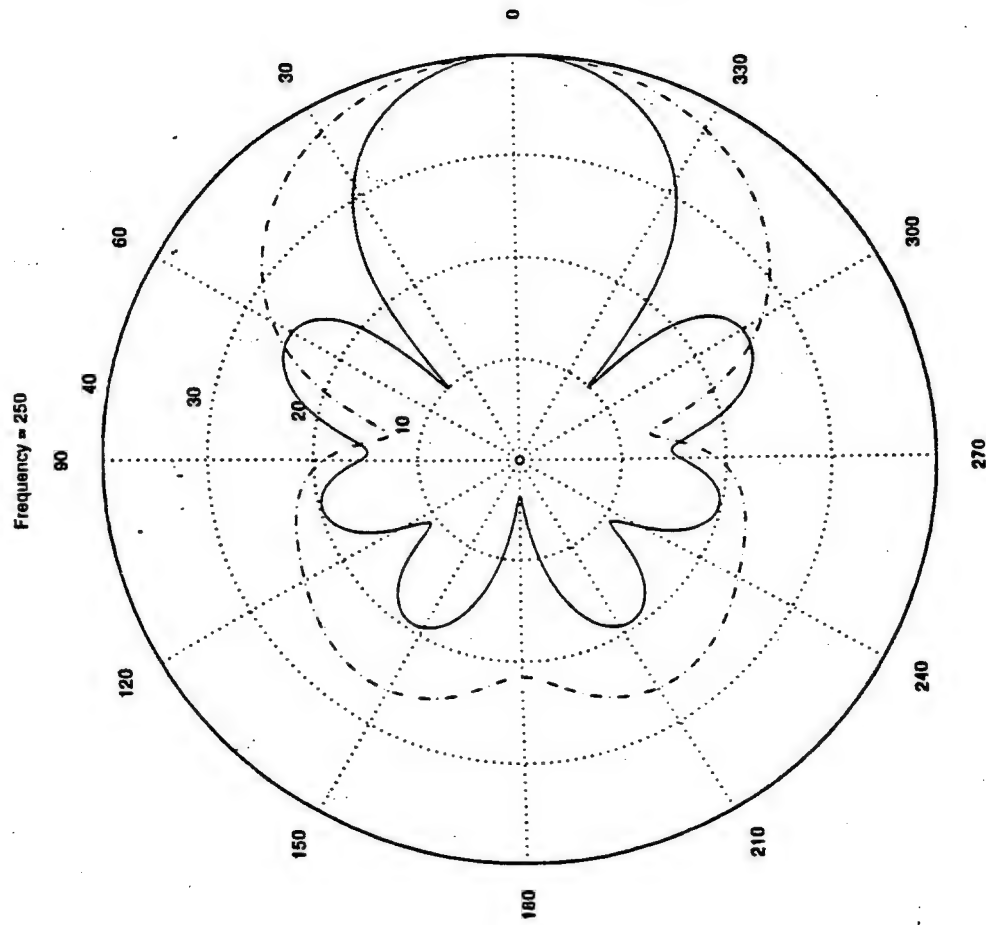
- YES:
 1. MODEL-BASED WHITENING OR SLOWLY ADAPTING
 2. DMR WITH THRESHOLD (RAPID ADAPTATION)



ABF

BEAM PATTERN COMPARISON

250 HZ



Array Gain = 12.7439 - Iso Opt
Array Gain = 7.4725 - Conventional



QUIESCENT PATTERN CONTROL

$$W = \frac{s - \sum_{i=1}^k \delta_i \beta_i (\mathbf{v}_i^* \mathbf{s}) \mathbf{v}_i}{|\mathbf{s}|^2 - \sum_{i=1}^k \delta_i \beta_i |\mathbf{v}_i^* \mathbf{s}|^2}$$

- USE DESIRED QUIESCENT COMPLEX SHADING WEIGHTS FOR \mathbf{s} .
- SET LARGENESS THRESHOLDS HIGH ENOUGH TO NULL ONLY STRONG INTERFERERS.
- SET CLOSENESS THRESHOLD γ CONSISTENT WITH BEAM PATTERN
- AND SHADING WEIGHT MISMATCH.

OR

- APPLY DMR AT BEAM OUTPUTS USING HIGH ENOUGH LARGENESS THRESHOLDS.



MULTI-RATE

TO OBTAIN GOOD ISOTROPIC GAIN WITH CLOSELY SPACED ELEMENTS OR GOOD BEAM PATTERNS

(1) APPLY PRE-COMPUTED (MODEL-BASED) SHADING WEIGHTS OR WHITENING.

- GIVES DESIRED RESPONSE IN ABSENCE OF STRONG INTERFERERS

(2) APPLY DMR WITH HIGH LARGENESS THRESHOLD TO BEAMS OR PRE-WHITENED ELEMENTS

- MAINTAINS DESIRED PATTERN UNLESS STRONG INTERFERENCE IS PRESENT, EVEN FOR NON-WHITE SPATIAL CORRELATION
 - PROTECTS MAINLOBE, RAPID CONVERGENCE
- (1A) REPLACE (1) WITH SLOWLY ADAPTING WEIGHTS
- MULTI-RATE



CONCLUSION

- DMR HAS DESIRABLE PROPERTIES: RAPID CONVERGENCE, FEW SNAPSHOTS REQUIRED.
- DMR CAN BE VIEWED AS COVARIANCE MATRIX APPROXIMATION USED IN MVDR
- SIMPLY SIDE CALCULATIONS PERMIT BEAM-BY-BEAM CONTROL OF WHITE NOISE GAIN AND MAINLOBE PROTECTION
- THRESHOLDS ON EIGENVALUE SIZE λ_i AND EIGENVECTOR DIRECTION $|\mathbf{v}_i^* \mathbf{s}|^2$ PROVIDE EXTRA CONTROL PARAMETERS WITH MULTIPLE USES INCLUDING:
 - MAINLOBE PROTECTION
 - QUIESCENT PATTERN CONTROL
 - MULTI-RATE ADAPTATION

Rapidly Adaptive Matched Field Processing for Nonstationary Environments

James Ward

MIT Lincoln Laboratory
244 Wood Street, Room J-149J
Lexington, MA 02173-9108
tel: (781) 981-0617
email: jward@ll.mit.edu

Arthur B. Baggeroer

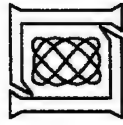
Depts. of Ocean Engineering and EECS
Massachusetts Institute of Technology
77 Massachusetts Avenue, Room 5-206A
Cambridge, MA 02139-4307
email: abb@arctic.mit.edu

Abstract Two of the most important concerns with matched field processing are the sensitivity to mismatch and the performance in the strong interference scenarios characteristic of shipping noise, and in active systems, reverberation. Furthermore, source/receiver motion limits the time that a target remains within a single resolution cell, and therefore the number of snapshots in which the field is stationary. The snapshot problem is compounded by the presence of the target signal in the sample covariance matrix, and its steering vector may not be known exactly due to uncertain propagation parameters.

In this talk we investigate adaptive matched field processing architectures for typical shallow water environments. The objective was to provide a fair comparison of different DOF reduction strategies based upon an SVD of the sample covariance matrix. Approaches considered include the well known principal components (PC) method, the recently published cross-spectral metric (CS), and other heuristic approaches that incorporate mismatch sensitivity directly in the DOF selection process. Comparisons with the old standby (but less analytically pleasing) white noise gain constrained MVDR (i.e. diagonal loading) are also performed. The trade-off is not a simple one that results in a single universally superior approach; it is shown how the relative performance results depend on the interference DOF (which can be large with extended surface interference), the adaptive DOF, the sample support, the signal strength, and the mismatch level. The CS approach, although optimum in a known covariance sense, is shown to offer benefits only when the adaptive DOF is less than the interference DOF and there is plenty of sample support. In many practical cases, principal components and other selection metrics can offer better performance because they are influenced less by the noise eigenvalue fluctuations. In very low sample support situations and where mismatch is present, the performance of the white noise gain constraint approach compares quite favorably with reduced DOF approaches. We hope to have additional results for broadband MFP scenarios by the time of the workshop.

[1] Goldstein and Reed, "Theory of Partially Adaptive Radar," October 1997 AES.

[2] H. Cox, "Further Results in Dominant Mode Rejection," IEEE Underwater Acoustics Signal Processing Workshop, October 8, 1997.



Rapidly Adaptive Matched Field Processing for Nonstationary Environments

James Ward¹
MIT Lincoln Laboratory

Arthur B. Baggeroer²

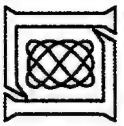
MIT
Departments of Ocean and Electrical
Engineering

Lisa Zurk¹
MIT Lincoln Laboratory

1998 Adaptive Sensor Array Processing Workshop
12 March 1998

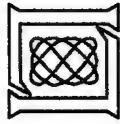
¹Opinions, interpretations, conclusions,
and recommendations are those of the
authors and are not necessarily endorsed
by the United States Air Force. This work
was sponsored by DARPA under Air Force
Contract F19628-95-C-0002

²Supported by ONR,
Code 321, #N00014-95-1-0362

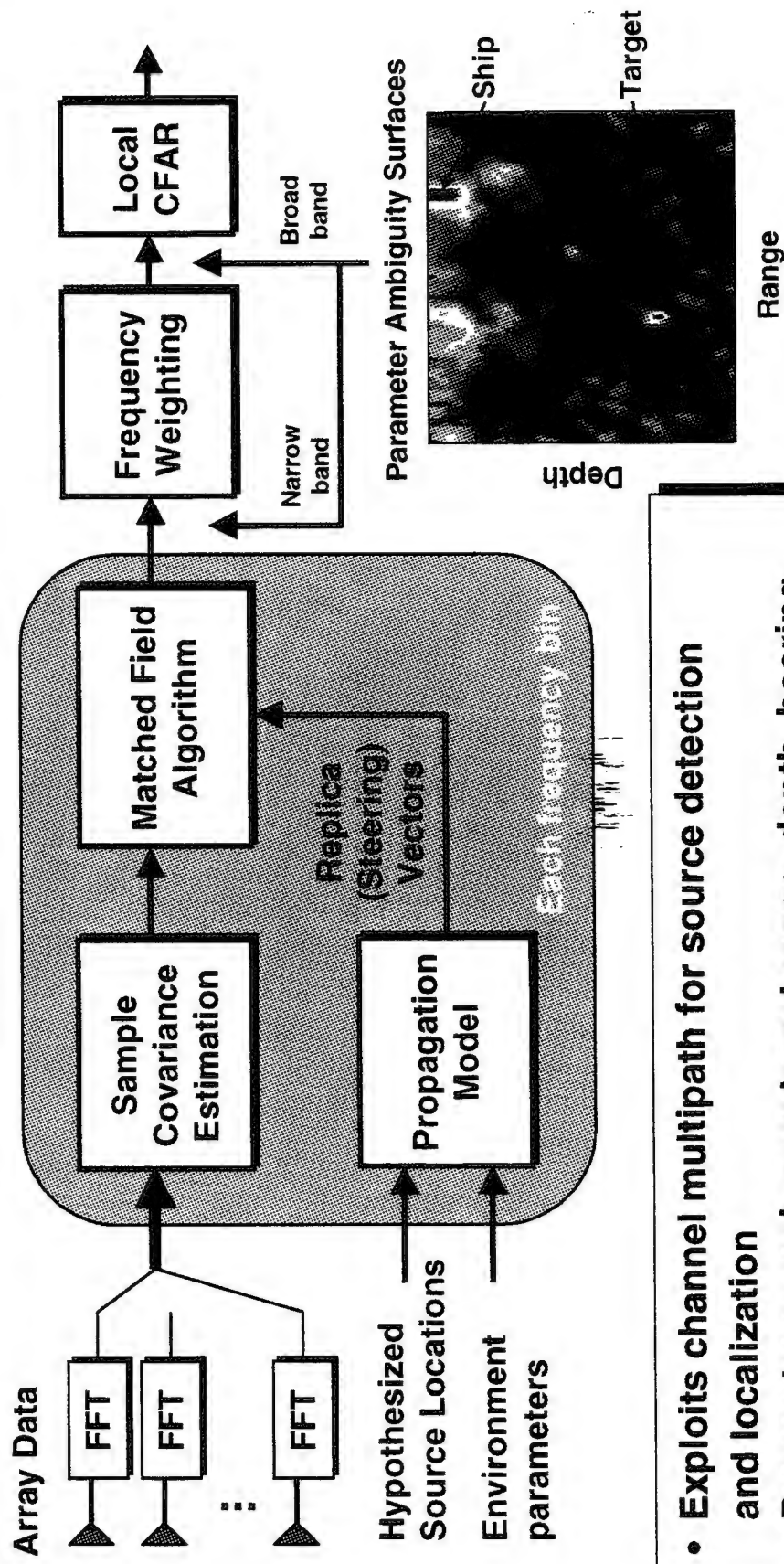


Outline

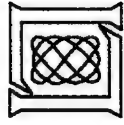
- Introduction
- Reduced Rank MFP Architectures
- Simulation Results
- Summary and Conclusions



Matched Field Processing (MFP)



- Exploits channel multipath for source detection and localization
- Parameter search over target range, depth, bearing
- Adaptive MFP reduces sidelobes of conventional MFP and rejects interference
- Main issue is robustness to environmental uncertainty



Motivation

Problem: Adaptive matched field processing when there are few snapshots for the sample covariance matrix

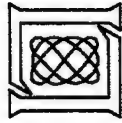
- Arrays with large numbers of sensors
- Transient, nonstationary noise fields
- Active systems (reverberation)

Solution: Reduced degree-of-freedom (DOF) adaptive processing

- Lessens required observation time
- Lessens computational complexity

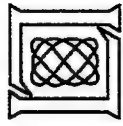
Goal: Comparative analysis of several reduced DOF architectures for the AMFP problem

- What's the best way to reduce DOF?



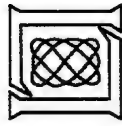
AMFP vs. Radar STAP

Matched Field Processing	Radar STAP
Passive / bistatic	Active / Monostatic
Target signal is continuous and always present in sample covariance matrix	Target-free range gates used to form background interference sample covariance matrix
Potentially large fractional bandwidths; frequency averaging used to lessen AMS sidelobes	Relatively narrowband, fractional bandwidths $< 1\%$
More difficult propagation Sophisticated models necessary for steering vectors; no SL control methods	Relatively simple propagation Easily implemented steering vectors Well known sidelobe control methods
Local CFAR across ambiguity surface for detection	CFAR across range in target filter for detection



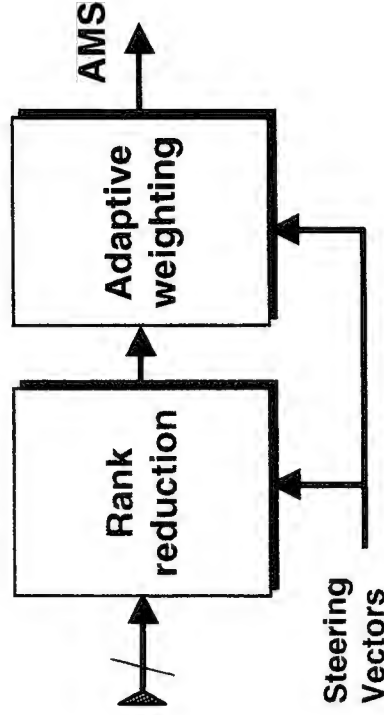
Outline

- Introduction
- Reduced Rank AMFP Architectures
- Simulation Results
- Summary and Conclusions



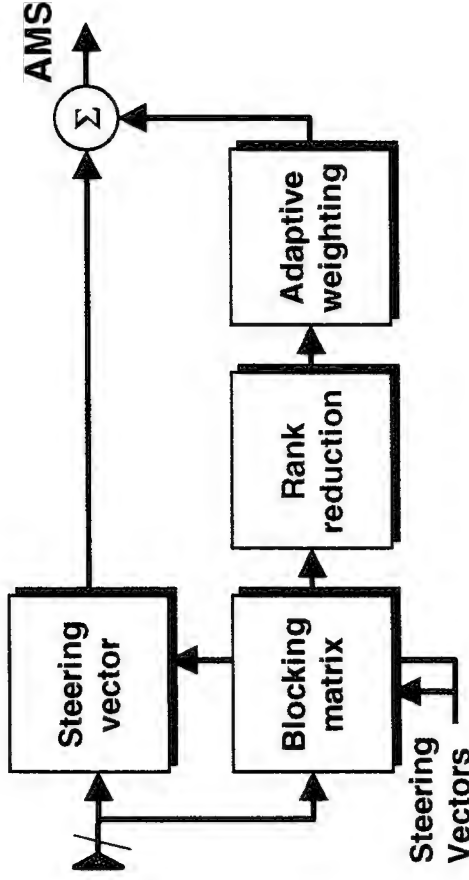
Two Adaptive MFP Architectures

Direct Form (DF)



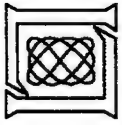
- Single covariance matrix inverted
- Constrain weights to preserve gain in steering vector 'direction'

Generalized Sidelobe Canceller (GSC)



- Blocking matrix removes signal of interest from adaptive weighting (in theory)
- Unconstrained adaptation in lower branch
- Requires separate blocking matrix and separate matrix inversion for every signal hypothesis

- Full rank performance of the two approaches are equal
- How do reduced rank approaches compare, for same DOF?



Full Rank MFP Algorithms

Ambiguity Surface	Array Sample Covariance Matrix	Weight Normalization
-------------------	--------------------------------	----------------------

$p(\bar{\theta}) = \bar{w}^H(\bar{\theta}) \hat{R} \bar{w}(\bar{\theta})$	$\hat{R} = \frac{1}{K} \sum_{k=1}^K \bar{x}_k \bar{x}_k^H = E \Lambda E^H$	$\bar{w}^H(\bar{\theta}) \bar{v}(\bar{\theta}) = 1$
---	--	---

- **Conventional MFP (CMFP)**

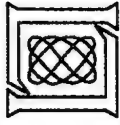
$$\bar{w}(\bar{\theta}) = \frac{\bar{v}(\bar{\theta})}{\bar{v}^H(\bar{\theta}) \bar{v}(\bar{\theta})}$$

- High sidelobes cause degraded performance in interference environments, potential for large location errors

- **MVDR with diagonal loading (FR-DL)**

$$\bar{w}(\bar{\theta}) = \frac{\hat{R}_L^{-1} \bar{v}(\bar{\theta})}{\bar{v}^H(\bar{\theta}) \hat{R}_L^{-1} \bar{v}(\bar{\theta})} \quad \hat{R}_L = \hat{R} + \sigma_L^2(\bar{\theta}) I$$

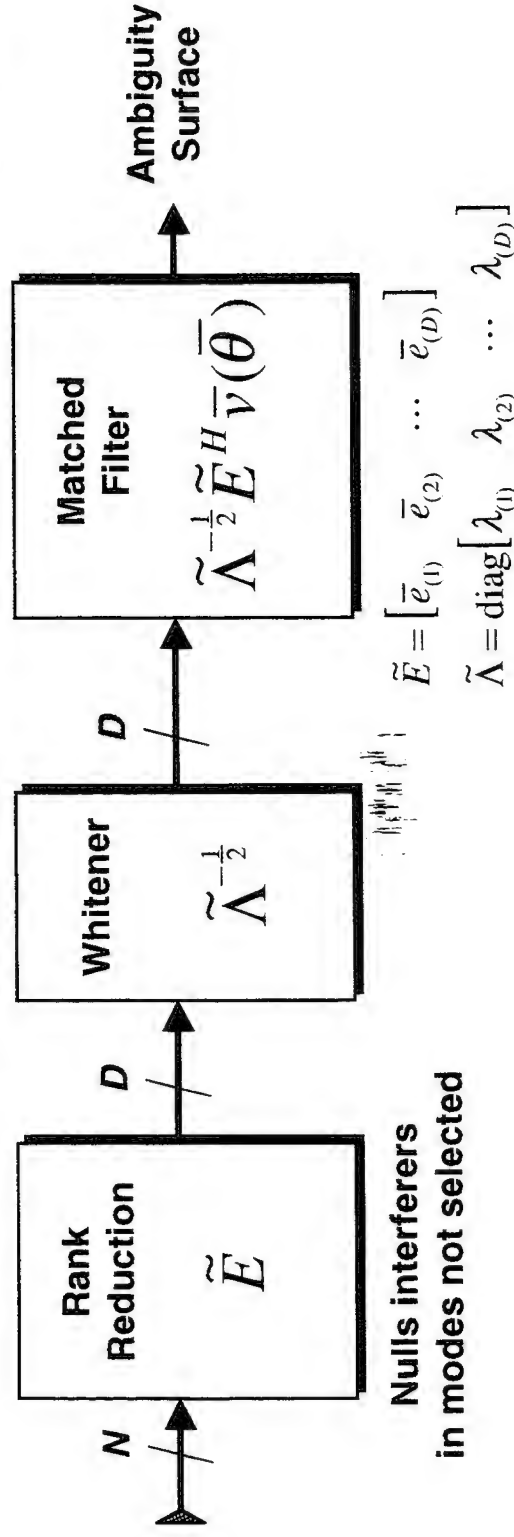
- Adaptation to environment mitigates high sidelobes of CMFP
- Loading provides robustness to mismatch and helps convergence with limited sample support



Direct Form Reduced Rank AMFP

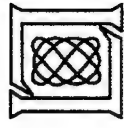
- Choose modes that maximize coherence with steering vector (DF-EC)¹

$$\{\bar{e}_{(n)}, \lambda_{(n)}\} = \max \frac{|\bar{v}^H \bar{e}_n|^2}{\lambda_n} \Rightarrow \bar{w}(\bar{\theta}) = \frac{\tilde{E} \tilde{\Lambda}^{-1} \tilde{E}^H \bar{v}(\bar{\theta})}{\bar{v}^H(\bar{\theta}) \tilde{E} \tilde{\Lambda}^{-1} \tilde{E}^H \bar{v}(\bar{\theta})}$$

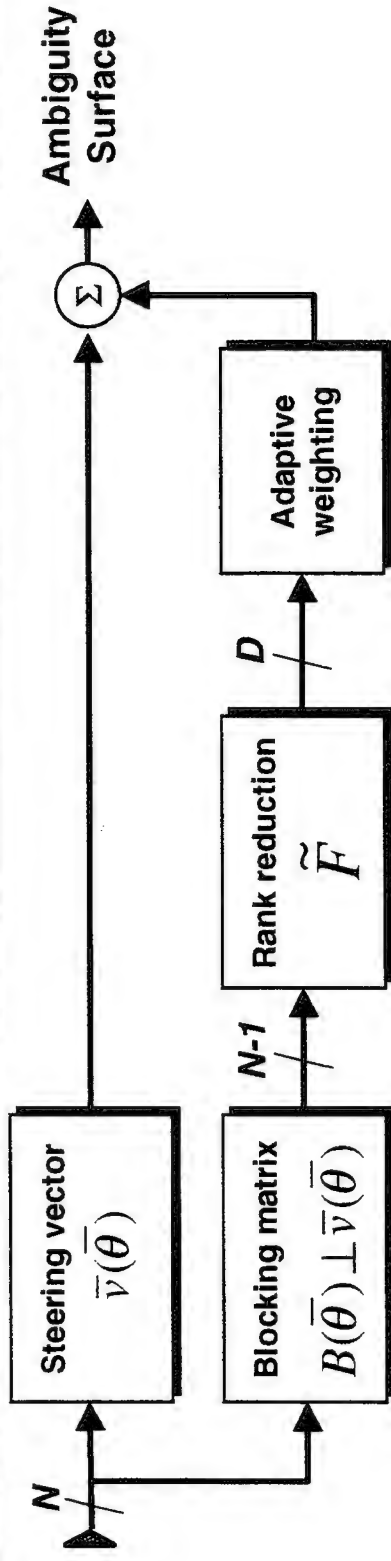


- Minimizes output power over all D -dimensional eigenvector bases
- Provides inherent robustness to mismatch

¹Lee, Mikhalevsky, et.al. (1993); Cox (1997); others?



GSC Reduced Rank AMFP Algorithms



- Rank reduction based on eigenanalysis after blocking matrix

$$\hat{R}_a = B^H \hat{R} B = F \Gamma F^H \Rightarrow \tilde{F} = [\tilde{f}_{(1)} \quad \tilde{f}_{(2)} \quad \dots \quad \tilde{f}_{(D)}]$$

- Cross-spectral metric¹:

$$\tilde{f}_{(n)} \Leftrightarrow \max_n \frac{|\tilde{r}^H \tilde{f}_n|^2}{\gamma_n}$$

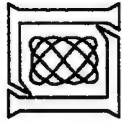
$$\tilde{r} = B^H \hat{R} \bar{v}$$

- Choose modes that maximally interfere with conventional MFP steering vector
- Minimizes output power for fixed DOF and eigenvector basis
- Principal components²:

$$\tilde{f}_{(n)} \Leftrightarrow \max \gamma_n$$

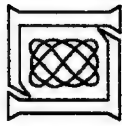
¹Goldstein, Reed (1997); others?

²Tufts, Kirshteins (1994), many others

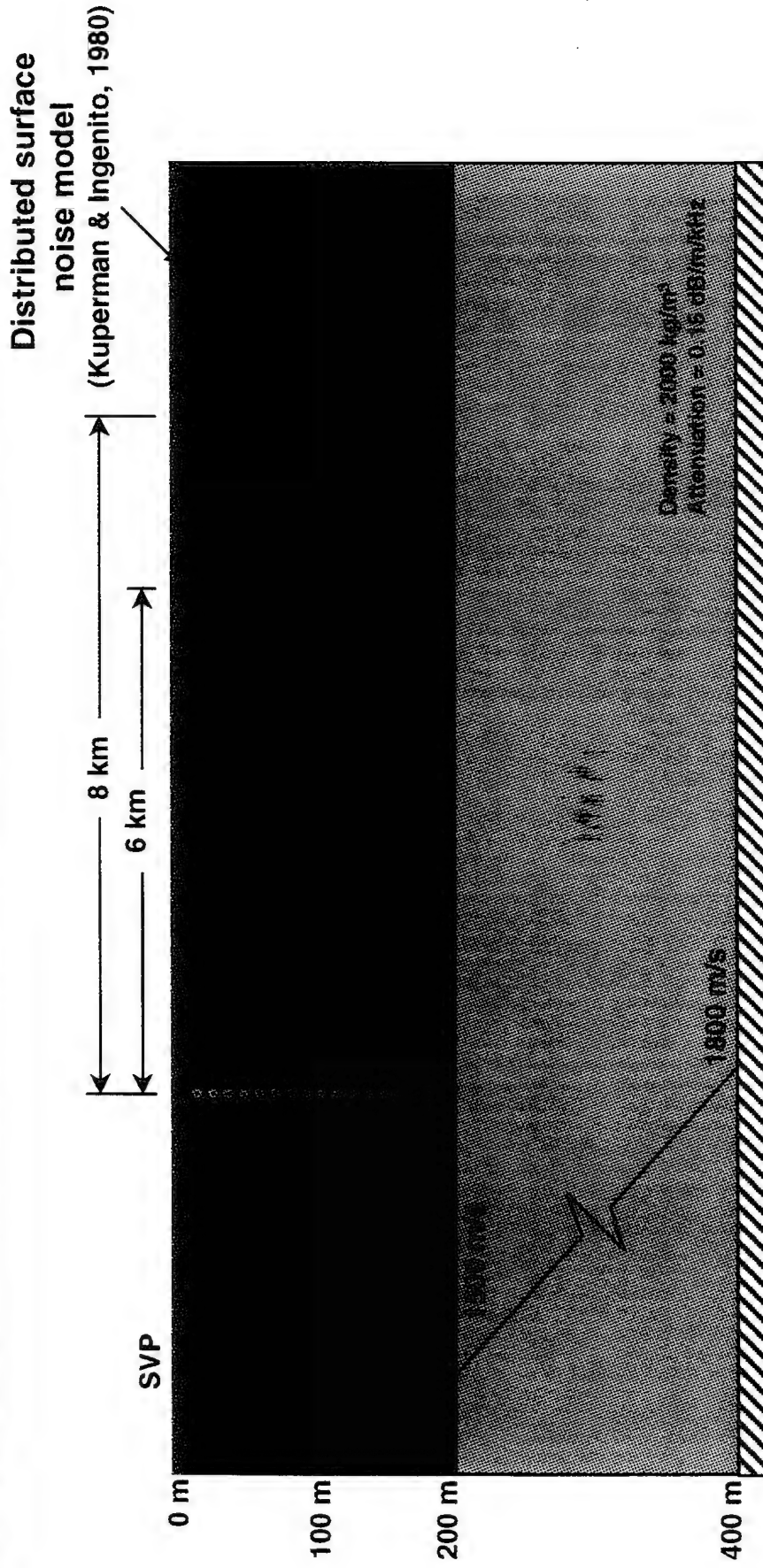


Outline

- Introduction
- Reduced Rank MFP Architectures
- ➔ Simulation Results
- Summary and Conclusions

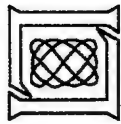


Example Shallow Water Environment

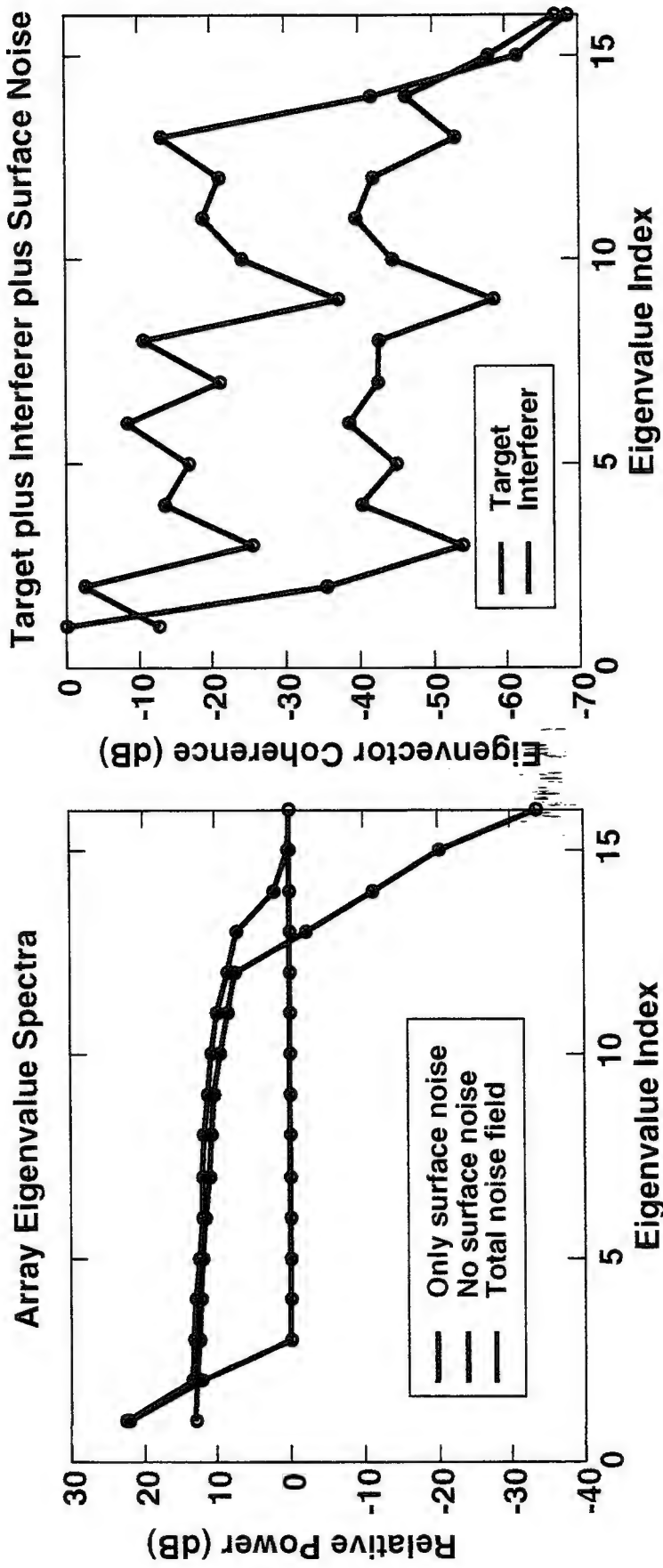


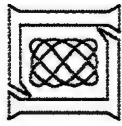
Frequency = 250 Hz

Case 1: Target + surface noise (no ship interferer)
Case 2: Target + surface noise + ship interferer

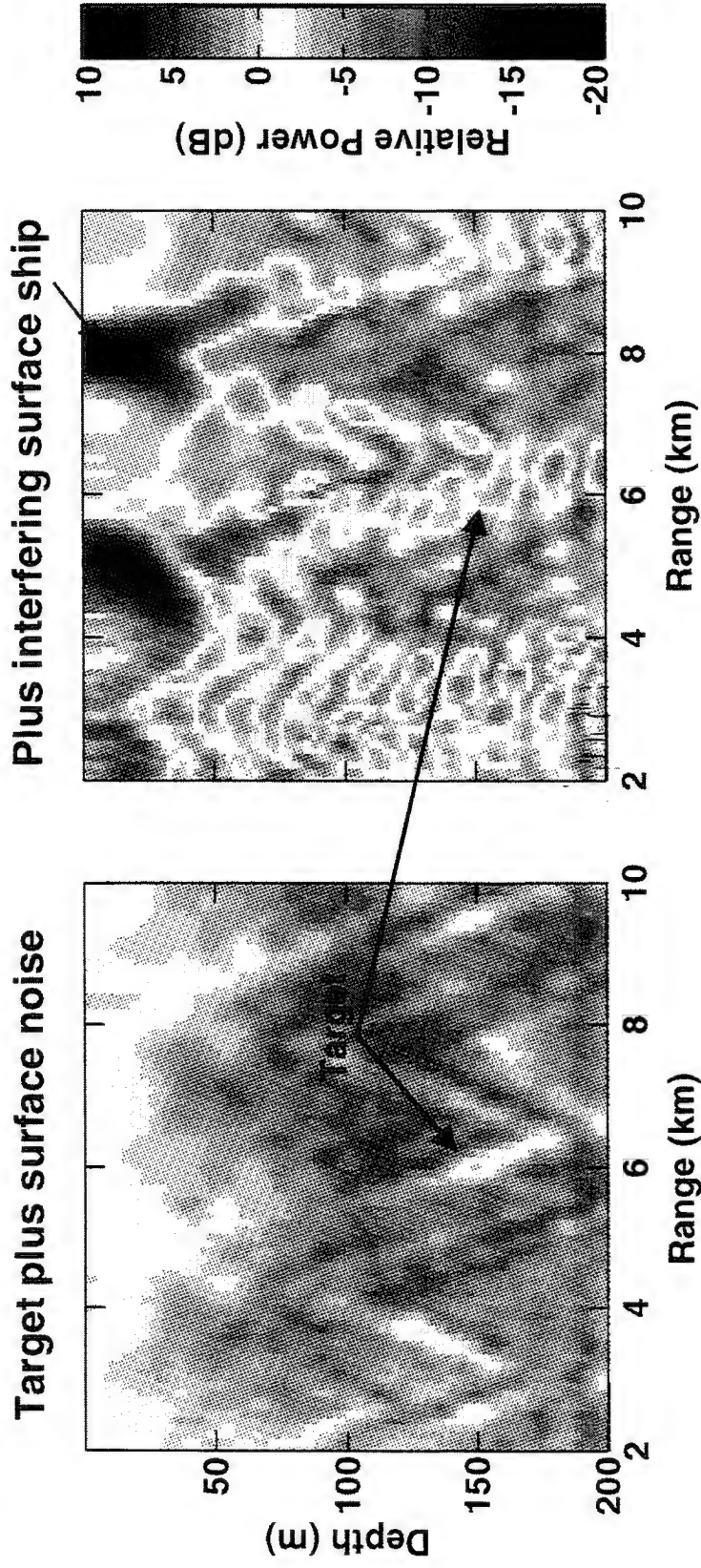


Direct Form Eigenvalue Spectra





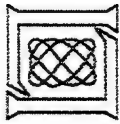
Conventional MFP Examples



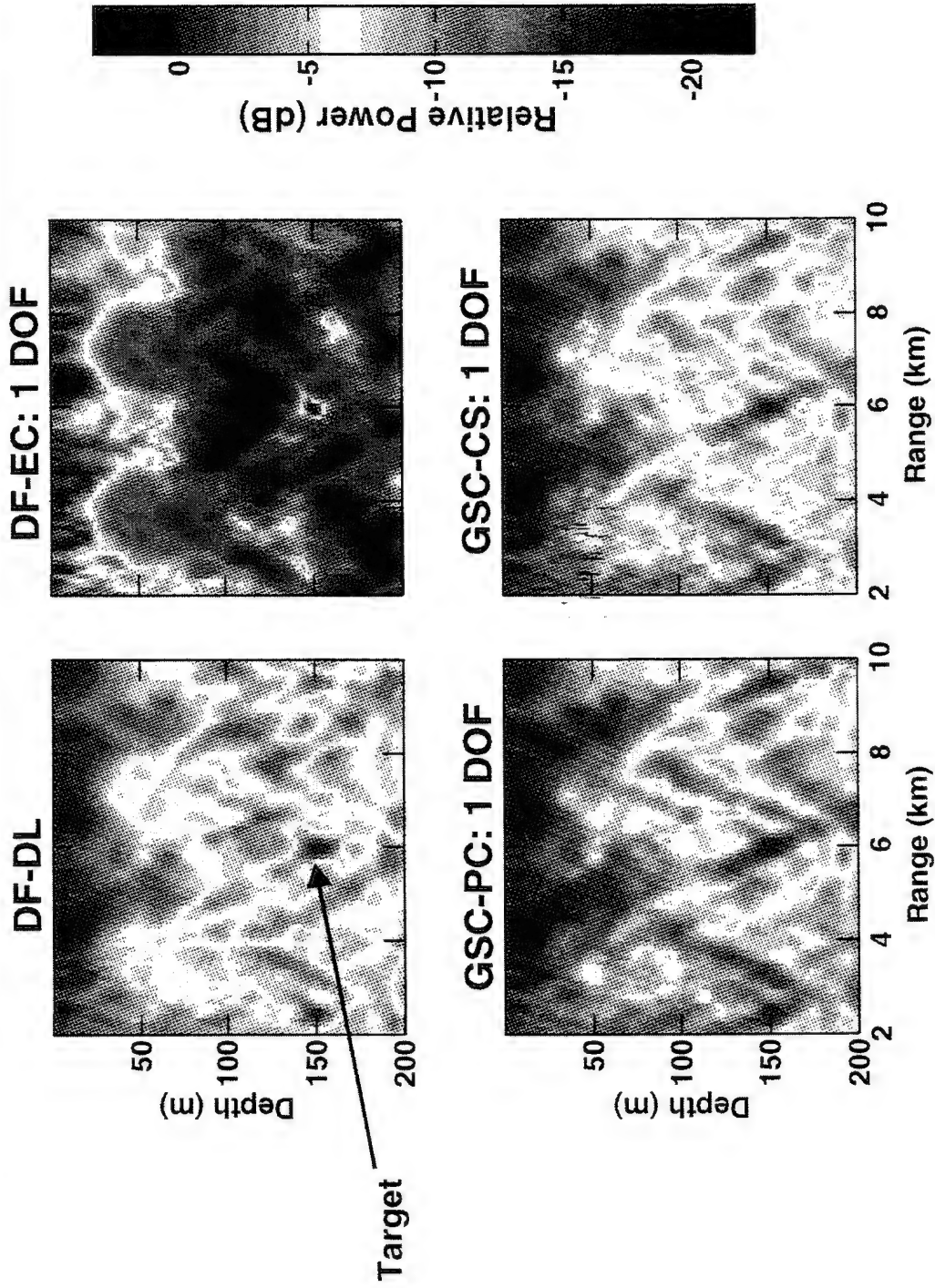
Surface noise level: 10 dBre white noise
Target ESNR = 0 dB
Interferer ESNR = 10 dB

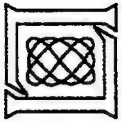
Interfering ship sidelobes obscure
submerged target with CMFP

48 snapshots



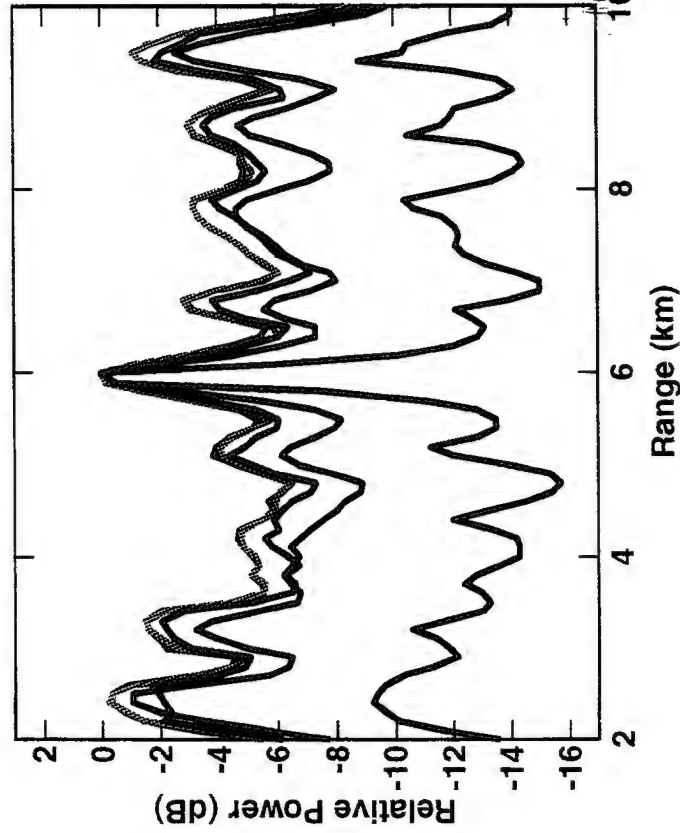
AMFP Results: No Interferer



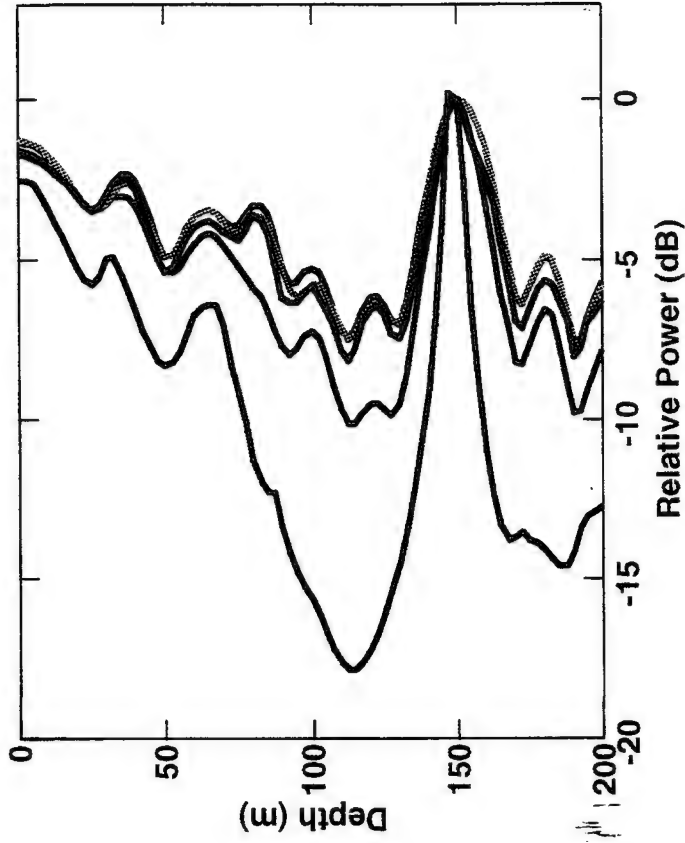


AMFP Slices: No Interferer

At target depth = 150 m



At target range = 6 km

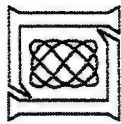


CMFP
DF-DL
GSC-PC: 1 DOF
GSC-CS: 1 DOF
DF-EC: 1 DOF

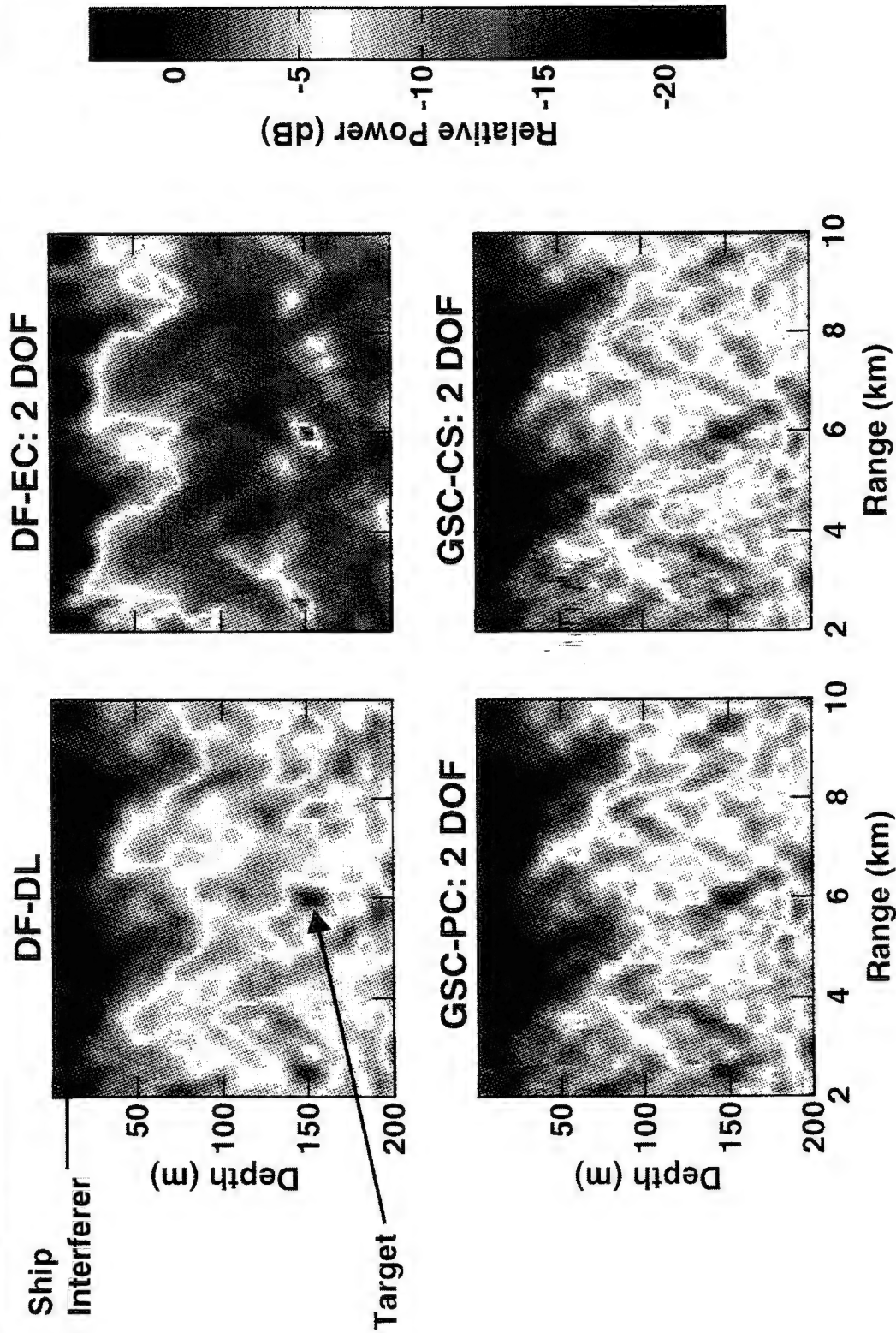
Surface noise level: 10 dBre white noise

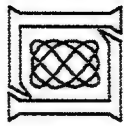
Target: 150 m, 6 km, ESNR = 0 dB

Sample covariance, 48 snapshots (3N)

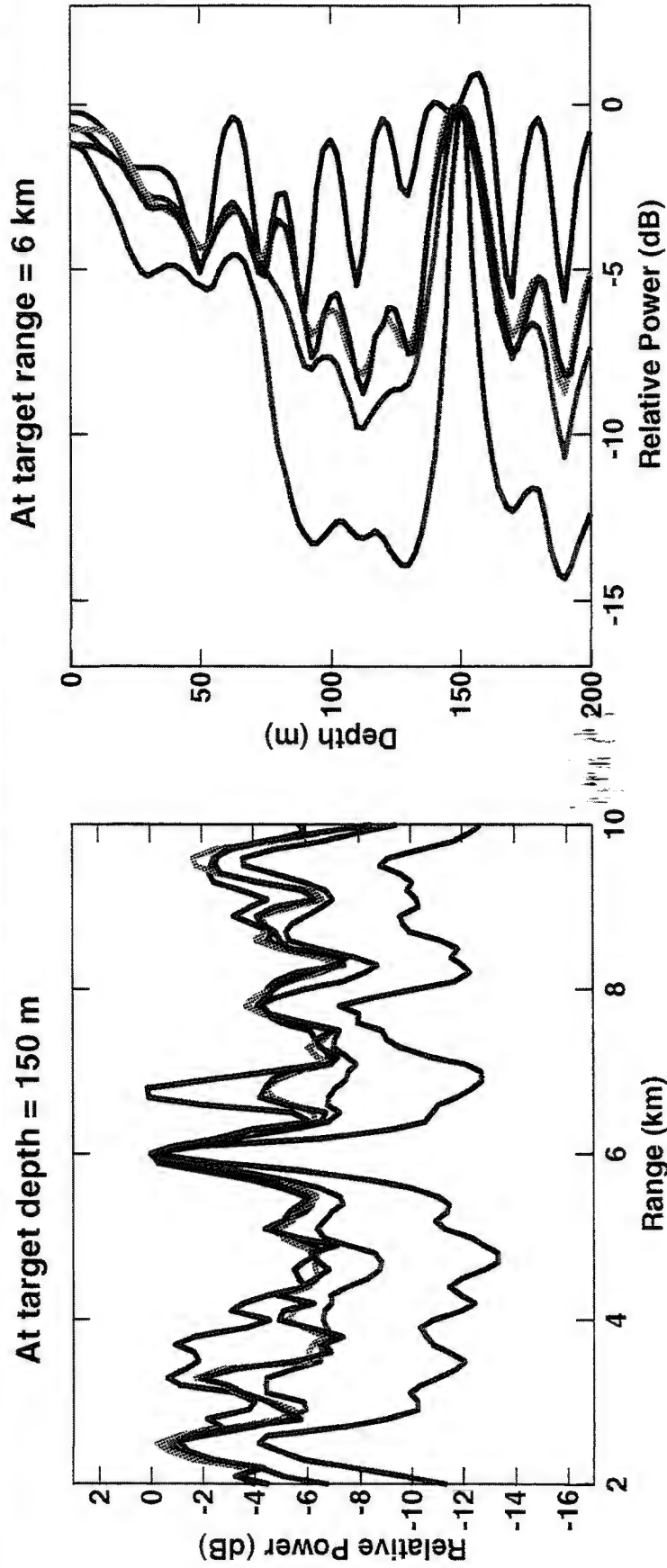


AMFP Results With Interfering Ship





AMFP Slices: With Interfering Ship



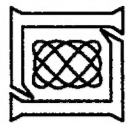
Surface noise level: 10 dB re white noise

Target: 150 m, 6 km, ESNR = 0 dB

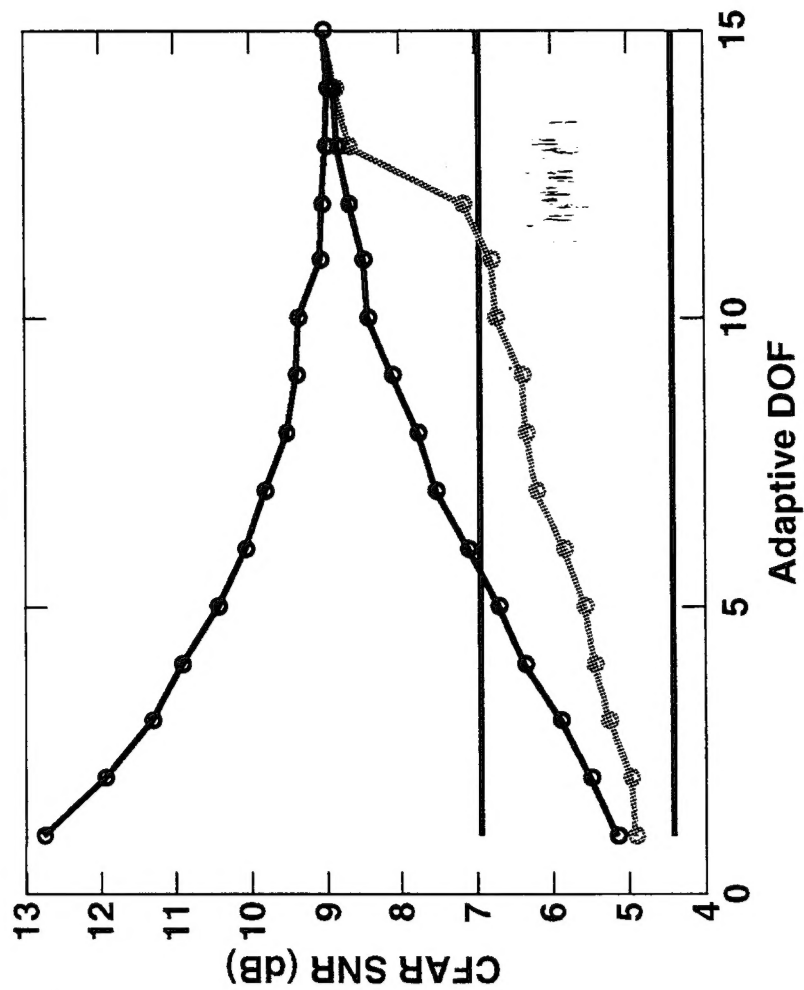
Interferer: 5 m, 8 km, ESNR = 10 dB

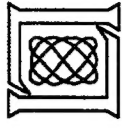
Sample covariance, 48 snapshots (3N)

CMFP
DF-DL
GSC-PC: 2 DOF
GSC-CS: 2 DOF
DF-EC: 2 DOF



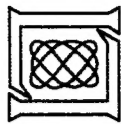
Local CFAR Performance Comparisons





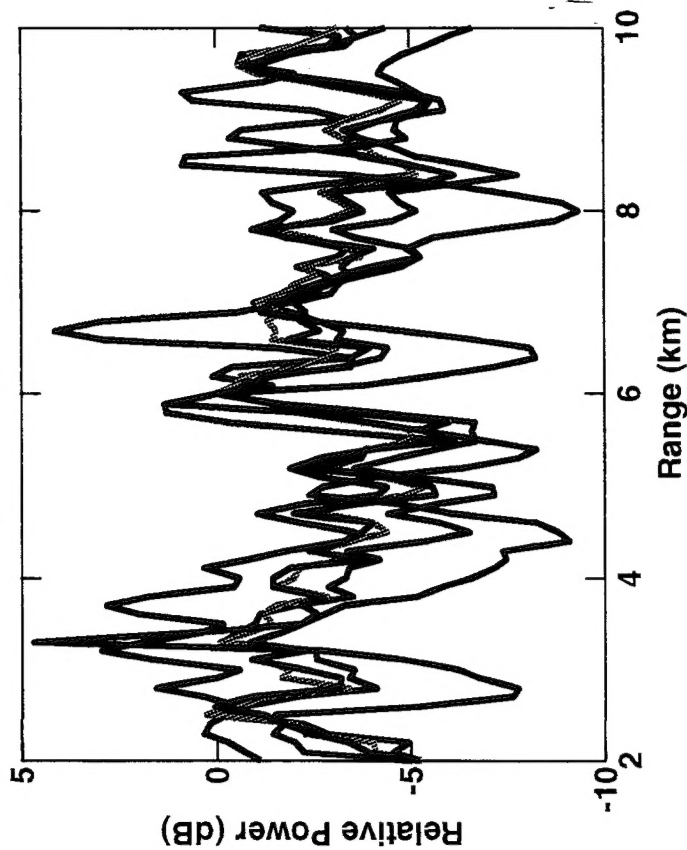
Summary and Conclusions

- Comparisons of reduced rank architectures for adaptive matched field processing were presented
 - Discrete noise and continuous surface noise model included in simulations
- Direct form reduced rank based on eigenvector coherence outperforms both MVDR with diagonal loading and GSC reduced rank architectures
- GSC architecture not recommended due to substantially increased computational complexity and inferior AMFP performance
- Future work area:
 - Extend reduced rank MFP concepts to active systems for noise and reverberation suppression

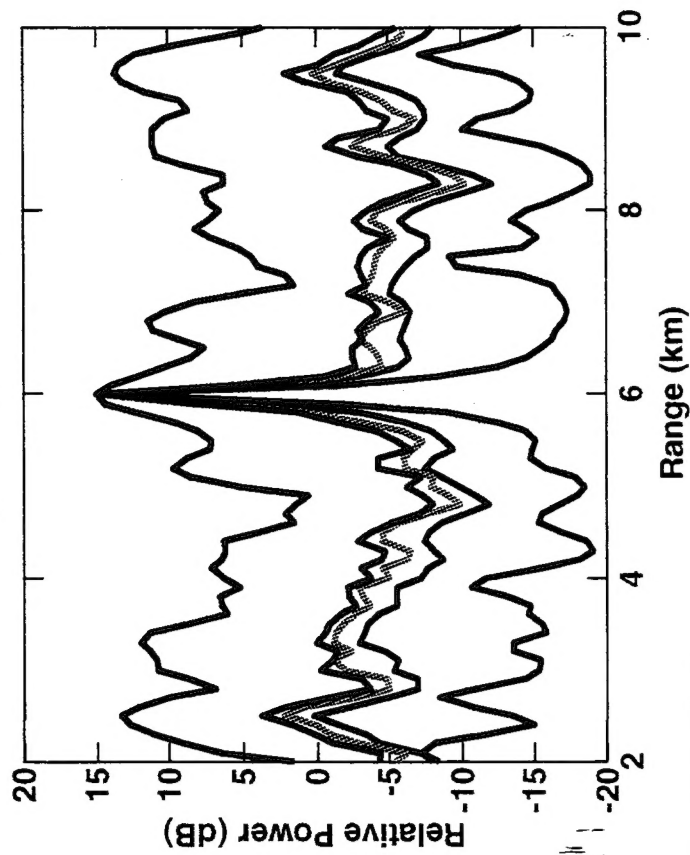


Sample Starved Example

Target ESNR = 0 dB



Target ESNR = 10 dB



AMS slices at target depth

Surface noise level: 10 dBre white noise

Target: 150 m, 6 km

Interferer: 5 m, 8 km, ESNR = 10 dB

Sample covariance, 16 snapshots

CMFP
DF-DL
GSC-PC: 3 DOF
GSC-CS: 3 DOF
DF-EC: 3 DOF

REPORT DOCUMENTATION PAGE

Form Approved
OMB No. 0704-0188

Public reporting burden for this collection of information is estimated to average 1 hour per response, including the time for reviewing instructions, searching existing data sources, gathering and maintaining the data needed, and completing and reviewing the collection of information. Send comments regarding this burden estimate or any other aspect of this collection of information, including suggestions for reducing this burden, to Washington Headquarters Services, Directorate for Information Operations and Reports, 1215 Jefferson Davis Highway, Suite 1204, Arlington, VA 22202-4302, and to the Office of Management and Budget, Paperwork Reduction Project (0704-0188), Washington, DC 20503.

1. AGENCY USE ONLY (Leave blank)		2. REPORT DATE 15 May 1998		3. REPORT TYPE AND DATES COVERED Project Report ASAP-6, Volume 1	
4. TITLE AND SUBTITLE Proceedings of the Adaptive Sensor Array Processing (ASAP) Workshop, 11-12 March 1998				5. FUNDING NUMBERS C — F19628-95-C-0002 PR — 682	
6. AUTHOR(S) Gina M. O'Donovan, Editor					
7. PERFORMING ORGANIZATION NAME(S) AND ADDRESS(ES) Lincoln Laboratory, MIT 244 Wood Street Lexington, MA 02173-9108				8. PERFORMING ORGANIZATION REPORT NUMBER ASAP-6, Volume 1	
9. SPONSORING/MONITORING AGENCY NAME(S) AND ADDRESS(ES) DARPA 3701 N. Fairfax Drive Arlington, VA 22203-1714				10. SPONSORING/MONITORING AGENCY REPORT NUMBER ESC-TR-97-115	
11. SUPPLEMENTARY NOTES None					
12a. DISTRIBUTION/AVAILABILITY STATEMENT Approved for public release; distribution is unlimited.				12b. DISTRIBUTION CODE	
13. ABSTRACT (Maximum 200 words) This year marks the sixth annual ASAP workshop, which is sponsored jointly by the DARPA Sensor Technology, Tactical Technology, and Information Systems Offices, and the Navy AEGIS and E2C Program Offices. This unique joint sponsorship is the result of this year's workshop focus and the many organizations that are developing adaptive signal processing technologies to address critical national defense concerns. In 1997 the workshop focused on the synergy between the sonar and radar communities and their approaches to adaptive signal processing problems. This year we will continue expanding this interaction by providing a forum in which important new developments may be presented and discussed within the context of national defense. The theme for this year's workshop will be adaptive sensor fusion, which extends the concept of an array to a "system of systems." This theme is strengthened by the inclusion of adaptive techniques for model-based image processing and SAR to complement sonar and radar.					
14. SUBJECT TERMS				15. NUMBER OF PAGES 516	
				16. PRICE CODE	
17. SECURITY CLASSIFICATION OF REPORT Unclassified	18. SECURITY CLASSIFICATION OF THIS PAGE Same as Report	19. SECURITY CLASSIFICATION OF ABSTRACT Same as Report	20. LIMITATION OF ABSTRACT Same as Report		